Superconducting Generator Design

EL-577
Research Project 429-1

Final Report, November 1977

Prepared by

DOE 5442

WESTINGHOUSE ELECTRIC CORPORATION
Large Rotating Apparatus Division
East Pittsburgh, Pennsylvania 15112

Principal Investigators
James H. Parker, Jr.
Raymond A. Towne

MASTER

Prepared for

Electric Power Research Institute
3412 Hillview Avenue
Palo Alto, California 94304

EPRI Project Manager
Mario Rabinowitz

DISTRIBUTION OF THIS DOCUMENT IS UNLIMITED

DISCLAIMER

This report was prepared as an account of work sponsored by an agency of the United States Government. Neither the United States Government nor any agency thereof, nor any of their employees, makes any warranty, express or implied, or assumes any legal liability or responsibility for the accuracy, completeness, or usefulness of any information, apparatus, product, or process disclosed, or represents that its use would not infringe privately owned rights. Reference herein to any specific commercial product, process, or service by trade name, trademark, manufacturer, or otherwise does not necessarily constitute or imply its endorsement, recommendation, or favoring by the United States Government or any agency thereof. The views and opinions of authors expressed herein do not necessarily state or reflect those of the United States Government or any agency thereof.

DISCLAIMER

Portions of this document may be illegible in electronic image products. Images are produced from the best available original document.

NOTICE

This report was prepared by Westinghouse Electric Corporation, as an account of work sponsored by the Electric Power Research Institute, Inc. (EPRI). Neither EPRI, members of EPRI, Westinghouse, nor any person acting on behalf of either: (a) makes any warranty or representation, express or implied, with respect to the accuracy, completeness, or usefulness of the information contained in this report, or that the use of any information, apparatus, method, or process disclosed in this report may not infringe privately owned rights; or (b) assumes any liabilities with respect to the use of, or for damages resulting from the use of, any information, apparatus, method, or process disclosed in this report.

FOREWORD

This is the final technical report under the Electric Power Research Institute (EPRI) Contract No. RP 429-1, "Superconducting Generator Design," as prepared by the Large Rotating Apparatus Division, Westinghouse Electric Corporation, Pittsburgh, Pennsylvania, for Dr. Mario Rabinowitz, the EPRI Project Manager for the program.

The technical work reported covers the period from September 1, 1975 to August 31, 1977.

The Westinghouse personnel who participated in this contract's effort are:

R. A. Towne (Principal Investigator)
J. H. Parker, Jr. (Principal Investigator)

A. S. Ying
G. D. Cooper
C. Flick
P. W. Eckels
G. R. Wagner
H. E. Haller, III
D. C. Litz
L. A. Kilgore
J. E. Luzader
C. C. Sterrett
R. C. Cheek
F. H. Wolff
H. S. Schenkel
A. C. Hagg
W. C. Brenner
R. L. Kolek
J. F. Ely
K. J. Baumann
R. Butterfield
F. W. Keay
A. M. Sletten
T. W. Dakin
M. Ashkin
R. H. Daugherty

Personnel from Helix Technology Corporation, who performed the work on the refrigeration system are:

R. W. Johnson
W. Toscano
D. Anenius
R. Morris

In accordance with contract requirements, progress in the technical work was reported periodically in Quarterly Reports and was summarized in a Preliminary Draft of the Final Report. There are numerous references in the text of this report to these earlier contributions. They are identified as follows:

Report	Period of Work	Date of Report
Quarterly Report No. 1	September 1, 1975 to December 1, 1975	
Quarterly Report No. 2	December 1, 1975 to March 1, 1976	April 19, 1976
Quarterly Report No. 3	March 1, 1976 to June 1, 1976	July 8, 1976
Quarterly Report No. 4	June 1, 1976 to September 1, 1976	
Quarterly Report No. 5	September 1, 1976 to March 1, 1977	March 10, 1977
Preliminary Draft - Final Report	September 1, 1975 to May 1, 1977	May 1977

In the aggregate, these reports contain information, some of which is not included in this Final Report. The information which has been omitted is usually of topical or temporary interest (in some cases it is obsolete or superseded) or is available from standard references. Those readers who require more information on this subject are referred to the above Quarterly Reports.

ABSTRACT

This report documents the principal results of a detailed conceptual design study of 300 and 1200 MVA turbine generators utilizing superconducting field windings as carried out by the Westinghouse Electric Corporation. Designs are reported that cover a range of reactances, e.g., the subtransient reactances range from 8 to 27% per unit. Design concepts utilized for the rotor involve an NbTi superconductor, a double-shield system, a flexible-disc thermal contraction concept, a convection-dominated helium circuit and an automatic helium level control. The armature designs are based on a new spiral winding concept which is applied at low voltage (14 kV) and at high voltage (up to 500 kV). Utilization of such a high voltage armature implies that the unit transformer can be eliminated. Refrigeration systems have been designed to match generators at both ratings. System studies have shown that the critical fault clearing time for the lower reactance superconducting generators can be appreciably longer than for conventional machines. The increased efficiency of the superconducting machines by about 0.5% plus elimination of the unit transformers with the high-voltage armature yields a life cycle savings for a utility that is equivalent to the original price of the generator. A development plan has been developed that lays out the tasks and schedule leading to the construction and utility test of a 300 MVA superconducting unit. It is concluded that the superconducting generator design is technically and economically attractive and sound; that its reliability can be made at least equal to that of present conventional units at a competitive price; and that its economic benefits extend to ratings as low as 300 MVA.

ACKNOWLEDGMENTS

We would like to acknowledge the support and encouragement that we have received from Dr. Mario Rabinowitz, the EPRI Project Manager for this program, and from Mr. Joseph Jackson, Manager, Rotating Machinery at EPRI.

We want to thank Drs. James Kirtley, Jr., Joseph Smith, Jr., Phillip Thullen, and Gerald Wilson from M.I.T. who in acting as EPRI consultants and reviewers of our progress on this program have given us valuable insight into many difficult technical problems. We also want to thank Dr. Charles Smith and Mr. James Edmunds of ERDA, Mr. Joseph Fitzgerald of Cleveland Electric Illuminating Company, and Mr. Mack Johnson of South Carolina Electric and Gas Company for their valuable questions and comments during the course of this program.

We also acknowledge the helpful suggestions and advice given by J. W. Batchelor, J. D. Davidson, D. H. Rielly, P. R. Heller, R. J. Hillen, L. A. Kilgore, D. L. Donatucci, G. W. Wiener, and S. Quick who formed the Westinghouse Design Advisory Committee.

CONTENTS

Section			Page
1.0	EXECUTIVE SUMMARY		1-1
2.0	TECHNICAL SUMMARY		1-1
	2.1	General Design Consideration	2-1
		2.1.1 Characteristic Data	2-2
		2.1.2 Major Configuration Selections	2-4
		2.1.2.1 Rotor Design	2-6
		2.1.2.2 Stator Design	2-15
		2.1.3 Performance Considerations	2-19
		2.1.3.1 Steady State Performance	2-19
		2.1.3.2 Consideration of Transients	2-21
		2.1.4 Generator Price	2-23
		2.1.5 Economic Evaluation	2-24
	2.2	Design Details	2-27
		2.2.1 Rotor Design	2-27
		2.2.1.1 Rotor Electrical Design	2-28
		2.2.1.2 Rotor Mechanical Design	2-33
		2.2.1.3 Helium Management System	2-41
		2.2.1.4 Rotor Instrumentation	2-42
		2.2.2 Stator Design	2-43
		2.2.2.1 Stator Electrical Design	2-43
		2.2.2.2 Stator Mechanical Design	2-49

Page

2.3 Auxiliaries 2-51
2.3.1 Exciter and Voltage Regulator 2-51
2.3.2 Generator Gas, Oil and Water Systems 2-51
2.3.3 Refrigeration System 2-51
2.4 Generator and System Interactions 2-53
2.5 Reliability 2-54
2.6 Manufacturing and Materials Development 2-55
2.7 Development Plan 2-55

3.0 REPORT OF WORK 3-1
3.1 General Design Considerations 3-1
3.1.1 Characteristic Data 3-1
3.1.2 Major Configuration Selection 3-1
3.1.3 Performance Considerations 3-16
3.1.3.1 Steady State Analysis 3-16
3.1.4 Explanation of Economic Estimates 3-23
3.2 Design Details 3-37
3.2.1 Rotor Design 3-37
General Introduction and Requirements 3-37
3.2.1.1 Rotor Electrical Design 3-38
Magnetic Field Distribution - Influence on Design . . . 3-42
Rotor Design: Electromagnetic Interactions 3-45
Factors in Selection of Detailed Winding Arrangement: Pole Angle and Thickness 3-53
Conductor Selection 3-65
Design Margins and Winding Stability 3-67
General Design Considerations for NbTi 3-73
Mixed-Matrix Conductors 3-77
Cable 3-83
All-Copper Matrix 3-85
Nb_3Sn Conductor Design 3-88
Damper Application 3-94
Thermal Design of Damper for Steady-State and Transient Conditions 3-107
Analysis of Magnetic Field Variations and Resultant Losses in Cryogenic Region During Transients with Cold Shield 3-111
Damper Distortion 3-112
Rotation of Inner Relative to Outer 3-126
Rotor Swings 3-127

Page

Steady State Fluctuations 3-129
Synchronous Flux Diffusion 3-129
Superconductor Loss 3-131
Attenuation and Loss of a Shield with a $\sigma = \infty$ Backup . 3-131
3.2.1.2 Rotor Mechanical Design 3-136
Rotor Configuration Selection 3-136
Outer Strongback Configuration 3-136
Inner Strongback Configuration 3-139
Assembly Procedure - Sequence 3-140
Design Criteria and Material Requirements 3-185
Damper Stresses and Deflections 3-186
Inner-to-Outer Rotor Attachment 3-189
Torsional Vibration 3-197
Rotor Lateral Vibration 3-204
Rotor Undamped Natural Frequencies and Mode Shapes . . 3-204
Response to Unbalance Conditions 3-209
Computer Modeling 3-223
Calculation of Mode Frequencies 3-224
Unbalance Calculations 3-227
Lateral Vibration Rotor Models 3-229
Whirl Dynamics of Liquid Helium 3-236
Helium Transfer System 3-241
Helium Transfer System Thermal Loss Analysis 3-248
3.2.1.3 Helium Management System 3-258
General Design Considerations 3-259
Physical Design Description 3-262
Component Performance Discussion 3-270
Design Calculations 3-271
Radial Heat Exchanger 3-272
Conductor Cooling 3-275
Cold Damper Cooling 3-276
Torque Tube Pumps 3-276
Torque Tube and Radiation Shield Cooling 3-277
Lead Analysis and Design 3-286
Field Winding Quench Analysis 3-289
Rotor Cooldown from Room Temperature 3-294
Effect of Transients on the Helium Management System . 3-294
Time Constants of the Cooling System 3-295

Page

3.2.1.4 Rotor Instrumentation 3-300
Quantities to be Measured and Telemetered 3-300
Cryogenic Sensors 3-301
Non-Cryogenic Sensors 3-304
3.2.2 Stator Design 3-316
General Introduction and Requirements 3-316
3.2.2.1 Stator Electrical Design 3-318
Increased Voltage Capability - EHV Turbine Generators . 3-319
Functional Evaluation of Insulation Systems 3-342
Magnetic Field Distributions in Superconducting Generators 3-344
Three-Dimensional Magnetic Field Calculation for a Finite Rotating Machine Enclosed by a Magnetic Boundary 3-344
Stator Winding Configuration Selection 3-358
Final Concept Evaluation and Selection 3-358
Spiral Pancake Winding 3-358
Application of the Spiral Pancake Winding Concept to High Voltage Armature 3-368
Terminal Arrangements for Large EHV Turbine Generators 3-372
Scaling of High-Voltage Design Criteria for Larger and Smaller Ratings 3-377
Reliability Factors for EHV Armature Windings: Test, Maintenance, and Fault Anticipation 3-380
Application of EHV Insulation: Comparison to Conventional Practice 3-380
Application of the Spiral Pancake Winding Concept to Low-Voltage Armature 3-386
Stator Winding Detail Design 3-388
Stranding and Transposition 3-389
Coordination between Insulation and Cooling Systems . . 3-393
Calculation of the Water Flow Path: Water and Surface Rises, Pressure Drop 3-398
Calculation of the Fluid Flow Path for High-Voltage Windings 3-399
Description of Stator Coils for Low-Voltage Windings . 3-400
Description of Stator Coils for High-Voltage Windings . 3-408
Shield Design 3-410
Calculation of Cooling Passages for Stator Shield for High-Voltage Windings 3-416

Page

3.2.2.2 Stator Mechanical Design 3-416
Spiral Pancake Winding and Its Support 3-421
3.3 Auxiliaries 3-425
3.3.1 Exciter and Voltage Regulator 3-425
Steady State Requirements 3-425
Excitation System Forcing Requirements 3-425
Operation of Excitation System and Voltage Regulator . 3-427
Quench Detection 3-434
Superconducting Machine Dynamic Stability 3-437
3.3.2 Generator Gas, Oil and Water Systems 3-457
3.3.3 Refrigeration System 3-458
System Design 3-461
Thermodynamic Process Cycle 3-462
System Description 3-465
Key Component Identification 3-479
Screw Compressor Operation 3-480
Cold Box Discussion 3-481
Heat Exchanger 3-483
Turbine Discussion 3-486
Reliability Overview 3-494
Reliability Analysis 3-495
Cost Evaluation 3-498
Conclusions and Recommendations 3-498
3.4 Generator and System Interactions 3-499
Introduction 3-499
The Parametric Study 3-501
Damping of Superconducting Generator Rotor Oscillations Following a Disturbance 3-510
Fault Torques and Further Results on CFCT 3-515
Steady State Stability 3-522
Regulation Under Load Change 3-523
Generator-Turbine Shaft Mode Damping 3-523
Impact of Flexible Shaft Oscillation on CFCT 3-539
Generator Transient Performance 3-550
3.5 Reliability 3-557
3.6 Material Selection 3-560
General Comments 3-560
Preliminary Material Selection 3-565

Page

Potential Future Materials 3-568

3.7 Development Plan 3-575

Introduction 3-575

Phase I - Premanufacturing Development 3-575

Phase II - Manufacture and Installation 3-576

Critical Component Development - Rotor 3-579

Critical Component Development - Stator 3-582

Engineering Development 3-584

Materials and Manufacturing Development 3-585

4.0 REVIEW QUESTIONS AND RESPONSES 4-1

LIST OF ILLUSTRATIONS

Figure No.	Title	Page
2-1	Longitudinal Section of Superconducting Generator	2-5
2-2	Longitudinal Section of Rotor	2-7
2-3	Cross Section of Rotor	2-9
2-4	Helium System Diagram	2-10
2-5	Details of Rotor Slots and Field Winding	2-12
2-6	View of Spiral Pancake Armature Winding and Coil	2-17
2-7	High Voltage Armature Winding	2-18
2-8	Generator Price Versus Rating	2-23
2-9	Generator Price Trends versus Synchronous Reactance	2-24
2-10	General Rotor Configuration	2-34
2-11	Longitudinal Section of Rotor	2-36
2-12	Side View of Torque Tube	2-37
2-13	Cross Section of Spiral Pancake Winding for EHV Superconducting Turbine Generator	2-46
2-14	Longitudinal Section of Superconducting Turbine Generator with EHV Armature Winding	2-47
3-1	Basic Generator Vector Diagram	3-17
3-2	kVa, X_d and V_T versus V_T	3-18
3-3	Generator Vector Diagram for Armature and Field Quantities	3-19
3-4	kVA, X_D and V_T versus V'_T	3-19
3-5	KVA, X_d and V_t versus V'_T	3-20
3-6	Generator Internal Voltage and kVA Capability as Functions of Winding Thickness and Superconducting Characteristics	3-21

Figure No.	Title	Page
3-7	Maximum E_f for NbTi and Nb_3Sn	3-22
3-8	Capital Expenditure Reduction Resulting from a Decrease in Generator Length	3-30
3-9	Capital Expenditure Reduction Resulting from a Decrease in Generator Weight	3-31
3-10	Generator Price versus Rating	3-35
3-11	Generator Price Trends versus Synchronous Reactance	3-36
3-12	Design Logic for Field Winding	3-41
3-13	Flux Map of Superconducting Turbine Generator under Load	3-44
3-14	Estimated Dependence of Subtransient Reactance to Proximity of Damper Winding to Armature Winding	3-46
3-15	Major Components of Superconducting Rotor	3-49
3-16	Racetrack Type Field Winding for Superconducting Generator	3-50
3-17	Final Rotor Configuration for 300 MVA Superconducting Turbine Generator	3-52
3-18	General Field Geometry	3-54
3-19	Maximum Flux Density in a Superconducting Field Winding as a Function of Pole Angle and Winding Thickness	3-55
3-20	Total Ampere-Turns in a Superconducting Field Winding as a Function of Pole Angle and Winding Thickness	3-56
3-21	Airgap Line and Superconductor Characteristic for a Superconducting Field Winding as Function of Pole Angle and Winding Thickness	3-58
3-22	Maximum Radial Component of Fundamental Field Flux Density at O.D. of Field Winding	3-59
3-23	Fraction of Maximum Flux Density Useful at O.D. of Field Winding	3-60
3-24	Location of Maximum Flux Density	3-61
3-25	Maximum Flux Density in a Superconducting Field Winding as a Function of Winding Thickness and Pole Angle	3-62
3-26	Amplitude of Field Harmonics of a Superconducting Field Winding as a Function of Pole Arc	3-64
3-27	Superconductor Limits	3-66

Figure No.	Title	Page
3-28	Magnetic Field and Temperature Degradation of the Current Carrying Capacity of NbTi Conductors	3-74
3-29	Temperature Rise of Conductor vs. Heat Input for Two Values of Helium Volume	3-76
3-30	Cross-section of Mixed-matrix Conductor	3-78
3-31	Comparison of Losses for Mixed-matrix Conductors for 300 MVA Machine	3-86
3-32	Cross Section of Proposed Copper Matrix, NbTi Superconductor.	3-89
3-33	Cross Section of Superconducting Rotor Illustrating Cold and Warm Damper Provisions	3-95
3-34	Attenuation Factor $\|K_{att}\|$ vs. Inner Radius R_1 and Thickness Δ of Damper	3-101
3-35	Attenuation Factor $\|K_{att}\|$ vs. Inner Radius R_1 and Thickness Δ of Damper	3-102
3-36	Attenuation Factor $\|K_{att}\|$ vs. Inner Radius R_1 and Thickness Δ of Damper	3-103
3-37	Two-Shell Configuration Diagram	3-106
3-38	Dimension of the Rotor Shells	3-121
3-39	General Rotor Configuration	3-137
3-40	Rotor Cross Section	3-138
3-41	Rotor Helium Management System	3-141
3-42	Rotor Helium Slot Circuit	3-142
3-43	Rotor Cross Section - 300 MVA	3-146
3-44	Rotor Cross Section - 1200 MVA~	3-147
3-45	Field Winding Slot	3-148
3-46	Torque Tube Design	3-151
3-47	SCTG Rotor Tube Stress Nomenclature	3-153
3-48	Model for Calculation of Torque Tube Stress due to Inner Rotor Weight	3-156
3-49	Effect of Bearing Pedestal Stiffness on Lateral Vibration of SCTG Rotor	3-158

Figure No.	Title	Page
3-50	Torque Tube Temperature Distribution - 300 MVA Rotor	3-161
3-51	Section through Radiation Shield - 300 MVA SCTG Rotor	3-164
3-52	Flex Ring Radiation Shield Mount	3-165
3-53	Radiation Shield Inner Shell Schematic of Cooling Grooves and Helium Flow	3-167
3-54	Flex Ring Radiation Shield Mount Axial Bending Stress Models - Straight Beam	3-174
3-55	Flex Ring Radiation Shield Mount Axial Bending Stress Models - Curved Beam	3-174
3-56	Short Circuit Torque on Flex Ring Radiation Shield Mount	3-180
3-57	Flexible Connection - 300 MVA	3-190
3-58	Flexure Dimensions	3-191
3-59	Sliding Support Scheme	3-195
3-60	Three-Inertia Model	3-198
3-61A	Lowest Lateral Vibration Modes - 1st Mode	3-206
3-61B	Lowest Lateral Vibration Modes - 2nd Mode	3-206
3-61C	Lowest Lateral Vibration Modes - 3rd Mode	3-206
3-62	Schematic of 1200 MVA SCTG Rotor Finite Element Model Used for Lateral Vibration Investigation	3-208
3-63A,	Lowest Three Lateral Vibration Modes - 1st	3-210
3-63B,	Lowest Three Lateral Vibration Modes - 2nd	3-210
3-63C,	Lowest Three Lateral Vibration Modes - 3rd	3-210
3-64	Vibration Responses of 300 MVA SCTG Rotors with 1.77 Nm (15.44 in. lb.) Static Unbalance on Outer Rotor	3-211
3-65	Vibration Responses of 300 MVA SCTG Rotors with 1.91 Nm (16.94 in. lb.) Static Unbalance on Inner Rotor	3-213
3-66	Vibration Responses of 300 MVA SCTG Rotors with 1.52 Nm (530 lb. in.^{2}) Dynamic Unbalance on Outer Rotor	3-214
3-67	Vibration Responses of 300 MVA SCTG Rotor with Out of Phase .27 Nm (2.35 in. lb.) Static Unbalances on Both the Inner and Outer Rotors	3-215
3-68	Vibration Responses of 1200 MVA SCTG Rotors with 5.54 Nm (49.01 in. lb.) Static Unbalance on Outer Rotor	3-217

Figure No.	Title	Page
3-69	Vibration Responses of 1200 MVA SCTG Rotors with 5.54 Nm (49.01 in. lb.) Static Unbalance on Outer Rotor	3-218
3-70	Vibration Responses of 1200 MVA SCTG Rotors with 5.28 Nm (46.69 in. lb.) Static Unbalance on Inner Rotor	3-219
3-71	Vibration Responses of 1200 MVA SCTG Rotors with 5.28 Nm (46.69 in. lb.) Static Unbalance on Inner Rotor	3-220
3-72	Vibration Responses of 1200 MVA SCTG Rotor with 1.01 Nm (8.91 in. lb.) Out of Phase Static Unbalances on Inner and Outer Rotor	3-221
3-73	Vibration Responses of 1200 MVA SCTG Rotors with Dynamic Unbalance of 6.79 Nm^2 (2366 lb. $in.^2$) on Outer Rotor	3-222
3-74	Schematic of Finite Element Model Used to Investigate Lateral Vibration of 300 MVA SCTG	3-230
3-75	Liquid Helium in a Rotating Eccentric Cylinder	3-238
3-76	Helium Transfer System	3-242
3-77	Static Joint for Transferring Liquid Helium	3-243
3-78	Rotating Helium Transfer System	3-243
3-79	Ferrofluidic Seal	3-245
3-80	Thermal Conductivity of 304 Stainless Steel versus Temperature. .	3-252
3-81	Temperature Distribution in 304 Stainless Steel due to Simple Conduction - Hot End at 300 K - Cold End at 4.2 K	3-254
3-82	Helium Management Diagram	3-263
3-83	Field Winding Slot Subassembly	3-264
3-84	Rotor End Sectional Showing the Helium Inlet Trough	3-265
3-85	Rotor Inlet "T" Tube and Trough Configuration Indicating the Control Volume for Eqs. 1 and 2	3-271
3-86	Delivery Temperature at the Outside Radius vs. Flowrate	3-273
3-87	Helium Evaporating Pressure and Exhaust Tube Pressure Drop . . .	3-278
3-88	Torque Tube Temperature Distribution as a Function of Flow Rate per End	3-279
3-89	Cold End Heat Leak through One Torque Tube as a Function of Flow Rate	3-280

Figure No.	Title	Page
3-90	Radiation Shield Inner Shell Schematic of Cooling Grooves and Helium Flow	3-282
3-91	Radiation Shield Temperature as a Function of Total Flow Rate	3-284
3-92	Torque Tube Temperature Distribution during a Fault Transient	3-285
3-93	Cold End Heat Leak vs. Area of Lead for Various Helium Flow Rates	3-288
3-94	Lead Temperature Distribution for Normal and Over Current Conditions	3-290
3-95	Field Coil Voltabe vs. Time During Quench	3-292
3-96	Field Winding Temperature at the Hot Spot vs. Time during the Quench Interval	3-293
3-97	Transmission Line MW Capability vs. Line Voltage Rating	3-321
3-98	Maximum Working Stress and Power Transmitted by Three Single-Core O.F. Cables of the 750 kV Class as a Function of the System Voltage	3-324
3-99	Comparison of Conventional Turbine Generator Installation with EHV Superconducting Generator Installation Concept	3-325
3-100	Dielectric Strengths of Oil-Treated Pressboard and Transformer Oil as Affected by Time	3-331
3-101	Impulse Voltage Breakdown of Oil Treated Pressboard with and without a Series Arranged Oil Duct	3-331
3-102	Impulse Flashover Characteristics of Oil Treated Pressboard Tested Under Oil	3-331
3-103	Equivalent Circuit of One Phase of Conventional Turbine Generator	3-336
3-104	Surge Voltage Distribution Along Phase Winding of Conventional Turbine Generator	3-336
3-105	Detailed Equivalent Circuit of 60 Portion of 2-Pole High Voltage Spiral Pancake Winding Concept.	3-337
3-106	Microscopic Field Enhancement as a Function of Geometry for an Ellipsoidal Projection on an Otherwise Flat Infinite Plane	3-338
3-107(a)	Dimensions of Magnetic Enclosure and Coil Layout	3-347
3-107(b)	Developed View of One Quarter of a Coil	3-347

Figure No.	Title	Page
3-108	Contour Plot of the Magnitude of the Armature Field $\|B\|$ at r = .597	3-352
3-109	Perspective Plot of the Magnitude of Armature Field $\|B\|$ at r = .597 m	3-353
3-110	Perspective Plot of the z-Component of the Armature Field B_z at r = .597	3-354
3-111	Perspective Plot of the θ-Component of the Armature Field B_θ at r - .597.	3-355
3-112	Transformation of an Element of a Ring-Wound Armature into a Drum-type Full Coil	3-362
3-113	Spiral Pancake Winding Concept	3-363
3-114	Cross Section of Spiral Pancake Winding for EHV Superconducting Turbine Generator Showing	3-364
3-115	Longitudinal Section of Superconducting Turbine Generator with EHV Armature Winding	3-365
3-116	Cross Section of Spiral Pancake Armature Winding for Low Voltage Application	3-366
3-117	Longitudinal Section of Superconducting Turbine Generator with Low-Voltage Armature Winding	3-367
3-118	Detail of Spiral Pancake Winding Concept for EHV Armature	3-371
3-119	Main Lead Terminal Arrangement for Large Conventional Turbine Generator	3-373
3-120	Conceptual Arrangement 2	3-375
3-121	Conceptual Arrangement 3	3-376
3-122	Interpretation of Voltage Rating, BIL, and Interphase Insulation Requirements for High Voltage Armature Windings vs. Rated MVA	3-378
3-123	General Arrangement of Spiral Pancake Winding for 2-pole Machine	3-390
3-124	Overall Appearance of Low-Voltage Spiral Pancake Stator Winding and of Single Spiral Pancake Coil	3-391
3-125	Concentrically Transposed Conductor with Water-cooled Subconductors	3-394
3-126	Details of Low Voltage Spiral Pancake Stator Winding	3-395

Figure No.	Title	Page
3-127	Details of High Voltage Spiral Pancake Armature Winding	3-397
3-128	Cross Sections of Stator Conductors for Low-voltage Armature Windings A, B, E, and F.	3-404
3-129(A)	Cross Sections of Stator Subconductors for Low-voltage Armature Windings A and B	3-405
3-129(B)	Cross Sections of Stator Subconductors for Low-voltage Armature Windings E and F	3-406
3-130	Experimental Stranded and Transposed Subconductor	3-407
3-131	Parallel-Series Connection with Transposition for Two Phase Coils of High Voltage Spiral Pancake Stator Winding	3-409
3-132	Radial Force Distribution	3-420
3-133	Field Winding Ripple Losses	3-430
3-134	Generator Control and Excitation System	3-433
3-135	Schematic of Quench Detection Scheme #1	3-438
3-136	Schematic of Quench Detection Method #2	3-439
3-137	Schematic of Quench Detection Method #3	3-440
3-138	Schematic of Field Coil Coupled to Armature and System	3-441
3-139(A)	Dynamic Stability Model for an Excitation Control System against an Infinite Bus with Electrical Torque Derived from Synchronous Machine Equivalent Circuits	3-443
3-139(B)	Dynamic Stability Model of an Excitation Control System against an Infinite Bus with Synchronizing and Damping Components of Electrical Torque Separated	3-444
3-140	Model of Conventional Synchronous Machine Against an Infinite Bus	3-445
3-141	Excitation System Model	3-446
3-142(a)	Synchronizing Torque: Excitation Control System with Conventional Generator	3-448
3-142(b)	Damping Torque: Excitation Control System with Conventional Generator	3-449
3-142(c)	Excitation Control System with Conventional Generator Ratio of Successive Oscillation Peaks	3-451
3-143(a)	Synchronous Torque: Excitation Control System with Superconducting Generator	3-452

Figure No.	Title	Page
3-143(b)	Damping Torque: Excitation Control System with Superconducting Generator	3-453
3-143(c)	Excitation Control System with Superconducting Generator Ratio of Successive Oscillation Peaks	3-454
3-144	Gas System for Use with Superconducting Generator	3-457
3-145	Diagram of Gland Seal Oil System	3-459
3-146	Diagram of Armature Cooling Water System	3-460
3-147	Thermodynamic Process Cycle for 300 MVA Generator	3-463
3-148	Thermodynamic Process Cycle for 1200 MVA Generator	3-464
3-149	Refrigeration System Block Diagram	3-466
3-150	Compressor System Block Diagram	3-468
3-151A	Compressor Flow Diagram	3-469
3-151B	Compressor Flow Diagram	3-470
3-152	Cold Box Block Diagram	3-473
3-153	Cold Box Flow Diagram	3-474
3-154	Process Control System Block Diagram	3-478
3-155	Compressor System	3-482
3-156	Cold Box	3-484
3-157	Gas Bearing Turbine	3-487
3-158	Turbine Exploded View	3-488
3-159	Control Panel	3-491
3-160	Storage Dewar	3-492
3-161	Critical Fault Clearing Time as a Function of Unit Inertia	3-503
3-162	Critical Fault Clearing Time as a Function of Generator Reactance	3-504
3-163	Critical Fault Clearing Time as a Function of Generator Subtransient Time Constant	3-506
3-164	Critical Fault Clearing Time as a Function of Exciter Ceiling Voltage	3-507

Figure No.	Title	Page
3-165	Diagram of System Analyzed	3-511
3-166	Rotor Angle versus Time	3-512
3-167	Rotor Angle versus Time	3-513
3-168	Rotor Angle versus Time	3-514
3-169	Air Gap Power versus Time (Fault Cleared at 0.23 sec.)	3-517
3-170	Shaft Torque versus Time (Fault Cleared at 0.23 sec.)	3-518
3-171	Torques versus Clearing Times 300 MVA Superconducting Generator	3-520
3-172	Generator Voltage versus Time 20% (60 MVAR) VAR Overload	3-524
3-173	Generator Voltage, Volts/Hz and Speed Following a Full Load Rejection-Superconducting	3-525
3-174	Generator Voltage, Volts/Hz and Speed Following a Full Load Rejection-Conventional	3-526
3-175	(a) Schematic of Generator - System (b) Steady State Phasor Diagram	3-532
3-176	Secondary Resistance and Skin Depth versus Frequency	3-536
3-177	Damping Constant versus Frequency - Open Circuit	3-537
3-178	Damping Constant versus Frequency - Full Load	3-538
3-179	Damping Constant versus Frequency - Low-voltage Spiral, Full Load	3-541
3-180	Damping Constant versus Frequency - High-voltage Spiral - 300 MVA, Full Load	3-542
3-181	Model System	3-543
3-182	CFCT Diagram	3-548
3-183	Development Plan	3-577
3-184	Critical Component Development - Rotor	3-580

LIST OF TABLES

Table No.	Title	Page
1-1	1200 MVA Comparison	1-4
2-1	Superconducting Generator Characteristic Data 3600 rpm 60 Hz - 0.90 Power Factor.	2-3
2-2	Low-Voltage Superconducting Generator Economic Benefits Relative to Conventional Generators Plant Rating - 1000 MWe	2-25
2-3	High-Voltage Superconducting Generator Economic Benefits Relative to Conventional Generators Plant Rating - 1000 MWe	2-26
2-4	List of Electrical	2-48
3-1	Generator Characteristic Data	3-2
3-2	Coal Plant Capital Cost Estimates	3-23
3-3	Nuclear Plant Capital Cost Estimates	3-23
3-4	Nuclear Plant Cost Breakdown 1000 MW - 1985 Commercial Operation	3-24
3-5	Projected Levelized Coal Prices	3-25
3-6	Nuclear Fuel Cycle Cost Estimate - 1985	3-25
3-7	High-Voltage Superconducting Generator Benefits Present Worthed to 1977 at 15%	3-28
3-8	Comparative Turbine Generator Prices (1976) 300 MVA - 3600 rpm	3-32
3-9	Comparative Turbine Generator Prices (1976) 1200 MVA - 3600 rpm	3-33
3-10	Comparative Turbine Generator Prices (1976) 3000 MVA - 3600 rpm	3-34
3-11A	Damper Shield Design Requirements Steady State Operation	3-39
3-11B	Damper Shield Design Requirements (Continued) Transient Conditions	3-40
3-12	Conductor Specifications	3-79

Table No.	Title	Page
3-13	Losses due to Transient Fields Created by a 66 msec Fault (Monolith)	3-82
3-14	Nb_3Sn Conductor Parameters	3-91
3-15	Losses due to Transient Fields Created by a 66 msec Fault (Nb_3Sn Monolith)	3-92
3-16	Damper Shield Equations	3-100
3-17	Determination of I_2^2t Capability	3-108
3-18	Determination of I_2 Capability Hydrogen Pressure 30 Psig	3-110
3-19	Skin Depth and Time Constants	3-123
3-20	Summary of Shield Heating	3-133
3-21	Generator Torque Tube Design Conditions	3-160
3-22	Torque Tube Stress Calculations (Warm End) 300 MVA SCTG	3-162
3-23	Radiation Shield Dimensions and Stresses SCTG Rotors	3-170
3-24	Flex Ring Data for Radiation Shield Mount	3-170
3-25	Thermal Expansions and Contractions (Axial) of Radiation Shield and Inner Rotor 300 MVA SCTG	3-172
3-26	Thermal Expansions and Contractions (Axial) of Radiation Shield and Inner Rotor 1200 MVA SCTG	3-173
3-27	Flexible Ring Axial Deflections and Stresses 300 MVA SCTG Radiation Shield Mount	3-177
3-28	Flexible Ring Axial Deflections and Stresses 1200 MVA SCTG Radiation Shield Mount	3-177
3-29	300 MVA Radial Free Body Deflections of Radiation Shield and Torque Tube	3-178
3-30	1200 MVA Radial Free Body Deflections of Radiation shield and Torque Tube	3-178
3-31	Flex Ring Combined Stresses 300 MVA SCTG Radiation Shield Mount	3-182
3-32	Flex Ring Combined Stresses 1200 MVA SCTG Radiation Shield Mount	3-182
3-33	Thick Damper Shield versus Thin Damper Shield	3-185
3-34	Damper Shield and Its Support Stresses and Deflections	3-187

Table No.	Title	Page
3-35	Damper Shield and Its Support Stresses and Deflections	3-188
3-36	Stresses in Radial Flexure	3-193
3-37	Shaft Torque at Short Circuit - 1200 MVA	3-203
3-38	Undamped Natural Frequencies (Lowest 3) for 300 MVA SCTG Rotor Model	3-205
3-39	Undamped Natural Frequencies (Lowest 3) for 1200 MVA SCTG Rotor Model	3-207
3-40	300 MVA SCTG Finite Element Properties	3-231
3-41	1200 MVA SCTG Rotor Finite Element Properties	3-234
3-42	1200 MVA SCTG Rotor Bearing Properties	3-233
3-43	EPRI-Westinghouse Superconducting Turbogenerator Cooling System Component Key	3-266
3-44	Heat Exchanger Data	3-275
3-45	Torque Tube Heat Transfer Data	3-281
3-46	SCTG Rotor - Quantities to be Telemetered	3-302
3-47	Power Limits for Transmission Lines	3-320
3-48	Capability and Rating of Circuit Breakers	3-322
3-49	Economic Evaluation of Some Alternative Superconducting Generator Terminal Voltages and Station Layouts	3-327
3-50	Insulation Classes and Dielectric Tests for Oil-Immersed Transformers	3-329
3-51	Maximum Field Strength E with a Potential Difference U between the Electrodes, for Several Electrode Configurations	3-333
3-52	300 MVA Spiral Winding "Solid" Rotor	3-348
3-53	Comparison of 3D and 2D Calculations	3-350
3-54	Spiral Pancake Winding Design Options	3-369
3-55	List of Electrical Designs	3-388
3-56	Armature Winding Design Data	3-402
3-57	Armature Winding Design Data	3-411
3-58	Flux Shield Ventilation for Low Voltage Stator Designs	3-414

Table No.	Title	Page
3-59	Flux Shield Cooling for High Voltage Stator Designs	3-417
3-60	Stator Core Vibration - 300 MVA	3-423
3-61	Stator Core Vibration - 1200 MVA	3-424
3-62	Constants Assumed for Dynamic Stability Analysis	3-447
3-63	System Concept Reliability Study.	3-496
3-64	Inspection Frequency Intervals	3-497
3-65	Price Breakdown	3-498
3-66	Superconducting Generator Electrical Constants Reference Design	3-502
3-67	Conventional Generator Electromechanical Constants	3-509
3-68	Comparison between Superconducting and Conventional Units	3-509
3-69	Generator Constants	3-515
3-70	Swing Frequency of Generator	3-515
3-71	Critical Fault Clearing Times for 300 MVA Generators	3-516
3-72	Rotor, Shaft, and System Constants	3-519
3-73	Fault Frequency	3-521
3-74	Frequency of False Line Interruptions	3-522
3-75	300 MVA Machine Parameters for Shaft Damping	3-540
3-76	Limited Failure - Repairable - Stator	3-558
3-77	Limited Failure - Repairable - Rotor	3-558
3-78	Limited Failure - Repairable - Auxiliaries	3-559
3-79	Required Material Properties	3-561
3-80	Preliminary Material Selections	3-562
3-81	Metal Alloy Designation Cross Reference	3-563
3-82	Room Temperature Properties of Several Current Metal Matrix Composites Reported in the Literature	3-572
3-83	Development Cost - 300 MVA - 3600 rpm	3-578

Section 1.0

EXECUTIVE SUMMARY

INTRODUCTION

Programs have been carried out throughout the world over the last decade to evaluate the technical and economic potential of turbine generators utilizing superconducting field windings. These programs have ranged from demonstrations of technical feasibility with small generators (ratings up to a few MVA) to paper studies on the design of larger machines and their system performance. Programs in the USA have been carried out at MIT under EPRI sponsorship and at Westinghouse and General Electric with "in house" funding.

In general, these programs have shown that superconducting generators have potential benefits relative to conventional units in terms of

- Reduced capital cost
- Lower losses leading to reduced life cycle costs
- Larger ratings
- Improved system performance
- Higher voltages

Based on the results of these earlier programs, the Electric Power Research Institute initiated a "next step" program in late 1975 with the objective of gaining further and more positive assurance as to the benefits of superconducting generators relative to conventional units.

The Westinghouse Electric Corporation was funded at that time under Contract RP429-1 to carry out a two-year program with the following objectives.

- Develop conceptual designs for 300 and 1200 MVA turbine generators (3600 rpm) utilizing superconducting field windings
- Compare the system performance of these machines with conventional units of the same ratings
- Compare capital and operating costs of these units with conventional units
- Lay out a development plan for proceeding through the design, construction and utility test of a 300 MVA unit.

The present report documents the principal results from the Westinghouse effort.

GENERAL APPROACH

In recognition of the fact that the program was directed toward generators for utility application, the Westinghouse group adopted a set of criteria as a basis for continual evaluation of the generator designs as they evolved. These criteria were

- Reliability
- Maintainability
- Manufacturability
- System compatibility
- High efficiency
- Minimum cost
- Compliance with industry standards

In addition, design concepts were to be accepted only if they could be shown to be technically feasibly for machines over the rating range of 300 to 3000 MVA. This criterion was critical in recognition that one of the long range goals of the program was to develop a design base for generators with ratings at the limit of present day machines and beyond.

DESIGN CONCEPTS

Rotor

- Triple shield system
  - -- Warm outer damper shield forms "strong back" of rotor
  - -- Intermediate vapor cooled radiation shield
  - -- Inner cold shield
- Field winding wound into radial slots and mechanically constrained
- Flexible, multiple disc design to accommodate thermal contraction of inner relative to outer rotor shell
- Automatic helium level control
- Radial heat exchangers within rotor to provide isothermal radial temperatures
- Field winding cooling by natural convection of supercritical helium

- Large helium storage within field winding for enhanced stability
- Ferrofluidic rotating seal design for transfer of helium into rotor

Stator

- New armature design utilizing a "spiral pancake" concept
  - -- Yields excellent end turn support
  - -- Applicable at both low and transmission level voltages
  - -- Low voltage utilizes water cooling
  - -- High voltage version uses oil cooled cable/transformer techniques.

Helium Refrigeration

- All rotary components
  - -- Screw compressor
  - -- Gas bearing turbine expanders
- Redundant compressor for reliability
- Full automatic controls

GENERATOR DESIGNS AND CHARACTERISTICS

Nine generator designs were developed based on the final design concepts outlined above. The set of designs covered a range of basic generator characteristics.

- Rating - 300, 1200 and 3000 MVA
- Voltage - Low and high (transmission level)
- Reactance - X''_d 8%, 16%, 27%

A complete set of generator design and performance characteristics were obtained for each generator design.

1200 MVA COMPARISON

An abbreviated comparison of a conventional unit with a specific low and high voltage superconducting generator for 1200 MVA, 3600 rpm is given in the following table.

Table 1-1

1200 MVA COMPARISON

	Conventional	Low S.C.	High S.C.
Voltage (kV)	26	30	500
X_d(%)	180	41	50
X'_d(%)	32	29	30
X''_d(%)	26	16	27
Total Losses (MW)	15.3	4.8	4.1
Efficiency (%)	98.6	99.6	99.6
Total weight (lbs.)	1,400,000	800,000	770,000
Length (ft.)	43	30	35

SYSTEM PERFORMANCE

The predicted system performance of the superconducting generators designed under this program can be summarized as follows.

- Will have no steady state or dynamic stability limit when operated within their MVA capability
- Critical fault clearing times are equal or longer than for conventional units with the same external system conditions
- Voltage regulation upon a Var overload or load rejection is equal to or better than a conventional unit response
- The damper system provides good positive damping for rotor swings

ECONOMIC BENEFITS

Superconducting generators have major economic advantages over conventional units due to

- Higher efficiency
- Lower generator cost
- Transmission level voltage capability

The mature cost of a low voltage 1000 MW generator and its auxiliaries is estimated to be 20% less than a conventional unit of the same rating. With a high voltage armature (transmission level) the cost is estimated to be equal to that of a conventional (low voltage) unit.

The total economic benefit (life cycle and capital) from using a low voltage superconducting generator (1000 MW) amounts to about 65% of the generator cost in a fossil plant to 48% in a nuclear plant.

The use of a high voltage armature eliminates the unit transformer and its losses, thus providing additional savings. The total economic benefit from using a high-voltage superconducting generator (1000 MW) amounts to about 90% of the generator cost for a fossil plant and 60% for a nuclear plant.

DEVELOPMENT PLAN

- Low voltage generator - Part A
  - -- Develop and test a 300 MVA unit with a low voltage armature
  - -- Estimated time - six years
  - -- Estimated cost - $12 x 10^6
- High voltage generator - Part B
  - -- Develop and test a 300 MVA unit with a high (transmission level) voltage armature. The effort for this part would be concentrated on the high voltage armature
  - -- Estimated time - six years
  - -- Estimated cost - $10.6 x 10^6
- Parts A and B could be scheduled in parallel or the start of B could be delayed
- Each part would consist of two phases
  - -- Phase 1, premanufacturing development
  - -- Phase 2, manufacturing and installation

CONCLUSIONS AND RECOMMENDATIONS

It is concluded that the superconducting turbine generator is

- Technically sound
- Economically attractive
- Can be made as reliable as present conventional units at a competitive price
- Economic benefits can extend to rating as low as 300 MVA
- In general, its system performance is superior to conventional units
- Ratings can be extended beyond that which is practical for present conventional units

There is considerable incentive, therefore, to continue support of this development both for the near term advantages utilities will achieve in using superconducting generators in place of conventional generators at present day ratings and for the push toward continuing to achieve "economies of size" at even larger ratings.

It is recommended, that as an extension to the present program, a 300 MVA unit be developed and utility tested, in order to further confirm the technical and economic benefits of the superconducting generator and to form the required base for the commercialization of this new technology.

Section 2.0

TECHNICAL SUMMARY

2.1 GENERAL DESIGN CONSIDERATION

Large turbine generators of conventional design are characterized by high efficiency, effective cooling practices and the utilization of high strength materials in critical rotating components. Present design and material practices will permit some further extension in maximum ratings that can thus be obtained, but no great increase can be expected. The use of superconducting field windings in turbine generators provides an opportunity for the advancement of design practice as follows:

- Major reduction in generator losses and size, leading to major economic benefits
- Freedom to select electrical characteristics more favorable to generator interactions with the transmission system
- Capability for design at transmission voltage levels, permitting the elimination of the main unit step up transformer and leading to further economic benefits
- Great extension in range of maximum rating.

In developing the optimum application of superconducting field windings for turbine generators, the maximization of economic benefits should be the final criterion in the process of selecting configurations and characteristics. Fortunately, the reduction of generator losses (relative to conventional generators) and the resulting economic benefit are not critically dependent on design choices over a wide range of variables. This provides the designer with the freedom to achieve the other objectives without jeopardizing the principal benefit.

Reliability is the most important single consideration in developing the superconducting generator design. This consideration has determined the selection of:

- Superconducting material, strand arrangement and matrix
- Superconductor design point (temperature margin)

- Superconducting field winding support system, and
- Armature configuration and support system.

The adequacy of these selections will ultimately be demonstrated by tests on full size component models and on prototype machines in actual service.

In the area of generator interaction with the connected power system there is an opportunity to provide better performance than can be obtained with conventional units by:

- Designing for lower reactance levels, and
- Providing increased damper shield thermal capability to absorb or dissipate losses due to line harmonics or negative sequence currents.

2.1.1 Characteristic Data

The major parameters of superconducting generator designs which illustrate these concepts are listed in Table 2-1.

Table 2-1

SUPERCONDUCTING GENERATOR CHARACTERISTIC DATA
3600 rpm - 60 Hz - 0.90 POWER FACTOR

MVA	300	300	300	300	1200	1200	1200	1200	1200*	3000
Line Volts - kV	13.8	13.8	230	230	29	30	500	500	26	34
Direct Axis Reactance (per unit) and Time Constants (seconds)										
X_d	0.225	0.417	0.249	0.492	0.221	0.405	0.261	0.497	1.810	0.600
X'_d	0.161	0.313	0.202	0.404	0.151	0.286	0.202	0.393	0.320	0.340
T'_{do}	5167	3920	7187	4990	19,060	12,217	23,263	17,123	4.7	87,200
X''_d	0.081	0.160	0.136	0.269	0.082	0.157	0.137	0.271	0.260	0.190
T''_{do}	0.248	0.259	0.228	0.237	0.293	0.298	0.271	0.276	0.040	0.260
I_2^2t Capability	20	20	20	20	15	15	15	15	7.5	
I_2 Capability	0.12	0.12	0.12	0.12	0.10	0.10	0.10	0.10	0.06	
H-Inertia Constant (kW-sec/kVA) Generator & Turbine	3.23	3.23	3.23	3.23	2.68	2.53	2.75	2.61		
Critical Fault Clearing Time	17.5	14.7	19.2	15.0	16.0	13.3	16.4	13.3	12.75	
Total F.L. Losses - kW (including refrigeration)	1563	1851	1435	1579	4433	4767	3874	4101		
Efficiency	99.42	99.32	99.47	99.42	99.59	99.56	99.64	99.62	99.59	99.67
Magnetic Flux Densities - T Maximum in Field Winding	5.560	5.680	5.620	5.620	5.540	5.620	5.540	5.610		5.220
Mean Radial in Armature	1.260	1.140	0.790	0.740	1.290	1.190	0.880	0.770		1.400
Overall Length - inch	250	225	290	250	433	360	505	420	510	487
Total Weight - lbs. x 10^3		324	399		800		773	1384		1673

*Conventional Generator Data for Comparison.

2.1.2 Major Configuration Selections

The principal design objectives for superconducting generators are

- To reduce losses so as to achieve the corresponding economic benefits
- To achieve reliability equal to or better than that obtained with conventional machines, and
- To achieve improved coordination of the generator and its characteristics with the requirements of the power system; e.g., voltage level, transient interactions.

Reduction of losses is accomplished mainly by utilizing the superconducting field winding to eliminate the ohmic loss that is associated with a conventional copper field winding. A further significant loss reduction may be obtained by matching machine and system voltage levels. Other losses are a function of machine size; the incremental savings in losses due to size reduction are not critical to a favorable economic evaluation, however. In selecting the major machine configurations, the other criteria are therefore given considerable weight.

The process of selecting the most appropriate machine configuration has gone through several stages, beginning with a very general analysis of the application of superconducting windings to the field and the armature, either one of which might be the rotating part of the machine. This was followed by more detailed examinations of field and armature winding configurations, helium management system options, performance, and cost, to obtain the final configuration. (This process is fully documented in the Quarterly Reports submitted under this contract.) A brief description of the final configuration and the general arrangement of the machine follows.

General Arrangement

In its major arrangement of parts and external appearance, the superconducting generator resembles a conventional machine. The active parts are similarly housed in a gas-tight enclosure which is equipped with bearing brackets and journal bearings at both ends for the support of the rotor. A coupling is provided in the usual manner on the turbine end of the rotor, which supports the field winding, the damper shields, the helium management and transfer system, the collector rings, and the field leads. The stator, which is flexibly mounted in the enclosure, includes an armature winding and a magnetic flux shield. This arrangement is shown in Figure 2-1. The component parts of both rotor and stator differ markedly, of course, from conventional practices.

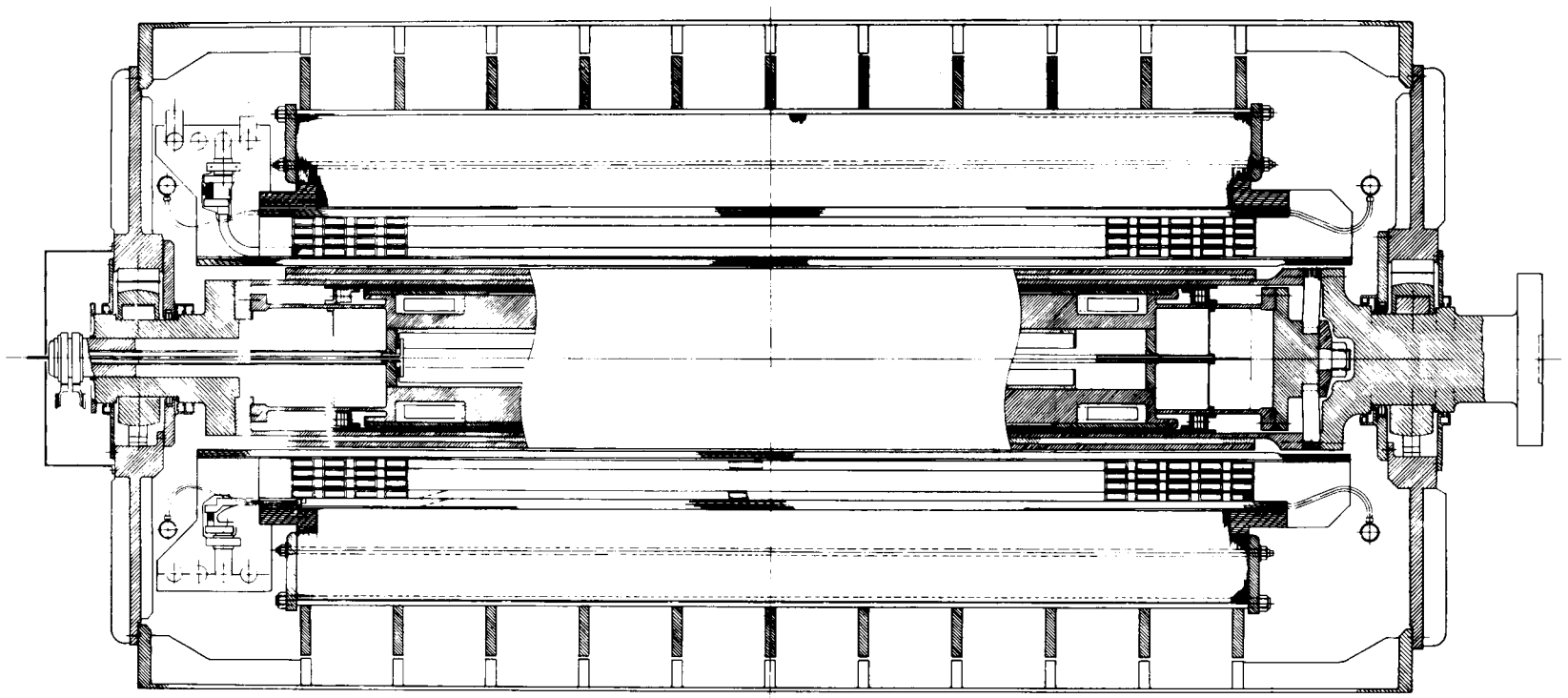

Figure 2-1. Longitudinal Section of Superconducting Generator

2.1.2.1 Rotor Design.

The preferred configuration of the rotor features a field winding of niobium-titanium superconducting wire that is contained in radial slots machined in a tubular rotor body forging and is shielded against external fields and heat transmission by an arrangement consisting of two damper shields and an electro-thermal shield. It has the following advantages:

- Use of well-proven superconductor type available in quantity with present technology
- Excellent mechanical support for superconductor against mechanical and electromechanical force effects
- Excellent shielding of superconductor against external fields
- Assured thorough flooding of winding with liquid helium
- Effective shielding with minimum loading of cryogenic system
- Simple and reliable construction of shield support system
- Simple and reliable construction of internal expansion joint
- Good space factor for windings.

The construction of the rotor is within the grasp of present manufacturing technology, but will require the development of tooling and techniques for installation of the windings. This is discussed in the section on "Development Plan".

A more detailed account of rotor construction follows:

The complete rotor assembly, shown in longitudinal section in Figure 2-2 consists of a "cold" inner rotor at liquid helium temperature, which is suspended within an outer rotor that operates at about 350 K under normal conditions. The suspension arrangement provides thermal isolation as well as control of the differential contraction that occurs during cooldown and of torsional and lateral vibration. It includes

- A rigid flange mount at the collector end
- A flexible connection to accommodate the contraction of the inner rotor, at the turbine end
- Helium-cooled torque tubes, at both ends, to minimize axial heat leaks into the field winding.

The inner rotor is further isolated from the outer rotor by means of thermal insulation that consists of a vacuum space and a thermal shield that is kept at an intermediate temperature (70 to 100 K).

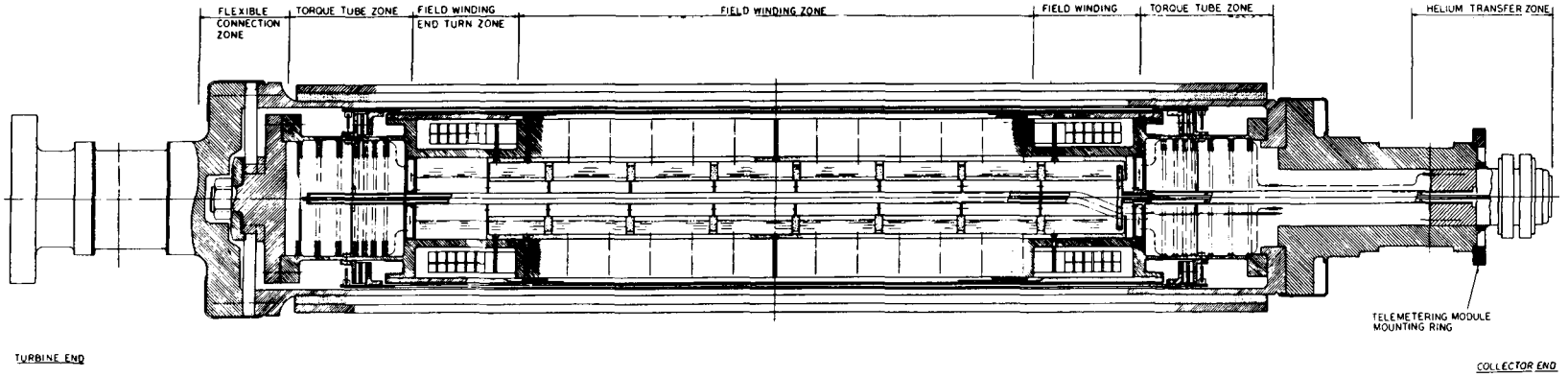

Figure 2-2. Longitudinal Section of Rotor

A solid forging with machined slots, not unlike those used in conventional machines except that it is non-magnetic, forms the basic part of the inner rotor, as shown in Figure 2-3. A large cavity in the center of this forging provides room for the helium management and distribution system, which connects to the field winding entrance ports by way of radial ducts. These are, at the same time, heat exchangers that return a portion of the heat of compression to the central pool of helium in the bore. A complete diagram of the helium system is shown in Figure 2-4.

The radial slots for the field winding, shown in detail in Figure 2-5, are designed to permit winding of the successive turns of small superconducting wire in situ, with sufficient spacers and ducts to obtain a thoroughly helium-permeable arrangement. Spacers provide also for tightening of the wires against local motion, and, in conjunction with an insulating liner, constitute the insulation of the winding to ground. All the slots connect to the helium management system at top and bottom. The slots are closed with metallic wedges, which are carefully fitted to confine the windings in all directions. The end turns are restrained by means of a retaining shell that extends past both sets of end turns and supports a "cold" damper that is bonded to its outer surface. The space between the inner diameter of this tube and the outer surface of the rotor forging is used for storage of reserve helium. Seal welding is used to provide helium and vacuum tight joints.

The outer rotor is the main structural member of the rotor assembly. It provides the major portions of mechanical rigidity and inertia, supports the inner rotor and the "warm" damper, and contains the vacuum which isolates the inner rotor. The ends of this structure are provided with bearing journals of the conventional type. Continuing past these journals, the ends of the outer rotor are equipped with the turbine coupling and the collector arrangement, which also includes the helium transfer system.

Field Winding

Several thousand turns of a multifilamentary copper-matrix superconducting wire make up the field winding. The possibility of utilizing a copper-matrix monolithic type of conductor, whose technology and use is well established, hinges on the utilization of a double damper (cold-warm) arrangement. (Earlier studies with only a warm damper had showed that the losses in the superconductors during

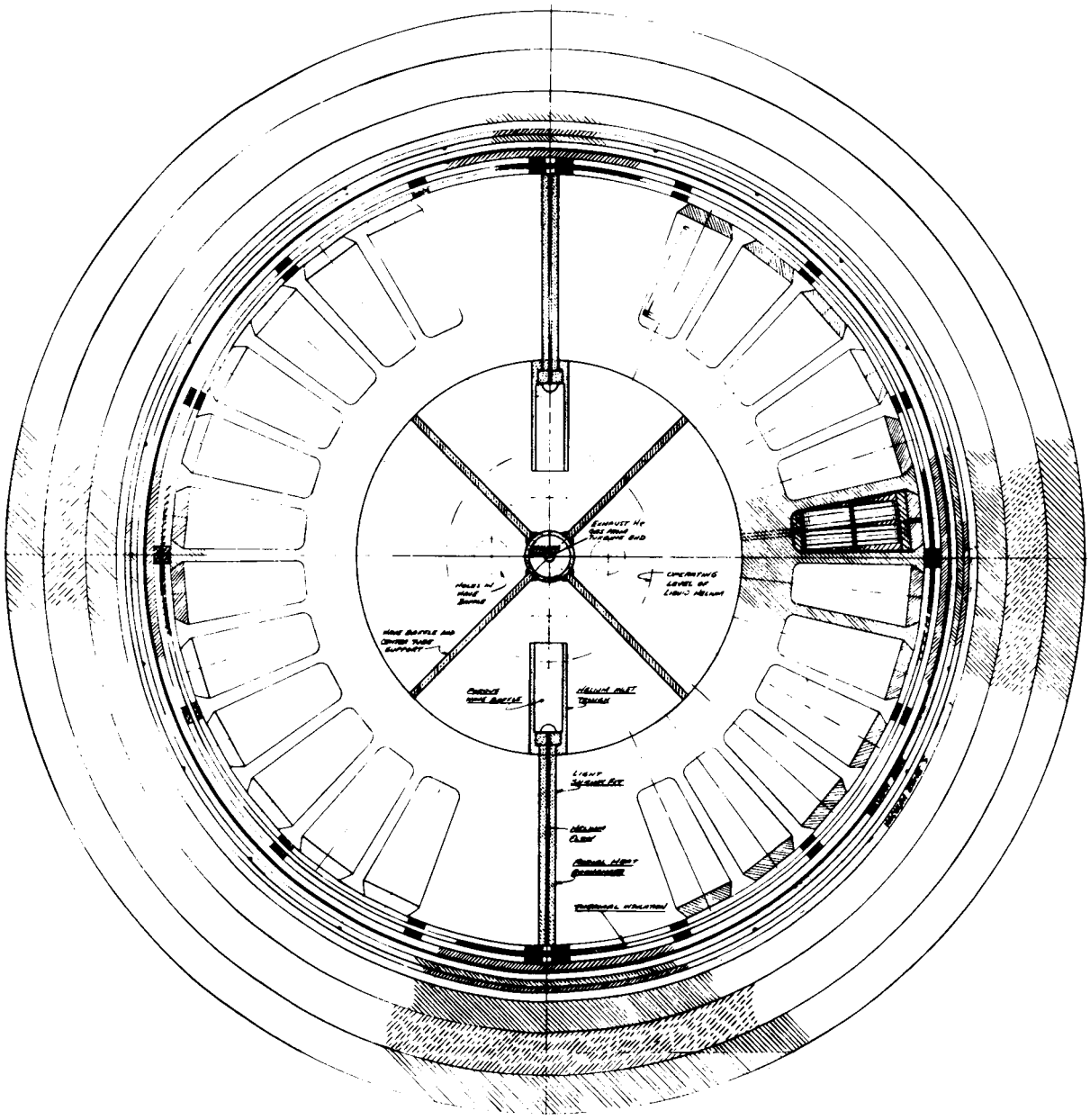

Figure 2-3. Cross Section of Rotor

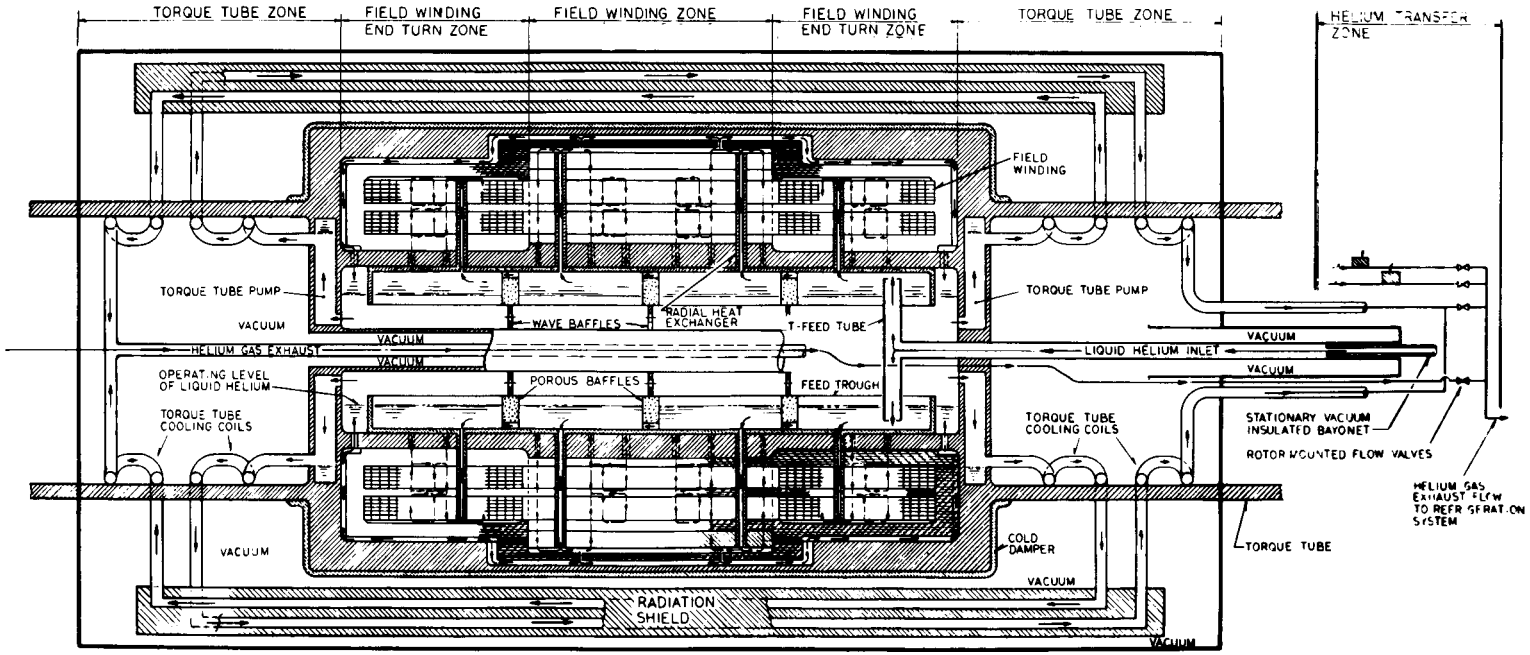

HELIUM MANAGEMENT DIAGRAM

Figure 2-4. Helium System Diagram

and after system faults would preclude the use of such a conductor, and require the use of cabled or mixed-matrix conductors.) The additional complications and costs resulting from these showed that the use of the double damper led to a more effective solution of the transient loss problem. The reference conductor is composed of niobium-tin filaments in a copper matrix, in the ratio of Cu:NbTi = 2:1, has an overall area of 7.36 mm^2, and a nominal current rating of 1000 amperes. Its rounded corners permit 10 percent of the winding volume to contain helium in direct contact with the conductor surface, which is covered only with a thin layer of insulating varnish. This excellent cooling arrangement will provide sufficient margin to assure against normalization of the conductors anywhere in the winding either during the permissible fault conditions or during field charging. As indicated in Figure 2-5, these conductors, after being preformed, are wound into the rotor slots together with the appropriate spacers and separators, and are finally wedged tight. Careful control of dimensions is required to obviate the possibility of localized motion leading to heating and a possible quench.

Damper Shield and Support

The severe and sometimes conflicting design requirements for the damper in superconducting generators can be met successfully with a combination of a rigidly supported outer damper at room temperature and a secondary cryogenic damper just outside the field winding. The former, near the outer diameter of the rotor, requires external supporting members which are amongst the most highly stressed parts in the machine. The conducting sheet of copper alloy is sandwiched between inner and outer non-magnetic supporting cylinders, as shown in Figure 2-3. The complete self-supporting structure is designed to withstand overspeeds at 120% of rated speed, and the stresses incident to short-circuits at the machine terminals. Under such short circuit conditions, the damper experiences strong ovalizing forces in the radial direction, and actually deforms by several millimeters in spite of its considerable thickness. This deformation impacts upon the design of the field winding in that it compresses the magnetic field that is present in its interior and thereby produces losses in the field conductors and support structure. The deformation must therefore be kept within rather narrow bounds and constitutes an important constraint on the overall design. The cold damper assists in keeping these losses at a low and acceptable level.

Losses are induced in the damper and its support structure by currents which flow in response to non-synchronous armature mmf excitations. These losses are

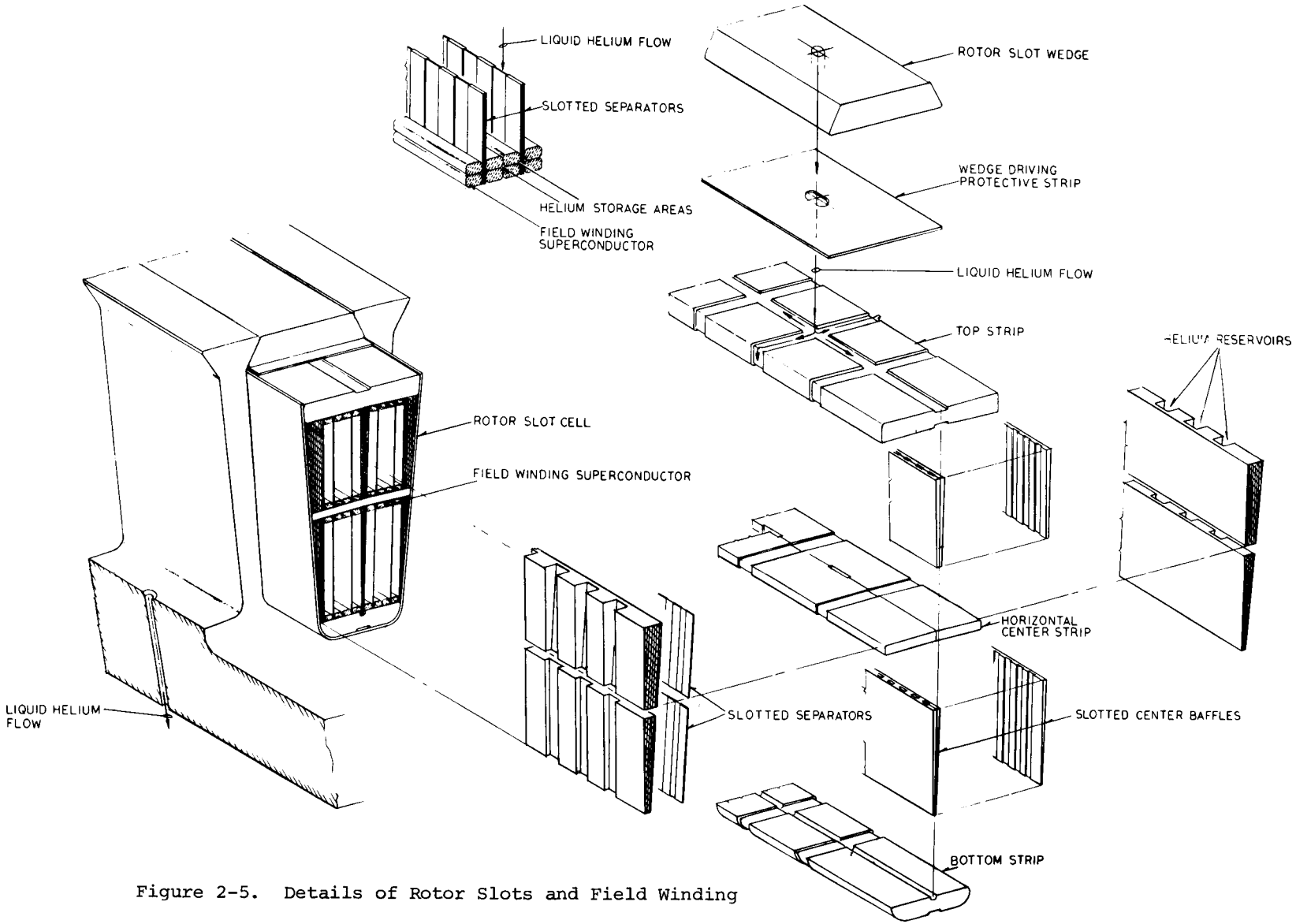

Figure 2-5. Details of Rotor Slots and Field Winding

relatively low during normal operation and can be easily removed by means of a fairly simple gas cooling system. Losses which result from fault conditions are relatively high, but the damping structure provides ample heat storage capability to maintain acceptable temperatures. The continuity of the structure, and relative freedom from current restrictions and joints, reduces the possibility of localized hot spots. A higher capability for unbalanced faults is expected than is provided by conventional construction.

An analysis of damper performance is given in Section 3.2.1.1.

Helium Management System

The complete helium system consists of the helium storage and distribution system within the rotor, the helium transfer system which supplies it, and the external refrigeration system which cools the spent helium back down to cryogenic temperature (4.2 K). The rotor portion has been described in detail elsewhere. It has the following important features:

- Isolation of alternator reliability from liquifier reliability by an intermediate, unregulated, atmospheric pressure liquid helium storage dewar
- Full self regulation of the helium flow
- Substmospheric pressure (3.6 K temperature), natural convection pool cooling of the winding
- Elimination of the neutral thermal lapse rate temperature rise of natural convection pool cooling systems by near isothermal compression-diabatic expansion type thermosyphon loops
- Isolation of structure loss induced coolant temperature rise from the winding by independent thermosyphon loops
- Mixed phase torque tube helium gas return pumps which eliminate instabilities associated with liquid ingestion in the return pumps
- Synergistically combined torque tube heat exchanger stations and radiation shield cooling paths control thermal stresses during steady and fault induced transient operations without additional fault transient mitigating equipment, e.g., valves, heat exchangers,... .
- A very reliable quench induced flow reversal that heats the conductor with helium compression work and increases the normal zone propagation velocity.

Reliability of the complete system also depends upon that of the transfer mechanisms which transport the liquid helium from the external supply to the rotating

reference frame of the field winding. Its design, illustrated in Figure 3-78 meets the following criteria:

- Reliable long term (5 year) operation
- Prevention of internal contamination
- Capability of operation for a specified period following primary seal failure
- Capability to survive a field winding quench without damage
- Capability to provide sufficient flow for rapid cooldown
- Capability to accept relative motions of rotor and stator
- High transfer efficiency
- Acceptable time cycle for replacement.

The long-term reliability is in part obtained by using a seal concept for the primary seal which avoids contact between the rotating and stationary parts, and thereby prevents wear. The small gap between the seal members is spanned by a ferromagnetic fluid under the action of a field set up by a permanent magnet. Functional testing of this type of seal at the R & D Center indicates that the required reliability is attainable. As a further means of assuring this, redundancy in the form of a backup seal is utilized. The primary seal, except for minute gas losses by diffusion, is a zero-leakage seal. The possibility of helium contamination by minute amounts of evaporation of the ferromagnetic fluid is counteracted by means of a face seal which also provides backup, especially during a quench. Its hydrodynamic action provides the desired separation of stationary and rotating parts during operation.

The helium refrigeration system is described under "Auxiliaries".

Provision for Differential Expansion

The use of a warm damper shield with a cryogenic inner rotor structure introduces the need to accommodate for the considerable differential expansion between the two components. In order not to complicate the outboard end of the rotor, where rotor electrical leads and helium lines are brought out, this end of the inner rotor is solidly attached to the shaft end. The damper shield is attached solidly to both shaft ends. The inboard end of the inner rotor then moves with respect to the shaft end and damper shield at that end. The inner rotor must be supported at that end so as to be concentric with the shaft, so as to transmit torque, and so as to have acceptable lateral and torsional vibration characteristics, as well as

to accommodate differential expansion. The proposed arrangement which meets these requirements consists of a series of thin disks, which are connected at their centers to the inner rotor support structure and at their outer peripheries to the inboard shaft end flange.

2.1.2.2 Stator Design

The stator and the armature winding are designed in accordance with new concepts which were developed in the course of the studies. A careful study of the problems encountered in attempting to apply modified airgap windings based on modifications of conventional winding and insulation technology led to the conviction that an innovative approach was also required in this area. An analysis of the design options eventually lead to the definition of a winding geometry which is new for turbine generator airgap windings. It substantially extends and enhances the potential of SCTG's for electric utility applications and makes it possible for the first time to give serious consideration to the design of SCTG's that can be directly connected to transmission lines without step-up transformers (EHV SCTG's). This geometry has the following attractive features:

- Most orderly configuration of conductors and insulation
  - -- Minimizes dielectric stress concentrations
  - -- Produces smooth, continuous, and overlapping spaces for insulation
  - -- Creates long paths to minimize surface creepage
  - -- Is compatible with high-voltage insulating materials
  - -- Results in excellent support for armature end turns
  - -- Results in simple and easily manufacturable coil shapes
- Versatility of concept allows application to high-voltage as well as low voltage windings and thus
  - -- Permits consideration of EHV turbine generators and substantial savings by elimination of main transformer
  - -- Permits consideration for HVDC transmission application (only candidate for this function)
  - -- Permits consideration for low voltage machines with low reactance design to improve critical fault clearing time
  - -- Is compatible with fully developed insulation technology for low voltage applications

The construction of the low voltage armature requires some manufacturing development, mainly in the area of forming the finely stranded conductors. Such development work would likewise be required if a more conventional concept had

been utilized for the armature winding, and the simpler geometry of the new "spiral pancake" winding will lend itself to limiting this work to a practical minimum. The high-voltage armature concept requires much more extensive development, inasmuch as it represents a much greater advance beyong conventional practices. The greater risk is accompanied by much larger potential benefits.

The detailed construction of the low-voltage armature winding is illustrated in Figure 2-6. The complete winding consists of six identical spiral pancake coils, each composed of several series connected turns, typically five to ten in number. These coils are separately constructed prior to assembly into a complete winding. This method permits manufacturing operations to be done in parallel, saves time, and helps to shorten the manufacturing cycle. The conductors of the winding are fully insulated with conventional micaceous-resin insulation (Thermalastic) which is completely cured into a void-free condition after vacuum-pressure impregnation. The coils are water-cooled with internal cooling tubes being provided within compressed bundles of stranded subconductors.

In the case, the spiral pancake geometry has the advantage that the straight end extensions of the coils can be effectively supported against an extension of the flux shield and avoid the rather complex support provisions that are required with conical involute end turns.

An illustration of the way in which the high-voltage winding concept uses the spiral-pancake geometry is given in Figure 2-7. In this case, the orderly arrangement and uniform spacing between coils is instrumental to the efficient use of high-voltage insulating materials in the form of laminated, permeable sheets. A dielectric fluid is used both to insulate and to cool the windings. Special arrangements have been devised to achieve a uniform distribution of dielectric stress and to minimize voltage differences across fluid-filled gaps.

Cooling of Armature Winding and Flux Shield

Close coordination has been achieved between the cooling of the stator flux shield and the overall machine design. For both the low- and the high-voltage armatures, the flux shield utilizes a cooling medium that is required for at least one other main machine member. Since the low-voltage winding utilizes water cooling, its flux shield is gas-cooled, utilizing the same coolant, hydrogen gas at several atmospheres, that is used for the gap and damper in exactly the same fashion as

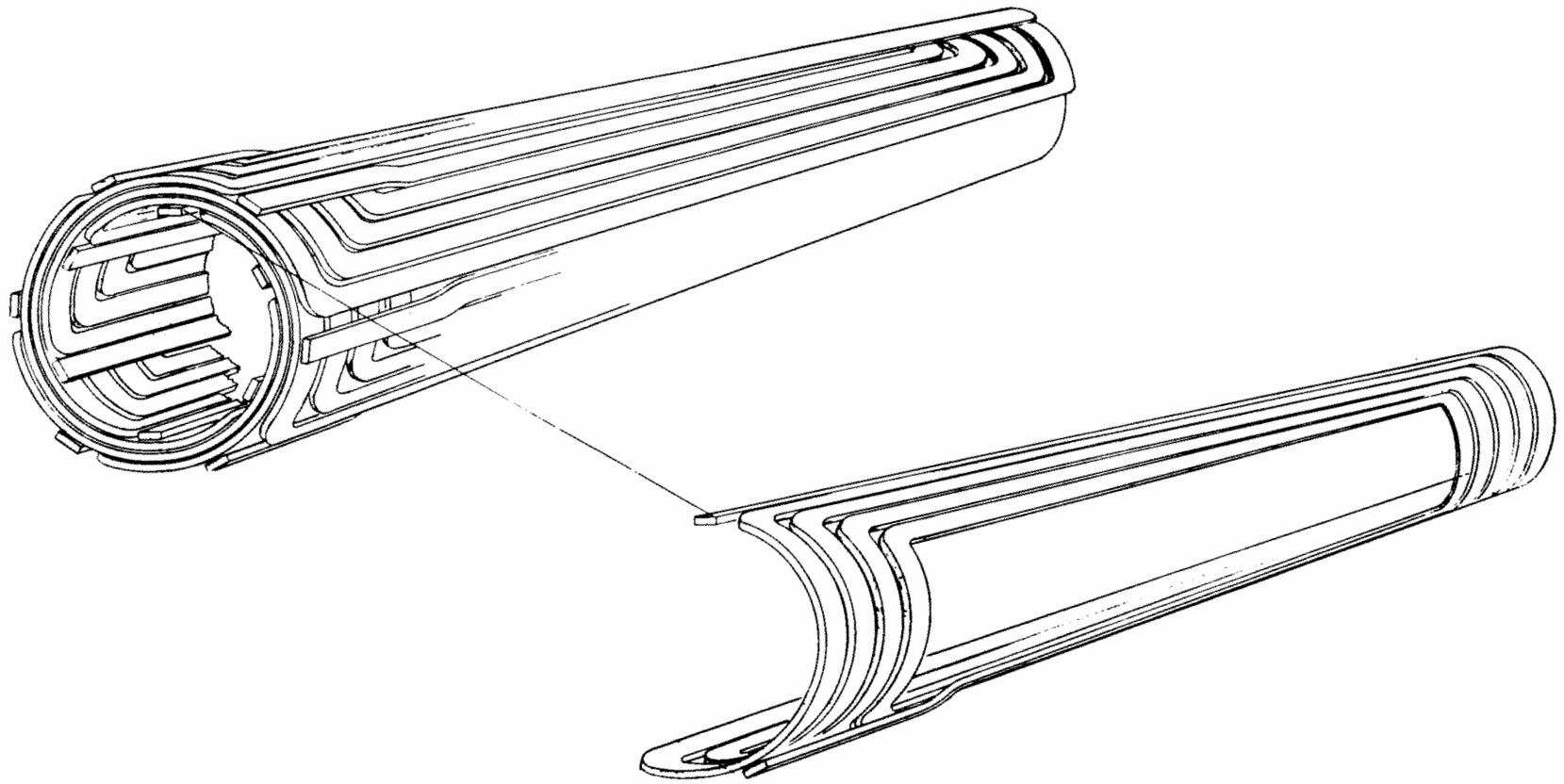

Figure 2-6. View of Spiral Pancake Armature Winding and Coil

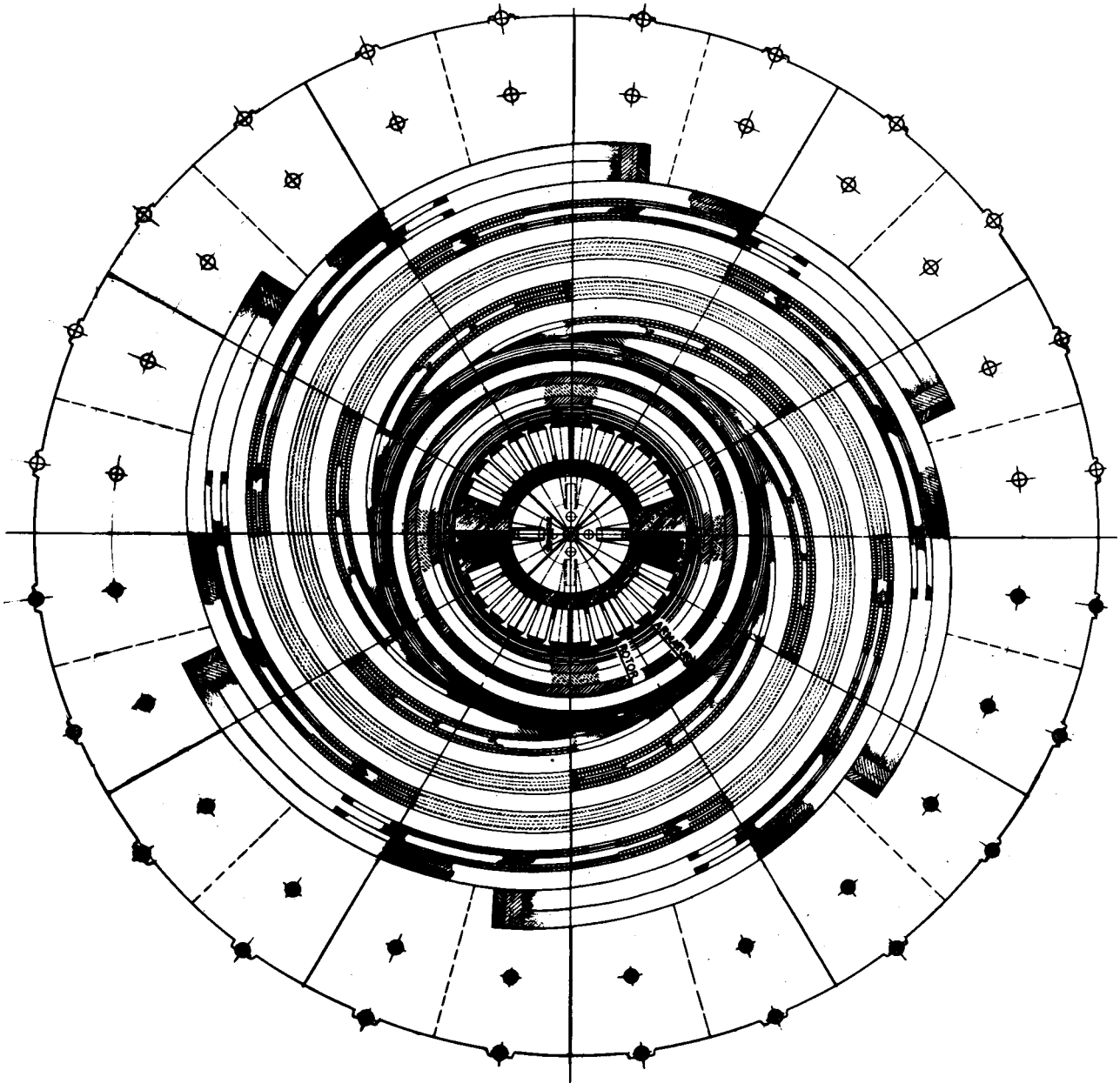

Figure 2-7. High Voltage Armature Winding

has been done for years in conventional machine practice. Parameters for the flux shield coolant passages are selected so as to match pressure drop requirements from inlet to discharge without the use of control orifices.

2.1.3. Performance Considerations

2.1.3.1 Steady State Performance.

Superconducting turbine generators will be operable in much the same manner as conventional machines, and will operate satisfactorily in parallel with other units in the same plant or on the same system. The methods of operation will resemble those used for conventional machines, i.e., steady-state loading will be done by means of capability curves furnished by the manufacturer. Operation of auxiliary systems will in the main be like that for conventional machines. The major new auxiliary is the helium refrigeration system. Westinghouse experience with such systems indicates that this will normally be operable by the usual grade of power station operating personnel.

The steady-state loading characteristics of superconducting turbine generators exhibit the following advantages over those of conventional machines:

- Steady-state stability limit well beyond maximum underexcited capability
- Increased capability for steady-state negative sequence current

Additionally, maintenance in normal service may be reduced because of the low excitation voltage and the small number of brushes required to satisfy the field excitation requirements.

Choice of Steady-State Operating Point - Short Circuit Ratio Optimization

In principle, superconducting turbine generators can be designed using a wide range of current densities and field strengths at the field winding. In a program of this type, it is necessary to select the most appropriate operating point for the most cost-effective design. While computer optimization procedures are required for a fully optimized detailed design, an idealized model can provide much insight into the choice of the operating point at a given combination of current density and field strength. Such a study was made, and resulted in definition of criteria for maximum power density. The criterion was found to be a value of synchronous reactance x_d = 1.0 p.u. This of course corresponds to a short-circuit ratio (SCR) of 1.0. Other observations which can be made on the basis of this study are:

- Power density is sensitive to the magnetic coupling between field and armature, to the superconductor characteristics, and to the amount of stabilizing material, cooling space, and design margin used in applying the superconductor

- Any desired reactance level can be achieved by the proper selection of the rated design point. For a given type of construction, (rigid warm damper vs. flexible cold damper, for example) the ratio of reactances tends to be fixed.

- While maximum power density occurs at $x_d = 1.0$, the penalty in power density incurred in going to $x_d = 0.5$ is not large and results in minimal cost penalties. Below that point, penalties increase rapidly.

2.1.3.2 Consideration of Transients.

System disturbances cause forces and losses in superconducting generator components that must be thoroughly analyzed and for which adequate accommodation must be provided to assure that normalization of the superconducting field winding does not occur and that damage does not occur to generator components.

Reduction of generator reactances improves steady state and transient stability with respect to performance on a power system, but also increases transient currents, forces and losses. The objective of the design effort is to obtain an acceptable balance between these conflicting considerations.

The steady state stability of a superconducting machine is extremely good for any practical design point, since the synchronous reactance (X_d) should not exceed 1.0 per unit (for maximum power density) and an optimum economic design point is in the range of X_d = .5 to .2; typical values of X_d for conventional machines are in the range of 1.7 to 2.0.

Transient stability is a function of both synchronous reactance and either transient reactance (in the case of conventional machine), or subtransient reactance (in the case of superconducting machines, due to the long subtransient time constant). By using sufficiently low values of reactance, the critical fault clearing time of superconducting generators can be made as long as, or longer than, the CFCT of conventional units, in spite of the lower rotor inertia of SCTG's. Designs have been developed for synchronous reactance values of .5 and .25, at which levels CFC times are comparable to those obtained for typical conventional generator applications. Corresponding transient forces and losses have been calculated and design provisions have been made to accommodate for them.

Transients that are considered are:

- Sudden short circuit at machine terminals
- System faults followed by clearing and reclosures
- Small variations in load during "steady state" conditions

Transients produce large induced currents which flow in all conducting parts, causing large torsional and radial forces and motions, and generating losses in various components.

Large compressive forces acting on the damper shield cause defections which compress magnetic fields inside the shield, resulting in fluctuations in magnetic field strength. The cold shield prevents these fluctuations from being seen by the field winding.

Torsional vibration of the shaft causes perturbations in the rotor position relative to the main flux field, and causes relative motion between the outer damper shield and the cold inner shield, again resulting in variations of the magnetic field strength.

Provisions are made in the design of components to provide long life in parts which are highly stressed during severe transients; such parts include the damper shield, the turbine end shaft, the flexible support between the cold inner rotor and the warm damper shield, the armature winding, and the armature support (armature shield and flexible mounting system).

Losses generated in the damper shield during severe transients are dissipated to the airgap cooling system. Losses in the radiation shield and cold inner shield are conducted to helium streams sufficiently separated from the field winding streams to provide effective thermal isolation. Losses in the field winding superconductors and in the field winding support structure are minimized by means of the cold inner shield so that the temperature rise will be small and several successive events can be sustained without loss of superconductivity. A short circuit at the machine terminals can probably also be endured without loss of superconductivity.

The cumulative effect of heavy fault forces on the life of the high voltage armature configuration proposed in this work cannot be predicted with presently available information. Experience with cable and transformer high voltage practice is not directly applicable. However, materials with mechanical and dielectric properties superior to those presently in use are available and there is a reasonable expectation that these can be developed successfully.

2.1.4 Generator Price

Superconducting generator prices have been estimated for 300, 1200 and 3000 MVA, and are shown in Figure 2-8. These prices represent the expected mature values after the heavy developmental costs have been paid off. The low voltage superconducting machines are slightly lower in price than conventional generators at 300 MVA and are about 20% lower in price at 1200 MVA. The price of high voltage (transmission level) superconducting generators is about 20% higher than conventionals at 300 MVA but drops below the price of conventionals at 1200 MVA.

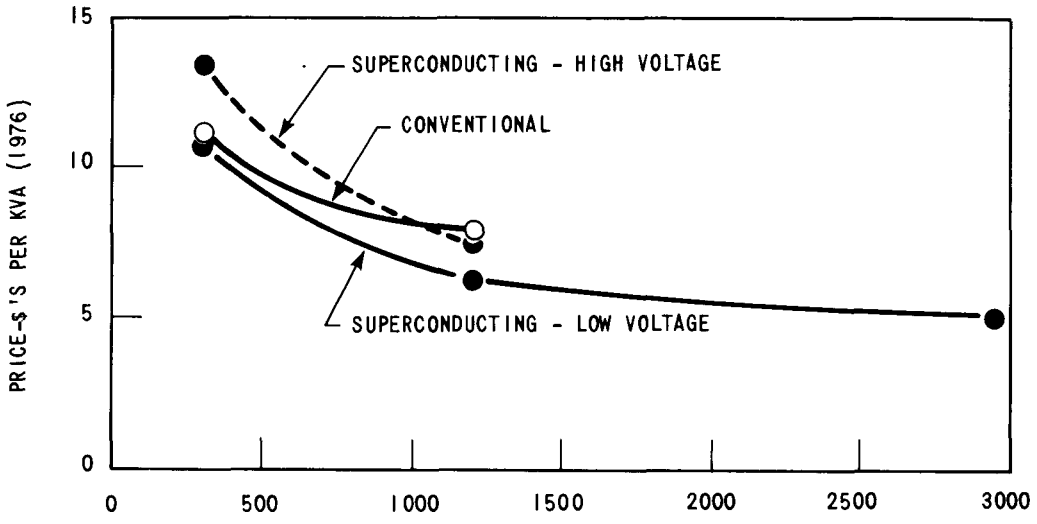

Figure 2-8. Generator Price Versus Rating

Generator cost is a function of reactance level. Between synchronous reactance values of 0.5 and 1.0 (P.U.) the cost is fairly constant, but for values less than 0.5 generator cost begins to increase rapidly. A trade-off between the value of system benefits obtained from low reactance levels, and the incremental cost premium to be paid for low reactance generators must be determined in each specific system application. A rough indication of generator price trend versus synchronous reactance is given in Figure 2-9.

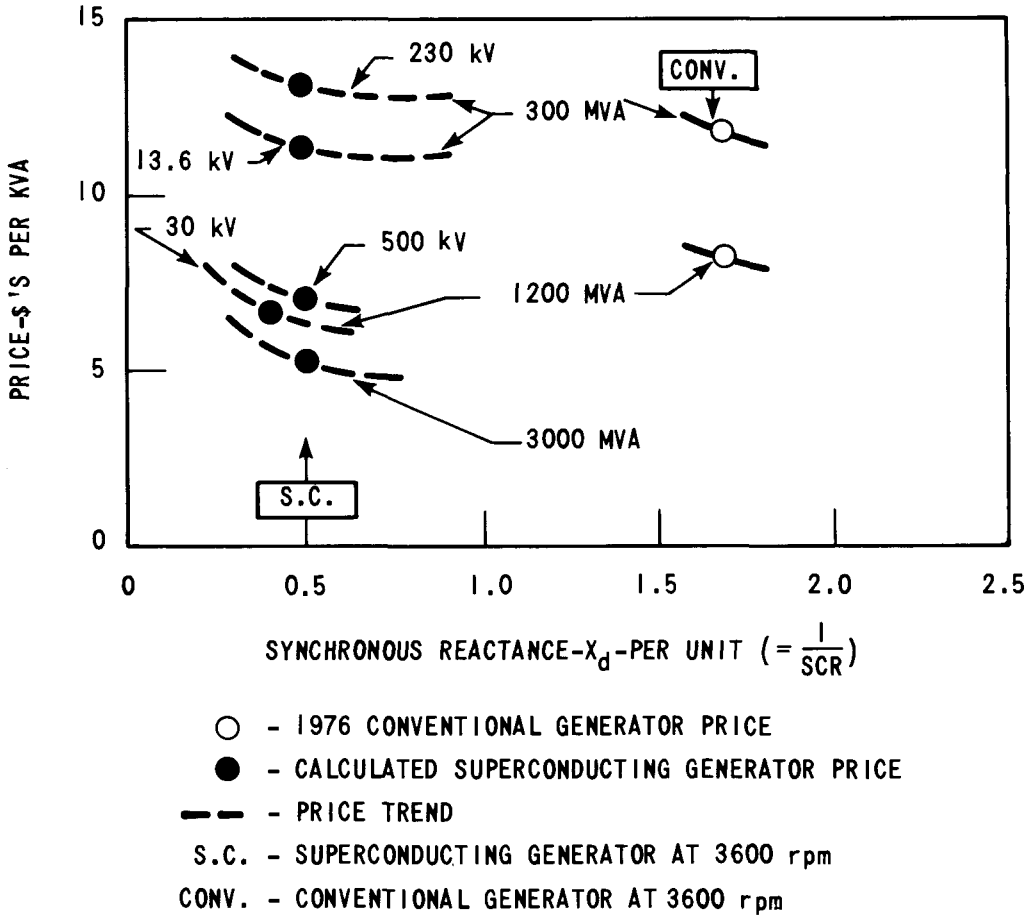

Figure 2-9. Generator Price Trends versus Synchronous Reactance

2.1.5 Economic Evaluation

Superconducting generators offer major cost savings relative to conventional units due to the following characteristic features:

- high efficiency
- competitive generator cost
- transmission level armature voltage capability
- freedom to select electrical characteristics to benefit system performance

Superconducting generators are inherently more efficient than conventional generators, principally because field winding losses are eliminated. The difference in kW loss is directly available as increased plant output without a corresponding increase in capital or fuel cost. A reduction in generator losses of about 60% (Δ efficiency = 0.7%) is expected in the proposed design; a conservative value of about 40% (Δ efficiency = 0.5%) has been used in the evaluation presented below.

Table 2-2 shows the details of this evaluation expressed in 1985 dollars, using projected 1985 plant and fuel costs.

Table 2-2

LOW-VOLTAGE SUPERCONDUCTING GENERATOR ECONOMIC
BENEFITS RELATIVE TO CONVENTIONAL GENERATORS
PLANT RATING - 1000 MWe
($/kwe 1985 Dollars)

PLANT TYPE	OIL	COAL	NUCLEAR
1. Plant Capital Cost	500	800	1000
2. Fuel Costs (mills/kwh)	30	20	11
		BENEFITS	
Generator Benefits (Δ efficiency 0.5%)			
3. Plant Capital Cost	2.50	4.00	5.00
4. Generator Cost 3600 rpm (reduction)	3.29	3.29	---
5. Generator Cost 1800 rpm (reduction)	---	---	4.73
6. Fuel Cost Savings (Δ effic. = 0.5%)	5.29	2.53	1.94
7. Operational Maintenance	0.53	0.88	0.53
8. Total Net Benefits	11.61	11.70	12.20
9. Generator Cost - 1985	17.80	17.80	25.60
10. Benefit as Percent of Generator Cost (%)	65.00	66.00	48.00
11. Benefit as Percent of Plant Cost (%)	2.32	1.46	1.22

The mature cost of a low voltage 1000 MW - 3600 rpm superconducting generator and its auxiliaries has been estimated to be about 20% less than the cost of a conventional unit of that rating. With a high voltage winding, the cost is about the same as conventional (low-voltage) unit. It has been assumed that a similar reduction would be obtained for 1800 rpm (nuclear) generators.

The economic benefits from using a low-voltage superconducting generator amount to about 65% of the generator cost in fossil installations and 48% in nuclear installations.

The use of high-voltage armatures permits the elimination of unit transformers and their power losses, thus achieving a further increase in plant output and providing additional savings in plant capital cost, transformer cost and fuel savings. The total economic benefits from using a high-voltage superconducting generator amount to about 90% of the generator cost in fossil installations and 60% in nuclear installations.

Table 2-3 shows the details of the high-voltage generator evaluation.

Table 2-3

HIGH-VOLTAGE SUPERCONDUCTING GENERATOR ECONOMIC BENEFITS RELATIVE TO CONVENTIONAL GENERATORS PLANT RATING - 1000 MWe ($/kwe 1985 Dollars)

PLANT TYPE	OIL	COAL	NUCLEAR
1. Plant Capital Cost	500	800	1000
2. Fuel Costs (mills/kwh)	30	20	11
		BENEFITS	
Generator Benefits (Δ efficiency 0.5%)			
3. Plant Capital Cost	2.50	4.00	5.00
4. Generator Cost 3600 rpm (reduction)	0.60	0.60	---
5. Generator Cost 1800 rpm (reduction)	---	---	0.86
6. Fuel Cost Savings (Δ effic. = 0.5%)	5.29	3.53	1.94
7. Operational Maintenance	0.53	0.88	0.53
Transformer Elimination Benefits (Δ efficiency 0.2%)			
8. Plant Capital Cost	1.00	1.60	2.00
9. Transformer Cost - 1985	3.50	3.50	3.50
10. Fuel Cost Savings (Δ effic. - 0.2%)	2.12	1.41	0.78
11. Operation and Maintenance	0.21	0.35	0.21
12. Total Net Benefits	15.75	15.87	14.82
13. Generator Cost - 1985	17.80	17.80	25.60
14. Benefit as Percent of Generator Cost (%)	88.00	89.00	58.00
15. Benefit as Percent of Plant Cost (%)	3.15	1.98	1.48

Expressed as a percent of plant capital cost, the low-voltage generator benefits are:

- 2.32% for an oil fuel plant.
- 1.46% for a nuclear plant.
- 1.22% for a nuclear plant.

Expressed as a percent of plant cost, the high-voltage generator benefits are:

- 3.15% for an oil fuel plant.
- 1.98% for a coal fuel plant.
- 1.48% for a nuclear fuel plant.

Reduction in weight and dimensions of the superconducting generator will produce benefits in foundation, building and shipping costs which are real but relatively small in comparison to the fuel and capital cost savings. A reduction in cost of the excitation system will also be obtained. The cost of the helium refrigeration system is included in the cost of the generator.

2.2 DESIGN DETAILS

2.2.1 Rotor Design

The overall design objectives for the rotor are:

- to secure optimum use of the superconductor so as to achieve maximum power density and lowest cost.
- to maintain the field winding in its superconducting state with all combinations of temperature, current density, and magnetic field strength which correspond to required operating states. These include both steady-state and transient operation.

2.2.1.1 Rotor Electrical Design. The complete electrical design of the rotor is an iterative procedure wherein the inherent J,B,T, properties of an available superconductor are matched against the transient field losses imposed by the steady-state and transient operating conditions of the machine and against the capabilities of the cryogenic cooling system to remove heat under all these conditions. The logic of this process is discussed in Section 3.2. Its implementation requires determination of varying magnetic field and current amplitudes in the region occupied by the field winding and its supporting structure. These amplitudes are determined by the rotor damper and excitation systems, which, in turn, must be designed in recognition of the requirements of the electrical power system and its stability criteria.

Detailed studies have been carried out on superconductor design, methods of shielding, structural support, and helium management design for cryogenic cooling. The design has evolved and matured through several stages which successively overcame serious problems, primarily with excess loss in the superconducting wire. The present design features a double damper structure (warm and cold dampers) that effectively shields the field winding and reduces internal loss generation to insignificant levels. With such shielding, it is possible to use a monolithic conductor support for the field winding and provide maximum support against transient forces as well restraint as other possible sources of motion. With such highly effective shielding it is also possible to consider the use of magnetic material for the field winding support, which may simplify and economize the material selection.

Selection of the superconductor, support structure, and helium management system parameters lead to a definition of overall current density in the field winding space, and thus to the detailed electrical design in which the available field mmf is matched to an armature winding to produce a desired rated output at a specified reactance level and specified maximum flux density. This process is carried out by computer with successive iteration of the machine dimensions to attain the specified characteristics. Calculations are subsequently performed to verify the maximum winding temperatures under all operating conditions, which are compared to the limiting value. An acceptable design results from actual temperatures less than limiting values.

Winding Configuration

A radial slot configuration has been adopted for the field winding (see figure in Section 3.2). It has significant advantages over other configurations that were considered in the course of the studies, particularly with respect to

providing support for the conductors of the field winding against mechanical and electromagnetic forces and torques that occur under fault conditions as well as in normal operation and during start-up. The confinement of the field winding coils in slots will provide the opportunity for ample support against motion of the superconductor, which is believed to produce losses and localized heating followed by possible normalization. This support method is therefore conducive to better superconductor stability.

Other configurations which have been considered include a parallel coil arrangement and a radial arrangement without teeth in the support structure. The parallel coil arrangement results in increased stresses in the support structure and shows little promise for application in large size machines. The radial configuration without teeth was initially adopted since it reduces losses in the cryogenic space and simplifies some aspects of rotor manufacture. Further studies have shown other methods of minimizing these losses (by means of cryogenically cooled dampers) and have indicated the necessity for better support than can be provided without the toothed support. The radial slot arrangement with cold damper also lends itself well to the use of a monolithic superconducting wire and to effective helium distribution.

Detailed studies were carried out on the configuration parameters of a radial slot winding with respect to pole angle and winding thickness. These have shown that the pole angle does not constitute a major parameter of the design within a range of values about 10 degrees on either side of the optimum value that is very close to 50 degrees. This is true with respect to both the utilization of the superconductor and with respect to harmonic side-effects. The thickness of the field winding (its radial depth) on the other hand, and its inner and outer radii constitute major parameters. A given element of the winding is more useful in producing output power the closer it is to the rotor periphery. The maximum radius of the field winding should therefore be as large as possible, consistent with the other design requirements for the support and electro-thermal shielding of the superconducting field winding.

Rotor Conductor Selection

During the early stages of design of the superconducting rotor, it was clear that an all-copper matrix conductor could not remain superconducting during a fault due to the high losses and subsequent temperature rise generated by the transient fields. As a result, mixed-matrix monolithic conductors and a cable of

mixed-matrix strands which have lower eddy current losses were considered to be the options available. The temperature rise expected during a fault for the mixed-matrix conductors was calculated on a conservative model assuming an adiabatic process and it was concluded that the mixed-matrix monolith would be marginally stable under fault conditions. The cable would survive, but a cabled conductor has many other disadvantages in this application so that if possible a monolith should be used. The rotor was subsequently redesigned with a cold shield to reduce the transients at the conductor. The result was such that the fields were reduced to a level that allowed the copper matrix conductor to be a viable candidate.

As a result of loss calculations using reliable theoretical models which have been proven successful in the past, we propose that a copper-matrix, multifilamentary conductor be used in the 300 MVA machine. The proposed conductor has Cu:NbTi = 2:1 with an overall area of 7.36 mm^2 yielding an operating current density of 1.36 (10^4) A/cm^2. It is rectangular with an aspect ratio of 1.5 and has rounded corners which will allow ten percent of the winding volume to contain helium in direct contact with the conductor. The helium will provide the necessary cooling to prevent normalization of the conductor during a fault or during ramp-up. The temperature rise expected during a fault has been calculated on a very conservative model assuming adiabatic conditions. The predicted value is $< 0.1°K$. Since the conductor is designed to allow a $\Delta T = 1.4°K$ before quench at the operating current of 1000A, it appears that it will be quite stable during a fault.

The conductor can be manufactured with state-of-the-art techniques so that no development work is required.

Rotor Damper Application

In a superconducting turbine generator, the damper arrangement first of all fulfills the critically important task of shielding the field winding and its cryogenic environment against external electromagnetic fields and disturbances. While doing so, it must also provide sufficient damping for shaft oscillations, and its supporting structure must resist the heavy crushing forces that are incident on it during fault conditions. These functions may, in principle, be performed by metallic shells or by polyphase insulated windings, which may be at the room-temperature surface of the rotor, or in its cryogenic environment, or both.

Evaluation of these concepts, in terms of the shielding afforded for the superconductors, the resultant choice of superconductor type and field winding support,

and of the damping of electromagnetic disturbances, has led to the choice of a combined damper system, consisting of one damper shell at room temperature, sandwiched between layers of high-strength supporting structure, and of a second damper at cryogenic temperature, located at the outer periphery of the field winding support. This combination has been shown to offer the required protection for the field winding as well as adequate damping of shaft oscillations following faults or other angular swings. This damper system also offers improved machine application characteristics in terms of higher negative sequence current capabilities for I_2^2t and for I_2. Calculations have shown that I_2^2t capability is twice that required by ANSI Standards for conventional turbine generators, while I_2capability is increased by 50 to 66 percent.

These conclusions are predicated on the results of a detailed calculation method for double-shell damper arrangements that was developed as part of the studies, and has been used to calculate performance of the damper and its supporting structure. A description of this method is given in Section 3.2.1.

Rotor Transient Heating

During and after fault periods, the rotor is subjected to large transient and oscillating forces and magnetic fields. These arise during the fault period due to the large armature currents that are associated with both the trapped flux and the short circuit synchronous currents. Besides the magnetic fields that are directly generated by the fault currents and which diffuse through the shield system and thereby lead to heating in the cold structure and field winding, there are fields that result from mechanical motion (deflection and rotation) of the outer warm shield relative to the inner cold rotor. These latter fields also lead to losses in the cold region. Additional time varying fields are generated after the fault has been cleared and during the "rotor swing" period. Reclosure can also lead to forces and fields that cause additional heat inputs.

It is of critical importance to limit the magnitude and the rate of change of time varying magnetic fields in the cryogenic inner rotor. This is not because of any penalty associated with refrigeration, but follows from the requirement that a high side fault must not lead to a sufficient temperature rise in the superconducting field winding as to cause a normalization of the field winding. Because of the very low specific heat of all materials at low temperatures, it is necessary to limit the heat input to a very low level.

It is the purpose of this section to give a brief review of the impact of these transient forces and fields on heating in the cryogenic inner rotor and cover the design features of the inner rotor that control and limit this heating to a level that will not cause field normalization. The impact of the fault forces on the mechanical design of the outer warm shield, the shaft system and the inner rotor are covered elsewhere in this report.

It is the shield system that controls and limits time varying fields in the region of the inner cryogenic rotor. The proposed shield system design is made of an outer warm shield (damper shield) and an inner cold shield at the OD of the field support cylinder.

The warm outer shield serves as the damper winding, serves as the main attenuator for higher frequency fields, e.g., 120 Hz phase unbalance, 60 Hz trapped flux and armature spacial harmonic fields, and helps to slow down the diffusion through the shield system of the synchronous fault fields.

During the fault period, the warm shield is subject to inward crushing forces which lead to a time varying distortion of this cylinder at 60 and 120 Hz (three-phase fault). Even though the deflection of the warm shield is only about 0.001 m, this is sufficient, through flux compression, to lead to magnetic fields between the OD of the warm shield and the OD of the cold shield of several hundred gauss.

In a similar way, fields are generated in this intershield space due to the relative angular oscillation of the inner rotor relative to the outer warm shield. This relative angular motion is driven by impulse and oscillating torques on the warm shield during the fault period.

Both of these "motional" fields are kept out of the field winding by the action of the cold shield. Further, it is the cold shield that acts as the main attenuator of the low frequency ($\sim$ 2 Hz) rotor swing fields.

For the 300 MVA machine, the total heat input to the cold shield and to the cold structural support for a three-phase, high side fault, has been calculated as $\sim$ 5000 Joules. This heat input covers both the fault period (0.07 sec) and the subsequent rotor swing period. The helium management system, as described later

in this section (and in 3.2) has been designed to handle this heat load without causing a significant rise in superconductor temperature.

Further, the heat input to the field winding due to conductor losses from all of the various time varying fields covered above, is such that the conductor temperature does not rise by more than 0.1 K during and after a fault. This aspect is covered more fully in Section 3.2, Conductor Selection section.

2.2.1.2 Rotor Mechanical Design. The general configuration of the rotor is shown schematically in Figure 2-10. The cold inner rotor consists of a field winding and a helium management system. The inner structure contains liquid helium at approximately 4.2 K and provides support of the winding. The support structure has axial extensions or "torque tubes" at each end of the winding annulus. One end is rigidly coupled to the outer rotor structure while the opposite end is supported so as to accommodate large thermal contraction of the cold inner rotor relative to the warm outer rotor. The torque tube is cooled by helium vapor to minimize heat flow from the warm outer rotor to the cold inner rotor. Radiation heat flow is limited by an inner cooled thermal radiation shield. A warm outer rotor consists of a damper shield and its support with rigidly attached shaft ends. It serves as the main structural element of the entire rotor and also as the vacuum enclosure around the field.

A different rotor construction in which the cold inner rotor served as the main structure, was previously considered. It is preferred that the outer rotor be designed to withstand the various loads and the inner one be protected against them.

The method of assembly of the built-up rotor has been considered continuously as the component layouts have been developed. Many configurations and dimensional restraints have been imposed by assembly requirements. In this way a practical rotor design has been developed which we will be able to assemble.

Details of the rotor configurations and the assembly sequence and procedure may be found in Section 3.2.

Inner Rotor

The inner rotor includes the superconducting field winding and its support, the torque tubes and the helium management system - a support system which distributes and controls the flow of helium through the rotor.

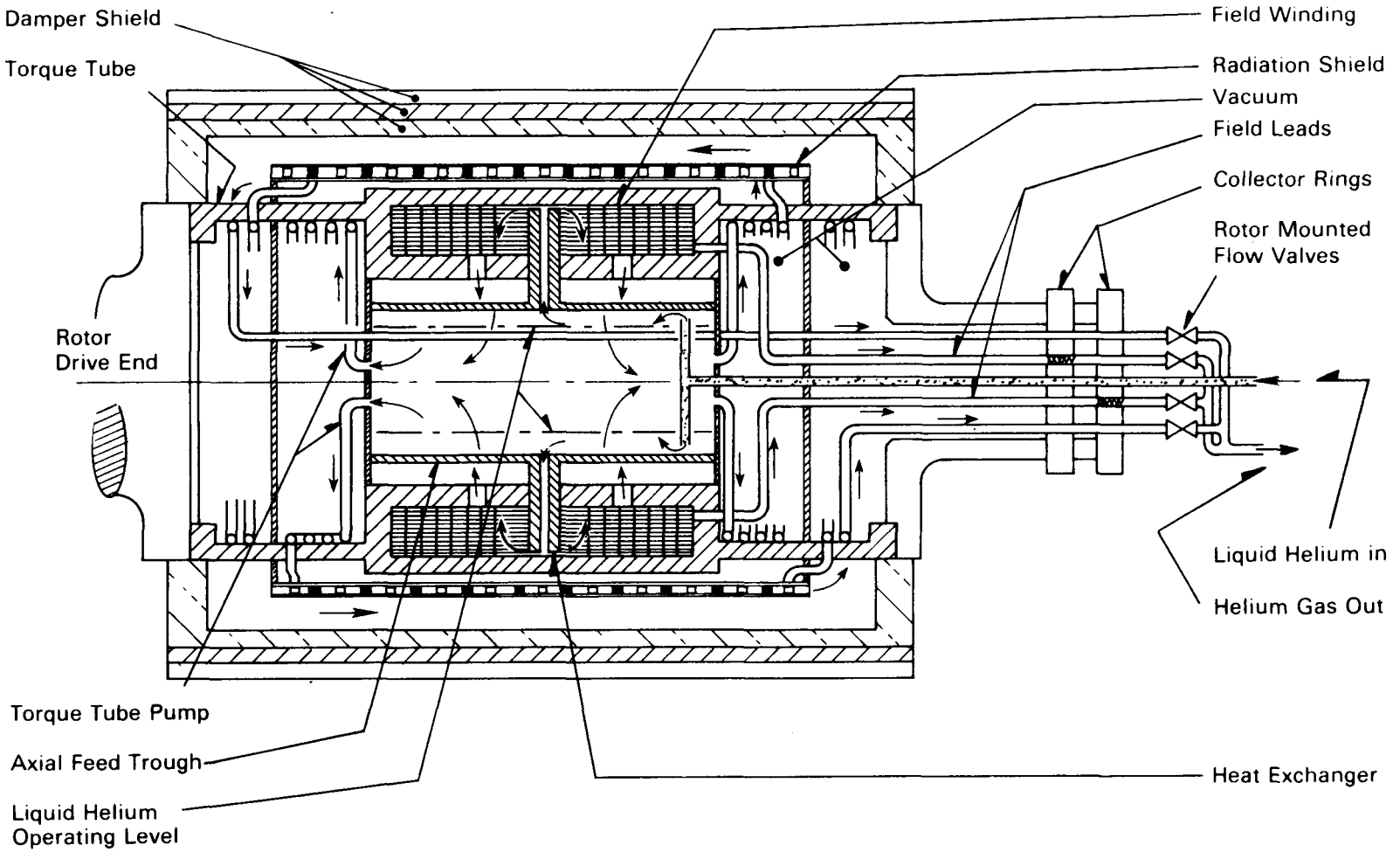

Figure 2-10. General Rotor Configuration

Toothless field winding support was considered at an early stage in order to minimize the losses due to magnetic flux variations. By utilizing a cryogenic damper shield in addition to the warm damper, the structural loss is reduced to such an insignificant value that a slot-tooth field winding support can be selected as feasible. Presently, the main body of the inner rotor structure is essentially a long thick cylinder with slots in the outer surface to contain the straight portions of the superconducting winding. The conductor will be wound into radial slots. Space will be available between turns for helium flow and storage. Slot wedges are used to hold the winding in place while end turns are retained by an external tube shrunk over the inner rotor body. The cryogenic damper shield is bonded to the outer surface of the tube. Clearance is provided for extra helium storage between the teeth and welded at each end and serves to contain the helium in the winding area. This arrangement which is close to present conventional generator design practice, will give excellent support for the conductor under rotational and magnetic forces.

Torque Tubes

The torque tubes mount the cryogenic inner rotor field winding region to the warm outer rotor. A configuration using two Inconel torque tubes (Figure 2-11) integral with the field winding support structure has been designed in some detail. Alternate schemes include welded on and bolted on torque tubes, and other materials such as composites. Calculations indicate that the tubes can be designed to transmit torque and exceed all other design requirements for all design conditions * without contributing excessively to the overall heat leak into the cryogenic region.

Boil-off gas from the helium space cools the torque tubes thereby reducing the conduction heat leak through the torque tubes. The boil-off gas is delivered to the torque tubes through metal tubes which are thermally and mechanically bonded to the inside surfaces of the torque tubes. Simple convention traps in the helium cooling tubes are made by periodically bending the paths of the torque tube cooling tubes to a smaller radius (Figure 2-12). The practicality of convection traps has

* See Section 3.2.

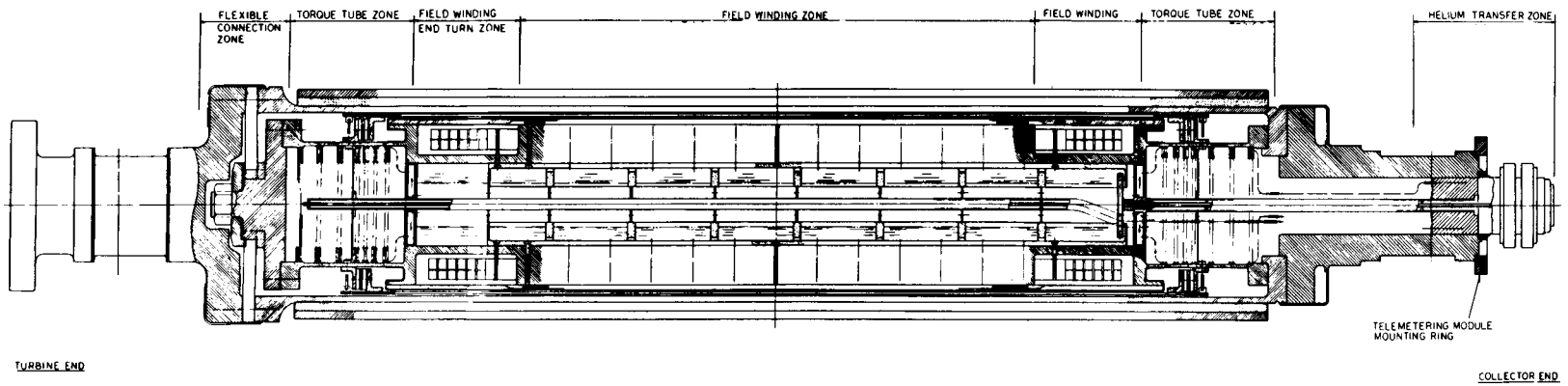

Figure 2-11. Longitudinal Section of Rotor

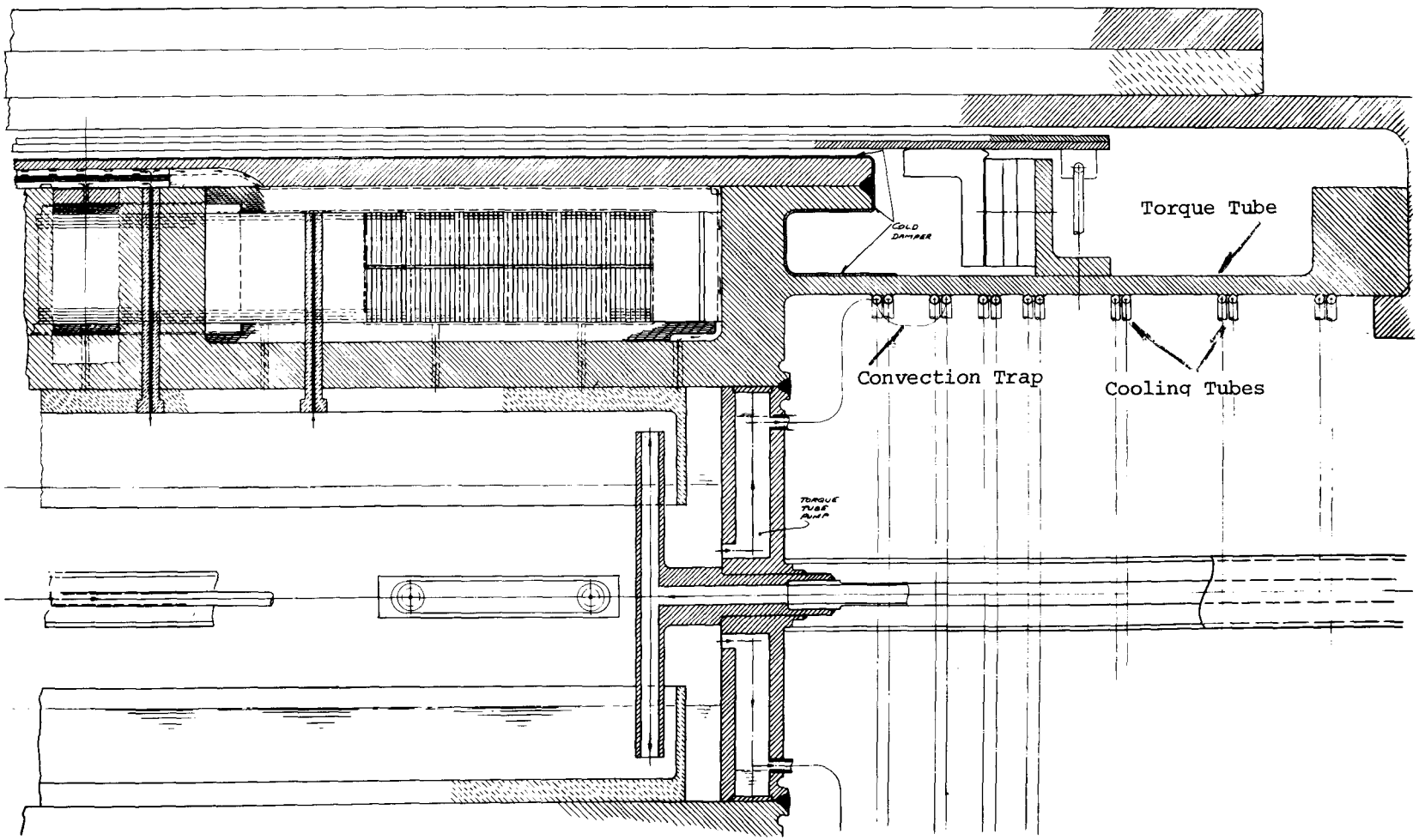

Figure 2-12. Side View of Torque Tube

been demonstrated by A. Bejan.** They prevent undesirable centrifugally induced natural convention loops**,+ within the cooling tubes.

Radiation Shield

An inner cooled radiation shield is located in the vacuum space between the warm outer rotor (damper) and cold inner rotor. It efficiently reduces the radiant heat leak into the cryogenic zone by shielding the inner rotor from heat radiated by the warm outer rotor. The shield also acts as a periodic heat exchanger by having sufficient thermal inertia to warm the exhausted helium and prevent the torque tubes from being overcooled during transients.

Several schemes have been considered. The configuration selected and designed in detail (patent disclosure has been written) consists of a relatively thin stainless steel shell shrunk over a thicker inner shell. Helium flow is accommodated by small axial grooves cut in the inner shell. Suitable flow paths are accomplished by circumferential and axial grooves and seal welds. The shield is fed helium by small metal tubing from the torque tubes.

A novel method (patent disclosure has been written) of mounting the radiation shield on the inner rotor using flexible rings has been developed after considering many other configurations.

Damper Shield and Support

The damper shield has significant losses generated in it during normal operation, making it reasonable and practical to locate a major damper outside the vacuum space at ambient temperature where it can be gas cooled rather than placing an unacceptable load on the refrigeration system. For such a room temperature damper, its electrical and thermal requirements can be met with suitable thickness and resistivity of highly conductive material of the shield.

Mechanically, the damper is designed for two conditions -- at 20% overspeed and under short circuit condition. It is generally the short circuit condition which determines the total damper thickness.

** "Improved Thermal Design of the Cryogenic Cooling System for the Rotor of a Superconducting Generator", Adrian Bejan, Ph.D., December 1974. (MIT Thesis).

+ "The Design and Testing of a Rotatable Liquid Helium Transfer Coupling for Use at 3600 RPM", P. Thullen, J.L. Smith, Jr., and W. D. Lee. Paper No. 1.20, Progress in Refrigeration Science and Technology, Vol. 1, Proceedings of the XIIIth International Congress of Refrigeration, Avi Publishing Co., Westport, Conn., 1973.

The damper shield can conceivably be made of a single cylinder of reasonable thickness. While a material, such as copper graphite composite, which will fulfill both the mechanical and electrical requirements, may be developed for our application in the future, the present damper shield is designed as a composite cylindrical shell of three cylinders. The inner and outer cylinders are of a high nickel alloy such an Inconel for support and the middle ring is of copper alloy for damping and shield. The rings must be shrunk or bonded together to act as a single ring in bending.

Calculations have shown that such a damper and its support can be satisfactorily designed. Detail damper description and configurations together with their maximum stresses and maximum deflections for the various designs of three ratings (300, 1200 and 3000 MVA) may be found in Section 3.2.

Inner to Outer Rotor Attachment

The superconducting generator rotor configuration must accommodate the differential thermal expansion and contraction between the cryogenic inner and warm outer rotors. The mechanism must be capable of withstanding axial movements on the order of 1.1 cm (.44 in.) for the 300 MVA machine and 2.0 cm (.80 in.) for the 1200 MVA machine. In addition it must be laterally stiff, torsionally stiff, and meet other requirements reliably.

Ten different schemes for solving the problem have been proposed. Of these ten, four received detailed calculation. A review of the advantages and disadvantages of each promising scheme has been made. The flexible connection design has been selected as the number one choice for development.

The flexible connection uses laminated radial going flexures which are preloaded. The scheme is advantageous in that it works in a vacuum and does not depend on control of friction. Long life and reliable operation are easily assured.

Details of this and the other schemes are presented in Section 3.2.

Torsional Vibration

One of the functions of the rotor structure is to transmit normal rated torque between the turbine coupling and the generator winding. In addition, a line-to-line short circuit can result in an ac torque with a main component at 60 Hz on

the generator with a peak amplitude approximately 8 times (for X_d = .4) rated torque. While the superconducting generator rotor can be designed to handle this torque, the problem lies in not exceeding approximately 3 per unit torque limit of the present turbine shaft design. It is believed that the 300 MVA model will be designed and built in the next five years and will probably couple to an existing turbine. Therefore, this torque limit criterion used to design the conventional generator, applies to the 300 MVA superconducting design. The required torque attenuation can be obtained by lowering the natural frequency of the system (approximately to 20 cycles) relative to the predominant 60 cycle exciting torque. This can be done by interposing a flex-shaft between the generator and the turbine coupling. The calculations and the flex-shaft details are given in 3.2.2.6.

An electrical mechanical system analysis has been made and is treated in a separate section. The results indicate that the maximum shaft torque experienced at reclosing after clearing a fault can be attenuated to the required value by using a suitable flex-shaft.

The design of a 1200 MVA superconducting machine is not subjected to this torque limit. The preliminary shaft torque at short circuit has been estimated and summarized in

Rotor Lateral Vibration

Lateral vibration characteristics of the proposed Westinghouse 300 and 1200 MVA SCTG rotors have been predicted by finite element computer modeling. Mode shapes, mode frequencies, and responses to both static and dynamic unbalances have been calculated. The encouraging results indicate that these rotors will have lateral vibration characteristics which are desirable for practical reliable machinery.

The models indicate that machines running steady state at 3600 rpm (60 Hz.) will be above the first critical (approximately 30 Hz.) and below the second critical speed (approximately 70 Hz.). The second critical speed is within the range of 120% overspeed (72 Hz.), however, calculations show that it will present no problems.

Whirl Dynamics of Liquid Helium

The present Westinghouse SCTG rotor cooling scheme employs liquid helium coolant. In the partially filled rotor, rotational forces establish a free cylindrical surface of liquid. A review has been made regarding possible effects of the

liquid on vibration of the rotor. It has been concluded that these effects will be negligible in the Westinghouse 300, 1200, and 3000 MVA rotors.

Helium Transfer System

A helium transfer system at the exciter end of the rotor has been designed to transfer the helium coolant into and out of the rotor. High inlet transfer efficiency is achieved by using a vacuum insulated bayonet concentric within a rotating tube aligned by bearings. A Ferrofluidic seal complemented by circumferential seals effectively prevents contamination and loss of the helium.

2.2.1.3 Helium Management System. A helium management system has been designed and analyzed for a 300 MVA generator that can be directly extrapolated to the largest superconducting generators yet conceived. The guiding principles for design of the helium cooling system were defined early in the program and adhered to throughout. They were to achieve the maximum reliability through simplicity of design and to maximize the use of cooling and flow techniques which have been proven experimentally. The resulting system design can be built within the present state of the art with no development program for materials, fabrication techniques or components. However model tests of the complete system will be required for design verification.

The helium management system combines the most desirable features of conduction, forced flow, natural convection, and evaporative cryogenic cooling systems for rotating apparatus identified in the existing literature. The combination is such that none of the cooling mechanisms is contrafunctional to the others. Steady heat generated within the rotor is transmitted to a boiling pool surface by high acceleration field assisted natural convection and high transient heat loads resulting from line faults are stored locally as a sensible temperature rise and transferred to the pool surface in a controlled release. Innovative design of the radiation shield and torque tube heat exchanger have produced a synergistic combination which effectively mitigates the thermal stress resulting from fault induced helium flow surges. Thus, a design is presented which has exceptionally large margin under fault conditions and relatively high reliability.

The features of the EPRI-Westinghouse superconducting field winding cooling system are the following:

- Isolation of alternator reliability from liquifier reliability by an intermediate, unregulated, atmospheric pressure liquid helium storage dewar.

- Full self regulation of the helium flow.
- Subatmospheric pressure (3.6 K temperature), natural convection pool cooling of the winding.
- Elimination of the neutral thermal lapse rate temperature rise of natural convection pool cooling systems by near isothermal compression-diabatic expansion type thermosyphon loops.
- Isolation of structure loss induced coolant temperature rise from the winding by independent thermosyphon loops.
- Mixed phase torque tube helium gas return pumps which eliminate instabilities associated with liquid ingestion in the return pumps.
- Synergistically combined torque tube heat exchanger stations and radiation shield cooling paths control thermal stresses during steady and fault induced transient operations without additional fault transient mitigating equipment, e.g., valves, heat exchangers,...
- A very reliable quench induced flow reversal that heats the conductor with helium compression work and increases the normal zone propagation velocity.

The design of any system that departs from conventional practice raises the question of what specialized auxiliary equipment will be required to operate reliably. Equipment unique to the superconducting generator consists of an eight hour helium supply storage dewar, a quench (transition to the resistive state) detection system, a dual compressor helium liquifier and certain instrumentation. The expected steady helium flow rate of 25 $\pm$ 5 l/hr is low in the range usually considered in generator economic analyses and leads to a storage dewar of 250 or more l -- a relatively standard low cost item. The quench detection system, which is based either on a machine simulation or tapped field winding approach, will be capable of detecting a quench before any irreversible damage can take place in the field winding.

Cool down from room temperature may be accomplished in 48 hours using only the plant liquifier or accomplished in less time using increased flow rates from stored or purchased liquid helium. In the following text instrumentation requirements are discussed. None of the novel features above present a significant impediment to the implementation of a superconducting generator.

2.2.1.4 Rotor Instrumentation. Instrumentation and telemetering system is required for design verification and performance monitoring of the superconducting rotor. Such instrumentation is most critical for model rotor tests in the early stages of the next phase of the development program. Here, the thrust would be design verification of rotor components, i.e., performance of the field winding, the helium management system, the shield system, etc. However, the rotor in the utility demonstration machine will also require instrumentation, though somewhat less than the model rotor, in order to monitor performance under system conditions.

The quantities to be measured and the sensor location are:

- Temperature (4 K to 300 K)

  Cryogenic - field winding
  - helium flow circuit
  - radiation shield
  - torque tube
  - field support shell and cold shield

  Room Temperature - damper shield.

- Flux Density - I.D. of damper shield
  - Within inner rotor.

- Displacement or Strain
  - inner rotor twist
  - inner rotor radial deflection
  - relative rotation of inner rotor to outer warm shield
  - outer warm shield radial deflection
  - flexible shaft twist.

- Vacuum Pressure - pressure in thermal isolation space between inner rotor and outer warm shield.

- Helium Level, Flow and Pressure
  - liquid level of helium in inner rotor
  - helium flow through field winding and exiting out of rotor
  - radial dependence of helium pressure.

The preferred sensors are listed below:

- Cryogenic Temperature - carbon-glass.
- Room Temperature - chromel/alumel thermocouple.
- Flux Density - magneto-resistors (dc)
  - search coils (ac).
- Deflection - resistance strain gauge.
- Vacuum - Phillips Ionization gauge.
- Helium Level - superconducting wire gauge.
- Helium Flow - (1) diaphragm pressure gauge with calibrated aperture
  - (2) heat pulse time of flight.
- Helium Pressure, Diaphragm Sensor.

A multiplexing F-M telemetering system will be utilized for transmitting the sensor signals from the rotating frame to the stationary frame, where the data can be processed and recorded.

2.2.2 Stator Design

2.2.2.1 Stator Electrical Design. The design opportunities offered by superconducting field windings have made possible new armature winding concepts which could

not be considered with conventional field conductors. The new types include air gap windings for direct generation of extra-high voltage at transmission system level with possible application to high-voltage DC transmission as well as low voltage windings.

The high mmf capability of the superconducting rotor winding reduces the need for magnetic material in the flux path and thus permits elimination of stator teeth. The space freed thereby can be used for increasing the cross section of the armature winding. This has provided opportunities as well as challenges to the designer:

1 - The ground plane no longer interpenetrates the winding. It is therefore possible to reorganize the insulation so as to obtain increased voltage capability.

2 - More uniform distribution of dielectric stress is made possible by the resulting more uniform spacing and winding capacitance distribution.

3 - Without the protection offered by teeth, the armature conductors are exposed to high magnetic fields and the resultant stray losses and electromagnetic effects.

4 - The steps required to control the losses and heating, such as fine stranding of the conductors, tend to reduce ability to withstand electromechanical force effects.

The electromechanical force effects produce vibration and impacts which work together with the normal heating and the dielectric stresses to deteriorate the stator insulation. All insulation has a useful service life that is limited by such effects. To avoid premature loss of life, the stator must be designed so as to control these effects and prevent damage to either the insulation or the conductors. This requires proper attention to electrical and mechanical stresses during both steady state and transient operating conditions for all parts of the armature winding, including end connections, phase leads, and terminals. Heating effects must likewise be properly controlled by appropriate cooling provisions.

The design criteria with regard to these effects are specified for windings in the conventional range of voltage ratings by American National Standards C50.10 and C50.13. Extra-high voltage windings, however, impose insulation requirements which are not covered by these turbine generator standards. Attainment of EHV ratings requires the application of high-voltage insulating materials in new arrangements not previously known in turbine generator design. Patent applications are being prepared for new winding arrangements which were invented in the course of this program.

Stator Configuration Selection

The initial requirements for EPRI Contract No. RP 429-1 included armature winding design for at least 70 kV voltage rating. Early in the work, this objective was revised upward to transmission line voltage. Though many were studied, no known design of turbine generator winding was demonstrably capable of meeting this objective. A study towards definition of a basically new concept was undertaken. This study succeeded in defining a unique "spiral pancake" concept with excellent potential for application to superconducting turbine generators in the size range of 300 to 3000 MVA at their respective transmission line voltages. At lower voltage levels, the spiral pancake configuration offers improved support against electromechanical force effects, and thus opens the way to low reactance designs more conducive to system stability and integrity. High voltage direct current transmission may also be considered.

A cross-sectional view of the new winding (previously disclosed to EPRI for patent application) is shown in Figure 2-13. The form of this winding intrinsically provides smooth, continuous, and overlapping insulating layers between the levels of conductors. This feature minimizes concentrations of dielectric stress and permits surface creepage paths of great length. These paths could, if necessary, be further elongated by special provisions. High-voltage insulating materials, such as are used in cables and transformers, can be applied in long, continuous, laminated layers of flat sheets. Dielectric voltage stresses are thus confined to insulation that can be designed to accommodate them. The gap is kept free of dielectric stresses by an electrostatic shield located near the inner surface of the armature winding insulation. Uniform mechanical support is provided by the extension of the stator shield over the end turns of the winding.

In the EHV application of this winding, a single dielectric liquid impregnates the solid insulation and cools the windings. Cooling, internal, and external connections are provided without interrupting the integrity of the insulating structure. This is readily observable in Figure 2-14, a longitudinal section.

In the low voltage version, conventional mica-resin insulation is used for the conductors, which are cooled with purified water. In this case, uniform support is offered by the straight-line continuation of the winding into the end turns and by the intrinsic wedging action against the stator shield.

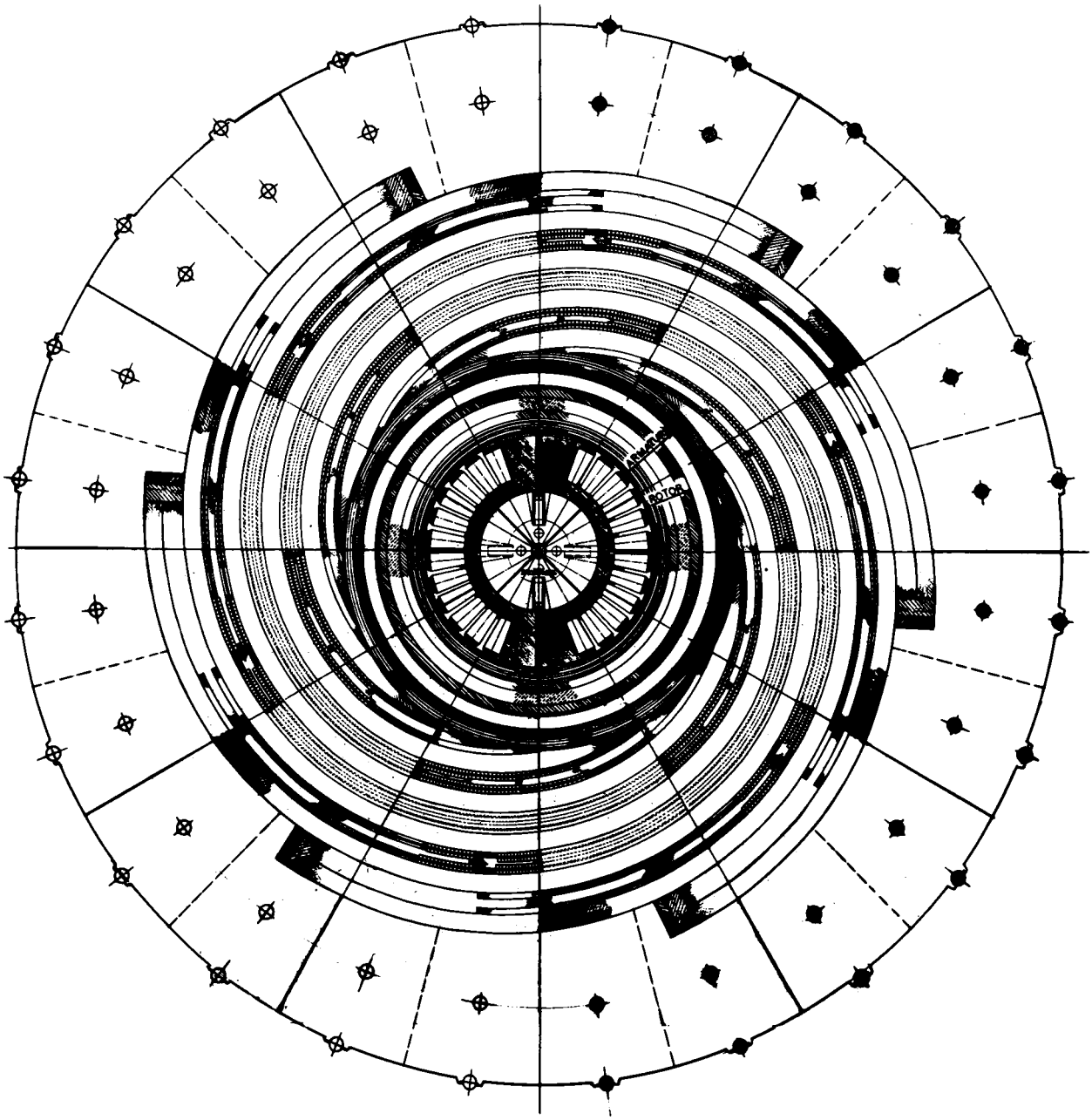

Figure 2-13. Cross Section of Spiral Pancake Winding for EHV Superconducting Turbine Generator

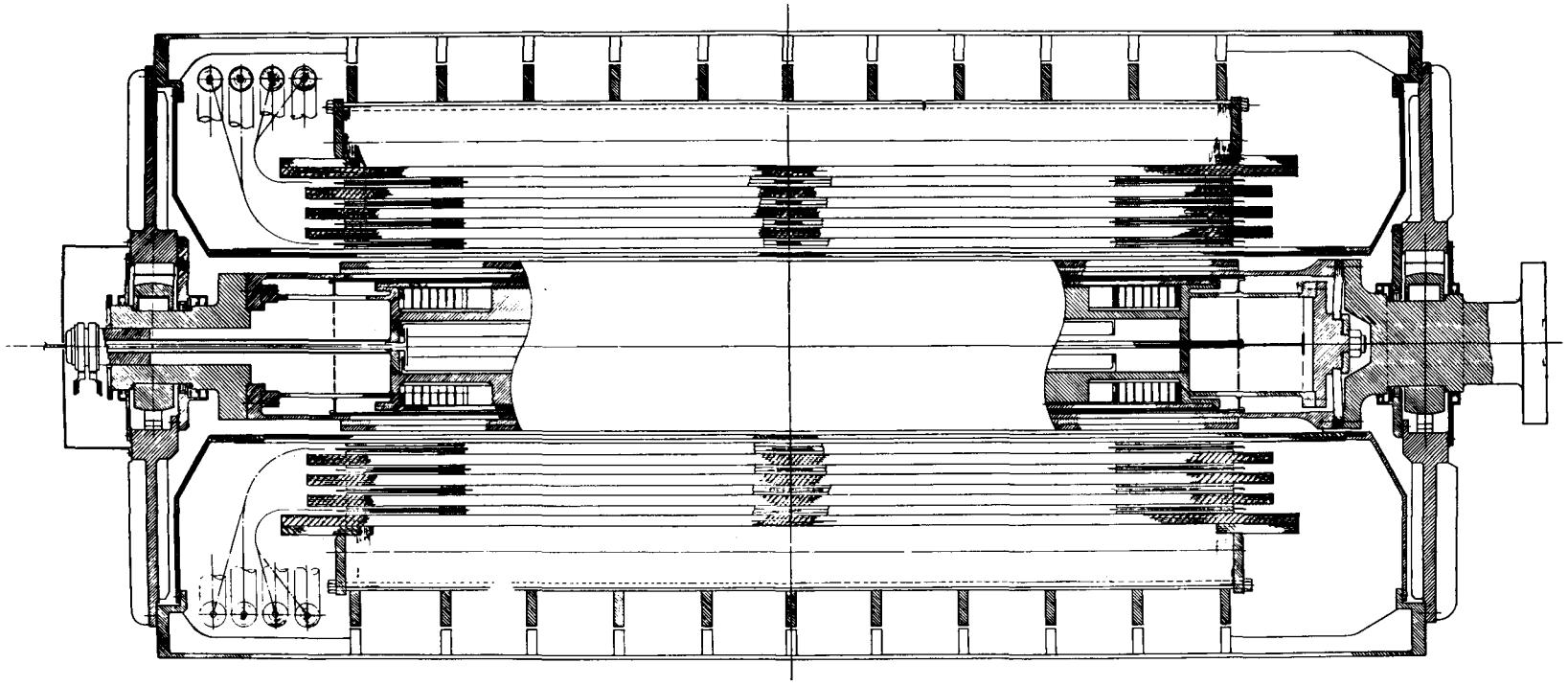

Figure 2-14. Longitudinal Section of Superconducting Turbine Generator with EHV Armature Winding

The spiral pancake winding, in its high-voltage and low-voltage forms, represents the final Westinghouse choice of armature winding concepts for development of superconducting turbine generators, and supersedes the modified airgap winding that was earlier identified as the best choice.

Stator Winding Detail Design

Detail design calculations were carried out for eight distinct electrical designs predicated on the final selection of armature winding configuration described in the previous section. These designs differ in output rating, voltage, and reactance level, as follows:

Table 2-4

LIST OF ELECTRICAL DESIGNS

RATED MVA	RATED VOLTAGE L-L	REACTANCES, PU		
		x_d	x_d'	x_d''
300	13800	.225	.161	.081
300	13800	.417	.313	.160
300	230000	.249	.202	.136
300	230000	.492	.404	.269
1200	29000	.221	.151	.082
1200	30000	.405	.286	.157
1200	500000	.261	.202	.137
1200	500000	.497	.393	.271

The armature conductors of the low voltage windings (13800 volts, 29000 volts, and 30000 volts) are water cooled by means of internal cooling tubes that are wound with the strands of which the coils are composed. The coils for the 230 and 500 kV windings are cooled by the same dielectric fluid that is used to insulate and impregnate the windings. The fluid has been assumed to be a low-viscosity hydrocarbon oil. The conductors of all coils are composed of fine stranding, of the order of 35 to 40 mils square, which is required to minimize the stray losses produced by the intense magnetic flux which is present at the winding.

A special internal construction has been devised for the coils of the high voltage armatures to minimize internal dielectric stresses across the oil ducts which are essential for cooling purposes. This is described in detail in Section 3.3.2. Further development is however, required for the precise control of dielectric stresses everywhere in the windings and the insulation. The development work required to achieve this is outlined in Section 3.7.

The results of detailed design calculations are presented in tabular form in Section 3.3.2.

Stator Shield Design

Flux shields were designed for each of the eight armature windings listed in the previous section. The flux shield not only serves as a return path for the main flux in the machine, but also provides a means of support for the armature winding, and must therefore be of sufficient cross section to offer the necessary rigidity. These purposes should be accomplished while achieving the best possible overall power density and highest efficiency, and without unduly complicating the construction of the machine.

This set of objectives has been accomplished for the eight flux shield designs by

1 - designing for maximum flux density

2 - checking for adequate rigidity

3 - coordinating the cooling method with other cooling provisions used in the machine.

The coolant used for the flux shield is the same as is used for at least one other major machine member. In the case of the high-voltage armature machines, the choice is obvious: the same dielectric fluid is used both for the stator coils and the flux shield. The low-voltage machines with water-cooled stator windings present a choice between water cooling and hydrogen cooling for the shield. In this case, good judgement and experience indicate that it is preferable to avoid a multiplicity of additional water passages and thereby the possibility of additional leaks. Therefore hydrogen cooling is chosen for these shield designs. In all cases, it has been found possible to match the pressure requirements for the two parallel cooling paths using the same medium quite closely. This avoids the need for special flow control orifices.

The detailed calculations of the shield designs and cooling are indicated in tabular form in Section 3.3.2.

2.2.2.2 Stator Mechanical Design.

Stator Winding and Support

The spiral pancake winding will be used in the superconducting generator stator. It consists of six phase windings or coils which are interleaved in a

spiral fashion to form the complete armature. The spaces in between the phase windings are impregnated with resin. The complete armature can be cured into a monolithic structure. For a high voltage machine, the insulation between the phase coils is provided by layers of oil-pregnated pressboard, and the entire winding assembly will be tightly clamped between the coils and the bore seal tube. The armature should be so positioned in the core that the operation of torque will tend to tighten the winding between the core and the bore ring against the vibrating forces. Provisions are also made to maintain the winding tight under normal operating conditions, to prevent excessive angular displacement of the coils during a short circuit and to retighten the armature, if necessary, during the life of the machine.

In a conventional stator, the straight portion of the coils is supported by the core and the frame, and their end turns are kept in place by the braces. Due to the difference in the spring constants of the core and the braces, the end turns are subjected to high stresses resulting from bending and twisting. While the conventional braces are strong enough for the generators of medium transient reactance, it remains to be proved that the similar bracing system will be sufficient for the low reactance machines. In the stator with spiral winding, the end turns are brought out on the same radius as the straight part of the coils so that the entire coil is continuously supported by the core and the cause for the high stress is eliminated. The end turns are subjected to forces equal to or less than those for the straight portion of the winding. Consequently, the stress and the displacement of the end turns will be no more than the corresponding values for the straight portions. Further discussions may be found in 3.3.2.

Shield, Frame and Bearings

The construction of the shield and frame of a superconducting generator is similar to that of a conventional generator except that the shield is extended to continuously support the end turns of the spiral winding. The core natural frequency together with its static and magnified displacements are calculated for various designs and their comparative conventional units. The results which can be found in 3.2 appear to be well within their allowable limit.

The 300 MVA generator requires a bearing of 35.6 cm(14 in) for all practical reactance levels while the 1200 MVA unit requires a bearing of 53.3 cm (21 in.) for X_d = .5 and of 58.4 cm (23 in.) for low reactance X_d = .22. Presently the largest tilting pad oil film bearing in operation is of 53.3 cm. It is conceivable that a 58.4 cm bearing required for the 1200 MVA generator with low reactance can be developed in the near future.

2.3 AUXILIARIES

2.3.1 Exciter and Voltage Regulator

The fact that the superconducting field winding has no ohmic resistance during normal operation results in very low steady-state demands on the excitation system. These are easily satisfied by a static system operating through slip rings. The steady-state power requirement is determined by brush and lead drops, and is about 3 kW for all ratings of 300 to 3000 MVA. The design of the exciter is thus mainly predicated on the transient requirements, which include both positive and negative field forcing at a ceiling of 400 volts. This voltage was selected in the basis of transient studies which showed that higher ceiling voltage provided no significant improvement in transient stability, and so as to limit losses in the field winding due to ripple voltages. The negative forcing is used to de-energize the field more rapidly in the event of a fault within the generator protective zone.

The static exciter is complemented by a voltage regulator and excitation protection devices of standard design, using static components. These include a minimum excitation limiter, a maximum instantaneous current limiter, a volts per hertz limiter, and instantaneous overexcitation protection. A quench detector is also required. Further studies will be needed to select the most desirable of several possible quench detection schemes.

2.3.2 Generator Gas, Oil and Water Systems

Gas supply and control systems will be of the conventional type, proven by decades of service experience. The gas circulated through the machine is required to remove miscellaneous losses, of which the loss in the damper is expected to be the largest. Gas cooling will also be used for the flux shield of the low voltage armature.

Oil systems are required for the generator bearings and gland seals, and for the high-voltage stator. The former will be of standard design. The high-voltage stator will require a dielectric fluid to be maintained at very high purity, and requires some engineering development.

The water system used for the low voltage armature coils and leads will be of standard design.

2.3.3 Refrigeration System

CTI-Cryogenics conducted a study to develop the conceptual design and cost estimate for a refrigeration system to satisfy the cryogenic cooling requirements of

a 300 MVA superconducting generator. The design concept can be expanded to satisfy the requirements of a 1200 MVA generator in the future.

The present conceptual design study indicates that a refrigeration system to meet the refrigeration capccity and operational requirements of the EPRI - Westinghouse 300 MVA generator is feasible and well within the state of the art. The study also shows that the same conceptual design can be applied to the 1200 MVA generator without further development.

In developing the conceptual design, we have taken into consideration the refrigeration requirements of the generator as well as the operational requirements of the refrigeration system. These requirements were reviewed with respect to performance, reliability, acceptable maintenance intervals and equipment service life.

Various cryogenic processes were analyzed to determine the optimum process to meet these requirements. Namely 47 liters per hour of liquid helium at 4.35 K for the 300 MVA generator and 79 liters per hour of liquid helium at 4.35 K for the 1200 MVA generator. These liquefaction requirements were specified by Westinghouse and include a 50% safety margin to allow for unpredictable losses and possible future changes in the superconducting generator cooling requirements.

A detailed process and instrumentation (P & I) diagram was prepared based upon the cycle selected and the above stated requirements. The developed P & I diagram was used to select the components and formed the basis for the component cost portion of the cost estimate.

The developed refrigeration system consists of a cryogenic cold box assembly containing heat exchangers and turbine expanders, a compressor assembly incorporating redundant compressors, an instrument panel containing a computer for process control and a helium storage dewar for back-up purposes during power outage or component replacement.

Each component within the system was reviewed to determine if redundancy was required in order to provide continuous cryogenic cooling to the generator.

An analysis of the system, as designed, leads to an estimated reliability of 96.6%, which would result in no more than one refrigeration system induced outage over the life of the superconducting generator system.

The cost estimate for the refrigeration system was developed for the design and manufacture of the first refrigeration system to meet the 300 MVA generator cooling requirements. The mature cost of a refrigerator system would be $600,000 in 1977 dollars.

2.4 GENERATOR AND SYSTEM INTERACTIONS

Several different aspects are involved in judging the performance of a superconducting generator with respect to its interaction with a power system. The most important characteristic is how the machine performs during system disturbances. Such disturbances can range from slow variations in load to sudden and severe load changes such as system faults. The basic question is whether the machine will be forced out of synchronism with respect to the system due to such disturbances. This event must be avoided, if at all possible, since it will probably require the machine to be temporarily disconnected from the system.

Certain parameters are used to characterize the performance of the machine and its ability to remain in synchronism with the system during and after disturbances. For very slow variations in load, the parameter is the "steady state stability limit" which is the maximum steady state power that the machine can deliver and remain in synchronous operation. For the severe case of faults, the parameter that is commonly used is the "critical fault clearing time." This is the maximum time that the machine can be subjected to a fault and still return to synchronous operation after the fault has been cleared. This parameter is said to characterize the "transient stability" of the generator.

One of the objectives of the present program was to compare superconducting generators to conventional generators with respect to their system performance. This was carried in the main for the 300 MVA units. In summary, this comparison is as follows.

Steady State Stability. The superconducting generator has a higher steady state stability limit because of its synchronous reactance is only about 1/3 of a conventional machine. This improvement is especially important for under-excited operation.

Dynamic Stability. Unlike a conventional machine, the superconducting generator will have no dynamic stability limit when operating within its MVA rating.

Transient Stability. In general, the critical fault clearing time for a superconducting generator is longer than for a conventional machine. How much of an increase can be realized depends mainly on the lower limit that can be achieved for the subtransient reactance. For example, the high voltage, spiral armature, superconducting generator with a X''_d = 0.16 pu has a CFCT of 19 cycles. This is to be compared with the CFCT of a conventional machine under the same system conditions of 14 cycles.

VAR Overload and Load Rejection. The superconducting generator has a better performance under a sudden VAR overload but has a somewhat poorer performance upon load rejection. However, peak voltage under load rejection is still within safe limits for auxiliary station transformers.

Rotor Swing Damping. Damping of the rotor swings is positive and adequate.

Flexible Shaft Mode Damping. A flexible shaft is utilized with the 300 MVA units between the generator rotor and the LP turbine shaft. The purpose of this flexible shaft is to attenuate fault torques from the generator to a level that can be handled by present day turbine shaft design limits (ν 3 pu). This is in anticipation that a 300 MVA demonstration unit will be tested in a utility system using an existing turbine. The flexible shaft introduces a new oscillatory mode at about 20 Hz. It has been shown that the electro-magnetic plus mechanical damping for this mode is positive.

2.5 RELIABILITY

Achieving a reliability that equals or surpasses that of conventional generators is mandatory for superconducting generators for utility application. There is no technical basis at this time for believing that this goal cannot be achieved. It will, of course, require a major long-term investment in engineering and manufacturing to push this technology toward commercial ratings and reliabilities. The question of reliability at this point is not so much can it be achieved, but how much will it cost and what are the consequent long range economic benefits if achieved.

It might be possible with further effort to extrapolate experience that does exist for certain components as utilized in other applications, e.g., stationary cryogenic dewars, refrigeration plants for liquification of gases and stationary superconducting coil systems. However, it was judged more expedient to expend the

funds under the present program in further engineering verification of the machine concepts being proposed rather than on a detailed reliability analysis of questionable long-range value.

2.6 MANUFACTURING AND MATERIALS DEVELOPMENT

Manufacturing methods and materials utilized in the superconducting generators must result in final fabricated and assembled parts meeting or exceeding required mechanical and physical properties.

A strong interdependence between design and materials and manufacturing has been recognized in the design process of the SCTG. In general the philosophy has been to use state of the art manufacturing and materials technology as much as possible, except in a few cases where the development of advanced SCTG's would be too severely limited or inhibited. The majority of the SCTG design which has been developed therefore uses straightforward state of the art technology.

In a few parts of the design, development of manufacturing methods or materials is anticipated. Section 3.6 of this report details these requirements and indicates machine parts which may be improved as more advanced materials are developed in the future.

2.7 DEVELOPMENT PLAN

The next step in the superconducting generator development is to build, test, and observe in service a prototype unit of sufficient size to credibly demonstrate the features of the design. A prototype will demonstrate:

1. That a full-size superconducting field winding, and its cryogenic system, can operate successfully under power system conditions.
2. That the armature configuration can withstand system transient forces, and
3. That the expected economic and system dynamic performance goals can be achieved.

It is proposed that both a low-voltage and a high-voltage (transmission level) prototype unit be developed. The development program would therefore be divided into two parts:

Part A: Develop and test a 300 MVA low-voltage generator. This part would involve the development of the cryogenic rotor, the low-voltage stator and generator auxiliaries.

Part B: Develop and test a 300 MVA high-voltage (transmission level) generator. This part would concentrate on the development of the high-voltage armature. The design of the rotor and auxiliaries for this second unit would depend on the work carried out in Part A.

Parts A and B would each take six years to completion. They could be run in parallel with Part A being initiated before the start of Part B.

Each part of this development is comprised of two phases. The first phase would consist of Premanufacturing Development and would be divided into Critical Component Development, Engineering Development and Material and Manufacturing Development. It is during this phase that all of the base data required for the detailed layout drawings of the generator are developed. This phase would include model tests of rotor and stator components, extensive analytical work and development of manufacturing methods.

The second phase, Manufacturing and Installation, would cover the manufacture of the generator and its installation and test on a utility system.

The total cost of Part A (low-voltage) is $\$12 \times 10^6$ and for Part B (high-voltage) is $\$10.4 \times 10^6$.

Section 3.0

REPORT OF WORK

The purpose of Section 2 was to give an extended summary covering all facets of the program. In addition, its first subsection 2.1, gives a broad introduction to general design considerations and economics. The present Section 3 is a detailed report on all of the work summarized in Section 2. Section 3 is therefore indexed to parallel the numbering system used for Section 2.

3.1 GENERAL DESIGN CONSIDERATIONS

3.1.1 Characteristic Data

Two major generator characteristics to be considered in evaluating generator design alternatives are voltage and reactance level. Table 3-1 presents general characteristic data for 300 and 1200 MVA designs for two voltage levels and two reactance levels. Data on a 1200 MVA conventional unit and a 3000 MVA superconducting design are also included.

3.1.2 Major Configuration Selection

This material is completely covered in Section 2.

Table 3-1

GENERATOR CHARACTERISTIC DATA

Generator Designation	A	B	C	D	E	F	G	H
RATING AND CAPABILITIES AT 30 PSIG HYDROGEN PRESSURE								
MVA	300	300	300	300	1200	1200	1200	1200
MW	270	270	270	270	1080	1080	1080	1080
Power Factor	0.9	0.9	0.9	0.9	0.9	0.9	0.9	0.9
Line Volts	13800	13800	230000	230000	29000	30000	500000	500000
Line Amperes	12551	12551	753	753	23890	23094	1386	1386
Phases	3	3	3	3	3	3	3	3
Frequency, Hz	60	60	60	60	60	60	60	60
Speed, R/min	3600	3600	3600	3600	3600	3600	3600	3600
Number of Poles	2	2	2	2	2	2	2	2
BIL, kV	N.A.	N.A.	900	900	N.A.	N.A.	1300	1300
I_2^2t Capability	20	20	20	20	15	15	15	15
Continuous I_2, per unit	0.12	0.12	0.12	0.12	0.10	0.10	0.10	0.10
EXCITATION DATA								
Field Amperes - No Load	887	827	877	773	903	860	873	781
Field Amperes - Full Load	990	1013	996	1000	1003	1055	997	1006
Charging Rate - %/sec.	2	2	2	2	2	2	2	2
CALCULATED TERMINAL VOLTAGE AND CURRENT								
Line Volts	13936	13628	230964	230074	28909	29671	501606	496846
Line Amperes	12428	12710	750	753	23966	23350	1381	1394

Table 3-1 - Continued

Generator Designation		A	B	C	D	E	F	G	H
CHARACTERISTIC CONSTANTS									
Per Unit Impedance, ohms		0.647	0.619	177.8	176.4	0.696	0.734	209.7	205.8
REACTANCES IN PER UNIT									
Direct Axis									
Synchronous	x_d	0.225	0.417	0.249	0.492	0.221	0.405	0.261	0.497
Transient	x_d	0.161	0.313	0.202	0.404	0.151	0.286	0.202	0.393
Subtransient	x''_d	0.081	0.160	0.136	0.269	0.082	0.157	0.137	0.271
Quadrature Axis									
Synchronous	x_q	0.225	0.417	0.249	0.492	0.221	0.405	0.261	0.497
Transient	x'_q	0.161	0.313	0.202	0.404	0.151	0.286	0.202	0.393
Subtransient	x''_q	0.081	0.160	0.136	0.269	0.082	0.157	0.137	0.271
Negative Sequence	x_2	0.081	0.160	0.136	0.269	0.082	0.157	0.137	0.271
Zero Sequence	x_o	0.049	0.087	0.046	0.091	0.047	0.083	0.047	0.088
Stator Leakage	x_1	0.025	0.065	0.080	0.160	0.034	0.080	0.089	0.183
RESISTANCES IN PER UNIT									
Armature	R_a	0.0024	0.0031	0.0018	0.0025	0.0015	0.0019	0.0009	0.0012
Positive Sequence	R_1	0.0025	0.0034	0.0019	0.0028	0.0017	0.0021	0.0012	0.0015
Negative Sequence	R_2	0.0111	0.0202	0.0101	0.0202	0.0133	0.0211	0.0088	0.0165
RESISTANCE IN OHMS									
Phase Resistance		0.0015	0.0020	0.312	0.444	0.0011	0.0014	0.196	0.245

Table 3-1 - Continued

Generator Designation		A	B	C	D	E	F	G	H
CHARACTERISTICS CONSTANTS - CONTINUED									
TIME CONSTANTS IN SECONDS									
Direct Axis									
Transient Open Circuit	T'_{do}	5167	3920	7187	4990	19060	12217	23263	17123
Subtransient Open Circuit	T''_{do}	0.248	0.259	0.228	0.237	0.293	0.298	0.271	0.276
Quadrature Axis									
Transient Open Circuit	T'_{qo}	0.422	0.440	0.388	0.403	0.498	0.507	0.461	0.469
Subtransient Open Circuit	T''_{qo}	0.248	0.259	0.228	0.237	0.293	0.298	0.271	0.276
Armature	T_a	0.090	0.137	0.200	0.285	0.145	0.219	0.404	0.599
Cold Damper		0.154	0.151	0.143	0.140	0.216	0.203	0.187	0.185
INDUCTANCES IN HENRY									
Self Inductances									
Field		15.50	11.76	21.56	14.97	57.18	36.65	69.79	51.37
Armature Phase x 10^3		0.258	0.456	78.43	153.6	0.272	0.526	100.3	181.0
Warm Damper x 10^5		0.301	0.256	0.328	0.266	0.513	0.387	0.527	0.411
Cold Damper x 10^5		0.274	0.234	0.310	0.252	0.473	0.358	0.502	0.393
Mutual Inductances									
Phase-Phase x 10^3		-0.129	-0.228	-39.22	-78.63	-0.136	-0.263	-50.13	-90.48
Field-Armature x 10^1		0.337	0.366	5.66	6.44	0.697	0.755	12.58	13.95
Field-Cold Damper x 10^2		0.452	0.334	0.574	0.401	1.243	0.820	1.40	1.02

Table 3-1 - Continued

Generator Designation	A	B	C	D	E	F	G	H
INDUCTANCES IN HENRY - CONTINUED								
Mutual Inductances - Continued								
Field-Warm Damper x 10^2	0.400	0.293	0.488	0.341	1.120	0.734	1.230	0.893
Armature-Warm Damper x 10^4	0.223	0.268	3.410	4.330	0.295	0.353	5.020	5.820
Armature-Cold Damper x 10^4	0.179	0.215	2.741	3.478	0.245	0.293	4.192	4.862
Warm Damper-Cold Damper x 10^5	0.242	0.206	0.263	0.214	0.426	0.311	0.440	0.343
CRITICAL FAULT CLEARING TIME								
Seconds	0.292	0.245	0.320	0.250	0.267	0.222	0.274	0.222
Cycles	17.5	14.7	19.2	15.0	16.0	13.3	16.4	13.3
INERTIA CONSTANT (H CONSTANT) - GENERATOR AND TURBINE								
KW Seconds/kVA	3.23	3.23	3.23	3.23	2.68	2.53	2.75	2.61
KINETIC ENERGY IN MW-SECONDS								
Generator	62.0	62.0	62.0	62.0	511.	337.	604.	433.
Turbine	908.0	908.0	908.0	908.0	2700.	2700.	2700.	2700.
Total	970.0	970.0	970.0	970.0	3211.	3037.	3304.	3133.

Table 3-1 - Continued

Generator Designation	A	B	C	D	E	F	G	H
MAJOR MACHINE DIMENSIONS IN METERS								
ARMATURE (STATOR) WINDING								
Mean Inner Radius	0.4978	0.4978	0.5418	0.5334	0.6477	0.6350	0.6629	0.6629
Mean Outer Radius	0.5588	0.5888	0.7912	0.7874	0.7671	0.7976	1.012	1.055
Length of Straight Part	2.733	1.906	3.747	2.506	5.792	3.768	6.947	4.874
Length of Mean Turn	9.45	8.25	12.25	9.95	17.2	12.95	19.80	15.80
FIELD (ROTOR) WINDING								
Inner Radius	0.1956	0.1930	0.1905	0.1905	0.2832	0.2819	0.2794	0.2781
Outer Radius	0.2682	0.2682	0.2682	0.2682	0.3531	0.3558	0.3531	0.3531
Length of Straight Part	2.733	1.906	3.747	2.506	5.792	3.768	6.947	4.874
Length of Mean Turn	6.13	4.47	8.14	5.65	12.8	8.80	15.1	11.0
WARM DAMPER								
Inner Radius	0.3493	0.3493	0.3493	0.3493	0.4636	0.4636	0.4604	0.4604
Outer Radius	0.3810	0.3810	0.3810	0.3810	0.4953	0.4953	0.4921	0.4921
Length	4.45	3.81	5.46	4.42	8.46	6.60	9.87	7.72
DAMPER SUPPORT STRUCTURE								
Inner Radius	0.3271	0.3271	0.3271	0.3271	0.4318	0.4318	0.4318	0.4318
Outer Radius	0.4097	0.4097	0.4097	0.4097	0.5461	0.5334	0.5207	0.5207

Table 3-1 - Continued

Generator Designation	A	B	C	D	E	F	G	H
MAJOR MACHINE DIMENSIONS IN METERS - CONTINUED								
STATOR FLUX SHIELD								
Inner Radius	0.6477	0.6777	0.8928	0.8890	0.8560	0.8865	1.1519	1.1951
Outer Radius	1.0523	1.0414	1.1946	1.2446	1.4038	1.3820	1.5646	1.5509
Length	4.173	3.532	4.986	3.944	7.390	5.531	8.407	6.464

Table **3-1** - Continued

Generator Designation	A	B	C	D	E	F	G	H
MAJOR MACHINE DIMENSIONS IN INCHES								
ARMATURE (STATOR) WINDING								
Mean Inner Radius	19.60	19.60	21.33	21.00	25.50	25.00	26.10	26.10
Mean Outer Radius	22.00	23.18	31.15	31.00	30.20	31.40	39.85	41.55
Length of Straight Part	107.61	75.03	147.53	98.67	228.04	148.34	273.50	191.88
Length of Mean Turn	372.0	325.0	483.0	392.0	677.0	510.5	780.5	621.5
FIELD (ROTOR) WINDING								
Inner Radius	7.70	7.60	7.50	7.50	11.15	11.10	11.00	10.95
Outer Radius	10.56	10.56	10.56	10.56	13.90	14.01	13.90	13.90
Length of Straight Part	107.61	75.03	147.53	98.67	228.04	148.34	273.50	191.88
Length of Mean Turn	241.4	175.8	320.3	222.5	505.6	346.5	595.9	432.4
WARM DAMPER								
Inner Radius	13.75	13.75	13.75	13.75	18.25	18.25	18.13	18.13
Outer Radius	15.00	15.00	15.00	15.00	19.50	19.50	19.38	19.38
Length	175.3	150.0	215.0	174.0	333.0	260.0	388.5	304.0
DAMPER SUPPORT STRUCTURE								
Inner Radius	12.88	12.88	12.88	12.88	17.00	17.00	17.00	17.00
Outer Radius	16.13	16.13	16.13	16.13	21.50	21.00	20.50	20.50

Table 3-1 - Continued

Generator Designation	A	B	C	D	E	F	G	H
MAJOR MACHINE DIMENSIONS IN INCHES - CONTINUED								
STATOR FLUX SHIELD								
Inner Radius	25.50	26.68	35.15	35.00	33.70	34.90	45.35	47.05
Outer Radius	41.43	41.00	47.03	49.00	55.27	54.41	61.60	61.06
Length	164.3	139.1	196.3	155.3	290.9	217.7	339.0	254.4

Table 3-1 - Continued

Generator Designation	A	B	C	D	E	F	G	H
GENERATOR LOSSES, KW								
No-Load Losses								
Core	357.7	275.2	391.5	205.4	1140.0	774.7	1175.0	787.0
Windage	30.2	23.8	45.9	33.1	159.0	110.9	191.2	145.0
Bearing	200	200	200	200	500	500	500	500
Stator I^2R	705.8	948.9	526.6	755.1	1826.5	2314.8	1121.0	1430.0
Stray Load Loss	176.	310.	178.	292.	654.	914.	734.	1086.
Excitation Loss	3.	3.	3.	3.	3.	3.	3.	3.
Refrigeration Loss	90.	90.	90.	90.	150.	150.	150.	150.
Total Losses, F.L.	1562.7	1850.9	1435.0	1578.6	4432.5	4767.4	3874.2	4101.

Table 3-1 - Continued

Generator Designation	A	B	C	D	E	F	G	H
WINDING PARAMETERS - FIELD								
Overall Current Density, MAmps/m^2	80.97	80.97	80.97	80.97	80.97	78.60	80.97	81.48
Conductor Current Density, MAmps/m^2	134.6	137.7	135.4	136.0	136.4	143.4	135.6	136.8
No. of Turns	3119	3210	3300	3300	4114	4032	4312	4378
Total Conductor Length, m	19125	14331	26846	18654	52835	35482	65265	48078
Space Factor	0.596	0.596	0.596	0.596	0.596	0.552	0.596	0.596
Stored Magnetic Energy, MJ	7.748	5.879	10.781	7.483	28.592	20.137	34.896	25.683

Table 3-1 - Continued

Generator Designation	A	B	C	D	E	F	G	H
WINDING PARAMETERS - ARMATURE								
Overall Current Density, MAmps/m^2	2.95	2.95	0.56	0.90	1.63	1.92	0.51	0.70
Current Density in Copper, MAmps/m^2	11.95	11.99	6.98	7.61	11.75	12.16	5.75	5.71
Cross Section of Copper in Conductor x 10^4, m^2	10.4	10.6	0.537	0.495	10.2	19.2	1.20	1.22
Series Turns/Phase	8	12	130	210	6	10	112	178
Connection	Y	Y	Y-Y	Y-Y	YY	Y	Y-Y	Y-Y
Phase Belt Angle, electrical deg.	60	60	60	60	60	60	60	60
Fractional Pitch	0.833	0.833	0.833	0.833	0.833	0.833	0.833	0.833
Overall Space Factor	0.245	0.245	0.074	0.115	0.135	0.159	0.079	0.110
Total Conductor Length, m	227.	297.	9555.	12537.	619.	389.	13306.	16874.

Table 3-1 - Continued

Generator Designation	A	B	C	D	E	F	G	H
MAGNETIC FLUX DENSITIES, PEAK VALUES IN TESLA								
Maximum in Field Winding	5.555	5.675	5.616	5.619	5.543	5.621	5.543	5.605
Radial at O.D. of Field Winding	3.781	3.743	3.718	3.639	3.952	3.904	3.875	3.837
Maximum at Mean I.D. of Armature Winding	1.397	1.346	1.080	1.084	1.474	1.475	1.262	1.257
Mean Radial at Armature Winding	1.261	1.140	0.790	0.738	1.286	1.187	0.883	0.773
Radial at I.D. of Flux Shield	1.003	0.874	0.541	0.491	1.030	0.912	0.576	0.479
Fundamental of Armature Reaction	0.245	0.361	0.179	0.292	0.268	0.422	0.222	0.345

Table 3-1 GENERATOR CHARACTERISTIC DATA - CONTINUED

Generator Designation	A	B	C	D	E	F	G	H
Load Angle, degrees	10.5	17.6	11.5	20.1	10.3	17.2	11.9	20.2
Torque x 10^{-7}, lbf-in.	0.634	0.634	0.634	0.634	2.53	2.53	2.53	2.53
Torque x 10^{-6}, N-m	0.716	0.716	0.716	0.716	2.86	2.86	2.86	2.86
PER UNIT TORQUE COMPONENTS FOR LINE-TO-LINE CIRCUIT								
For Short Circuit at Terminals								
Line Frequency Torque	14.53	7.79	8.98	5.05	14.27	7.94	8.97	4.99
Double-Line Freq. Torque	-7.27	-3.90	-4.49	-2.52	-7.14	-3.97	-4.49	-2.50
Unidirectional Torque	0.77	0.34	0.20	0.10	0.48	0.23	0.14	0.06
Decrement Factors for:								
Line Frequency Torque	19.04	13.69	8.90	6.77	11.21	8.20	4.78	3.46
Double Line Freq. Torque	1.53	1.43	0.80	0.82	1.14	1.11	0.70	0.65
Unidirectional Torque	5.91	5.96	3.81	3.93	5.09	4.99	3.22	2.77
For Short Circuit at High-Side of Transformer								
Line Frequency Torque	8.98	5.94			8.88	6.02		
Double-Line Frequency Torque	4.49	2.97			4.44	3.01		
Unidirectional Torque	0.38	0.23			0.27	0.17		
Decrement Factors for:								
Line Frequency Torque	20.99	16.18			16.09	12.06		
Double-Line Frequency Torque	0.96	1.09			0.71	0.84		
Unidirectional Torque	4.03	4.83			3.41	4.20		

Table 3-1 - Continued

Generator Designation	A	B	C	D	E	F	G	H
MISCELLANEOUS DATA - CONTINUED								
CRUSHING FORCES ON DAMPER DURING THREE-PHASE SHORT CIRCUIT - FORCES IN PSI								
For Short Circuit at Terminals								
σ_{r1}	2959.8	1879.5	951.7	733.2	3458.4	2630.9	1386.4	992.9
σ_{r2}	2966.0	1893.2	955.8	743.1	3465.7	2648.7	1392.5	1006.4
For Short Circuit at High-Side of Transformer								
σ_{r1}	752.7	849.1			895.4	1159.3		
σ_{r2}	756.8	859.1			900.1	1172.5		

3.1.3 Performance Considerations

3.1.3.1 Steady State Analysis. The use of a superconducting field winding instead of a conventional field winding in a turbine generator makes available a greatly increased ampere-turn capability. However, practical application considerations limit the potential benefit of this capability.

In contrast to the construction used in conventional machines the main flux paths in superconducting generators require no magnetic iron paths. At the high flux densities which are induced by superconducting windings, iron paths are neither useful nor desirable, except for the return path through the flux shield. If magnetic iron were present in the rotor, it would be heavily saturated and offer no appreciable reduction in reluctance; if in the armature winding, it would also be saturated, would experience losses, and would detract from the space available for windings. The superconducting generator is therefore designed ab initio on the basis of:

- a greatly increased effective "air gap"
- partial magnetic coupling between the field and armature windings

Both of these effects act to reduce the practical electrical output capability of the superconducting generator below what may be expected from a simple consideration of the considerable ampere-turn capability available. Nevertheless, a large increase in capability can still be achieved.

The optimal design of a superconducting generator may be determined by various appropriate techniques. For the exact determination of a design to be manufactured, the mass of information involved requires that the calculations be handled by computer. However, for the purpose of obtaining a good overall picture of the effect of major design parameters on the optimization of a design, a simplified and idealized machine model can be analyzed and displayed graphically, providing an easily comprehended and fairly accurate representation.

An effective machine design should utilize the full capabilities of its components. The following optimization study explores the potential capability of superconducting field windings and assumes an armature to match this capability. It relates the generator output capability (kVA) to the superconductors' intrinsic capability, as described by its J, B characteristic. Maximum power density is determined as a function of two major parameters, B and $[r_{fo} - r_{fi}]$ (radial depth of field winding). Minimum cost ($/kVA) is found to occur at lower values of B

and $[r_{fo} - r_{fi}]$ than for maximum power density. A sufficiently high evaluation of critical fault clearing time (CFCT) would cause a further shift in the optimum design point.

The basic generator vector diagram is as follows:

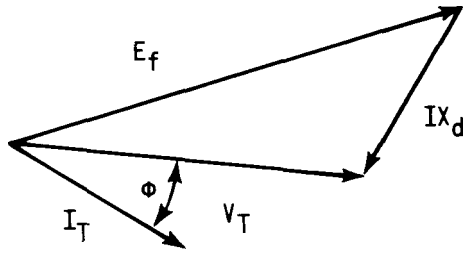

Figure 3-1. Basic Generator Vector Diagram

Assume an idealized model of unit length and fixed armature turns, wherein the armature and field windings are sinusoidally distributed, have no radial depth (no thermal limitation) and are located at identical diameters. Arbitrarily fixed values of field amperes and field winding turns are used.

E_f = open circuit armature voltage at fixed field excitation = (constant) x (total rotor flux)

X_d = synchronous reactance in ohms (= constant)

I_T = line amperes

V_T = terminal voltage $\propto$ net flux linking armature

ϕ = generator power factor angle (maintained constant)

The output of the generator is:

$$kVA = \frac{V_T \times I_T}{1000}$$

or

$$kVA \quad K_1 \times \frac{V_T \times I_T X_{d(ohms)}}{1000}$$

where

$$K_1 = \frac{1}{X_{d(ohms)}}$$

Note that, by definition:

$$X_{d(per\ unit)} = \frac{I_T X_{d(ohms)}}{V_T}$$

I_T is varied from open circuit ($I_T = 0$) to short circuit ($I_T = \frac{E_f}{X_{d(ohms)}}$) with excitation ($E_f$) and power factor maintained constant. kVA, V_T and $X_{d(per\ unit)}$ are plotted as functions of V_T in Figure 3-2 , where kVA and V_T are normalized to their maximum value.

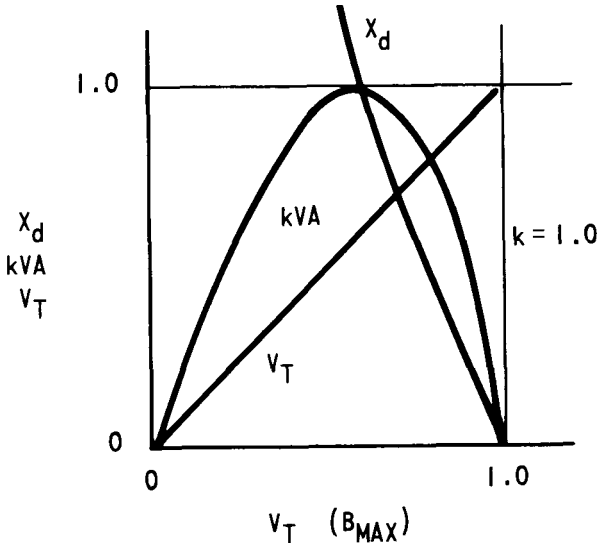

Figure 3-2. kVA, x_d and V_T versus V_T

Observe that kVA is a maximum when $X_{d(\text{per unit})} = 1.0$, in which case the external and internal impedances are equal

$$(Z_{external} = \frac{V_T}{I_T} = Z_{internal} = \frac{I_T X_{d(ohms)}}{I_T}),$$

and maximum power transfer is obtained.

It is useful, in the case of superconducting generators, to consider kVA, V_T and X_d as functions of the maximum flux density existing at any point in the field winding configuration. In this way, the generator output characteristics can be related to the superconductors inherent performance characteristic (J, B curve).

The field and armature winding each produce a uniform magnetic field distribution within their inside diameter. The resultant flux density and net armature flux linkages for any load condition are therefore exactly proportional to the vector sum of the field and armature mmf's. The armature terminal voltage is proportional to the net flux linkages, and therefore, to the flux density inside the windings. The flux density inside the windings in the maximum density existing in this ideal machine. In a practical machine end effects must be considered, but the correction is relatively small. In view of the exact linear relation between V_T and B_{max} at the superconductor when armature and field windings have the same diameter, we can express the abscissa of Figure 3-2 as B_{max} as well as V_T.

Observe that output capability is proportional to the square of E_f, and therefore to the square of maximum useable current density of the superconductor.

Consider an ideal machine, identical to the preceding case, except that the armature diameter is larger than the field diameter. Note that, for windings

of negligible radial depth, the coefficient of magnetic coupling k, is exactly equal to the ratio of field to armature diameters:

$$k = \frac{\text{field diameter}}{\text{armature diameter}} = \text{magnetic coupling coefficient}$$

A generator vector diagram may be drawn indicating both field and armature quantities, thus again relating generator output capabilities to the superconductor characteristic. Figure 3-3 shows the vector diagram.

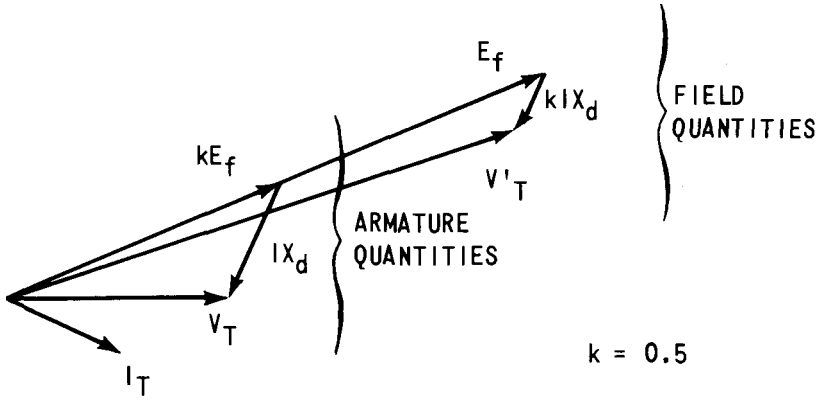

Figure 3-3. Generator Vector Diagram for Armature and Field Quantities

Note that the machine output capability is proportional to the square of E_f and of k, and that the maximum flux density at the superconductor B_{max} is proportional to V'_T. The armature quantities kVA, V_T and X_d are plotted against B_{max} in Figure 3-4, with excitation amperes (E_f) still maintained constant.

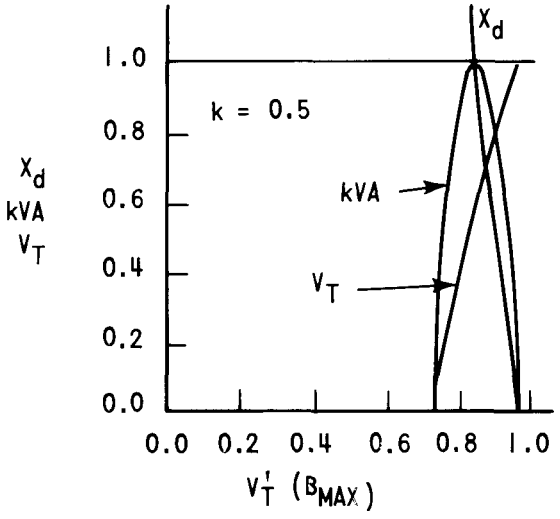

Figure 3-4. kVA, x_d and V_T versus V'_T

Allow the excitation (E_f) to vary with B_{max} corresponding to the characteristic curve of the superconductor material. A plot of armature quantities is then shown in Figure 3-5.

kVA_1 - constant excitation (from Figure 3-4)

kVA_2 - excitation per J, B characteristic of superconductor

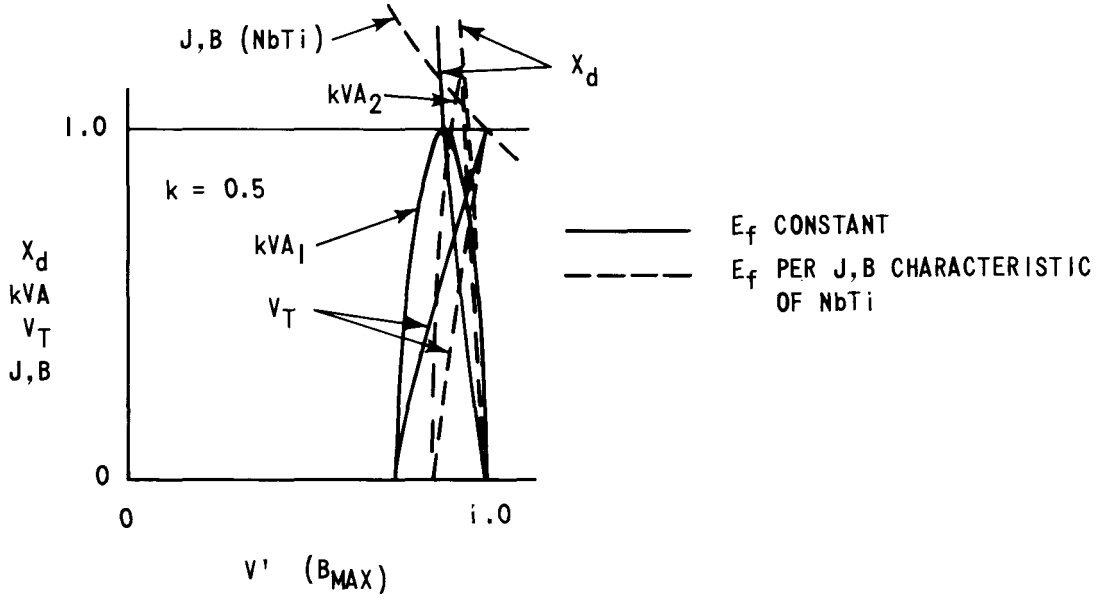

Figure 3-5. kVA, x_d and V_T versus V_T'

The power density obtainable from a field winding of a given outside diameter in a practical machine is a function of the radial depth ($r_{fo} - r_{fi}$) of the winding. As the radial depth is increased, the maximum flux density at the winding inside diameter increases at first almost linearly with depth and the kVA output capability increases nearly as the square. Maximum power density occurs when incremental increases in field winding depth are balanced by reductions in field winding current density required to satisfy the superconductor J, B characteristic for increasing values of B_{max}, by increase in reluctance of flux path due to reduction of field winding inside diameter, and reduction in the armature coupling coefficient, such that no increase in flux linking the armature is obtained. Refer to Figure 3-6. An economic design point occurs before the maximum power density point, since an appreciable increase in winding depth (and cost) produces a relatively small increase in power density.

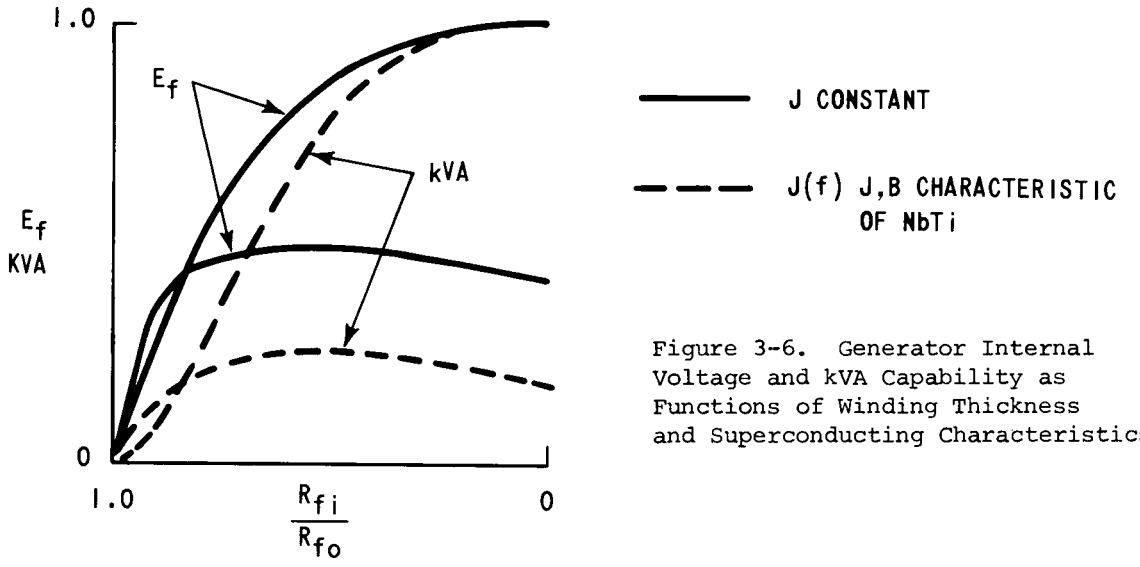

Figure 3-6. Generator Internal Voltage and kVA Capability as Functions of Winding Thickness and Superconducting Characteristics

The following general observations regarding practical machines may be made:

1. The kVA capability of the armature varies as the square of kE_f, thus power density is sensitive to both the magnetic coupling between the field and the armature, to the characteristic curve of the superconductor, and to the amount of design margin that is teken in utilizing the superconductor.

2. Any desired reactance level can be obtained by appropriately selecting B_{max} for the rated design point.

Synchronous, transient and subtransient reactances vary together in approximately the same ratios at any desired reactance level provided that consistent design practice is followed; that is, provided that the ratios of the diameters of the field winding, damper shield and armature winding are fairly constant. Where these ratios are different, for instance, in the use of a thin cold damper as compared to a thick warm damper, or in the case of a relatively thin low voltage armature versus a thick transmission voltage armature, the reactance ratios would change markedly.

3. The power density is a maximum at X_d = 1.0 (P.U.) and decreases as X_d is decreased below 1.0, but initially it decreases at a much slower rate than X_d, so that there is only a small penalty in power density in going down to X_d = .5; below that point, the penalty increases rapidly.

Optimization of field winding pole face angle for maximum power density is not critical and has been compromised to favor minimization of armature flux harmonics.

A niobium titanium superconductor has been selected for the prototype machine because of its good windability and service experience. Niobium tin has higher performance capability, but at present does not have sufficiently good windability or stability of performance to be considered for application to a rotating machine. Further development can be expected to make it acceptable for future applications. Figure 3-7 shows the J,B characteristics of the two materials, with a generator open-circuit characteristic curve indicated. The intersection of the open-circuit characteristic and the J,B characteristic lines establishes the design point corresponding to E_f, the generator internal voltage. Niobium tin would operate at about 150% of the niobium titanium design point and would have about 225% of the power density capability of niobium titanium.

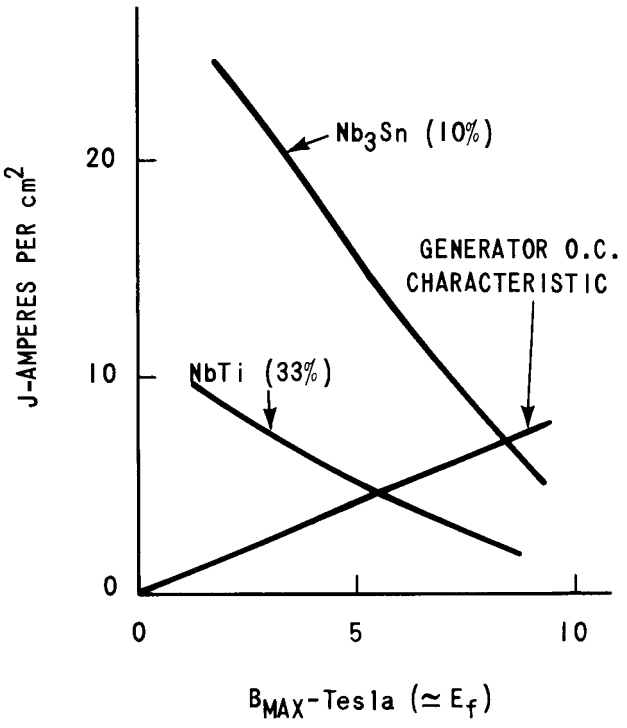

Figure 3-7. Maximum E_f for NbTi and Nb_3Sn

3.1.4 Explanation of Economic Estimates

Plant Capital Cost

a. A nominal capital cost of $500 is assumed for oil-fueled plants* even though such plants will probably not be built after 1985.

b. Coal-fueled power plant capital cost estimates adjusted (8%/year) to 1985 are given in Table 3-2 as calculated recently by five different organizations. The two values show estimates with and without SO_2 removal equipment costed an $160/kwe. Since environmental equipment will usually be required, $800/kwe is taken as the nominal capital cost.

c. Nuclear power plant capital cost estimates adjusted (8%/year) to 1985 are given in Table 3-2 as calculated recently by five different organizations. A cost breakdown is given in Table 3-3 $1000/kwe is taken as the nominal capital cost.

Table 3-2

COAL PLANT CAPITAL COST ESTIMATES
(DOLLARS PER KW)

SOURCE	DATE OF STUDY	COST ESTIMATE	SCHEDULE C.O. (LENGTH)	ADJUSTED TO 1985
Ebasco	10-76	1036/775	1987 (10 years)	890/670
Sargent & Lundy	9-76	906/740	1985 (-)	906/740
United Engineers	4-76	726/620	1985 (5.3 years)	726/620
Bechtel	1-76	850/690	1985 (7 years)	850/690
A. D. Little	3-75	697/565	1984 (5.4 years)	750/610

C.O. (Years to Commercial Operation) Average 825/665

Table 3-3

NUCLEAR PLANT CAPITAL COST ESTIMATES
(DOLLARS PER KW)

SOURCE	DATE OF STUDY	COST ESTIMATE	SCHEDULE C.O. (LENGTH)	ADJUSTED TO 1985
Ebasco	10-76	1216	1987 (10 years)	1050
Sargent & Lundy	9-76	1047	1985 (9 years)	1047
United Engineers	4-76	830	1955 (10 years)	830
Bechtel	1-76	1030	1985 (10 years)	1030
A. D. Little	3-75	863	1984 (8 years)	935

C.O. (Years to Commercial Operation Range 830/1050
Average 980

* Reference: Federal Energy Administration release of January 13, 1977 referring to city of Gainsville, Florida plant, Deerhaven No. 2, costing $116 million and rated 236 megawatts, or $492/kwe.)

Table 3-4

NUCLEAR PLANT COST BREAKDOWN
1000 MW-1985 COMMERCIAL OPERATION

COST ITEM	PERCENT	MILLIONS OF DOLLARS
Reactor plant equipment	8	78
Turbine generator	5	50
Balance of plant equipment	6	59
Construction materials and structures	6	59
Construction labor	13	129
Professional services	6	59
Owner's cost	1	10
Contingency	3	30
Escalation and IDC	52	505
TOTAL	100	980

Fuel Cost

a. Oil Fuel costs in 1985 are assumed as 30 mills/kwh based on residual oil at $20/bbl (333¢/MBTU) and a heat rate of 9,000 BTU/kwh.

b. Coal prices which depend on sulfur content and shipment distance vary as indicated in Table 3-5. Because averages are not significant, a nominal value fuel cost for coal is taken as 20 mills/kwh. This assumes a price of $45 per ton, a heat energy cost of 200¢/MBTU, and a heat rate of 10,000 BTU/kwh with SO_2 removal equipment.

c. A nuclear fuel cycle cost estimate is given in Table 3-6 with unit costs for the various parts of the cycle which may be appropriate in 1985. The price taken for uranium is the spot market for delivery of U_3O_8 in 1985 based on a 1977 price of $40/lb. U_3O_8 escalated at 6% per year to 1985. Since reprocessing with its associated uranium and plutonium credit is uncertain, a nominal nuclear fuel cost of 11 mills/kWh is assumed.

Efficiency

Increased efficiency of the superconducting generator is conservatively taken as 0.5% based on calculated increased efficiencies which are 0.7 to 1.0%.

Capital Cost Benefits

Plant capital cost benefits are taken equal to the increase in generator efficiency because the power output of the entire plant could be built to produce the same power, hence saving capital cost. For example for nuclear: 0.5% x $1000/kwe = $5/kwe.

Table 3-5

PROJECTED LEVELIZED COAL PRICES

Region	As Burned Mid-1986 (C/MMBTU)	6% Escalated Mid-1986 (¢/MMBTU)	10 Year Levelized Mid-1986	
			(¢/MMBTU)	(Mills/KWH)
Northeast	125	224	298	29.8
East	95	170	227	22.7
Central	80	143	191	19.1
West (300 Mile Haul)	55	98	131	12.4
Western Coal (1000 Mile Haul)	100	179	239	22.7
AVERAGE	91	163	217	21.3

Table 3-6

NUCLEAR FUEL CYCLE COST ESTIMATE - 1985

PRICE	PRICE	CONTRIBUTION (MILLS/KWH)
Mining & Milling	($64/lb)	7.3
Conversion to UF_6	($5/kg)	0.2
Enrichment	($120/SWU)	2.7
Fabrication	($145/kg)	0.8
Reprocessing Shipping & Waste Disposal	($357/kg)	1.1
PU Credit	($34/grm)	-1.0
Uranium Credit		-1.1
TOTAL		10.0

Generator Cost

Generator cost estimates have been based on detailed cost evaluations of the cost of material per pound installed in conventional generators where comparable manufacturing is involved and cost estimates for superconducting components. These cost estimates include a cryogenic refrigerator at $500,000 for a 1000 MWe generator.

Fuel Cost Benefits

Fuel cost benefits result from the reduction in fuel costs because of the increased generator efficiency capitalized at 17% assuming 6000 hours/year (68%) of full power operation.

a. Oil: $\frac{30 \text{ mills}}{\text{kWh}} \times 0.1765 = \$5.29/\text{kWe}$

b. Coal: $\frac{20 \text{ mills}}{\text{kWh}} \times \frac{6000 \times 0.005}{0.17} = \$3.53/\text{kWe}$

c. Nuclear: $\frac{11 \text{ mills}}{\text{kWh}} \times 6000 \frac{\text{hrs.}}{\text{year}} \times 0.5\% = \$1.94/\text{kWe}$

Operation and Maintenance Benefits

Operation and maintenance benefits result from such costs being distributed over the larger number of kWh produced because of the incremental generator efficiency. O and M costs are taken as 3 mills/kWh for nuclear and oil but as 5 mills/kWh for coal because of the need for SO_2 removal. Benefits are capitalized the same as above:

a. Oil: $\frac{3 \text{ mills}}{\text{kWh}} \times 6000 \frac{\text{hrs.}}{\text{year}} \times \frac{1}{17\%} \times 0.5\% = \$0.53$

b. Coal: $\frac{5 \text{ mills}}{\text{kWh}} \times 0.1765 = \$0.88$

c. Nuclear: $\frac{3 \text{ mills}}{\text{kWh}} \times 0.1765 = \$0.53$

Transformer Elimination Benefit

Transformer elimination benefits result from the fact that the station step-up transformer can be eliminated because a superconducting generator with a high-voltage armature winding would be able to produce line voltage. The value of the increased power and energy output obtained because the transformer losses of 0.2% are eliminated can be capitalized as benefits. Other system advantages occur because of the elimination of the impedance of the transformer, but these are not quantified. In a manner similar to the above, plant capital cost benefits resulting from the 0.2% efficiency improvement which is obtained by eliminating the station main step-up transformer are calculated. For example, for nuclear:

$$0.2\% \times \$1000/\text{kWe} = \$2.00/\text{kWe}$$

Transformer Cost Benefit

Transformer cost benefit is taken as the price of the station step-up transformer in 1985 which is the 1977 price escalated at 6% to the year 1985.

Transformer Loss Elimination Benefit

Fuel cost benefits from the increased 0.2% efficiency realized by transformer elimination are calculated in a manner analogous to the above, for example,

$$\text{nuclear: } \frac{11 \text{ mills}}{\text{kwh}} \times \frac{6000 \text{ hrs.}}{\text{year}} \times \frac{1}{17\%} \times 0.2\% = \$.78/\text{kwe}$$

Transformer Operation and Maintenance Benefit

Operation and maintenance benefits from transformers elimination and hence 0.2% increased efficiency are calculated in a manner similar to the above, for example,

$$\text{nuclear: } \frac{3 \text{ mills}}{\text{kwh}} \times 6000 \frac{\text{hrs.}}{\text{year}} \times 0.2\% = \$.21/\text{kwe}$$

High Voltage Superconducting Generator Benefits

The benefits shown in Table 3-7 for superconducting generators assume a market capture increasing from the first 300 MWe unit on line in 1985 (1% of market) to 75% of new generators added in the year 2000 with a capitalized benefit from Table 2-3 of $16/kwe. The cumulative capitalized benefit is calculated and then the revenue requirements to support it at a 17% cost of capital. The revenue requirements are presently worthed to 1977 at 15% as an indication of what could be spent based on economic logic, to develop the superconducting generator. Comparing these present worthed benefits with the present worthed development costs of about $7 million, the benefits would exceed development costs in 1994. This means that a 15% return on development costs would be received by the utility industry by 1994 with return on investment increasing thereafter. Total energy conservation from 1985 through the year 2000 would be 310^{12} kwh or 310^{16} BTU which is 50% more energy than the U. S. Utility industry consumed in 1976.

Foundation and Building Cost Evaluations

The superconducting generator will be both shorter and lighter than a conventional machine of the same rating. Because the machine is shorter than a conventional unit, the power plant building can be shortened. This will result in a savings to the utility. The lighter superconducting machine will result in

Table 3-7

HIGH-VOLTAGE SUPERCONDUCTING GENERATOR BENEFITS
PRESENT WORTHED TO 1977 AT 15%

YEAR	TOTAL GENERATOR ADDED (GWE)	SCG ADDED		CAPITALIZED BENEFIT AT $16/KWe ($ MILLIONS)	CUMULATIVE CAPITAL ($ MILLIONS)	REVENUE REQUIREMENTS AT 17% ($ MILLIONS)	PRESENT WORTH FACTOR AT 15%	PRESENT WORTH ($ MILLIONS)
		(% OF MKT.)	(GWE)					
1985	32	1	0.3	5	5	0.85	0.327	0.278
1986	29	0	0	0	5	0.85	0.284	0.242
1987	32	0	0	0	5	0.85	0.247	0.210
1988	36	3	1.0	16	21	3.57	0.215	0.770
1989	45	0	0	0	21	3.57	0.187	0.670
1990	40	5	2.0	32	53	9.01	0.163	1.470
1991	47	0	0	0	53	9.01	0.141	1.270
1992	47	10	4.7	75	128	21.80	0.123	2.680
1993	50	15	8.0	128	256	43.50	0.107	4.650
1994	50	20	10.0	160	416	70.70	0.093	6.580
1995	52	25	13.0	208	624	106.00	0.081	8.590
1996	51	35	18.0	288	912	155.00	0.071	11.000
1997	54	45	24.0	384	1296	220.00	0.061	13.400
1998	54	55	30.0	480	1776	302.00	0.054	16.300
1999	56	65	36.0	576	2352	400.00	0.046	18.400
2000	59	75	44.0	704	3056	520.00	0.040	20.800
TOTAL								107.31×10^6

foundation savings. This assumes that additional foundation support is not needed to brace against short circuit forces.

The curves of Figures 3-8 and 3-9 depict the expected capital expenditure decrease resulting from a reduction in generator length and weight, respectively. The cost estimates were obtained from Sargent and Lundy Engineers.

A 1000 mw superconducting generator may be 12 feet shorter than a conventional machine of similar rating. From Figure 3-8 , this will result in a capital reduction of about 160,000 dollars. The reduction in generator weight may be as much as 300 tons. This will result in a capital reduction of 30,000 dollars. All dollar amounts in this section are 1975 dollars.

Economic Evaluation of High-Voltage Armature

An economic evaluation of high-voltage armatures is made in the discussion of "Stator Design," q.v.

Generator Price

Details of conventional and superconducting generator mature cost estimates are shown in Tables 3-8 , 3-9 and 3-10. Major component weight are tabulated for 300, 1200, and 3000 MVA designs. Costs per pound are derived from various sources: stator frame costs (including the flux shield) are well known from current practice; armature costs are estimated from present generator and transformer experience, and are projected with less accuracy than frame costs; rotor mechanical parts require expensive materials and advanced fabricating techniques which are within existing capabilities and costs are based on quotations from qualified suppliers; rotor winding costs are based on projected future cost trends in superconducting material and on present in-house experience with winding superconducting magnet coils and small generator superconducting field coils. The cost of auxiliaries, including the helium refrigerator, is considered to be reasonable and conservative.

An estimate of the margin of error that may be expected in the costs is obtained as follows: (1) the cost of all structural parts and auxiliaries is considered accurate and (2) the cost margin of armature and field windings is taken to be (+) 50% and (-) 25%.

The margin of error in overall cost for the 1200 MVA superconducting machine is then (+) 15% and (-) 7.5% for the low-voltage version and (+) 20% and (-) 10% for the high-voltage version.

Figures 3-10 and 3-11 show plots of generator prices (in 1976 dollars) as functions of MVA ratings and synchronous reactance.

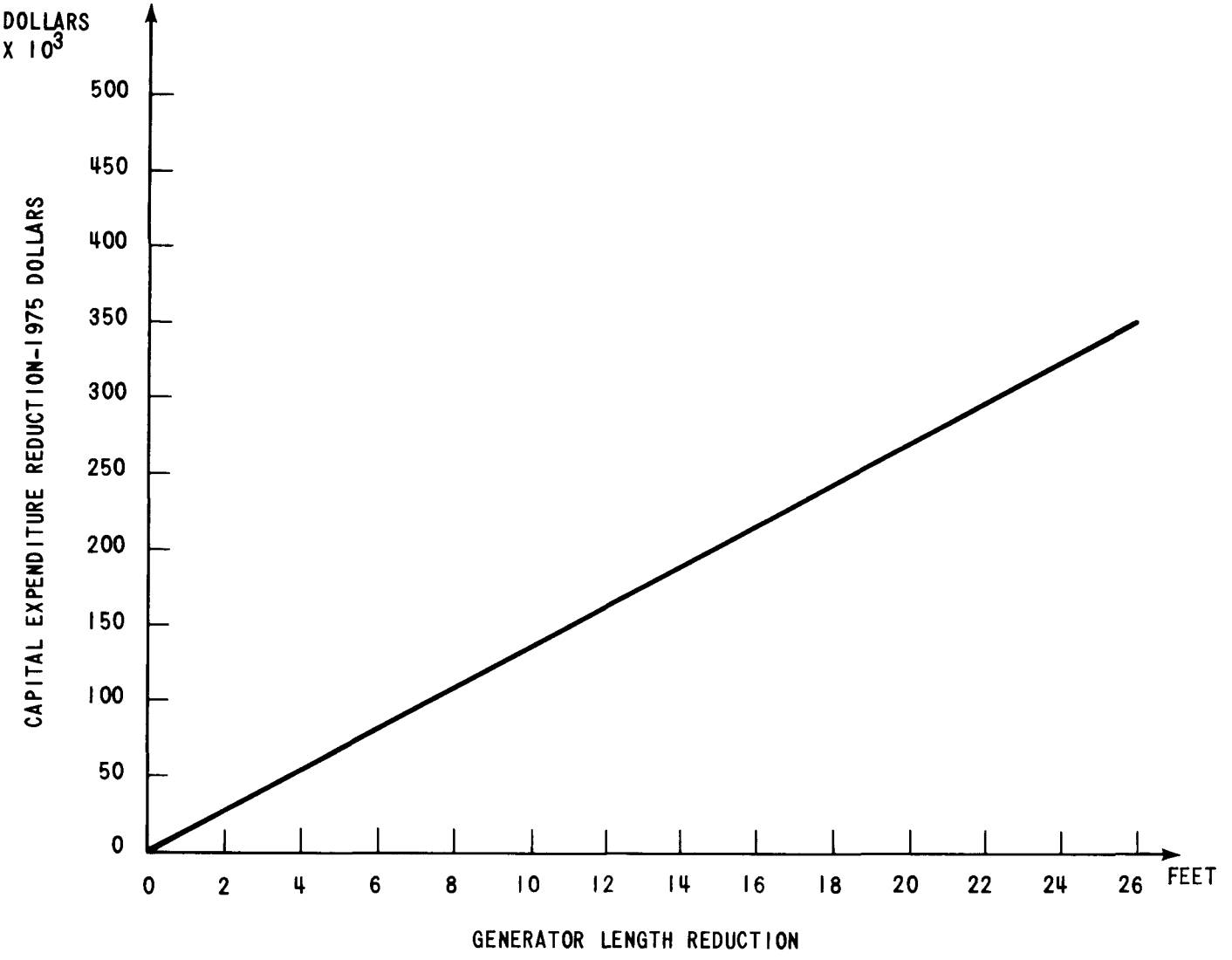

Figure 3-8. Capital Expenditure Reduction Resulting from a Decrease in Generator Length

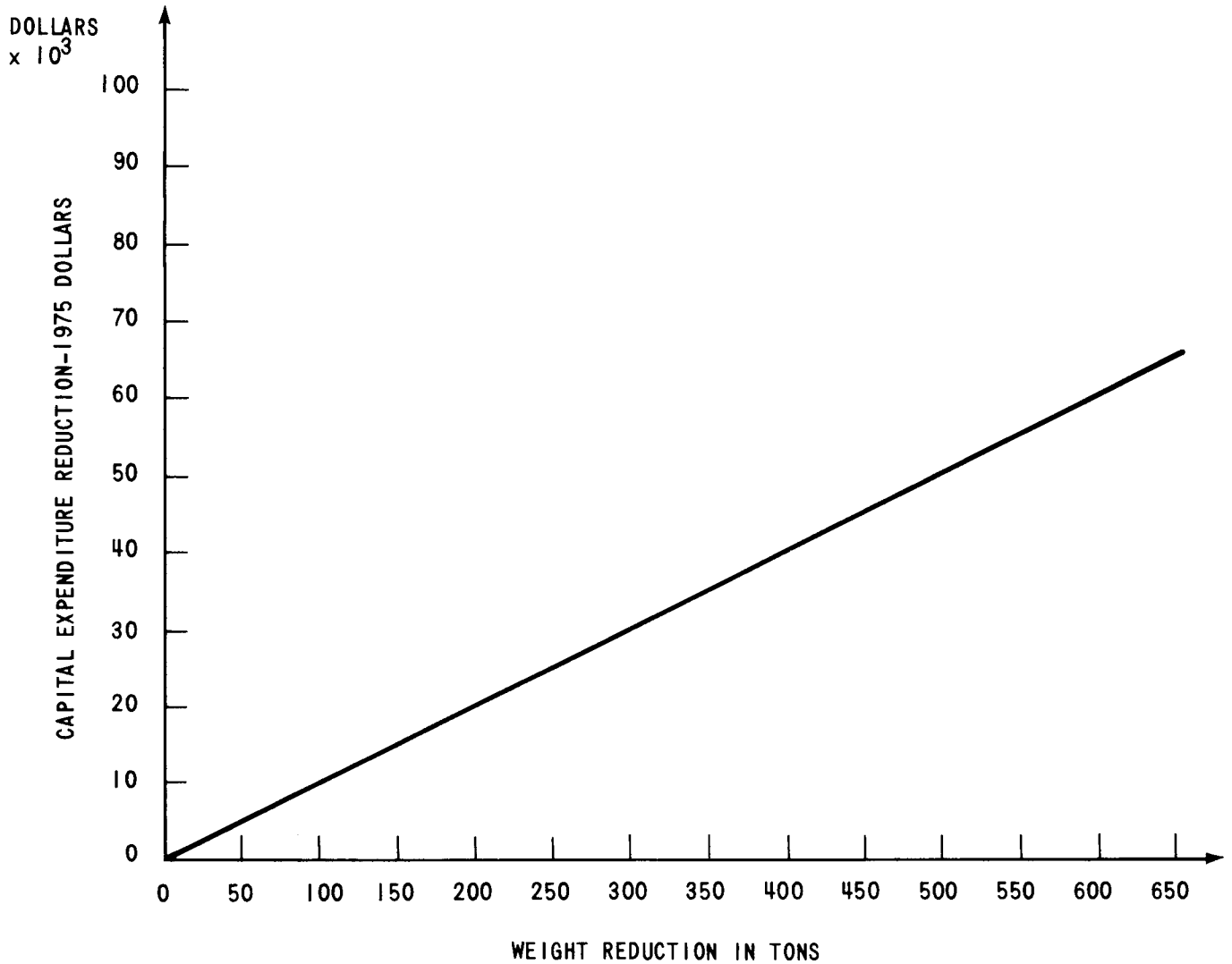

Figure 3-9. Capital Expenditure Reduction Resulting from a Decrease in Generator Weight

Table 3-8

COMPARATIVE TURBINE GENERATOR PRICES (1976)

300 MVA - 3600 RPM

TYPE	CONVENTIONAL $X_d = 1.70$ $X''_d = .24$			SCTG - 13. kV $X_d = 0.50$ $X''_d = .16$			SCTG - 230 kV $X_d = 0.50$ $X''_d = .27$		
	wt.	$/#	Price in $1,000's	wt.	$/#	Price in $1,000's	wt.	$/#	Price in $1,000's
Armature	60,000	11.7	700	38,500	13.5	520	56,000	13.5	756
Frame	425,000	2.88	1,225	254,500	2.88	733	284,000	2.88	818
Total Stator	485,000	3.47	1,925	293,000	4.28	1,253	363,000	4.48	1,574
Rotor Winding	11,000	31.8	350	2,430	250	608	3,330	250	833
Rotor Mechanical Parts	64,000	8.20	525	28,570	25	714	32,570	25	814
Total Rotor	75,000	11.67	875	31,000	42.65	1,322	35,900	45.88	1,647
Exciter	---	---	350	---	---	150	---	---	150
Auxiliaries	---	---	350	---	---	350	---	---	350
Refrigerator	---	---	---	---	---	300	---	---	300
TOTALS	560,000	6.25	3,500	324,000	10.42	3,375	398,900	10.08	4,021
$/KVA		11.67			11.25			13.40	

Table 3-9

COMPARATIVE TURBINE GENERATOR PRICES (1976)

1200 MVA - 3600 RPM

TYPE	CONVENTIONAL			SCTG - 30 kv			SCTG - 500 kV		
CONSTANTS	$X_d = 1.81$ $X''_d = 0.24$			$X_d = 0.41$ $X''_d = 0.16$			$X_d = 0.50$ $X''_d = .27$		
	wt.	$/#	Price in $1,000's	wt.	$/#	Price in $1,000's	wt.	$/#	Price in $1,000's
Armature	130,000	13.27	1,725	70,500	15.3	1,079	149,000	15.30	2,280
Frame	1,070,000	3.19	3,410	650,000	3.20	2,080	533,500	3.20	1,707
Total Stator	1,200,000	4.28	5,135	720,500	4.38	3,159	682,500	5.84	3,987
Rotor Winding	25,000	35.4	885	4,900	250	1,225	6,260	250	1,565
Rotor Mechanical Parts	159,000	9.94	1,580	74,600	30	2,238	84,240	30	2,527
Total Rotor	184,000	13.4	2,465	79,500	43.56	3,463	90,500	45.22	4,092
Exciter	---	---	1,000	---	---	200	---	---	200
Auxiliaries	---	---	1,000	---	---	500	---	---	500
Refrigerator	---	---	---	---	---	500	---	---	500
TOTALS	1,384,000	6.94	9,600	800,000	9.78	7,822	773,000	12.00	9,279
$/kVA		8.00			6.52			7.73	

Table 3-10

COMPARATIVE TURBINE GENERATOR PRICES (1976)

3000 MVA - 3600 RPM

TYPE CONSTANTS	CONVENTIONAL	SCTG X_d = .52 X''_d = .15 wt.	 $/#	 Price in $1,000's
Armature		93,600	15.5	1,451
Frame		1,418,000	3.5	4,963
Total Stator		1,512,000	4.24	6,414
Rotor Winding		9,950	250	2,488
Rotor Mechanical Parts	Not Available	151,050	35	5,285
Total Rotor		161,000	48.3	7,773
Exciter		---	---	250
Auxiliaries		---	---	650
Refrigerator		---	---	700
TOTALS		1,673,000	9.44	15,787
$/kVa			5.26	

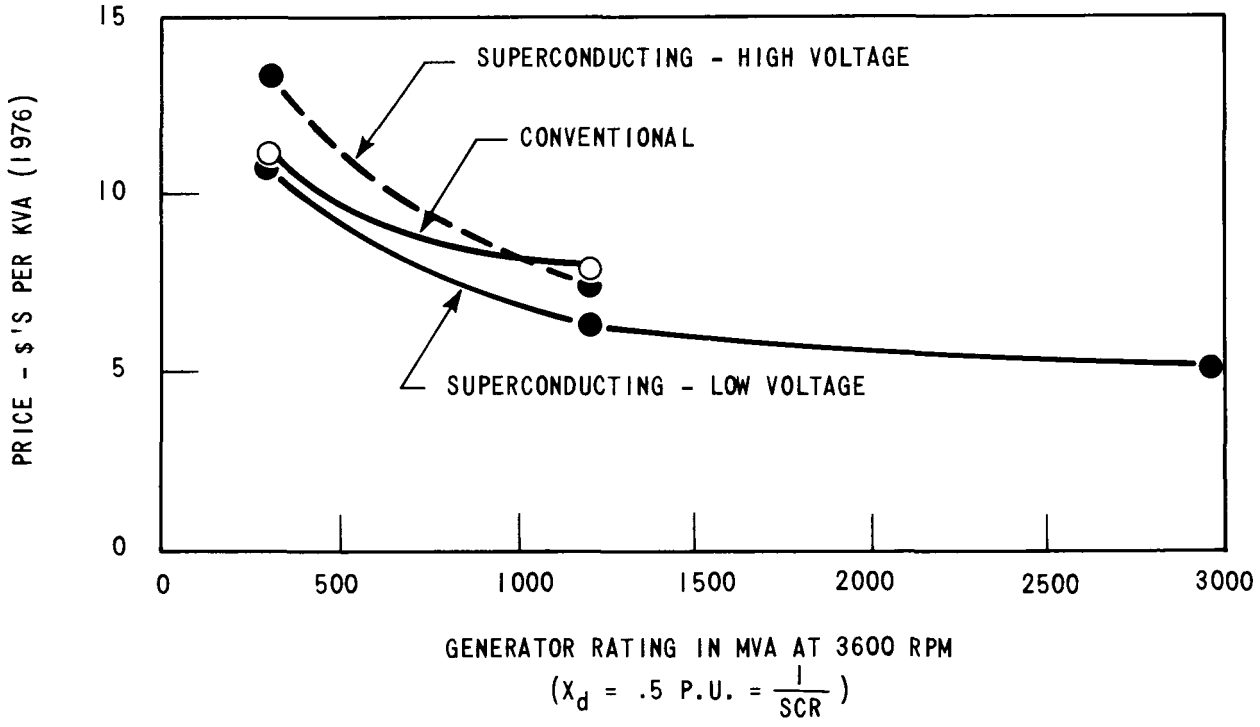

Figure 3-10. Generator Price versus Rating

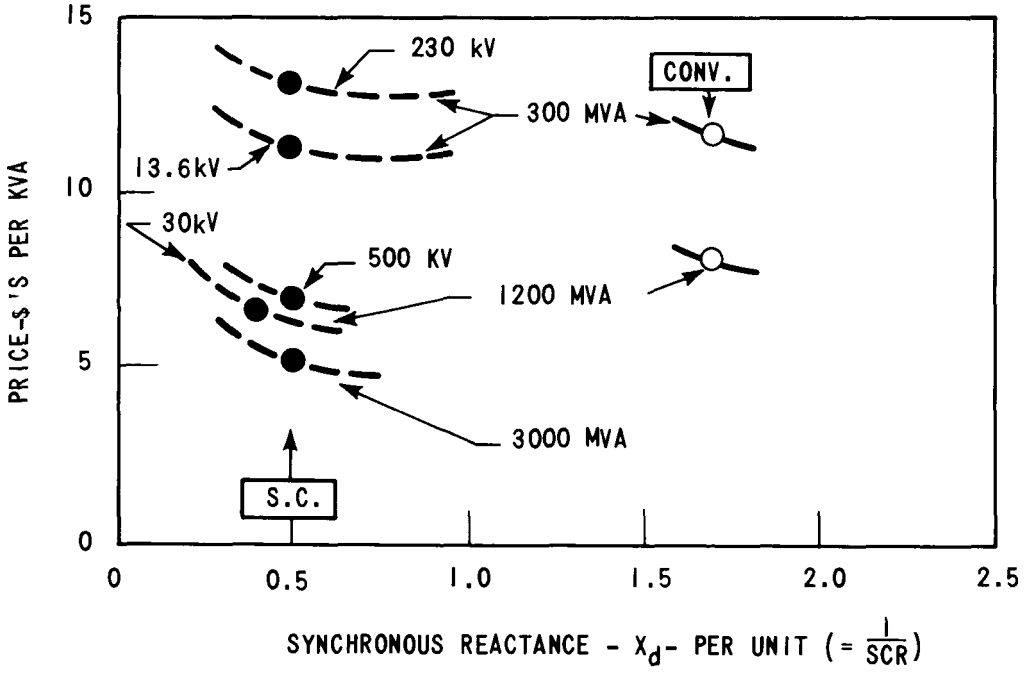

Figure 3-11. Generator Price Trends versus Synchronous Reactance

3.2 Design Details

3.2.1 Rotor Design

General Introduction and Requirements

Application of superconducting field windings to electric utility turbine generators offers several important potential benefits:

- Elimination of I^2R loss in the field winding.
- Simplification and size reduction in the excitation system.
- Size and weight reduction in the main generator - or, larger rating for a given size.
- Reduced generator cost.

On the basis of the studies conducted during the present contract, this list may now be extended to include:

- Extra-high-voltage armature winding capability.
- Potential for application to high-voltage DC transmission.
- Elimination of main power transformer for AC transmission.
- Further loss reduction and consequent fuel savings.
- Elimination of converter transformer for HVDC transmission.
- Improved I_2 and I_2^2t capability.
- Potential for improved critical fault clearing time.
- Further cost improvements.

The successful implementation of superconducting turbine generator concepts requires, first of all, correct application of the superconductors so as to assure stable and reliable operation under all required conditions. The following criteria have been defined in the EPRI Specification for Contract RP 429-1 to evaluate the superconducting field winding design:

- Helium transfer couplings (rotating seals) and transfer lines.
- Stability margin of field winding under anticipated operating and fault conditions.
- Specification of AC field tolerance of field winding.
- Specify all AC field losses in the rotor, (to be considered in refrigeration requirements).
- Mechanical support of field winding (banding, potting, etc.), mechanical stresses under normal and three phase fault conditions and critical speed prediction.
- Field winding refrigerant flow passage geometry and predicted flow patterns. Comparison of impregnated rotor winding with flooded winding.
- Thermal isolation and refrigeration requirement of field winding.

- Specification of field insulation requirements and operating voltages.
- Lead design stability, cooling.
- Helium supply system for steady state, cool-down, and transient conditions (refrigerator, liquefier, dewars, etc.).
- Specification of field winding techniques to be used.
- Number of helium supply and discharge passages on the rotor; method of control and metering of flow in stationary frame.
- Cooldown and warm-up specifications, auxiliary refrigerants (i.e., LN_2).
- Slip ring design.

Specific industry standards do not exist at this time for superconducting field windings. Standards do apply to other aspects of the rotor design, particularly the fault capability and the unbalanced load capability. These affect, in the first instance, the design of the damper shield. The requirements, including EPRI objectives for better than standard performance, are summarized in Tables 3-11A and 3-11B. These tables include as well the entire range of circumstances that must be considered in the damper shield design.

The basic requirements for the design of the field winding and its supporting systems may be stated rather simply:

- to secure optimum use of the superconductor for maximum power density and lowest machine cost.
- to prevent normalization of the superconductor under any required operating condition by any combination of temperature, current density, and magnetic field strength.

3.2.1.1 Rotor Electrical Designs

The complete electrical design of the rotor is an iterative procedure wherein the intrinsic J,B,T (current density - flux density - temperature) characteristics of an available superconductor are matched against the restraints imposed by mechanical limitation, steady-state and transient operating conditions of the machine, the electrothermal shielding for the cryogenic environment of the field winding, and the heat removal ability of the cryogenic cooling system. The logic of this process is illustrated in Figure 3-12. Its implementation requires that several disciplines be brought to bear simultaneously and cooperate towards a common solution of the design problem. At this time there is no computational process available whereby all aspects of the design might be simultaneously synthesized or optimized.

Table 3-11

DAMPER SHIELD DESIGN REQUIREMENTS

A - STEADY STATE OPERATION ORIGIN	DESCRIPTION	DESIGN OBJECTIVES
ARMATURE WINDING	SPACE HARMONICS (5th, 7th, 11th, 13th, etc.). ROTATE BACKWARDS AND FORWARDS WITH RESPECT TO FUNDAMENTAL. INDUCE DAMPER CURRENTS AT 6, 12, ETC. TIMES FUNDAMENTAL FREQUENCY. CONTINUOUS, PROPORTIONAL TO LOAD.	SHIELD FIELD WINDING AND CRYOGENIC STRUCTURE AGAINST PENETRATION OF SPACE HARMONIC FIELDS AND THUS PREVENT GENERATION OF LOSSES IN CRYOGENIC CONTAINMENT.
SYSTEM LOAD UNBALANCE	NEGATIVE SEQUENCE FLUX WAVE INDUCED IN GAP. ROTATES IN DIRECTION OPPOSITE TO ROTOR TO PRODUCE DAMPER CURRENTS AT TWICE LINE FREQUENCY. CONTINUOUS, PROPORTIONAL TO NEGATIVE SEQUENCE CURRENT I_2.	MINIMUM VALUES OF CONTINUOUS NEGATIVE SEQUENCE CURRENT I_2 DEFINED BY ANSI STANDARD C50.13: GENERATOR MVA — I_2 (PERCENT) To 960 — 8 961 to 1200 — 6 1201 to 1500 — 5 Above 1500 — Not defined. EPRI CONTRACT OBJECTIVE IS IMPROVED I_2 CAPABILITY.

Table 3-11 (cont'd)

DAMPER SHIELD DESIGN REQUIREMENTS

B - TRANSIENT CONDITIONS ORIGIN	DESCRIPTION	DESIGN OBJECTIVES
THREE-PHASE TERMINAL OR SYSTEM FAULTS	TRANSIENT AC AND DC CURRENTS IN DAMPER, WHICH EXPERIENCES TORQUES AND CRUSHING FORCES.	FIELD WINDING TO REMAIN SUPERCONDUCTING DURING AND FOLLOWING THREE-PHASE FAULT ON HIGH SIDE OF 0.1 P.U. REACTANCE TRANSFORMER, LASTING 66 msec. CAPABLE OF WITHSTANDING TERMINAL FAULT WITHOUT DAMAGE. ANSI C50.13 ARMATURE WINDING SHORT-TIME THERMAL REQUIREMENTS.
UNBALANCED TERMINAL OR SYSTEM FAULTS	NEGATIVE SEQUENCE CURRENTS IN DAMPER, HEAT DISSIPATION, DOUBLE FREQUENCY TORQUES AND FORCES.	NO DAMAGE IN GENERATOR FOR MINIMUM I_2^2t - 10 - 0.00625 (MVA - 800). EPRI OBJECTIVE IS IMPROVED I_2^2t CAPABILITY
LOSS OF FIELD LOSS OF SYNCHRONISM	ASYNCHRONOUS OPERATION AT ABOVE SYNCHRONOUS SPEED. LOW (SLIP) FREQUENCY CURRENTS IN DAMPER.	NONE DEFINED.
SYSTEM RESONANCES (MAY BE SUBSYNCHRONOUS)	ASYNCHRONOUS FIELDS SET UP, CAUSING CURRENTS IN DAMPER AND ASYNCHRONOUS ROTOR TORQUES.	NONE DEFINED.
POWER TRANSIENTS (FAULT CLEARING, LOAD SWINGS, ETC.)	OSCILLATIONS ABOUT STEADY-STATE LOAD ANGLE PRODUCE EDDY CURRENTS AND HEATING IN CRYOGENIC PARTS OF ROTOR.	REDUCE LOAD SWINGS RAPIDLY TO MINIMIZE HEAT DISSIPATION IN ROTOR PARTS. OPTIMIZED CRITICAL FAULT CLEARING TIMES. NO LOSS OF STABILITY.
FIELD CHARGING	DAMPER CURRENTS OPPOSE BUILDUP OF FLUX IN FIELD, DELAYING CHARGING.	CHARGING TIME NOT TO BE EXCESSIVE.

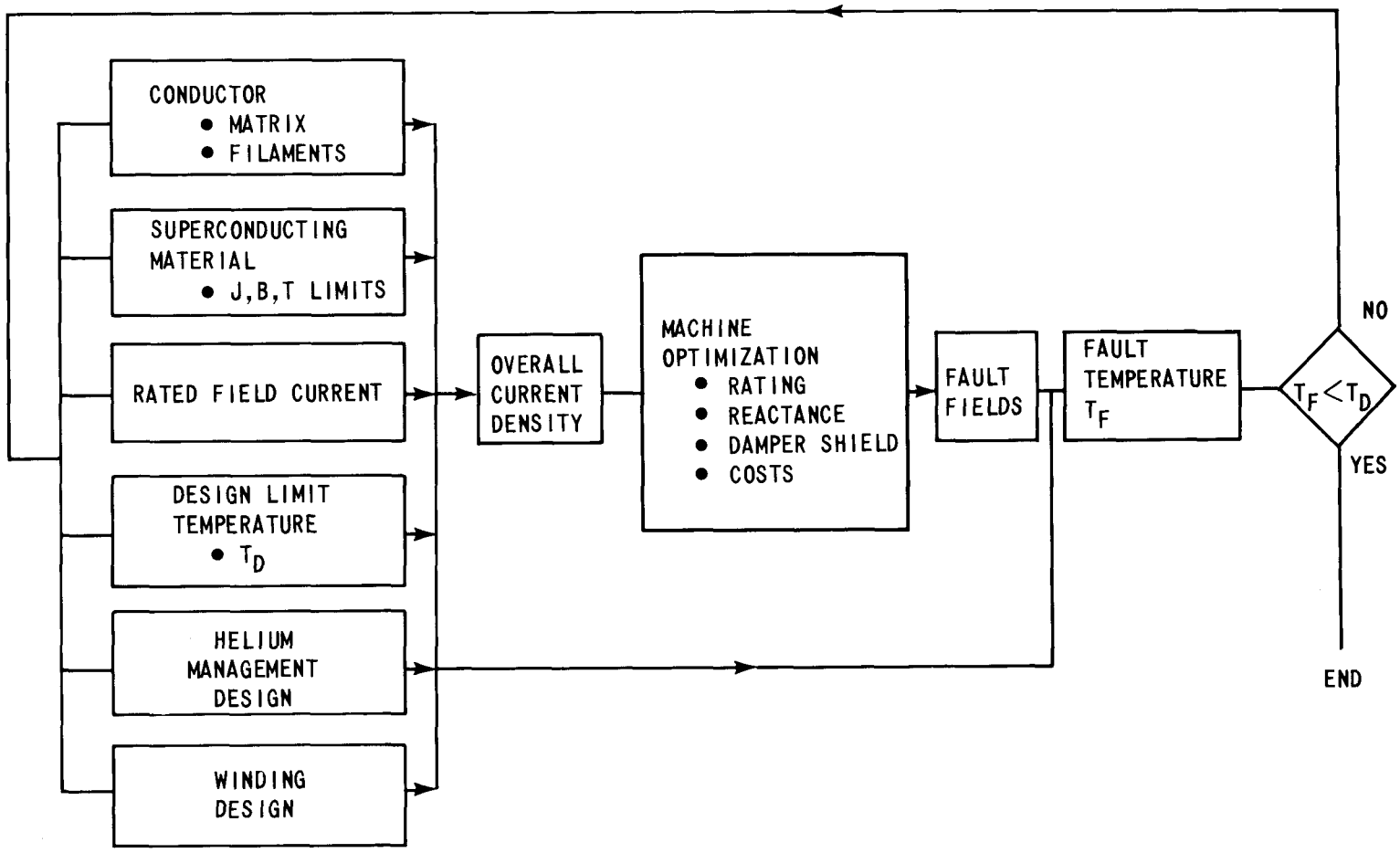

Figure 3-12. Design Logic for Field Winding

One part of this process may be called the electrical design proper. Its main function is to determine a set of dimensions for the complete machine, including the field winding, that is consistent with the specified requirements and the internal restraints that arise, for example, from metallurgical limitations on support materials. This process is represented by the "winding design" and "machine optimization" blocks in Figure 3-12. Its point of departure is a definition of the superconducting wire in terms of its size and its J,B,T characteristics. The objective of this process is the optimization of the machine in terms of rating, power density, costs, and characteristics that affect power system performance and cost, for example, reactance values. Much of this electrical design process is now done by computer. It is adaptable to rigorous optimization procedures.

The selection of the superconducting wire which precedes this electrical design is discussed in the Conductor Selection section below.

A major part of the electrical design deals with determination of magnetic fields and their distributions in the several parts of the machine under various operating conditions. The knowledge of these field distribution leads directly to an understanding of power densities, reactances, losses and heating due to electromagnetic induction, and force effects on conductors such as the armature winding and the damper at the outer periphery of the rotor. Analysis of the consequences of the losses and force effects then leads into a determination of the J,B,T profile at the superconductor, and to a conclusion or possible reiteration of the design process.

Magnetic Field Distribution - Influence on Design

It is usual in electric machine design practice to consider first the two-dimensional problem presented by the uniform cross-section of the machine. This, in effect, treats the machine as if it were infinitely long. For many design purposes, this is sufficiently accurate, especially for relatively long machines. When end effects must be considered, this can often be done by empirical correction factors. The complete three-dimensional solution of the magnetic fields in electrical machines is a relatively complex problem that is usually not undertaken until there is a clear need for the information. Chronologically, the analysis of superconducting generators has proceeded much along the same lines.

The complete solution of the magnetic field distribution in two dimensions has been given by Dr. J. L. Kirtley, Jr.[1] Empirical factors for effective lengths

must be used in conjunction with these expressions to represent an actual machine design. So far, these factors have been checked against few test results that may not be representative of the various proportions that may be required for different designs.

Many other methods, including graphical, analog, and digital computer methods have been developed to solve Laplace's equation in electric machine geometries, both with and without magnetic boundaries. Modern studies often utilize finite element methods with digital computers. Such an approach was used to generate the typical flux map of a superconducting generator under load shown in Figure 3-13. It will be observed from this figure that the main flux in the machine, that is the flux which links both the armature and field windings, and is useful in producing output power, is effectively channeled in the interior of the field, but begins to diverge rapidly to lower densities as it leaves the confines of the field. The flux density is essentially constant at radii less than the inner radius of the field, and falls off inversely with the radius at radii greater than the outer radius of the field. These simple observations make it possible to define rough criteria for the electrical design of the machine so as to obtain the largest power density:

- All conductors of the field winding should be located at the largest possible radius.
- The armature winding should be located at the smallest possible radius.
- The magnetic shield should be located at the smallest possible radius.

Obviously, many limitations will determine to what extent this placement of conductors can be realized in practice. Amongst the most important of these limitations are:

- Radial distance required for mechanical support of field winding
- Radial distance required for thermal shielding
- Radial distance required for the electromagnetic shielding and its supporting structure(s)
- Minimum gap between rotor and stator
- Radial distance required for mechanical support of armature winding at its inner and outer radii
- Maximum permissible current density in field winding
- Maximum permissible current density in armature winding.

In many respects, these various limitations interact, sometimes in unexpected ways, so that the complete design must consider as well how these interactions affect the complete machine and its performance with respect to the power system. Some of these interactions will be discussed in the following. Nevertheless, it

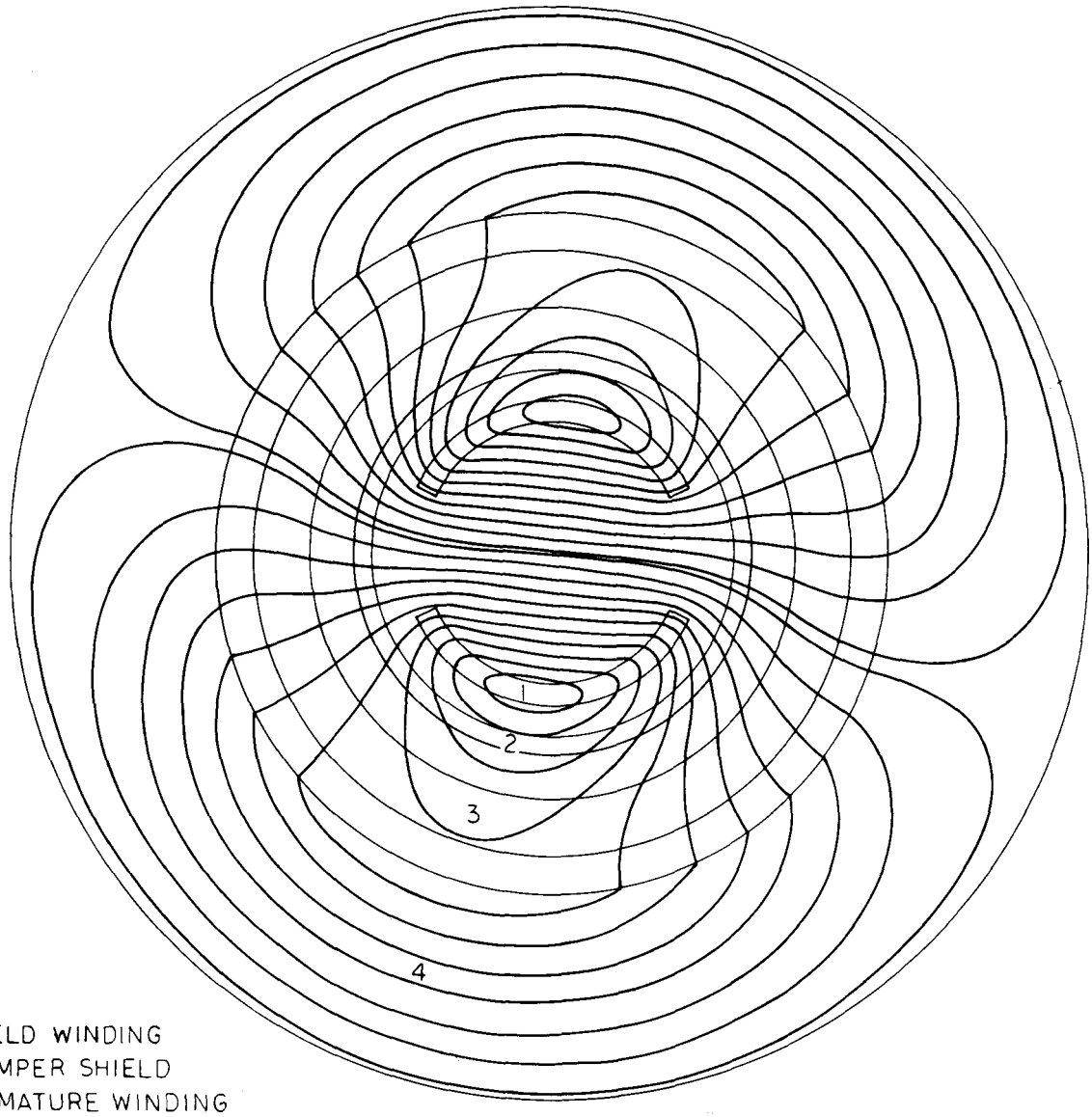

1. FIELD WINDING
2. DAMPER SHIELD
3. ARMATURE WINDING
4. STATOR FLUX SHIELD

Figure 3-13. Flux Map of Superconducting Turbine Generator under Load

remains true that the design is favored by placing the field conductors as near the rotor periphery as is permissible.

Subtransient Reactance

To evaluate the variation of subtransient reactance with rotor proportions, a study was made varying the proportions over a maximum practical range permissible by limitations imposed by the field and its support and by the armature. The results are shown in Figure 3-14. They illustrate the very strong dependence of subtransient reactance of damper position. These results also show that the ratio of subtransient reactance to transient reactance is a strong function of the geometry of the part of the machine between the armature and field windings, and cannot be greatly changed by the geometry of those windings themselves.

The detailed calculation of reactances has also been given by Dr. Kirtley[1] and will not be reproduced here. For design purposes, it is included in a computer program that was written prior to the initiation of the present studies in connection with the 5 MVA prototype superconducting generator built by Westinghouse.

Rotor Design: Electromagnetic Interactions

In accordance with the design logic shown in Figure 3-12, the determination of reactance coefficients leads into a block titled "fault fields". This aspect of the design relates particularly to the field winding, but in an actual design process it is more general and also involves the determination of force and torque patterns that stress the various structural parts of the machine. The following specific calculations are made in this part of the design:

- Fault currents - magnitude and time dependence
- Airgap torques during and after clearing fault - magnitude and time dependence
- Rotor dynamics for torsional oscillations
- Motions of rotor components relative to synchronous frame and relative to each other during and after clearing fault
- Radial forces on damper - magnitude and time dependence
- Deformation of damper structure - magnitude and time dependence
- Penetration of fault fields by diffusion through damper
- Propagation of fault fields by electromechanical deformation of damper.

The results of these calculations are applied to the mechanical and thermal analysis of the rotor summarized in the logic diagram under "fault temperature".

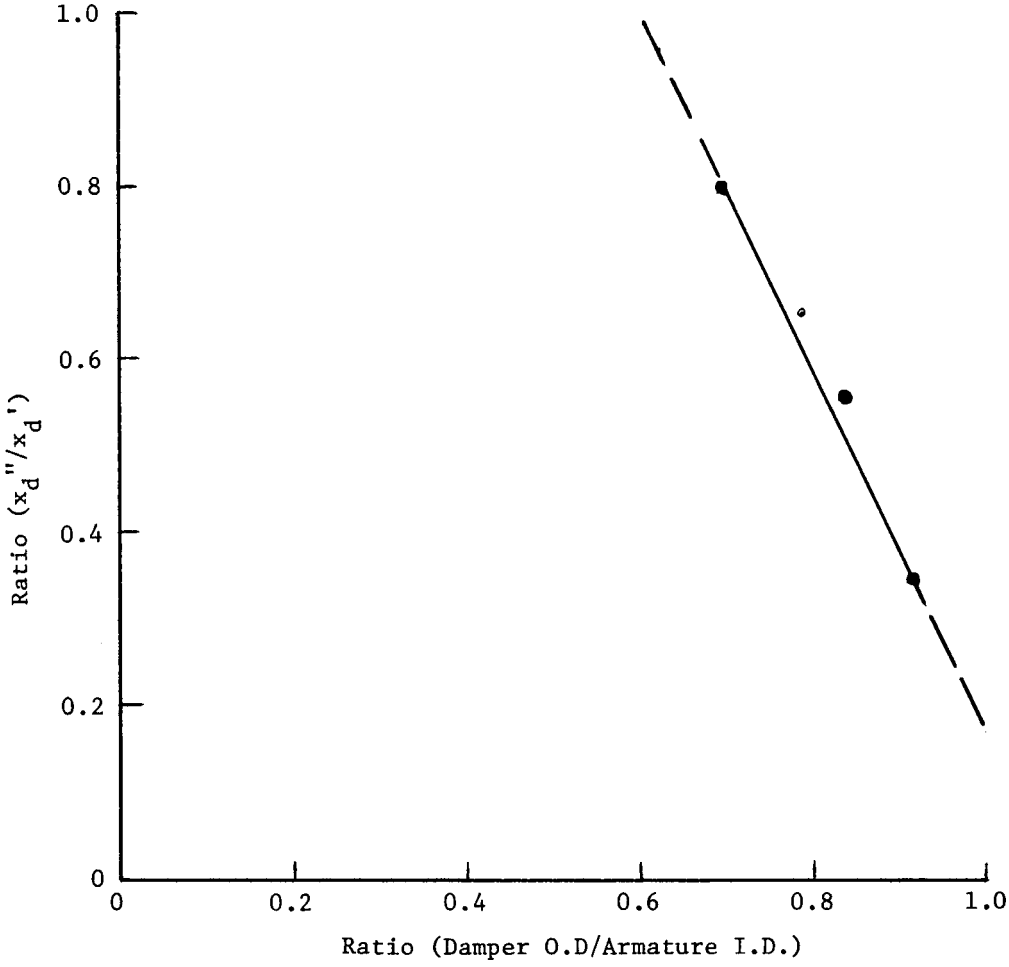

Figure 3-14. Estimated Dependence of Subtransient Reactance to Proximity of Damper Winding To Armature Winding

As indicated, if all phases of this analysis prove acceptable and compatible, the design is complete. If this is not the case, one or more of the initial assumptions are revised, and another iteration is performed.

The propagation of fault fields past the damper is discussed below in section "Damper Application".

REFERENCES

1. J. L. Kirtley, Jr., "Basic Formulas for Air-Core Synchronous Machines", IEEE Conference Paper 71 CP 155 - PWR, presented at IEEE PES Winter Power Meeting, New York, N.Y., January 31 - February 5, 1971.

Winding Configuration

The major components of a superconducting rotor are illustrated in Figure 3-15 . This figure shows schematically the interdependence of the electrical design represented by the field winding and the damper, the mechanical design, represented by the supporting structures including that in the pole arc, and the thermal design which concerns the liquid helium system and the radiation shield.

The preponderance of practical turbine generator designs are based on a configuration of field conductors known as the "radial slot" arrangement. An alternative "parallel slot" design enjoyed considerable popularity in the early years of the industry, but had limitations with respect to the mechanical design of the teeth and with respect to flux harmonics. It became obsolete after the invention of the radial slot design solved these problems in large measure.

Nearly all turbine generator rotors have concentrated coil windings. In principle, it is perfectly possible to wind rotors with distributed windings; in practice this has only proven advantageous in special cases, such as certain water-cooled rotor windings where the diamond type end turns facilitate the water flow connections.

In the development of superconducting turbine generator fields, the parallel slot geometry has once more found application in prototype generators. It has been utilized in the form of stacked pancake or racetrack coils, as illustrated in Figure 3-16 . It has the advantage that such flat coils are relatively easier to form and consolidate against internal motion than coils of more complex shape. If applied to larger machine sizes, this concept encounters limitations with respect to the mechanical support of tangential as well as radial stresses due to centrifugal force.

Consequently, the radial slot geometry was identified as best suited for meeting the varied design requirements of the rotor as early as the proposal stage of the present contract. There has been no need to change this selection since then. It constitutes the basis for the final design.

Iterations in Rotor Winding Configuration

The most significant iterations that occurred during the conduct of the studies with respect to field winding configuration were occasioned by changes in field winding support, field winding conductor, and damper concepts. These are well documented in the quarterly progress reports, and will be only briefly summarized here:

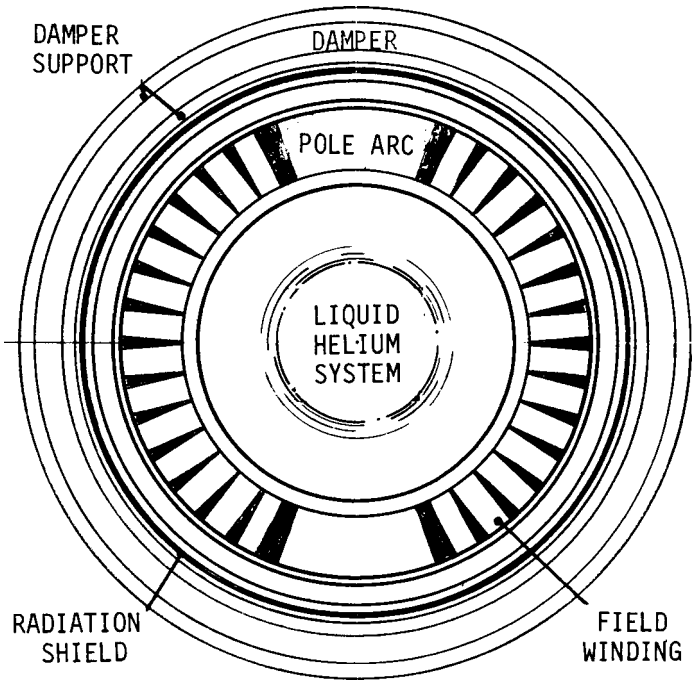

Figure 3-15. Major Components of Superconducting Rotor

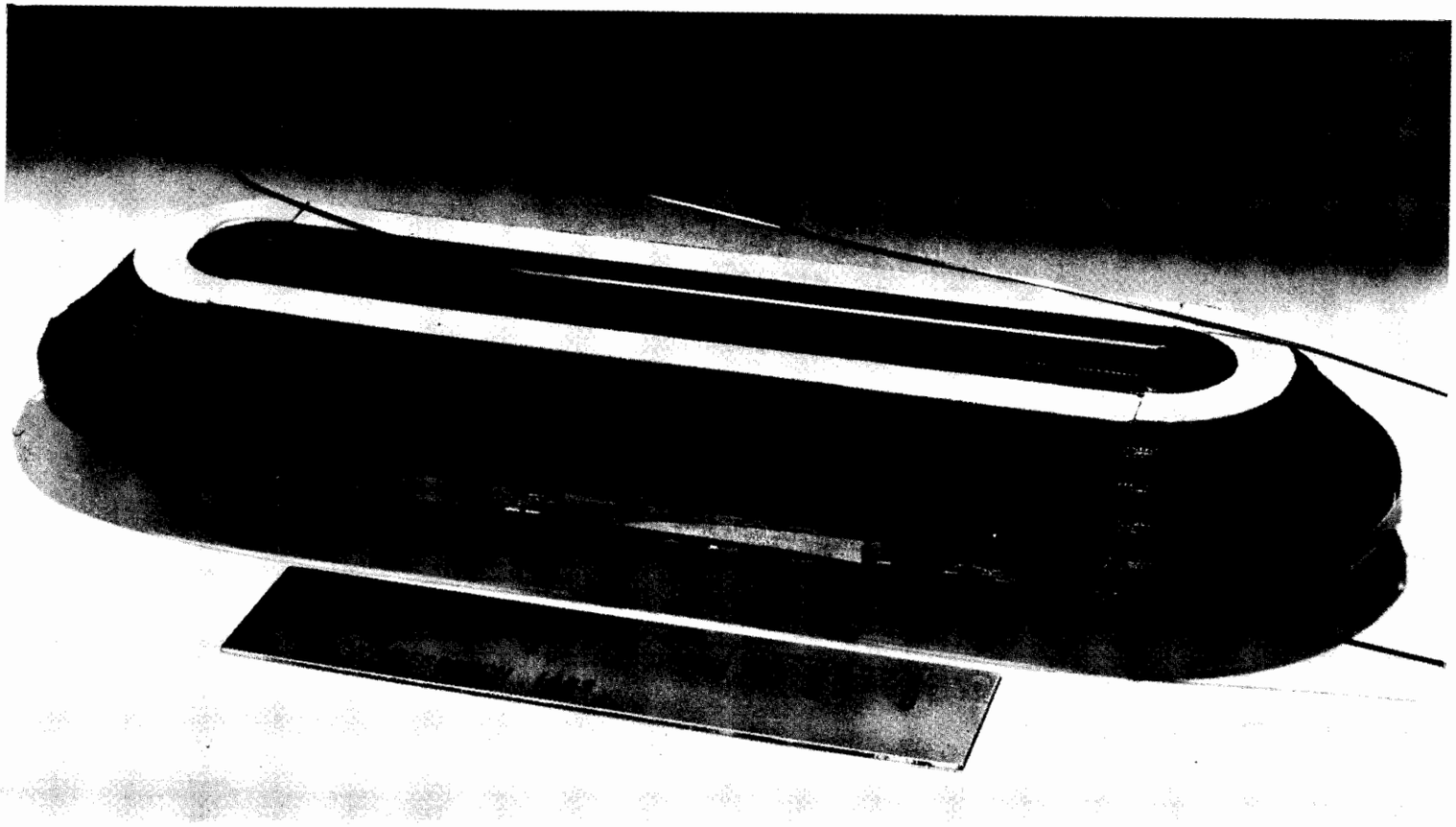

Figure 3-16. Racetrack Type Field Winding for Superconducting Generator

- First quarter studies re-examined the rotor configuration described in the proposal, which had slots for the conductors separated by metallic teeth. Advantages ascribed to an alternate design without teeth were:
  - -- More winding space
  - -- Elimination of heat losses in the teeth
  - -- Ability to use preformed coils or coil assemblies

  The studies on damper design indicated that, with such an inner rotor structure, a room temperature damper would probably satisfy the attenuation and damping requirements.
- In the second quarter, a specific albeit approximate calculation of losses in the field winding support indicated that these were acceptable in terms of the cryogenic design and the specified fault duration.
- Conductor selection studies reported in the third quarter showed unacceptably high losses during fault conditions in the conductor that had been assumed for the reference design. The following options were available to overcome this problem:
  - -- Redesign of damper shield to reduce penetration of fault effects
  - -- Change to a cabled conductor
  - -- Use of Nb_3Sn conductors
- The complete design logic and margins in the use of superconductors were reported in the fourth quarter. The significance of possible conductor motion on the required design margins was discussed and the need for adequate restraint against conductor motion to secure high current density reliably was noted.
- Superconductor selection was further examined in the fifth quarter. Addition of a cold damper was mentioned as a viable solution to the superconductor loss problem.
- A cold damper shield has been added to the design. The additional attenuation offered by this shield to disturbances of various modes that penetrate through the warm damper, and the losses in the cold damper itself have been determined. The loss reduction in the field winding support structure is large enough to permit the reconsideration of a toothed, slotted, support assembly similar to that described in the proposal. Such a support provides much better restraint against conductor motion than would be possible with the alternative cylindrical shell support without teeth. The winding space is less than would be available in the absence of teeth, but a higher current density is possible with the improved shielding and support system, so that little change occurs in the power density of the complete machine. Finally, this design appears more conducive to application of existing rotor winding techniques used in conventional radial slot rotors.

The final rotor configuration is illustrated in Figure 3-17. In this arrangement, the conductors are located in slots machined in a hollow cylindrical rotor body which provides a means of transmitting torque as well as mechanical support for the superconductors against centrifugal and electromagnetic forces.

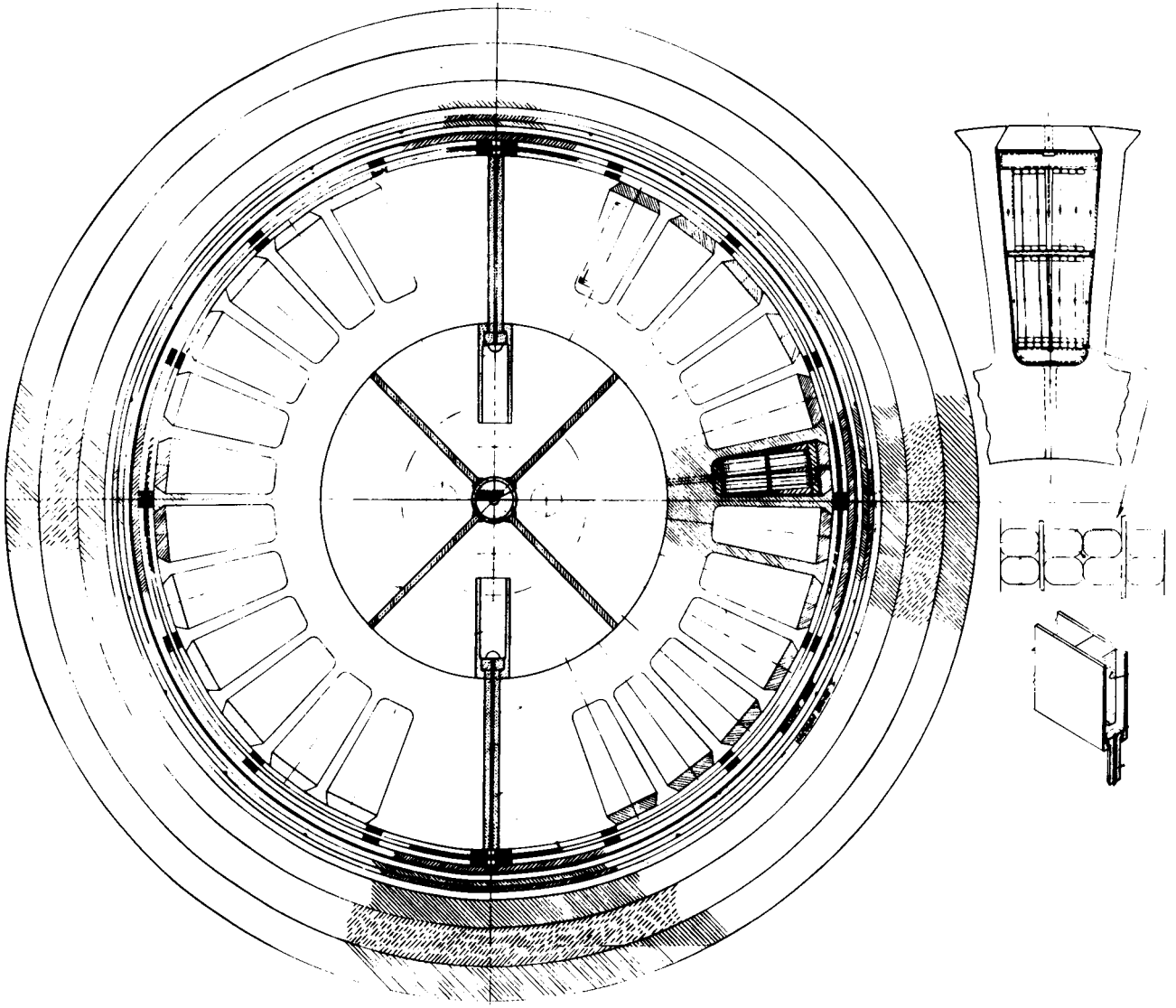

Figure 3-17. Final Rotor Configuration for 300 MVA Superconducting Turbine Generator

The solid body also resists bending due to the weight of the rotating parts. The outlines of the slots are tapered from top to bottom. This permits the use of internal tightening wedges and facilitates the design of the helium distribution system. Each of the slots is lined with a slot cell, which insulates the winding from ground potential. The bottom of the cell is pierced at intervals to permit the passage of helium coolant. Within the slot, the individual conductors are arranged in columns. Spacers which have passageways for helium flow are inserted at intervals between the columns of superconducting wires. The individual wires are monolithic superconductors of composite construction (see conductor section) and are mutually insulated with a synthetic varnish treatment. The top of the slot is tightly wedged to contain the coil assembly. End turns of the winding will generally conform to a saddle shape and will be supported by extensions of the outer field support cylinder and by sidewise blocking.

Factors in Selection of Detailed Winding Arrangement: Pole Angle and Thickness

The intuitive judgment that the field winding should be at as large a radius as possible and occupy maximum space consistent with other design requirements was tested by means of a parametric study relating the capability of the field winding to pole angle and winding thickness. The analysis used the basic equations for air-core synchronous machines. As is explained in the discussion on three-dimensional flux distribution studies included below, these equations are rigorously correct only for the ideal case of an infinitely long machine. They will be nearly correct, however, for machines of normal proportions of length to diameter as is typical of turbine generators in larger sizes. This analysis was also useful in demonstrating the interrelation of winding thickness and pole angle, and in identifying the location of the limiting flux density at the superconductor. The procedure and results of the analysis follow.

The general geometry is illustrated in Figure 3-18. The outer radius of the field winding R_{fo} was considered fixed, as was the nominal current density in the field winding space. The pole angle θ_p and the radial thickness of the winding were varied. The resulting maximum flux density values and total ampere-turns as functions of pole angle and thickness are plotted in Figures 3-19 and 3-20 respectively. It can be seen from these plots that both flux density and mmf of the winding depend much more critically on winding depth than on pole angle. At constant t, increasing the pole angle reduces the space available for conductors and, as might be expected, produces corresponding reductions in flux density and mmf.

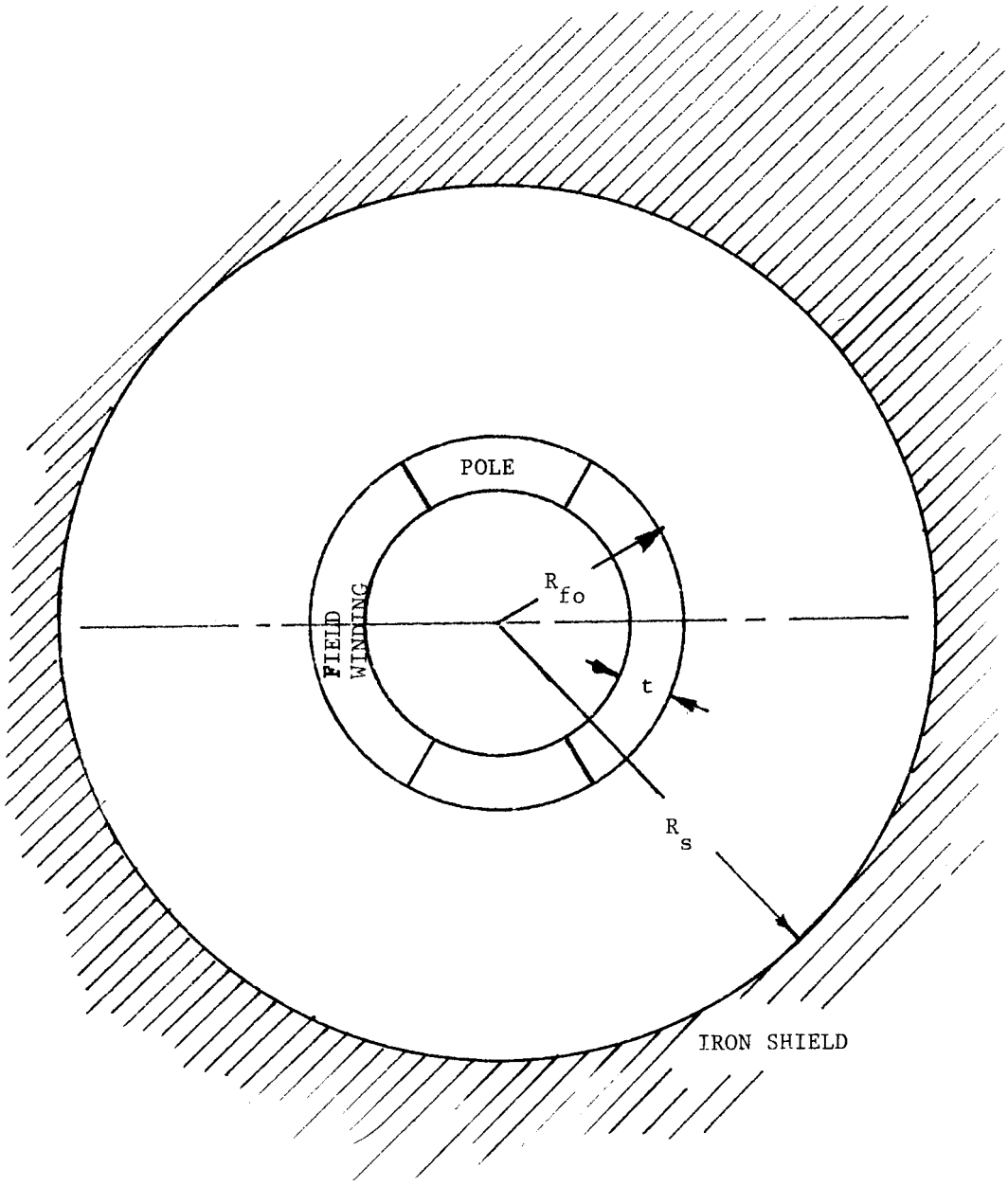

R_{fo} = Outside Radius of Field Winding

R_s = Inside Radius of Flux Shield

t = Thickness of Field Winding

Figure 3-18. General Field Geometry

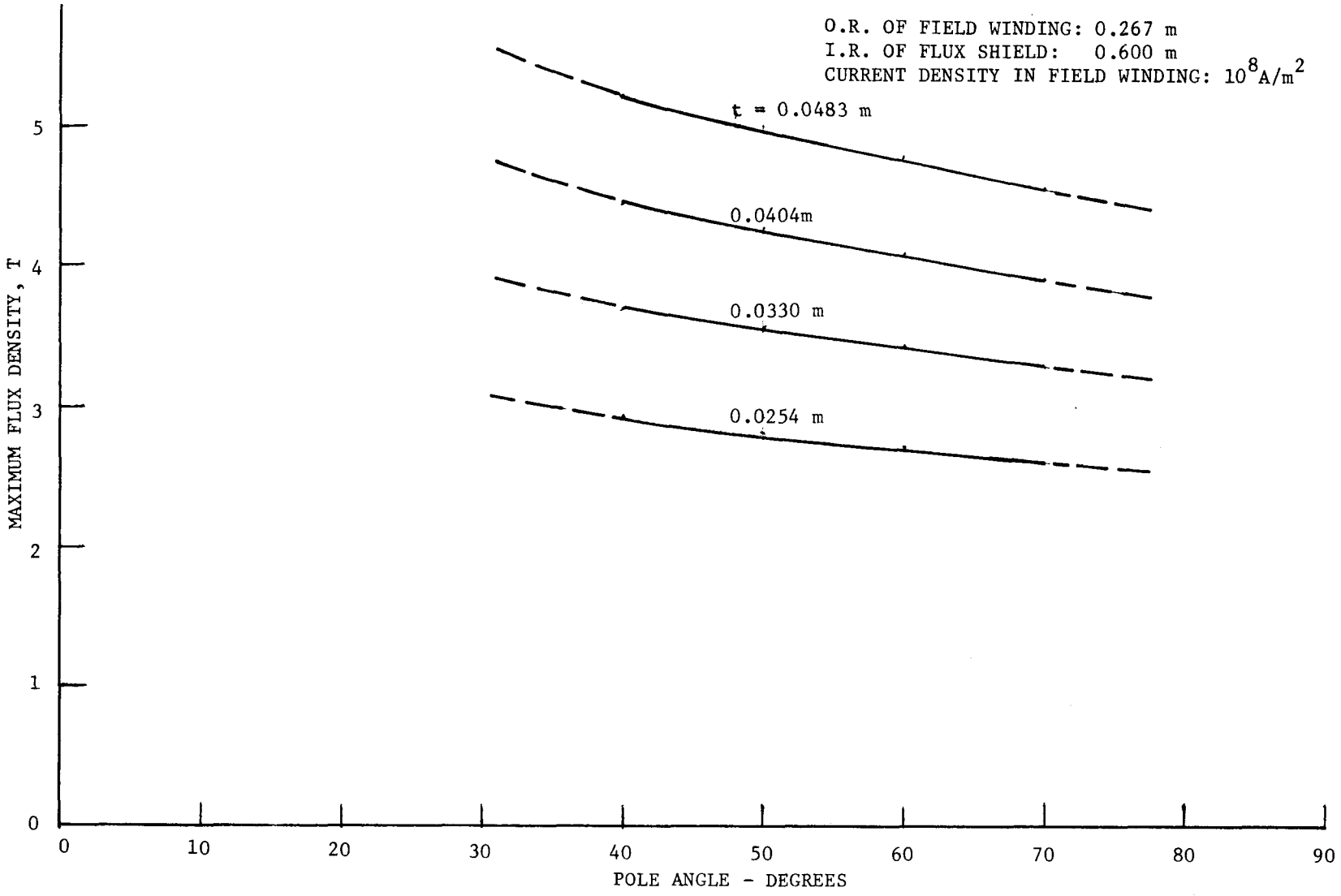

Figure 3-19. Maximum Flux Density in a Superconducting Field Winding as a Function of Pole Angle and Winding Thickness.

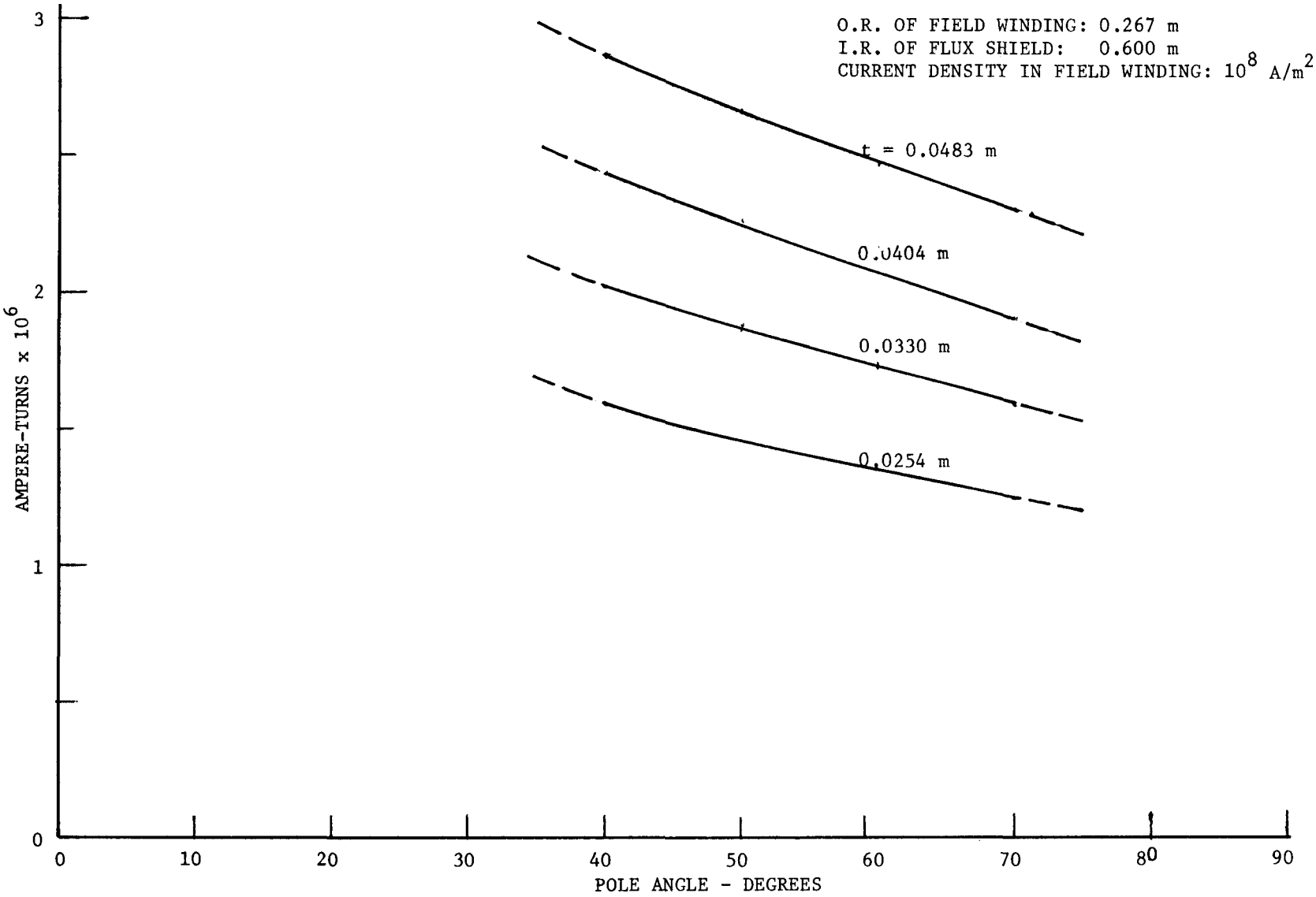

Figure 3-20. Total Ampere-Turns in a Superconducting Field Winding as a Function of Pole Angle and Winding Thickness.

These results can be combined, as in Figure 3-21, to produce the air gap line for the winding. In the same figure, the air gap lines for several different combinations of pole angle and winding thickness are superimposed on superconductor characteristics for the same combinations. (Inherent superconductor characteristic and utilization is assumed.) The intersection of these characteristics, for a given combination, represents the no-load flux density in the machine, while the difference between these curves at a constant flux density represents the mmf available to overcome armature reaction. It can be seen from Figure 3-21 that the maximum flux density provided by the field is proportionately more sensitive to depth of field winding than to pole angle.

The percentage of the maximum flux density that is useful in producing output MVA was also checked. The useful flux density, defined as the magnitude of the radial component, was calculated at the outer radius of the field winding and is plotted in Figure 3-22. The ratio of useful flux density to maximum flux density is shown in Figure 3-23. Since the maximum flux density at the superconductor constitutes one of the limits in its utilization, the ratio plotted in Figure 3-23 is a measure of the overall utilization of the superconductor in the given geometry. It will be seen that this ratio is nearly constant at about 0.7, and nearly independent of winding geometry within the limits of variation. From this viewpoint, pole angle exerts only a very weak influence over the utilization of the active parts of the machine, and thus is not a major parameter of the design. The maximum, although it is not a pronounced one, occurs at a pole angle of 50 degrees. This value has been used or closely approximated in all design studies.

Finally, the point of maximum flux density given by the basic equations for the idealized machine was determined. The maximum flux density is found at the inner radius of the field winding, about 2 to 3 degrees from the edge of the pole. See Figure 3-24.

The data plotted in Figure 3-19 can easily be interpreted to extract the effect of winding depth more explicitly. As shown in Figure 3-25, the maximum flux density increases with increasing coil depth, but less than linearly. Over the range that was considered, the flux density at maximum thickness is only about 95% of what would be expected from a linear extrapolation. If this result is combined with the reduction in useful flux density shown in Figure 3-25, the overall effectiveness of a winding of maximum depth of 0.0483 m is seen to be only about 93% of

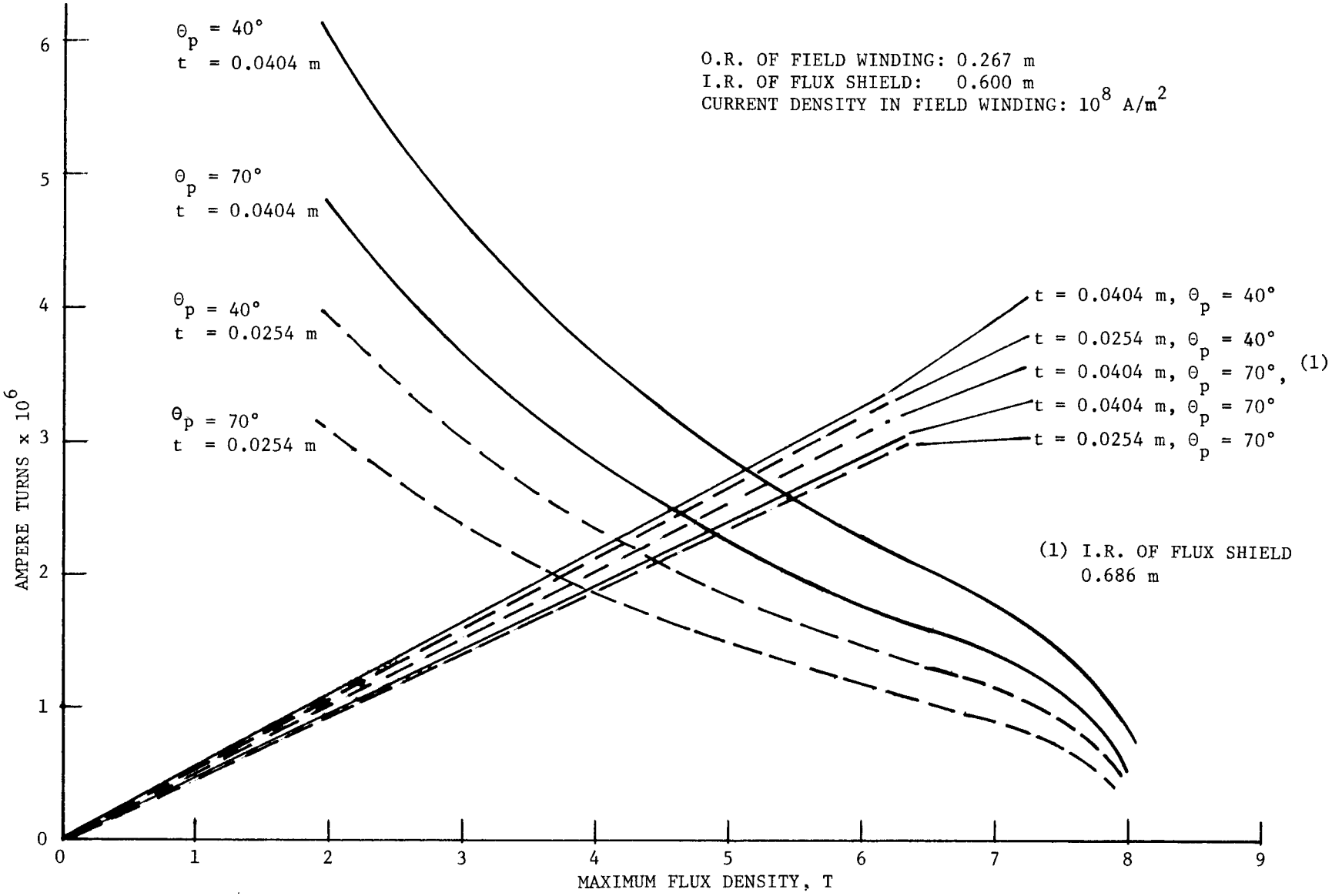

Figure 3-21. Air Gap Line and Superconductor Characteristic for a Superconducting Field Winding as a Function of Pole Angle and Winding Thickness.

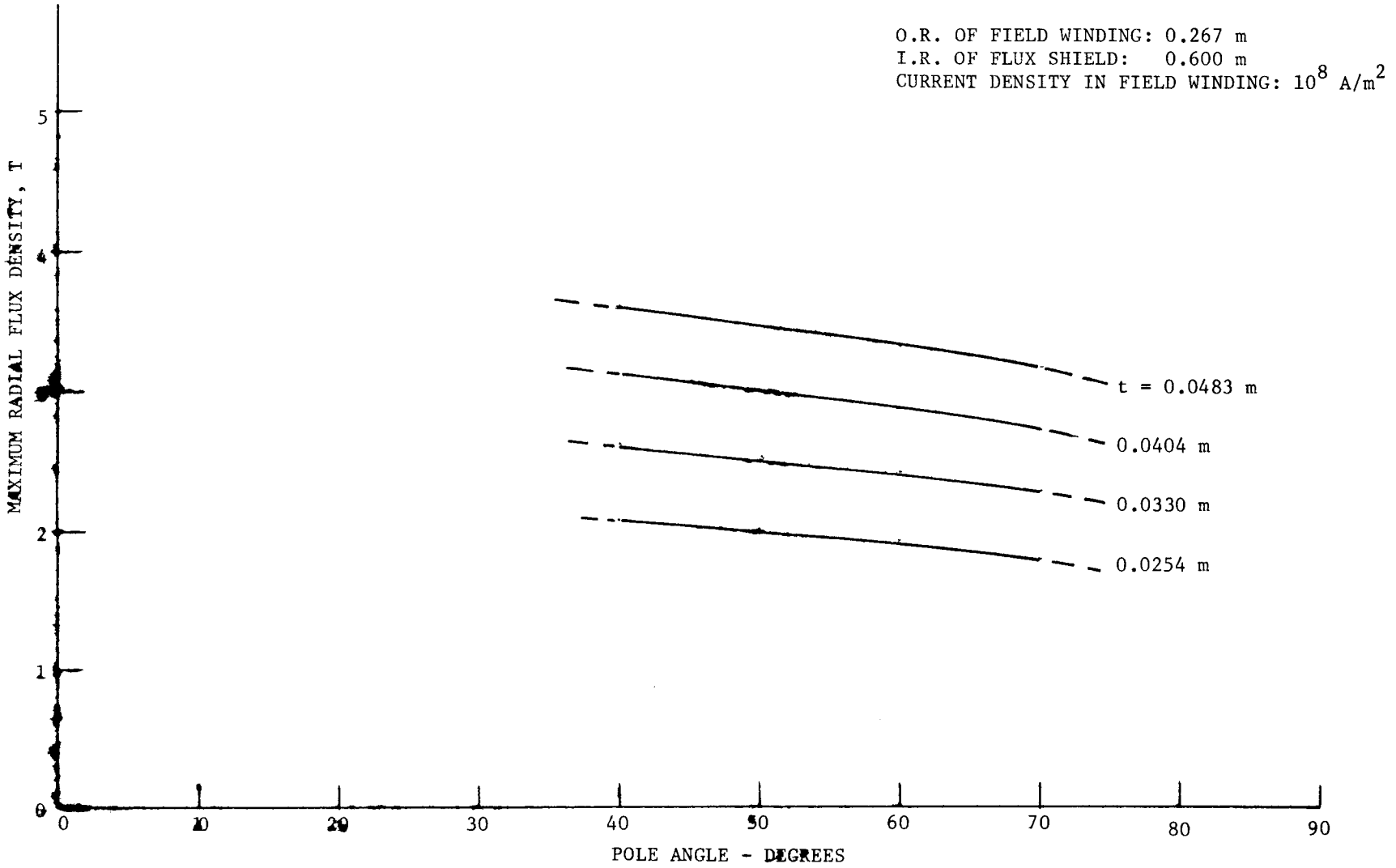

Figure 3-22. Maximum Radial Component of Fundamental Field Flux Density at O.D. of Field Winding.

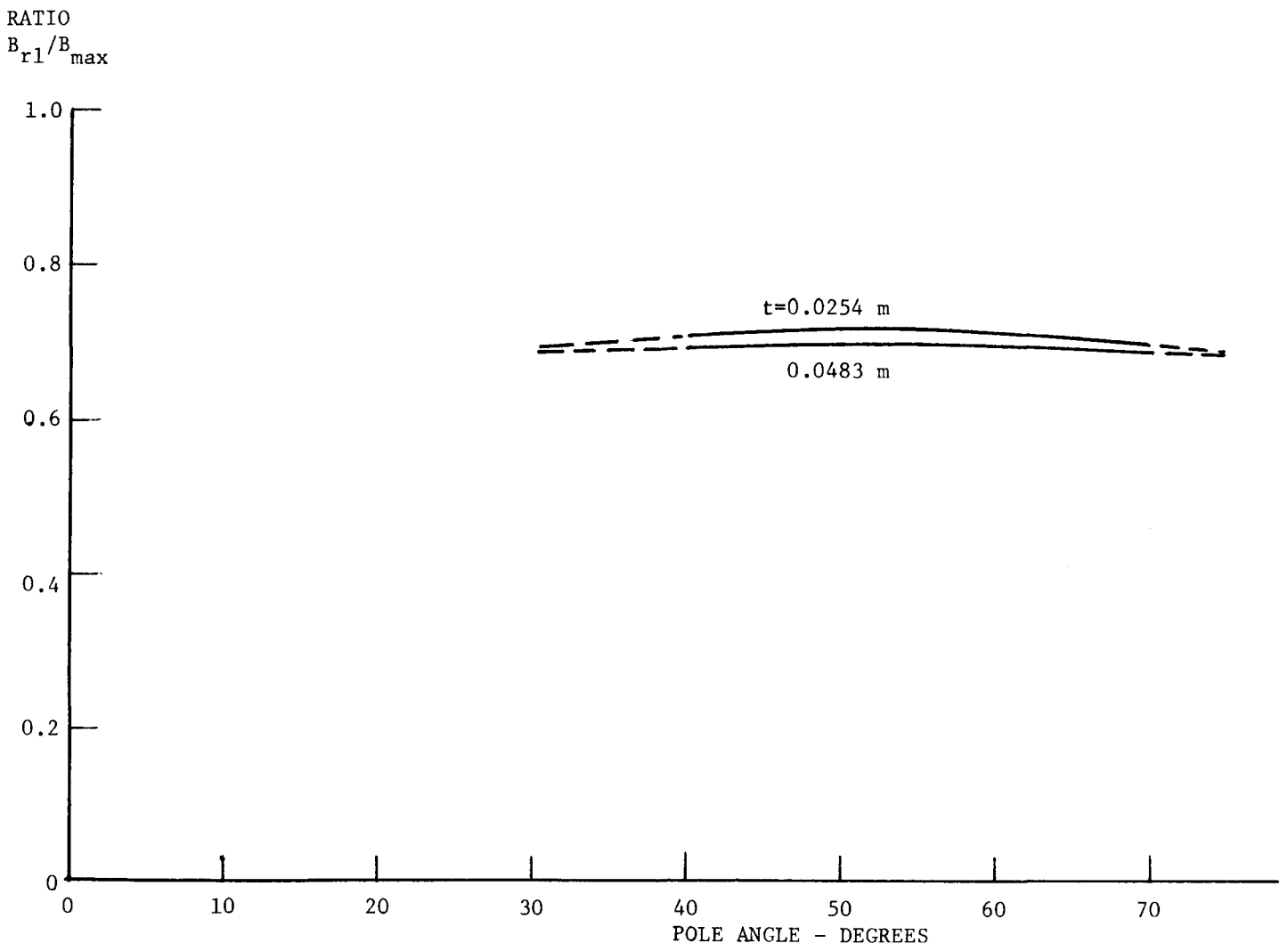

Figure 3-23. Fraction of Maximum Flux Density Useful at O.D. of Field Winding.

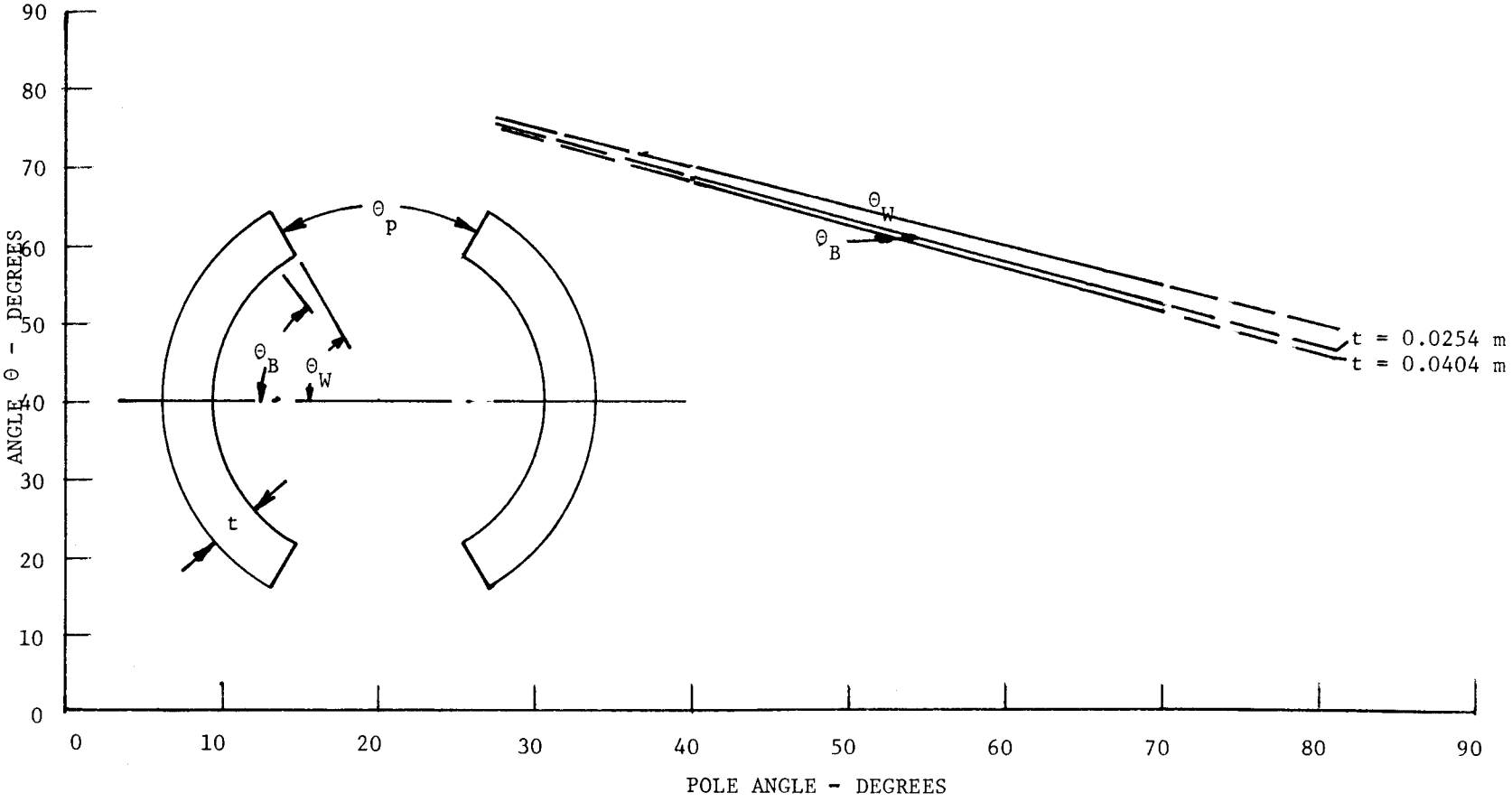

Figure 3-24. Location of Maximum Flux Density.

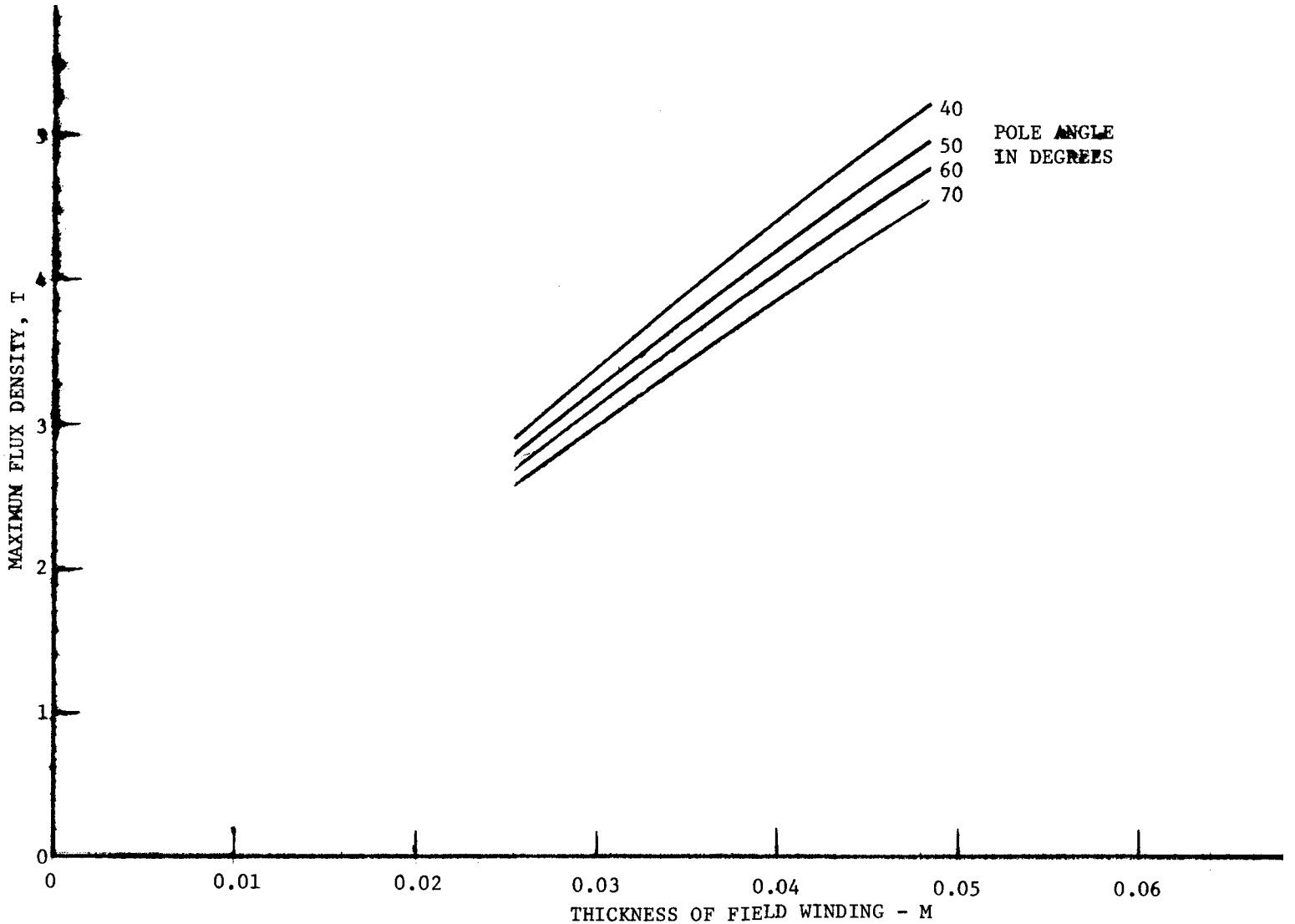

Figure 3-25. Maximum Flux Density in a Superconducting Field Winding as a Function of Winding Thickness and Pole Angle.

the overall effectiveness of a thinner winding of 0.0254 m depth. The thicker winding has, of course, more output capability than the thinner winding, but not as much as if it had been possible to locate the conductors further out towards the periphery at a higher current density. This confirms the intuitive approach to winding design.

The possible influence of pole angle selection on practically significant flux and voltage harmonics in the armature winding was also investigated. It is well known that conventional machines with large gaps usually have less need for measures to counteract harmonic effects due to field windings than machines with small gaps. This is because, with the larger gaps, the effective interlinkages with harmonic field flux distributions are reduced. This is even more the case in superconducting generators which have, in effect, gaps extending throughout the space of the active windings. The actual magnitudes of harmonic flux density components may be calculated from the basic formulas. If this is done, it is found that harmonic flux densities decrease very rapidly as the order of the harmonic increases. For higher order harmonics, the decrease is faster than the cube of the order. As a result, only the first few harmonics are of any practical significance. The relative importance of these to the overall design depends primarily on the extent to which they can effectively interact with the armature winding. Three-phase star connection of the armature winding eliminates any third-harmonic flux density effects in the line voltages, and thereby makes the third harmonic of the field form practically insignificant. Selection of 5/6 pitch for the armature winding provides reduction of the effects of the 5th and 7th harmonics. It will later be shown that a concentrated coil armature winding of the spiral pancake type does not behave in this respect in the identical fashion as a distributed winding, and the differences will be discussed in Section 3.2.2. Nevertheless no practical significant effects of the design are expected from either the amplitudes of these harmonics or the changes in amplitude as a function of the pole angle.

The amplitudes (normalized to unity) of the 3rd through 11th odd harmonics of the field form are shown in Figure 3-26 as a function of the pole angle. It will be readily observed that a pole angle of 50 degrees nearly eliminates the 7th harmonic but not the 5th. The latter harmonic, however, is not strongly responsive to slot angle over the entire range from 40 to 60 degrees, which was previously shown to give the best utilization of the field winding capability. It is therefore concluded that the choice of a pole angle of approximately 50 degrees represents an excellent compromise of the power density and harmonic considerations.

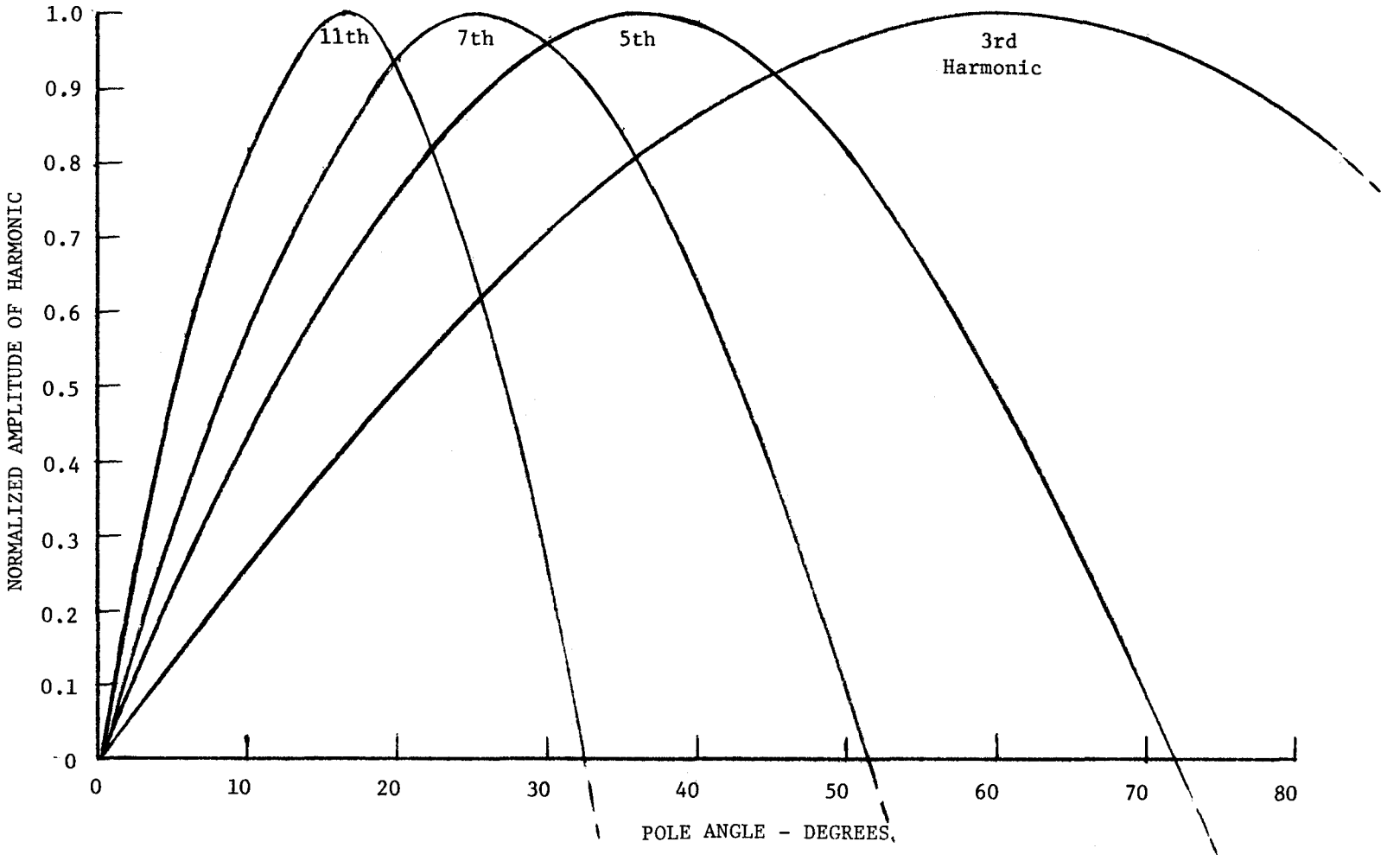

Figure 3-26. Amplitude of Field Harmonics of a Superconducting Field Winding as a Function of Pole Arc.

Conductor Selection

Superconducting wires which are suitable for high field, high current application in rotating machinery are necessarily complex multifilamentary structures. They consist of a large number of fine, superconducting filaments imbedded in a matrix of normal conducting material. The filament diameter is required to be small ($\lesssim$ 50 μm for NbTi) for adiabatic (flux jump) stability and for low hysteretic losses induced by time varying transverse magnetic fields which fully penetrate the filaments. The matrix should contain a significant amount of high conductivity material such as copper to provide further stability against normalization due to mechanical motion of the conductor as well as other effects.

The superconducting material to be used for a first large demonstration machine is certain to be NbTi because of extensive experience that exists with it in terms of conductor fabrication and utilization in large magnets and prototype machines. While Nb_3Sn has appreciably higher current, field, and temperature capability than NbTi, and Nb_3Sn multifilamentary conductors are commercially available, as yet there is little experience with them in magnet systems. Therefore they most probably will be utilized in later machines.

Selecting the superconducting material sets the limiting performance capability of the conductor in terms of temperature, magnetic field and current density. Figure 3-27 illustrates the type of limitations for the superconductor. Each curve is to be interpreted as the boundary below which the material is in a superconducting state and above which it is in a normal metal state. Each curve corresponds to a given temperature that has relevance to the design of the field winding. Rated operation, T_R, is the temperature during steady state operation; fault conditions, T_F, corresponds to the fault period; and design limit, T_D corresponds to the temperature that can result from both fault and frictional heating (conductor motion). How these intrinsic limits factor into and affect the field winding design is discussed below.

The eddy currents which are induced to flow through the matrix due to coupling of the filaments by time varying, transverse magnetic fields generate heat in the conductor. For low frequency fields, this loss is reduced by twisting the conductor about its axis, thus forming helical filaments, and may be further reduced by dividing up the copper martix with a high resistivity material, such as copper-nickel, to reduce the coupling currents. The dependence of these eddy current losses on twist length, matrix conductivity, and the amplitude and frequency of the time varying field has been treated theoretically by Carr using an anisotropic

continuum model. The theory has been very successful in explaining experimental data on many and varied conductors.[1-11] The theory usually predicts losses which are higher, but within a factor of two, of the experimentally determined values over a wide frequency range.

Cabled or braided conductors made of several smaller wires which are fully insulated from each other will have lower losses than a larger monolithic conductor, but will be difficult to constrain for mechanical integrity under the high stress levels found in rotating machinery.

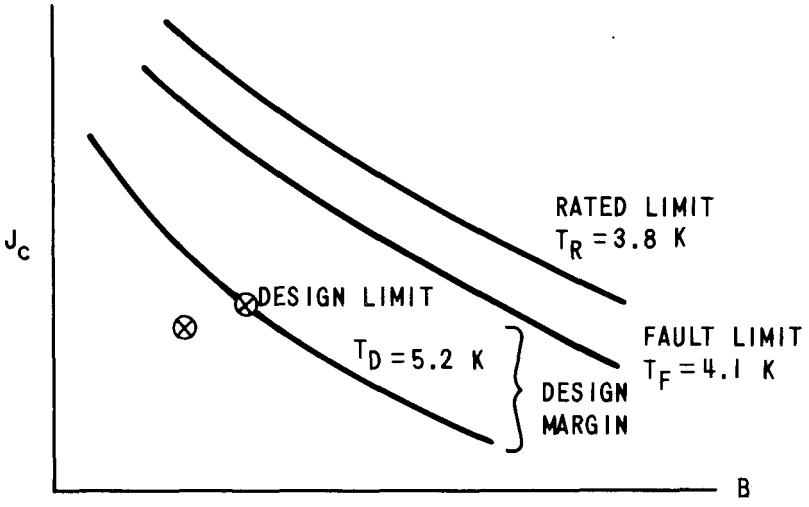

Figure 3-27.
Superconductor Limits

In this section we review the conductors which have been considered to date for use in the rotor of the 300 MVA generator. Monoliths using NbTi with an all copper matrix or with a copper-copper-nickel mixed matrix are discussed as well as a cabled conductor using strands of the mixed matrix conductor. The feasibility of using a Nb_3Sn conductor is considered and a possible conductor design is presented.

The conductor candidates have been chosen to be made as simply as possible consistent with the requirements for current density, mechanical stability, ac losses, and state-of-the-art manufacturing techniques. Since it is essential that the conductor remain superconducting during fault conditions, a crucial part of the conductor design involves the calculation of losses incurred in the conductor and the resultant temperature rise. For this reason we devote part of this section to a brief review of the loss theory developed by Carr and co-workers at Westinghouse which has been used successfully in predicting losses.

During the early stages of design of the rotor it appeared that the amplitudes of the transient fields occurring at the conductor during a fault would be much greater than necessary to quench a copper matrix conductor. For this reason,

only mixed-matrix conductors were considered and we designed a monolith and a cable. But even the lowest-loss mixed-matrix monolith was marginally stable during fault so that the shielding scheme for the rotor had to be redesigned. It was found that it was possible to add a cold shield which would reduce the transient fields enough to allow the use of a copper matrix conductor. Thus, although we include here a discussion of the mixed matrix conductors which we have considered, it is for comparison only and we propose that the all copper matrix monolith be used in the final rotor design.

Design Margins and Winding Stability

The combined conductor winding and cooling design must assure that under worst case conditions, the field winding will either remain superconducting or, if some portion of the winding goes normal, that portion will return to the superconducting state without inducing a normalization or quench of the entire winding. This type of outage must be avoided. The superconductor will go normal if current density, magnetic field or temperature goes above the worst design limit curve shown in Figure 3-27.

Providing margin for worst case current and field excursions is straightforward and is based on determining limits for these quantities during transient and fault periods.

Providing margin for temperature excursions is not as straightforward. The two important causes for temperature changes are

- Rapid magnetic field changes during fault periods that lead to heating of the superconductor or adjacent metallic structures.
- Sudden mechanical motion of the conductor due to mechanical or electromagnetic forces leading to frictional heating.

Field induced heating can be predicted if the transient fields are known using superconductor ac loss theory. The temperature rise then follows from heat transfer calculations for the specific cooling system that is utilized. Therefore, safe margins can be set for this case with acceptable confidence.

Two different approaches have been used over the last decade to design superconducting magnets that are stable against wire motion and frictional heating effects.

The first approach, which is the most conservative, is to provide sufficient copper shunting of the superconductor and sufficient copper such that if a major

portion of the winding goes normal, the current can transfer to and be carried by the copper while the winding cools down to the superconducting state. This approach, which is called "cryostability," provides in essence, a copper winding in parallel with a superconducting winding. Current densities of the order of 2 kA/cm^2 can be realized.

This approach, while still having the advantages of low field winding losses under steady state, has the disadvantage of requiring about the same volume of winding as a conventional generator of the same rating. Therefore the same upper limits to ratings of conventional machines would apply to superconducting machines using the cryostable concept.

The alternate approach is to utilize much higher current densities by using less copper shunting and designing the winding so that conductor movement is minimized. The winding in this case must be either subjected to heavy mechanical clamping or be bonded together by an organic binder in order to restrict motion. For NbTi conductors, current densities of about 10^4 A/cm^2 can be obtained by this approach.

Even with the greatest care in the design and fabrication of the field winding, some conductor motion may still occur. Providing helium within the winding to take advantage of its high specific heat (in comparison to solids at low temperatures) and designing with an additional temperature margin beyond that required for fault conditions, are means of controlling the temperature rise due to residual motion. In addition a certain amount of copper as part of the conductor matrix will function in the same way as in the cryostable case, where the event may be limited to normalizing a few filaments on a short section of the conductor.

While the cryostable approach has been evaluated in the present program in terms of its impact on generator characteristics, the main thrust of the program is toward higher current density designs. A sizable effort will be required to develop reliable, high current density designs. However, the benefits of developing the capability to build large rating machines (3000 to 5000 MVA) justify the additional development effort.

Hysteresis Losses

The hysteresis loss per unit volume in a cylindrical multifilamentary superconductor for field changes large enough to fully penetrate the filaments is given by (MKS units are used throughout):[11]

$$\frac{P_h}{V} = \frac{2\dot{B}\,\lambda_{s.c.}\,j_c\,d}{3\pi} \tag{1}$$

where $\lambda_{s.c.}$ is the volume fraction of the filaments, $\dot{B}$ is the rate of change of the field and d is the filament diameter. For sinusoidally varying fields of amplitude B_m and frequency f, the quantity $\dot{B}$ is replaced by $4fB_m$ in Eq. (1). The field change necessary for full penetration is given by[3]

$$\Delta B_p = 4 \times 10^{-7}\, d\, j_c. \tag{2}$$

Equation (1) is derived from Maxwell's equation, curl $\underline{E} = -\dot{\underline{B}}$, by assuming an isotropic j_c which is nearly constant during the change in field and integrating $\underline{J} \cdot \underline{E}$ over the filament cross-section.

The case of solid rectangular filaments has been treated by Walker and Murphy.[9] Again, for full field penetration the result is

$$\frac{P}{V} = \frac{\lambda_{s.c.}\,j_c\,\dot{B}\,v}{2} F\left(\theta, \frac{s}{v}, \frac{j}{j_c}\right) \tag{3}$$

This equation has been derived by treating the filaments as elliptical with 2s and 2v the lengths of the major and minor axes respectively and θ the angle between the magnetic field and the major axis. The function F has been derived for $\theta = 0$ and $\theta = \pi/2$, viz:

$$F = \frac{s}{v}\left[1 + \left(\frac{j}{j_c}\right)^2\right], \quad \theta = \frac{\pi}{2}$$

and

$$F = 1 + \left(\frac{j}{j_c}\right)^2, \quad \theta = 0 \tag{4}$$

In the case that the field change is not large enough to fully penetrate the filaments, the hysteresis loss for round filaments is given by:

$$\frac{P_h}{V} = \frac{256}{9\pi} \frac{\lambda_{s.c.}\,B_m^{\,3}\,f}{\mu_o^{\,2}\,d\,j_c} \tag{5}$$

This formula will apply to the calculation of losses for the ac fields with amplitudes less than ΔB_p given by Eq. (2).

Eddy Current Losses

The anisotropic continuum model developed by Carr and coworkers to calculate the losses in multifilamentary superconductors has been used successfully to explain the experimental results on several and varied conductors. Usually the theoretical predictions overestimate the losses, but are within a factor of two or less of the experimentally measured value. For this reason we have confidence that an upper limit to the losses in multifilamentary superconductors can be obtained using this model.

The model assumes an anisotropic conductivity with $\sigma_{||}$ parallel to the filaments and $\sigma_{\perp}$ transverse to them and an anisotropic permeability with components $\mu_{r_{||}}$ and $\mu_{r_{\perp}}$. The transverse conductivity is given by[1]

$$\sigma_{\perp} = \left(\frac{1-\lambda}{1+\lambda}\right) \sigma_m \tag{6}$$

if there is a thin, high resistance layer between filament and matrix, as is usually the case for an all copper matrix; or by

$$\sigma_{\perp} = \left(\frac{1-\lambda}{1+\lambda}\right) \sigma_m \tag{7}$$

if there is no contact resistance, as for mixed matrix conductors. Here σ_m is the matrix conductivity and λ is the fraction of high conductivity material in the conductor. For mixed matrix conductors, λ is the fraction of copper plus superconductor, but for all-copper matrix $\lambda = \lambda_{s.c.}$.

For the case where the magnetic field change is large enough to fully penetrate the filaments $\Delta B > 4 \times 10^{-7}\ d\ j_c$, we can take $\mu_{r_{||}} = \mu_{r_{\perp}} = 1$. Otherwise we have

$$\mu_{r_{||}} = 1 - \lambda_{s.c.} \quad \text{and} \quad \mu_{r_{\perp}} = \frac{(1-\lambda_{s.c.})}{(1+\lambda_{s.c.})} \tag{8}$$

There are three frequency regions of loss behavior for applied alternating magnetic fields. The low frequency region is defined by $f < f_{t1}, f_{t2}$ where[1,5]

$$f_{t1} = \frac{4\pi}{(\mu_o\ \mu_{r_{\perp}}\ \sigma_{\perp}\ L^2)} \tag{a}$$

and (9)

$$f_{t2} = (\pi R_o^2 \mu_o \mu_{r_{||}} \sigma_\perp)^{-1} \qquad \text{(b)}$$

where L is the 360° twist length and R_o is the radius of the active area of the conductor.

For transient fields to be in the low frequency limit, the field changes should occur in times long compared to the relaxation time of the eddy currents; i.e., in times long compared to $\tau_1 = (2\pi f_{t1})^{-1}$ and $\tau_2 = (2\pi f_{t2})^{-1}$. We will show this to be the case for the transient fields caused by a fault for both the copper matrix and the mixed matrix conductors.

For a round conductor in the low frequency limit, the losses are given by[1,5]

$$\frac{P_e}{V} = \left(\frac{R_o}{R_t}\right)^2 \dot{B}^2 \sigma_\perp \left[\left(\frac{L}{2\pi}\right)^2 + \frac{R_o^2}{4}\right] \qquad (10)$$

where R_t is the total wire radius - in case there is a non-superconducting sheath of thickness $R_t - R_o$ on the wire. As Walker points out, this equation is true for $\mu_{r_\perp} \cong 1$ and for the case that most of the conductor is unsaturated. Current saturation of the outer filaments due to eddy currents occurs to a depth w_o given by[1]

$$W_o = \frac{2\mu_{r_\perp}}{\mu_{r_\perp} + 1} \left(\frac{L}{2\pi}\right)^2 \frac{\sigma_\perp \dot{B}}{\lambda_{s.c.} j_c} \qquad (11)$$

and we require $w_o << R_o$ for Equation (10) to apply.

For the case where $\Delta B < B_p$, $\mu_r \neq 1$ and Eq. (10) becomes

$$\frac{P_e}{V} = \left(\frac{R_o}{R_t}\right)^2 \dot{B}^2 \sigma_\perp \left(\frac{2\mu_{r_\perp}}{1 + \mu_{r_\perp}}\right)^2 \frac{L^2}{4\pi^2} \qquad (11a)$$

At intermediate frequencies for which $f_{t1} < f < f_{t2}$, the inner filaments are shielded by the currents induced in the outer layers of filaments and the eddy current loss is given by

$$\frac{P}{V} = \left(\frac{R_o}{R_t}\right)^2 \frac{B_m^2 \ (10^{14})}{2\sigma_\perp L^2} \tag{12}$$

Note that the loss is inversely proportional to $\sigma_\perp$ and L^2. Thus, if a conductor is subjected to more than one time varying field, designing for a low loss due to one will yield a higher loss from the other if they occur on different sides of f_{t1}.

At very high frequencies, $f > f_{t2}$, the skin effect region occurs and the loss is given by

$$\frac{P_e}{V} = \left(\frac{R_o}{R_t}\right)^2 \frac{R_o}{L^2} \left(\frac{64\pi^5 \mu_{r\perp} f}{\sigma_\perp \mu_o^3}\right)^{1/2} B_m^2 \tag{13}$$

Again, the loss is inversely proportional to L^2.

Eddy current losses in rectangular conductors have been treated by Murphy, et al.[7,9] by using the anisotropic continuum model and approximating the conductor cross section as an ellipse with major and minor axes of length 2a and 2b respectively. In the low frequency limit for full field penetration ($\mu_{r_\perp} \cong 1$), the loss is given by

$$\frac{P_e}{V} = \frac{\sigma_\perp \dot{B}^2}{4} \left(\left(\frac{L}{\pi}\right)^2 \left[\left(\frac{b}{a}\right)^2 \cos^2\theta + \left(\frac{a}{b}\right) \sin^2\theta \right] + b^2 \cos^2\theta + a^2 \sin^2\theta \right) \tag{14}$$

where θ is the angle between the transient field and the major axis of the conductor cross section.

For linearly polarized sinusoidally varying fields the quantity $\dot{B}^2$ in the eddy current loss equations is averaged over a cycle and $\dot{B}^2$ as replaced by $2\pi^2 B_m^2 f^2$. For rotating fields, as is the case in the machine for some transients, the result must be multiplied by two. This may be seen by noting that an oscillating field may be considered to be made up of two circulating fields of half amplitude rotating

in opposite directions. Each contributes half of the eddy current loss so that a circulating field of full amplitude will produce twice the loss. Since the hysteresis loss is linear in B_m, a circulating field produces the same loss as an oscillating one.

General Design Considerations for NbTi

State-of-the-art manufacturing techniques allow production of multifilamentary NbTi superconductors in long lengths with acceptably uniform filament cross-sections having minimum filament diameters of about 5 μm. The maximum number of filaments which can be achieved in a single bundling for extrusion is about 2100. Over the years a rule of thumb has developed that says the ratio of stabilizer (Cu) to superconductor (NbTi) should be about 2:1 for stability. This rule is based on experience and seems to be successful even though it has not been justified theoretically. We will design our conductors with this ratio. Another constraint to be considered for mixed-matrix conductors is the minimum amount of Cu-Ni that can be used in the conductor. For a single extrusion ($\leq$ 2100 filaments) the minimum amount is about 27% of the conductor volume in order to maintain the integrity of the Cu-Ni between filaments. Of this 27%, about 17% is contained in the conductor interior between filaments and 10% is in a sheath around the outside of the conductor. If less than this amount is used, the Cu-Ni barriers between filaments become too thin. If a conductor of more than 2100 filaments is to be made, rebundling is required, and then 40% by volume is about the minimum amount of Cu-Ni that can be used. A single extrusion is preferred because it yields a smaller conductor and a higher overall current density. The trade-off is an increase in hysteresis loss due to the necessarily larger size filament.

The conductor for the 300 MVA machine will be designed for an operating current of 1000 A. In order to allow for a reasonable temperature margin during fault conditions and a 30% margin for over current, the conductor is designed to carry 1300 A at 5.2°K and 5 tesla. This allows a temperature rise of 1.4°K from the operating temperature of 3.8°K. Figure 3-28 shows the scaling law for NbTi. At 5 tesla and 5.2°K the critical current is 62% of the value at 4.2°K and 5 T. Thus we want I_c (4.2°K, 5 T) = 2100 A.

For ease of winding and a greater packing factor, the conductor should not be round, but rectangular, However, the ac losses in a rectangular conductor are increased over a round conductor by the square of the aspect ratio for fields normal to the wide side of the conductor [compare Eqs. (10) and (12)]. An aspect ratio of 1.5 has been chosen as a reasonable value to compromise these two considerations.

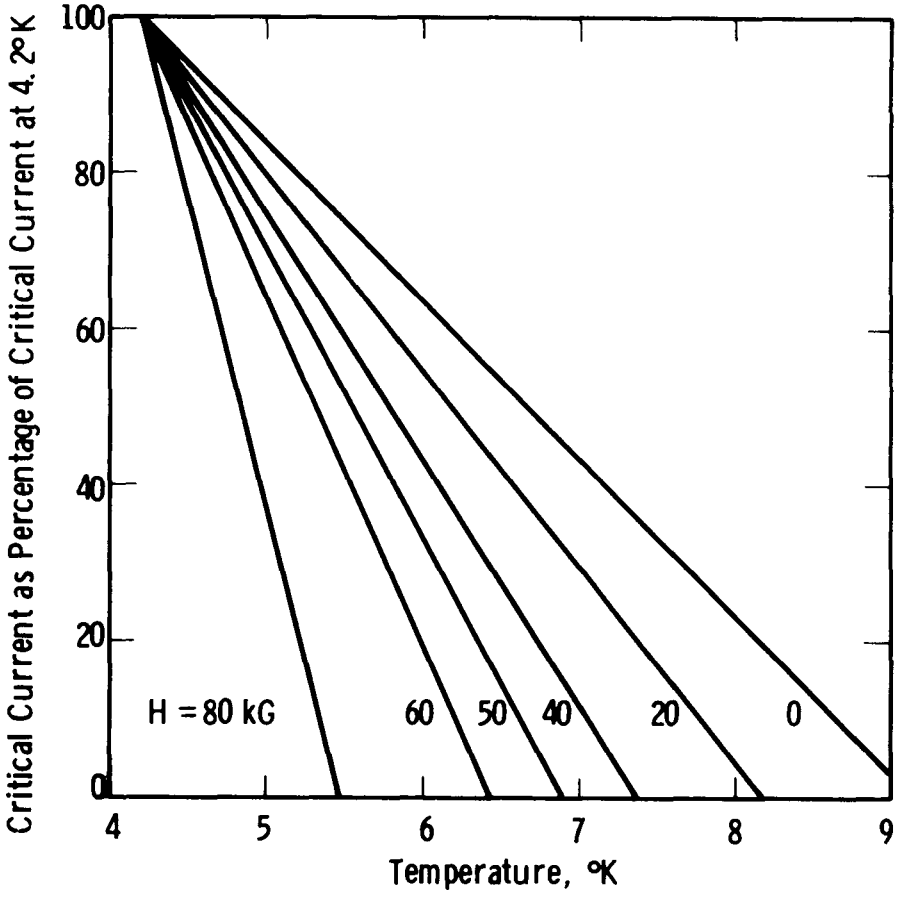

Figure 3-28. Magnetic Field and Temperature Degradation of the Current Carrying Capacity of NbTi Conductors

As noted earlier, twisting the conductor about its axis reduces the eddy current losses in the low frequency region. As we shall see, the transient fields of importance occur in the low frequency region so that the conductor should have as tight a twist as possible. The 360° twist length is limited to about ten wire diameters by manufacturing techniques with a lower limit for small wires of about 1 cm. Besides being restricted by physical limitations, a twist tighter than this reduces the axial current density significantly and creates a significant component of current tangential to the wire.

Adiabatic Temperature Rise Due to Fault

In anticipation of the loss estimates which follow for each conductor, we calculate here a conservative estimate of the upper limit to the allowable heat input during a fault or during ramp up. We do this by finding the temperature rise of the winding assuming that the heat generated in the conductor by the transient fields escapes rapidly to the helium which is locally in contact with the conductor. This assumes negligible heat transfer down the conductor. Since the heat capacity of the helium is roughly two orders of magnitude larger than that of the conductor, the latter will be ignored. At a pressure of 100 psi and in the temperature range 3.9°K to 5°K, the heat capacity of liquid helium is given approximately by

$$C_p = 71.7\ T^{1.3}\ \text{mJ/cm}^{-3}\text{-°K} \tag{15}$$

If Δh is the energy input per unit volume of the conductor, and β is the volume ratio of conductor to helium, the temperature rise from T_1 to T_2 will be found from the following equation

$$\Delta h = \frac{1}{\beta} \int_{T_1}^{T_2} C_p\ dT \tag{16}$$

Using Eq. (15) for C_p we find

$$\Delta T = T_2 - T_1 = \left[\frac{\Delta h\ \beta}{31.2} + T_1^{2.3}\right]^{0.435} - T_1 \tag{17}$$

In Figure 3-29 we have plotted ΔT vs. Δh for 2 values of β, $\beta = 19$ and $\beta = 9$, corresponding to 5% and 10% helium by volume, respectively. A value of $T_1 = 3.8$°K has been used. Figure 3-29 shows that for $\Delta T = 1.4$°K (i.e., $T_2 = 5.2$°K) the heat generated in the conductor must be less than 80 mJ/cm^3 or 37 mJ/cm^3 for 10% and 5% helium, respectively. As we shall see, ten percent is about the maximum amount of helium we can get in the winding by rounding the corners of the conductor to create channels.

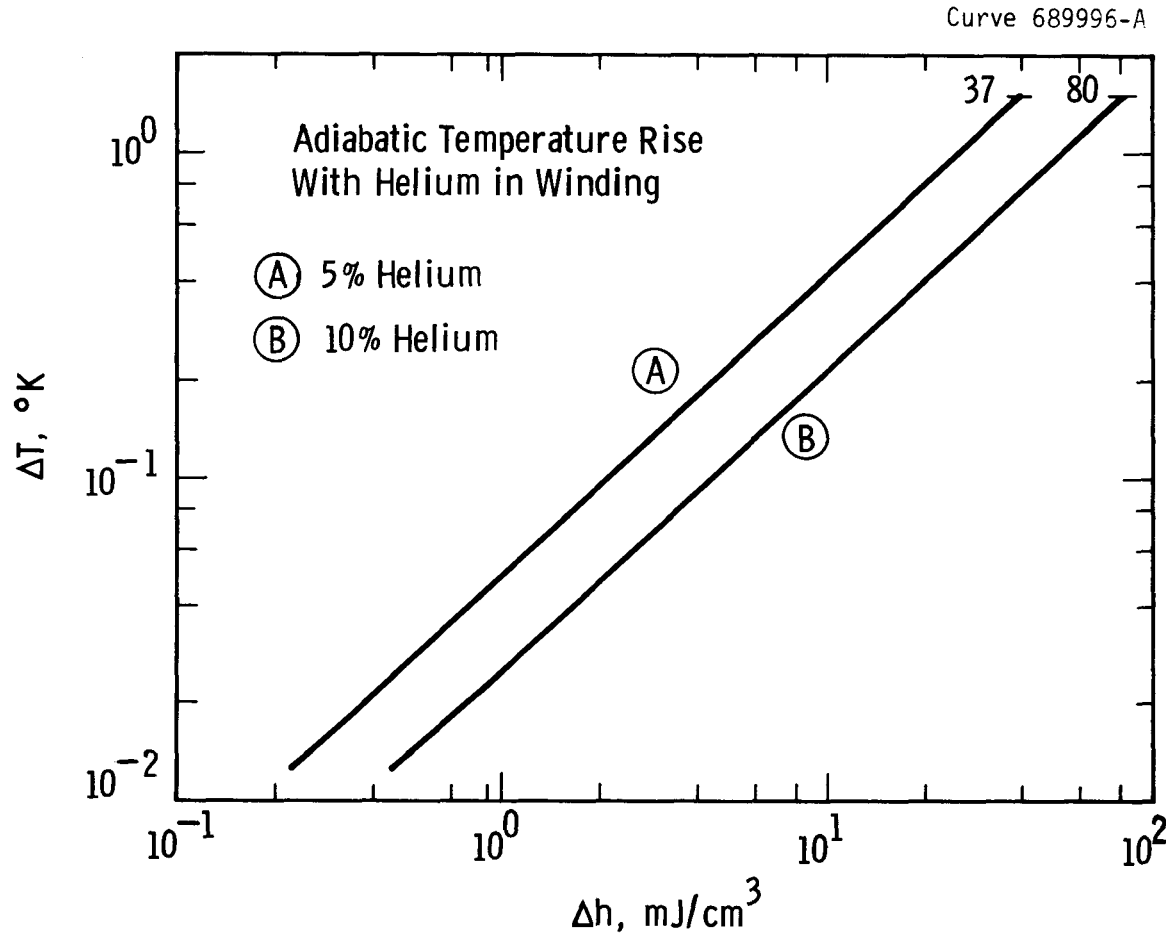

Figure 3-29. Temperature Rise of Conductor vs. Heat Input for Two Values of Helium Volume

Mixed-Matrix Conductors

Monoliths

In the past, conductor manufacturers have preferred to work with $Cu_{0.9}Ni_{0.1}$ because the commercially available $Cu_{0.7}Ni_{0.3}$ alloy is rather impure and presents problems during the manufacturing process. However, for large quantities of conductor, as we need for the 300 MVA machine, it is understood that conductor manufacturers will produce their own cupronickel and no other special problems are anticipated in the manufacturing process. As we will show later, the higher electrical resistivity of the $Cu_{0.7}Ni_{0.3}$ will yield lower ac losses than $Cu_{0.9}Ni_{0.1}$ and will be preferred. However, we have calculated losses for both alloys.

Figure 3-30 shows a cross section of the proposed conductor. The rounded corners allow liquid helium to flow through the windings for direct contact to the conductor. The value of r to be chosen depends upon the amount of helium required in the winding. For example, r = 1.09 mm would allow 10% helium by volume in the winding, while r = 0.79 would allow 5%. Ten percent helium is about the maximum allowable because this leaves a flat on the narrow side of the conductor of 0.42 mm. A larger radius would reduce the bonding surface. As we show later, 10% helium by volume will provide adequate cooling.

Table 3-12 gives the specifications for $Cu_{0.7}Ni_{0.3}$ conductor. The $Cu_{0.9}Ni_{0.1}$ conductor would have the same specifications except that $\sigma_m = 7.09\ (10^6)$ mho/m and $\sigma_\perp = 6.75\ (10^7)$ mho/m. These values will be used in calculating the ac losses.

Using Eqs. (9a) and (9b) and the parameters given in Table 3-12 we find that $f_{t1} = 165$ Hz for the Cu-$Cu_{0.9}Ni_{0.1}$ matrix and $f_{t1} = 408$ Hz for the Cu-$Cu_{0.7}Ni_{0.3}$ matrix. Both of these have been caluclated for the case that $\mu_{r\perp} = 1$ which is true for $\Delta B > \Delta B_p$ where ΔB_p the change necessary for full penetration of the filaments. From Eq. (2) we have $\Delta B_p = 1.44\ (10^{-2})$ tesla for d = 36 μm and $j_c = 10^9$ A/m^2. For $\Delta B < \Delta B_p$, we have from Eq. (8) $\mu_{r\perp} = 0.575$ and $\mu_{r\parallel} = 0.73$ yielding $f_{t1} = 287$ Hz for Cu-$Cu_{0.9}Ni_{0.1}$ and $f_{t1} = 710$ Hz for Cu-$Cu_{0.7}Ni_{0.3}$.

For the low frequency formulas to apply for the calculation of losses, the field changes during a fault must occur in a time long compared to $\tau_1 = (2\pi\ f_{t1})^{-1}$ The maximum τ_1 is for $\mu_{r\perp} = 1$ when $f_{t1} = 165$ Hz. In this case $\tau_1 = 9.6\ (10^{-4})$ sec. This time is much shorter than the 66 msec fault clearing time.

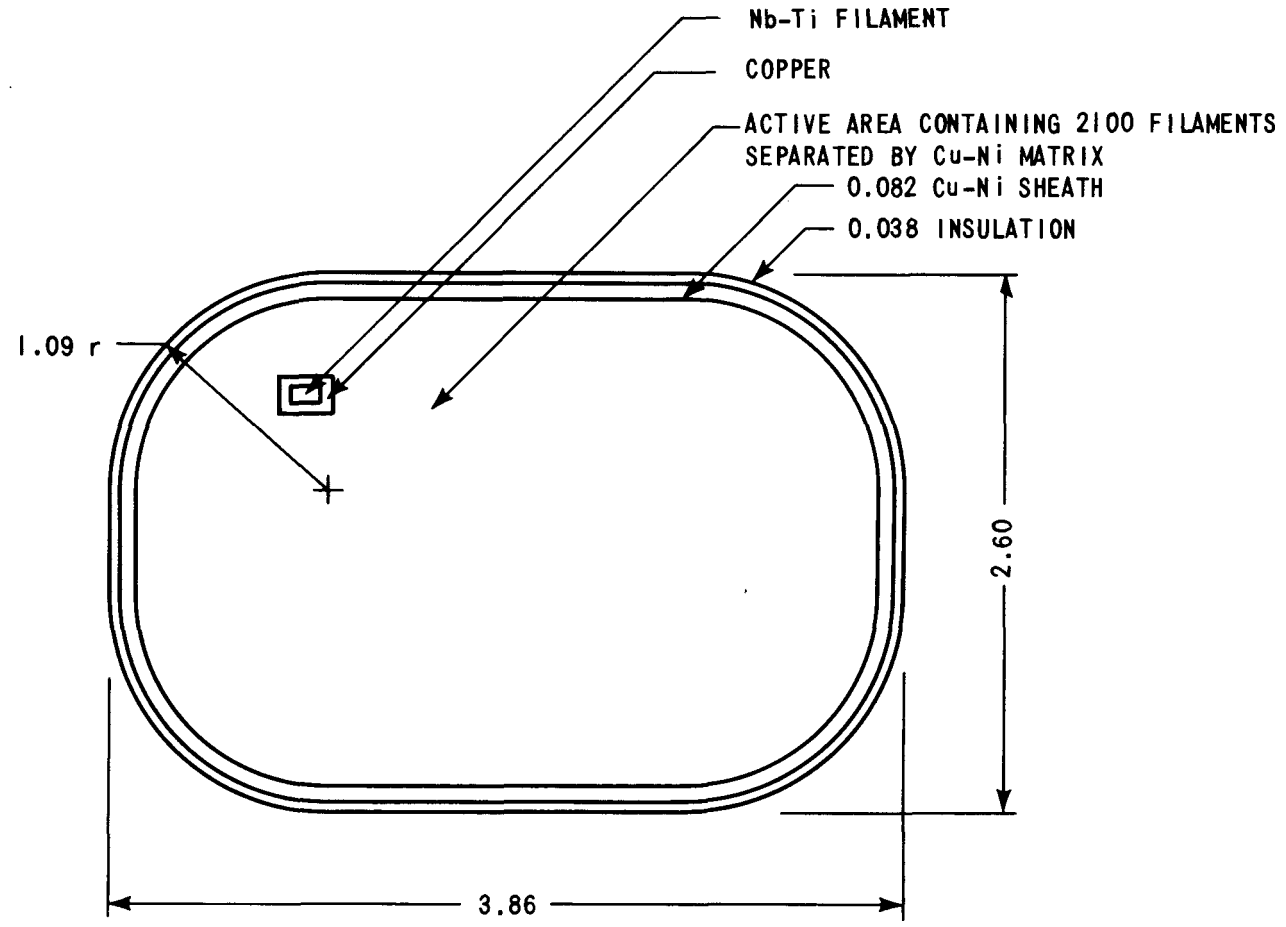

NOTE: Dimensions in mm

Figure 3-30. Cross Section of Mixed Matrix Conductor

Table 3-12

CONDUCTOR SPECIFICATIONS

QUANTITY	SYMBOL	MIXED-MATRIX MONOLITH	CABLE 10 STRAND (MIXED-MATRIX)	ALL COPPER MATRIX MONOLITH
Conductor[1] Dimensions mm	2a 2b	3.86 2.60	3.86 2.60	3.30 2.23
Matrix Conductivity[2] mho/m	σ_m	2.86 (10^6)	2.86 (10^6)	2 (10^9)
Fraction of NbTi Overall[3]		0.24	0.24	0.33
Fraction of NbTi in Active Area[4]	$\lambda_{s.c.}$	0.27	0.27	0.33
Fraction of Cu + NbTi[5]	λ	0.81	0.81	--
Transverse Conductivity mho/m	$\sigma_\perp$	2.72 (10^7)	2.72 (10^7)	1.0 (10^9)
Twist Pitch cm	L	3	1 cm in strand	3
Equivalent Round Radius mm	R_o	1.70	0.5 mm/strand	1.45
Filament Dimensions μm	2s 2v	39 26	11 μm diameter	22 14
Number of Filaments	n	2100	2100 strand 21,000 total	6684
Overall J_c[6] A/cm^2	J_c	2.1 (10^4)	2.1 (10^4)	2.85 (10^4)
Overall J[6] A/cm^2	J	9.5 (10^3)	9.05 (10^3)	1.36 (10^4)
Operating I Amps	I	1000	1000	1000
Critical Current Amps	I_c	2100	2000	2100

(1) Includes 0.003" (0.08 mm) insulation buildup for monoliths. Assumes 100% compaction for cable.

(2) The monolith and cable mixed-matrix conductors use $Cu_{0.7}Ni_{0.3}$. The all copper matrix uses RRR = 64 and a factor of two for magnetoresistance at 5 T.

(3) This is the fraction of NbTi in conductor including Cu-Ni sheath but excluding insulation.

(4) This is the fraction of NbTi in active area excluding Cu-Ni sheath and insulation. This quantity $\lambda_{s.c.}$ is used in determining hysteresis losses.

(5) λ is used to determine $\sigma_\perp$ for loss calculations.

(6) Includes helium space and insulation. Calculation is for $j_c = 10^5$ A/cm^2 at 4.2°K and 5 tesla.

The last relationship we must show to be satisfied for use of the low frequency formulas is that $w_o << R_o$ where w_o is given in Eq. (11). Using the values given in Table 3-12 and $\mu_{r_\perp} = 1$ we find $w_o = 5.7\ (10^{-6})\ \dot{B}$. Now $R_o \cong 2 \times 10^{-3}$ m and for $w_o = R_o$ we would require $\dot{B} = 351$ T/sec. There are no transients this fast present in the machines, so indeed $w_o << R_o$.

Fault Losses

To calculate the loss associated with each of the transients we use Table 3-12 and Eqs. (3) and (14). Equations (3) and (14) give the loss in terms of $\dot{B}$ and to get the loss for a sinusoidal field we simply average $\dot{B}$ over a cycle for the hysteresis loss and average $\dot{B}^2$ for the eddy current loss. This means replacing $\dot{B}$ by $4f B_m$ in Eq. (3) and $\dot{B}^2$ by $2B_m^2 \pi^2 f^2$ in Eq. (14), where B_m is the amplitude of the sinusoidal field. Thus we have for the losses in the case of the $Cu\text{-}Cu_{0.9}Ni_{0.1}$ matrix:

$$\left.\begin{aligned}
\left(\frac{P_e}{V}\right)_{radial} &= 3.52\ \dot{B}^2 \text{ mw/cm}^3 && \text{(a)}\\
&= 69.5\ f^2\ B_m^2 \text{ mw/cm}^3 && \text{(b)}\\
\left(\frac{P_e}{V}\right)_{tang.} &= 0.711\ \dot{B}^2 \text{ mw/cm}^3 && \text{(c)}\\
&= 14.0\ B_m^2\ f^2 \text{ mw/cm}^3 && \text{(d)}
\end{aligned}\right\} \qquad (18)$$

and

$$\left.\begin{aligned}
\left(\frac{P_h}{V}\right)_{radial} &= 3.29\ \dot{B} \text{ mw/cm}^3 && \text{(a)}\\
&= 13.2\ B_m\ f \text{ mw/cm}^3 && \text{(b)}\\
\left(\frac{P_h}{V}\right)_{tang.} &= 2.20\ \dot{B} \text{ mw/cm}^3 && \text{(c)}\\
&= 8175\ B_m\ f \text{ mw/cm}^3 && \text{(d)}
\end{aligned}\right\} \qquad (19)$$

where $\dot{B}$ is in T/ sec, B_m in tesla, and f in Hz. In Eq. (19) we have taken $j_c = 10^9$ A/sec and $j/j_c = 0.5$. Equations (18) and (19) can be used to calculate the losses for this conductor for any transient field provided $\Delta B \gtrsim 1.44\ (10^{-2})$ T and that it occurs in a time longer than 1 msec. For a sinusoidal field we require $B_m \gtrsim 1.44\ (10^{-2})$ T and $f < 165$ Hz for these equations to be valid.

Since $P_e/V \propto \sigma_\perp$, we multiply Eq. (18) by 0.403, the ratio of the conductivities, to get the results for the $Cu\text{-}Cu_{0.7}Ni_{0.3}$ matrix. The hysteresis losses do not depend upon $\sigma_\perp$ so that Eq. (19) is valid for both matrices.

For partial penetration losses when $B_m < B_p$, Eqs (18b) and (18d) should be multiplied by the factor $\left(2\mu_{r_\perp}/(1 + \mu_{r_\perp})\right)^2 = 0.533$ and the hysteresis losses should be calculated from Eq. (5) which yields

$$\frac{P_h}{V} = 4.3\ (10^4)\ B_m^{\ 3}\ f,\ mW/cm^3$$

where B_m is in tesla.

We repeat briefly the description of the transients which occur due to a fault. The amplitudes and time constants are discussed subsequently under "Damper Application".

- The transient field due to decay of damper currents which sustain the flux wave which travels synchronously with the rotor. The magnitude decays with the subtransient time constant. The amplitude at the rotor has been found to be 0.047 tesla. This decays in 66 msec yielding $\dot{B}$ = 0.712 T/sec. (Type A.)
- Rotation of inner shield relative to outer. This occurs at 20 Hz with $B_m = 2\ (10^{-4})$ T and lasts for 5 sec. (Type B.)
- Due to deflection of damper produced by crushing force. There are two components; one rotates at 120 Hz with respect to rotor with $B_m = 5\ (10^{-5})$ T and the other rotates at 60 Hz with $B_m = 4\ (10^{-5})$ T. Each lasts for 66 msec. Again, calculate for radial component. (Type C.)
- Due to rotor swings which occur at 2.5 Hz with an amplitude at the rotor of $B_m = 6\ (10^{-3})$ T. Calculate loss for three swings ($\sim$ 0.6 sec duration). (Type D.)

The losses for each of these transients are given in Table 3-13 along with the heat input due to each. From Figure 3-29 we see that the ΔT for either conductor for the total Q given in Table 3-13 is about 0.02°K. The conductor will remain superconducting.

Steady-State Losses

The negative sequence field rotates at 120 Hz relative to the damper shield and the field winding. We previously calculated the losses in the mixed matrix conductor for a 10% negative sequence which produced an amplitude of 0.5 gauss inside the warm shield. (See Quarterly Report No. 3). The losses were found

Table 3-13

LOSSES DUE TO TRANSIENT FIELDS CREATED
BY A 66 msec FAULT (MONOLITH)

LOSS TYPE		$Cu\text{-}Cu_{0.9}Ni_{0.1}$	$Cu\text{-}Cu_{0.7}Ni_{0.3}$	ALL COPPER
A.	Hyst.	2.3	2.3	1.5
	Eddy	1.8	0.7	27
	Total	4.1	3.0	28.5
	Q	0.3	0.2	1.9
B.	Hyst.	Negligible	Negligible	Negligible
	Eddy	0.004	0.002	$8\ (10^{-3})$
	Total	0.004	0.002	$8\ (10^{-3})$
	Q	0.02	0.01	0.04
C.	Hyst.	0.08	0.08	Negligible
	Eddy	0.002	0.001	0.02
	Total	0.082	0.081	0.02
	Q	0.005	0.005	10^{-3}
D.	Hyst.	0.20	0.20	0.05
	Eddy	0.02	0.01	0.11
	Total	0.22	0.21	0.16
	Q	0.13	0.13	0.10
TOTAL Q		0.46	0.35	2.0

All P/V are given in mw/cm^3 and all Q's are mJ/cm^3.

to be small. The cold shield which has been added inside the warm damper will attenuate the negative sequence fields even further so that the heat input to the conductor will be the order of 10^{-9} W/cm^3. This can be neglected.

Ramp-Up Losses

The charging rate for the machine during turn-on is estimated to be 2% per second (i.e., the field current will be increased from zero to full value in about 50 sec.) Maximum losses during this ramp will be found from Eqs. (18a) and (19a) for $\dot{B}$ = 0.10 T/sec. We have for both matrices:

$$\frac{P_h}{V} = 0.3 \text{ mw/cm}^3$$

and

$$\frac{P_e}{V} = 0.04 \text{ mw/cm}^3 \ (\text{Cu-Cu}_{0.9}\text{Ni}_{0.1})$$

$$\frac{P_e}{V} = 0.02 \text{ mw/cm}^3 \ (\text{Cu-Cu}_{0.7}\text{Ni}_{0.3})$$

Over the 50 sec. charging period, the total heat input will be 17 mJ/cm^3 for the $Cu_{0.9}Ni_{0.1}$ matrix and 16 mJ/cm^3 for the $Cu_{0.7}Ni_{0.3}$ matrix. The ΔT, from Figure 3-29, will be $\sim$ 0.8°K and neither conductor should normalize.

Cable

A cabled conductor made up of several small strands will have lower losses than a monolith. For minimum losses the strands should be insulated to prevent coupling currents between strands and the associated eddy current losses. Using small wires in the cable allows the tightest twist pitch to be used which minimizes the low frequency eddy current losses, and also allows a reduction in filament size which reduces the hysteresis losses.

Compacted cables containing many fully insulated strands of fine wire are presently being made with reliable techniques. Filling factors as high as 90% may be achieved. We consider here the losses associated with such a cable which is designed to have the operating characteristics required for the 300 MVA machine.

Each strand in the cable will have the minimum reasonable twist length of 1 cm. With L = 1 cm, the maximum allowable strand diameter is about 1 mm.

Making the strands smaller than this will increase the number of strands required and reduce their individual strength, so we will use R_t = 0.5 mm. Using a mixed matrix as for the monolith with Cu:Cu-Ni:NbTi = 2:1.1:1 and 2100 filaments we find that the filament diameter is d = 11 μm. For $J_c = 10^9$ A/m^2 at 4.2°K and 5 T, the critical current in each strand will be 200 A. Therefore, a ten stranded cable will have I_c = 1000 A. The specifications for this conductor are given in Table 3-12.

Fault Losses

The individual strand losses during a fault may now be calculated using Eqs (1) and (10). The results are

$$\left.\begin{aligned} \frac{P_h}{V} &= 0.57\ \dot{B}\ \text{mw/cm}^3 \qquad \text{(a)} \\ &= 2.28\ B_m\ f\ \text{mw/cm}^3 \qquad \text{(b)} \end{aligned}\right\} \tag{20}$$

and

$$\left.\begin{aligned} \frac{P_e}{V} &= 0.171\ \dot{B}^2\ \text{mw/cm}^3 \qquad \text{(a)} \\ &= 3.38\ B_m^2\ f^2\ \text{mw/cm}^3 \qquad \text{(b)} \end{aligned}\right\} \tag{21}$$

where again $\dot{B}$ is in T/sec, B_m in Tesla, and f in Hz. Equation (21) is for Cu-$Cu_{0.9}Ni_{0.1}$ and must be multiplied by 0.403 to get the losses for Cu-$Cu_{0.7}Ni_{0.3}$. Again, the eddy losses given in Eq. (21) are for an oscillating field and must be doubled for a rotating field.

Comparing Eqs. (20) and (21) to Eqs. (19) and (18) we find that the hysteresis losses in the cable are 17% of those in the monolith while the eddy losses are only 5% of the monolith.

Steady-State Losses

As for the monolith, the losses due to a 10% negative sequence are negligibly small due to the attenuation of the 120 Hz field by the two shields.

Ramp-Up Losses

For a charging rate of 2%/sec we have $\dot{B}$ = 0.1 T/sec. Losses are calculated with Eqs. (20a) and (21a). The results are

$$\frac{P_h}{V} = 0.06 \text{ mw/cm}$$

and

$$\frac{P_e}{V} = 0.002 \text{ mw/cm}^3 \ (\text{Cu-Cu}_{0.9}\text{Ni}_{0.1})$$

and

$$\frac{P_e}{V} = 0.001 \text{ mw/cm}^3 \ (\text{Cu-Cu}_{0.7}\text{Ni}_{0.3})$$

The total heat input during the 50 sec. charge time is roughly 3 mJ/cm^3 for each matrix.

All Copper Matrix

The advantages of using an all copper matrix, monolithic conductor over a mixed-matrix monolith or a cable are many. The conductor would: be cheaper; be easier to manufacture with more reliabiltiy; have better thermal characteristics; and probably be more stable. In addition, we have had more experience in loss measurements in copper matrix conductors so that once we satisfy ourselves that we know the field transients with confidence, we will have a higher degree of confidence in the loss calculations than for the mixed-matrix monolith or the cable.

The problem arises as to whether the losses in an all copper matrix are too high during a fault to preclude a quench. We have included in Table 3-12 the characteristics of a copper matrix conductor which we recommend be used with the cold magnetic shield described earlier incorporated in the rotor. Using the parameters given in Table 3-12, we find from Eq. (2) that the full penetration field is $B_p = 80$ gauss (assuming $j_c = 10^9$ A/m^2). For the sake of comparison to the mixed-matrix monolith we have plotted the eddy current losses for both in Figure 3-31 , assuming round conductors in the full penetration region ($\Delta B > B_p$). Equations (10), (12) and (13) were used. The important features to note are that the copper conductor has higher losses in the low frequency region ($f < 60$ Hz) but actually has lower losses for $f > 60$ Hz. The reason for this is that the higher copper conductivity causes the shielding region to begin at $f \cong 11$ Hz and the skin effect region at $f \cong 60$ Hz whereas the shielding region in the mixed matrix begins at $f \cong 400$ Hz. Thus, the eddy losses due to the damper shield distortion at 120 Hz are less in the copper matrix conductor than in the mixed-matrix. However, the rotor swings which occur at 2.5 Hz will produce a loss which is about forty times greater

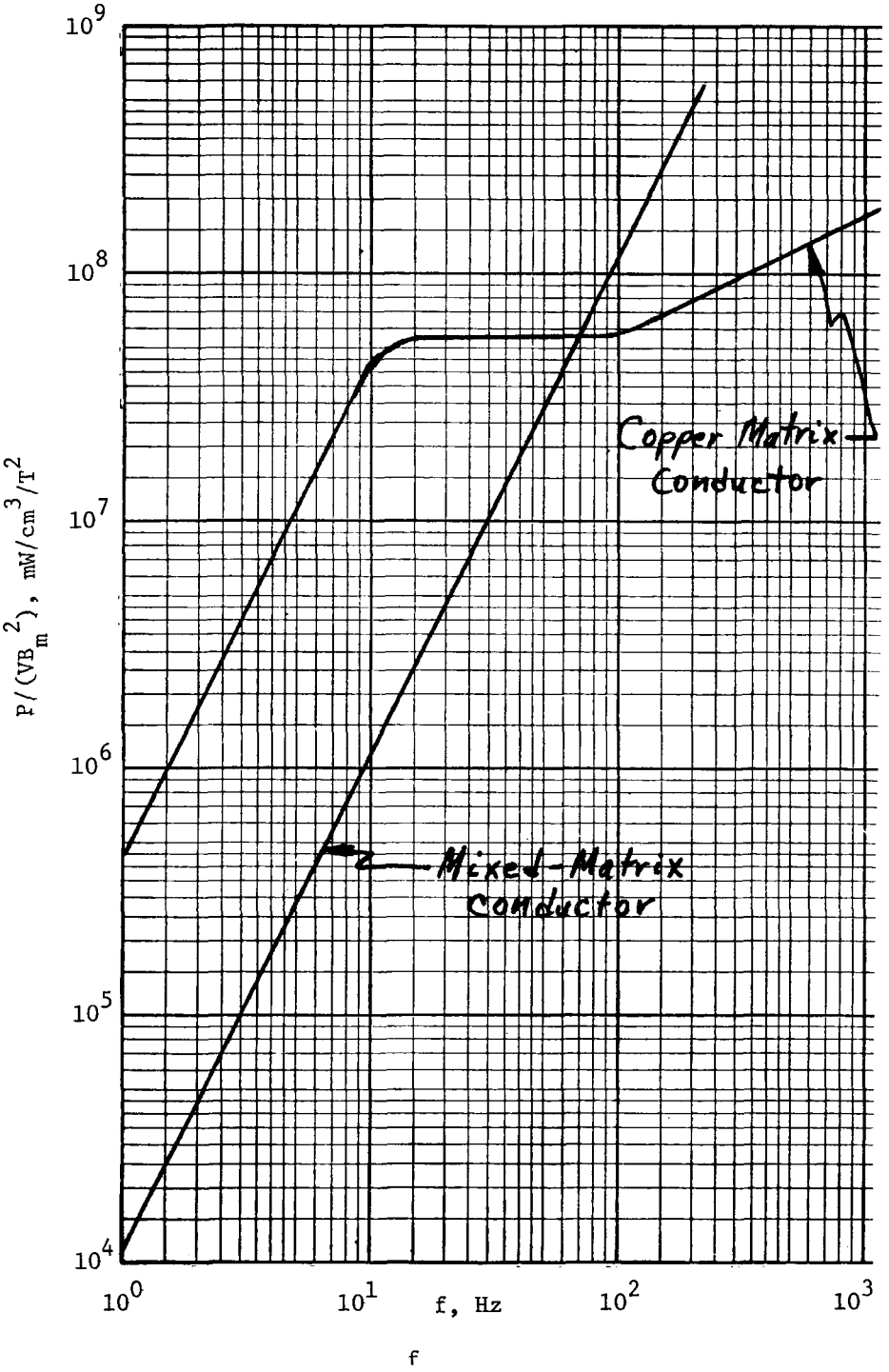

Figure 3-31. Comparison of Losses for Mixed Matrix (Cu:Cu-Ni:NbTi = 2:1.1:1) and Copper Matrix (Cu:NbTi = 2:1) Conductors for 300 MVA machine

in the copper-matrix conductor. A cold magnetic shield which reduces the amplitude of the field due to the damper distortion to an acceptable level for the mixed-matrix monolith will be even slightly more effective for the copper-matrix conductor.

Fault Losses

The losses for this conductor under the fault conditions described earlier are calculated from the following equations and given in Table 3-13. For partial penetration (B_m < 80 gauss):

Eddy Current Losses

$$\left.\begin{aligned} \left(\frac{P_e}{V}\right)_{radial} &= 469\ B_m^{\,2}\ f^2,\ mw/cm^3 \\ \left(\frac{P_e}{V}\right)_{tang.} &= 93\ B_m^{\,2}\ f^2,\ mw/cm^3 \end{aligned}\right\} \qquad (22)$$

Hysteresis Losses

$$\frac{P_h}{V} = 9.5\ (10^4)\ B_m^{\,3}\ f,\ mw/cm^3 \qquad (23)$$

For full penetration (B_m > 80 gauss):

Eddy Current Losses

$$\left.\begin{aligned} \left(\frac{P_e}{V}\right)_{radial} &= 1.1\ (10^3)\ B_m^{\,2}\ f^2,\ mw/cm^3 \\ \left(\frac{P_e}{V}\right)_{tang.} &= 2.1\ (10^2)\ B_m^{\,2}\ f^2,\ mw/cm^3 \end{aligned}\right\} \qquad (24)$$

Hysteresis Losses

$$\left.\begin{aligned} \left(\frac{P_h}{V}\right)_{radial} &= 18\ B_m\ f,\ mw/cm^3 \\ \left(\frac{P_h}{V}\right)_{tang.} &= 12\ B_m\ f,\ mw/cm^3 \end{aligned}\right\} \qquad (25)$$

The total of 2 mJ/cm^3 will yield an adiabatic temperature rise of less than 0.1°K even for 5% helium in the winding. (See Figure 3-29) Thus, the conductor should easily remain superconducting during a fault.

Steady-State Losses

The negative sequence field occurs at 120 Hz which is at the upper end of the shielding region for this conductor. As seen from Figure 3-31 the eddy current losses will be less in the copper conductor than in the mixed-matrix. Thus, the losses are negligible.

Ramp-Up Losses

At 0.1 T/sec we find the eddy current losses from Eq. (24), after replacing $B_m^2 f^2$ by $\dot{B}^2 (2\pi^2)$, to be:

$$\frac{P_e}{V} = 0.56 \text{ mw/cm}^3$$

The hysteresis losses are found from Eq. (25) by replacing $B_m f$ by $\dot{B}/4$.

$$\frac{P_h}{V} = 0.45 \text{ mw/cm}^3$$

Thus, the total loss during a ramp time of 50 sec will yield

$$Q_T = 50 \text{ mJ/cm}^3$$

According to Figure 3-29 the winding temperature will rise by $\sim$ 1°K if there is 10% helium in the winding. This is acceptable and should be an upper limit since the adiabatic approximation is a very conservative one over a 50 sec time span.

A cross-section of the proposed conductor is shown in Figure 3-32 . The corner radius r is shown as 0.92 mm which provides for 10% of the volume to be filled with helium. We recommend this value to allow for the largest margin of safety during a fault.

Nb_3Sn Conductor Design

Multifilamentary Nb_3Sn conductors are presently being made by several manufacturers, both here and abroad. These conductors have not been tested

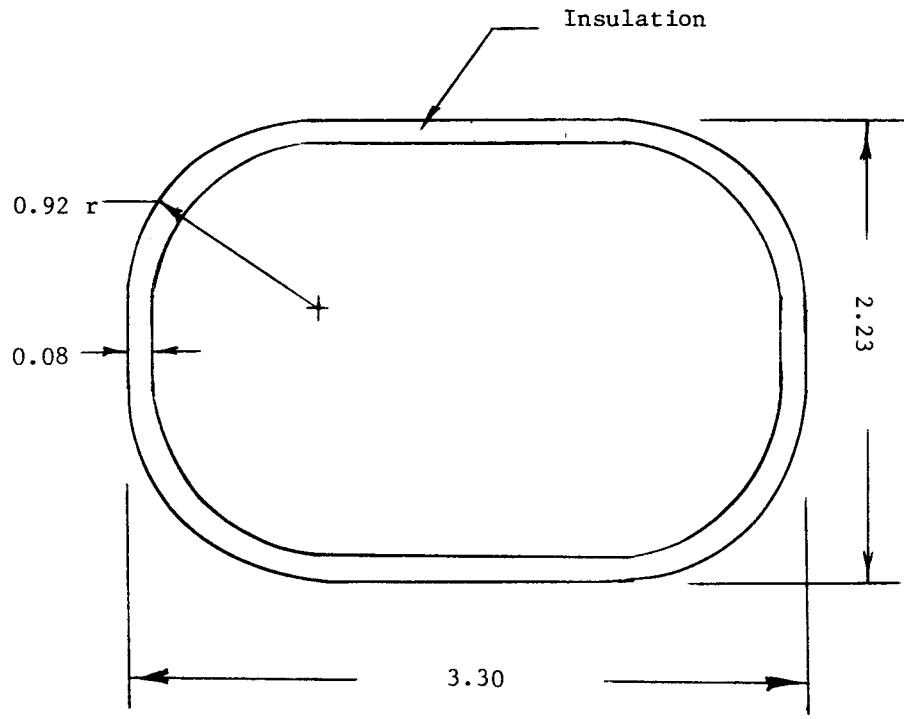

NOTE: Dimensions are in mm.

Figure 3-32. Cross Section of Proposed Copper Matrix NbTi Superconductor

thoroughly in large coil configurations. Some small magnets (1-10 cm size) have been made to operate successfully with critical currents reaching 100% of short sample. Due to the brittleness of Nb_3Sn, some of these small coils are made by the wind and react technique.

Currently, Airco, IGC, and Supercon are under contract to Lawrence Livermore Laboratories to develop techniques for producing high current (10,000 amps), high field Nb_3Sn conductors for use in large fusion reactors. In addition, IGC has a contract with Wright-Patterson to develop multi-filamentary Nb_3Sn for use in future, high power, airborne generators. The progress of all these programs seems to indicate that conductors suitable for use in large generators will be manufactured and tested within the next few years. Accordingly it is reasonable at this time to consider a Nb_3Sn conductor for the 300 MVA machine. The conductors which are discussed in this report are of the type which have been made in limited quantities. Whether they can be manufactured reliably in large enough quantities and whether they can perform reliably in full size coils needs to be determined.

Monolith Design

The NbTi conductor which was described above was designed to have a critical current of 1300A at 5 Tesla and 5.2°K. This allows a temperature rise during fault of $\sim$ 1.4 K from the operating temperature of 3.8°K and an overcurrent of 30%. The result is a conductor with $I_c \simeq$ 2000A at 5 T and 4.2°K. Because the superconducting properties of Nb_3Sn do not degrade as rapidly with temperature as for NbTi, a Nb_3Sn conductor with I_c (5T, 4.2°K) = 2000A would have I_c = 1300A at 7°K and 5 T. This allows a thermal margin of $\sim$ 3.2°K.

Niobium-tin conductors are usually made by putting Nb rods in a bronze billet and then extruding and drawing into wire. The Nb_3Sn is formed on the Nb filaments by reacting the wire at $\sim$ 700°C for several hours. The filaments are usually the order of 2-3 μm in diameter and the Nb_3Sn layer on the filaments is 0.5-1 μm thick. Copper may be added as rods in the original billet but must be protected by a diffusion barrier such as tantalum to prevent the Sn from poisoning the copper during heat treatment.

Manufacturers are currently achieving $j_c = 10^{10}$ A/m^2 in the Nb_3Sn layer at 4.2°K and 5 T. Thus, if we design the 300 MVA conductor to have I_c (5T, 4.2°K) = 2500A we need $2.5(10^{-7})$ m^2 of Nb_3Sn. Taking d = 3 μm and w = 1 μm we have n = 39,789 filaments. This number of filaments requires a double extrusion but is routinely attained. Table 3-14 describes the conductor parameters and gives

values for a 2500 amp conductor. This conductor will have I_c = 1300 A @ 8.3°K giving a thermal margin of 4.5°K.

Table 3-14

Nb_3Sn CONDUCTOR PARAMETERS

Symbol	Description	Value
a,b	Conductor dimensions	1.45 mm, 0.97
2s, 2v	Filament dimensions	3.26 μm, 2.17 μm
n	Number of filaments	39,789
w	Nb_3Sn layer thickness	1 μm
d	Equivalent round filament diameter	3 μm
R_o	Equivalent round cond. dia.	0.67 mm
L	Twist length	1.2 cm
α	Aspect ratio	1.5
I_c(5T, 4.2°K)	Critical current at 5T, 4.2°K	2500 Amps
I_c(5T, 8.3°K)	Critical current at 5T, 8.3°K	1300 Amps
J_c(5T, 4.2°K)	Overall critical current density at 4.2°K and 5T	2×10^9 A/m^2

The minimum bend diameter for bends in the plane of the conductor would be 48.3 cm (19 in.) for 0.2% strain. For bends normal to the plane, the minimum diameter would be 72.4 cm (28.5 in.). Bends tighter than this probably would degrade the critical current of the Nb_3Sn and so this conductor would have to be reacted after winding. Harwell is having a good deal of success making coils this way using an E-glass insulation on the conductor. Winding the coils in modular form, reacting, and then inserting in the rotor would be the procedure to use.

Monolith Losses

Losses are calculated as for the NbTi conductor. The pertinent parameters for this Nb_3Sn conductor are $\sigma_m \simeq 10^8$ mho/m (conductivity of bronze), λ = 0.200 yielding $\sigma_\perp$ = 1.5 (10^8) mho/m. Eddy current losses in the low frequency region are:

Full Penetration

$$\left(\frac{P_e}{V}\right)_{radial} = 1.31\ \dot{B}^2 \text{ mW/cm}^3$$

$$= 25.9\ f^2\ B_m^{\ 2} \text{ mW/cm}^3$$

$$\left(\frac{P_e}{V}\right)_{tang.} = 0.28\ \dot{B}^2\ mW/cm^3$$

$$= 5.5\ f^2\ B_m^{\ 2}\ mW/cm^3$$

$$\left(\frac{P_h}{V}\right)_{radial} = 4.08\ \dot{B}\ mW/cm^3$$

$$= 16.3\ B_m\ f\ mW/cm^3$$

$$\left(\frac{P_h}{V}\right)_{tang} = 2.72\ \dot{B}\ mW/cm^3$$

$$= 10.9\ B_m\ f\ mW/cm^3$$

Partial Penetration

$$\left(\frac{P_e}{V}\right)_{radial} = 16.6\ f^2\ B_m^{\ 2}\ mW/cm^3$$

$$\left(\frac{P_e}{V}\right)_{tang.} = 3.5\ f^2\ B_m^{\ 2}\ mW/cm^3$$

$$\left(\frac{P_h}{V}\right) = 3.8\ (10^4)\ B_m^{\ 3}\ f\ mW/cm^3$$

Thus, the losses during a fault for the various transient fields which occur are given in Table 3-15.

Table 3-15

LOSSES DUE TO TRANSIENT FIELDS CREATED BY A 66 msec FAULT
(Nb_3Sn Monolith)

LOSS TYPE/ TRANSIENT EFFECT	A	B	C	D	A + B + C + D
Hyst (mW/cm^3)	2.9	N	N	0.02	
Eddy (mW/cm^3)	0.7	N	N	0.004	
Total (mW/cm^3)	3.6	N	N	0.024	
Total Heat Input (mJ/cm^3)	0.24	N	N	0.014	0.25

N = Negligible

The total heat input is roughly the same as for the NbTi monolith described above using $Cu_{0.7}Ni_{0.3}$ in the matrix. The value of 0.25 mJ/cm^3 will yield $\Delta T < 0.1°K$ for 10% helium in the winding. Since we have allowed a $\Delta T = 4.5°K$, we find this conductor to be quite stable during a fault.

REFERENCES

1. For a review see, M.S. Walker, J.H. Murphy, and W.J. Carr, Jr., Proceedings of the Fifth International Magnet Technology Conference, Rome, Italy, April 1975 and references therein.
2. J.H. Murphy, W.J. Carr, Jr., and M.S. Walker, IEEE Transactions MAG 10, p. 868 (1974).
3. W.J. Carr, Jr., M.S. Walker, and J.H. Murphy, J. Appl. Phys. 46. 4048 (1975).
4. W.J. Carr, Jr., Phys. Rev. B. 11, 1547 (1975); W.J. Carr, Jr., JPA, 46, 4043 (1975); W.J. Carr, Jr., J. Appl. Phys. 45. 020 and 935 (1974).
5. M.S. Walker, J.H. Murphy, and W.J. Carr, Jr., Papers S-1 through S-3, Proc. of the Applied Superconductivity Conf., Oakbrook, Illinois, October 1974, IEEE Trans. MAG-11, 309-320.
6. M.S. Walker, W.J. Carr, Jr., and J.H. Murphy, IEEE Trans. MAG-11, 1475 (1975).
7. J.H. Murphy, W.J. Carr, Jr., M.S. Walker, and P.D. Vecchio, "Field Orientation Dependence of Losses in Rectangular Multifilament Conductors," to be published in the Proceedings of the International Cryogenic Materials Conference, Kingston, Ontario (July 1975).
8. J.H. Murphy and W.J. Carr, Jr., "Eddy Current Losses in Twisted Multifilamentary Superconductors - Part I," Westinghouse Paper 73-9J2-MACON-P3.
9. M.S. Walker and J.H. Murphy, "Superconducting Windings," Final Report, Office of Naval Research Contract N00014-73-C-0461 (with corrections, December 1975).
10. J.H. Murphy and M.S. Walker, "Losses in Superconductors for the Energy Doubler," Fermi National Accelerator Laboratory, No. 50213.
11. J.H. Murphy, D.W. Deis, B.J. Shaw, and M.S. Walker, IEEE Trans. on Magnetics, Vol. MAG-11, #2, March 1975, p. 317.
12. The work has been discussed recently at the Symposium on Stress Effects in Superconductors, Third NBS/ARPA Workshop, Vail, Colorado, April 1976.

Damper Application

Damper windings used in superconducting turbine generators must meet somewhat more critical design requirements than those applied to machines of conventional design. The design objectives that relate to transient as well as to steady-state operating conditions were listed in Tables 3-11A and 3-11B above.

Amongst these requirements, adequate shielding of the field winding and its cryogenic environment is imperative. It is essential to the maintenance of superconductivity, and hence to the operation of the machine. One requirement for successful damper application is thus to provide sufficient shielding so that the propagation of electromagnetic disturbances into the field winding zone is limited to levels that can be handled by the helium management system and the superconductor design.

Transient as well as steady-state magnetic fields may penetrate past the damper by the usual process of electromagnetic diffusion.[1-6] They may also propagate by an electromechanical interaction involving the displacement of parts of the rotor structure.[7] An analysis of the effects on the field winding containment must take all possible mechanisms into account.

The damper arrangement must not only limit the propagation of fields and electromechanical effects into the cryogenic zone, but must also provide sufficient damping for machine-system interactions to assure stability of the machine with respect to the system. To some extent, these requirements conflict, inasmuch as damper parameters that favor isolation of the field winding tend to result in reduced damping of system disturbances.[10, 12-13] The present studies indicate that successful compromise solutions can be based on the use of no more than two damper shells, one located in the room temperature zone, and the other at or near the temperature of the field winding.

The physical arrangement that is used to accomplish this purpose consists of one or more damper structures, which are typically cylindrical shells of conducting material placed concentric with the rotor axis and supported by means of the rotor mechanical structure. See Figure 3-33. Consideration has been given to dampers made in the form of polyphase windings,[8] but there appears to be insufficient justification for this, which would increase the cost and structural problems of the rotor.

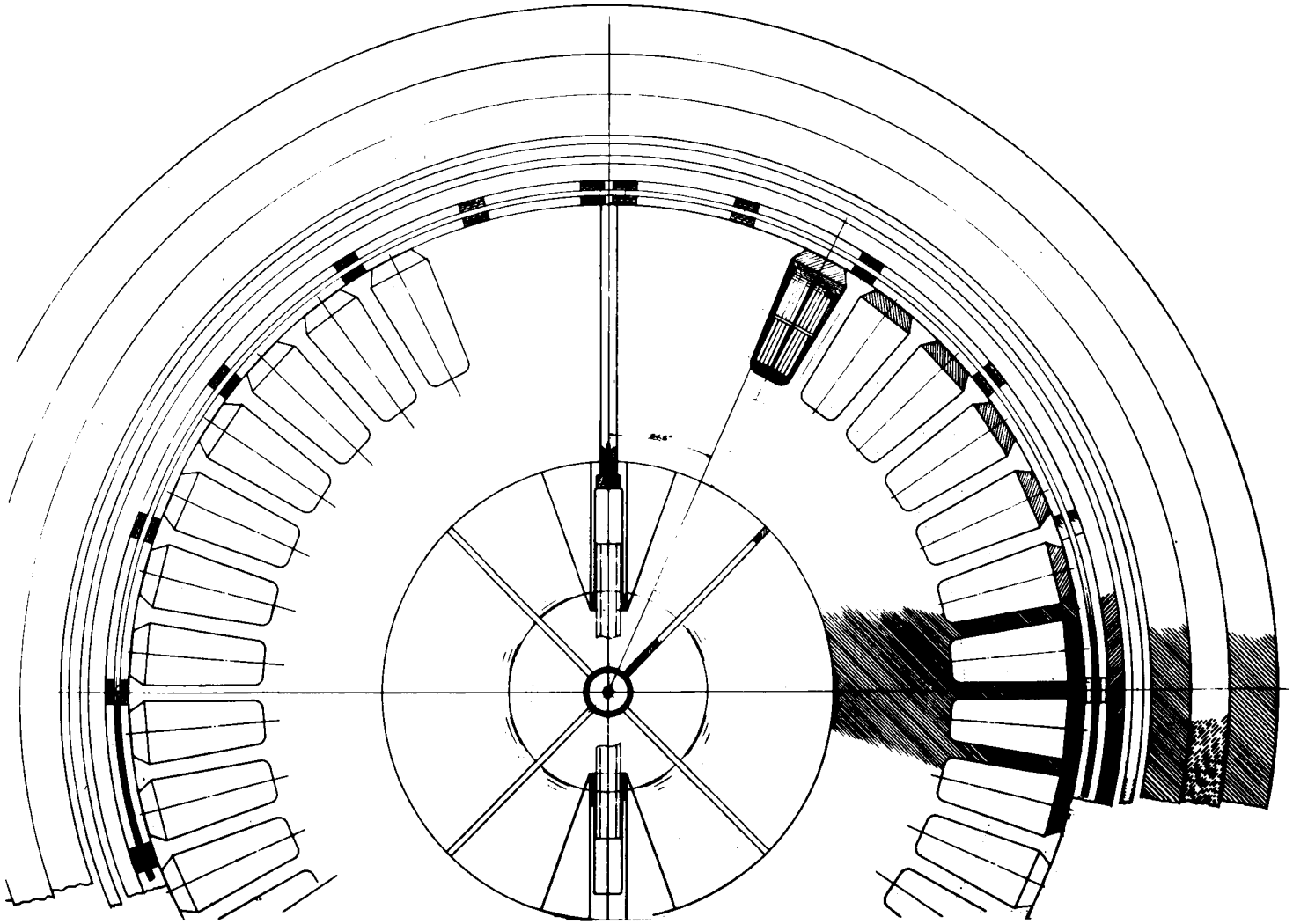

Figure 3-33. Cross Section of Superconducting Rotor Illustrating Cold and Warm Damper Provisions

Because the structural support for the damper must resist the forces and torques that the damper experiences due to electromagnetic interactions, which can be severe, consideration has been given to special constructions of damper supports or field winding supports that permit rotation of the damper or the field winding during fault conditions.[9-11] These concepts were evaluated during the present studies, and it was concluded that the problems introduced by the required complex mechanical support could not, at this time, be solved with adequate expectation of high reliability. A solid support arrangement for the damper(s) was selected.

Consideration has been given to dampers located in the following manner:

- Low-temperature dampers located in the cryogenic environment at a few to several tens °K
- Room-temperature dampers located in the warm part of the rotor outside the radiation shield and thermal isolation of the field winding
- Combinations of both.

As described above, original design work proceeded on the basis of a single room-temperature damper which appeared to provide enough isolation to keep losses in the field winding support structure acceptably low. Further calculations, however, indicated problems with losses in the superconductor. Moreover, the achievement of acceptable structural losses entailed compromises in the design of the mechanical support for the field winding. The addition of a second low-temperature or "cold" damper at the outer periphery of the field winding support cylinder overcame this difficulty, and has permitted the use of an acceptable monolithic superconductor as well as of an integral field winding support in which the conductors are tightly contained in slots machined to close tolerances. This construction is shown in Figure 3-33.

Analysis of Damper Performance

The basic electromagnetic problem of shielding by conducting shells has received attention for many years.[1, 18-19] Applications to the theory of rotating electrical machines have not been extensive, however, since solid cylindrical structures of appreciable thickness have not found too many applications in rotating machines of conventional types. Even some of these applications have been analyzed by other means. Superconducting generator design therefore required an extension of the analysis, particularly since dampers made up of two or more concentric shells are under consideration. The present studies have extended the theory of shielding and losses for double-shell arrangements. The results are stated subsequently in this section.

The propagation of electromagnetic disturbances past the damper through electromechanical effects involving its physical displacement is unique to superconducting machines. Although similar forces exist in conventional machines at the surface of the rotor, the rigidity of the rotor structure prevents any significant displacement. The forces leading to this deformation of the damper support structure arise normal to the damper surface during fault conditions. An analysis of these effects has been made, and it has been found that the "crushing" of the damper produces flux compression effects at the outer periphery of the field winding which lead to heating that can contribute a major part of the total heat input to the cryogenic environment. This important effect was studied in detail. It constitutes a design restraint that affects the overall rotor design with respect to the mechanical support requirements as well as the choice which led to selection of a double damper arrangement.

The induction of losses in the cryogenic environment by diffusion and by electromechanical effects has been studied by means of an approximate analysis that resolves the complex interactions taking place during a transient into a number of discrete "events" which are assumed to take place independently. The losses due to each of these effects are summed to obtain the total losses liberated to the cryogenic environment. This analysis is also reported in this section.

Steady State Conditions

During steady state operating conditions, the damper acts primarily as an electromagnetic shield for the field winding and its support structure. It shields these parts against alternating magnetic fields which would otherwise produce losses therein. These fields include the space harmonics produced by the armature winding as well as any negative sequence field that may be present as a result of the imbalance of the armature phase currents. Such an imbalance can occur on normal electric utility systems. It can be produced, for example, by the presence of untransposed or imperfectly transposed transmission lines. ANSI Standard C50.13 defines the minimum negative sequence current of which turbine generators in the size range up to 1500 MVA must be capable. Numerical values are given in Table 3-11A. The objective of these studies has been to attain a degree of negative sequence capability over and above that required by ANSI Standards. This has been accomplished.

Of the above-mentioned fields, the negative sequence field is potentially the largest and most important. With stator windings that can be designed to approximate sinusoidal distribution of the fundamental MMF very closely, the

harmonics of the MMF wave can be reduced to very small amplitudes. The negative sequence wave is, however, determined by system conditions and not within control of the designer. It can therefore be expected that the shielding requirements for steady-state operation will be primarily determined by the required negative sequence capability.

The exclusion of magnetic fields from the interior of the rotor is a function of the attenuation factor of the damper shield.[1, 6] The attenuation factor has been calculated over a range of dimensions for copper alloy of 80% of the conductivity of copper at 350°K and for frequencies corresponding to negative sequence and to the first four non-vanishing harmonics of the stator MMF. These are the 5th, 7th, 11th and 13th harmonics. Each pair of adjacent harmonics produces a reaction on the rotor at a frequency which is equal to their average order multiplied by line frequency and modulated by a spacial distribution which depends on their relative magnitudes.

Consider, for example, the pair of 5th and 7th harmonics:

$$B = C_5[i_a \cos 5\theta_s + i_b \cos 5(\theta_s - 120) + i_c \cos 5(\theta_s + 120)]$$

$$+ C_7[i_a \cos 7_s + i_b \cos 7(\theta_s - 120) + i_c \cos 7(\theta_s + 120)]$$

where θ_s is a reference angle around the air gap in the stator reference frame.

For fundamental armature currents

$$i_a = I \cos \omega t \quad i_b = I \cos(\omega t - 120) \quad i_c = I \cos(\omega t + 120)$$

then

$$B = \frac{3C_5 I}{4} \cos(5\theta_s + \omega t) + \frac{3C_7 I}{4} \cos(7\theta_s - \omega t)$$

If we now re-express this field in the rotor reference frame for a 2-pole machine

$$\theta_s = \omega t + \theta_r$$

then

$$B = \frac{3C_5 I}{4} \cos(6\omega t + 5\theta_r) + \frac{3C_7 I}{4} \cos(6\omega t + 7\theta_r)$$

Now if the amplitudes of the harmonics are assumed equal (in general they are not) then

$$B = \frac{3C_5 I}{2} [\cos(6\omega t + 6\theta_r) \cdot \cos \theta_r]$$

Then the field varies at 6 times line frequency but has a twelve pole MMF modulated by a two pole spatial wave.

The limiting equations for calculating the attenuation factor and losses in an isolated damper cylinder are listed in Table 3-16. The results for calculations of the attenuation factor in the thick shell limit are plotted in Figures 3-34, 3-35, and 3-36. It will be observed that attenuations down to 1/1000 or less of the incident MMF can be obtained with a warm damper and practical values of thickness of conducting material. Attenuation improves for a given thickness of conducting material with increasing inner radius, so that for the same attenuation it is possible to reduce the thickness as the radius increases.

In producing this attenuation, the damper shield and its supporting structure experience losses which must be continuously dissipated. The losses in the damper proper are an inevitable consequence of its shielding function. The losses in the support structure are, however parasitic. They can be reduced with careful design.

The warm damper proposed in these studies is of composite construction, with the high-conductivity material sandwiched between two layers of structural support material. The outer layer of support material is exposed to the magnetic fields before these can be attenuated by the damper. The inner support is shielded by the damper, and its losses may be considered negligible. Fortunately, the presence of the damper material substantially reduces the losses in the support shell, if this is of moderate thickness and high resistivity. The loss reduction in a cylindrical shell produced by the presence of an internal, highly conductive cylinder is significant. This effect was first derived by postulating the internal cylinder to be of infinite conductivity. At a later date, the derivation was generalized to an inner cylinder of arbitrary conductivity and permeability. These derivations and results are stated in the following. They provide the means for calculating the losses in the component parts of the damper system and in cylindrical support shells used in the rotor structure. Thus, they permit evaluation of the steady-state heating and of continuous negative-sequence current capability. These results have also been used for approximate evaluations of losses under transient conditions, using a quasi-static (AC) simulation. This includes evaluation of the $I_2^2 t$ capability.

Table 3-16

DAMPER SHIELD EQUATIONS

STEADY STATE DAMPER SHIELD EQUATIONS

CASE	TYPE	ATTENUATION (MAGNITUDE)	TIME-AVERAGE POWER DISSIPATION
1	Thin Damper	$\frac{1}{\{1 + [(\omega)T_{sn}]^2\}^{1/2}}$	$\frac{2\pi\mu_o}{n} \frac{R^2}{[1 \pm (\frac{R}{T})^2]} \frac{1}{T_{sn}} \frac{[(\omega)T_{sn}]^2}{\lvert 1 + [(\omega)T_{sn}]^2 \rvert} \ell H_o^2$
	$\delta > \Delta$	$T_{sn} = \frac{1}{2} \frac{\Delta\sigma\mu_o}{n} R[1 \pm (\frac{R}{T})^2 n]$	
2	Thick Damper	$2\sqrt{2} \frac{\delta}{R} e^{-\frac{\Delta}{\delta}}$	$\frac{4\pi\ell}{\sigma\delta} \frac{R}{[1 \pm (\frac{R}{T})^{2n}]^2} H_o^2$
	$\delta < \Delta$	$\delta = (2/\omega\sigma\mu_o)^{1/2}$	
3	Thin Shell with Internal Damping Cylinder	$\tau = \frac{\mu_o \sigma d R_s}{2n} [1 - (R/R_s)^{2n}]$	$\frac{2\pi R_s}{\sigma d} \frac{(\omega\tau)^2}{1 + (\omega\tau)^2} H_o^2$

Note: ω is angular frequency relative to rotor surface and n is the order of space harmonic, also relative to to the rotor surface.

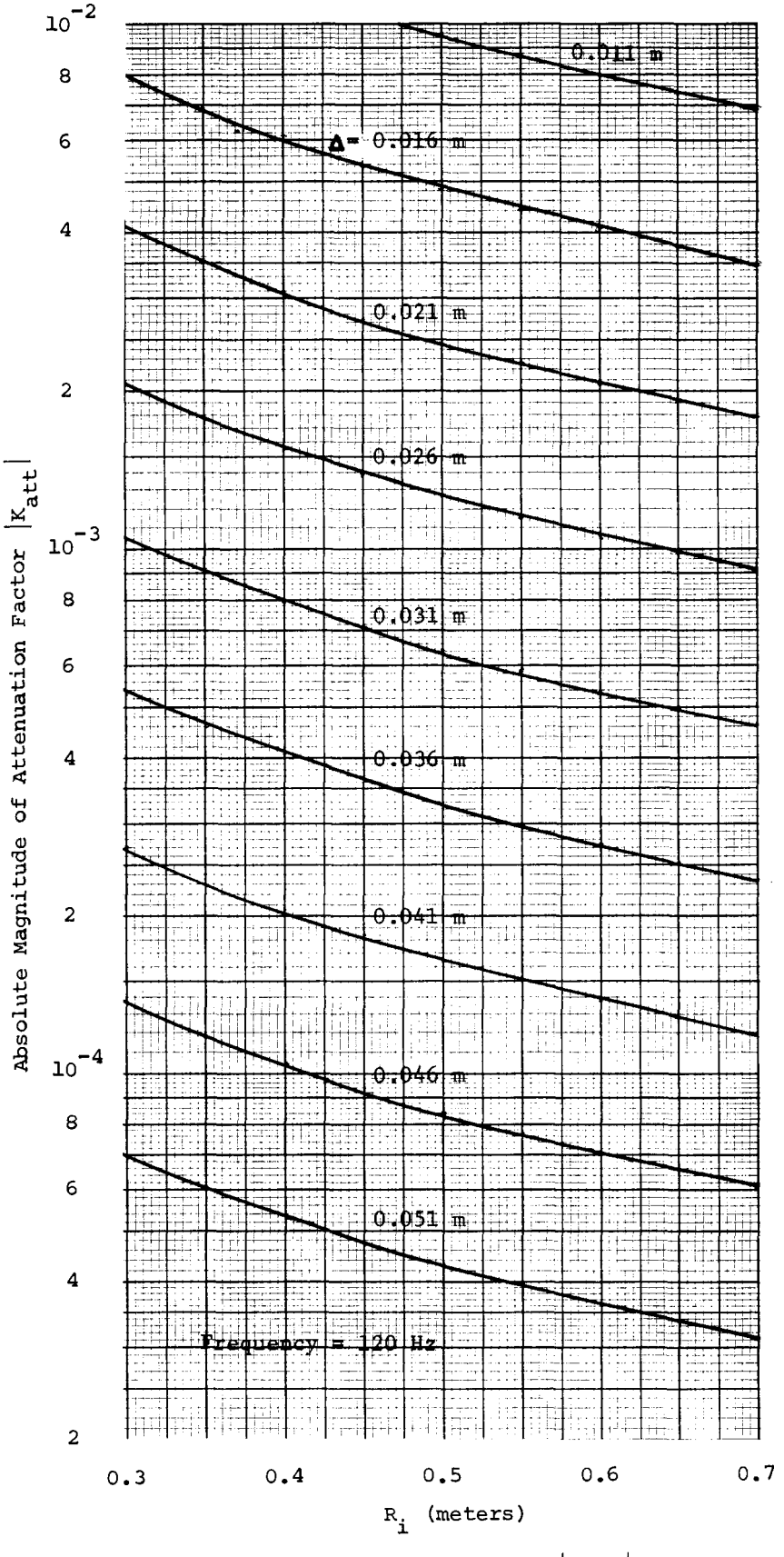

Figure 3-34. Attenuation Factor $|K_{att}|$ vs. Inner Radius R_i and Thickness Δ of Damper

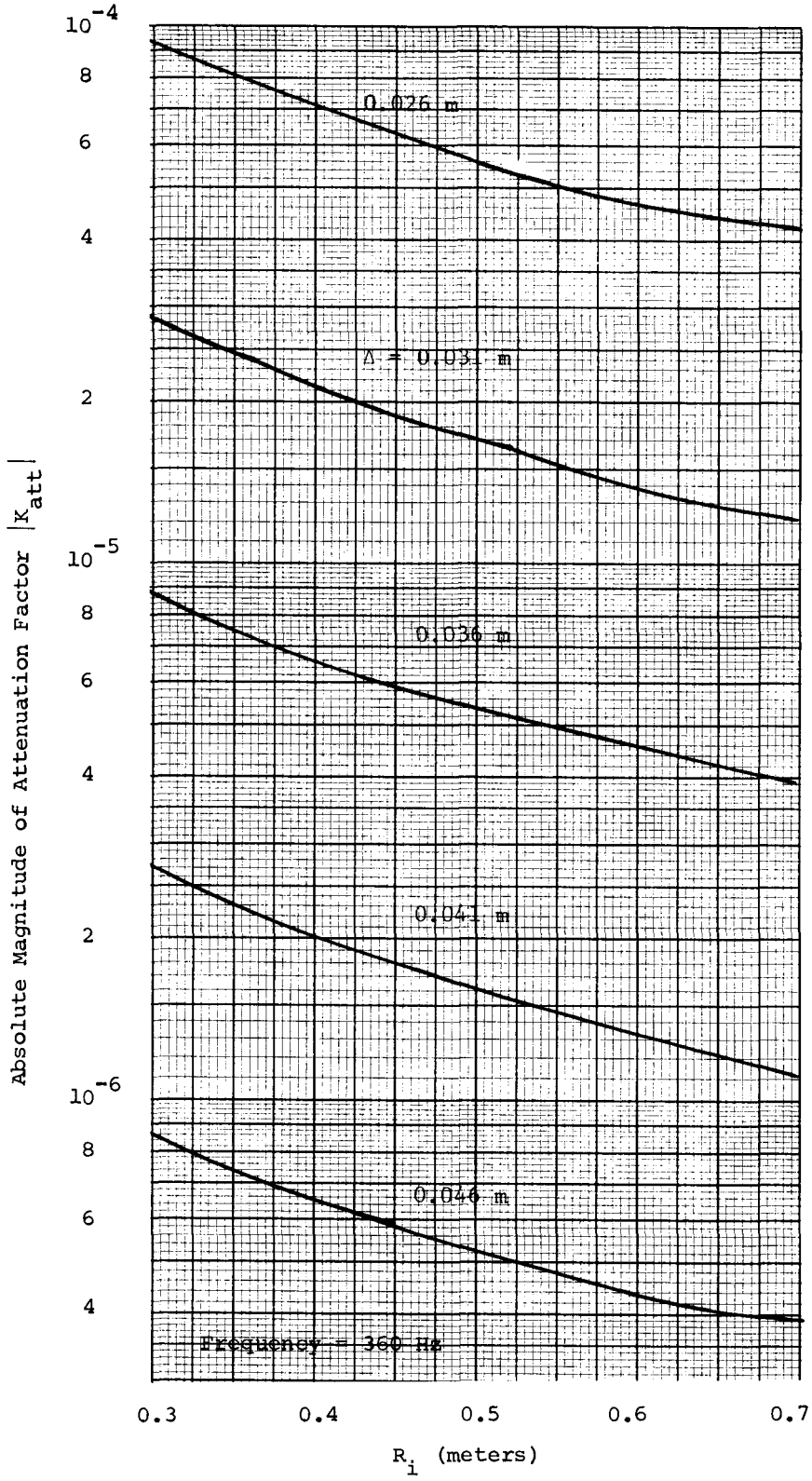

Figure 3-35. Attenuation Factor $|K_{att}|$ vs. Inner Radius R_i and Thickness Δ of Damper

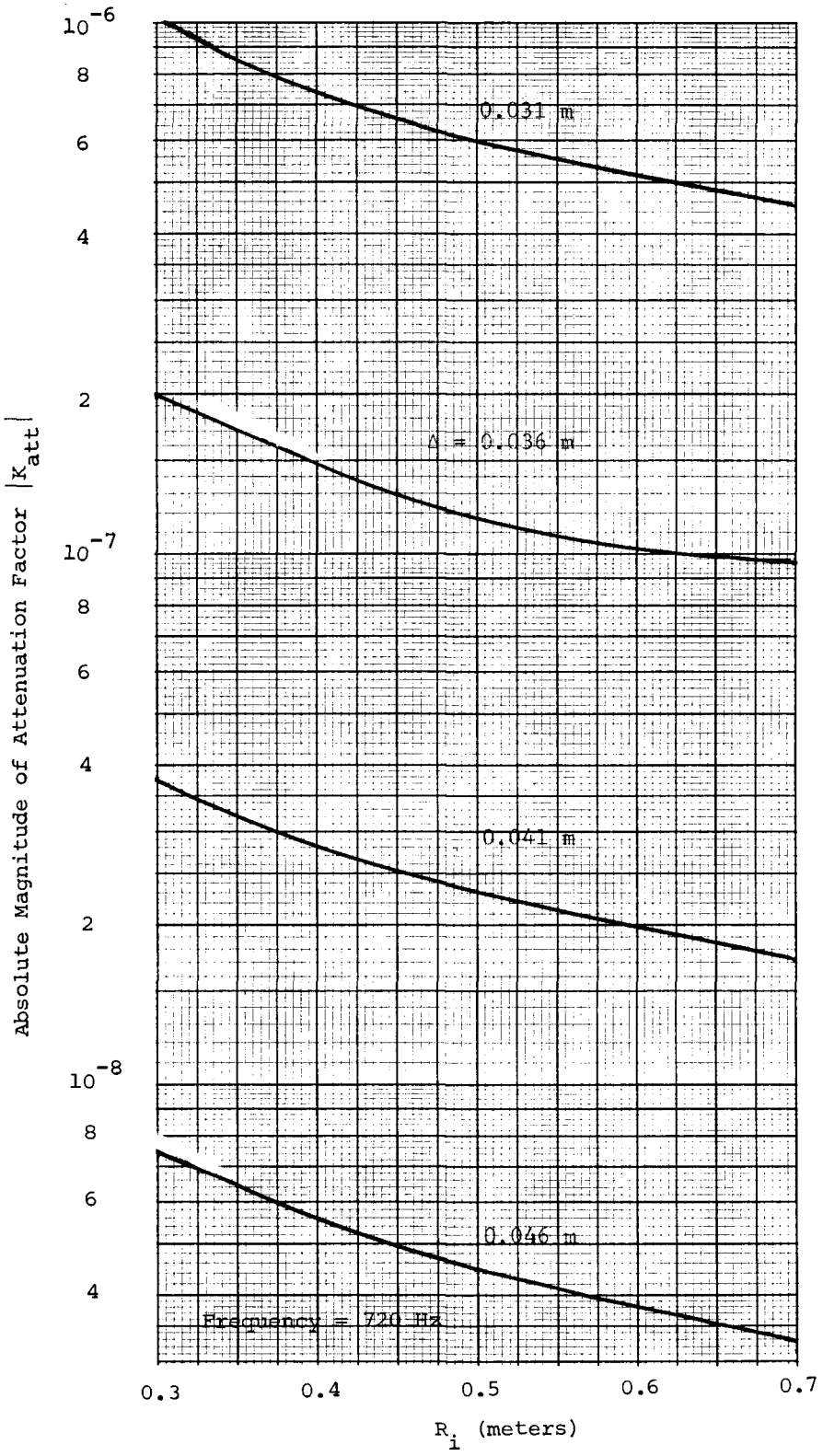

Figure 3-36. Attenuation Factor $|K_{att}|$ vs. Inner Radius R_i and Thickness Δ of Damper

The losses in structural support parts can be reduced by

- Improved shielding
- Subdivision of the eddy current paths

For the outer support of the warm damper, this can be done by grooving the support shell with parallel peripheral grooves, or even by subdividing it into separate support rings.

Derivation of Loss in Structural Shell

In order to evaluate the losses in the Inconel structural shell outside the damper shield, it is necessary to include a consideration of the damper shield current. Because the skin depth in Inconel is large compared to the thickness of the shell, it can be modeled as a current sheet. Because the skin depth in copper is small compared to the damper shield thickness, it can be modeled as an infinitely conducting boundary. The fields both inside and outside the structural shell are found by taking solutions to LaPlace's equation in cylindrical coordinates. Boundary conditions are then applied at the radii of the two shells in order to solve for the constants in the field solutions. Finally, Maxwell's equation

$$\nabla \times \underline{E} = - \frac{\partial \underline{B}}{\partial t}$$

is applied in the one dimensional geometry of the structural shell to find the last constant.

The electric field is found from the relationship

$$\underline{K} = \Sigma \underline{E}$$

and the loss is found by integrating $\frac{1}{2} \sigma E^2$ over the volume of the shell. (The model of the structural shell as a current sheet implies that there is no radial variation in E through the shell.)

A complete derivation of the loss is to be found in Appendix II of the First Quarterly Report as well as in the Preliminary Draft of the Final Report. The results of this derivation give the loss as:

$$P/\ell = \frac{(\omega\tau)^2}{1 + (\omega\tau)^2} \quad \frac{2 \pi R_s}{\sigma d} H_o^2$$

$$\tau = \frac{\mu_o \sigma d R_s}{2n} \left[1 - (R/R_s)^{2n}\right]$$

Double-Shell Damper Model

The damper and support construction actually used in the designs utilizes several concentric shells of different conductivities, some of which are intimately bonded. A more precise model was analyzed to simulate this construction.

The configuration studied is shown in Figure 3-37. This is a two dimensional analysis, with no variation in the z direction. The permeability of the iron shield is considered to be infinite. All other regions are considered as free space. The conductivities of the two shells may be independently specified, while all other regions have no conductivity. The number of poles, n, the frequency ω, and the amplitude, K_o, of the current sheet may all be specified.

The complete derivation is given in Quarterly Report No. 2 as well as in the Preliminary Draft of the Final Report. The resulting expressions for power dissipation (for large arguments of Bessel functions used in the derivation) are:

$$\frac{P}{l} = \frac{\pi R_4 \left(\frac{R_4}{R_a}\right)^{2n-2} \left[1 + \left(\frac{R_a}{R_s}\right)^{2n}\right]^2 K_o^2}{2\sigma_o \delta_o \left[1 + \left(\frac{R_4}{R_s}\right)^{2n}\right]^2} \quad \frac{\sinh 2\frac{d_o}{\delta_o} + \sin 2\frac{d_o}{\delta_o}}{\cosh 2\frac{d_o}{\delta_o} - \cos 2\frac{d_o}{\delta_o}} \qquad (1)$$

for the outer shell, and

$$\frac{P}{l} = \frac{2\pi R_2 R_4 \delta_i n^2 (R_2 R_4 / R_3 R_a)^{2n-2} \left[1 + \left(\frac{R_a}{R_s}\right)^{2n}\right]^2 K_o^2}{R_3^3 \sigma_o \left[1 - \left(\frac{R_2}{R_3}\right)^{2n}\right]^2 \left[1 + \left(\frac{R_4}{R_s}\right)^{2n}\right]^2}$$

$$\times \frac{\sinh 2\frac{d_i}{\delta_i} + \sin 2\frac{d_i}{\delta_i}}{\left(\cosh s\frac{d_o}{\delta_o} - \cos 2\frac{d_o}{\delta_o}\right)\left(\cosh 2\frac{d_i}{\delta_o} - \cos 2\frac{d_i}{\delta_i}\right)} \qquad (2)$$

for the inner shell.

Where

$d_o = R_4 - R_3$ = thickness of outer shell

$\delta_o = \left[\frac{2}{\mu_o \sigma_o \omega}\right]^{1/2}$ = skin depth is outer shell

$d_i = R_2 - R_1$ = thickness of inner shell

$\delta_i = \left[\frac{2}{\mu_o \sigma_i \omega}\right]^{1/2}$ = skin depth in inner shell

A computer program which evaluates the Bessel functions and finds the loss by integration was used for detailed calculations of damper performance.

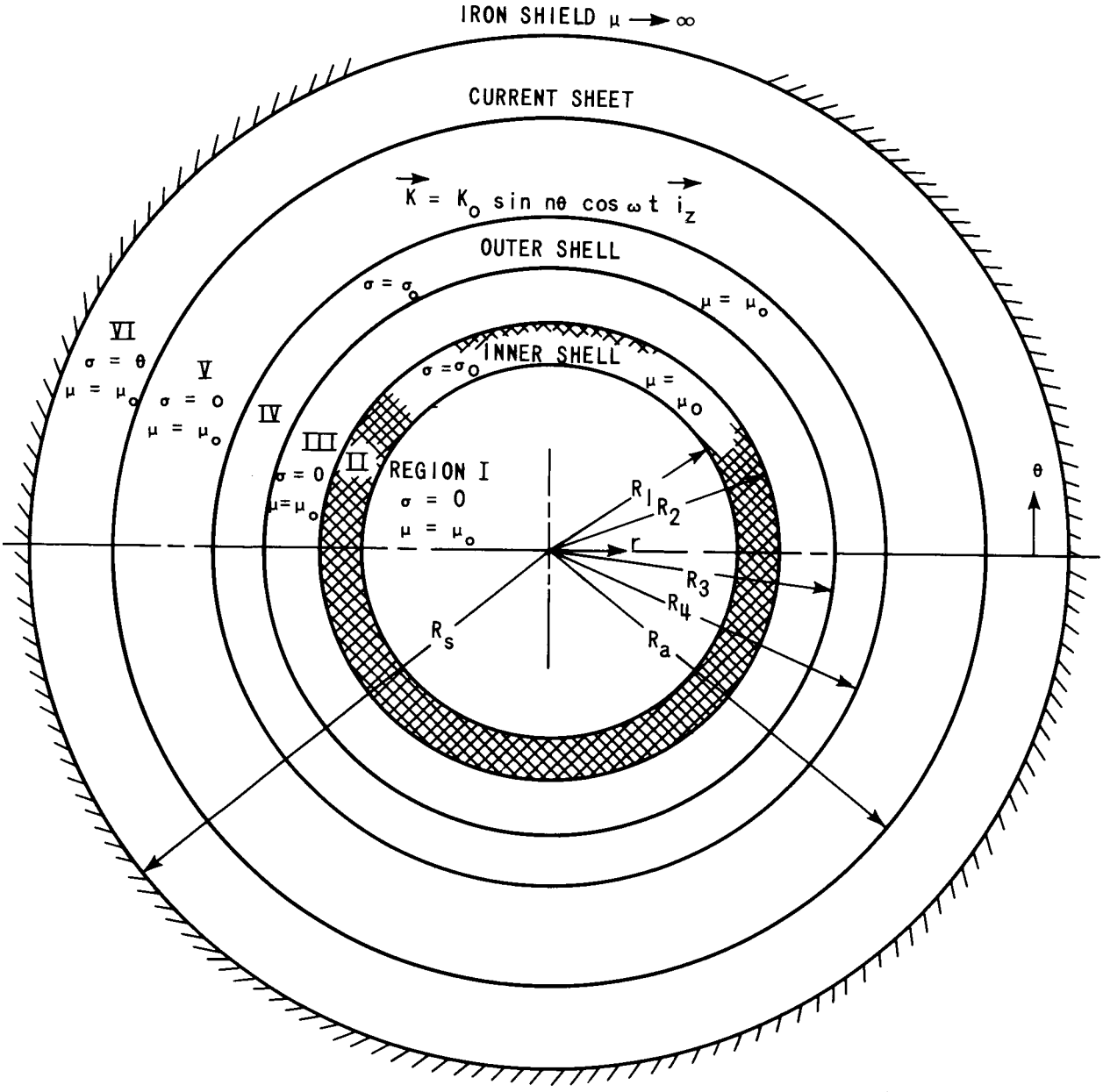

Figure 3-37. Two-Shell Configuration Diagram

As might be expected, the loss in the outer shell is independent of the inner shell if the outer shell is "thick".

Thermal Design of Damper for Steady-State and Transient Conditions

Section 3.2, under "General Introduction and Requirements", makes note of the interest of the electric utility industry in improved negative sequence capabilities for I_2 and I_2^2t. This interest is also reflected in the EPRI requirements for RP-429-1. The limits on negative sequence capability are primarily thermal; i.e., the damper and its support structure must be protected against excess temperature rise during transient as well as during steady state conditions. Using the results of the double-shell damper model analysis given in the above, losses were calculated for the eight designs (designated A through G) which are tabulated in Section 3.1. These losses were then used to study heating effects in the damper and its support structure, as follows:

I_2^2t Heating: It was assumed that all heat liberated during the transient interval for which the I_2^2t limit applies would be stored in the thermal capacity of the damper and its outer support. It was further assumed that the heat liberated in the support structure must be stored there, and that no transfer takes place across the damper-support interface. Since, in all cases, the damper rise is substantially lower than the rise of the support structure, this is a pessimistic assumption, and the capability of the composite would be expected to be somewhat greater than that determined on the basis of these assumptions. The results of this calculation are listed in Table 3-17. They show that it is feasible to assign an I_2^2t capability of 20 to the 300 MVA designs and of 15 to the 1200 MVA designs. These values are twice those required for conventional generators.

The physical constants used in the above calculation are:

- Conductivity of damper material: 80% of copper conductivity
- Conductivity of support material: 2% of copper conductivity
- Specific heat of damper material: 400 J/kg-°K
- Specific heat of support material: 452 J/kg-°K

I_2 Heating: It is assumed that all heat liberated due to the flow of continuous negative sequence currents in the damper and its support structure will be liberated to cooling gas from the peripheral surface of the support. This surface is part of the annular region of the gap. The design equations for pressure drop and heat transfer coefficient in an annular region between cylindrical surfaces are:

Table 3-17

DETERMINATION OF I_2^2t CAPABILITY

GENERATOR DESIGNATION	A	B	C	D	E	F	G	H
MVA	300	300	300	300	1200	1200	1200	1200
Radius R_1 * m	0.3493	0.3493	0.3493	0.3493	0.4636	0.4636	0.4604	0.4604
Radius R_2 * m	0.3810	0.3810	0.3810	0.3810	0.4953	0.4953	0.4921	0.4921
Radius R_3 * m	0.3810	0.3810	0.3810	0.3810	0.4953	0.4953	0.4921	0.4921
Radius R_4 * m	0.4907	0.4907	0.4907	0.4907	0.5461	0.5334	0.5207	0.5207
Radius R_a * m	0.4978	0.4978	0.5418	0.5334	0.6477	0.6350	0.6629	0.6629
Radius R_s * m	0.6477	0.6777	0.8930	0.8890	0.8560	0.8865	1.152	1.195
K_o Amperes/m	249244	382335	224417	369641	277559	459806	293901	469952
LOSSES IN MW/m								
Damper	0.2212	0.5104	0.1728	0.4616	0.1462	0.6818	0.3630	0.9158
Support	0.9168	2.1160	0.7160	1.9140	3.1380	6.2300	1.4860	2.7500
HEAT LIBERATION IN MJ/m FOR I_2^2t								
I_2^2t	20	20	20	20	15	15	15	15
Damper	4.4240	10.2100	2.4540	9.2320	2.1800	10.2300	5.4460	13.7380
Support	18.3360	42.3200	14.3200	38.2800	62.7600	93.4600	29.7200	56.2600
LINEAR MASS DENSITY, kg/m								
Damper	645.2	645.2	645.2	645.2	847.1	847.1	841.5	841.5
Support	558.4	558.4	558.4	558.4	1301.8	964.5	712.2	712.2
TEMPERATURE RISE, °K								
Damper	17.2	39.6	13.4	35.8	6.4	30.2	16.2	40.8
Support	72.6	167.6	56.8	151.6	80.0	214.4	69.2	173.0

*See Figure

$$f_z = \frac{0.3164}{Re_z^{.25}} (1 + 2(Re_p/Re_z)^2)^{0.35}$$

and

$$h = \frac{kf_z}{16b} Re_z \, Pr^{0.333}$$

where

Re_z = Reynolds number for flow in axial direction

Re_p = Reynolds number for peripheral velocity

f_z = friction factor for axial flow

k = thermal conductivity

b = length of annular gap

Pr = Prandtl number.

Assuming the use of high-purity hydrogen gas for gap ventilation (as is done in nearly all types of conventional machine designs), the data for the temperature rise of the damper support surface can be calculated and collected. These data are tabulated in Table 3-18 and show that with respect to I_2 capability the superconducting turbine generator also performs better than is required by ANSI standards for conventional turbine generators. The improvement is about 50% in this case.

Table 3-18

DETERMINATION OF I_2 CAPABILITY - HYDROGEN PRESSURE 30 PSIG

GENERATOR DESIGNATION	A	B	C	D	E	F	G	H
Windage Loss, kW	30.22	23.77	45.92	33.10	159.02	110.92	191.17	145.00
Negative Sequence Current I_2, per unit	0.12	0.12	0.12	0.12	0.10	0.10	0.10	0.10
Damper Loss Intensity, kW/m	16.38	37.82	12.80	34.18	32.84	69.12	18.50	46.66
Damper Length, m	4.45	3.81	5.46	4.42	8.46	6.60	9.87	7.72
Damper Loss, kW	72.90	144.1	69.88	151.1	277.8	456.2	182.5	360.2
Total Loss in Annulus	103.1	181.9	115.8	184.2	436.8	567.1	373.7	505.2
Total Gas Flow, m^3/sec	2.05	2.05	2.05	2.05	6.0	6.0	5.1	5.1
Axial Velocity in Gap, m/sec	40.85	40.85	40.85	40.85	67.27	68.84	59.91	59.91
Re_z	39348	39348	39348	39348	86396	88421	76943	76493
Re_p	74389	74389	74389	74389	132207	129132	126058	126058
f_z	0.047	0.047	0.047	0.047	0.034	0.033	0.036	0.036
h	773.3	773.3	773.3	773.3	920.5	909.7	880.7	880.7
Surface Rise, °K	8.2	19.0	7.4	17.2	16.0	34.2	9.2	23.4
Gas Rise °K	14.5	25.6	16.3	26.0	21.3	27.6	18.1	24.6
Total Rise, °K	22.7	44.6	23.7	43.2	37.3	61.8	27.3	48.0
L/D_h ratio	116.9	100.	143.	116.	167.	130.	194.	152.
Friction drop, velocity heads	5.48	4.69	6.71	5.44	5.66	4.26	7.02	5.50
Total drop, velocity heads	7.48	6.69	8.71	7.44	7.66	6.26	9.02	7.50
Differential Pressure, mm H_2O	708.7	637.5	828.	704.9	1508.	1200.	1433.	1123.

Analysis of Magnetic Field Variations and Resultant Losses in Cryogenic Region during Transients with Cold Second Shield

The conceptual designs as initially developed by Westinghouse have utilized a single warm shield to serve both as the damper winding and as the eddy current shield under steady state and fault conditions.

The single shield in combination with the proposed helium management system and the cabled, mixed matrix superconductor has been shown in earlier reports to perform as follows:

- Provides sufficient shielding under steady state negative sequence conditions to limit heating in the cold rotor to a low level.
- Provides good damping for rotor swings.
- Provides positive damping at turbine-shaft frequencies.
- Provides sufficient shielding or limits the rate change of flux within cold structure and field winding region so that a normalization will not occur during or after a "high side" fault.
- Limits damper distortion to a sufficiently low level so that flux compression fields will not lead to a normalization.

The single shield rotor as proposed does require a quite sophisticated and complex superconductor. This has meant somewhat lower current densities than can be attained with a copper matrix, monolithic conductor. Also it can be anticipated that coil winding will be more complicated with a cabled than with a monolithic conductor.

It appeared that it might be possible to return to the copper matrix conductor if a second cold shield was introduced into the design. This would consist of a thin copper layer on the O.D. of the inner rotor support cylinder. The effect of this shield would be to further attenuate ac fields and consequently decrease the heating in the cold region both in the structural support and in the field winding.

The cold shield is to be a thick copper plating on the O.D. of the outer field support cylinder with a thickness of 2.54×10^{-3} m (0.10"). This type of shield fabrication was successfully utilized for the Phase I AF rotor.

The purpose of this section is to report on the performance of the double shield system in terms of shielding and heating of the cold shield support structure and the superconductor. The performance will be evaluated with respect to the following fault effects:

- Damper shield distortion
- Rotation of the inner cold relative to the outer warm shield
- Rotor swings
- Synchronous flux diffusion through the shields.

Also the heating due to steady state system fluctuations will be evaluated.

Damper Distortion

During a system fault the damper shield is subject to large ovalizing forces. The distortional motion resulting from these forces leads to ac magnetic fields inside the damper shield due to compression and dilation of the fields initially inside the damper.

The purpose of this section is to evaluate these ac magnetic fields and the associated heat generated in the cold structure and field winding.

The physics of the problem can be described as follows. Initially there are no currents flowing in the damper and the magnetic field that exists inside the damper material is the sum of the steady synchronous fields due to the field and armature windings under load condition. The fault then occurs and large fault currents flow in the armature. Currents are then induced in the damper that act to exclude the incremental armature flux from entering the interior of the shield. The shielding currents interacting with the armature currents result in ovalizing forces which cause the shield to distort. The resulting motion of the shield in the magnetic field induces additional currents which flow such as to conserve flux linkage. It is this last action which generates the motional (ac) magnetic fields inside the damper.

In the following analysis it is assumed, for simplicity, that the fault occurs from open circuit at rated voltage rather than from full load. The analysis can be readily extended to the full load case if required.

Approach

In a two-dimensional field analysis the problem can be expressed in terms of the z-component of the vector potential. The field equations with moving media can be written as ($\mu = 1$):

$$\nabla \cdot \underline{B} = 0$$

$$\nabla \times \underline{B} = \mu_o \underline{j}$$

$$\nabla \cdot \underline{E} = 0$$

$$\nabla \times \underline{E} = -\frac{\partial \underline{B}}{\partial t} + \nabla \times \underline{v} \times \underline{B}$$

where $\underline{E}$ in the electric field as measured by a moving observer and $\underline{v}$ is the moving media (damper shield)velocity. When expressed in terms of the vector potential ($\underline{B} = \nabla \times \underline{A}$) and recognizing that there is no z dependence, the equations reduce to

$$\nabla^2 \underline{A} = -\mu_o \underline{j} \tag{1}$$

$$\nabla \times \left(\underline{E} + \frac{\partial \underline{A}}{\partial t} - \underline{v} \times \nabla \times \underline{A} \right) = 0 \tag{2}$$

where $\underline{A} = A\hat{k}$ and $\underline{E} = E\hat{k}$ and $A = A_z$.

Now Eq. (2) is satisfied if we take E as given by

$$\underline{E} = -\frac{\partial \underline{A}}{\partial t} + \underline{v} \times \nabla \times \underline{A}$$

and the current in the moving media is then given by

$$\underline{j} = \sigma \underline{E} = \sigma \left(-\frac{\partial \underline{A}}{\partial t} + \underline{v} \times \nabla \times \underline{A} \right) .$$

Then the equation for A is

$$\nabla^2 \underline{A} + \mu_o \sigma \left(-\frac{\partial \underline{A}}{\partial t} \times \underline{v} + \nabla \times \underline{A} \right) = -\mu_o \underline{j}_{ext} . \tag{3}$$

Now for small deflections of the damper shield the fields associated with currents induced in the damper shield due to its motion are small in comparison to the field produced by the field winding or by the short circuit armature currents. Therefore the calculation will be carried out to first order in $\underline{v}$. It will be shown that this motional field is about 1% of the other fields. Therefore $\underline{A}$ can be expressed as

$$\underline{A} = \underline{A}_o + \underline{A}_1$$

where $\underline{A}_o$ represents the zero order fields due to field and armature currents ($v = 0$) and $\underline{A}_1$ is produced by the motion. With small deflection it follows that the mechanical motion is determined by $\underline{A}_o$ and the mechanical properties of the shield, i.e., the magnetic spring can be neglected. Then Eq. (3) breaks up into

two equations, the zero and first order parts,

$$\nabla^2 \underline{A}_o - \sigma\mu_o \frac{\partial \underline{A}_o}{\partial t} = -\mu_o \underline{j} \tag{4}$$

and

$$\nabla^2 \underline{A}_1 + \sigma\mu_o \left(- \frac{\partial \underline{A}_1}{\partial t} + \underline{v} \times \underline{B}_o \right) = 0. \tag{5}$$

Now the solution to Eq. (4) covers the fields produced initially by the field winding before the fault and after the fault includes the additional fields due to the armature short circuit currents and the shielding currents induced in the damper and in the field winding. This part, to the accuracy required, can be handled by a combination of machine lumped parameter representation supplemented by cylindrical shield relationships. It is the solution to Eq. (5) that is required for the present discussion.

We can now introduce another approximation due to the high σ of the damper shield. Then to zero and first order, Eq. (5) becomes

$$\underline{A}_1 = \underline{A}_{10} + \underline{A}_{11}$$

$$- \frac{\partial \underline{A}_{10}}{\partial t} + \underline{v} \times \underline{B}_o = 0 \tag{6}$$

and

$$\sigma\mu_o \frac{\partial \underline{A}_{11}}{\partial t} = \nabla^2 \underline{A}_{10} \, . \tag{7}$$

The meaning of this approximation is that to first order, E = 0 inside the shield because σ is large. This can be said in another way, that when the shield starts to move the motional electric field, $\underline{v} \times \underline{B}$ causes currents to flow. These currents, in turn, produce changing magnetic fields and thereby electric fields that oppose the motional electric field. If the conductivity is high, this cancellation is almost perfect and $E \sim 0$, i.e., the shield is almost purely <u>reactive</u> in response to the motion.

Then Eq. (6) gives $\underline{A}$ to first order in the shield and yields a boundary condition for determining $\underline{A}_{10}$, inside the shield where $\nabla^2 \underline{A}_1 = 0$ (i.e., $\sigma = 0$),

$$\left. \frac{\underline{A}_{10}}{\partial t} \right]_{\text{Boundary}} = \left. \underline{v} \times \underline{B}_o \right]_{\text{Boundary}} \tag{8}$$

with $\nabla^2 \underline{A}_1 = 0$ gives $\underline{A}_1$ uniquely. Then

$$\underline{A}_{1o}\Big)_{\text{Boundary}} = \int \underline{V} \times \underline{B}_o \, dt = \delta \underline{R} \times \underline{B}_o$$

Equation (7) can then be used, if desired, to give the electric field and motionally induced currents. However, we are only interested in obtaining the fields between the outer warm damper and the inner cold shield, and therefore Eq. (7) will not be needed. Also, in limit of small deflections the boundary on which Eq. (8) applies can be taken as cylindrical in place of the true distorted boundary. This approximation should be valid since the deflection turns out to be small in comparison to the spacing between the I.D. of the warm damper and the O.D. of the inner cold shield. Taking the boundary as cylindrical means that cylindrical harmonic functions can be utilized insteady of distorted cylindrical harmonic functions.

Damper Shield Motion

The electromagnetic stress on the damper shield can be obtained by using the Maxwell stress tensor. The net stress on the outer shield at the beginning of the of the fault period ($t < \tau_d$") and for a shield thickness small in comparison to the shield radius is given by

$$\sigma_{rr} \simeq \frac{1}{2\mu_o} (B_A^2 + B_A B_F)$$

where B_A is the θ component of B due to armature and shield currents ($V = 0$) and B_F is the θ component of B at the shield radius due to field winding currents. Now

$$B_A = B_{AS} \sin \theta - B_{AT} \sin (\omega t + \theta)$$

and

$$B_F = B_{FO} \sin \theta$$

where B_{AS} and B_{AT} are the synchronous and "trapped flux" components of the armature (and shield) fault fields.

Then the time and space varying components of σ_{rr} are

$$\sigma_{rr} = \frac{1}{4\mu_o} \left[B_{AT} (B_F + 2B_{AS}) \cos(\omega t + 2\theta) - B_{AT}^2 \cos 2(\omega t_o + \theta) \right] \qquad (9)$$

Now $\left| B_{AT} \right| = \left| B_{AS} \right|$ for a 3ϕ fault from an open circuit condition (at rated voltage).

For a thin shell the deflection is given by

$$\delta R_o = \frac{4\sigma_{rr} R^4}{3E\Delta^3} . \tag{10}$$

The shell has a $\delta\theta$ deflection in addition to the δR deflection on the assumption that the circumference of the shell is constant during distortion, then if δR has the form of

$$\delta R = \delta R_o \cos 2\theta,$$

then $\delta\theta$ is given by

$$\delta\theta = \frac{\delta R_o}{2R_W} \sin 2\theta.$$

Magnetic Fields

The magnetic fields associated with damper distortion will be derived following the approach outlined above.

Using the notation introduced earlier,

$$\delta \underline{A}_{10}\Big|_{\text{Boundary}} = \delta \underline{R} \times \underline{B}_o$$

now

$$\delta \underline{R} = \delta R\, \hat{r} + R_W \delta\theta \hat{\theta}.$$

While $\underline{B}_o$ should include contributions both from field and armature currents, for the present only B_F will be considered (good for $t < \tau_d''$) and later the effect of the adding in the armature fault fields that get through the damper during the subtransient period will be commented on.

Then taking $\underline{B}_o$ as

$$\underline{B}_o = B_\theta^{(F)} \sin\theta\hat{\theta} + B_r^{(F)} \cos\theta \hat{r}$$

then

$$\delta A_{10} = \delta R B_\theta^{(F)} \sin\theta - R_W \delta\theta B_r^{(F)} \cos\theta$$

δR can be expressed as

$$\delta R = \delta R_o^{(60)} \cos(\omega_o t + 2\theta) + \delta R_o^{(120)} \cos(2\omega_o t + 2\theta)$$

and a similar expression applies for $\delta\theta$, but with half the amplitude and with sin functions.

Then

$$\delta A_{10} = \delta R_o^{(120)} \left(B_\theta^{(F)} + \frac{B_r^{(F)}}{2}\right) \sin(2\omega_o t + 3\theta) + \delta R_o^{(120)} \left(-B_\theta^{(F)} + \frac{B_r^{(F)}}{2}\right) \sin(2\omega_o t + \theta) + \delta R_o^{(60)} \left(B_\theta^{(F)} + \frac{B_r^{(F)}}{2}\right) \sin(\omega_o t + 3\theta) + \delta R_o^{(60)} \left(-B_\theta^{(F)} + \frac{B_r^{(F)}}{2}\right) \sin(\omega_o t + \theta)$$

This expression for δA_{10} is evaluated at I.D. of the damper shield and used as a boundary condition for A_{10} between the I.D. of the damper and the O.D. of the cold shield.

Using the boundary condition of $B_r = 0$ on the cold shield surface, which should be a good assumption, since δ (skin depth) at 60 and 120 Hz is smaller than the thickness of the cold shield. Then B_θ for the flux density at the surface of the cold shield is

$$\begin{aligned} B_\theta = & \frac{-3\left(B_\theta^{(F)} + \frac{B_r^{(F)}}{2}\right)}{1-\left(\frac{R_c}{R_W}\right)^6} \left(\frac{\delta R_o^{120}}{R_W}\right)\left(\frac{R_c}{R_W}\right)^2 \sin(2\omega_o t + 3\theta) \\ & - \frac{\left(-B_\theta^{(F)} + \frac{B_r^{(F)}}{2}\right)}{1-\left(\frac{R_c}{R_W}\right)^2} \left(\frac{\delta R_o^{120}}{R_W}\right) \sin(2\omega_o t + \theta) \\ & - \frac{3\left(B_\theta^{(F)} + \frac{B_r^{(F)}}{2}\right)}{1-\left(\frac{R_c}{R_W}\right)^6} \left(\frac{\delta R_o^{60}}{R_W}\right)\left(\frac{R_c}{R_W}\right)^2 \sin(\omega_o t + 3\theta) \\ & - \frac{\left(B_\theta^{(F)} + \frac{B_r^{(F)}}{2}\right)}{1-\left(\frac{R_c}{R_W}\right)^2} \left(\frac{\delta R_o^{60}}{R_W}\right) \sin(\omega_o t + \theta) \end{aligned} \qquad (11)$$

where R_c = radius of cold shield

and R_W = radius at I.D. of damper.

Numerical Results

Using Eqs. (9) and (10) the damper shield radial stress and deflection can be calculated.

Using the dimensions and electrical characteristic of the 300 MVA low-voltage (spiral armature) design, the following results are obtained for a high-side fault. Then

$$B_{AS} = 2.7 \text{ T}$$

$$B_F = 0.83 \text{ T}$$

evaluated at the damper shield. Then

$$\sigma_{rr} \text{ (60 Hz)} = 3.3 \times 10^6 \text{ N/m}^2$$
$$= 476 \text{ psi}$$

and

$$\sigma_{rr} \text{(120 Hz)} = 1.45 \times 10^6 \text{ N/m}^2$$
$$= 210 \text{ psi}$$

Then

$$\delta R_o \text{ (60)} = 6.9 \times 10^{-4} \text{ m}$$
$$= 0.027"$$

and

$$\delta R_o \text{ (120} = 2.8 \times 10^{-4} \text{m}$$
$$= 0.011".$$

Now

$$\left(B_\theta^{(F)} + \frac{B_r^{(F)}}{2} \right) = 2.1 \text{ T}$$

and

$$\left(- B_\theta^{(F)} + \frac{B_r^{(F)}}{2} \right) = - 0.012 \text{ T} \quad \text{(Neglect)}.$$

With these numbers the ac field at the surface of cold shield due to damper distortion is

$$B_\theta^{(60)} = 0.01 \text{ T}$$

$$B_\theta^{(120)} = 0.004 \text{ T}.$$

The above calculation assumed that $\underline{B}_o$ in the damper resulted from field currents alone. However, armature short circuit fields penetrate into the damper during the subtransient period. Taking the fault period as 0.07 sec, which is about 1/2 of τ_d", at the end of the fault period an additional field of about 1T should be combined with the 2T field from the field winding. This would change the motional flux density by about 50%.

Rotation of Inner Relative to Outer Rotor

The approach to calculating the magnetic fields generated by the inner cold structure oscillating relative to the warm outer shell during a fault follows a similar path as the calculation for the damper distortion fields.

In this case there is only a $\delta\theta$ motion. Again the $\delta\underline{A}$ that sets a boundary condition for the motional field is given by

$$\delta\underline{A} = \delta\underline{R} \times \underline{B}_o$$

Now

$$\delta\underline{R} = R_W \delta\theta \sin \omega t \, \hat{\theta}$$

and the r component of $\underline{B}_o$ is

$$\underline{B}_o = B_r^{(F)} \cos \theta \, \hat{r}$$

Then

$$\delta A = R_W \, \delta\theta \, B_r^{(F)} \cos \theta \sin \omega t$$

at the ID of the warm damper.

Again taking $B_r = 0$ on the cold inner shield gives A between the warm and cold shield as,

$$A = \frac{\delta\theta \, B_r^{(F)}}{1 - \left(\frac{R_c}{R_W}\right)^2} \left(r - \frac{R_c^2}{r}\right) \sin \omega t \cos \theta$$

and then

$$B_\theta = - \frac{\partial A}{\partial r}$$

$$B_\theta \Big|_{r = R_c} \simeq \frac{- 2\delta\theta \, B_r^{(F)}}{1 - \left(\frac{R_c}{R_W}\right)^2} \sin \omega t \cos \theta$$

We take from Quarterly #2, P 3-72

$$\delta\theta = 0.25°$$

$$\omega = 20 \text{ Hz}$$

$$B_r^{(F)} = 2.0 \text{ T (open circuit)}$$

then B_θ at the surface of the cold shield is

$$B_\theta = 0.06 \text{ T (quadrature axis)}$$

Rotor Swings

The model to obtain the ac fields due to rotor swings is as follows. It is assumed that the rotor swings around the armature field by $\sim \pm 20°$ at 2.5 Hz for three swings (1.5 cycles). The armature field upon clearing the fault was e imated in Quarterly #3 P 3-46, as 2.5 pu. Now B_A (1 pu) = 0.36 T and therefore

$$B_q = 0.9 \sin 20° \quad = 0.31 \text{ T at 2.5 Hz}$$

$$B_d = 0.90 (1-\cos 20°) = 0.027 \text{ T at 5 Hz}$$

These are the uniform fields outside the warm damper.

Field Penetration through Shield System and Heating

The rotor now has a quite complicated and multiple shield system. This is evident in Figure 3-38 which shows a schematic cross section of the shields and their dimensions (300 MVA, high voltage). While shielding action comes from the warm outer shield and the cold inner shield, it is still necessary to also consider the radiation shield and the field support cylinder in evaluating heat generation in the cold region during faults. Also the field winding play a significant role as a long time constant back up in the direct axis.

The simple attenuation and loss formulas applicable to a single isolated shield are not directly useful for this more complicated shield assembly. While it is possible to go "brute force" to a field solution for this assembly, it has not been carried to completion as yet and even when it is, it will not give the physical insight that more approximate approaches can give. Therefore in the present section, the evaluation of the fields and losses appropriate to the various metallic

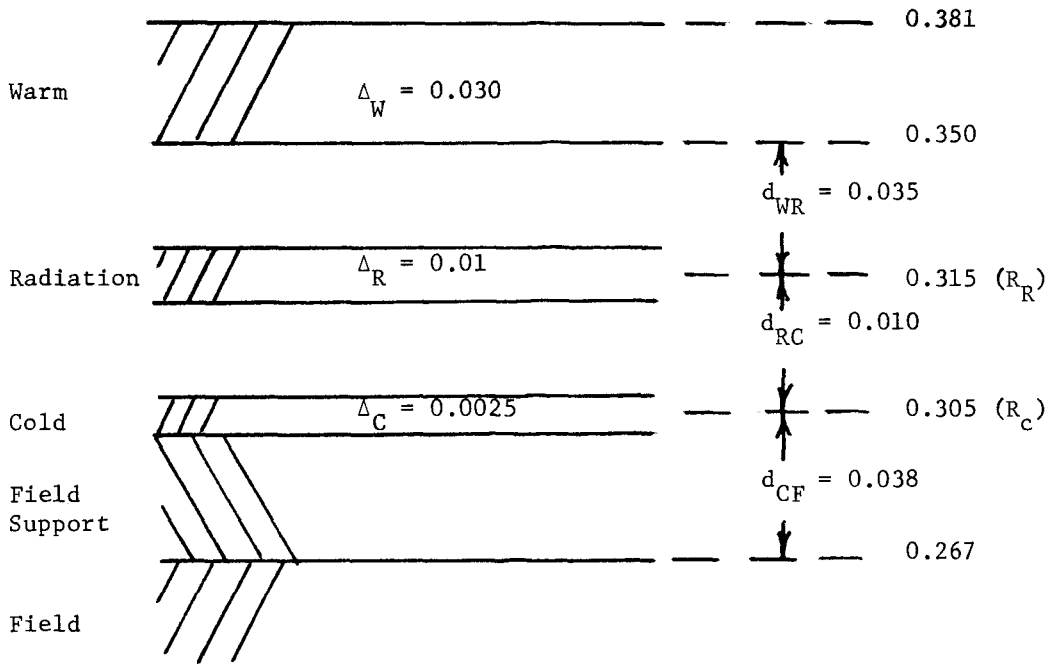

NOTE: Dimensions in meters

Figure 3-38. Dimensions of the Rotor Shells

cylinders for each of the cases under consideration in this section will be carried out by such an approximate approach. We also will evaluate superconductor loss for the cold shield case. We will not evaluate the warm shield loss as this has been covered on page 3-124 and is not directly related to cold region heating.

The approximate formulas that will be used below depend on the thickness, the spacing between, and the skin depth for each cylindrical shell being small in comparison to the radius of the shell. That these ratios are small is evident in Figure 3-38 which gives the thickness (Δ) and the shell spacings (d) and from Table 3-19 which lists skin depths frequencies of relevance to the present discussion. Only for inconel at 2.5 Hz is there an exception with $\delta \sim R$.

The time constants of the various shells are also useful in deciding the approximation approach. These are also listed in Table 3-19 .

These time constants include the effect of coupling to neighboring shells or windings, i.e., reduction of the shell inductance through mutuals with other shells or windings. The warm shell couples to the armature and to the cold shell. The radiation shell couples to the warm and the cold, the cold couples to the warm and the field winding and the structure couples to the cold and the field winding. The factor by which the isolated shell time constant is multiplied by, to obtain the reduced time constant is

$$\left(\frac{2d}{R}\right)$$

where R is the radius of the shell and d is the spacing to the nearest outer (or inner) shell with a larger time constant. For example, the time constant for the radiation shell is

$$\tau_R = \left(\frac{2d_{WR}}{R_R}\right)\left(\frac{2d_{RC}}{R_R}\right) \quad \tau_R \text{ (isolated)}.$$

The present section does not cover the synchronous flux diffusion case, which is handled separately below.

Damper Distortion

Radiation Shield. In obtaining the magnetic field between the warm damper and the inner cold shield due to damper distortion, it was implicitly assumed that

Table 3-19

SKIN DEPTH AND TIME CONSTANTS

Frequency (Hz)	2.5	20	60	120
Skin Depth (m)				
• Inconel	0.32	0.11	0.065	0.046
• Warm Copper (300 K)	0.052	0.018	0.011	0.0075
• Cold Copper (4 K)	0.0052	0.0018	0.0011	0.00075
	Time Constants			
Warm	0.13 sec			
Radiation	2.8×10^{-5} sec			
Cold	0.22 sec			
Cold Structure	1.4×10^{-4}			

Note: $\rho_{inconel} = 10^{-6}$ Ω-m

$\rho_{copper} = 2.7 \times 10^{-10}$ Ω-m

at 4 K, 4 T

the presence of the radiation shield in this space could be ingored. This is justified since $\omega\tau < 1$. The vector potential in this space is of the form,

$$A = \frac{B_\theta}{2}\left[r - \frac{R_c^2}{r}\right] e^{i(\omega t + n\theta)}$$

where B_θ is the magnetic induction at the surface of the cold shield, given above as

$$B_\theta(60\ \text{Hz}) = 0.01\ \text{T}$$

and

$$B_\theta\ (120\ \text{Hz}) = 0.004\ \text{T}.$$

Then the power/unit vol, $P_V = EE^*/2\rho$, with $E = -\partial A/\partial t$, can be integrated over the volume of the radiation shield to yield the formula for total heat input during the fault period, t, as

$$Q \simeq \frac{\pi R_R B_\theta^2 d_{RC}^2 \Delta_R \omega^2 \ell t}{\rho_R}$$

Evaluating this expression with t = 0.066 S and ℓ = 2 m, gives

$$Q = (60) = 2\ \text{J}$$

$$Q = (120) = 0.3\ \text{J}$$

Cold Shield. Since $\Delta/\delta > 1$ for the cold shield, the limiting formula for a thick shield can be used, but expressed in terms of B_θ, i.e.,

$$Q = \frac{\pi R_c \rho_c B_\theta^2 t \ell}{\mu_o^2 \delta}$$

When evaluated this gives

$$Q\ (60) = 3\ \text{J}$$

$$Q\ (120) = 0.7\ \text{J}$$

Attenuation Through Cold Shield. Again, because $\Delta/\sigma > 1$, limiting thick shield formulas can be used.

For the quadrature axis with no field winding underneath, the attenuation K is

$$K = \frac{B_{uniform} \text{ (Inside Cold)}}{B_\theta \text{ (outside cold)}}$$

$$= \sqrt{2}\,\frac{\delta_c}{R_c}\, e^{-\Delta_c/\delta_c}$$

Note that this formula is expressed in terms of B_θ outside going to $B_{uniform}$ inside instead of the more familiar formula for uniform-outside to uniform-inside. This removes a two as a factor, i.e., $B_\theta/2 = B_{uniform}$.

Then

$$K_q\ (60) = 5 \times 10^{-4}$$

$$K_q\ (120) = 2 \times 10^{-4}$$

For the direct axis the effect of the field winding underneath the cold shield must be taken into account. As will be derived further on this report, the attenuation for a thick shield backed up by a $\sigma = \infty$ shield ($\Delta/\delta > 1$) is

$$K_d = \frac{B_\theta \text{ (surface of } \sigma = \infty \text{ shield)}}{B_\theta \text{ (outside of cold shield)}}$$

$$= \sqrt{2}\,\frac{\delta}{d}\; e^{-\Delta/\delta}$$

where d is the spacing between the outer thick shield and the inner $\sigma = \infty$ shield.

When this is evaluated for the present case

$$K_d\ (60) = 5 \times 10^{-4}$$

$$K_d\ (120) = 2 \times 10^{-4}$$

The fields in the cold structure and in the field winding can be obtained using these attenuations. For the direct axis the field at the surface of the field winding is,

$$B_d\ (60) = 4 \times 10^{-5}\ T$$

$$B_d\ (120) = 8 \times 10^{-7}\ T.$$

For the quadrature axis the field (uniform) in the winding is

$$B_q\ (60) = 5 \times 10^{-6}\ T$$

$$B_q\ (120) = 8 \times 10^{-7}\ T.$$

Cold Structure. With the very small fields as given above, the heating in the cold structure is negligible.

Rotation of Inner Relative to Outer

Radiation Shield. The flux density for this case outside of the cold shield was given above as

$$B_\theta = 0.060\ T\ \text{(Quadrature axis)}.$$

The relationship used for the radiation shield heating for the damper distortion case can be used here. However, it is divided by two to hold for the present unidirectional field (non-rotating). With an estimate of 100 for the Q of the shaft-turbine mode, the time for heating is 5 sec. The total heat is evaluated as

$$Q = 283\ J.$$

Cold Shield. Now Δ/δ is still > 1 and a quadrature axis field, the thick shield formula for a non-rotating field is applicable. This gives

$$Q = 1400\ J.$$

Attenuation Through Cold Shield. Using the thick shield formula

$$K = 4.2 \times 10^{-3}.$$

Then B in the cold structure and the field winding is

$$B \text{ (inside cold shield)} = 1.3 \times 10^{-4} \text{ T}$$

Cold Structure. With the above uniform quadrature field, the heat into the cold structure is

$$Q = 17 \text{ J}$$

Rotor Swings

The fields given above for the direct and quadrature axes resulting from rotor swings were,

$$B_q = 0.31 \text{ T at } 2.5 \text{ Hz}$$

$$B_d = 0.027 \text{ T at } 5 \text{ Hz}$$

These were the uniform fields outside the warm shield with the shield removed. The cold shield inside the warm shield can again be taken as a $B_r = 0$ boundary for both the d and q axes. This is not as good an approximation as for the higher frequency cases, however as will be seen below, the attenuation through the cold shield is still quite large, $K < 0.1$.

Since $\Delta/\delta \sim 0.58$ for the warm shield, the attenuation must be obtained from a more exact attenuation expression than used above when $\Delta/\delta > 1$. This expression, as mentioned above, is derived further on in this report, an expression in this case for a shield with a $\sigma = \infty$ back up. Using this more complete formula gives for the warm shield

$$\frac{B_\theta \text{ (cold surface)}}{B_{\text{uniform}} \text{ (outside warm)}} = K$$

$$K = 1.0$$

This is very close to what is obtained using the thin shield formula, i.e.,

$$K = \frac{2}{\sqrt{1 + (\omega\tau)^2}}$$

$$= 0.88$$

Therefore the warm shield does not attenuate the rotor swing fields.

Radiation Shield. Heating in the radiation shield is calculated as before. The results are

$$Q_q = 14 \text{ J}$$

and

$$Q_d = 0.4 \text{ J}$$

Using the more complete isolated shield formula (quadrature) and the formula for the $\sigma = \infty$ backing, the cold shield heats are,

$$Q_q = 2630 \text{ J}$$

and

$$Q_d = 76 \text{ J}$$

Attenuation of Cold Shield. The attenuation of the cold shield is

$$K_q = \frac{B_{\text{uniform}}}{B_\theta \text{ (outside cold)}} = 0.018$$

$$K_d = \frac{B_\theta \text{ (outside field)}}{B_\theta \text{ (outside cold)}} = 0.13$$

These give the field in the cold structure and in the field as

$$B_q \text{ (uniform in field)} = 0.0053 \text{ T}$$

$$B_{d\theta} \text{ (outside field)} = 0.0072 \text{ T}$$

Cold Structure. The heat in the cold structure are

$$Q_q = 13 \text{ J}$$

and

$$Q_d = 8 \text{ J}$$

Steady State Fluctuations

The steady state system fluctuations are represented by a ± 5% variation in machine angle at 2.5 Hz. With a machine angle of 20°, this gives the fields outside the warm shield as

$$B_q = \sin (1°)\ 0.36 = 6 \times 10^{-3}\ T$$

$$B_d = \left(1 - \cos (1°)\right)\ 0.36 = 3 \times 10^{-5}\ T$$

The steady state heating of the cold shield is

$$P_q = 1.8\ \omega$$

$$P_d = \text{negligible}$$

The radiation shield heating is also very small.

The fields in the field winding are (same attenuation as for rotor swings)

$$B_q = 1.1 \times 10^{-4}\ T$$

$$B_d = 6.5 \times 10^{-6}\ T$$

The cold structure heat is negligible ($\sim$ 0.04 watts).

Synchronous Flux Diffusion

Approach

After a fault has occurred, the synchronous flux produced by the armature diffuses through the shield shells in succession. The field diffusion process is in reality represented by a sum of radial modes, each with its own time constant. However, an approximate approach can be taken that recognizes that all the higher modes decay at least ten times faster than the lowest (L/R) mode which possesses an almost uniform radial current distribution. Therefore it is appropriate to consider only the lowest mode and to represent it by a perfectly uniform current distribution in the shell. This is like a thin shell approximation. The fault produces a field of

$$B = \frac{B_A\ (1\ pu)}{X''_d} = 1.38\ T$$

outside the warm shield. The field then penetrates through the warm shield, governed by a time constant of $\tau_W = \tau_d'' = 0.13$ sec. Since we are considering the fault to be cleared by 0.066 sec, we can take a linear approximation for the growth of the field inside the warm shield.

Then

$$B \text{ (inside warm)} = \frac{t}{\tau_d''} B \text{ (outside warm)}$$

This gives the field outside the cold shield (B_θ) and the field that penetrates through the radiation shield.

Radiation Shield. The instantaneous power going into the radiation shield can be written as

$$P_e = \frac{\pi \dot{B}_o^2 R^3 \Delta}{2\rho}$$

using B (t) as given above, the heat input is evaluated as Q = 325 J for the 0.066 sec period.

Cold Shield. We assume that during the 0.066 sec period, the current in the cold shield exactly follows the field at its surface. This means that we ignore its own decay time or assume for this calculation that $\tau_c > \tau_\omega$. Then integrating $J^2\rho$ over the volume of the shield and over the 0.066 sec period,

where $$J = \frac{2B_o}{\Delta \mu_o}$$

Then the heat input is

$$Q = \frac{4\pi \rho R B_o^2 t^3 \ell}{3\Delta \mu_o^2 \tau_d'' 2}$$

and gives

$$Q = 275 \text{ J}$$

Field Penetration Through Cold Shield. In calculating the heat input to the cold shield, we ignore the decay time of the cold shield. However in

estimating the field within the cold shield (in the structural and field winding) the τ_c must be taken into account. For time short in comparison to τ_ω and τ_c the field inside the cold shield can be written as

$$B \text{ (inside cold)} \approx \frac{t^2}{2\tau_c \tau_\omega} B \text{ (outside warm)}$$

Cold Structure. The heat input to the cold structure is calculated using the above time dependent field and the same type of relationship as used for the radiation shield. This gives

$$Q \approx 1 \text{ J}$$

Superconductor Loss

The time varying fields that exist inside the field winding during and after a fault were obtained above for all the different cases. One of the main purposes of going to the two-shield system was the possibility of being able to return to a simple copper-matrix conductor for the generator.

With the previous single-shield system, the damper distortion fields were one of the main reasons for having to use a cabled mixed-matrix conductor. These distortion fields along with the rotation of the inner relative to the outer fields are now reduced to a very low level.

Using the several fields obtained above, the losses in the copper matrix superconductor as specified in Report #5 were calculated. For the case of 10% stored helium adjacent to the conductors, the maximum temperature rise during and after the fault is predicted to be < 0.1 K. Therefore we conclude that the double-shield system does easily permit utilization of the copper-matrix conductor. The 300 MVA generator with the high-voltage armature has been designed on this basis.

Attenuation and Loss of a Shield with a $\sigma = \infty$ Backup

For the above calculations for the double-shield system, it was important to have formulas applicable to one shield backed up with a high conductivity second shield.

As was pointed out earlier for the shells that form the shield system, the thickness, the skin depth, and the spacing are in general small in comparison

to their radius. With δ/R and $\Delta/R < 1$, the vector potential inside the shell can be expressed, to a good approximation, as

$$A = a\, e^{\beta r} + b\, e^{-\beta r}$$

where

$$\beta = \frac{1 + i}{\delta}$$

On this basis the case of a shield backed up by a $\sigma = \infty$ shell was treated to obtain the attenuation and loss. This is an extension of thin shield case treated in an earlier report. A fuller discussion of the derivations of the formulas given below will be presented in a later report.

The attenuation is given by

$$\frac{1}{K^2} = \frac{1}{4}\left(\frac{d}{\delta}\right)^2 \left[\left\{ 1 + \frac{1}{2}\left(\frac{\delta}{d}\right)^2 \right\} \cosh \frac{2\Delta}{\delta} - \left\{ 1 - \frac{1}{2}\left(\frac{\delta}{2}\right)^2 \right\} \cos \frac{2\Delta}{\delta} + \left(\frac{\delta}{d}\right) \sin \frac{2\Delta}{\delta} - \left(\frac{\delta}{d}\right) \sin \frac{2\Delta}{\delta} \right]$$

where Δ is the thickness of the shield, d the spacing between the shield and the $\sigma = \infty$ backup and the δ the skin depth. This gives the attenuation of an outside uniform field to an inside B_θ at the surface of the $\sigma = \infty$ inner shield.

Note that in the limit of $\Delta/\delta \to 0$

$$K = \frac{2}{\sqrt{1 + \omega\tau^2}}$$

where $\tau = \Delta d\, \mu_o\, \sigma$ and in the limit of $\Delta/\delta > 1$ and $\delta/d < 1$

$$K = 2\sqrt{2}\, \frac{\delta}{d}\, e^{-\Delta/\delta}$$

For $\delta/d > 1$

$$K = 2\sqrt{2}\, e^{-\Delta/\delta}.$$

The power loss/unit length in the shield is given by (non-rotating field)

$$P_e = \frac{2\pi R B^2 \rho}{\mu_o^2 \delta} x$$

$$\frac{1 + \frac{1}{2}\left(\frac{\delta}{d}\right)^2 \sinh\frac{2\Delta}{d} + 2\left(\frac{\delta}{d}\right)\sinh^2\frac{\Delta}{\delta} + \left\{1 - \frac{1}{2}\left(\frac{\delta}{d}\right)^2\right\}\sin\frac{2\Delta}{\delta} + \frac{2}{d}\sin^2\frac{2\Delta}{\delta}}{\left\{1 + \frac{1}{2}\left(\frac{\delta}{d}\right)^2\right\}\cosh\left(\frac{2\Delta}{d}\right) - \left\{1 - \frac{1}{2}\left(\frac{\delta}{d}\right)^2\right\}\cos\left(\frac{2\Delta}{\delta}\right) + \frac{\delta}{d}\sinh\frac{2\Delta}{\delta} - \frac{\delta}{d}\sin\left(\frac{2\Delta}{\delta}\right)}$$

Results Summary

Table 3-20 gives a summary of the results for the cold shield and support heating.

Table 3-20

SUMMARY OF SHIELD HEATING

	FREQUENCY AND DURATION	COLD SHIELD	COLD STRUCTURE	RADIATION SHIELD
Damper Distortion	60 Hz 120 Hz 0.066 sec	3.7 J	N	2 J
Rotor Swings	2.5 Hz 0.6 sec (3 swings)	2700 J	21 J	13 J
Synchronous Flux Diffusion	Step Function	275 J	1 J	325 J
Rotation of Inner Relative to Outer	20 Hz 5 sec	1400 J	17 J	283 J
Steady State Fluctuations	Continuous	1.8 J	N	N

N = negligible.

REFERENCES

1. Magnetic Screening by Hollow Circular Cylinders, J.C. Jaeger, Philosophical Magazine, Vol. 29, No. 192, January 1940, pp. 18-31.

2. P. J. Lawrenson and M. C. Ralph, "General 3-dimensional Solution of Eddy-Current and Laplacian Fields in Cylindrical Structures." IEE Proceedings, Vol. 117, No. 2, pp. 467-472 (February 1970).

3. Ralph, M. C.: "Eddy-current Effects in the Cylindrical Members of Rotating Electrical Machinery", Ph.D. thesis, Leeds University, 1968.

4. T. J. E. Miller, P. J. Lawrenson, "Penetration of Transient Magnetic Fields through Conducting Cylindrical Structures with Particular Reference to Superconducting A.C. Machines", Proc. IEE, Vol. 123 No. 5, pp. 437-443 (May 1976).

5. T. Bratoljic, "Electromagnetic Transients in Superconducting Turbogenerators", International Conference on Electrical Machines, City University, London, England, September 1974, paper A7.

6. Electromechanical and Thermal Effects of Faults Upon Superconducting Generators, D. L. Luck, Ph.D. Thesis, MIT Department of Electrical Engineering, June 1971.

7. A Design Concept of a Damper Shield of a Superconducting Alternator, M. Furuyama, M.S. Thesis, MIT Department of Mechanical Engineering, August 1974.

8. S. H. Tan, "A Design of Superconducting Generators with Wound Electrothermal Shields", M.S. Thesis, Department of Electrical Engineering and Computer Science, MIT, January 1976.

9. Electromechanical Design for an Inertial Spool Superconducting Generator, N. Dagalakis, Ph.D. Thesis, MIT Department of Mechanical Engineering, September 1974.

10. T. Bratoljic, H. Fursich, H. W. Lorenzen, "Transient and Small Perturbation Behavior of Superconducting Turbogenerators,", IEEE Paper F 77 069-8, presented at 1977 PES Winter Meeting.

11. C. Pinet, "Transients in Superconducting Alternators with Torque Compensating Shells," Electric Machines and Electromechanics, Volume 1, No. 2, January-March 1977.

12. Einstein, Thomas H., "Excitation Requirements and Dynamic Performance of a Superconducting Alternator for Electric Utility Power Generation", December 1970. (MIT Sc.D. thesis).

13. P. J. Lawrenson, T. J. E. Miller, J. M. Stephenson, "Damping and Screening in the Synchronous Superconducting Generator," Proc., IEE, Vol. 123, No. 8, August 1976, pp. 787-794.

14. Luck, D. L., and Thullen, P., "Double Shielded Superconducting Field Winding", U.S. Patent No. 3,764,835, October 9, 1973.

15. Kirtley, J. L., Jr., and Dagalakis, N., "Protection of Superconducting Field Windings for Electrical Machines by the Use of an Inertial Free Electro-mechanical Shield", IEEE Trans. on Magnetics, Vo.l MAG-11 No. 2, March 1975, pp.650-652.

16. Kirtley, J. L., and Smith, J. J., "Superconducting Machine Having Wound Damper-shield Winding", U.S. Patent Application S.N. 523,604, November 13, 1974.

17. Kirtley, J. L., and Wilson, G. L., "Superconducting Machine Having Flexible Shield Means Operation to Protect the Superconducting Field Winding Against Transient", U.S. Patent Application S.N. 523,603, November 13, 1974.

18. Theory of the Induction Machine with Conducting Sleeve Rotor, Edward C. Guilford, AIEE Transactions, pt. III (Power Apparatus and Systems), Vol. 80, 1961 (Feb. 1962 section) pp. 1129-36.

19. Theorie und Berechnung von Ferraris-Motoren mit unmagnetischen, zylindrischen Laeufern in Mantel und Glockenform, W. H. Koch, Dissertation, Technische Hochschule, Hannover, Germany, 1961.

3.2.1.2 Rotor Mechanical Design

Rotor Configuration Selection

Efforts have been made to examine the range of possible configurations of the rotor. The most advantageous configuration has been selected and designed in detail. The general configuration of this rotor is shown schematically in Figure 3-39.

The required functions of the rotor have dictated the need for and to some extent the arrangement of specific rotor components. In particular, the following general functions must be accomplished by the rotor:

- Mechanically support the field winding
- Maintain the field winding at cryogenic temperature
- Protect the field winding from transients
- Transmit machine torque, steady state and short circuit.

Two basic configurations for the rotor have been developed from these requirements, along with many possible detailed variations.

Outer Strongback Configuration

Figure 3-40 is the most viable configuration. A warm outer rotor structure serves as the main structural element (strongback) of the total rotor. It also serves as the vacuum enclosure around the field, and as a support for the damper shield which surrounds the field winding. During a sudden short circuit, large air gap torques are applied to the damper as well as large radial crushing forces. The outer rotor structure which includes the damper and damper support is designed to withstand these forces, while the inner cold rotor is largely protected against them. Additional protection is provided by a second damper. This cryogenic damper is bonded to the outer surface of the inner rotor.

Concentrically mounted within the warm strongback is the cryogenic inner rotor supporting the field winding. The cryogenic inner rotor is a thick cylinder having slots machined into its outer surface to support the superconducting winding. A multipurpose thin cylinder surrounds the slotted inner rotor. The thin cylinder retains the helium, serves as retaining rings for the winding end turns, and supports the integral cold damper. A liquid helium refrigeration system maintains the inner rotor at approximately 4.2°K. Care has been taken to reduce the heat leak into the cryogenic zone. Thermal radiation from the warm strongback to the cold inner rotor is minimized by locating an inner cooled radiation shield in the annulus between the inner and outer rotors, and by axial shields. Conduction

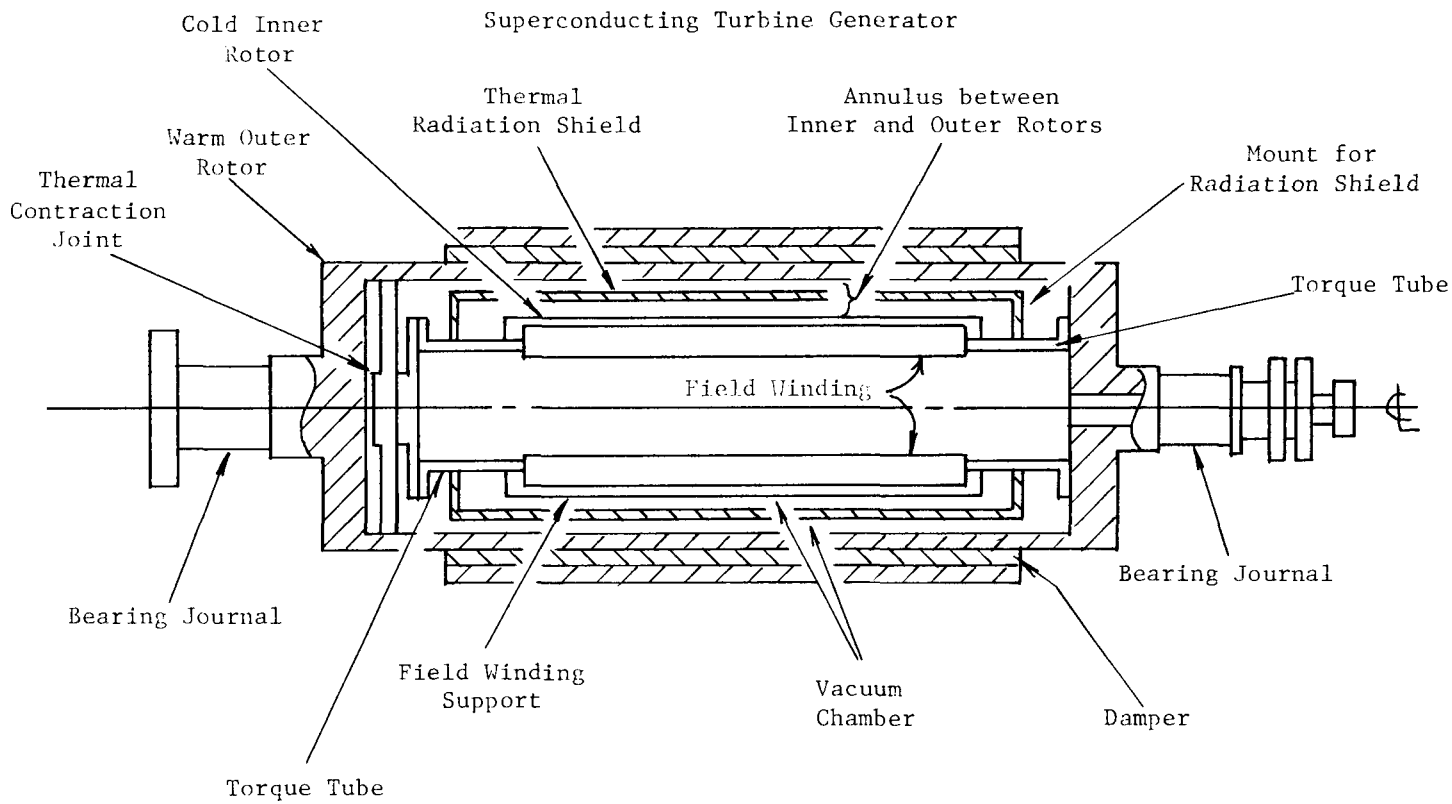

Figure 3-39. General Rotor Configuration

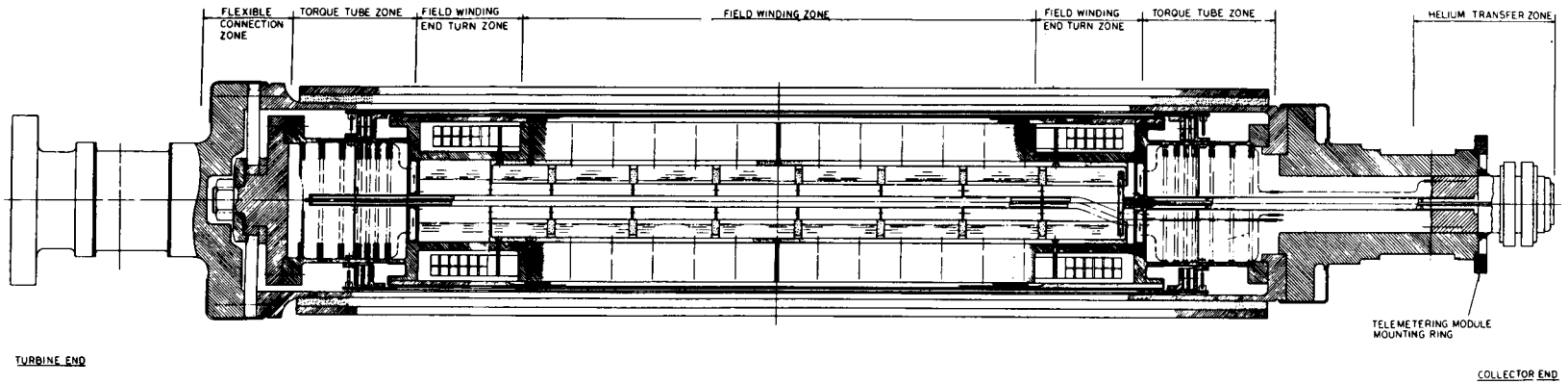

Figure 3-40. Rotor Cross Section

is reduced by having only long, vapor cooled small area torque tubes at each end of the inner rotor connecting it to the outer rotor. Convection is minimized by removing most of the ambient gas from the space around the inner rotor, that is, by pulling a high vacuum between the two rotors.

The mechanical support requirements between the inner and outer rotors to resist short circuit torque and provide stability against vibrations were in conflict with differential thermal expansion and contraction requirements. This problem has been solved by having a reliable flexible connection between the inner and outer rotors at the turbine end only.

Rigid stub shafts at each end of the rotor connect the major rotor configuration components into an assembly capable of providing the proper electromagnetic, mechanical, and thermal environments necessary for the superconducting field winding.

It has been shown that the entire assembly can be designed to have desirable vibration characteristics.

Variations of this basic configuration which have been considered have been similar except without slots. The inner rotor was a thinner cylinder and was considered placed at both the I.D. and O.D. of field winding. Helium management devices change accordingly with each variation.

Inner Strongback Configuration

In the Westinghouse proposal, a different rotor construction was described in which the cold inner rotor was continuous between bearings, and thus was the main structural element of the overall rotor. The damper shield was attached rigidly to the cold rotor at the outboard end but simply supported at the drive end so that it was free to rotate relative to the inner rotor. This construction was believed to offer several advantages but further study has now led us to believe that it introduced more problems than it solved. Its main purpose was to attenuate air gap torque by utilizing the torsional flexibility of the cold inner rotor between the drive shaft and the damper shield. In addition, it did not require provision for axial thermal contraction of the cold inner rotor within the rotor itself where it would be inaccessible. These possible advantages are more than offset by the following disadvantages:

- The outer rotor cannot be used as the vacuum enclosure.
- Excessive lateral flexibility of the inner rotor relative to the outer must be accommodated at the attachment between the two.

- The inner rotor structure including the torque tubes must be designed to take short circuit torques.
- Twisting of the inner rotor during faults may produce excessive heat or result in damage to the winding.

For these reasons, the outer strongback configuration is now believed to be the best.

Rotor Dimensions of 300, 1200 and 3000 MVA Generators

In order to make a direct comparison, dimensions are listed in Table 3-1 for 300 and 1200 superconducting generators, all with toothless rotor and involute stator winding.

Assembly Procedure - Sequence

The method of assembly of the rotor has been considered continuously as the general layout of components has been developed and has restrained the rotor design in some areas. The rotor assembly procedures described here apply to the present 300 MVA and 1200 MVA superconducting generator design.

A. Field Winding and Helium Management System Assembly

This assembly consists of the collector shaft, the inner collector ring sub-assembly, field leads and helium transfer system as well as the field winding and the helium management system.

The components of the field winding and the helium management system are shown in Figures 3-40 , 3-41 and 3-42 and can be assembled in the following sequence.

1. Start with inner helium management support cylinder which includes torque tubes and cooling coils.
2. Install axial feed troughs and heat exchanger assemblies in the support cylinder.
3. Assemble E.E. end feed troughs and connect tube to the axial feed trough.
4. Fit and weld center tube and wave baffles in place.
5. Assemble T.E. end feed troughs and connect tubes between the end feed troughs and the axial feed troughs.
6. Install "T" feed tube.
7. Fit and weld E.E. end plate helium pump.
8. Fit and weld T.E. end plate helium pump.
9. Make helium tube connections between pump and cooling coils.

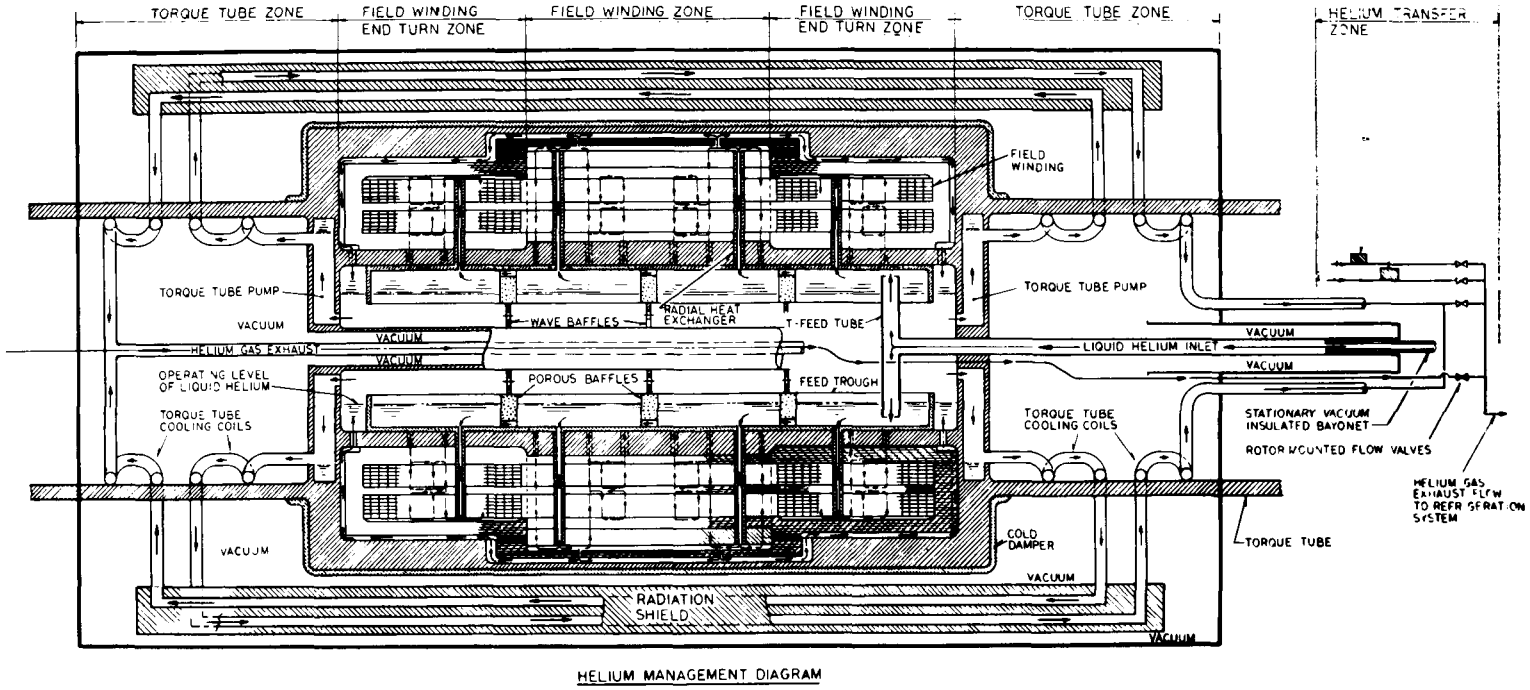

HELIUM MANAGEMENT DIAGRAM

Figure 3-41. Rotor Helium Management System

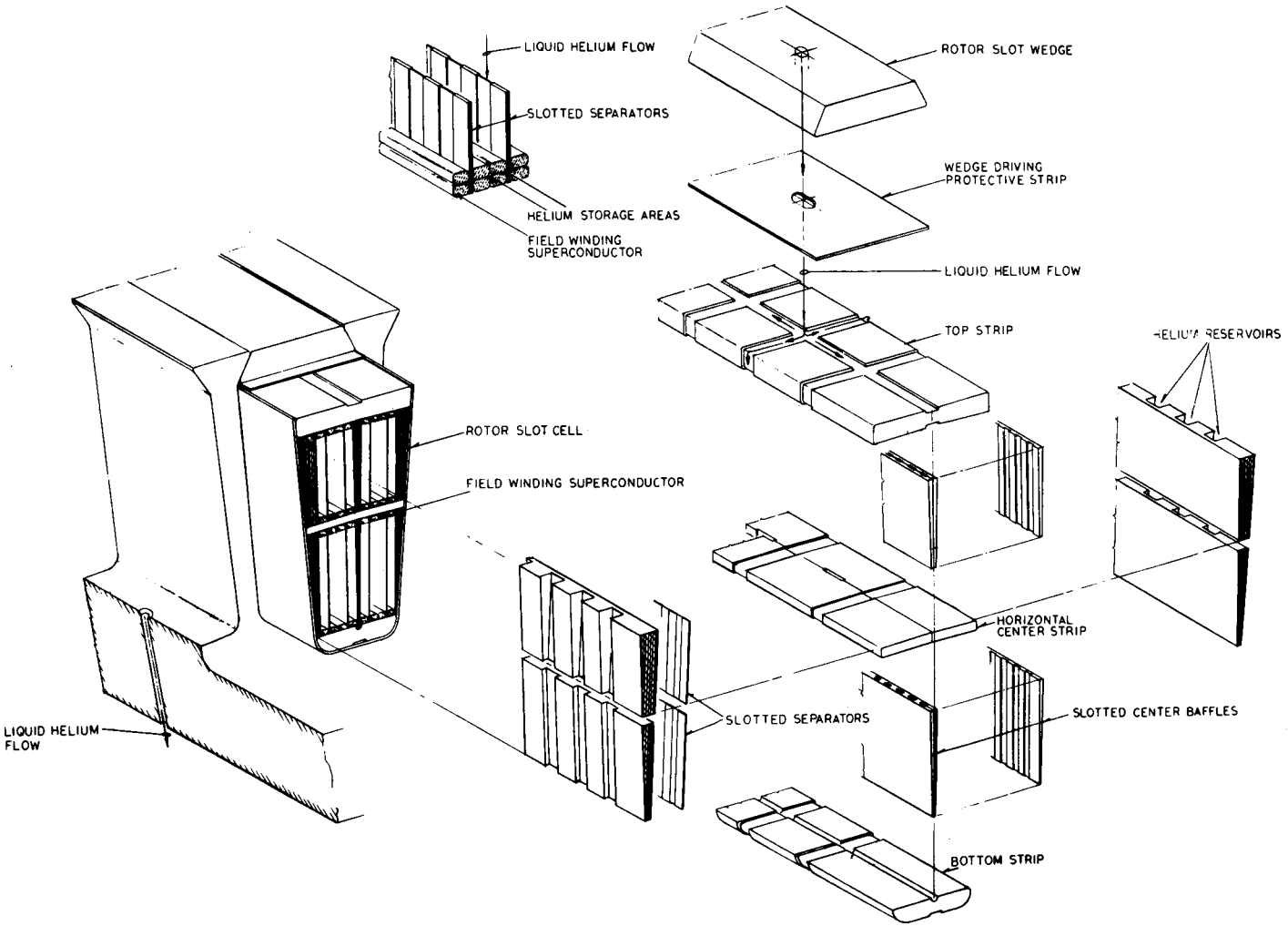

Figure 3-42. Rotor Helium Slot Circuit

are slotted to allow helium storage and flow. Cooling ducts, similar to those used on the Westinghouse 5 MVA machine, will be wound into the coil.

For a 300 MVA generator, there are 24 slots that accommodate six coils per pole and there are 8 columns of conductors in each slot. See Figure 3-43. Each column is divided into top and bottom conductors separated by a horizontal center strip in order to facilitate their winding. The conductors are wound with the side parallel to the bottom of the slot. This winding configuration was chosen because the predominate force is radial, thus resulting in a more stable mechanical structure. All the bottom conductors will be wound first starting from the smallest turns (nearest to the pole head) to the largest turns. Tools can be developed to overbend the conductor corners so that the conductors will fit tightly against the pole head and the filler blocks. Since the crown on the conductor is only 0.023 cm (.009 in.) wide separators may be required between every column of the conductors. The top conductors will be wound in similar fashion. The conductors should be compressed during winding before positioning of the horizontal center strips and wedging of the slots. Filler strips installed below the wedges will ensure a tight radial fit. The circumferential tightness will be ensured by fitting the filler and conductor dimension to the finished slot size.

A superconducting joint may be required for each half column of conductors with a possible maximum total of 200 and 250 joints for the 300 and 1200 MVA machines respectively. The joint design will be based on the state of art, i.e., a soldered lap or ultrasonic welded joint with resistance of 10^{-8} to 10^{-9} . The design field current is 1000 amps. The total loss of the joints is acceptable if the joints are suitably located and distributed. As the winding technique is developed and improved, it is anticipated that the total number of joints will be in a relatively low field area beyond the end turns where ample helium can be provided along the joint to remove the joint losses.

During the cooldown to liquid helium temperature a slight difference in thermal expansion may occur between the superconductor and the radial teeth. In both the 300 MVA and 1200 MVA designs this difference is no more than a mil, which indicates that a tight room temperature wedging procedure will keep the field winding tight throughout the operating temperature range. The axial thermal contraction difference will increase the axial tension in the superconductor due to its higher percentage of thermal contraction during cooldown. This difference is of the order of .08 cm (.030 in.) and .15 cm (.060 in.) for the 300 and 1200 MVA machines for a total strain of 0.35% which is acceptable for this material.

10. Assemble field leads, collector shaft and helium transfer system. Since this part of the assembly is slender and weak, temporary support should be provided. An alternate procedure is to install these parts at a later stage, probably after the field coils are wound.
11. Install field winding lay-up support on I.D. of end windings.
12. Wind coils progressively from the smallest coil to the largest coil, installing spacers and blocks.
13. Wedge rotor winding.
14. Cap end winding with ground insulation.
15. Install temporary supports on ends.

B. Inner Rotor Assembly

This assembly comprises the field winding support, torque tubes and the flexible connection in addition to the previous assembly. In order to facilitate the provision of balancing weights the radiation shield will be mounted after balancing. The assembly sequence is presented in the following:

1. Shrink the retaining ring over the previous assembled field winding and helium management assembly.
2. Seal weld the ring at each end.
3. Attach end (axial) radiation plates.
4. Attach flexible connection to turbine end torque tube.

The complete inner rotor is ready to be prepared for balancing.

C. Balance of Inner Rotor

It is highly recommended that the rotor be balanced twice, one for the inner rotor and the other for the complete rotor. Means must be provided at this stage to support the inner rotor in the balance rig. One way to do this is to use the existing shaft ends which can be rigidly bolted to the inner rotor with suitable spacers to form a continuous structure. Special bolts must be provided. Shear sleeves will not be installed. Balance holes or grooves can be provided in the torque tube flanges and at the ring-shaped sections between the torque tubes and the field winding support.

D. Complete Rotor Assembly

This assembly consists of the damper shield and support, the radiation shield, the shaft ends and the inner rotor.

1. Disassemble the balanced inner rotor from the shaft ends and the spacers. Replace and tighten all the bolts between the flexible connection and the torque tube.
2. Mount the radiation shield to its supports on the torque tubes.
3. Make helium pipe connections to radiation shield.
4. Slide the damper and support over the inner rotor from the excitation end.
5. Assemble the E.E. shaft end. Fit shear sleeves and tighten bolts. Install vacuum seal.
6. Loosely assemble the T.E. shaft end. Fit shear sleeves but do not tighten bolts.
7. Contract the inner rotor to one half of its total thermal contracted length at 4.2°K. This may be done by temporarily using liquid nitrogen in the helium management system. Some heat may be required to keep the damper up around room temperature. The flexible connection should now be undeflected; shim or make final adjustments as necessary.
8. While the inner rotor is at liquid nitrogen temperature, tighten the bolts connecting the turbine end stub shaft, the flex connection, and the damper assembly. Allow rotor to warm up. Install vacuum seal.

The complete rotor, shown in Figure 3-40 , is ready for final machining and balancing.

Inner Rotor

The inner rotor includes the superconducting field winding and its support, the torque tubes and the helium management system - a support system which distributes and controls the flow of helium throughout the rotor. The helium management system will be treated in a separate section.

Field Winding Support

Three different arrangements have been considered and are described in the following paragraphs.

Toothed Rotor Design

The main body of the field winding support is essentially a long thick cylinder with slots in the outer surface. The rotor cross sections for the 300 and 1200 MVA generators are shown in Figures 3-43 and 3-44. The superconductors are wedged into slots in the same manner as in conventional generators. The conductors are wound in a slot cell and the bottom and side filler strips as shown in Figure 3-45. The strips, which are provided to protect the winding and the ground insulation from the differential movements between the conductors and the structure,

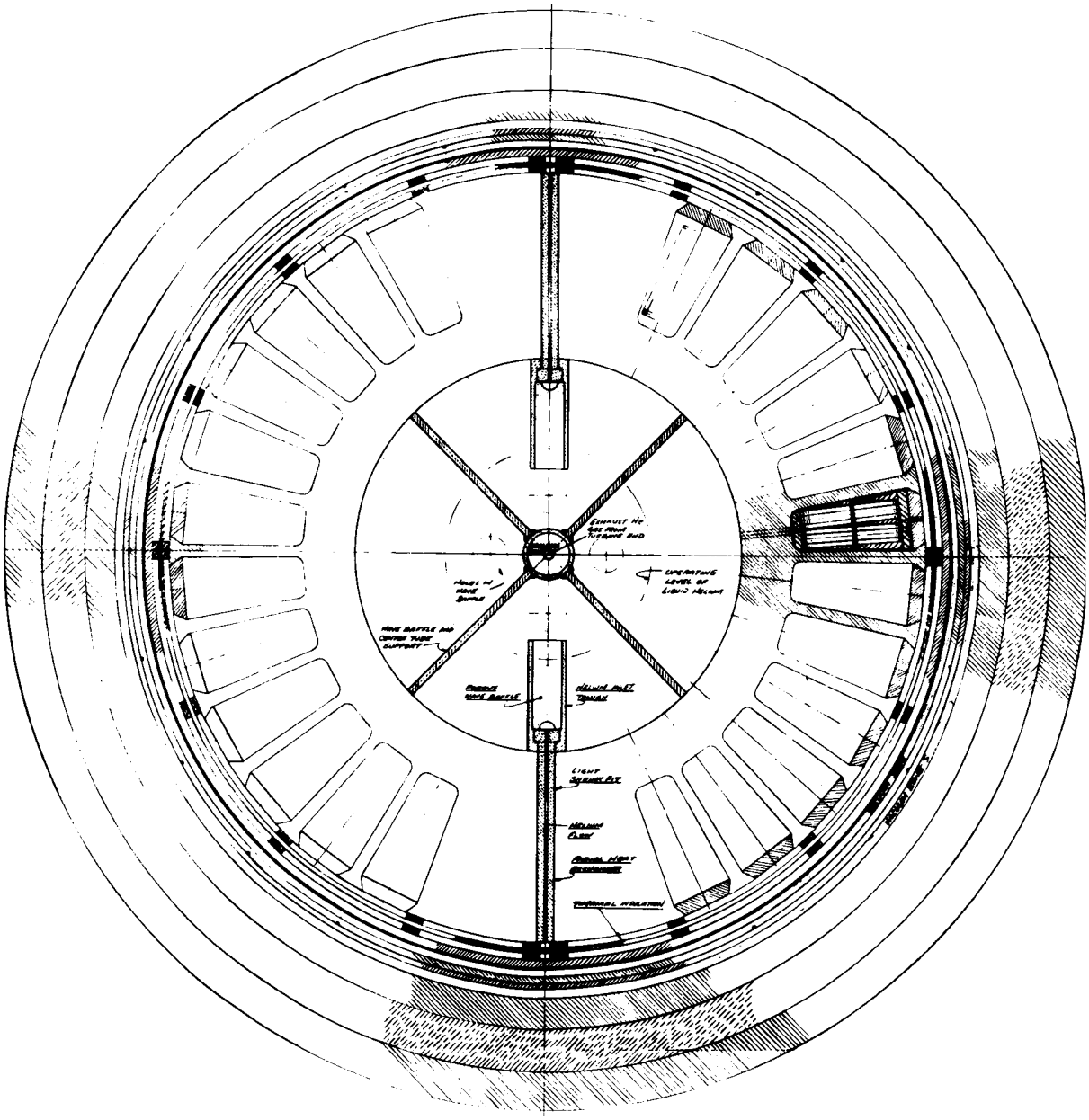

Figure 3-43. Rotor Cross Section - 300 MVA

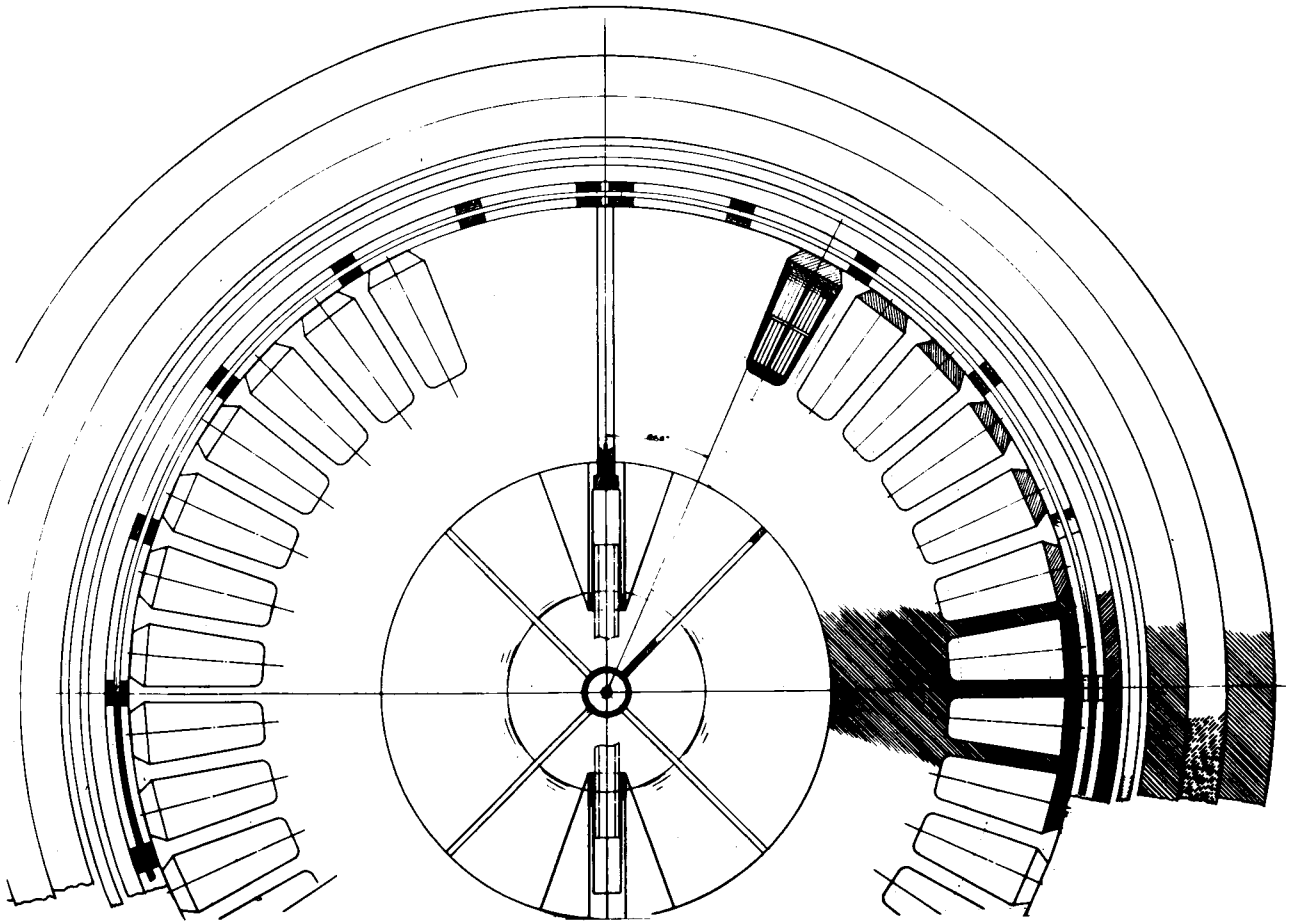

Figure 3-44. Rotor Cross Section - 1200 MVA

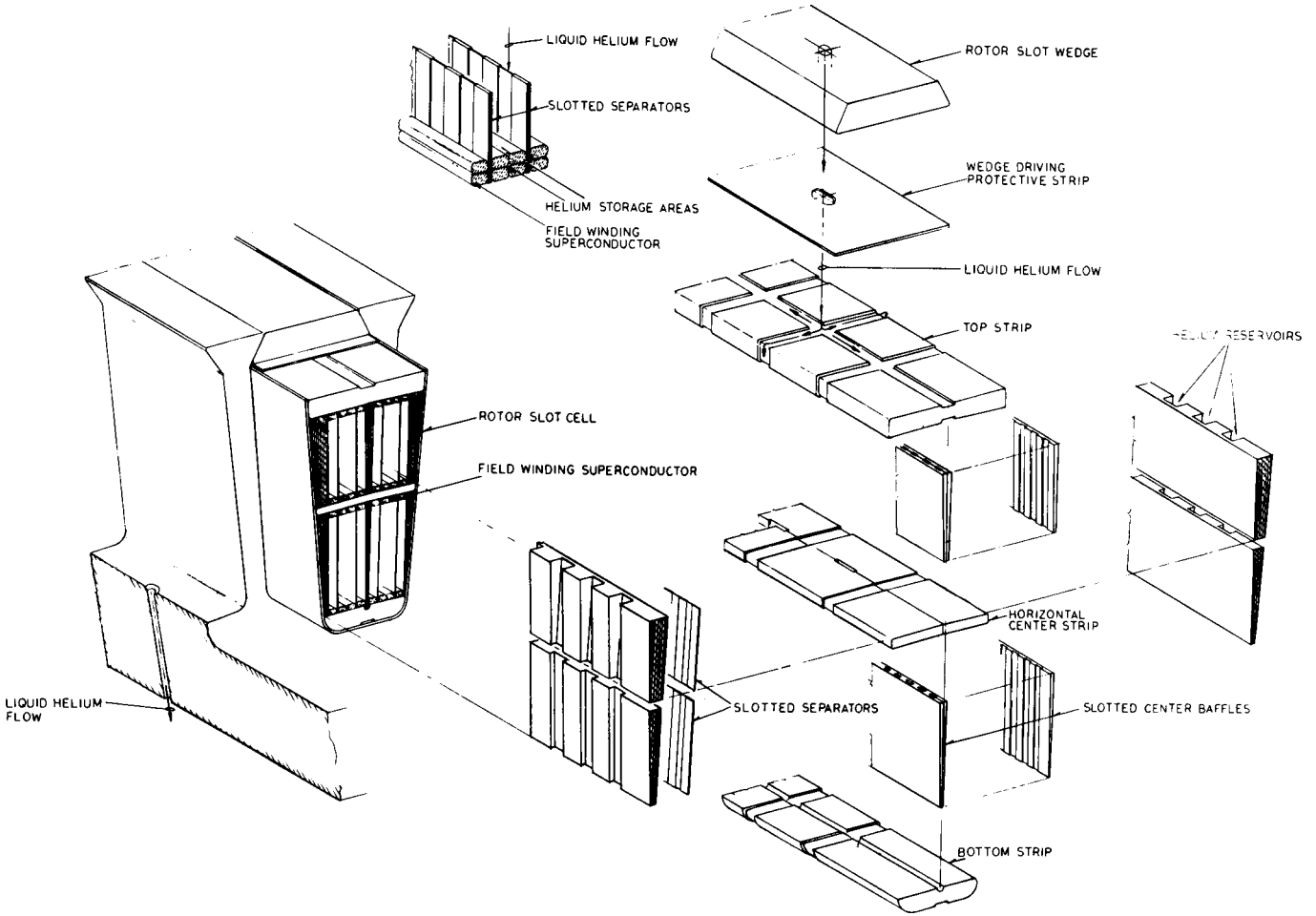

Figure 3-45. Field Winding Slot

The torque reaction of the machine, which will be supported by a pressure between the conductors and the teeth, results in a conductor tooth pressure less than 1.4 MPa (200 psi). The centrifugal pressure between the conductors and the wedges is of the order of 21 MPa (3000 psi) and 28 MPa (4000 psi) at operating speed for the 300 and 1200 MVA machines, respectively. This pressure is within the compressive strength of the superconductor, conductor insulations and slot fillers.

Radial forces of the conductors will be supported by the wedge-tooth structure. The wedge thickness is sized to limit the maximum wedge bending stress to 400 MPa (60,000 psi) at 20% overspeed. Combined stress at the root of the tooth due to the torque reaction and radial forces at 20% overspeed is below 70% of the material yield strength at 4.2 K.

The end turns are retained by an external tube shrunk over the inner rotor body. The end turns are bonded first with a fiber reinforced plastic to provide a smooth cylindrical surface to seat the end turn retaining tube. The tube is seal welded at each end and also serves to contain the helium in the winding area. Clearance is provided for thermal insulation and extra helium storage between the teeth and the tube over the straight portion of the winding. This clearance also facilitates the shrink of the long tube over the rotor body. A cryogenic damper shield is bonded to the outer surface of the inner rotor. By utilizing the cryogenic damper shield, the losses in the rotor teeth and the structural cylinder can be reduced to such an insignificant value that the slot-tooth field winding support can be selected as feasible. Radial helium passages must be provided probably in the form of a few holes in the rotor body. This arrangement which is close to present conventional generator design practice, will give excellent support for the conductor under rotational and magnetic forces and will be used in the future superconducting generators.

Rotor Torque Tube

Design objectives for the SCTG rotor torque tube are:

1. Transmit torque
2. Minimize or optimize conduction heat leak
3. Sustain centrifugal loads
4. Sustain end conditions
5. Accommodate internal connections (helium, leads, etc.)
6. Provide mount for radiation shield
7. Provide needed lateral stiffness

8. Provide needed torsional stiffness
9. Support inner rotor mass
10. Sustain temperature gradients
11. Avoid critical buckling stress
12. Sustain vibration loads
13. Consider variable (temperature dependent) material properties
14. Maintain fracture toughness

Torsional vibration, lateral vibration, and other considerations have demonstrated the desirability of an arrangement using two Inconel torque tubes. An alternative which has been considered is a single torque tube configuration. Titanium and composite materials have been considered as alternate torque tube materials.

Because of titanium's lower modulus, titanium torque tubes are subject to approximately twice the torsional deflection as Inconel tubes. Desire to minimize losses due to torsional deflections therefore has led to the consideration of other materials, including composites.

Problems associated with the use of high modulus reinforced composite materials for the SCTG rotor torque tube application include:

1. Difficulty of maintaining sealed vacuum due to material outgassing.
2. Difficulty of developing end transitions from reinforced composites to metal.
3. High cost (would expect future decrease). This material was therefore given no further consideration.

The two torque tubes are of similar general dimensions. The cold (field winding) end conditions of each torque tube differ in that there are two different mounting methods. The torque tube at the exciter end of the rotor is bolted to the stub shaft and the outer rotor assembly, while the torque tube at the turbine end of the rotor is connected to the mechanism for accommodating differential thermal expansion and contraction. The exciter end torque tube has been studied for design purposes. Its warm end connection to a very stiff member is expected to be a worse case than the end mounting of the turbine end torque tube.

Heat leak considerations demonstrate the need for helium cooling of the torque tubes. This cooling will maintain the desired temperature gradient in the torque tube. The brazed-in cooling tube is shown in Figure 3-46.

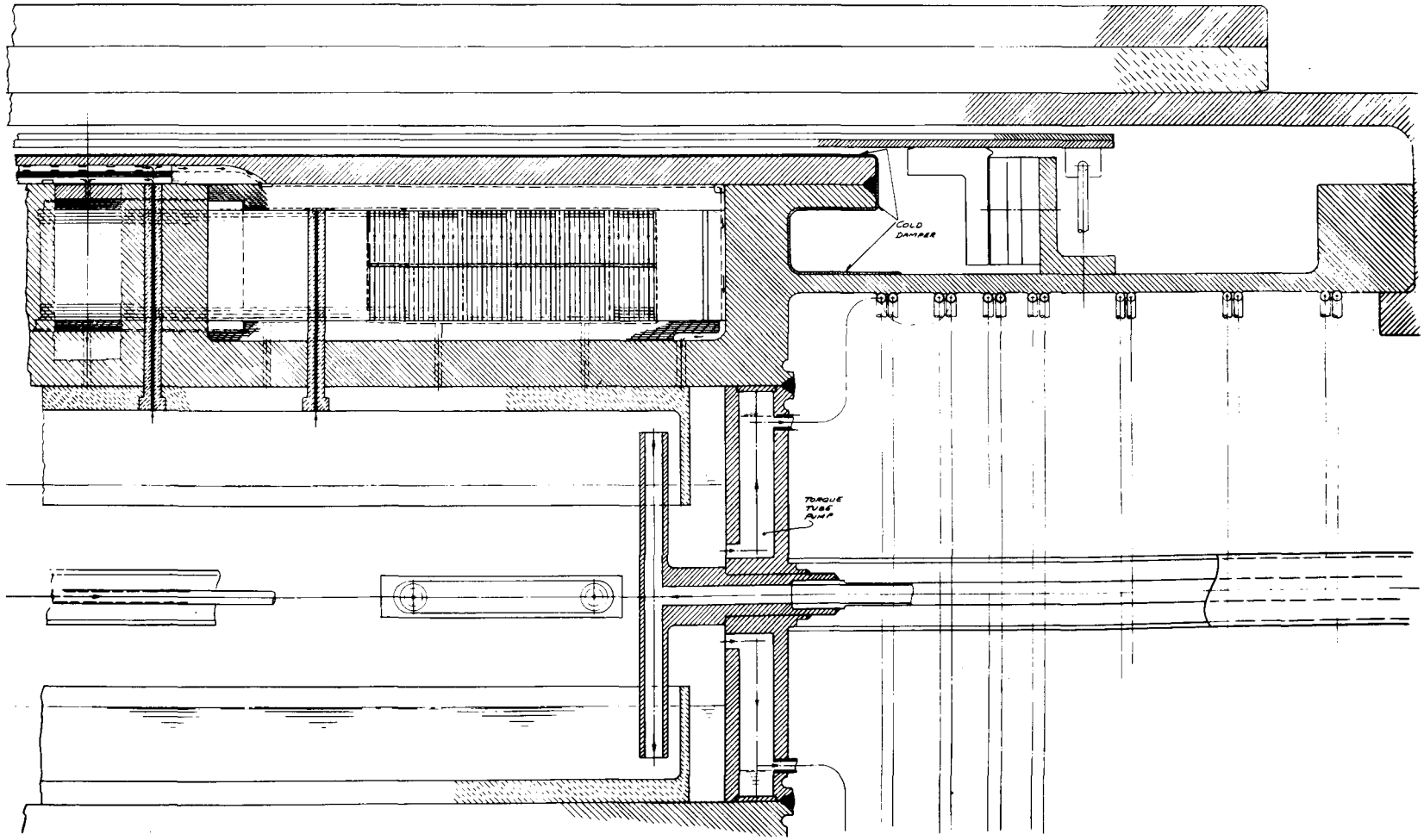

Figure 3-46. Torque Tube Design

The 300 MVA torque tube mean radius used for analysis was 21.6 (8.5 in.), thickness was 1.27 cm (.5 in.), and length was 43.2 cm (17 in.). Loads acting on the torque tube, shown in Fig. 3-47 include torque, centrifugal forces, end restraints, inner rotor weight, lateral vibration, and longitudinal thermal gradients. Stress calculation nomenclature is shown in Figure 3-47.

Stress calculations in the torque tube have been made for all conditions including standstill, running, overspeed, short circuit, quench, and test conditions. Calculated triaxial component stresses include rotational, thermal, end condition (forces and moments), torque, weight, and vibration stresses.

The torque tube analysis completed within the framework of the present contract has proven that the general configuration shown in Figure 3-47 is feasible. Additional detailed analysis, which is beyond the scope of the present contract, should be made to finalize the torque tube design in the 120°K area where the radiation shield is mounted. Four holes for radiation shield helium supply and return tubes are needed in each torque tube. Also bolt holes or welds will probably be required for the flex ring mounts. Future analysis should be made using the latest torque tube dimensions and temperature curves. Alternate schemes including welded-on and bolted-on torque tubes may be developed to circumvent possible material problems, In particular, the toothed inner rotor may not be available with integral torque tubes in Inconel 718. No insurmountable problems in this area are anticipated.

τ_{lr} (Figure 3-47) varies through the wall thickness. At the inner and outer surfaces, $\tau_{lr} = 0$. Also, at the inner and outer surfaces, bending stresses are maximum. In this way $\tau_{lr} = \sigma_r = \tau_{tr} = 0$. In Figure 3-47 it is shown that torque load produces $\tau_{lt} = \tau_{tl}$ shear stress. This stress reaches a maximum at the outer surface. Because the tube diameter is large relative to its thickness this shear stress varies only slightly through the wall thickness.

Axial thermal gradients produce thermal bending stresses in the σ_l and σ_t directions. It has been assumed that the mechanism accommodating differential thermal expansion creates some axial force in the inner and outer rotors. This is described as σ_l direct tensile stress in the torque tube. The inner rotor weight produces a rotating σ_l bending stress in the torque tube. Lateral vibration deflections also cause σ_l bending stress. Centrifugal loads cause σ_t tensile stress.

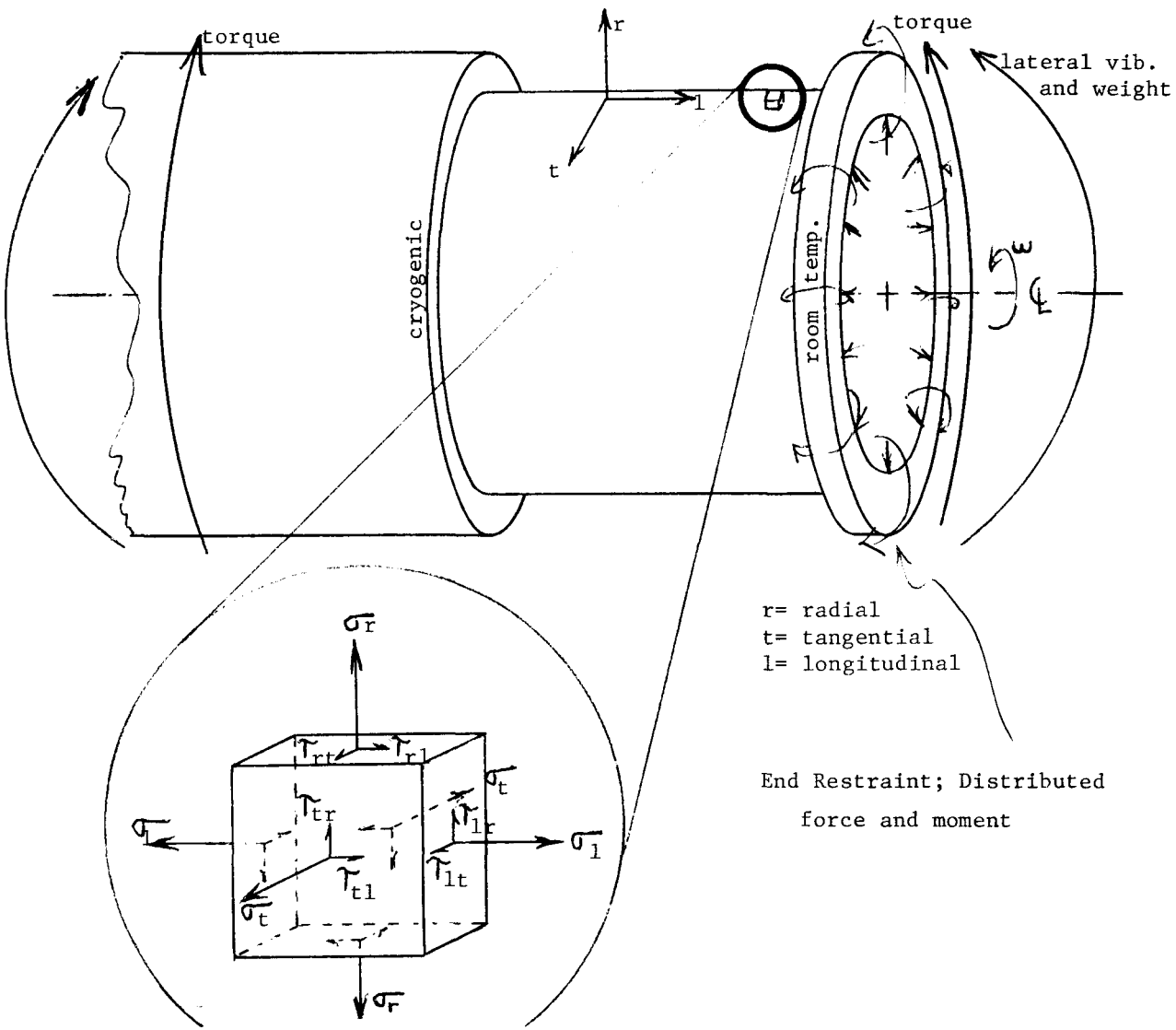

Figure 3-47. Rotor Torque Tube Stress Nomenclature

The warm end condition is a bolted connection to the stub shaft and outer rotor assembly. The relative stiffness of the stub shaft compared to the torque tube leads to the assumption that the torque tube warm end will follow deflection of the stub shaft. Because of the bolted connection, slope of the tube wall at this end must be zero; that is it must parallel the rotor axis. The presence of the warm end connection is represented by distributed forces and moments at that end. The effect of these warm end conditions on the other (cold) end of the torque tube is negligible. This is a result of the torque tube being a long beam[1] having Bl > 5. The value of Bl is found using:

$$B = \sqrt[4]{\frac{3(1-\mu^2)}{r^2h^2}} = \sqrt[4]{\frac{3(1-.3^2)}{(8.5)^2(.5)^2}} = .62$$

for l = 16.8 inch; Bl = (.62) (16.8) = 10.42 > 5.

Thermal and centrifugal stresses have been calculated using computer program PH0719.[2] Material properties which vary with temperature are used.

Rotor torque is obtained as follows (for unit MVA):

$$\text{torque}_{\text{rotor}} = (300 \text{ MVA}) \left(\frac{10^6}{\text{mega}}\right) \left(\frac{\text{watt}}{\text{VA}}\right) \left(\frac{.7376 \text{ ft lb}}{\text{watt sec}}\right) \left(\frac{\text{min}}{3600 \text{ rev}}\right) \left(\frac{60 \text{ sec}}{\text{min}}\right) \left(\frac{\text{rev}}{2\pi \text{ rad}}\right) \left(\frac{12 \text{ in}}{\text{ft}}\right) =$$

$$\text{torque}_{\text{rotor}} = 7.97 \times 10^5 \text{ Nm } (7.05 \times 10^6 \text{ in. lb.})$$

Torque is assumed to be equally divided between the two torque tubes:

$$\text{torque}_{\substack{\text{torque tube} \\ \text{steady state}}} = \frac{7.97 \times 10^5 \text{ Nm}}{2} = 3.99 \times 10^5 \text{ Nm } (3.53 \times 10^6 \text{ in. lb.})$$

Short circuit torque, 3T, on the inner rotor is obtained from torsional analysis in Quarterly Report No. 2. Short Circuit torque is assumed equally divided between the torque tubes:

$$\text{torque}_{\substack{\text{torque} \\ \text{tube} \\ \text{short circuit}}} = \frac{3}{2} (7.97 \times 10^5 \text{ Nm}) = 1.20 \times 10^6 \text{ Nm } (1.06 \times 10^7 \text{ in. lb.})$$

Shear stress in the torque tube is given by:

$$\tau_{\substack{\text{steady}\\\text{state}}} = \frac{T}{J}\frac{c}{} = \frac{(3.53 \times 10^6 \text{ in. lb.})\ (8.5 \text{ in.})}{1610 \text{ in.}^4} = 1.28 \times 10^8 \text{ pascal}\ (18637 \text{ psi})$$

$$\tau_{\substack{\text{short}\\\text{circuit}}} = \frac{(1.06 \times 10^7)(8.5)}{1610} = 3.86 \times 10^8 \text{ pascal (56000 psi)}$$

Stress in the torque tube due to the inner rotor weight is calculated using a simple beam approximation as shown in Figure 3-48. This rotating bending type (cyclic)stress is found using:

$$\sigma_1 = \frac{M}{I}\frac{c}{} = \frac{(\frac{3}{16})\ (6000)(120)(8.25)}{805} = 9.54 \times 10^6 \text{ pascal (1384 psi)}$$

For all conditions it is assumed that the inner rotor mass, weighing 2.67×10^4 N (6000 lb.) is 254 μm (.010 inch) eccentric. The unbalance forces at 3600 rpm and 4320 rpm (overspeed) are used in calculating σ_1 stress in the torque tube. Again the inner rotor is modeled as a beam in Figure 3-48. Assuming 25.4 μm (.010 inch) eccentricity the unbalance forces are:

$$F = mr\omega^2 = \frac{(6000 \text{ lb})(.010 \text{ in})\ (\frac{3600 \text{ rev}}{\text{min}})(\frac{\text{min}}{60 \text{ sec}})(\frac{2\pi \text{ rad}}{\text{rev}})^2}{386 \text{ in./sec.}^2} = 98270 \text{ N}\ (22093 \text{ lb})\ @\ 3600 \text{ rpm}$$

$$F = \frac{(6000)(.010)\ \left(\frac{4320\ (2\pi)}{60}\right)^2}{386} = 141500 \text{ N (31812 lb.) @ 4320 rpm}$$

Using Figure 3-48,the stresses in the torque tube due to the assumed unbalance are then:

$$\sigma_1 = \frac{(\frac{3}{16})(22093)(120)(8.25)}{805} = 3.51 \times 10^7 \text{ pascal (5094 psi) @ 3600 rpm}$$

$$\sigma_1 = \frac{(\frac{3}{16})(31812)(120)(8.25)}{805} = 5.06 \times 10^7 \text{ pascal (7336 psi) @ 4320 rpm}$$

These stresses due to rotor unbalance are in general not of a cyclical nature. An observer on a stationary reference sees the spinning rotor vibrating

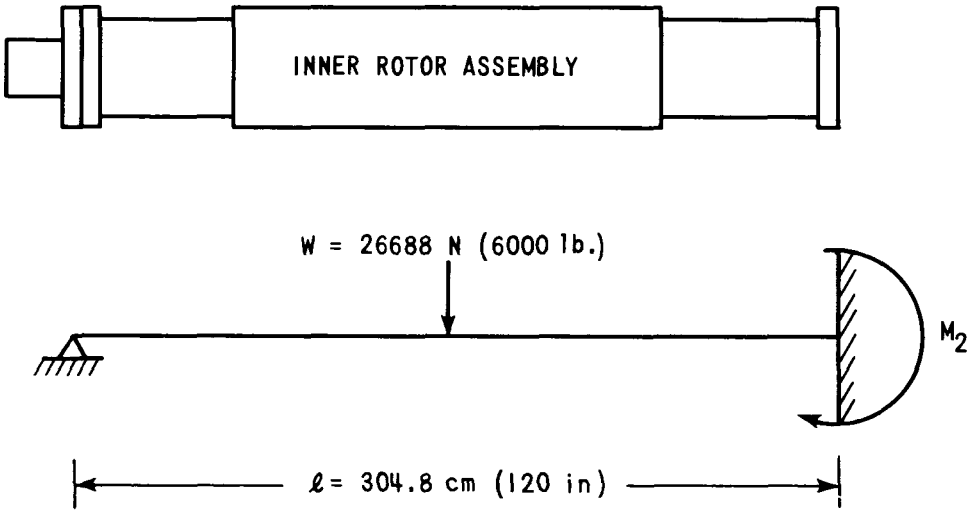

$$I = \frac{\pi}{64}(16.5^4 - 15.5^4) = 5194 \text{ cm}^4 \ (805 \text{ in}^4)$$

$$M_2 = \frac{3}{16} W\ell$$

$$\sigma = \frac{Mc}{I}$$

Figure 3-48. Model for Calculation of Torque Tube Stress due to Inner Rotor Weight

due to unbalance. However, if an observer were able to spin with the ω of the rotor and observe the unbalance deflection, the deflection would appear to be a static deflection.

It is assumed above that the bearing pedestals have horizontal and vertical stiffnesses nearly equal. If these stiffnesses are significantly unequal, the unbalance deflection might have a static component and a large cyclic component which varies with each revolution as the pedestal and rotor interact. Generally, a tall slender pedestal would be expected to deflect more horizontally than it would vertically. This might give rise to an elliptical rather than round deflection orbit. Cyclical inbalance stresses on the rotor are minimized by proper pedestal design. See Figure 3-49.

Maximum shear stresses in the highest stressed regions (near the warm end) of the torque tube have been calculated from component stresses using a Mohr's circle calculation:

$$\tau_{max} = \sqrt{\left(\frac{\sigma_l - \sigma_t}{2}\right)^2 + \tau_{tl}^2}$$

For all conditions except short circuit maximum shear stress is limited to 70% of the shear yield. For short circuit, maximum shear stress is limited to 80% of shear yield.

Principal tensile stresses are:

$$\sigma_1 = \frac{\sigma_l + \sigma_t}{2} + \tau_{max}$$

$$\sigma_2 = \frac{\sigma_l + \sigma_2}{2} - \tau_{max}$$

For all conditions except short circuit, the maximum tensile stress is limited to 70% of the tensile yield. For short circuit, maximum tensile stress is limited to 80% of tensile yield.

Calculations indicate that helium flow rate in the torque tubes varies with transient conditions such as short circuit and quench. Increased helium flow rates in the torque tubes cause steeper temperature gradients near the warm ends. This causes higher thermal bending stresses.

UNDESIRABLE PEDESTAL SHAPE (END VIEW)

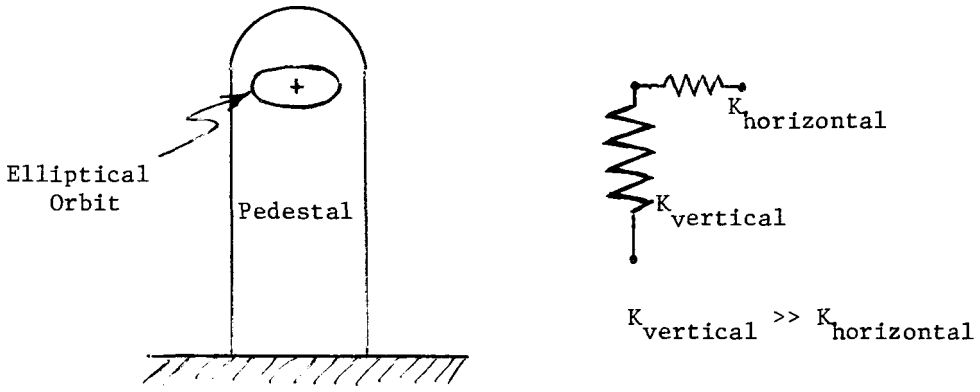

Horizontal Pedestal Stiffness << Vertical Pedestal Stiffness

For an unbalanced rotor, this may cause an elliptical rotor orbit as the pedestal deflects more horizontally than it does vertically with each revolution. Cyclical stress arises from unbalance.

DESIRABLE PEDESTAL SHAPE

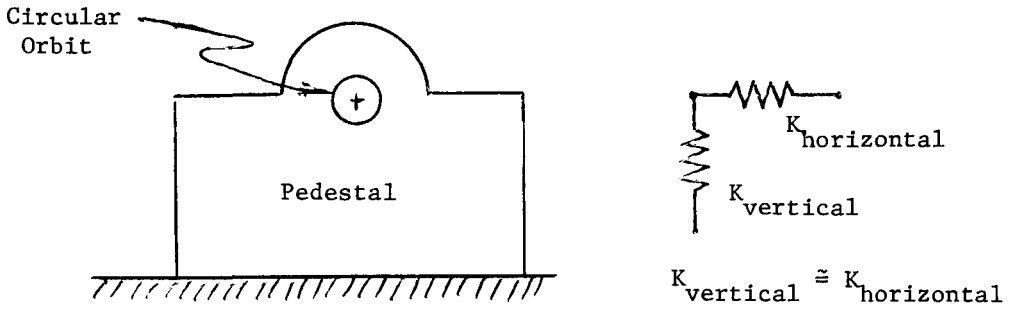

Horizontal Pedestal Stiffness ≅ Vertical Pedestal Stiffness

This results in a nearly circular rotor orbit. Unbalance stress is static stress.

Figure 3-49. Effect of Bearing Pedestal Stiffness on Lateral Vibration of SCTG Rotor

Torque tube stresses are calculated for conditions shown in Table 3-21. Steady state (normal running) calculations, are made assuming a temperature profile (Figure 3-50) which approximates a 1.07 kg/hr. (2.35 lb./hr.) helium flow rate through each torque tube. Short circuit calculations are made using a temperature profile (Figure 3-50) which approximates a helium flow rate through each torque tube of 2.25 kg/hr. (4.95 lb./hr.). It is conservatively assumed that this helium flow rate occurs simultaneously with the maximum short circuit torque.

Calculated stresses and criteria stress limits are listed in Table 3-22.

REFERENCES

1. Timoshenko, S., "Strength of Materials Part II", 3rd Edition, Van Nostrand Co., 1956.

2. Barton, S., "Shells of Revolution Program PH0719, Westinghouse Steam Division Proprietary Computer Program, 1960.

Table 3-21

GENERATOR TORQUE TUBE DESIGN CONDITIONS

Load Condition	Load #	RPM	Temperature Distribution	Torque	Lateral Vibration Load	Stress Criteria
Standstill A)	1	0	Uniform	0	0	$\sigma_{max}=(.70)(\sigma_y)$ $\tau_{max}=(.70)(\tau_y)$
Standstill B)	2	0	See Figure 3-50	0	0	
Spinning (R.T. Test)	3	3600	Uniform	0	98270 N (22093 lb)	
Normal Running	4	3600	See Figure 3-50	$\frac{T}{2}$		
Short Circuit	5	3600	See Figure 3-50	$\frac{3}{2}$ T		$\sigma_{max}=(.80)(\sigma_y)$ $\tau_{max}=(.80)(\tau_y)$
120% Overspeed A) Test	6	4320	Uniform	0	141500 N (31812 lb)	$\sigma_{max}=(.70)(\sigma_y)$ $\tau_{max}=(.70)(\tau_y)$
120% Overspeed B)	7	4320	See Figure 3-50 (assumed same as short circuit)	0		
Quench	8	3600	Requires further study		98270 N (22093 lb)	

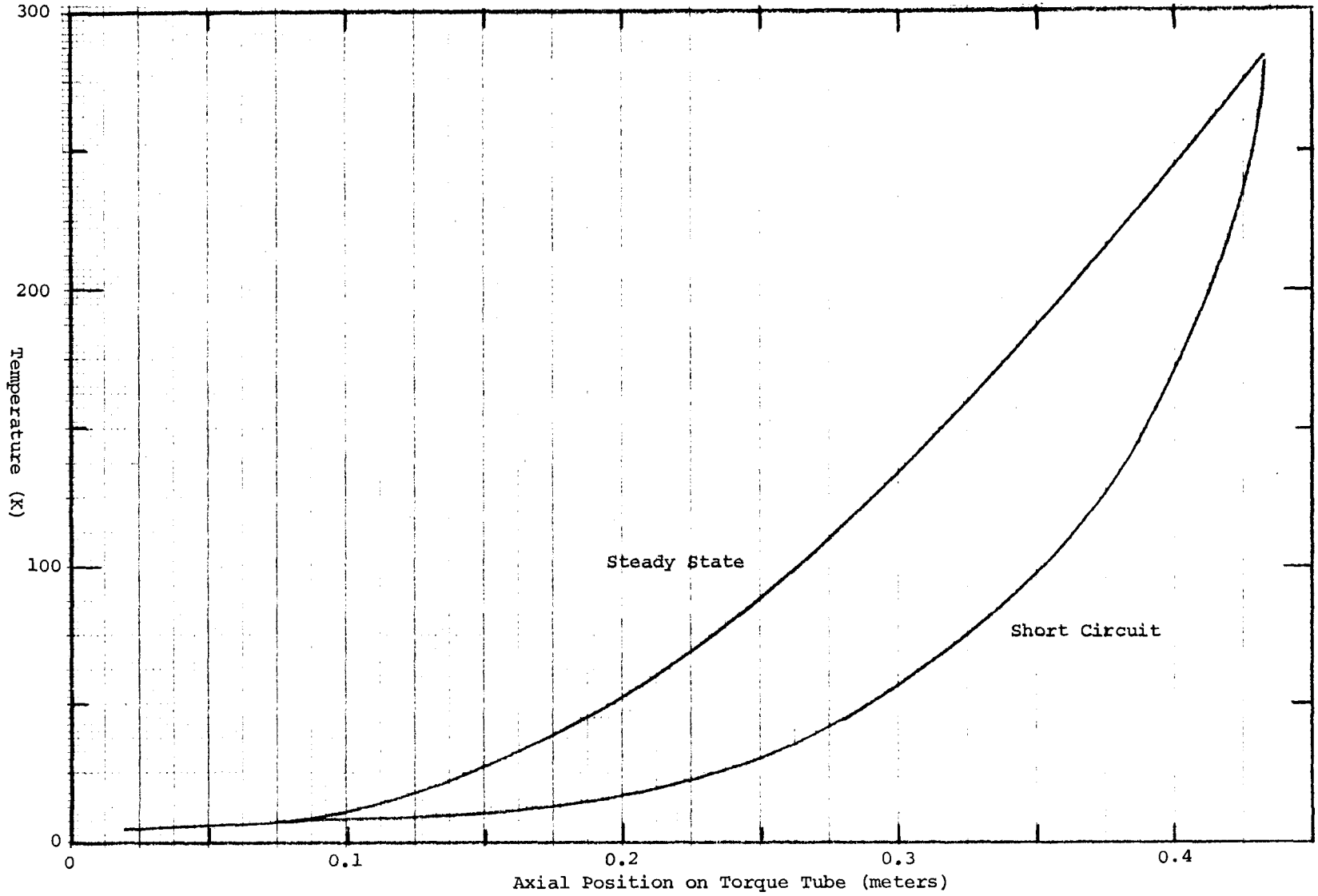

Figure 3-50. Torque Tube Temperature Distribution - 300 MVA Rotor

Table 3-22

TORQUE TUBE STRESS CALCULATIONS (WARM END)

300 MVA SCTG

Load		σ_1 Components						σ_t Components										
								Direct		Bending								
Cond.	#	σ_1 Rotor Weight	σ_1 Unbal-ance	σ_1 Sliding Joint	σ_1 Cent. Force	σ_1 Thermal	σ_1 Total	σ_t Cent. Force	σ_t Thermal	σ_t Cent. Force	σ_t Thermal	σ_t Total	τ_{t1} Torque	τ_{max}	σ_1	σ_2	$\tau_{criteria}$	$\sigma_{criteria}$
Stand-still	1	9.54×10^6 ±1384	0	-1.38×10^7 -2000	0	0	2.33×10^7 3384	0	0	0	0	0	0	1.17×10^7 1692	2.33×10^7 3384	0	4.40×10^8 63840	7.72×10^7 112000
↓	2		0	1.38×10^7 +2000	0	-1.04×10^8 -15120	-1.0×10^8 -14504	0	-1.89×10^8 -27461	0	-3.13×10^7 -4536	-2.21×10^8 -31997	0	6.03×10^7 8747	-1.0×10^8 -14504	-2.21×10^8 -31998	↓	↓
Spinning	3		3.51×10^7 ±5094	-1.38×10^7 -2000	-8.35×10^7 -12108	0	-1.42×10^8 -20586	4.81×10^7 6977	0	-2.50×10^7 -3632	0	2.31×10^7 3345	0	8.25×10^7 11966	2.31×10^7 3346	-1.42×10^8 -20587	↓	↓
Normal Running	4		↓	1.38×10^7 +2000	↓	-1.04×10^8 -15120	-2.19×10^8 -31706	↓	-1.89×10^8 -27461	↓	-3.13×10^7 -4536	-1.98×10^8 -28652	1.29×10^8 186 37	1.29×10^8 18699	-7.92×10^7 -11480	-3.37×10^8 -48878	↓	↓
Short Circuit	5		↓	1.38×10^7 +2000	↓	4.14×10^8 60112	3.89×10^8 56482	↓	-1.89×10^8 -28641	↓	1.24×10^8 18034	-5.04×10^7 -7312	3.86×10^8 56000	4.44×10^8 64447	6.14×10^8 89082	-2.75×10^8 -39862	5.03×10^8 72960	8.83×10^8 128000
120% Over-speed	6		5.06×10^7 ±7336	-1.38×10^7 -2000	-1.20×10^8 -17435	0	-1.94×10^8 -28155	6.93×10^7 10050	0	-3.61×10^7 -5230	0	3.32×10^7 4820	0	1.14×10^8 16488	3.32×10^7 4821	-1.94×10^8 -28156	4.40×10^8 63840	7.72×10^8 112000
↓	7		↓	1.38×10^7 +2000	↓	-1.04×10^8 -15120	-2.71×10^8 -39275	6.93×10^7 10050	-1.89×10^8 -27461	-3.61×10^8 -5230	-3.13×10^7 -4536	-1.87×10^8 -27177	0	4.17×10^7 6049	-1.87×10^8 -27177	-2.71×10^4 -39285	↓	↓
Quench	8	↓																

criteria (.57)(.70)(160000) = 4.40×10^8 pascal (63840 psi) shear
(.70)(160000) = 7.72×10^8 pascal (112000 psi) tensile

short circuit criteria (.57)(.80)(160000) = 5.03×10^8 pascal (72960 psi) shear
(.80)(160000) = 8.83×10^8 pascal (128000 psi) tensile

Radiation Shield and Mounting

A strong and cost effective radiation shield design and a method of mounting the shield in the rotor have been developed. The radiation shield has been designed to meet the following objectives:

1. Intercept and minimize losses due to radiation between the warm outer rotor and cold inner rotor.
2. Maintain 120°K steady state temperature.
3. Maintain low emissivity.
4. Maintain dynamic stability.
5. Sustain short circuit forces.
6. Does not contaminate vacuum.
7. Withstand centrifugal force.
8. Withstand non-uniform electromagnetic pressure.
9. Sustain thermal excursions, including loss of coolant.
10. Use state-of-the-art technologies.

Consideration was given to having one shield at a freely floating intermediate temperature, having one inner cooled shield at various temperatures, having two shields at freely floating intermediate temperatures, and having two inner cooled shields at various temperatures. Thermal analysis indicated the scheme having one inner cooled shield as being the most advantageous. This fortunately avoided the added mechanical complexity inherent in a two-shield system, but the inner cooling did create some design challenges.

Radiation Shield

Two basic inner-coiled constructions have been considered for the radiation shield. One is a honeycomb and the scheme chosen for development is two essentially solid shells shrunk together (Figure 3-51 and 3-52). Problems envisioned with the honeycomb scheme include difficulty of manufacture, cost, low thermal damping for the helium management systems, and manifolding difficulties.

The most severe problem with the honeycomb is the manufacture of a cylindrically curved, inner cooled honeycomb shape to the required overall strength level. Honeycomb manufacturers indicate that the 300 MVA size honeycomb radiation shield concept is beyond the present day honeycomb technology.

The scheme does have the advantage of having less mass than a more solid configuration. If lateral vibration of the radiation shield or other problems arise, the honeycomb holds promise as a possible but expensive solution requiring manufacturing development.

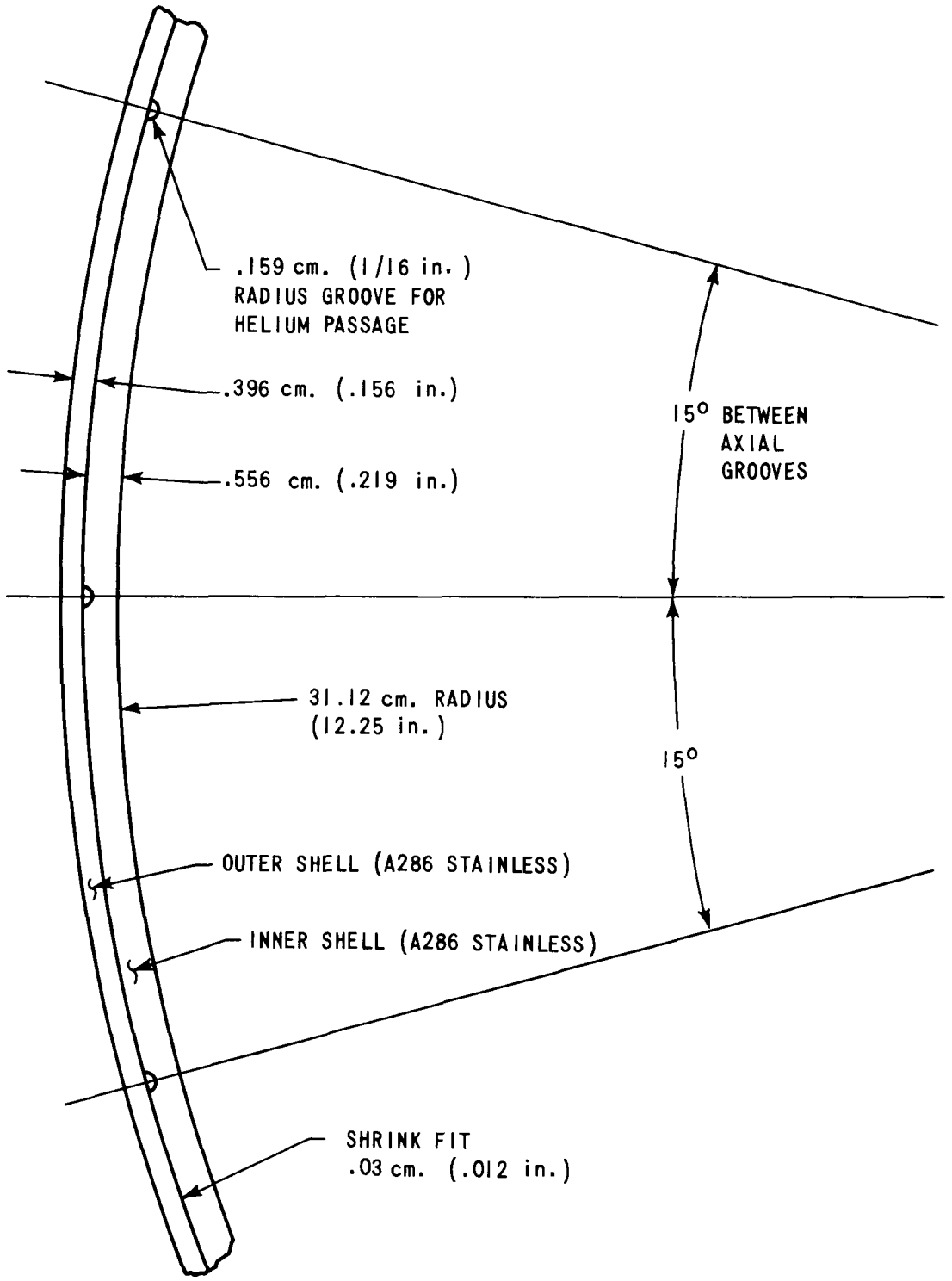

Figure No. 3-51. Section through Radiation Shield
300 MVA SCTG Rotor

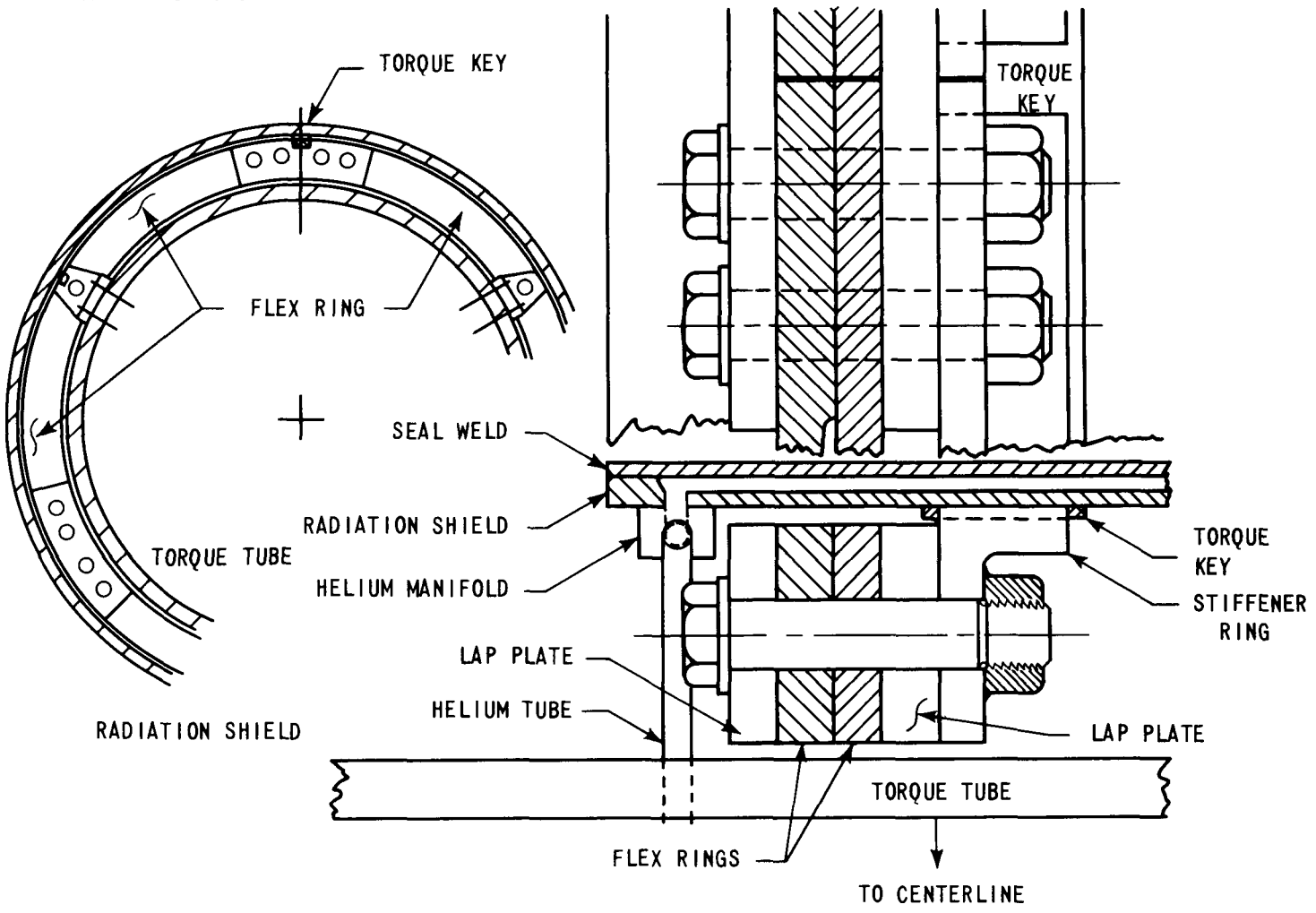

Figure 3-52. Flex Ring Radiation Shield Mount

The developed radiation shield configuration is shown in Figures 3-51 and 3-52 . Manufacturing will be straightforward and much less expensive. The result will be a strong shield with excellent structural integrity. The 300 MVA shield consists of a thin .396 cm (.156 in.) solid A 286 stainless steel outer cylinder shrunk onto a thicker .556 cm (.219 inch) layer in which helium passages have been machined.

Twenty-four grooves are cut with equal spacing (15°) around the circumference. Each groove is semicircular or oval in cross section rather than rectangular to reduce stress concentration. These slots are sized to provide cross sectional flow area approximately equal to the area of the torque tube helium supply and return pipes. They are fed by a low helium velocity plenum. For the 300 MVA machine with .64 cm x .081 cm wall (.25 inch x .032 inch wall) helium pipes, each semicircular slot radius is .159 cm (1/16 inch). Near each end of the shield is a large circumferential groove 1.27 cm (.5 in.) in axial width which connects the 24 axial grooves. For ease of manufacture, proper flow paths in each circumferential groove are obtained by welding 4 plugs in each circumferential groove so as to block helium flow to the adjacent set of grooves. The end result is 4 sets of 6-parallel grooves (Figure 3-53).

Before shrinking on the outer shell, four radial holes (Figure 3-53) are drilled through the inner shell into each circumferential groove. These holes are sized to accommodate the 4 helium tube manifolds (Figure 3-52) which will be brazed onto each end of the shield after the shield is mounted on the rotor. This provides two helium feed paths and two helium return paths at each end to match up with the four helium pipes coming through each torque tube.

After shrinking on the outer shell, both ends of the inner and outer shells are seal welded together to prevent helium leakage to the rotor vacuum. The shield is plated to reduce radiation heat transfer, and mounted on the rotor.

The .030 cm (.012 inch) shrink fit between the radiation shield shells produces stresses of 1.17×10^8 pascal (17000 psi) tension in the outer member and 8.27×10^7 pascal (12000 psi) compression in the inner member. The interface pressure is 1.45×10^6 pascal (211 psi) which gives sufficient heat transfer. Shear stress due to the shrink fit is 5.93×10^7 pascal (8600 psi).

Centrifugal stress in the shield is 1.12×10^8 pascal (16200 psi) at 3600 rpm and 1.60×10^8 pascal (23200 psi) at 4320 rpm.

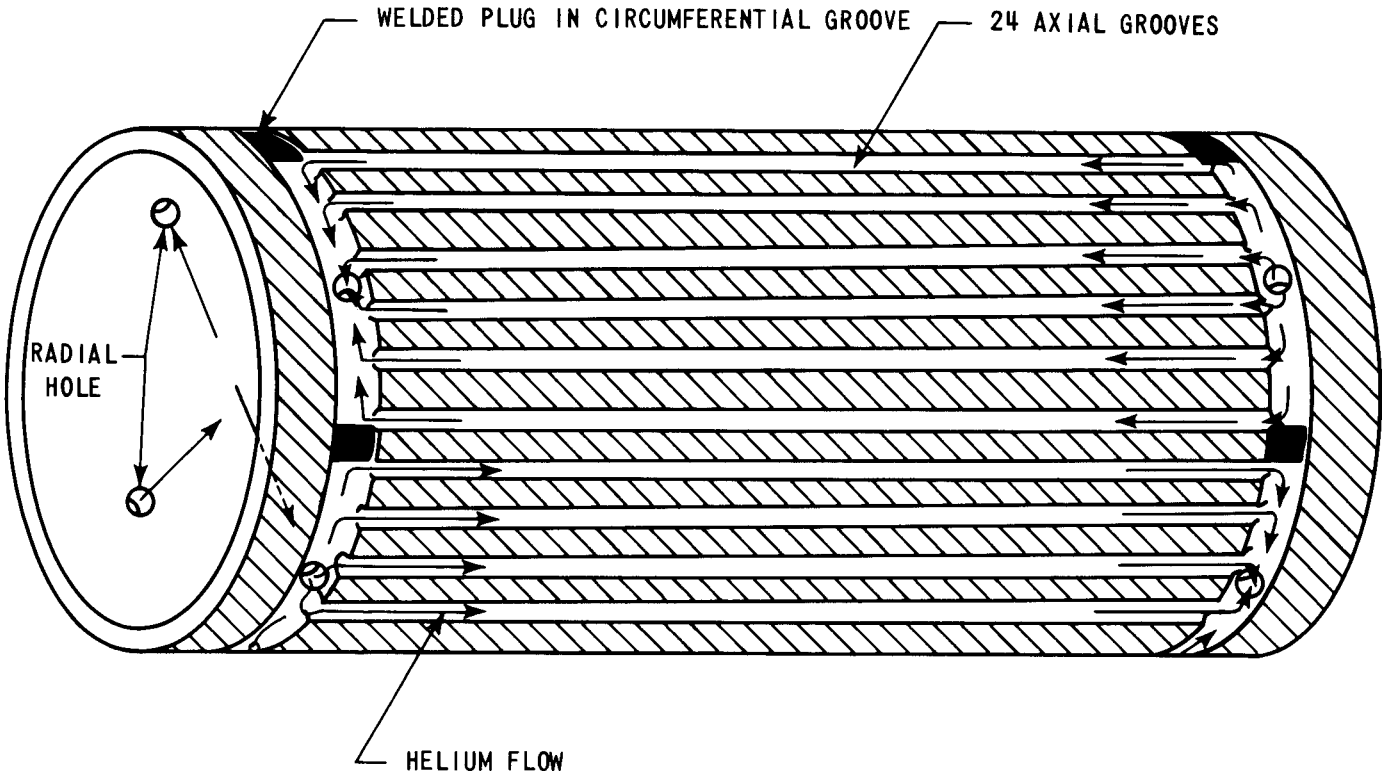

Figure 3-53. Radiation Shield Inner Shell Schematic of Cooling Grooves and Helium Flow

Bending stress due to short circuit nonuniform electromagnetic radial force, 8.27×10^4 pascal (12 psi) maximum single amplitude is 1.77×10^8 pascal (25600 psi). The corresponding maximum outward single amplitude radial deflection of the radiation shield is .53 cm (.21 inch). When added to the maximum inward .41 cm (.16 inch) radial deflection of the damper shield, the total .94 cm (.37 inch) exceeds the .64 cm (.25 inch) clearance. The phase relationship of these deflections has not been determined. The need for additional work in this area is indicated.

Near the ends of the radiation shield, the out-of-circle bending stress is reduced by stiffening and segmented rings pressed into the shield. The rings also serve the dual purpose of providing, without stress concentration, attachment points for the flexible mounting rings. The stiffener ring geometry is shown in Figure 3-52. The .015 cm (.006 inch) on the radius press fit between the stiffener ring and the shield creates a tensile stress of 6.69×10^7 pascal (9700 psi) in the radiation shield. The stiffener ring's corresponding compressive stress is 3.79×10^7 pascal (5500 psi). This fit is sufficient to hold the radiation shield and stiffener ring in contact for all conditions except loss of coolant to the shield. During loss of coolant, a gap of approximately .076 (.030 in.) opens up between the ring and shield. The 6 torque keys at each end then hold the shield centered upon the rings.

Thermal stresses in the shield due to its own non-uniform temperature distribution are expected to be rather small, corresponding to the low thermal expansion coefficients at low temperatures.

Shear stress in the shield during short circuit due to rotor twist of .15" is 2.41×10^7 pascal (3500 psi).

Maximum shear stresses in the highest stressed regions of the shield are calculated from component stresses using Mohr's Circle calculation:

$$\tau_{max} = \sqrt{\left(\frac{\sigma_l - \sigma_t}{2}\right)^2 + \tau_{tl}^2}$$

For all conditions except short circuit and loss of coolant, maximum shear stress is much less than 70% of the shear yield. Specifications and combined stresses are listed in Table 3-23 for the 300 and 1200 MVA SCTG radiation shields.

The calculations should be redone to reflect the stress change in the shield as the press fit tightness varies during the various conditions.

Radiation Shield Mount

The severe requirements for the radiation shield mount must be satisfied within a very restricted geometry. The mount must support the radiation shield within acceptable limits of torsional, lateral, and axial vibrations. It must withstand short circuit torques. Large relative axial thermal deflections between the shield and the inner rotor must be accommodated. Relative thermal and centrifugal radial deflections must also be accommodated. The mount must be positioned on the torque tube at an axial position having a steady state temperature of about 120°K. Stress concentrations imposed on the torque tube must be within acceptable limits. All of this must be accomplished within a small annulus and high vacuum. With these requirements in mind, a unique, workable scheme has been developed for flexibly mounting the radiation shield upon the inner rotor. The mount, used at both ends of the radiation shield, is illustrated in Figure 3-52. Other schemes which have been considered but have not been made workable include spokes, rigid breech lock mounting, bellows, diaphragm, and combinations of these schemes.

The radiation shield mount uses intermediate flexible ring members in the annulus between the shield and torque tube. The radiation shield and torque tube are attached to the rings at alternate points around their circumferences. Three equally spaced attachments are to the shield and midway between these are three torque tube attachments. Axial deflection is accommodated by out of plane bending of the flexible ring members.

The ring segments are sized to be flexible for out of plane bending and stiff for in plane (lateral) bending. Two sets of ring segments are used in parallel on each end in order to limit short circuit stresses to an acceptable level. Another possible method of reducing short circuit stresses is to use more than three point mounting. Four point mounting would have this

Table 3-23

RADIATION SHIELD DIMENSIONS AND STRESSES

SCTG ROTORS

		300 MVA		1200 MVA	
Inside radius	cm (in)	31.12	12.25	41.28	16.25
Total thickness	cm (in)	.95	.375	.95	.375
Outer shell thickness	cm (in)	.396	.156	.36	.14
Inner shell thickness	cm (in)	.556	.219	.60	.235
Length	cm (in)	275.6	108.5	487.7	192.0
Weight	dyne (lb)	4.0×10^8	900	9.3×10^8	2100
No. of axial grooves		--	24	--	24
No. of circumferential grooves		--	2	--	2
Groove radius	cm (in)	.159	1/16	.24	.093
Material		--	A286	--	higher strength
Shrink fit between shells	cm (in)	.030	.012	.041	.016
Shrink fit stress in inner shell	pascal (psi)	-8.27×10^7	-12000	7.58×10^8	-11000
Shrink fit stress in outer shell	pascal (psi)	1.17×10^8	17000	1.24×10^7	+18000
Shear stress due to shrink fit	pascal (psi)	5.93×10^7	8600	6.21×10^8	9000
Centrifugal stress 3600 rpm	pascal (psi)	1.12×10^8	16200	1.93×10^8	28000
120% overspeed 4320 rpm	pascal (psi)	1.60×10^8	23200	2.76×10^9	40500
Bending stress due to short circuit σ_{r2}	pascal (psi)	1.77×10^8	25600	4.21×10^8	61000
Electromagnetic pressure short circuit σ_{r2}(s.a.)	pascal (psi)	8.27×10^4	12	1.10×10^5	16
Radial deflection due to σ_{r2}	cm (in)	.53	.21	2.49	.98
Stress due to stiffener ring press fit	pascal (psi)	6.69×10^7	9700	1.02×10^8	14800
Press fit with stiffener ring	cm (in)	.015	.006	.025	.010
Short circuit shear stress in shield	pascal (psi)	2.41×10^7	3500	--	--
τ_{max} loss of coolant	pascal (psi)	1.29×10^8	18700	1.72×10^8	25000
τ_{max} short circuit	pascal (psi)	2.48×10^8	36000	4.21×10^8	61000
τ_{max} overspeed	pascal (psi)	1.79×10^8	26000	2.62×10^8	38000

Table 3-24

FLEX RING DATA FOR RADIATION SHIELD MOUNT

	300 MVA	1200 MVA
Number of rings at each end of shield	2	2
Number of segments per ring (to facilitate assembly)	3	3
Axial thickness of each ring cm (in)	1.0 (.4)	1.0 (.4)
Outside radius of ring cm (in)	30.0 (11.8)	40.9 (16.1)
Inside radius of ring cm (in)	25.9 (10.2)	33.3 (13.1)
Radial depth of ring cm (in)	4.1 (1.6)	7.6 (3)
Span of each flexible arc degrees	45	45
Inside radius of radiation shield cm (in)	31.1 (12.25)	41.3 (16.25)
Outside radius of torque tube cm (in)	25.6 (10.06)	33.0 (13.0)
E, Young's modulus of ring pascal (psi)	2.07×10^{11} (30×10^6)	2.07×10^{11} (30×10^6)

advantage and would match the number of helium flow tubes at each end. Four point mounting would however increase stresses due to out-of-plane bending.

Design calculations have been made for three point mounting Figures 3-54, 3-55) using straight beam approximations and some curved beam calculations. Complete detailed analysis should be made using curved beam theory. Calculations are based on dimensions listed in Table 3-24.

The principle of superposition is used in combining stresses and deflections. The mount is designed to accommodate conditions including short circuit, loss of coolant to the radiation shield, room temperature standstill, steady state, and loss of vacuum in the rotor. For ease of assembly it is assumed that the mount is unstressed when the entire rotor is assembled at room temperature. No preload is used on the flex rings. It is assumed that short circuit and loss of coolant to the radiation shield do not occur simultaneously. The length of the 300 MVA radiation shield and of the inner rotor between mounting points is taken as 275.6 cm (108.5 inches). It is assumed that the inner rotor is Inconel 718 and the radiation shield is A 286 stainless steel. The temperatures and relative axial thermal expansions and contractions between the radiation shield and the inner rotor during all the anticipated conditions are listed in Tables 3-25 and 3-26. Notice that the difference between steady state and loss of coolant conditions dictates the maximum stroke 1 cm (.39 inch ≈ .4 inch) that the mount must accommodate.

Flexible mounts are used at both ends of the radiation shield to allow for differences in slope and radial and axial thermal deflections. The maximum axial deflection of each mount, .51 cm (.2 inch) is half of the maximum expected thermal differential 1 cm (.4 inch).

Deflection in the axial direction of the flexible ring segment is calculated using a ring segment which covers an arc of 22-1/2°. This 22-1/2° arc is one half of the beam's active length in bending which covers a 45° arc. One might expect the active length of the ring to be $\frac{360°}{6 \text{ beams}} = 60°$. Size effects of the necessary bolted connections in the ring reduce the available bending length from 60° to approximately 45°.

Using Figure 3-54, axial bending stress is calculated using

Table 3-25

THERMAL EXPANSIONS AND CONTRACTIONS (AXIAL) OF
RADIATION SHIELD AND INNER ROTOR

300 MVA SCTG

Condition	Temperature °K (°F) assumed uniform		Thermal ΔL cm (in.) referenced to room temp.		$\Delta L_{RS} - \Delta L_{IR}$ cm (in)	Length Differential to be Taken by Mounts
	Inner Rotor	Shield	Inner Rotor	R. Shield		
Assembly at Room Temp.	293 (68)	293 (68)	0	0	0	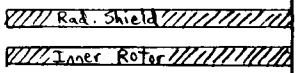
Steady State	4 (-451)	120 (-244)	-.69 (-.27)	-.66 (-.26)	.03 (+.01)	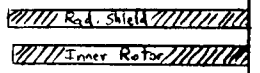
Short Circuit	4 (-451)	100 (-280)	-.69 (-.27)	-.71 (-.28)	-.03 (-.01)	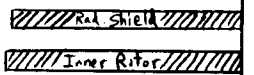
Loss of Vacuum	4 (-451)	173 (-148)	-.69 (-.27)	-.51 (-.20)	+.18 (+.07)	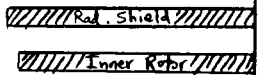
Loss of Coolant to Radiation Shield	4 (-451)	356 (181)	-.69 (-.27)	+.28 (+.11)	+.97 (+.38)	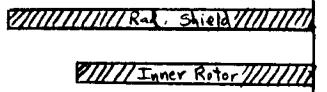

Length of radiation shield between mounts = 275.6 cm (108.5 in.)

Length of inner rotor between mounts = 275.6 cm (108.5 in.)

Radiation shield A286

Inner rotor Inconel 718

Table 3-26

THERMAL EXPANSIONS AND CONTRACTIONS (AXIAL) OF
RADIATION SHIELD AND INNER ROTOR

1200 MVA SCTG

Condition	Temperature °K (°F) assumed uniform		Thermal ΔL cm (in.) referenced to room temp.		$\Delta L_{RS} - \Delta L_{IR}$ cm (in.)	Length Differential to be Taken by Mounts
	Inner Rotor	Shield	Inner Rotor	R. Shield		
Assembly at Room Temp.	293 (68)	293 (68)	0	0	0	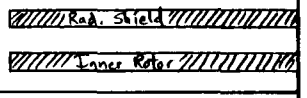
Steady State	4 (-451)	120 (-244)	-1.24 (-.49)	-1.19 (-.47)	+.05 (+.02)	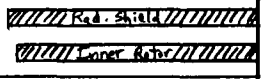
Short Circuit	4 (-451)	100 (-280)	-1.24 (-.49)	1.30 (-.51)	-.05 (-.02)	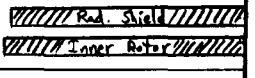
Loss of Vacuum	4 (-451)	173 (-148)	-1.24 (-.49)	-.84 (-.33)	.41 (.16)	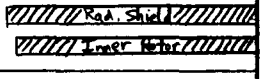
Loss of Coolant to Radiation Shield	4 (-451)	356 (181)	-1.24 (-.49)	+.51 (+.20)	1.75 (+.69)	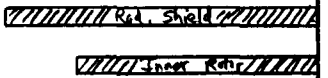

Length of radiation shield between mounts = 495.3 cm (195 in.)

Length of inner rotor between mounts = 495.3 cm (195 in.)

Radiation shield A286 assumed

Inner Rotor Inconel 718

STRAIGHT BEAM

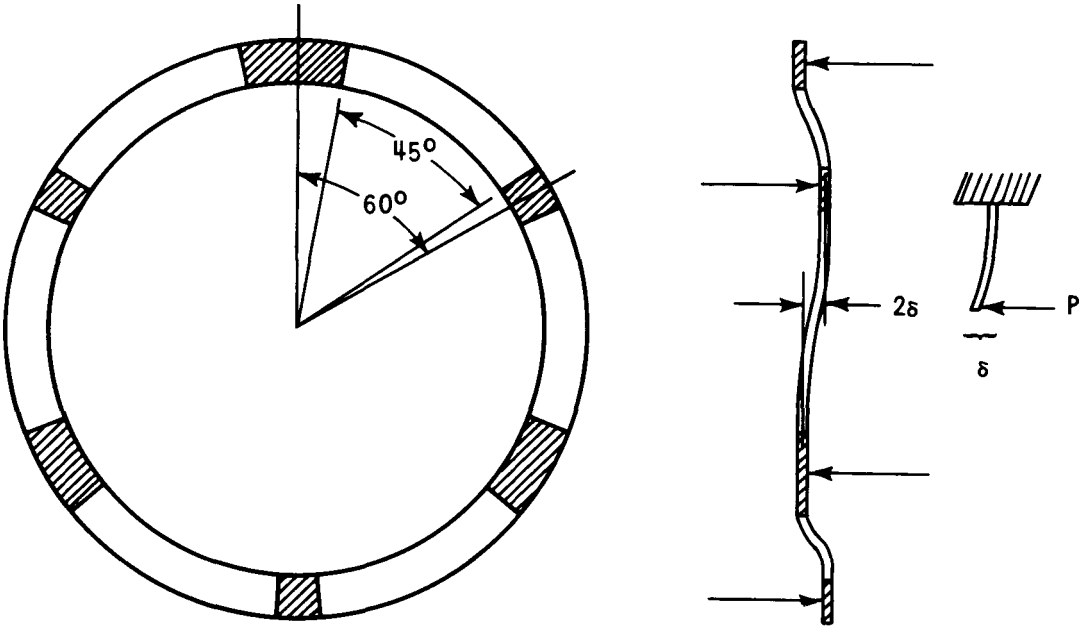

Figure 3-54. Flex Ring Radiation Shield Mount Axial Bending Stress Models - Straight Beam

CURVED BEAM

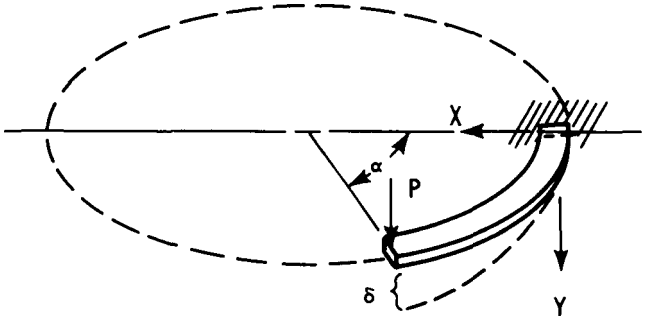

Figure 3-55. Flex Ring Radiation Shield Mount Axial Bending Stress Models - Curved Beam

straight beam theory. The worst case loss of coolant to the 300 MVA radiation shield is used as an example:

$$\delta = \frac{Pl^3}{3EI}$$

$$.1 = \frac{P[(\sin 22.5)(11)]^3}{3(30 \times 10^6)\frac{(1.6)(.4)^3}{12}}$$

$$P = 4577 \text{ N } (1029 \text{ lb.})$$

$$\sigma = \frac{Mc}{I} = \frac{(1029)(4.21)(.2)}{\frac{(1.6)(.4)^3}{12}} = 7.03 \times 10^8 \text{ pascal } (102{,}000 \text{ psi})$$

The straight beam estimate is used to check the following curved beam calculation (neglecting twist) using Figure 3-55 from Timshenko[2]

$$\delta = \frac{Pr^3}{EI_x} \int_0^{\alpha} \{\sin^2(\alpha-\phi) + \frac{EI_x}{C}[1 - \cos(\alpha-\phi]^2\} \, d\phi$$

or

$$\delta = \frac{Pr^3}{EI_x}[(\frac{\alpha}{Z} - \frac{\sin 2\alpha}{4}) + \frac{EI_x}{C}(\frac{3\alpha}{2} - 2\sin + \frac{\sin 2\alpha}{4})]$$

For the case at hand, referring to Figure 3-55 , we have

$$I_x = \frac{(1.6)(.4)^3}{12} = .0085$$

$$\alpha = \frac{\pi}{8} = 22.5°$$

$$C = 3.32 \times 10^5 \text{ from Timoshenko}^3,\ \frac{b}{c} = \frac{1.6}{.4} = 4 \quad \beta = .281$$

$$C = \beta bc^3 G$$

$$C = (.281)(1.6)(.4)^3(1.15 \times 10^7)$$

$$.1 = \frac{P(11)^3}{(30 \times 10^6)(.0085)}\left[\left(\frac{\pi}{16} - \frac{\sin\frac{\pi}{4}}{4}\right) + \frac{(30\times10^6)(.0085)}{(3.32\times10^5)}\left(\frac{3\pi}{16} - 2\sin\frac{\pi}{8} + \frac{\sin\frac{\pi}{4}}{4}\right)\right]$$

giving P = 4279 N (962 lb.)

$$M_{Xmax} = (962)(11)\left(\sin\frac{\pi}{8}\right) = 458 \text{ Nm} \quad (4050 \text{ in. lb.})$$

$$M_{Zmax} = (962)(11)\left(1 - \cos\frac{\pi}{8}\right) = 91 \text{ Nm } (806 \text{ in. lb.})$$

$$\sigma = \frac{M_x c}{I_x} = \frac{(4050)(.2)}{.0085} = 6.57 \times 10^8 \text{ pascal } (95{,}300 \text{ psi})$$

$$\tau_{max} = \frac{M_Z}{\frac{1}{3}bc^2} = \frac{806}{\frac{1}{3}(1.6)(.4)^2} = 6.55 \times 10^7 \text{ pascal } (9500 \text{ psi})$$

Axial deflections and the resulting stresses for the other design conditions are listed in Tables 3-27 and 3-28.

The free radial thermal and centrifugal deflections of the flex ring, torque tube, radiation shield, and radiation shield stiffener ring want to be different for certain conditions. The postulated free deflections are listed in Tables 3-29 and 3-30.

Consideration of Tables 3-29 and 3-30 shows that in certain conditions the press fit gets tighter and in others it is partly relieved. The press fit between the shield and ring remains in contact during all conditions except loss of coolant. In loss of coolant, a gap will open up between the shield and ring. The six torque keys on each end then center the shield.

Table 3-27

FLEXIBLE RING AXIAL DEFLECTIONS AND STRESSES

300 MVA SCTG RADIATION SHIELD MOUNT

Condition	Length Differential		1/2 Beam Deflection		Tensile Stress				Shear Stress	
					Straight Beam		Curved Beam			
	cm	in	cm	in	pascal	psi	pascal	psi	pascal	psi
Room Temperature	0	0	0	0	0	0	0	0	0	0
Steady State	+.03	+.01	+.01	+.003	2.11×10^7	+3060	1.97×10^7	2859	1.97×10^6	285
Short Circuit	-.03	-.01	-.01	-.003	-2.11×10^7	-3060	1.97×10^7	2859	1.97×10^6	285
Loss of Vacuum	+.18	+.07	+.05	+.02	1.41×10^8	+20400	1.31×10^8	19060	1.31×10^7	1900
Loss of Coolant	+.97	+.38	+.25	.1	7.03×10^8	102000	6.57×10^8	95300	6.55×10^7	9500

Table 3-28

FLEXIBLE RING AXIAL DEFLECTIONS AND STRESSES

1200 MVA RADIATION SHIELD MOUNT

Condition	Length Differential		1/2 Beam Deflection		Tensile Stress				Shear Stress	
					Straight Beam		Curved Beam			
	cm	in	cm	in	pascal	psi	pascal	psi	pascal	psi
Room Temperature	0	0	0	0	0	0	0	0	0	0
Steady State	+.05	+.02	.013	+.005	1.93×10^7	2800	—		1.91×10^6	277
Short Circuit	-.05	-.02	-.013	-.005	-1.93×10^7	-2800	—		-1.91×10^6	-277
Loss of Vacuum	+.41	+.16	.10	.04	1.53×10^8	22200	—		1.52×10^7	2200
Loss of Coolant	+1.75	+.69	.44	.173	6.63×10^8	96100	—		6.62×10^7	9600

Table 3-29
300 MVA RADIAL FREE BODY DEFLECTIONS OF RADIATION SHIELD AND TORQUE TUBE

Condition	RPM	$\delta_{\Delta T}$ cm (inch)		δ_{CF} cm (inch)		$\delta_{Total} = \delta_{\Delta T} + \delta_{CF}$ cm (inch)		$\delta_{Total\ Shield} - \delta_{Total\ TT}$ cm (inch)
		Torque Tube	Shield	Torque Tube	Shield	Torque Tube	Shield	
Room Temperature	0	0	0	0	0	0	0	0
Steady State	3600	-.053 (-.021)	-.074 (-.029)	.008 (+.003)	.018 (+.007)	-.046 (-.018)	-.056 (-.022)	-.010 (-.004)
Short Circuit	3600	-.064 (-.025)	-.079 (-031)	.008 (.003)	.018 (.007)	-.056 (-.022)	-.061 (-.024)	-.005 (-.002)
Loss of Vacuum	3600	-.053 (-.021)	-.056 (-.022)	.008 (.003)	.018 (.007)	-.046 (-.018)	-.038 (-.015)	.008 (+.003)
Loss of Coolant	3600	-.053 (-.021)	+.030 (+.012)	.008 (.003)	.018 (.007)	-.046 (-.018)	.048 (+.019)	.094 (+.037)
Overspeed	4320	-.053 (-.021)	-.074 (-.029)	.013 (.005)	.025 (.010)	-.041 (-.016)	-.048 (-.019)	-.008 (-.003)

Table 3-30
1200 MVA RADIAL FREE BODY DEFLECTIONS OF RADIATION SHIELD AND TORQUE TUBE

Condition	RPM	$\delta_{\Delta T}$ cm (inch)		δ_{CF} cm (inch)		$\delta_{Total} = \delta_{\Delta T} + \delta_{CF}$ cm (inch)		$\delta_{Total\ Shield} - \delta_{Total\ TT}$
		Torque Tube	Shield	Torque Tube	Shield	Torque Tube	Shield	
Room Temperature	0	0	0	0	0	0	0	0
Steady State	3600	-.064 (-.025)	-.097 (-.038)	.015 (+.006)	.038 (+.015)	-.048 (-.019)	-.058 (-.023)	-.010 (-.004)
Short Circuit	3600	-.076 (-.030)	-.104 (-.041)	.015 (+.006)	.038 (.015)	-.061 (-.024)	-.066 (-.026)	-.005 (-.002)
Loss of Vacuum	3600	-.064 (-.025)	-.074 (-.029)	.015 (.006)	.038 (.015)	-.048 (-.019)	-.036 (-.014)	+.013 (+.005)
Loss of Coolant	3600	-.064 (-.025)	+.041 (+.016)	.015 (.006)	.038 (.015)	-.048 (-.019)	+.079 (+.031)	+.127 (+.050)
Overspeed	4320	-.064 (-.025)	-.097 (-.038)	.023 (.009)	.056 (.022)	-.041 (-.016)	-.041 (-.016)	0 (0)

Flex ring bending stresses due to radial deflections are neglected. This stress is expected to be less than 6.90×10^7 pascal (10000 psi). It is recommended that this stress be included in a more detailed analysis.

Short circuit torque on the radiation shield is assumed proportional to its inertia:

$$\frac{3T_{rotor}}{t_{shield}} = \frac{I_{rotor}}{I_{shield}}$$

$$t_{shield} = \frac{(3)(7.04 \times 10^6)\ 362}{7700} = 1.13 \times 10^6 \text{ pascal } (1 \times 10^6 \text{ in. lb.})$$

Friction will be sufficient to prevent the outer shell of the shield from rotating with respect to the inner shell of the shield. Friction may not be sufficient to prevent the entire shield from sliding on its press fit stiffener rings during short circuit. Six torque keys per end are therefore provided (Figure 3-48) between the shield and rings to positively lock the rings and shield. Bearing stress in the keys is 5.24×10^8 pascal (76000 psi) and shear stress is 8.96×10^7 pascal (13000 psi) during short circuit.

The effects of short circuit torque on the flex rings has been described using Castigliano's Theorem and Figure 3-56.

$$M_{max} = .414\ P_r$$

$$\sigma_{max} = \frac{P}{A} + \frac{2.484\ P_r}{bh^2}$$

$$P = \frac{1 \times 10^6 \text{ in. lb.}}{(2 \text{ ends})(6 \text{ beams})(11 \text{ in.})} = 3.37 \times 10^4 \text{ N } (7576 \text{ lb.})$$

$$\sigma_{max} = \frac{7576}{(2)(.4)(1.6)} + \frac{(2.484)(7576)(11)}{(2)(.4)(1.6)^2} = 7.38 \times 10^8 \text{ pascal } (107{,}000 \text{ psi})$$

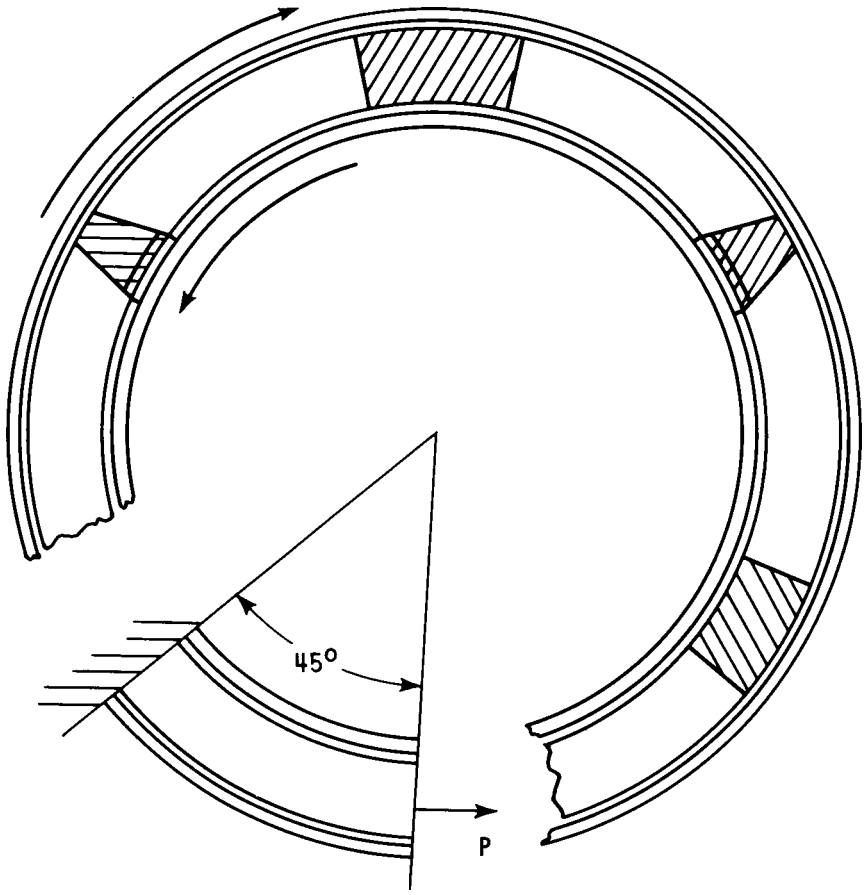

FORCE ON ONE FLEX RING SEGMENT

Figure 3-56. Short Circuit Torque on
Flex Ring Radiation Shield Mount

This short circuit torque requires the strength of two flex rings acting in parallel at each end of the 300 MVA shield.

The short circuit tangential load P acting at a shield mount radius different than the torque tube creates a moment at each of the three torque tube shield mounts. This causes bending stress of approximately 3.17 x 10^8 pascal (46000 psi) in the torque tube.

The bolts in the radiation shield stiffener rings serve several purposes. They reform the stiffener segments into rings for assembly reasons using lap plates, connect the flex rings to the stiffener rings, and form the flex rings into hoops to carry their own centrifugal loading. The bolts are sized to carry centrifugal loads, couples due to radial loads, and short circuit loads. Additional work is needed to finalize this design.

Combined stresses in the flex rings for the 300 and 1200 MVA machines under all conditions are listed in Tables 3-31 and 3-32. In these tables, stresses due to radial loads are omitted.

The following details will have to be considered when parts drawings are made for manufacture:

- Additional study of the joint in the flex rings is needed to finalize the design.
- Detailed design of the torque tube must be made in the area where holes are drilled to pass the shield mounting bolts and helium pipes. Reinforcements might be needed.
- The acceptable lower bound of the lateral spring constant of the flex rings should be found. The work required has been outlined making use of the existing WECAN finite element lateral vibration models. It is expected that the lower bound needed for suitable vibration characteristics will not affect the present design.
- Study should be made to determine whether additional damping is needed to prevent axial oscillations of the shield on its mounts. The magnitude of axial excitation of the shield is needed for this analysis.
- Helium connections between the shield and the torque tube must be designed.
- Radial deflection of the shield relative to the damper requires additional study. In particular, indications are that the 1200 MVA shield thickness and clearance will have to be increased.

Table 3-31

FLEX RING COMBINED STRESSES

300 MVA SCTG Radiation Shield Mount

Condition	Centrifugal Stress σ		Torque Load Stress σ		Axial Load Stress σ		Axial Load Stress τ		Combined Stress τ_{max}	
	pascal	psi	pascal	psi	pascal	psi	pascal	psi	pascal	psi
Room Temp.	0	0	0	0	0	0	0	0	0	0
Steady State	1.11×10^8	16100	0	0	1.97×10^7	2859	1.97×10^6	285	6.55×10^7	9500
Short Circuit	1.11×10^8	16100	7.38×10^8	107000	1.97×10^7	2859	1.97×10^6	285	4.34×10^8	63000
Loss of Vacuum	1.11×10^8	16100	0	0	1.31×10^8	19060	1.31×10^7	1900	1.22×10^7	17700
Loss of Coolant	1.11×10^8	16100	0	0	6.57×10^8	95300	6.55×10^7	9500	3.90×10^8	56500
Overspeed	1.60×10^8	23200	0	0	1.97×10^7	2859	1.97×10^6	285	2.96×10^7	13000

Table 3-32

FLEX RING COMBINED STRESSES

1200 MVA SCTG Radiation Shield Mount

Condition	Centrifugal Stress σ		Torque Load Stress σ		Axial Load Stress σ		Axial Load Stress τ		Combined Stress τ_{max}	
	pascal	psi	pascal	psi	pascal	psi	pascal	psi	pascal	psi
Room Temperature	0	0	0	0	0	0	0	0	0	0
Steady State	1.94×10^8	28100	0	0	1.93×10^7	2800	1.91×10^6	277	1.07×10^8	15500
Short Circuit	1.94×10^8	28100	6.61×10^8	95800	1.93×10^7	2800	1.91×10^6	277	4.37×10^8	63400
Loss of Vacuum	1.94×10^8	28100	0	0	1.53×10^8	22200	1.52×10^7	2200	1.74×10^8	25200
Loss of Coolant	1.94×10^8	28100	0	0	6.63×10^8	96100	6.62×10^7	9600	4.33×10^8	62800
Overspeed	2.79×10^8	40500	0	0	1.93×10^7	2800	1.91×10^6	277	1.50×10^8	21700

- Detailed study of radial loads and resulting stresses in shield, flex rings, and torque tube should be made.

REFERENCES

1. J. H. Parker, Jr. and R. A. Towne, Superconducting Generator Design, Quarterly Report No. 3, July 8, 1976, p. 3-50.
2. Timoshenko, Strength of Materials, Part I, D. Van Nostrand Co., Inc., N.Y., 1955, p. 412.
3. Timoshenko, Strength of Materials, Vol. II, Van Nostrand Co., Inc., 1956, p. 240.

Damper Shield and Support

Description

The main damper shield has significant losses generated in it during normal operation, making it reasonable and practical to locate it outside the vacuum space at ambient temperature where it can be gas cooled rather than placing an unacceptable load on the refrigeration system. If such a room temperature damper is used, its electrical and thermal requirements can be met with suitable thickness and resistivity of highly conductive material of the shield.

Mechanically, the damper shield must be supported against its centrifugal force and must resist large torque and large crushing forces which occur under the short circuit conditions. The damper shield can conceivably be made of a single cylinder of reasonable thickness. While a material, such as copper graphite composite, which will fulfill both the mechanical and electrical requirements, may be developed for our application in the future, the present damper shield is designed as a composite cylindrical shell of three cylinders. The inner and outer cylinders are of a high nickel alloy (Inconel) for support and the middle ring is of copper alloy for damping and shielding. The rings must be shrunk or bonded to act as a single ring in bending. The shield thickness is calculated to be 3.2 cm (1.25 in.).

The inner support cylinder is mechanically connected to the shaft ends to serve as the main structural part of the rotor and must be rigid enough to prevent excessive rotor deflection. The inner cylinder also serves as a vacuum enclosure.

The outer cylinder for generators of 1200 and 3000 MVA will probably require a series of deep circumferential grooves to reduce electrical heating in itself.

Thick Damper Shield vs. Thin Damper Shield

The damper can be designed either as a thick, self-supporting structure or a thin one. The thick damper is one which will not contact the inner rotor structure when subjected to gap crushing forces during fault conditions. The thin damper will contact and be supported by the

rotor during a fault. In the latter case, a difficult problem must be solved in preventing heat flow from the damper assembly to the cryogenic region from normalizing the field winding. The thin damper would be permitted to contact the rotor during a three-phase fault at the generator terminals, but it must not contact and normalize the field winding during a three-phase fault on the high voltage side of the transformer. Comparison of mechanical features of the two design concepts are listed in Table 3-33.

Table 3-33

THICK DAMPER SHIELD VERSUS THIN DAMPER SHIELD

Advantages of Thick Damper Shield	Advantages of Thin Damper Shield
1. More rigid rotor	1. Lighter
2. Simpler inner rotor structure	2. Reduced shaft torque during fault
3. Increased WR^2 to attenuate torque	3. Reduced crushing forces during fault

Calculations indicate that the reduction of shaft torque and crushing forces during fault due to closer distance between the field winding and the shield is only 10-15% for the thin damper design. The thick structure is being considered because of its simpler rotor design and better shaft torque attenuation.

Design Criteria and Material Requirements

The damper shield and its support are mechanically designed for two conditions. The maximum hoop stresses in the damper shield and its support calculated at 20% overspeed, are limited to 70% of the material yield strength. In this case it is assumed that only the outer support cylinder helps to carry the copper centrifugal force. Under short circuit condition large torque and large crushing radial pressures will arise in addition to the centrifugal force. The calculation of the shaft torque is referred to in Table 3-43, "Shaft Torque at Short Circuit". The radial pressures can be given by

$$\sigma_r = \sigma_{r_1} + \sigma_{r_2} \cos 2\theta$$

where θ = angular position around the shield

Using Mohr's circle and the maximum shear failure theory, the shear stress condition for both the steel support and the copper shield, is

$$\sigma_{yp} = \sqrt{\sigma^2 + 4\tau^2}$$

where σ_{yp} = yield stress
σ = total tangential stress due to centrifugal forces plus radial pressures
τ = torsional shear stress.

It should be noted that the short circuit condition determines the total damper thickness required and that the bending stress due to non-uniform radial force has, by far, the largest value of all component stresses. The damper must be supported at the ends of the rotor body with a continuous radial clearance from the inner rotor structure greater than its maximum deflection.

The damper support is non-magnetic and has high electrical resistivity, to limit electrical loss. The material must have high toughness and a yield strength of 830 x 10^6 pascals (120,000 psi) for 300 MVA and 1170 x 10^6 (170,000 psi) for 1200 MVA and 3000 MVA units. The damper shield is supported by the inner and outer steel support cylinders. However, to prevent yielding during short circuit and at 20% overspeed, it must have a yield strength of 280 x 10^6 pascals (40,000 psi) for 300 MVA and approximately 410 x 10^6 pascals (60,000 psi) for 1200 MVA and 3000 MVA units. The shield material must have high electrical conductivity (80% IACS) and high specific heat (0.1 cal/gm C°). Operating temperature is in the range of 0 to 200°C.

Quotations have been obtained for the material and the manufacture of the damper shield and its support of a 300 MVA machine. While the material for the 1200 MVA unit is commercially available, the manufacture of the damper for the size in this application must be developed.

Damper Stresses and Deflections

The following table gives the damper configurations together with the maximum stresses and maximum deflections for the various designs of the three ratings (300, 1200 and 3000 MVA) under the design criteria previously described. The location and the proportioning of the damper shield and its support dimensions represent a compromise between electrical and mechanical requirements. It is obvious that the damper dimensions are mainly determined by the loads under short circuit conditions.

Table 3-34

Damper Shield and Its Support Stresses and Deflections

(Toothed Rotor - Spiral Winding Stator)

	300 MVA X''_d = .16, Low Voltage		300 MVA X''_d = .27, High Voltage	
Damper Configuration	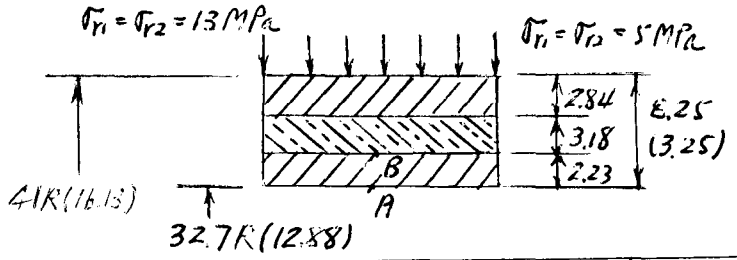			
At 20% Overspeed	In Outer Cyl.	In Copper	In Outer Cyl.	In Copper
Max. Tensile, MPa (psi)	365 (53000)	170 (25000)	365 (53,000)	170 (25000)
Deflection	.07	(.028)	.07	(.028)
At Short Circuit	In Steel at A	In Copper at B	In Steel at A	In Copper at B
Max. Tensile, σ, MPa (psi)	662 (96000)	200 (29000)	372 (54000)	140 (20400)
Max. Shear, τ, MPa (psi)	78 (11400)	40 (6070)	78 (11400)	40 (6070)
$\sigma_{yp} = \sqrt{\sigma^2 + 4\tau^2}$, MPa (psi)	690 (100000)	216 (31400)	410 (59000)	165 (24000)
Max. Deflection	.30	(.12)	.10	(.04)

All dimensions are in centimeters. Dimensions in parentheses are inch equivalents.

Table 3-35

Damper Shield and Its Support Stresses and Deflections

(Toothed Rotor - Spiral Winding Stator)

	1200 MVA X''_d = .16, Low Voltage		1200 MVA X''_d = .27, High Voltage	
Damper Configuration	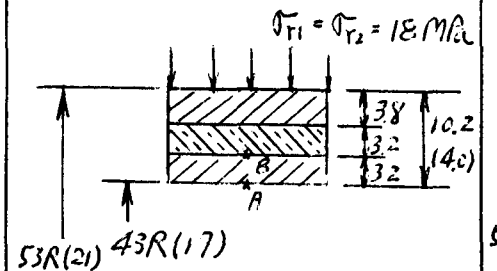		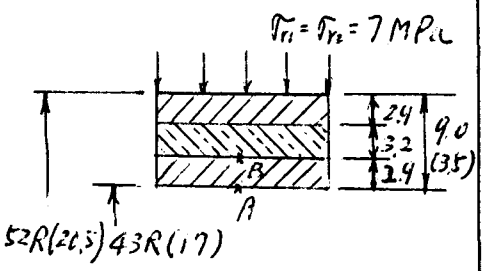	
At 20% Overspeed	In Outer Cyl.	In Copper	In Outer Cyl.	In Copper
Maximum Tensile, MPa (psi)	530 (77000)	280 (41000)	540 (78600)	290 (42000)
Deflection	.13	(.052)	.13	(.052)
At Short Circuit	In Steel at A	In Copper at B	In Steel at A	In Copper at B
Maximum Tensile, σ, MPa (psi)	1030 (150,000)	280 (40700)	690 (100,000)	220 (32400)
Maximum Shear, τ, MPa (psi)	190 (27800)	100 (15000)	200 (29500)	72 (10400)
$\sigma_{yp} = \sqrt{\sigma^2 + 4\tau^2}$, MPa (psi)	1100 (160,000)	345 (50000)	790 (115,000)	265 (38500)
Max. Deflection	.60	(.24)	.36	(.14)

All dimensions are in centimeters. Dimensions in parentheses are inch equivalents.

Inner-to-Outer Rotor Attachment

The problem was to design a reliable inner rotor to outer rotor support configuration capable of accommodating the differential thermal expansion between the cold inner and warm outer rotors while at the same time meeting these other design objectives:

- Meet stress and deflection limits -- loads include centrifugal, torque, weight, unbalance, electromagnetic forces, as well as thermal
- Provide lateral stability and stiffness
- Provide torsional stability and stiffness
- Pass connections such as He, leads, instrumentation at exciter end
- Efficiently maintain inner rotor at cryogenic temperature (low heat leak)
- Be machinable and formable
- Be able to be assembled

The problem is inherent in the general SCTG rotor configuration chosen by Westinghouse. This configuration uses a warm outer strongback and cold inner rotor winding support. Other general rotor configurations, which may or may not have this same problem, are judged to have more severe problems.

Eight different concepts or schemes for designing the attachment between the inner and outer rotors were described and discussed in the fourth Quarterly Report. Two additional schemes were presented the fifth Quarterly Report. The final configuration is based on the "tenth scheme", which now appears to be the most effective solution to the attachment problem. For comparison, an alternate scheme, which represented the first choice during much of the duration of the studies, is also presented.

Scheme 1 - Flexible Connection

The first scheme uses multiple thin disks or laminated warm radial going flexures for supporting the free end of the inner rotor within the outer rotor. One design has been developed for the generators as shown in Figure 3-57.

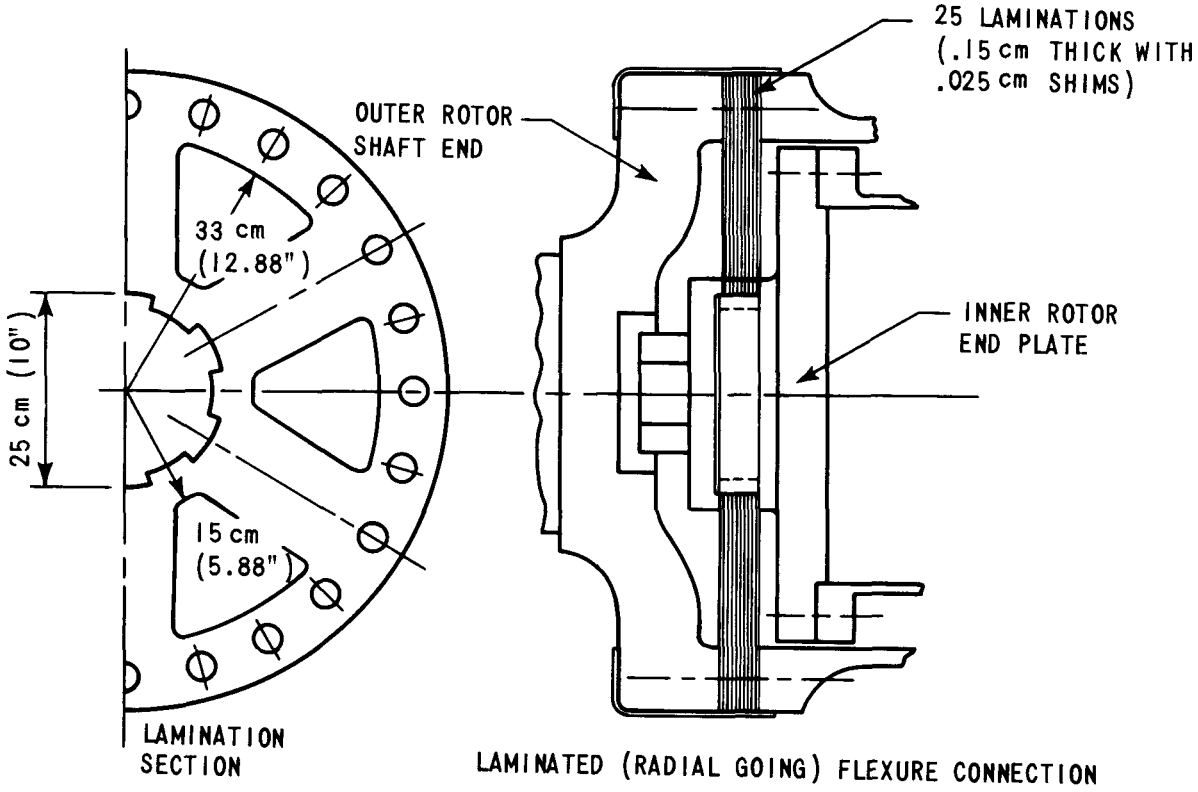

Figure 3-57. Flexible Connection - 300 MVA

The laminated radial going flexures are made in the form of thin slotted disks. The central part of the disks are rigidly attached to the shaft portion of the inner rotor end plate. This shaft portion and the total thickness of laminations must be deisgned to withstand the short circuit torque. The torque is transmitted between the laminations and the inner rotor by splines or keys. The disks are tightly clamped at their outer rims between the damper shield and the outer rotor shaft end. Shims or spacers will be placed between laminations at the I.D. and O.D. portions of the disks to prevent fretting between disks. The laminations and the shims may be brazed together to form a rigid part of the shaft. Provision such as a spigot fit or brazing must be made between the rigid rim and the damper shield and the outer rotor shaft end to avoid overloading the connecting bolts and the shear sleeves.

The thermal contraction of the inner rotor relative to the

warm outer rotor is calculated to be 1.1 and 2.0 cm (.44 and .80 in.) for the 300 and 1200 MVA generators, respectively. If the laminations are assembled at their unstrained state in the middle position with the inner rotor at liquid nitrogen temperature, the maximum displacement to be accommodated by each lamination will be one half of the thermal contraction. The thickness of the lamination is taken as .15 cm (.060 in.). Since the lamination displacement is large in comparison with its thickness, the effect of the stretching force, S, of the radial flexure on the bending must be considered. Assuming that each flexure is fixed at both O.D. and I.D. of the disk, the stresses are calculated and summarized together with the dimensions and values of constants used. See Figure 3-58. The formulas used are also included..

l = Length of radial going flexure

y_{max} = Half of flexure displacement

E = Modulus of elasticity

I = Section moment of inertia

h = Lamination thickness

R = Reaction force

S = Tensile force

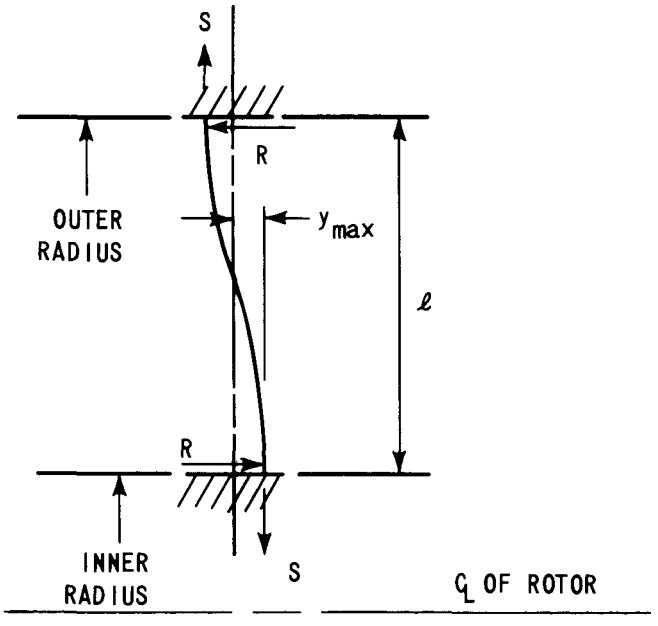

Figure 3-58 Flexure Dimensions

a) Direct tensile stress*

λ = elongation of flexure = $\frac{\pi^2 y_{max}^2}{4l}$

σ_t = tensile stress = $E \frac{\lambda}{l}$

b) Bending stress*

$$y_{max} = \frac{Rl^3}{24EI} \frac{u-\tanh u}{\frac{1}{3}u^3}$$

$$M_{max} = \frac{Rl}{2} \frac{\tanh u}{u} = \frac{12EI\, y_{max}}{l^2} \frac{u^2 \tanh u}{3(u-\tanh u)}$$

where $u^2 = \frac{Sl^2}{4EI} = \frac{3\sigma t l^2}{Eh^2} = \frac{3}{4} \frac{\pi^2 y_{max}^2}{h^2}$

$$\sigma_b = \text{bending stress} = k \frac{6Ey_{max}h}{l^2}$$

where $k = \frac{u^2 \tanh u}{3(u-\tanh u)}$

c) Total stress

σ_T = total stress = $\sigma_t + \sigma_b$

It is seen that the bending stress is obtained by multiplying the simple bending stress without the stretching force by the factor k which depends on the magnitude of the ratio, y_{max}/h. The value of k will increase as the ratio increases. k becomes 1 when the ratio or u is small in comparison with one.

The resulting stress as shown in Table 3-36 in the steel flexures for a 300 MVA generator is reasonable and practical, while that for a 1200 MVA unti appears to be excessive. The stress is directly proportional to the modulus of elasticity of the material and can be reduced by using a material with low modulus. In case of titanium laminations with a modulus of 110 GPa (16 x 10^6 psi), the stress in a

---

*Reference 2 on page 3-272.

1200 MVA generator will be 517 MPa (75000 psi), which amounts to 60% of its yield strength.

Table 3-36

STRESSES IN RADIAL FLEXURE

	300 MVA		1200 MVA	
	Metric Units	Engrg. Units	Metric Units	Engrg. Units
l	17.8 cm	7 in.	21.6 cm	8.5 in.
y_{max}	.28 cm	.11 in.	.51 cm	.2 in.
E	200 GPa	30 x 10^6 psi	200 GPa	30 x 10^6 psi
σ_t	124 MPa	18000 psi	280 MPa	41000 psi
h	.15 cm	.06 in.	.15 cm	.06 in.
u	5	5	9	9
k	2.1	2.1	3.4	3.4
σ_b	345 MPa	5000 psi	690 MPa	100,000 psi
σ_t	470 MPa	58000 psi	970 MPa	141,000 psi

Additional stresses due to various loads have been calculated for a 300 MVA generator.

- σ_1 = Stress due to centrifugal force of its own weight = 24 MPa (3500 psi)
- σ_2 = Stress due to inertia load of inner rotor = 10 MPa (1500 psi)
- σ_3 = Stress due to flexural bending of inner rotor = 1 MPa (110 psi)
- σ_4 = Bending stress due to short circuit torque = 275 MPa (40,000 psi)

The total stress on the flexure at short circuit will be 676 MPa (98,000 psi) which is permissible. The stress at short circuit is limited to the yield strength of the material. The flexure should not buckle laterally during short circuit due to the large tensile force S (see Figure 3-58).

The flexible connection which can be designed without excessive stress, is simple and practical in manufacturing and operation. It is expected that lateral vibration characteristics of the rotor with the flexible connection will be satisfactory. The scheme works in a vacuum. The operation is independent of control of friction on which the second scheme (sliding support) depends, therefore no long time test is required. Based on the analysis, the flexible connection is believed to be the best for the inner to outer rotor attachment and will be used in the future superconducting generators.

The design can be improved, if necessary, by utilizing preformed laminations which are not flat in the unstressed condition. In the simplest case, the laminations may be dished slightly so that they will "oil can" through a compression condition during cooldown. This should reduce the large radial force at operating conditions. The initial deflection of the laminations must be determined in such a way that the laminations will not be buckled and damaged through the compression condition. The embodiment shown in Figure 3-46 is sufficient as shown.

Scheme 2 - Sliding Support

The sliding support scheme, Figure 3-59, uses a rigid bolted connection at the exciter end and a sliding support at the turbine and so as not to interfere with the helium inlet parts. In this scheme, a shaft end which is hollow and segmented, is keyed and fitted into the outer structure so that torsional slip will not occur. Axial sliding occurs during cooldown and warmup. The sliding support is designed to utilize centrifugal force as a means of keeping a positive pressure between the support fingers and the outer structure. The wedge and spring help to maintain this positive pressure so that no slip, thus no fretting occurs at the surfaces during normal operating conditions. At standstill or low speeds the pressure will be lower than the pressure at speed to allow axial sliding caused by thermal contraction during cooldown.

The inner rotor shaft end has been designed to transmit a torque equal to 1.5 times rated torque per end. The diaphragm provides sufficient flexibility to take up small differences in flexural angularity of the cold inner and warm outer rotors caused by rotation and differences in flexural rigidity of the two members. This diaphragm is designed to impose only a small static moment on the shaft end to minimize fretting. Constant positive pressure maintained on the sliding fit by the wedge and spring is designed

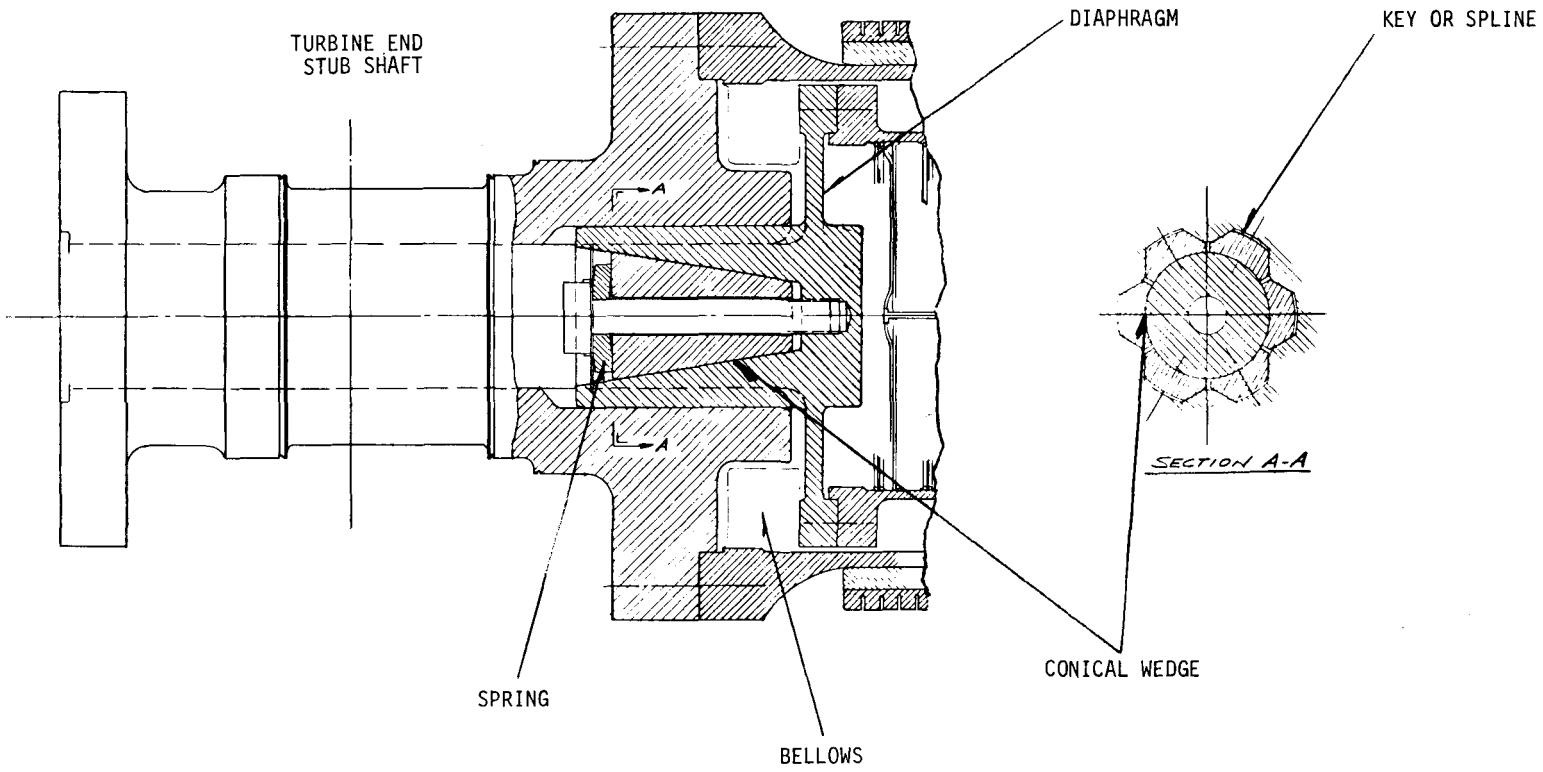

Figure 3-59. Sliding Support Scheme

to resist 3 times the static moment. The shaft end is long to reduce tilting and requires surfaces which will not gall. The bellows which serves as a vacuum seal must accommodate the thermal contraction without excessive stresses. The sliding support is located outside the vacuum enclosure.

The shear stress in the bellows around the sliding joint due to torsional deflection of the bellows during short circuit is approximately 3.45×10^8 pascal (50000 psi) or less. This corresponds to the total angular twist of .062° which the bellows must take. The twist angle is calculated by considering shear and bending deflections of the sliding joint fingers. A laboratory test of the bellows is needed to study its performance.

The bolted connection between the turbine end stub shaft and the outer rotor has been designed in detail. Thirty (30) bolts and shear sleeves are used on a 37.48 cm (14.755 inch) bolt circle radius. The bolts are 2.54 cm (1 inch) diameter, with a .079 cm (.03 inch) radial clearance to the 2.032 cm (.8 inch) O.R., 1.349 cm (.531 inch) I.R. shear sleeve. The flange should be shrunk fit approximately .025 cm (.010 inch) onto the stub shaft to prevent excessive stress in the shear sleeves at speed. The ring (outer rotor shell) tends to expand faster than the stub shaft.

The bolted connection between the turbine end torque tube and the sliding support has been designed. Thirly-six (36) 2.54 cm (1 inch) diameter shoulder bolts on a 28.58 cm (11.25 inch) radius are called for.

Lateral vibration characteristics of the sliding support have been studied using computer finite element models. The results indicate that no lateral vibration problems should be expected with the sliding support.

Advantages

- Little or no stress in rotors due to thermal expansions
- Workable scheme expected to fulfill all requirements
- Lateral vibration characteristics are suitable

Disadvantages

- Depends on control of friction
- Difficult machining job
- Not operable in vacuum.

Based on the detailed analysis done to date, the sliding support scheme is presently judged to be the second best scheme with which to proceed. It has potential of being a good practical solution to the SCTG differential thermal expansion problem.

Recommendations

The flexible connection is recommended as the first choice based on its many advantages and lack of significant disadvantages. If the second choice is ever developed, it is recommended that the performance of the sliding support should be evaluated as soon as possible. A laboratory test could be used to develop confidence in, verify and if needed develop analysis concerning fretting, conical wedge performance, bellows performance and spring constants for moment, torsion and lateral deflections of the sliding support.

Torsional Vibration - 300 MVA

On the assumption that the 300 MVA model will be designed and built in the next several years and will probably couple to an existing turbine, the 3 per unit torque limit criterion used to design conventional generators applies to the 300 MVA superconducting design. The required torque attenuation can be obtained by lowering the natural frequency of the system (approximately to 20 cycles) relative to the predominant 60 cycle exciting torque. This can be done by interposing a flex-shaft between the generator and the turbine coupling. A "Three Inertia Model" as shown in Figure 3-60 is used in the following analysis.

In the model, separate moments of inertia are used for the inner and outer rotor structures to study the relative torsional displacement between the inner and the outer structures. The outer structure is the damper shield and its support while the inner one is the rotor winding supporting structure. The outer structure is further divided into two parts to study the effect of the twist in damper shield on the torque tubes.

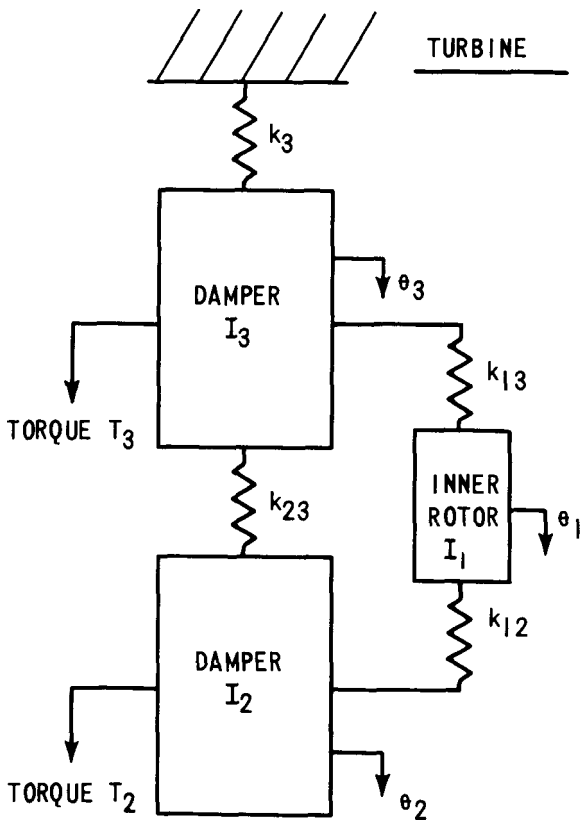

Figure 3-60. Three-Inertia Model

The magnetic spring constant between the damper shield and the inner rotor has been estimated to be small in comparison with the corresponding mechanical spring constant. See numerical values of the spring constant in next section. These considerations include some of the valuable suggestions and direct questions of the EPRI reviewers brought out in the course of the November 21, 1975 quarterly review. Hunting at low frequency and self-excited instability problems are treated in Section 3.4.

Assuming an infinite inertia of the turbine, the three inertia model can be illustrated by Figure 3-60. Let θ_1, θ_2, and θ_3 be the angles of displacement of inertias I_1, I_2, and I_3 respectively from the unstrained positions, in radians. The differential equations of motion in the case under consideration are

$$\left.\begin{aligned} &I_1\ddot{\theta}_1 + k_{12}(\theta_1 - \theta_2) + k_{13}(\theta_1 - \theta_3) = 0 \\ &I_2\ddot{\theta}_2 + k_{12}(\theta_2 - \theta_1) + K_{23}(\theta_2 - \theta_3) = T_2 \\ &I_3\ddot{\theta}_3 + k_3\theta_3 + k_{13}(\theta_3 - \theta_1) + k_{23}(\theta_3 - \theta_2) = T_3 \end{aligned}\right\} \quad (1)$$

Without considering the decrement and damping, the external torque can be approximated by

$$T_2 = T_3 = T_0 \ (4 \sin \omega t - 2 \sin 2\omega t) \quad (2)$$

where T_0 is rated torque.

The general solution of the equations will be of the form

$$\theta_i = a_i \sin \omega t - b_i \sin 2\omega t + \Sigma A_i \sin p_2 t, \ i = 1, 2, 3 \quad (3)$$

where p is the circular critical speed in radian per second. Substituting the solutions (3) into differential equations (1) and equating the corresponding coefficients of sin ωt and sin $2\omega t$ on both sides, we can solve for the constants a's and b's.

$$
\left.
\begin{aligned}
(-I_1\omega^2 + k_{12} + k_{13})\, a_1 - k_{12}\, a_2 - k_{13}\, a_3 &= 0 \\
-k_{12}\, a_1 + (-I_2\omega^2 + k_{23} + k_{12})\, a_2 - k_{23} a_3 &= 4T_0 \\
-k_{13} a_1 - k_{23} a_2 + (-I_3\omega^2 + k_3 + k_{13} + k_{23}) a_3 &= 4T_0
\end{aligned}
\right\} \quad (4)
$$

and

$$
\left.
\begin{aligned}
(-4I_1\omega^2 + k_{12} + k_{13})\, b_1 - k_{12} b_2 - k_{13} b_3 &= 0 \\
-k_{12} b_1 + (-4I_2\omega^2 + k_{23} + k_{12})\, b_2 - k_{23} b_3 &= 2T_0 \\
-k_{13} b_1 - k_{23} b_2 + (-4I_3\omega^2 + k_3 + k_{13} + k_{23}) b_3 &= 2T_0
\end{aligned}
\right\} \quad (5)
$$

The general solution should satisfy two initial conditions, namely

$$\text{at } t = 0,\ \theta_i = 0 \text{ and } \theta_i = 0$$

The first condition is satisfied by using sine function in the solution and the second condition can be satisfied by taking

$$A_i = -\frac{\omega}{p}\,(a_i - 2b_i) \quad (6)$$

p can be solved from the frequency equation $\theta(p^2) = 0$ which is the determinant of equation (4) with p^2 instead of ω^2.

With values of inertias and spring constants for 300 MVA generator as follows

I = Turbine Inertia = 12700 N-M-sec.^{2}

I_1 = Inertia of inner rotor = 150 N-M-sec.^{2}

$I_2 = I_3$ = Half of damper inertia = 360 N-M-sec.^{2}

$k_{12} = k_{13}$ = Spring constant between inner rotor and damper

$k_{12} = k_{13}$ = Spring constant between inner rotor and damper
= 130×10^6 N-M per radian (mechanical)
= 2×10^6 N-M per radian (magnetic)

k_{23} = Damper spring constant = 450×10^6 N-M per radian

k_3 = Spring constant between turbine and generator
= 14×10^6 N-M per radian

ω = Forcing frequency = 377 radian per second.

We find the solutions for θ_1, θ_2 and θ_3.

$$\theta_1 = (-.07797 \sin \omega t + .01132 \sin 2\omega t + .1643 \sin pt) \times 10^{-6} T_0$$

$$\theta_2 = (-.07219 \sin \omega t + .00773 \sin 2\omega t + .1685 \sin pt) \times 10^{-6} T_0$$

$$\theta_3 = (-.07117 \sin \omega t + .00760 \sin 2\omega t + .1662 \sin pt) \times 10^{-6} T_0$$

where p is calculated to be 127 radians per second or 20 Hz.

$(\theta_3)_{max.}$ $0.24 \times 10^{-6} T_0$ (approximately 11°)

$(\theta_1 - \theta_3)_{max,} = 0.010 \times 10^{-6} T_0$

$(\theta_1 - \theta_2)_{max.} = 0.011 \times 10^{-6} T_0$ (approximately 0.5%)

Torque on damper = $k_3(\theta_3)_{max.} = 3.4 T_0$

Torque on torque tube = $k_{12}(\theta_1 - \theta_2)_{max.} = 1.4 T_0$

Assume the spring constant between the generator and the turbine are the same as that of the conventional unit, i.e., 44×10^6 N-N per radian. A flux shaft with spring constant of 20.5×10^6 N-M per rad. is required to yield a value of $k_3 = 14 \times 10^6$ N-M per rad. The flex-shaft should be made of material with low modulus of elasticity such as titanium which has a tensile yield of 930×10^6 pascals (135,000 psi) and a shear modulus of 45×10^9 pascals

(6.6×10^6 psi). In this case the flex-shaft will be of 28 cm. in diameter and 132 cm. of effective length. High strength material can also be used to obtain maximum flexibility for the flex-shaft.

The calculations have indicated that attenuation of the transient torque to a reasonable value is possible, if the other associated problems can be satisfactorily solved.

Torsional Vibration - 1200 MVA

The design of a 1200 MVA superconducting machine is not subjected to torque limit criteria. The preliminary shaft torque at short circuit has been estimated as shown in Table 3-37 with a simple inertia-spring model for the conceptual design.

The data for the conventional units are obtained from Westinghouse Electric Corporation's Large Rotating Apparatus and Steam Turbine Divisions for 300 MVA and 900 MVA machines and are extrapolated for 1200 MVA unit. The moments of inertia, I, of the superconducting generators are calculated from the dimensions shown in the layouts. The spring constants, k, are assumed to be same for all three generators. Assuming an infinite turbine inertia, the natural frequency is calculated from

$$f_n = \frac{1}{2\pi} \sqrt{\frac{k}{I}}$$

The air gap torques are calculated in accordance with Section 3.4. The maximum shaft torque can be approximated by

$$T_{shaft} = \frac{T_{air\ gap}}{1 - \left(\frac{f}{f_n}\right)^2} \left(\sin 2\pi ft - \frac{f}{f_n} \sin 2\pi f_n t\right) \text{ and}$$

$$\text{Max. } T_{shaft} \simeq \frac{T_{air\ gap}}{1 - \left(\frac{f}{f_n}\right)^2} \text{ where f = line frequency}$$

Table 3-37

SHAFT TORQUE AT SHORT CIRCUIT

1200 MVA - 3600 RPM

	Conventional	Superconducting $X_d = .4$	Superconducting $X_d = .22$
*Gen. I. N-M-sec.^{2} (lb-in-sec^2)	12400 (110,000)	4750 (42,000)	7200 (64,000)
Spring Const. k, kN-M/rad. (lb-in/rad.)	100 (900×10^6)	100 (900×10^6)	100 (900×10^6)
Response Freq. f_n, Hz	14.4	23.3	18.9
$T_{air\ gap}$, per unit	5.5	7.6	14.3
Max. T_{shaft}, per unit	1.7	4.5	6.5
$\theta_{max.}$, degrees	3	8	11.5

*Turbine I = 38000 N-M-sec.^{2}

The maximum rotation is defined as

$$\theta_{max} = \frac{\text{max. } T_{shaft}}{k}$$

Rotor Lateral Vibration

Lateral vibration characteristics of the proposed Westinghouse 300 and 1200 MVA SCTG rotors have been predicted by finite element computer modeling. Mode shapes, mode frequencies, and responses to both static and dynamic unbalances have been calculated. The encouraging results indicate that these rotors will have lateral vibration characteristics which are desirable for practical, reliable machinery.

Finite element models were constructed using rotor drawings which have since been superseded by later drawings featuring design improvements. Because of time spent on other studies within the scope of the present contract, the models have not been kept up to date with all the latest modifications. These calculations must be updated before parts drawings are made.

The work presented here is the result of the development of a method of calculation of an unprecedented rotor geometry. Use of new models in the calculations will give results basically similar but slightly different than those presented here. In particular, mode frequencies are sensitive to rotor dimensions. Work has proceeded assuming that updated rotor dimensions for a given machine size can be varied sufficiently to obtain acceptable lateral vibration characteristics.

Rotor Undamped Natural Frequencies and Mode Shapes

300 MVA

The 3 lowest natural frequencies are listed in Table 3-38 for the 300 MVA rotor:

- on rigid bearings and simple support at left connection on inner and outer rotor
- with a bearing stiffness of 3.50×10^8 N/m/bearing (2×10^6 lb./in./bearing) and simple support at left connection of inner and outer rotors

- with a bearing stiffness of 3.50×10^8 N/m/bearing (2×10^6 lb./in/bearing) and moment spring of 4.52×10^7 N/m/rad. (400×10^6 in/lb./rad.) at the left connection of inner and outer rotors

Table 3-38

UNDAMPED NATURAL FREQUENCIES
(LOWEST 3) FOR 300 MVA SCTG ROTOR MODEL

Case No.	Bearing Stiffness		Moment Spring		Lowest 3 Natural Frequencies (Hz)		
	lb/in/bearing	N/m/bearing	in lb/rad	Nm/rad	(1)	(2)	(3)
1	rigid	rigid	free	free	40	99	155
2	2×10^6	3.5×10^8	free	free	30	70	98
3	2×10^6	3.5×10^8	400×10^6	4.52×10^7	30	70	107

Bearing characteristics were varied in order to study the sensitivity of the model to the bearing representation. The moment spring characteristics were varied to study the effects of the moment spring on rotor lateral vibrations.

The effect of the bearing flexibility (Case 2): lowers the first mode, which involves in phase bending of the inner and outer rotors, from 40 Hz to 30 Hz (Fig. 3-61A); introduces a rocking mode on the bearing supports at 70 Hz (Fig. 3-61B); and changes the out of phase vibration mode of the inner and outer rotors from 155 Hz to 98 Hz (Fig. 3-61C).

The addition of the moment spring between the inner and outer rotors (nodes 109, 209) has little effect on the three lowest natural frequencies; the third mode frequency is raised to 107 Hz. The 300 MVA model without the moment spring which is slightly more pessimistic was investigated during the subsequent unbalance calculations.

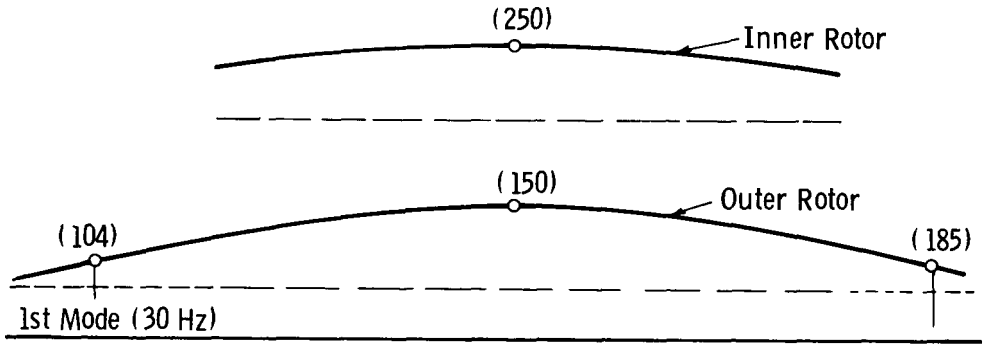

Figure 3-61A

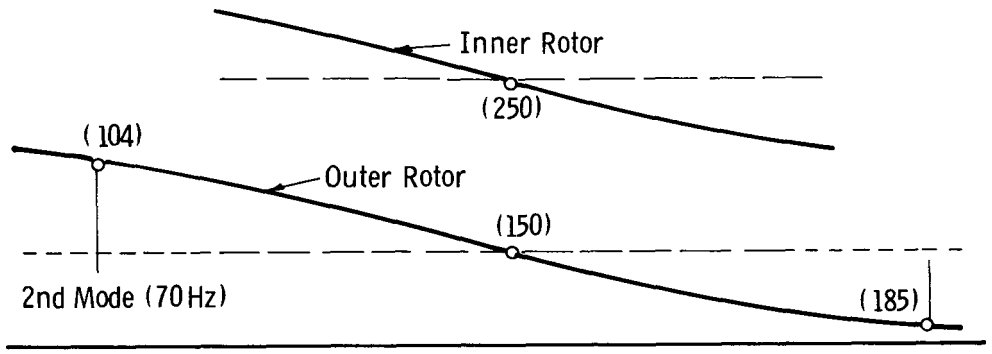

Figure 3-61B

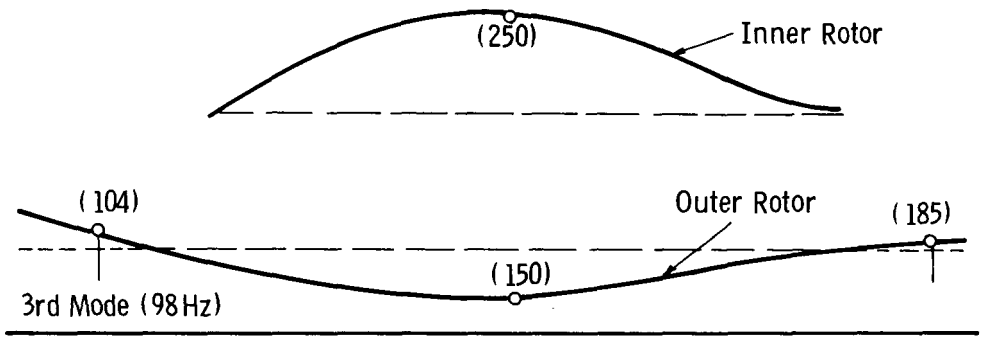

Figure 3-61C

Lowest Lateral Vibration Modes - 1st Mode
Lowest Lateral Vibration Modes - 2nd Mode
Lowest Lateral Vibration Modes - 3rd Mode

1200 MVA

The three lowest natural frequencies are listed in Table 3-39 for the 1200 MVA SCTG:

- With a bearing stiffness of 8.83×10^8 N/m/bearing (5.04×10^6 lb./in./bearing) and simple support at left connection of inner and outer cylinder. For this case, element 16 moment spring (Figure 3-62) has no stiffness.
- With a bearing stiffness of 8.83×10^8 N/m/bearing (5.04×10^6 lb./in./bearing) and a moment spring of 2.83×10^8 Nm/rad. (25×10^8 in. lb./rad.) between the inner and outer cylinders.

Table 3-39

UNDAMPED NATURAL FREQUENCIES
(LOWEST 3) FOR 1200 MVA SCTG ROTOR MODEL

Case No.	Bearing Stiffness		Moment Spring		Lowest 3 Natural Frequencies (Hz)		
	lb/in/bearing	N/m/bearing	in lb/rad	Nm/rad.	(1)	(2)	(3)
1	5.04×10^6	8.83×10^8	0	0	30	68	81
2	5.04×10^6	8.83×10^8	25×10^8	2.83×10^8	30	68	88

Again, the moment spring characteristics were varied to study the effects of the moment spring on mode shapes and frequencies.

It is apparent from Table 3-45 that the larger size of the 1200 MVA machine presents no significant lateral vibration problems. In general, the same basic design scheme being used on the 300 MVA rotor is seen applicable to the larger 1200 MVA machine. The large machine may require a larger number of thinner flex rings to provide additional lateral support to the radiation shield. Future work should include the shield as a beam in the models with spring (flex rings) mounting.

The mode shapes are shown in Figure 3-61 The addition of the moment spring to the analysis has little effect on the three lowest

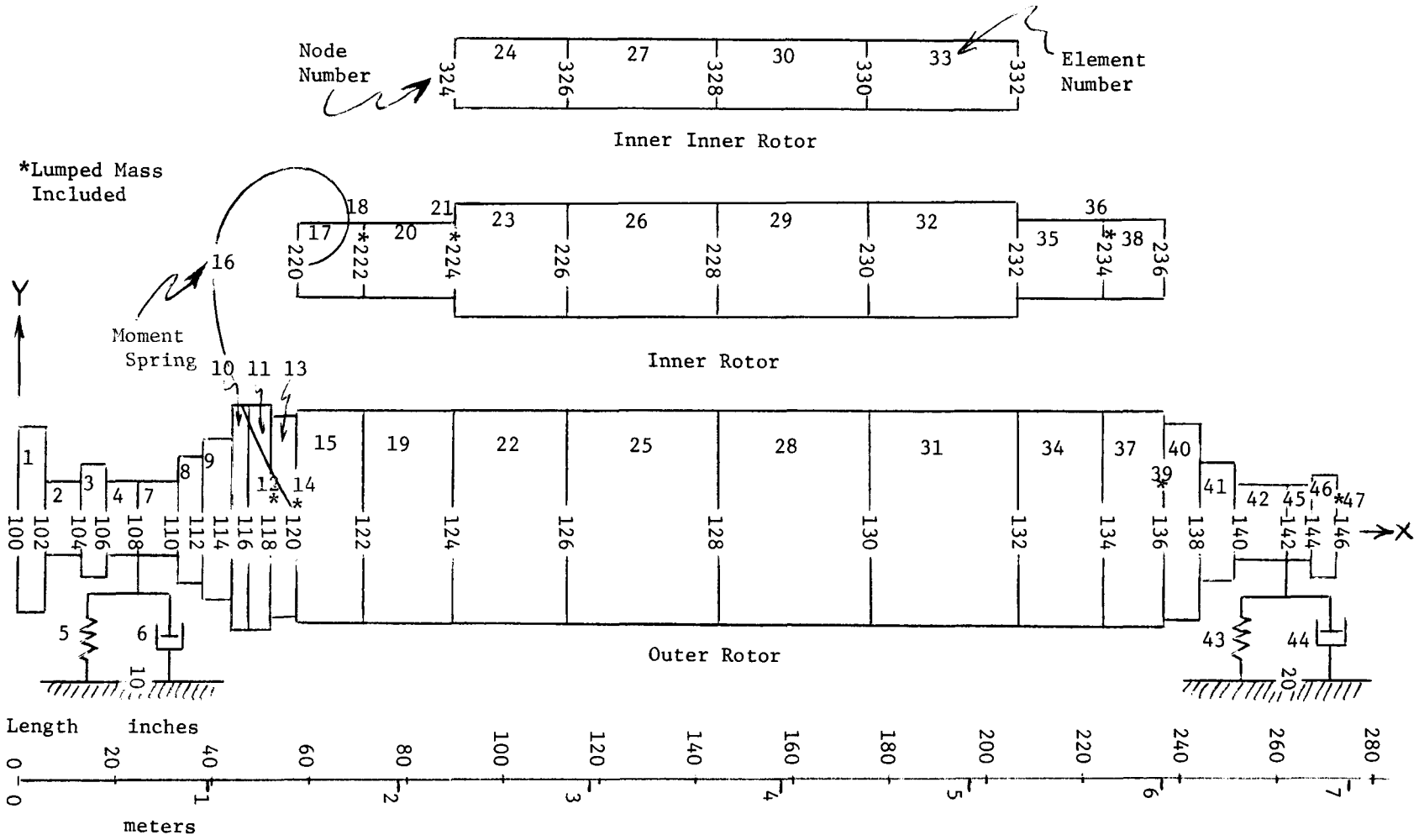

Figure 3-62. Schematic of 1200 MVA SCTG Rotor Finite Element Model Used for Lateral Vibration Investigation

natural frequencies. The third natural frequency is raised from 81 Hz to 88 Hz with the addition of the moment spring. For subsequent unbalance calculations, the 1200 MVA rotor model with the moment spring was used.

Study of the mode shapes in Figure 3-63 leads to several observations:

- Mode 1 (Figure 3-63A) and mode 2 (Figure 3-63B) have relatively large bearing motions. Therefore damping in the bearings is expected to be very effective in modes 1 and 2. Bearing damping is less effective in mode 3. (Figure 3-63C).
- In all 3 modes the inner inner rotor, which was to have been for helium management, tends to move in phase with the inner rotor. The latest construction eliminates the inner inner rotor altogether.
- Only in the third mode do the inner and outer rotors tend to move out of phase.

By comparing Figure 3-61 with Figure 3-63 the following comparisons can be made between the 300 and 1200 MVA rotors:

- The 300 MVA and 1200 MVA SCTG rotors have 1st and 2nd modes and frequencies which are very similar. The resulting similarity is due to various geometrical similarities and differences. In particular the 1200 MVA rotor is longer and more massive than the 300 MVA, but it also has a larger diameter and hence a larger moment of inertia to resist bending.
- The 1200 MVA outer rotor in the 3rd mode is behaving differently than the 300 MVA outer rotor in the 3rd mode.

Response to Unbalance Conditions

To investigate the effect of possible unbalance conditions during start up, running, and overspeed of the 300 MVA and 1200 MVA SCTG units, the responses to static and dynamic unbalance forces have been computed using the harmonic analysis capability of WECAN.[2]

300 MVA

The single amplitude responses of the center of the outer rotor (node 150), center of inner rotor (node 250), and the left bearing (node 104) to a static unbalance of 1.77 Nm (15.64 in. lbs.) distributed over the outer rotor are shown in Figure 3-64. The 1.77 Nm (15.64 in. lb.) unbalance

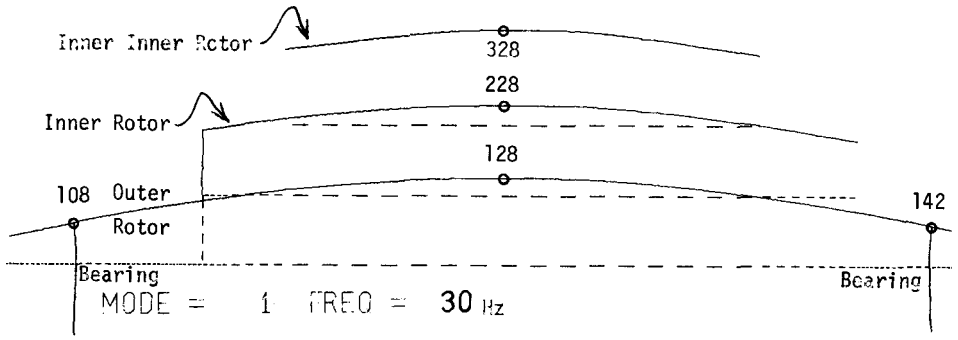

Figure 3-63A

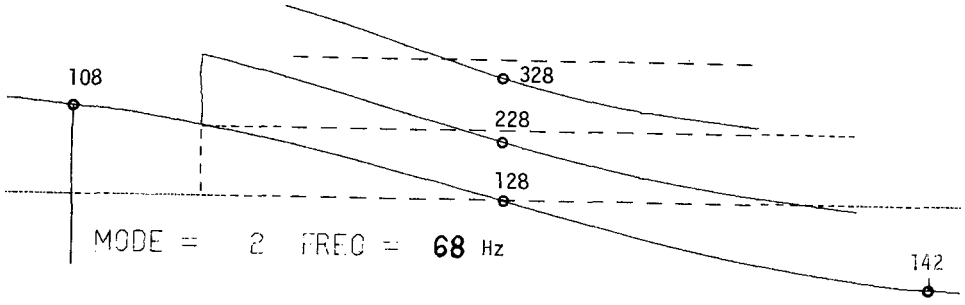

Figure 3-63B

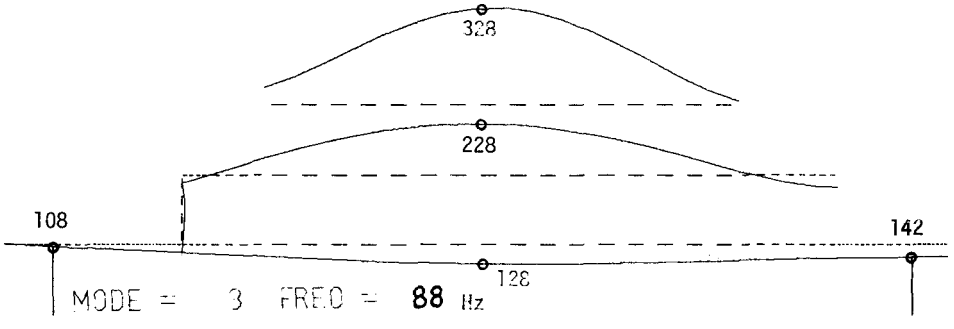

Figure 3-63C

Lowest Three Lateral Vibration Modes - 1st Mode
Lowest Three Lateral Vibration Modes - 2nd Mode
Lowest Three Lateral Vibration Modes - 3rd Mode

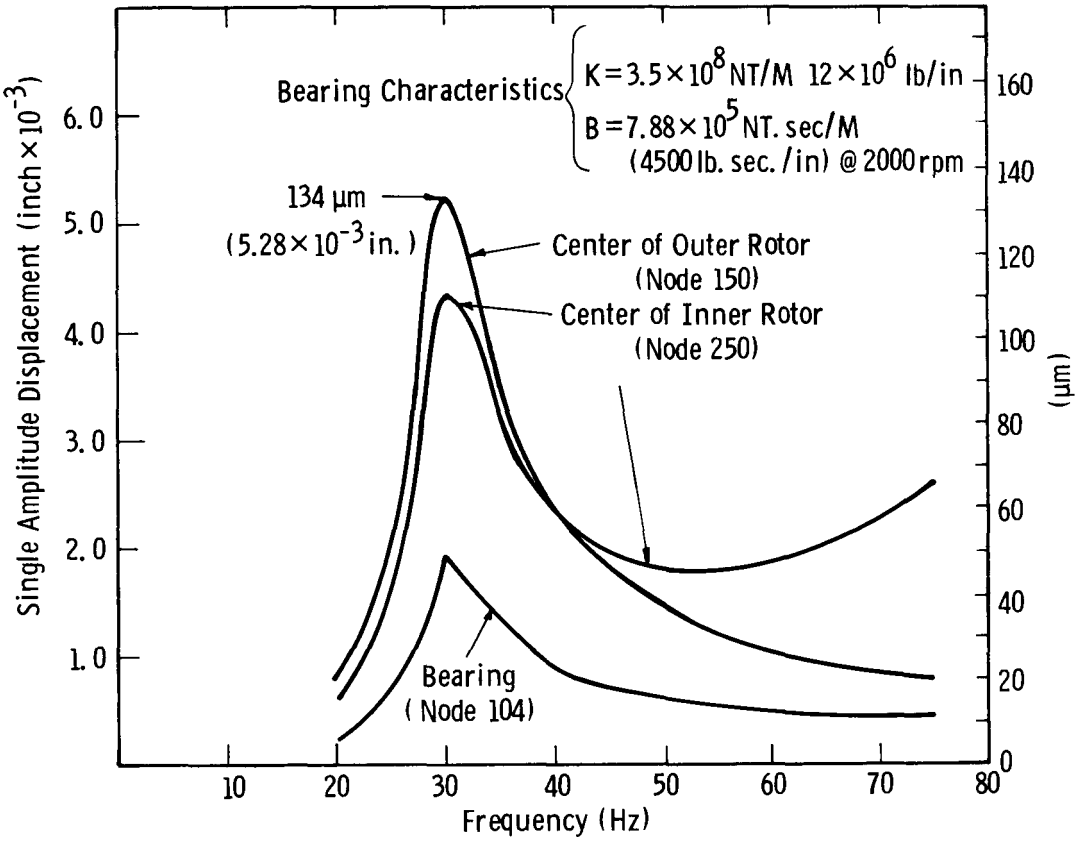

Figure 3-64. Vibration Responses of 300 MVA SCTG Rotors with 1.77 Nm (15.44 in. lb.) Static Unbalance on Outer Rotor

is chosen to give a 25.4 μm (0.001 in.) eccentricity of the outer rotor mass axis with respect to its geometric axis. The peak displacement of node 150,134 μm (0.00528 in.), therefore represents not only response but also amplification of $\frac{5.28}{1.00} = 5.28$ as the 30 Hz mode is traversed with the effective bearing damping constant being 7.88×10^5 N sec./m (4500 lb. sec./in./bearing). Significant motion at the bearings during the first mode vibration as indicated in Fig. 3-61A causes damping at the bearings to be effective in the first mode and therefore limits first mode vibration buildup. First mode damping is:

$$\S_1 \simeq \frac{1}{2 \times 5.28} = 0.095 \text{ or } 9.5\% \text{ of critical.}$$

A static unbalance of 1.91 Nm (16.94 in. lbs.) has been distributed over the inner rotor to produce 25.4 μm (0.001 in.) eccentricity of the outer rotor mass and geometric axes. The single amplitude peak of 175 μm (0.00683 in.) of node 150 (Fig. 3-65) represents an amplification of 6.83 with the effective bearing damping constant being 5.95×10^5 N/sec/m (3400 lb. sec./in./bearing).

Since the 70 Hz mode is within the range of overspeed, a dynamic unbalance condition, which would be most effective in exciting this mode, has been simulated. A dynamic unbalance of 1.52 Nm^2 (530 lb. $in.^2$) was applied to the outer rotor to produce a 25.4 μm (0.001 in.) eccentricity at the left journal (bearing node 104). Although this second mode is heavily damped by the 5.95×10^5 N sec/m/bearing (3400 lb. sec./in./bearing) damping constant a rather large buildup was evidenced as the third mode (98 Hz) is approached (Fig. 3-66). Damping is

$$\S_2 = \frac{1}{2 \times 1.5} = 33\% \text{ of critical.}$$

Even though the 98 Hz mode is well above operative frequency it is necessary to investigate the amount of buildup one could expect from this type of mode. The mode shape (Fig. 3-61C), which shows the out-of-phase vibration of the two rotor cylinders, indicates that because of the small motion at the bearings, the bearings would be of limited effect in damping this mode. A distributed out-of-phase unbalance totaling 0.266 Nm (2.35 in. lbs.) was applied to both inner and outer rotors to produce a total 25.4 μm (.001

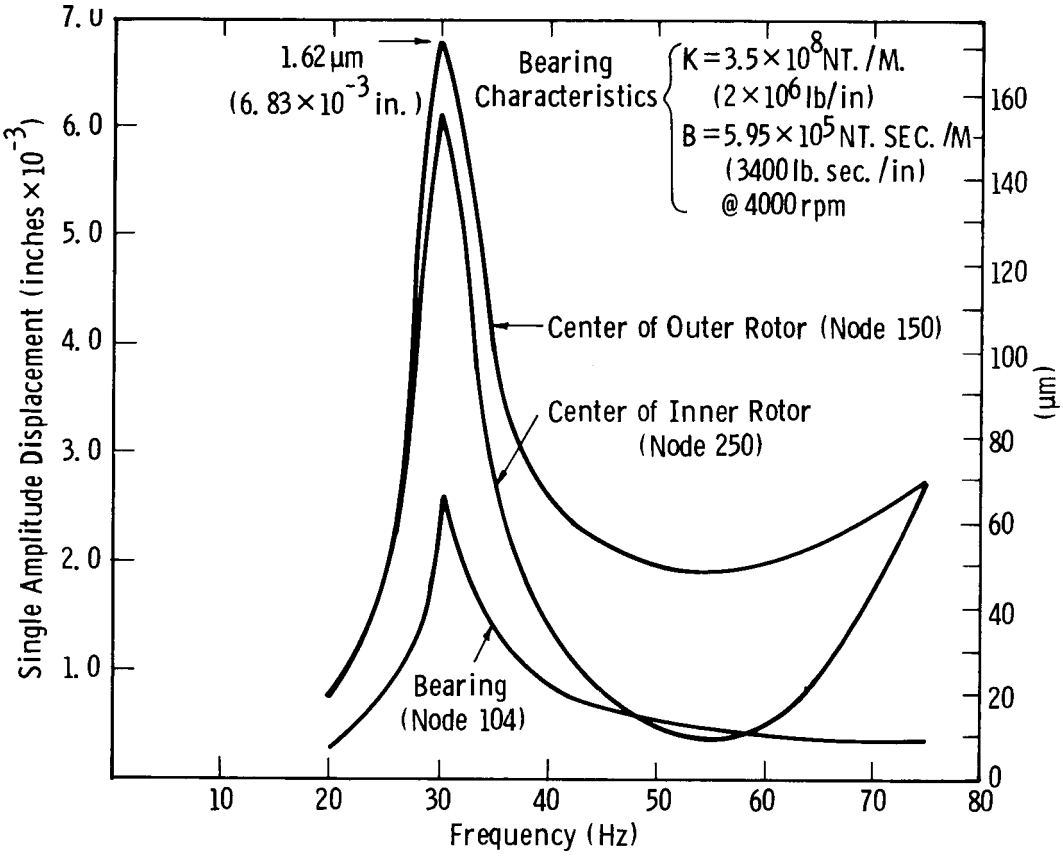

Figure 3-65. Vibration Responses of 300 MVA SCTG Rotors with 1.91 Nm (16.94 in. lb.) Static Unbalance on Inner Rotor

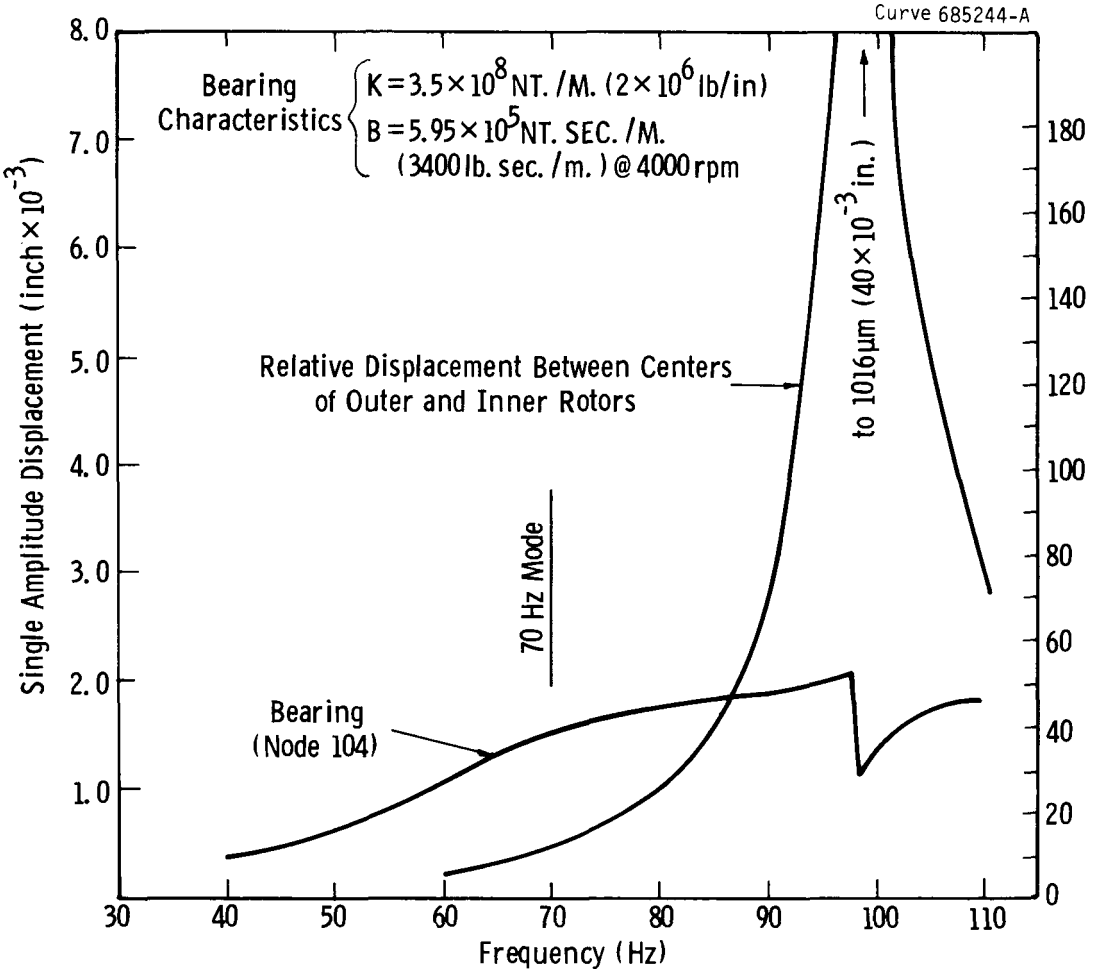

Figure 3-66. Vibration Responses of 300 MVA SCTG Rotors with 1.52 (530 lb. in.^{2}) Dynamic Unbalance on Outer Rotor

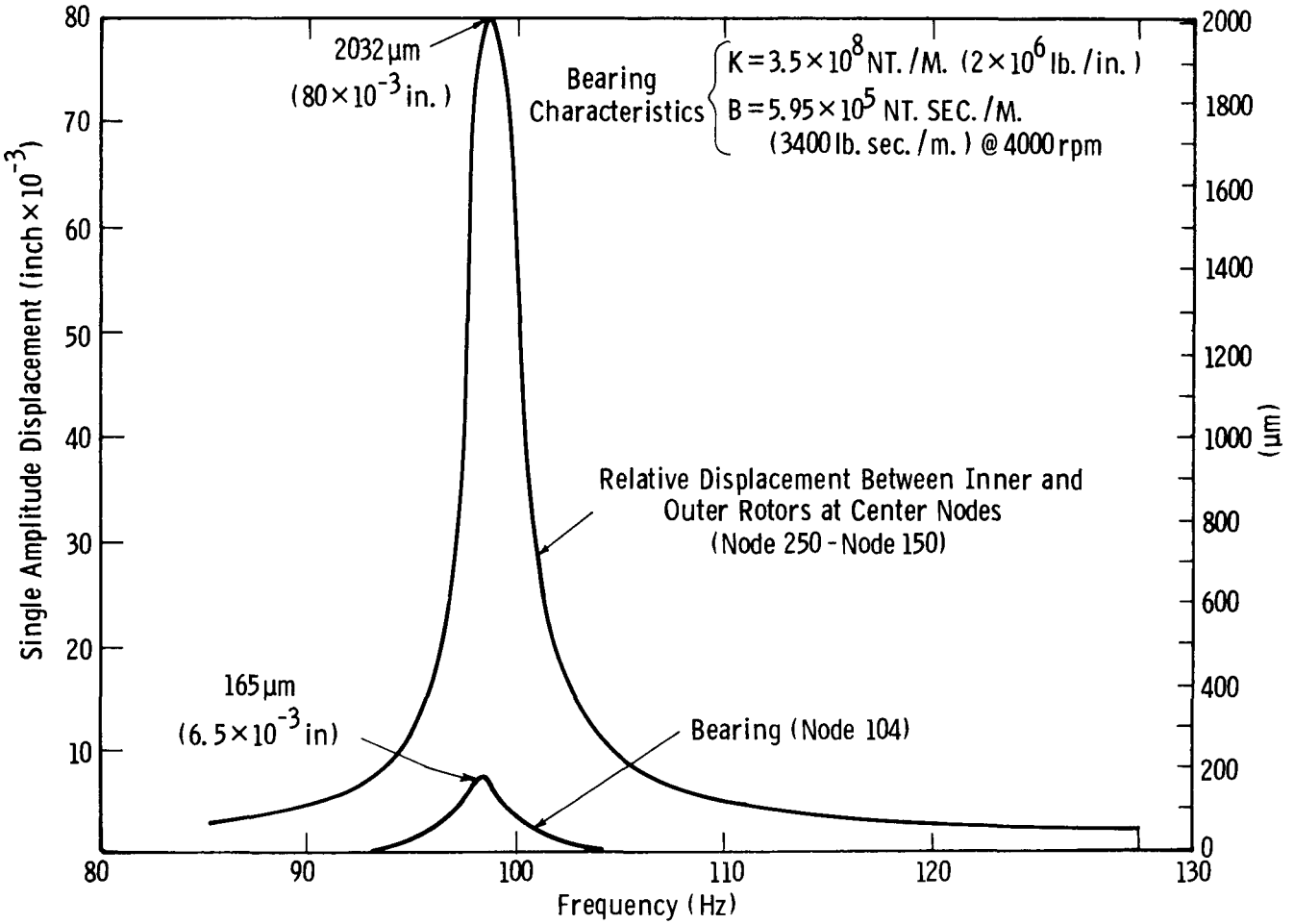

Figure 3-67. Vibration Responses of 300 MVA SCTG Rotor with Out of Phase .27 Nm (2.35 in. lb.) Static Unbalances on Both the Inner and Outer Rotors

inch) eccentricity of both rotors' mass axes with respect to their geometric axes. A large buildup (80x) was exhibited (Fig. 3-67) by the relative displacement between the centers of the inner and outer rotors as the lightly damped third mode (98 Hz) was passed through. Damping is:

$$\zeta_3 = \frac{1}{2 \times 80} = 0.0063 \text{ or } 0.63 \text{ of critical}$$

Fortunately, the 98 Hz third mode is well above operating range for the 300 MVA unit; however, any deviation in design that could significantly lower this mode has to be carefully investigated. See figure 3-67.

1200 MVA

Static unbalances for the 1200 MVA SCTG rotor which have been investigated include 5.54 Nm (49.01 in. lb.) distributed on the outer rotor (Figures 3-68 and 3-69, 5.28 Nm (46.69 in. lb.) distributed on the inner rotor (Figures 3-70 and 3-71), and 1.01 Nm (8.91 in. lb.) distributed on each of the inner and outer rotors 180° apart (Figure 3-72). Dynamic unbalance was investigated using 6.79 Nm^2 (2366 lb. $in.^2$) on the outer rotor (Figure 3-73).

Examing Figures 3-68, 3-69, 3-70 and 3-71, it can be seen that the displacement amplitudes peak at 30 Hz, the first natural frequency of the system. Because these static unbalances approximate 25.4 μm (.001 inch) eccentricity of the rotor mass, these curve peaks may be used to roughly approximate the displacement amplification expected as 30 Hz is traversed. Using Figures 3-69 and 3-71, the largest amplification is approximately $\frac{0.0063}{0.001} \simeq 6.3$. This indicates that the buildup of vibration in the first mode is effectively limited by damping in the bearings. Note from Figure 3-63 that the first mode shape involves relatively large motion at the bearings, hence bearing damping was expected to be effective in this mode.

From Figure 3-72 it can be concluded that the buildup of vibration in the third mode should present no problem over the 0-72 Hz speed range of the unit, providing that this out of phase unbalance on the inner and outer rotors is not excessively large. This type of unbalance may be more difficult than usual to measure and correct, due to the geometry of the

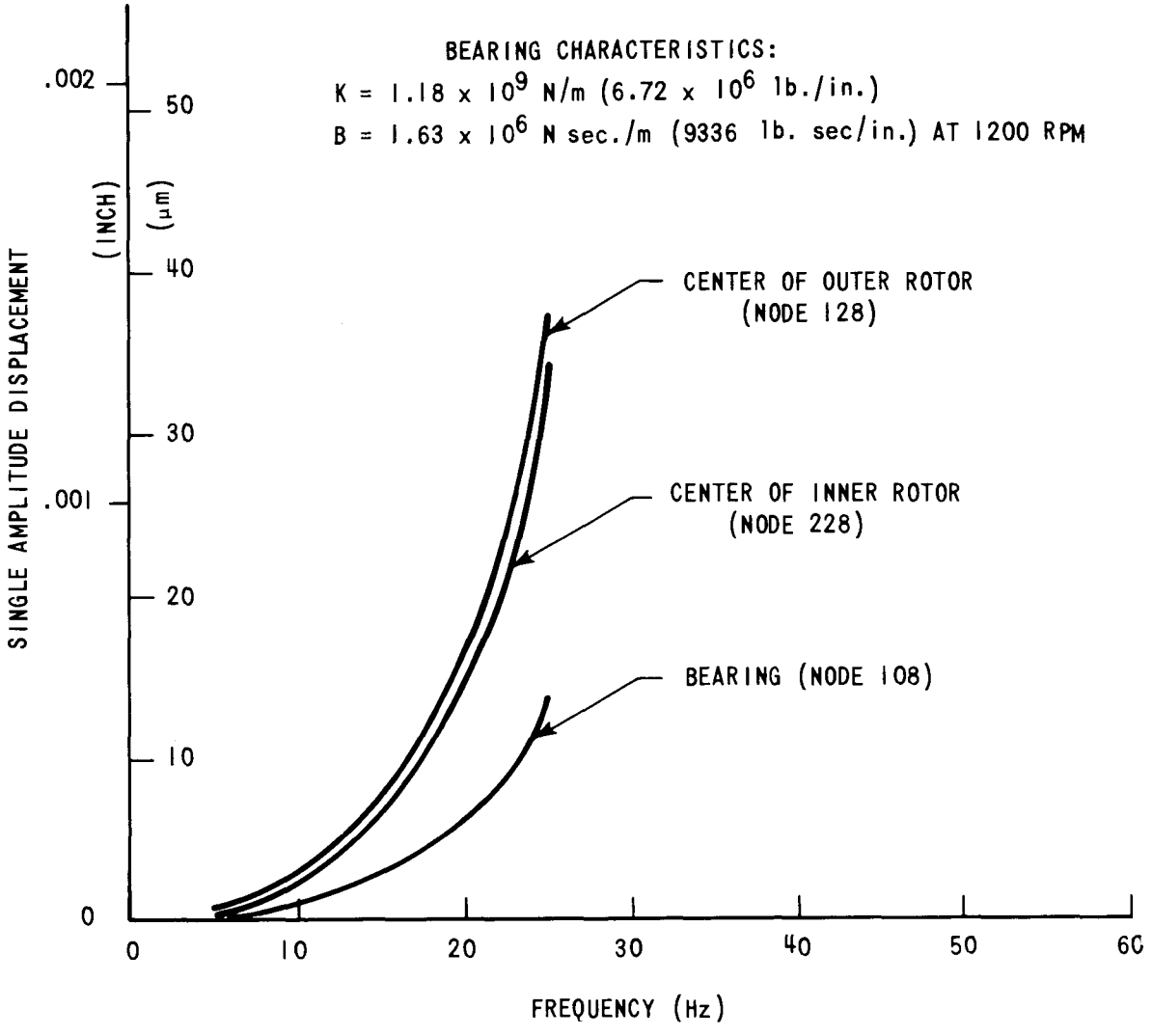

Figure 3-68. Vibration Responses of 1200 MVA SCTG Rotors with 5.54 Nm (49.01 in. lb.) Static Unbalance on Outer Rotor

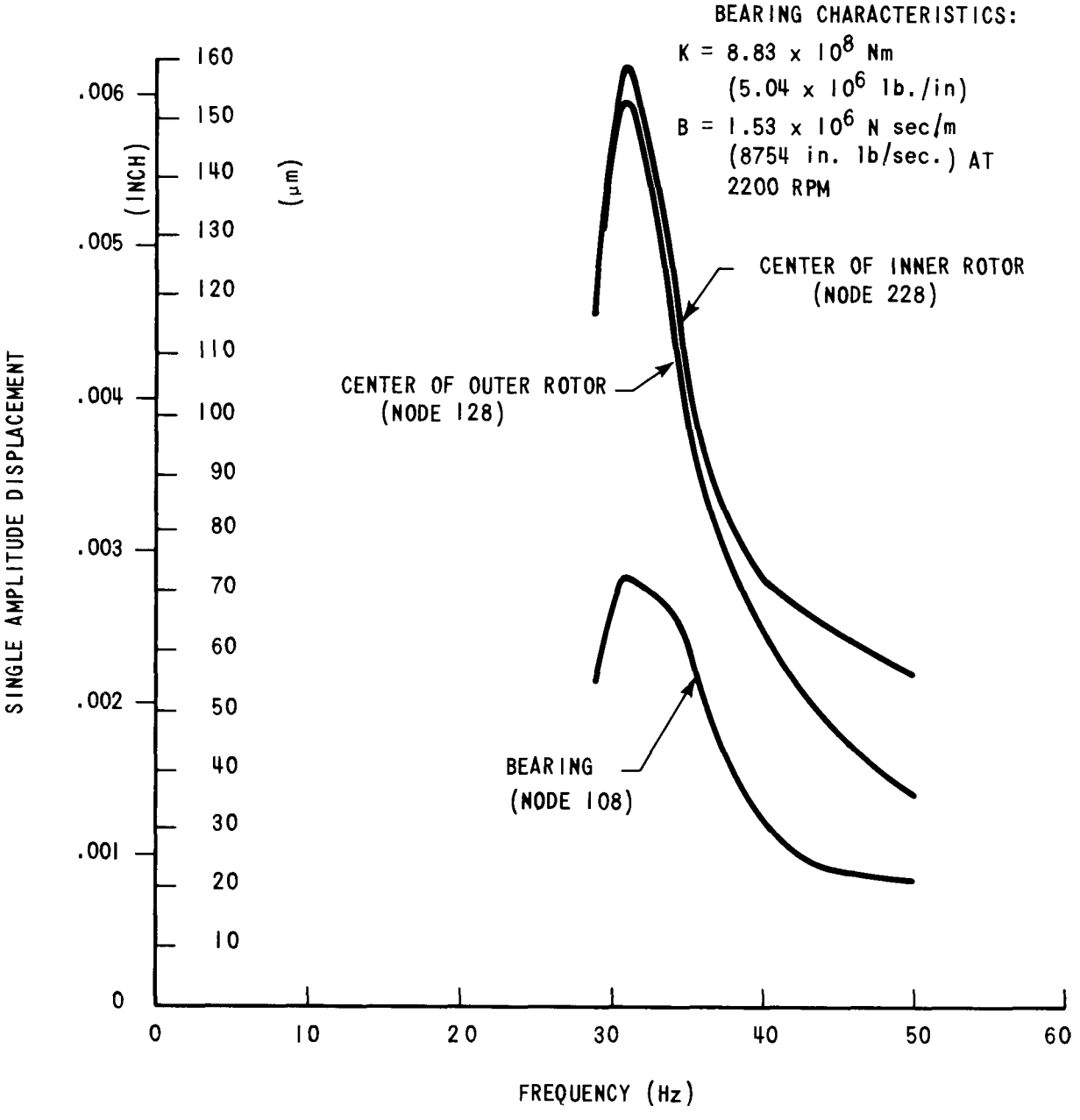

Figure 3-69. Vibration Responses of 1200 MVA SCTG Rotors with 5.54 Nm (49.01 in. lb.) Static Unbalance on Outer Rotor

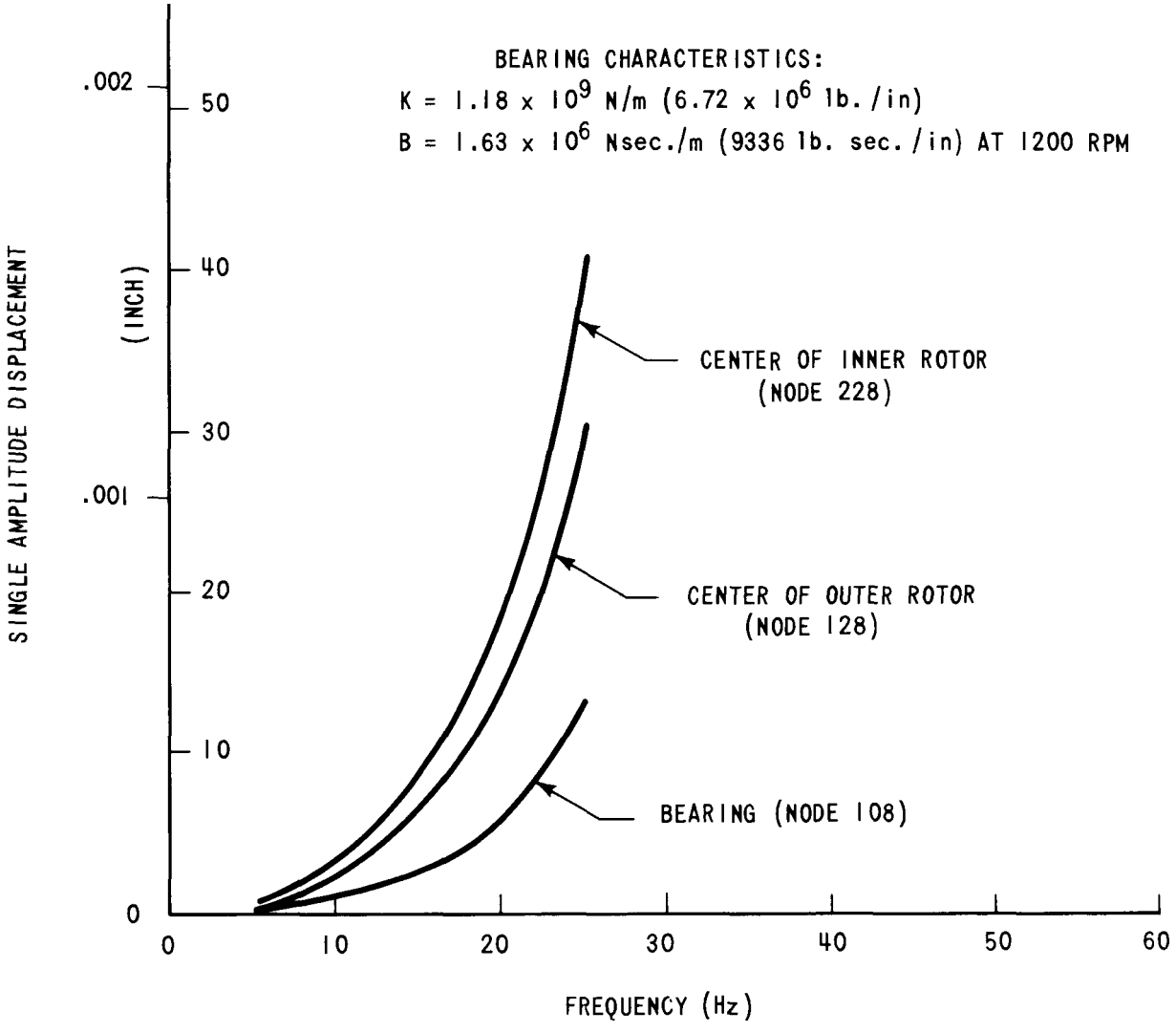

Figure 3-70. Vibration Responses of 1200 MVA SCTG Rotors with 5.28 Nm (46.69 in. lb.) Static Unbalance on Inner Rotor

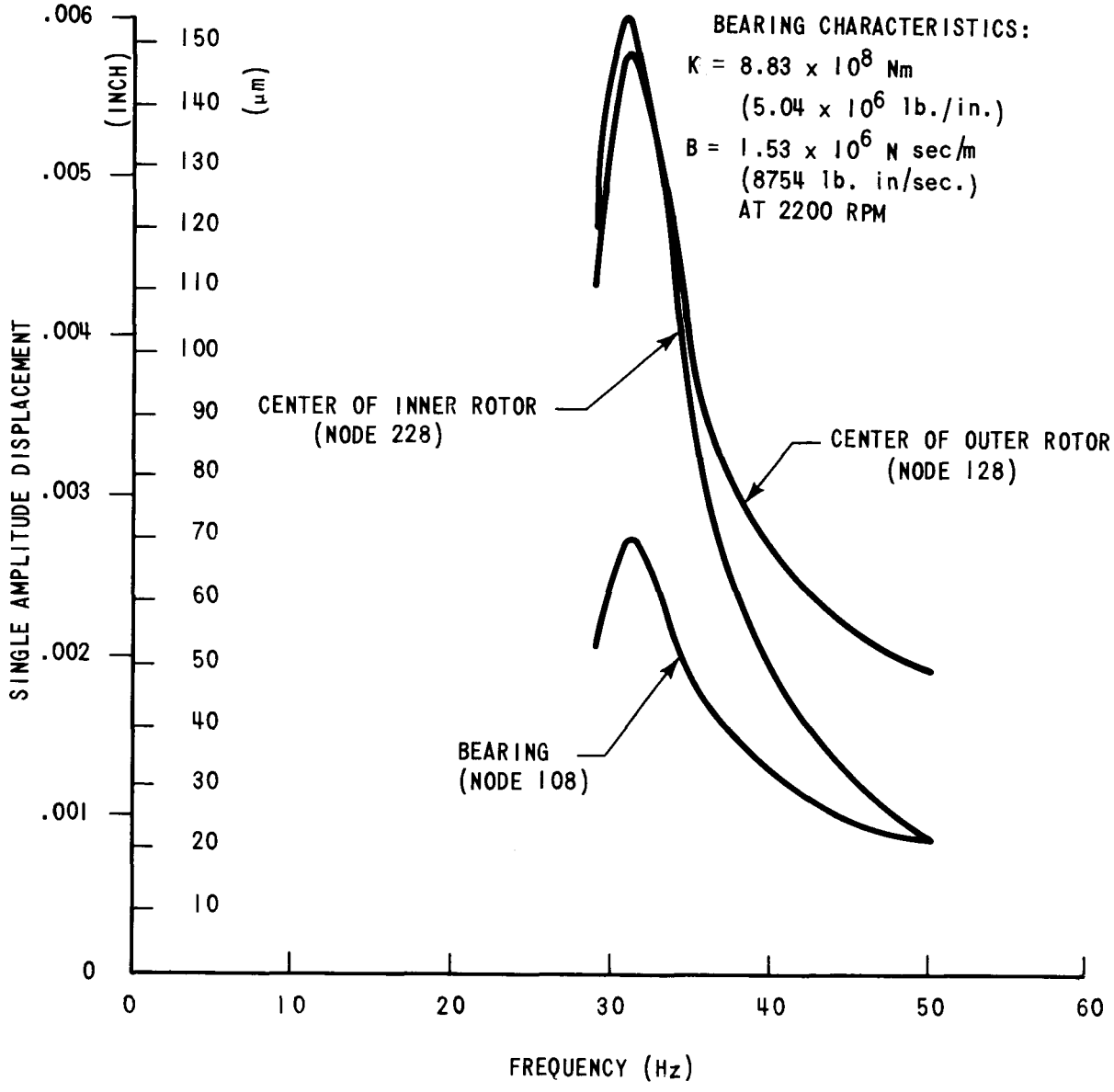

Figure 3-71. Vibration Responses of 1200 MVA SCTG Rotors with 5.28 Nm (46.69 in. lb.) Static Unbalance on Inner Rotor

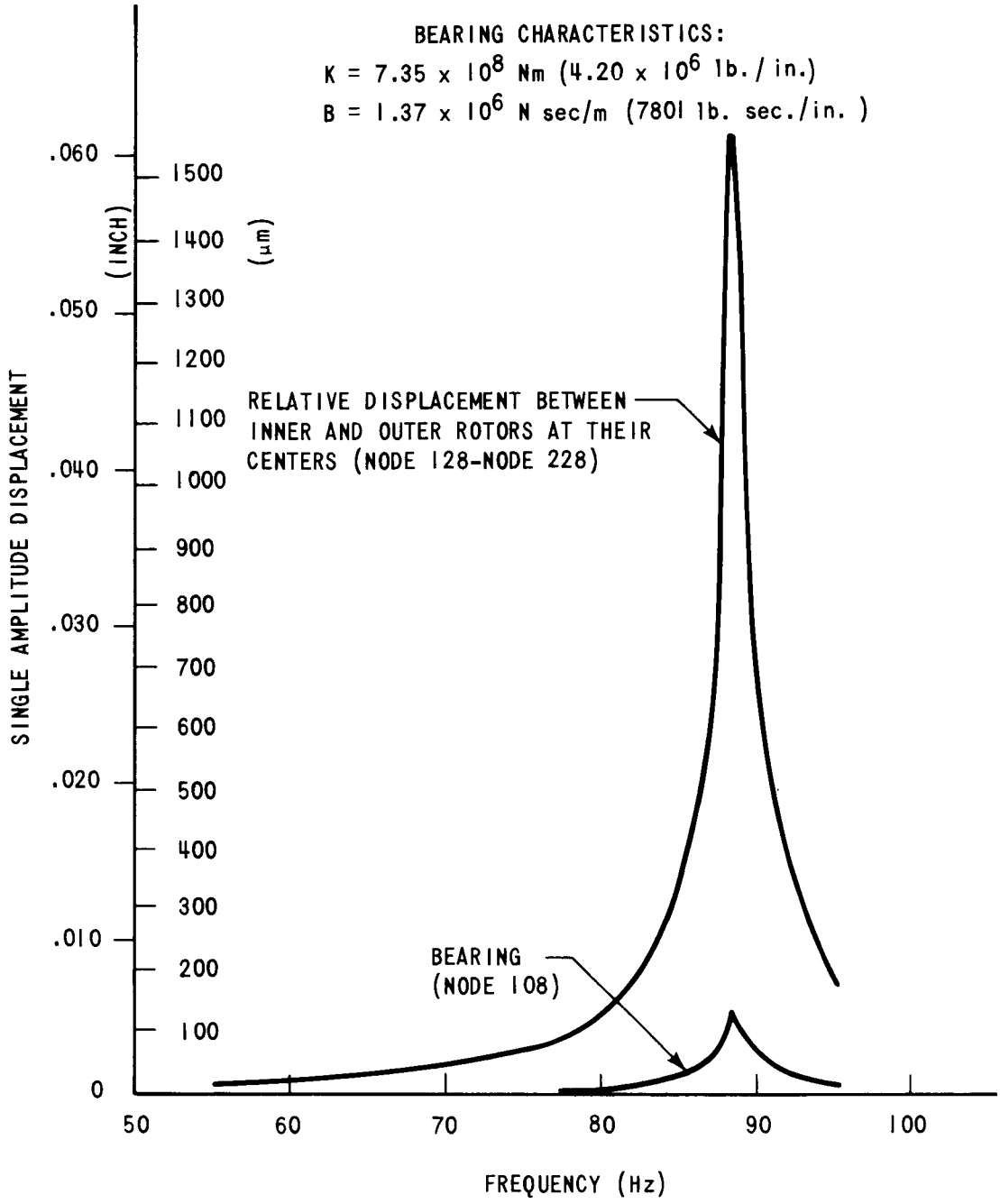

Figure 3-72. Vibration Responses of 1200 MVA SCTG Rotor with 1.01 Nm (8.91 in. lb.) Out of Phase Static Unbalance on Inner and Outer Rotor

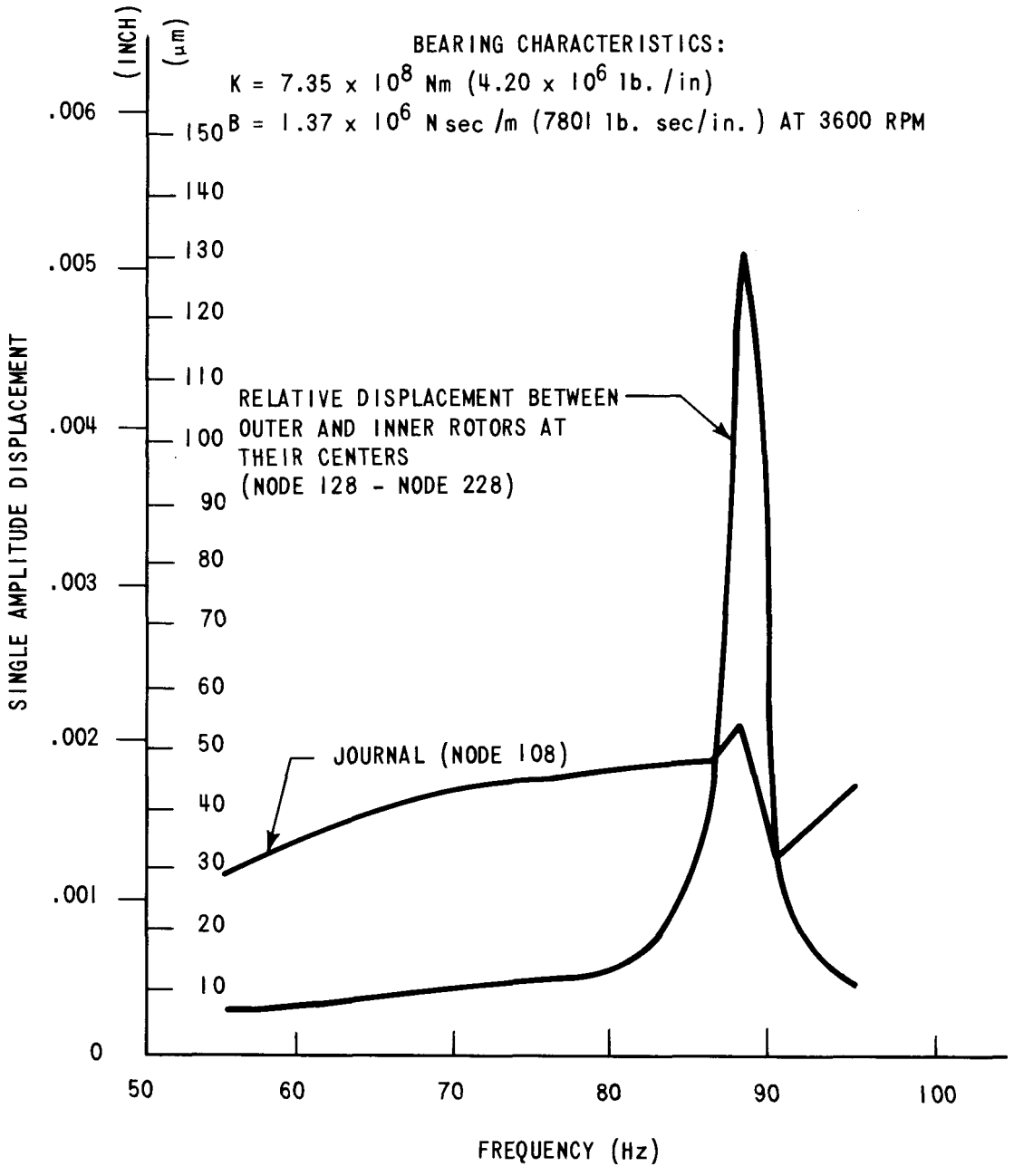

Figure 3-73. Vibration Responses of 1200 MVA SCTG Rotor with Dynamic Unbalance of 6.79 Nm^2 (2366 lb. $in.^2$) on Outer Rotor

SCTG rotor. Note also from Figure 3-72 that this type of unbalance is very ineffective in exciting the 2nd mode at 68 Hz.

Figure 3-73 shows that 6.79 Nm^2 (266 in. $lb.^2$) dynamic unbalance causes very little vibration buildup in the 2nd (68 Hz) mode. From Figure 3-63 it would be expected that the 2nd mode (68 Hz) is heavily damped in that it is characterized by large bearing motions. Figure 3-73 shows that a dynamic unbalance excites the third mode (88 Hz). However, the peak relative displacement between inner and outer rotors is only 127 μ m (.005 in.) at 88 Hz for a 6.79 Nm^2 (2366 lb. $in.^2$) dynamic unbalance. Again, this 88 Hz is well above the 73 Hz overspeed.

Computer Modeling

The WECAN computer program used to study rotor lateral vibration characteristics is based on the finite element method of analysis. The analyst must model, or idealize, the structure in terms of discrete elements and apply loadings and boundary conditions to these elements. The stiffness matrix for each element is assembled into a system of simultaneous linear equations for the entire structure. This set of equations is then solved by a variation of the Gaussian elimination method known as the wave front technique. This type of solution makes it possible to solve systems with a large number of degrees of freedom using a minimum amount of core storage.

In the SCTG lateral vibration models, most elements are 2D beams. The model also makes use of moment spring, linear spring, damper and concentrated mass elements. The following is a brief description of each element:

2D Beam Element (WECAN Element #3)

The two dimensional beam is a uniaxial element with tension-compression and bending capabilities. The displacement functions are a first order polynomial in the axial direction and a cubic polynomial in bending. The effect of shear deformation is not included in the element stiffness. The beam is defined by its two nodal points, cross-sectional area, cross-sectional moment of inertia, thickness from top to bottom, and material properties. The beam can have any cross-sectional shape for which the moment of inertia can be computed. The mass matrix computed for this element is a consistent mass matrix.

2D Mass Element (WECAN Element #16)

The two-dimensional mass element contributed only to the structural mass matrix. The element has no displacement functions, but has two translational degrees of freedom in the global X and Y directions.

The mass element is defined by a single nodal point and its concentrated mass.

2D Spring element (WECAN Element #18)

The two-dimensional spring is a uniaxial tension-compression element with two translational degrees of freedom, in the global X and Y directions. The displacement function is a linear polynomial in the axial direction. No bending is considered. This element has no mass, and its spring constant is specified directly.

The element is defined by its two nodal points and a spring constant.

2D Damper Element (WECAN Element #19)

The two-dimensional damper is a uniaxial element with two translational degrees of freedom, in the global X and Y directions. The element contributes only damping coefficients to the structural damping matrix.

The damper is defined by its two nodal points and a damping coefficient in units of force-time/length.

2D Rotary Spring Element (WECAN Element #45)

The two-dimensional rotary spring has only one degree of freedom per node, rotation about the global Z axis.

The element is defined by its two nodal points and rotary spring constant.

Calculation of Mode Frequencies

The reduced modal analysis option in WECAN is used to determine the natural frequencies and mode shapes for the linear elastic, undamped structure.

This analysis requires the specification of dynamic or active degrees of freedom. The dynamic degrees of freedom are chosen so as to characterize the deformations of the structure in the various modes of interest.

The structure must be a linear elastic structure. If damping is present in the model it is ignored, and any nonlinear elements present are treated as linear, with their stiffness depending on their initial state.

The basic equations for the reduced modal analysis are the same as those for a standard modal analysis except that the mass and stiffness matrices are reduced to contain only the specified dynamic degrees of freedom.

The basic equation for the dynamic behavior of a structure is:

$$[M]\ \{\ddot{x}\} + [C]\ \{\dot{x}\} + [K]\ \{x\} = \{F(t)\} \qquad (1)$$

where

- [M] is the total mass matrix of the structure, the sum of the individual element masses,
- [C] is the total viscous damping matrix of the structure, the sum of the individual element damping matrices,
- [K] is the total stiffness matrix of the structure, the sum of the individual element stiffness matrices,
- $\{x\}$ is the nodal point displacement vector,
- $\{\dot{x}\}$ is the nodal point velocity vector, and
- $\{\ddot{x}\}$ is the nodal point acceleration vector, and
- F(t) is the vector of applied nodal forces as functions of time, t.

In the case of an undamped structure under free vibrations Equation 1 becomes

$$[M]\ \{\ddot{x}\} + [K]\ \{x\} = 0 \qquad (2)$$

If it is assumed that the motion is harmonic of the form

$$\{x\} = \{x_o\} \cos \omega t$$

Equation 2 becomes

$$[K]\ \{x_o\} = \omega^2\ [M]\ \{x_o\}$$

which is an eigenvalue problem, and is often written

$$[K]\ [\Psi] = [\lambda]\ [M]\ [\Psi]$$

where

[Ψ] is the modal matrix,

[λ] is the diagonal matrix whose terms are the squares of the natural frequencies.

The Guyan reduction scheme[1] is employed to calculate these matrices. In order to properly use the reduction scheme, the degrees of freedom retained (i.e., dynamic degrees of freedom), must be those associated with the lowest modes and frequencies of the structure and those eliminated are associated with the higher modes and frequencies. The user can only rely on his engineering judgement and expertise to make the proper selection of the dynamic degrees of freedom. The frequencies calculated are always increased by this reduction process. Referring to Figure 3-62, and Table 3-39, the active degrees of freedom used in the 1200 MVA modal and analyses are:

Active D.O.F. For Dynamic Reduction

No.	Node	D.O.F.
	(See Figure 3-62)	
1	100	UY
2	102	UY
3	104	UY
4	106	UY
5	110	UY
6	112	UY
7	114	UY
8	116	UY
9	118	UY
10	120	UY
11	122	UY
12	124	UY
13	126	UY
14	128	UY
15	130	UY
16	132	UY
17	134	UY
18	136	UY
19	138	UY
20	140	UY
21	144	UY
22	146	UY
23	222	UY
24	224	UY
25	226	UY
26	228	UY
27	230	UY
28	232	UY
29	234	UY
30	326	UY
31	328	UY
32	330	UY

Note that these 32 active D.O.F. are reduced from a gross total of 107 in the complete model. A similar reduction is used on the 300 MVA model.

The reduced stiffness matrix can be thought of as the matrix of the influence coefficients of the structure at the points and in the directions of the dynamic degrees of freedom, while the reduced mass matrix results from a redistribution of the mass to the dynamic degrees of freedom in a manner consistent with the possible static deformations of the structure due to imposed deformations along the dynamic degrees of freedom.

Unbalance Calculations

The harmonic response analysis option in WECAN is used to calculate unbalance responses of the rotor. The harmonic response analysis is a steady state solution of a linear elastic system under a set of harmonic loads of known amplitude and frequency. These boundary loads are specified as forces. All forcing functions for a given analysis must be at the same frequency and in phase. Damping is included in the system as discrete viscous dampers.

As in the modal analysis, the basic equation for the dynamic behavior of a structure is:

$$[M]\{\ddot{x}\} + [C]\{\dot{x}\} + [K]\{x\} = \{F(t)\} \qquad (3)$$

where the terms are defined as in Equation (1).

Assuming the forcing function is of the form

$$\{F(t)\} = \{F_o\}\, e^{j\omega t}$$

and the displacement is of the form

$$\{x\} = \{x_o\}\, e^{j\omega t}$$

then Equation (3) becomes

$$-\omega^2 [M] + j\omega [C] + [K]\{x_o\} = \{F_o\}$$

This is a set of simultaneous linear equations of the same form as for the static elastic solution, except that the matrix is complex.

The solution has a displacement vector x_o which is complex, having a real and an imaginary portion, representing an amplitude and a phase angle.[2]

REFERENCES (COMPUTER MODELING)

1. R. Guyan, "Reduction of Stiffness and Mass Matrices," AIAA Journal, Vol. 3, p. 380, 1965

2. WECAN, Westinghouse Electric Computer Analysis, Westinghouse Proprietary Computer Program, 1973.

Lateral Vibration Rotor Models

300 MVA

The WECAN[1] finite element model (Fig. 3-74) identifies all the elements according to node and element numbers with the x,y coordinate system. Two parallel branches consisting of 2-D beam elements are used to represent the inner and outer rotor cylinders. The discretization of beam elements is based upon geometric considerations as well as obtaining an accurate representation of the modes of vibration.

Two different constraints for the left end (nodes 109, 209) connection between the outer and inner rotors have been studied. The translational degrees of freedom for both nodes are coupled; however, the two nodes are free to rotate independent of each other in one case (simple support -- no transmitted moment) while in the second case an estimated moment spring of 4.52×10^7 Nm/rad. (400×10^6 in. lb./rad.) is inserted to allow a moment to be transmitted. In all cases the right end connection between the inner and outer rotors (nodes 181, 281) is fixed (translation and rotation degrees of freedom coupled).

Table 3-40 lists the geometric and material properties required for each beam element-area, area moment of inertia, and mass distribution. The lowest natural frequency of the radiation shield on simple supports is estimated to be 230 Hz which is much higher than the inner rotor; hence, adding one-half the radiation shield mass at both nodes 210 and 280 simulates the mass effect of the shield following the inner rotor vibration. The mass of the winding, winding support, field support tube, and the T.E. and E.E. torque tubes is distributed over the center 81 inches of the inner rotor (elements 26 through 29).

The outer rotor is a composite cylinder member with concentrically arranged steel-copper-steel layers. In addition, at the time of modeling the outermost steel cylinder contained 3.18 mm (1/8 inch) wide slots which were 2.54 cm (1 inch) deep and spaced 2.54 cm (1 inch) apart. An equivalent homogeneous beam element was used which contained the same mass as the outer rotor but an effective area moment of inertia based on an outer radius consistent with 30° stress lines. Even if the outermost radius is taken, the inertia is only 10% greater indicating that the frequencies are rather insensitive to the judgment as to how much material between the slots is effective in bending.

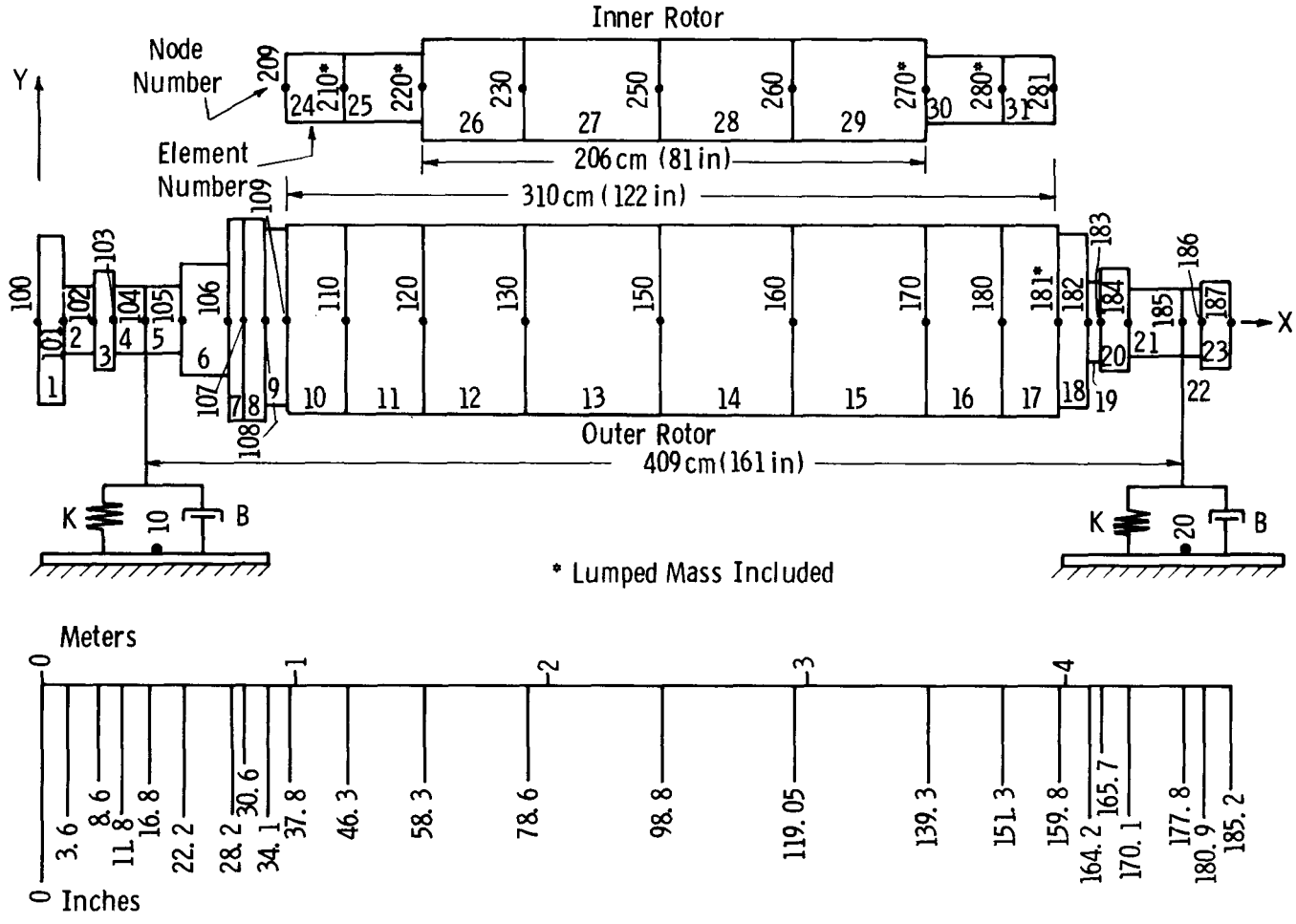

Figure 3-74. Schematic of Finite Element Model Used To Investigate Lateral Vibration of 300 MVA SCTG Rotor

Table 3-40

300 MVA S.C.T.G. FINITE ELEMENT PROPERTIES

Element No.	Length in.	Length cm.	Nodes	Area $in.^2$	Area cm^2	Inertia $in.^4$	Inertia cm^4	Mass Density $\frac{lb.\ sec^2}{in.^4}$	Mass Density $\frac{gram\ sec^2}{cm^4}$	Weight/Length lb./in.	Weight/Length dyne/cm	Weight lb.	Weight dyne
1	3.6	9.1	100-101	544.3	3511.8	26023	1083293	.000733	.00799	154.0	2.71×10^7	554.4	2.47×10^8
2	5.0	12.7	101-102	108.6	700.7	1427	59404			30.7	5.40×10^6	153.5	6.83×10^7
3	3.2	8.1	102-103	143.9	928.4	2292	95412			40.7	7.16×10^6	130.2	5.79×10^7
4	5.0	12.7	103-104	108.6	700.7	1427	59404			30.7	5.40×10^6	153.5	6.83×10^7
5	5.4	13.7	104-105	↓	↓	↓	↓			↓	↓	165.8	7.37×10^7
6	6.0	15.2	105-106	144.0	929.1	3310	137790			40.8	7.18×10^6	244.8	1.09×10^8
7	2.8	7.1	106-107	682.4	4402.8	44916	1869777			193.1	3.40×10^7	540.7	2.41×10^8
8	3.5	8.9	107-108	292.9	1889.8	28358	1180495			82.9	1.46×10^7	290.2	1.29×10^8
9	3.7	9.4	108-109	153.9	993.0	13197	549369			↓	↓	161.1	7.17×10^7
10	8.5	21.6	109-110	355.1	2291.1	4289	178544			100.5	1.77×10^7	854.0	3.80×10^8
11	12.0	30.5	110-120	↓	↓	↓	↓			↓	↓	1205.7	5.36×10^8
12	20.25	51.4	120-130									2034.7	9.05×10^8
13	20.25	↓	130-150									↓	↓
14	20.25		150-160										
15	20.25		160-170										
16	12.0	30.5	170-180									1205.7	5.36×10^8
17	8.5	21.6	180-181	↓	↓	↓	↓			↓	↓	854.0	3.80×10^8
18	4.4	11.2	181-182	496.7	3204.7	18645	776160			140.6	2.47×10^7	618.6	2.75×10^7
19	1.5	3.8	182-183	98.6	636.2	1309	54491			27.9	4.91×10^6	41.8	1.86×10^7
20	4.4	11.2	183-184	133.2	859.4	2137	88960			37.7	6.64×10^6	163.7	7.28×10^7
21	7.7	19.6	184-185	98.6	636.2	1309	54491			27.9	4.91×10^6	214.8	9.55×10^7
22	3.1	7.9	185-186	↓	↓	↓	↓			↓	↓	86.5	3.85×10^7
23	4.3	10.9	186-187	133.2	859.4	2137	88960			37.7	6.64×10^6	162.1	7.21×10^7
24	8.5	21.6	209-210	24.3	156.8	732	30472			6.9	1.21×10^6	58.6	2.61×10^7
25	12.0	30.5	210-220	↓	↓	↓	↓			↓	↓	82.8	3.68×10^7
26	20.25	51.4	220-230	33.8	218.1	1952	81258	.003426	.03734	44.7	7.87×10^6	905.2	4.03×10^8
27	20.25	↓	230-250	↓	↓	↓	↓	↓	↓	↓	↓	↓	↓
28	↓		250-260										
29			260-270										
30	12.0	30.5	270-280	24.3	156.8	732	30472	.00073	.00799	6.9	1.21×10^6	82.8	3.68×10^7
31	8.5	21.6	280-281	↓	↓	↓	↓	↓	↓	↓	↓	58.6	2.61×10^7

The bearing stiffness and damping coefficients have been calculated for oil film journal bearings which are of the tilted pad type. The weight load acts between pads. For a journal radius of 16.5 cm (6.5 in.) and radial clearance of .254 mm (.01 in.), the damping coefficients are 7.88×10^5 N sec/m/bearing (4500 lb. sec/in./bearing) and 5.95×10^5 N sec/m/bearing (3400 lb. sec./in./bearing) for the speeds of 2000 rpm and 4000 rpm, respectively.[2] A stiffness coefficient of 3.50×10^8 N/m bearing (2×10^6 lb./in./bearing) is used for the bearings at both speeds.

1200 MVA

Because the 300 MVA rotor is being developed as a prototype for larger machine sizes, it was possible to develop the 1200 MVA rotor model using essentially the same modeling techniques employed on the 300 MVA rotor. These are some notable differences between the 1200 and 300 MVA rotor models:

- The inner inner rotor was added as another (3rd discrete branch inside the 1200 MVA rotor system. This inner inner rotor (Figure 3-40) represented the cylinder upon which the helium distribution troughs would have been mounted. Although there would have been more than two axial locations of radial support between this inner inner rotor and the inner rotor, the 1200 MVA model assumed there was support only at each end of the inner inner cylinder. An estimate of the nature of the mimimum required radial support would then be gained from the model. The inner inner rotor was subsequently eliminated to simplify the rotor.
- The 1200 MVA model represented a 27,433 kg (60,500 lb.), 6.2 m (243") between bearings, 1.1 m (43.3") O.D. rotor system while the 300 MVA model represented a 9526 kg (21,000 lb.), 4.1 m (161") between bearings, .8 m (31.3") O.D. rotor system.
- Again two different constraints for the left end (nodes 120, 220, Figure 3-63) connection between the outer and inner cylinders were studied. The moment spring rate studied for the 1200 MVA rotor is 2.83×10^8 Nm/rad. (25×10^8 in. lb./rad.). The 1200 MVA rotor harmonic analyses (unbalance calculations), however, were made using the model with the moment spring, whereas the 300 MVA harmonic analysis used the model without the moment spring.

The study without the moment spring is more conservative than the study with the moment spring. This moment spring is a more detailed model of the turbine end sliding support between the inner and outer rotors. This difference in the models results from a refinement in modeling technique

used when making the second (1200 MVA) model. The 300 MVA rotor was the first unit to be modeled. Future models must mimic the latest differential expansion design.

The 2-D beam finite element properties are found in Table 3-41. The 1200 MVA model node and element numbers are shown in Figure 3-62. Note that element and node numbering differs for the 300 MVA and 1200 MVA machines.

The lowest natural frequency of the 454 kg (1000 lb.) radiation shield on simple supports is estimated to be 100 Hz. It is mounted upon the 5443 kg (12000 lb.) inner rotor which has an estimated lowest natural frequency of 66 Hz. The model assumes that the radiation shield acts as a mass distributed on the inner rotor. Further development of the model can show whether the 1200 MVA radiation shield requires additional support between its end points.

Tilted pad bearing properties were calculated at 1200, 2200, and 3600 rpm, using bearings which are 45.7 cm (18") diameter, 25.4 cm (10") pad length, and .457 cm (.018") radial clearance. The properties are shown in Table 3-42.

Table 3-42

1200 MVA SCTG ROTOR BEARING PROPERTIES

RPM	Spring Constant		Damping	
	lb/in	N/m	lb sec/in	$\frac{\text{N sec}}{\text{m}}$
1200	6.72×10^6	1.18×10^9	9336	1.63×10^6
2200	5.04×10^6	8.83×10^8	8754	1.53×10^6
3600	4.20×10^6	7.35×10^8	7801	1.37×10^6

REFERENCES

1. WECAN, Westinghouse Electric Computer Analysis, Westinghouse Proprietary Computer Program, 1973.

2. Hagg, A. C. and Sankey, G. O., "Elastic and Damping Properties of Oil-Film Journal Bearings for Application to Unbalance Vibration Calculations," Journal of Applied Mechanics, 1958.

Table 3-41

1200 MVA ROTOR FINITE ELEMENT PROPERTIES

Element No.	Length in.	Length cm.	Nodes	Area $in.^2$	Area cm^2	Inertia $in.^4$	Inertia cm^4	Mass Density $\frac{lb.\ sec^2}{in.^4}$	Mass Density $\frac{gram\ sec^2}{cm^4}$	Weight/Length lb./in.	Weight/Length dyne/cm	Weight lb.	Weight dyne
1	4.0	10.2	100-102	664	4283.9	40415	1.68×10^6	.000733	.00799	188	3.31×10^7	752	3.34×10^8
2	6.0	15.2	102-104	204	1316.1	4952	2.06×10^5	↓	↓	58	1.02×10^7	348	1.55×10^8
3	4.0	10.2	104-106	259	1671.0	7405	3.08×10^5			73	1.28×10^7	292	1.30×10^8
4	5.36	13.6	106-108	204	1316.1	4952	2.06×10^5			58	1.02×10^7	311	1.38×10^8
5	Spring		108-10	$K=8.83\times10^8$ N/m (5.04×10^6 lb/in)									
6	Damper		108-10	$B=1.53\times10^6$ N sec/m (8754 lb sec/in)									
7	11.12	28.2	108-110	204	1316.1	4952	2.06×10^5	.000733	.00799	58	1.02×10^7	645	2.87×10^8
8	5.04	12.8	110-112	257	1658.1	8118	3.38×10^5	↓	↓	73	1.28×10^7	368	1.64×10^8
9	6.00	15.2	112-114	331	2135.5	15518	6.46×10^5			94	1.65×10^7	564	2.51×10^8
10	4.80	12.2	114-116	1337	8625.8	169646	7.06×10^6			378	6.65×10^7	1814	8.07×10^8
11	3.80	9.7	116-118	596	3845.2	110749	4.61×10^6	↓	↓	169	2.97×10^7	642	2.86×10^8
12	Mass		118									1471	6.54×10^8
13	5.60	14.2	118-120	288	1858.1	46517	1.94×10^6	.000733	.00799	82	1.44×10^7	459	2.04×10^8
14	Mass		120									1471	6.54×10^8
15	7.44	18.9	120-122	601	3877.4	56302	2.34×10^6	.000733	.00799	167	2.94×10^7	1242	5.52×10^8
16	Moment	Spring	220-120	$K=2.83\times10^8$ Nm/rad		(25×10^8 in lb/rad)							
17	7.44	18.9	220-222	60	378.1	4894	2.04×10^5	.000733	.00799	17	2.99×10^7	126	5.60×10^7
18	Mass		222									923	4.11×10^8
19	16.00	40.6	122-124	601	3877.4	56302	2.34×10^6	.000733	.00799	167	2.94×10^7	2672	1.19×10^9
20	16.00	40.6	222-224	60	387.1	4894	2.04×10^5	.000733	↓	17	2.99×10^6	272	1.21×10^8
21	Mass		224									405	1.80×10^8
22	33.60	85.3	124-126	601	3877.4	56302	2.34×10^6	.000733	.00799	167	2.94×10^7	5611	2.50×10^9
23	33.60	↓	224-226	96	619.4	11132	4.63×10^5	.00198	.02158	86	1.51×10^7	2890	1.29×10^9
24	33.60		324-326	38	245.2	683	2.84×10^4	.00133	.01449	19	3.34×10^6	638	2.84×10^8
25	33.84	86.0	126-128	601	3877.4	56302	2.34×10^6	.000733	.00799	167	2.94×10^7	5651	2.51×10^9
26	33.84	↓	226-228	96	619.4	11132	4.63×10^5	.00198	.02158	86	1.51×10^7	2910	1.29×10^9
27	33.84		326-328	38	245.2	683	2.84×10^4	.00133	.01449	19	3.34×10^6	643	2.86×10^8
28	33.20	84.3	128-130	601	3877.4	56302	2.34×10^6	.000733	.00799	167	2.94×10^7	5544	2.47×10^9
29	33.20	↓	228-230	96	619.4	11132	4.63×10^5	.00198	.02158	86	1.51×10^7	2855	1.27×10^9
30	33.20		328-330	38	245.2	683	2.84×10^4	.00133	.01449	19	3.34×10^6	631	2.81×10^8
31	33.44	84.8	130-132	601	3877.4	56302	2.34×10^5	.000733	.00799	167	2.94×10^7	5584	2.48×10^9
32	33.44	↓	230-232	96	619.4	11132	4.63×10^5	.00198	.02158	86	1.51×10^7	2876	1.28×10^9

1200 MVA ROTOR FINITE ELEMENT PROPERTIES (CONTINUED)

Element No.	Length in.	Length cm.	Nodes	Area in^2	Area cm^2	Inertia in^4	Inertia cm^4	Mass Density $\frac{lb\ sec^2}{in^4}$	Mass Density $\frac{gram\ sec^2}{cm^4}$	Weight/Length lb/in	Weight/Length dyne/cm	Weight lb	Weight dyne
33	33.44	84.9	330-332	38	245.2	683	2.84×10^4	.00133	.01449	19	3.34×10^7	635	2.82×10^9
34	16.40	41.7	132-134	601	3877.4	56302	2.34×10^6	.000733	.00799	167	2.94×10^6	2739	1.22×10^8
35	16.40	41.7	232-234	60	387.1	4894	2.04×10^5	.000733	.00799	17	2.99×10^6	279	1.24×10^8
36	Mass		234									923	4.11×10^8
37	11.52	29.3	134-136	601	3877.4	56302	2.34×10^6	.000733	.00799	167	2.94×10^7	1924	8.56×10^8
38	11.52	29.3	234-236	60	387.1	4894	2.04×10^5	.000733	.00799	17	2.99×10^6	196	8.72×10^7
39	Mass		136									575	2.56×10^8
40	4.64	11.8	136-138	968	6245.1	82247	3.42×10^6	.000733	.00799	274	4.82×10^7	1271	5.65×10^8
41	6.40	16.3	138-140	259	1671.0	7405	3.08×10^5	↓	↓	73	1.28×10^7	467	2.08×10^8
42	10.00	25.4	140-142	204	1316.1	4952	2.06×10^5			58	1.02×10^7	580	2.58×10^8
43	Spring		142-20	$K = 8.83 \times 10^8$ N/m (5.04×10^6 lb/in)									
44	Damper		142-20	$B = 1.53 \times 10^6$ N sec/m (8754 lb sec/in)									
45	5.60	14.2	142-144	204	1316.1	4952	2.06×10^5	.000733	.00799	58	1.02×10^7	325	1.45×10^8
46	4.64	11.8	144-146	259	1671.0	7405	3.08×10^5	.000733	.00799	73	1.28×10^7	339	1.51×10^8
47	Mass		146									112	4.98×10^7

Whirl Dynamics of Liquid Helium

The present Westinghouse SCTG rotor cooling scheme employs liquid helium coolant. In the partially filled rotor, rotational forces establish a free cylindrical surface of liquid. A review has been made regarding possible effects of the liquid free surface on vibration of the rotor. It has been concluded that these effects will be negligible in the Westinghouse 300, 1200, and 3000 MVA rotors.

There is limited experience with rotors partially filled with liquid. A literature review indicates some experience with trapped oil,[1] a clothes washing machine rotor, spinning liquid rockets, centrifuges, and liquid cooled gas turbine rotors.[2]

A review of experiences with superconducting rotating machinery includes MIT machines and Westinghouse machines. The first Westinghouse 12,000 rpm Air Force superconducting generator had a limited free surface composed of many small passages. Waves could not travel circumferentially in this geometry. A second Westinghouse 12,000 rpm Air Force superconducting generator is being built essentially without a free surface. The Westinghouse 5 MVA superconducting generator also had essentially no free surface. All of these Westinghouse machines have significant damping built in at the bearings or bearing supports.

The first MIT superconducting rotor had a free surface. During balancing operation at a speed somewhat above 600 rpm, excessive rotor vibration resulted in damaged spokes connecting inner and outer rotors. The damage is attributed to the whirl instability of a partially (liquid nitrogen) filled rotor mounted on soft supports. The self centering spherical ball bearings were mounted upon stiff blocks which in turn were mounted upon laterally soft 8.26 cm (3.25 in.) long sections of 31 lb/ft I beams.

The second MIT superconducting rotor has essentially no free surface. MIT is in the process of building an experimental liquid helium system machine which will have a free surface. The concern is therefore one in which limited, yet significant, experience has been gained. Analysis of the phenomenon is in a development stage. References on the subject are generally theses or published papers.

The following calculation of the unbalance of liquid helium in a rotating eccentric cylinder under steady state shows that it is very small -- about 1-2% of the 300 MVA S.C.T.G. existing rotor unbalance and about 1% of the 1200 MVA S.C.T.G. rotor unbalance corresponding to the eccentricity at a critical speed and less at other speeds. This (favorable) result follows from the low density of the liquid and the small radius of the free surface.

It is noted that the free surface of the liquid is established at about 108 rpm. This means that at a critical speed -- say 1800 rpm and at higher speeds (400 g's) -- the equilibrium time should be very small and the free surface will follow the relatively slow changes in magnitude and phase of the eccentricity. Additionally, even if a transient flow effect did occur and was several times the steady state effect, the resulting unbalance would still be relatively small.

A rotor cylinder as shown in Figure 3-75 but without liquid is eccentric because of (existing) unbalance. If U_r is the unbalance (in-lbs/per unit length of rotor)

$$U_r = \frac{W\varepsilon}{q}$$

where W is the weight of the rotor per unit length, $\frac{\varepsilon}{q}$ is the eccentricity of the center of gravity (of the rotor unit length) with respect to the geometric axis, and q is the vibration magnification.

The additional unbalance, U_l per unit length caused by the liquid is evaluated as follows:

$$\Delta U_l = \gamma R\varepsilon \quad \sin\theta \; R d\theta \quad (\varepsilon << R)$$

$$\Delta F_x = \frac{\gamma}{g} R\varepsilon \quad \sin^2\theta \; R d\theta \; \omega^2$$

where γ = wt. (mass) of helium per unit vol.

$$F_x = \frac{\gamma}{g} R^2 \varepsilon \omega^2 \int_o^{2\pi} \sin^2 \theta d\theta = \frac{\gamma}{g} \pi R^2 \varepsilon \omega^2$$

$$(F_y = 0)$$

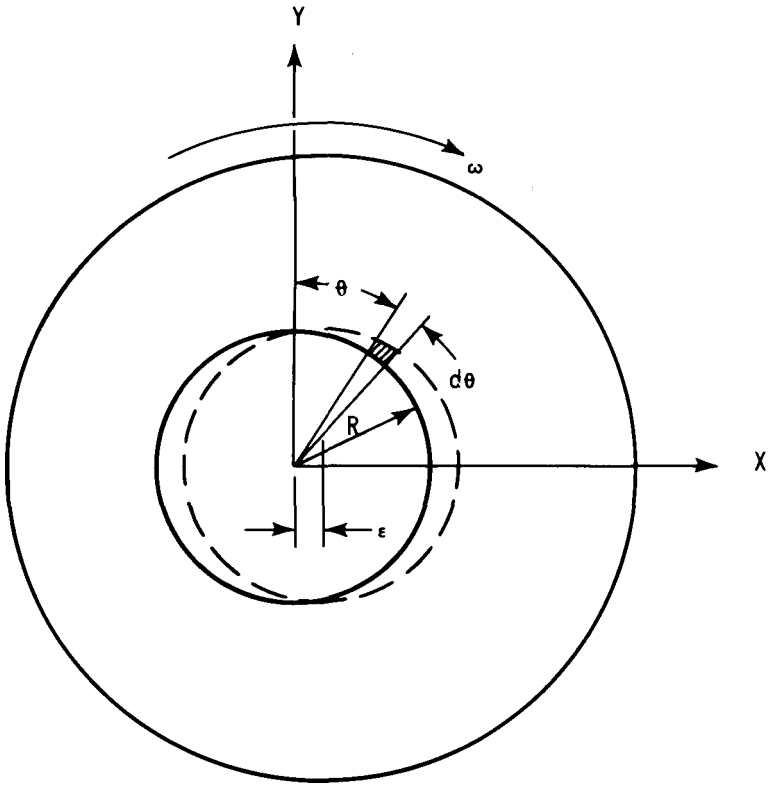

Figure 3-75. Liquid Helium in a Rotating Eccentric Cylinder

and

$$U_l = \gamma \pi R^2 \varepsilon$$

The ratio U_l/U_r is

$$\frac{U_l}{U_r} = \frac{\gamma \pi R^2 \varepsilon q}{W\varepsilon} = \frac{\gamma \pi R^2 q}{W}$$

For the case at hand

300 MVA

$\gamma = 4.4 \times 10^{-3}$ lbs/in^3 = 0.122 gms/cm^3

R = 3 in. = 7.62 cm

q ≃ 10 at critical speed

W ≃ 100 lbs/in (est) = 17.9 kg/cm

and

$$\frac{U_l}{U_r} = \frac{4.4 \times 10^{-3} \times \pi \times 9 \times 10}{100} = .0124 = 1\text{-}2\%$$

The contribution of the liquid to the unbalance already existing is very small for the 300 MVA machine such that the effect can be neglected.

1200 MVA

$\gamma = 4.4 \times 10^{-3}$ lb/in^3 = 0.122 gms/cm^3

R = 3 in. = 7.62 cm

q ≃ 10 at critical speed

W = 225 lbs/in = 40.2 kg/cm

$$\frac{U_l}{U_r} \quad \frac{(4.4 \times 10^{-3})(\pi)\ (3)^2\ (10)}{225} = .0055 = .5\text{-}1\%$$

The contribution of the liquid to the unbalance, .5-1%, is even less for the 1200 MVA machine.

The free surface of the liquid is established at $\frac{R\omega^2}{g} > 1$ or

rpm > $\frac{60}{2\pi}\sqrt{\frac{g}{R}}$ or rpm > 108 for R = 3 in. = 7.62 cm. Because there was concern regarding the dynamic behavior of the liquid helium, additional consideration has been made using existing literature.

The J. A. Wolf, Jr. thesis[3] cannot be used to obtain significant conclusive results for the SCTG because external damping is specifically excluded, and no amplitudes of vibrations are derived. The SCTG has external damping of significant magnitude applied to the system by tilting pad oil film journal bearings at all frequencies. The SCTG machine also differs from the Wolf model in that small passages and helium troughs would interfere with wave motion.

A calculation using the F. F. Ehrich analysis[4], indicates that the liquid causes no significant change in vibration at the critical speed. The whirl amplitude at speeds above the critical by the Ehrich calculation is 3.04×10^{-9} cm (1.2×10^{-9} inch).

External positive damping, which is estimated to be very large compared to the negative damping of the liquid will eliminate any asynchronous motion altogether. No vibration problem will be experienced with a SCTG rotor partially filled with nitrogen or helium. In view of the calculations, consideration was given to eliminating the wave baffles presently shown on layouts. They have been left in to provide piping support.

REFERENCES

1. Ehrich, F. F., "The Influence of Trapped Fluid on High Speed Rotor Vibration," Journal of Engineering for Industry, Trans. ASME, Vol. 89, Series B, 1967, pp. 806-812.

2. Wolf, J. A., Jr., "Whirl Dynamics of a Rotor Partially Filled with Liquid," Sc.D. Thesis, MIT, Cambridge, Mass., September, 1968.

3. Wolf, J. A., Jr., Ibid.

4. Ehrich, F. F., op.cit.

Helium Transfer System

The primary function of the helium transfer system is to transfer liquid helium coolant into and out of the machine rotor. In addition to this primary function, other objectives must be met to allow satisfactory operation of the generator including:

- High transfer efficiency
- Reliable long term (5 year) operation
- Prevention of internal contamination
- Ability to survive a quench without damage
- Capability of operation for a specified period following a primary seal failure
- Capability to accept rotor-stator motions
- Capability to provide sufficient flow for cooldown
- Acceptable maintenance time cycle for seal replacement

A design, shown in Figure 3-76 , has been prepared that will achieve these objectives.

- Transfer efficiency. A measure of liquid lost in the joint, is a function of the flow through the system and the heat leak from the warm zone to the cold zone.

  High inlet transfer efficiency is achieved using an insulated bayonet concept similar to static liquid helium joint. Figure 3-77 shows schematically a static bayonet joint. Concentric vacuum insulated tubes provide the necessary thermal insulation while the sealing function is provided by an "O" ring seal in the room temperature part of the assembly. A thermal gradient from the tip of the bayonet to the seal area determines the heat loss in the joint.

  The rotating seal, shown schematically in Figure 3-78, uses essentially the same principle with the stator "O" ring seal replaced with a dynamic seal and alignment bearings provided to ensure concentricity of the bayonet.

  Two exhaust channels are shown in Figure 3-73. These channels use circumferential seals to prevent channel-to-channel leakage. The channels are placed between the alignment bearings and the Ferrofluidic seal to prevent contamination of the Ferrofluid by the bearing oil lubricant. This is acceptable since the boiloff gas in the exhaust channels will be returned to a refrigerator where it will be cleaned prior to re-liquification.

- Long term operation. To satisfy the long-life requirement, it is believed that contact of the sealing surface with its mating runner must be avoided during operation. In this way, seal wear is eliminated and an extended operating life

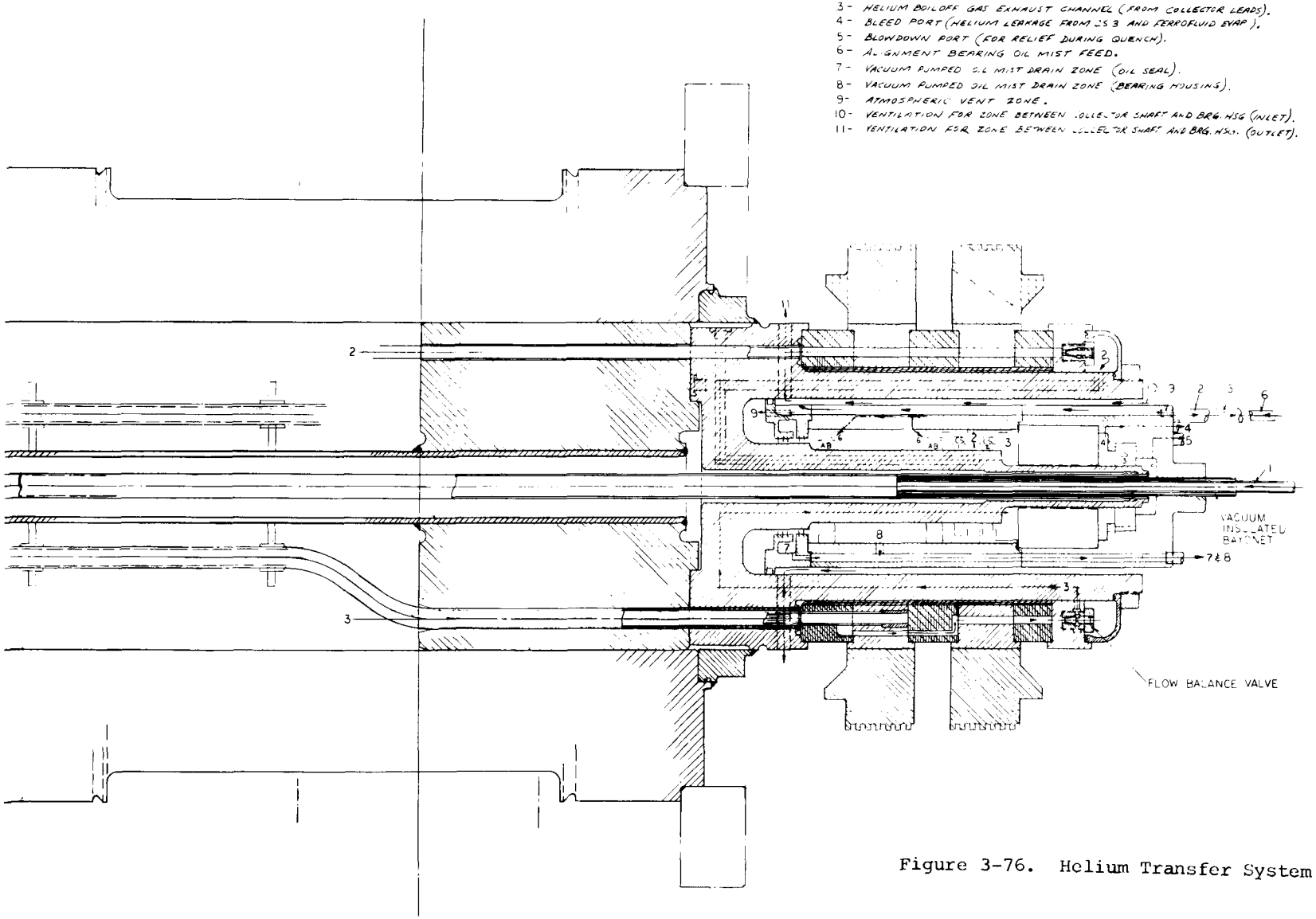

Figure 3-76. Helium Transfer System

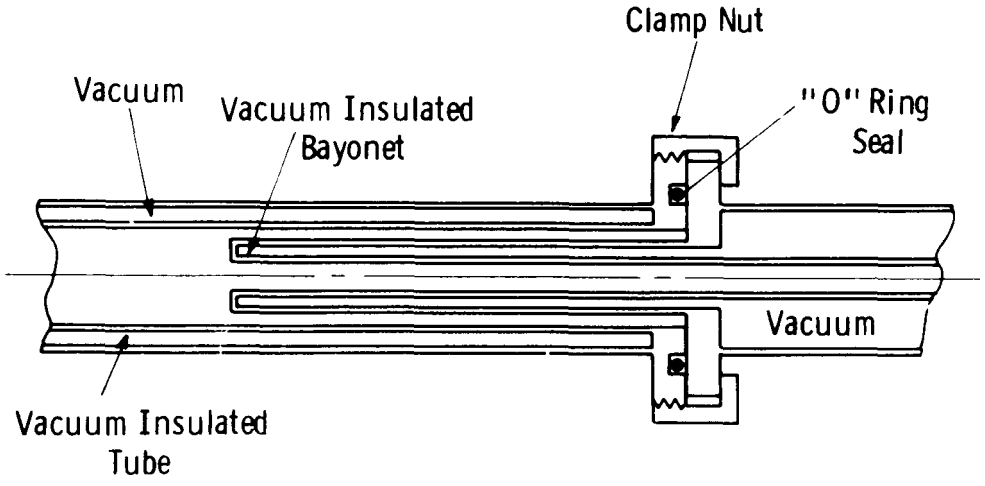

Figure 3-77. Static Joint for Transferring Liquid Helium

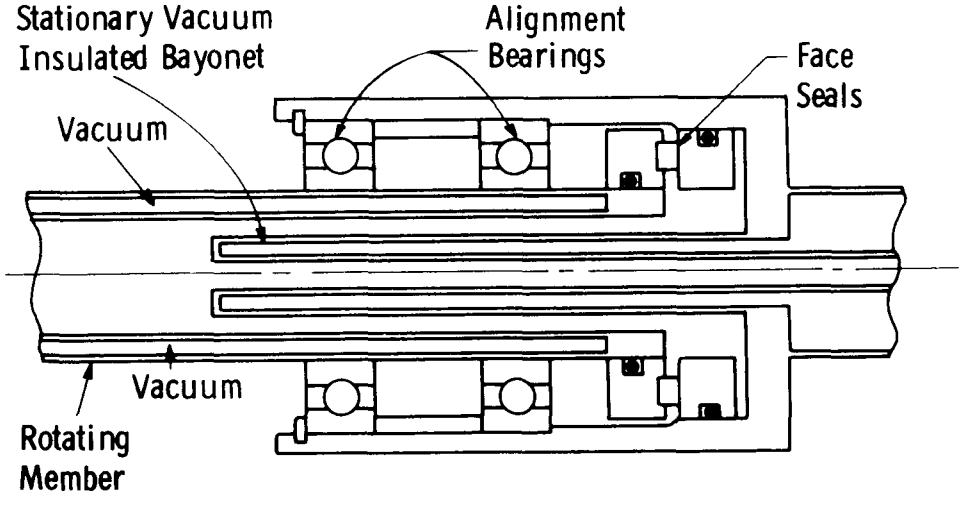

Figure 3-78. Rotating Helium Transfer System

capability becomes feasible. A relatively new sealing concept that is believed to offer potential in this regard is a seal employing a ferromagnetic fluid, or Ferrofluid*. A ferromagnetic fluid is a suspension of submicron ferrite particles dispersed in a carrier, such as lubricating oil, water, or diester fluid. By maintaining the particle size to less than 100 Angstroms, and coating the particles with an organic material, settling and agglomeration of the particles in the carrier fluid is prevented. When a magnetic field is applied to such a fluid, a body force is developed within the fluid which, if applied properly, can elevate its free surface. This characteristic has been utilized by the Ferrofluidics Corporation to design an effective circumferential shaft seal for use as vacuum feedthroughs. At the seal location, the surface of the shaft to be sealed is provided with a series of pointed ridges along its axis. A magnetic fluid is painted onto these ridges, as shown schematically in Figure 3-79. When the fluid is exposed to a magnetic flux -- provided by a permanent magnet and pole blocks in the seal housing -- it forms continuous, annular, fluid rings at the ridge peaks and the seal housing. Each ring is capable of providing approximately a 3 lb/in^2 pressure drop, which is cumulative for each "ridge". Thus, a seal containing ten to twelve "ridges" has a sealing capability of 30 lb/in^2 gauge. Since there is no physical contact between the rotating (shaft) and stationary members (seal housing) that require sealing, no component wear can occur. As a result, this seal concept offers the potential of achieving many years of reliable performance.

The Westinghouse Research Laboratories is currently engaged in investigating various schemes for adapting the Ferrofluidic seal concept for use in the helium transfer systems of superconducting machinery. Over 5000 hours of functional test experience has been accumulated on various ferrofluidic seal designs at speeds up to 3600 rpm and helium gas pressures of 30 lb/in^2 gauge. The seals demonstrated their zero-leakage capability over this period of time.

Following the 5000 hour test, a seal failure occurred due to evaporation of the Ferrofluid carrier. Initial studies on changes that would improve life have indicated several potential solutions.

Increased cooling, possibly with water, will lower the temperature of the Ferrofluid and reduce the evaporation of the carrier. The carrier fluid can be replaced with one having a lower evaporating rate at operating conditions. Finally, provisions can be made to replace the Ferrofluid while the seal is operating.

- Prevention of internal contamination. Contamination of the superconducting generator's internals by air, moisture, or bearing lubricants must be prevented. These seals, except for minute gas losses by diffusion, are zero-leakage seals.

  Although the evaporation rates are low in a Ferrofluidic seal, some internal contamination may occur due to diffusion or back streaming to the cold zone. In the conceptual design for the helium transfer system, Figure 3-76, an auxiliary circumferential seal has been added between the Ferrofluidic seal and the cold

*Registered Trademark - Ferrofluidic Corp.

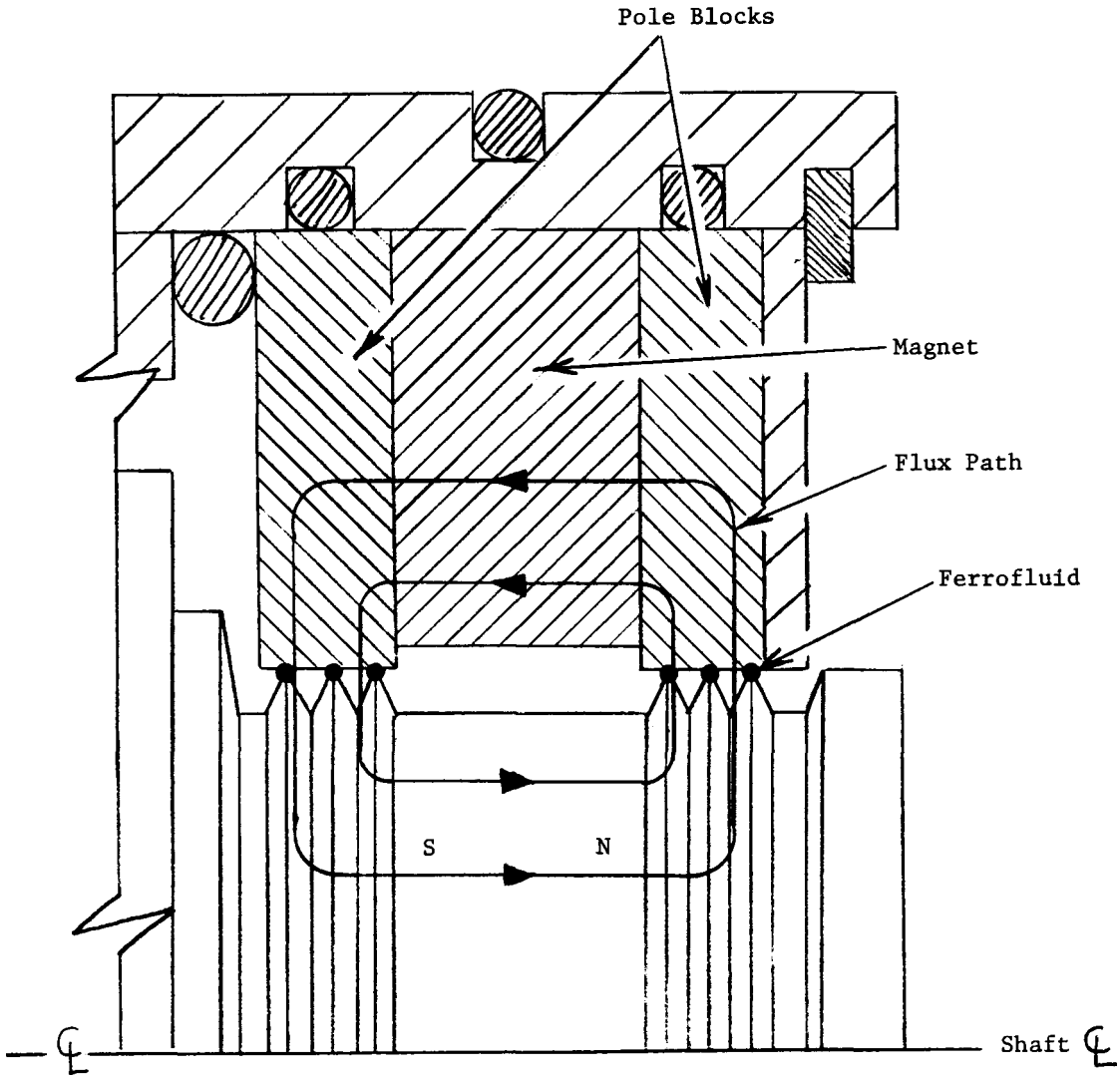

Figure 3-79. Ferrofluidic Seal

zone as a barrier to possible contamination of the inlet channel. The design of this seal is such that it offers the capability of withstanding high-velocity rubbing at primary sealing surfaces, and also provides a high degree of sealing ability. In addition, it allows for considerable relative axial motion between rotating and stationary members. The general configuration of a typical circumferential seal consists of relatively stationary segmented rings which mate with a rotating member on their bore. The rings are loosely keyed to the stationary member by rotating locks. Circumferential garter springs are used to maintain contact under static conditions. Under dynamic conditions, incorporation of appropriate seal life configuration results in the separation of the sealing surfaces from the rotating member by hydrodynamic means. The amount of separation is on the order of 1000 to 500 micro-inches.

The circumferential seal does allow a small amount of leakage because of the separation of the seal mating parts. In its position in the helium transfer system, however, the leakage is into warm boil-off gas from the helium inlet port. It is removed through a bleed port. This continual flow into and out of the cavity between the two seals removes evaporation products from the Ferrofluidic seal.

- Quench capability. This circumferential seal provides an additional function during a machine quench. Internal pressures may reach 40 psi following a quench. If the Ferrofluidic seal was designed to withstand this pressure differential, as many as fourteen stages at 3 psi/stage are required. If a seal is too long it may become undesirable from a loss and alignment standpoint. In a quench, the circumferential seal combined with relief valve in the blow down port prevent high pressure from reaching the Ferrofluidic seal. The flow impedance of the relief port is designed to ensure acceptable pressure rise between the Ferrofluidic and circumferential seal. Further relief protection can be provided in the bleed port and supply line as a safety measure if needed.

- Redundancy. The double-seal concept also provides redundancy in operation should a seal failure occur. Failure of the Ferrofluidic seal would result in a loss of the vapor barrier between the output and input channels. Failure of the circumferential seal would allow potential contamination of the inlet channel. Either of these failures would however allow short term operation of the system eliminating the potential of an unscheduled shutdown.

- Dynamic mounting. The helium transfer system is dynamically mounted to the rotor shaft to provide the alignment of the various sealing systems to ensure design life requirements can be met. The transfer piping will have to be capable of withstanding motion between rotor and stator indicating a flexible connection. Roller bearings positively align the bayonet members, and cause the light transfer system to follow the more massive rotor.

- Sufficient cooldown flowrate. The inlet bayonet has been sized at 0.250 inch inside diameter. This is a design tradeoff between convective losses and flow rate available for cooldown at a

velocity of 10 ft/sec. A 0.25 inch pipe can transfer 350 liters/hr. of liquid helium. If cooldown requires more flow a larger bayonet can be used.

- Low cycle time for maintenance. Provisions can be developed to replace the Ferrofluid while the seal is operating. This could be accomplished with a double seal so that sealing is maintained in one section while the Ferrofluid is being replaced in the other section. Alternately, the design can be made to minimize the effort required to replace the fluid while the machine is stopped during scheduled downtime.

Helium Transfer System Thermal Loss Analysis

The thermal losses in the helium transfer system are as follows:

- Radiation across vacuum gap
- Residual gas conduction in the vacuum gap
- Axial conduction through the metallic walls
- Axial conduction through the helium in the annulus between the stationary and rotating parts of the system
- Convection losses in the helium annulus due to rotation

These losses must be evaluated to insure that the entry quality requirements for its helium management system are met.

The work presented is based on analytical techniques developed for the Westinghouse 5 MVA superconducting generator by T. J. Fagan of the Westinghouse Research Center.

- Radiation Losses. The radiant heat transfer per unit time, Q_{rad}, between two gray surfaces at uniform temperature is given by:

$$Q_{rad} = A_1 \zeta_{1-2} \sigma (T_h^4 - T_c^4) \quad (1)$$

where

A = cold surface area

ζ_{1-2} = gray body shape factor

σ = Stefan-Boltzman constant

T_h = hot surface temperature

T_c = cold surface temperature

The gray body shape factor ζ_{1-2} is given by

$$\zeta_{1-2} = \frac{1}{\frac{1}{\varepsilon_1} - 1 + \frac{A_1}{A_2}\left(\frac{1}{\varepsilon_2} - 1\right) + \frac{1}{F_{1-2}}} \quad (2)$$

where

A_2 = warm surface area

ε_1 = cold surface emissivity

ε_2 = warm surface emissivity

F_{1-2} = geometric shape factor (unity for long concentric tubes).

Barron[1] gives an emissivity ε for polished 304 stainless steel of .15 at 300°K and .061 at 78°K. Since the emissivity tends to decrease with decreasing temperature, the value at liquid helium temperature 4.2°K is expected to be somewhat less than .061. Lacking specific data, a conservative value of .061 has been used. Based on these values, the radiation heat loss was calculated assuming a transfer line length of 0.5 feet.

The radiation loss in the bayonet area is complex since a thermal gradient exists from room temperature to liquid helium temperature. A conservative assumption will include the bayonet area with the full temperature difference across the vacuum gap. Based on these assumptions, the radiation loss is calculated as:

$$Q_{rad} = 0.37 \text{ watts}$$

- Residual Gas Conduction. Since it is impossible to produce a perfect vacuum, some gas molecules will remain in the vacuum space. Air will diffuse through the external tube walls and helium through the internal tube walls.

Since the inner walls will operate at temperatures near liquid helium temperature, all elements except helium will be deposited on the inner tube walls in solid form. This effect is commonly known as cryo-pumping. Thus, the gas molecules remaining will be primarily helium molecules.

Heat will be transported from the warm surface to the cold surface by free molecular conduction.

If the spacing between the surfaces is small compared to the mean free path, the heat leak, Q_{gcon}, can be estimated by the method of Knudsen:[2]

$$Q_{gcon} = GpA_1 (T_h - T_c) \tag{3}$$

where

P = absolute pressure

$$G = \frac{\gamma + 1}{\gamma - 1} \left(\frac{g_c R}{8\pi M T_m} \right)^{1/2} F_a \tag{4}$$

γ = specific heat ratio

g_c = gravitational constant

R = universal gas constant

T_m = gage temperature

M = gas molecular weight

$$F_a = \frac{1}{\frac{1}{a_1} + \frac{A_1}{A_2}\left(\frac{1}{a_2} - 1\right)} \tag{5}$$

Scott[3] gives the following values for the accommodation coefficient of helium:

T°R	a
540	.3
136.8	.4
36	.6

Scott indicates that the accommodation coefficient, a, will approach unity as the temperature approaches the critical temperature of the gas. For helium the critical temperature is 5.20°K. Thus, the accommodation coefficient for the cold wall, a_1. should be very near to unity.

Again using the assumption that the full temperature gradient is maintained across the vacuum in the bayonet area, the residual gas conduction loss is

$$Q_{gcon} = 0.015 \text{ watts}$$

The mean free path is given by:

$$\lambda = \frac{3\mu}{P}\left(\frac{\pi R T_m}{8 g_c M}\right)^{1/2} \tag{6}$$

The minimum value of μ occurs at the lowest temperature. Thus, with both μ and T at a minimum the smallest mean free path will occur at the cold end. At 4.2°K where R, $\mu = 1.26 \times 10^{-5}$ gm/sec cm. The mean free path is

-- $\lambda = 16.6$ cm

Thus, the mean free path is much larger than the distance between the surfaces and the equations apply.

- Tube Wall Axial Conduction. In the areas where the stationary and rotating tubes overlap an axial temperature gradient will exist in the outer stationary tube and the inner rotating tube. This gradient will cause a flow of heat in the axial direction by conduction through the tube walls.

The transfer of heat, Q_{wcon}, by conduction in one dimension is described by the familiar Fourier equation:

$$Q_{wcon} = K_w A_c \frac{dT}{dx} \tag{7}$$

where

K_w = thermal conductivity

A_c = wall cross sectional area

dT/dx = thermal gradient

As shown in Figure 3-80, the thermal conductivity of 304 stainless steel is a strong function of temperature over the range of interest.

The variation in thermal conductivity can be accounted for in several ways. The simplest approach is to use an average value of thermal conductivity. Thus, Eq. (7) simplifies to:

$$Q_{wcon} = \frac{\bar{K}_w A_c}{L_w} (T_h - T_c) \tag{8}$$

By numerical integration of the data presented in Fig. 3-80 an average value of thermal conductivity of 5.95 Btu/hr-ft-°F was obtained.

With an overlap of six inches (.5 ft.)

$$Q_{wcons} = 0.78 \text{ watts}$$

An alternative approach is to describe the thermal conductivity as some mathematical function of temperature and integrate.

A polynomial curve fitting the experimental data is shown on Fig. 3-80. Substitution of this polynomial into Eq. (7) gives:

$$Q_{wcon} = [C_o + C_1 T + C_2 T^2 + C_3 T^3] A_c \frac{dT}{dx} \tag{9}$$

Since the heat transfer rate at all points in the tube must be the same, Q_{wcon} is a constant. Thus, separation of variables gives:

$$dx = \frac{A_c}{Q_{wcon}} [C_o + C_1 T + C_2 T^2 + C_3 T^3] dt \tag{10}$$

The boundary conditions are:

$T = T_c$ at $x = 0$

$T - T_h$ at $x = L_w$

Integration gives:

$$L_w = \frac{A_c}{Q_{wcon}} \left[C_o (T_h - T_c) + \frac{C_1}{2} (T_h^2 - T_c^2) + \frac{C_2}{3} (T_h^3 - T_c^3) + \frac{C_3}{4} (T_h^4 - T_c^4)\right] \tag{11}$$

Solving for Q_{wcon}:

$$Q_{wcon} = \frac{A_c}{L_w} \left[C_o (T_h - T_c) + \frac{C_1}{2} (T_h^2 - T_c^2) + \frac{C_2}{3} (T_h^3 - T_c^3) + \frac{C_3}{4} (T_h^4 - T_c^4)\right] \tag{12}$$

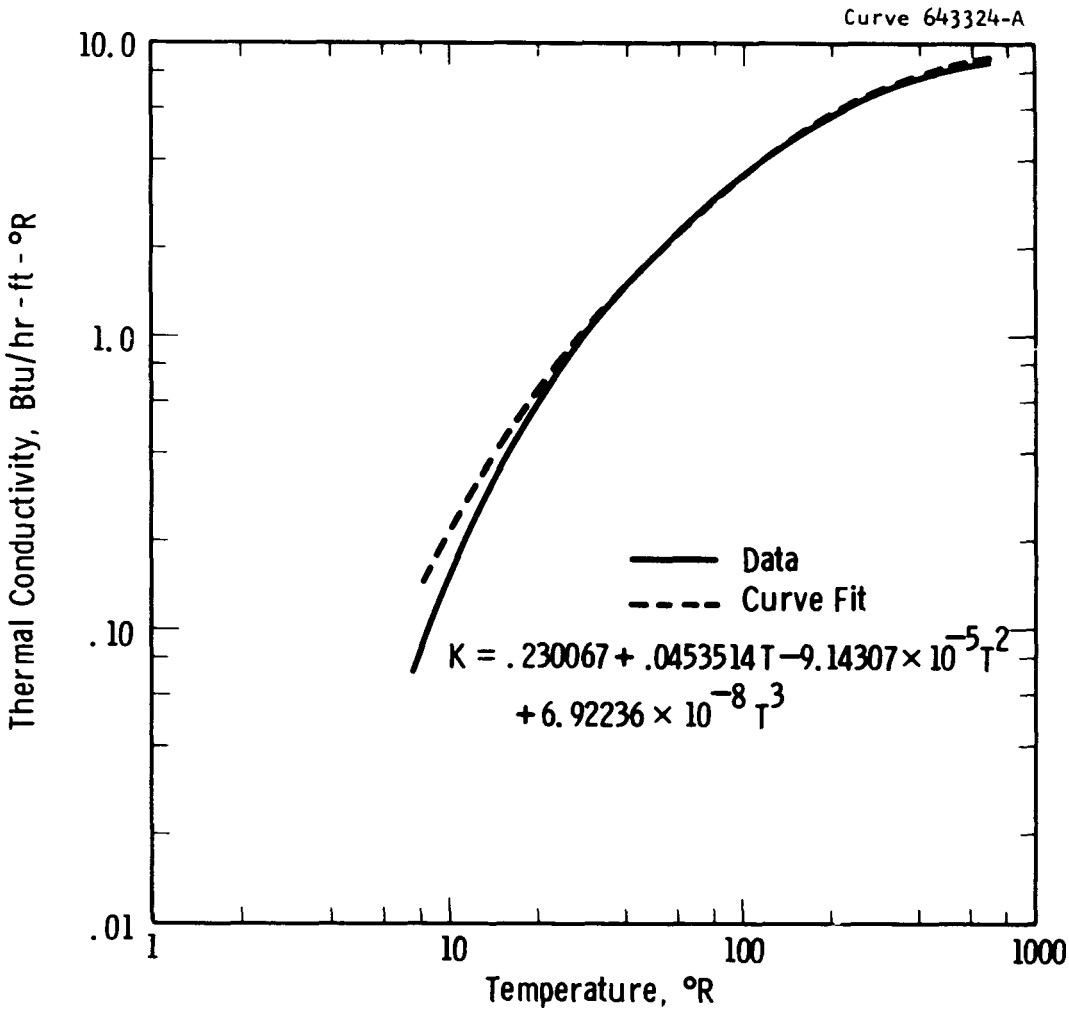

Figure 3-80. Thermal Conductivity of 304 Stainless Steel versus Temperature

Substitution of the constants, cross sectional area and length for the inner rotating tube gives:

$$Q_{wconr} = 0.89 \text{ watts}$$

This agrees with the heat leak predicted by the mean thermal conductivity method. However, the temperature distributions predicted by the two methods are quite different. The mean thermal conductivity method predicts a linear temperature distribution. Integration of Eq. (10) for an arbitrary value of x gives:

$$x = \frac{A_c}{Q_{wcon}} \left[C_o (T - T_c) + \frac{C_1}{2} (T^2 - T_c^2) + \frac{C_2}{3} (T - T_c^3) + \frac{C_3}{4} (T^4 - T_c^4)\right.$$

Substitution of Eq. (11) gives:

$$\frac{x}{L_w} = \frac{C_o(T - T_c) + \frac{C_1}{2}(T^2 - T_c^2) + \frac{C_2}{3}(T^3 - T_c^3) + \frac{C_3}{4}(T^4 - T_c^4)}{C_o(T_h - T_c) + \frac{C_1}{2}(T_n^2 - T_c^2) + \frac{C_2}{3}(T_n^3 - T_c^3) + \frac{C_3}{4}(T_h^4 - T_c^4)} \quad (13)$$

It is difficult to solve for T as a function of x but by substitution of various values of T a plot of temperature versus length can be constructed. An example is shown in Fig. 3-81. Obviously, the temperature distribution differs considerably from a linear distribution, particularly at the cold end.

- Helium Axial Conduction. Heat will also be transferred by axial conduction through the helium trapped in the annular space between the rotating and stationary tubes. Since the thermal conductivity of the helium is much less than that of the tube walls, it seems likely that the temperature distribution of the tube walls will be imposed upon the helium. Thus, the cold and temperature gradient of the helium will be the same as that of the tube walls. Equation (7) can be written as:

$$\left.\frac{dT}{dx}\right|_{4.2} = \frac{Q_{wcon}}{K_w A_c}$$

For $Q_{wcon} = 0.36$ watts (inner tube) and

$$K_w = 2.2 \times 10^{-3} \frac{\text{watts}}{\text{cm°K}}$$

$$\left.\frac{dT}{dx}\right|_{4.2} = 454 \frac{°K}{\text{cm}}$$

The thermal conductivity of helium vapor at 4.2°K and 1 atmosphere

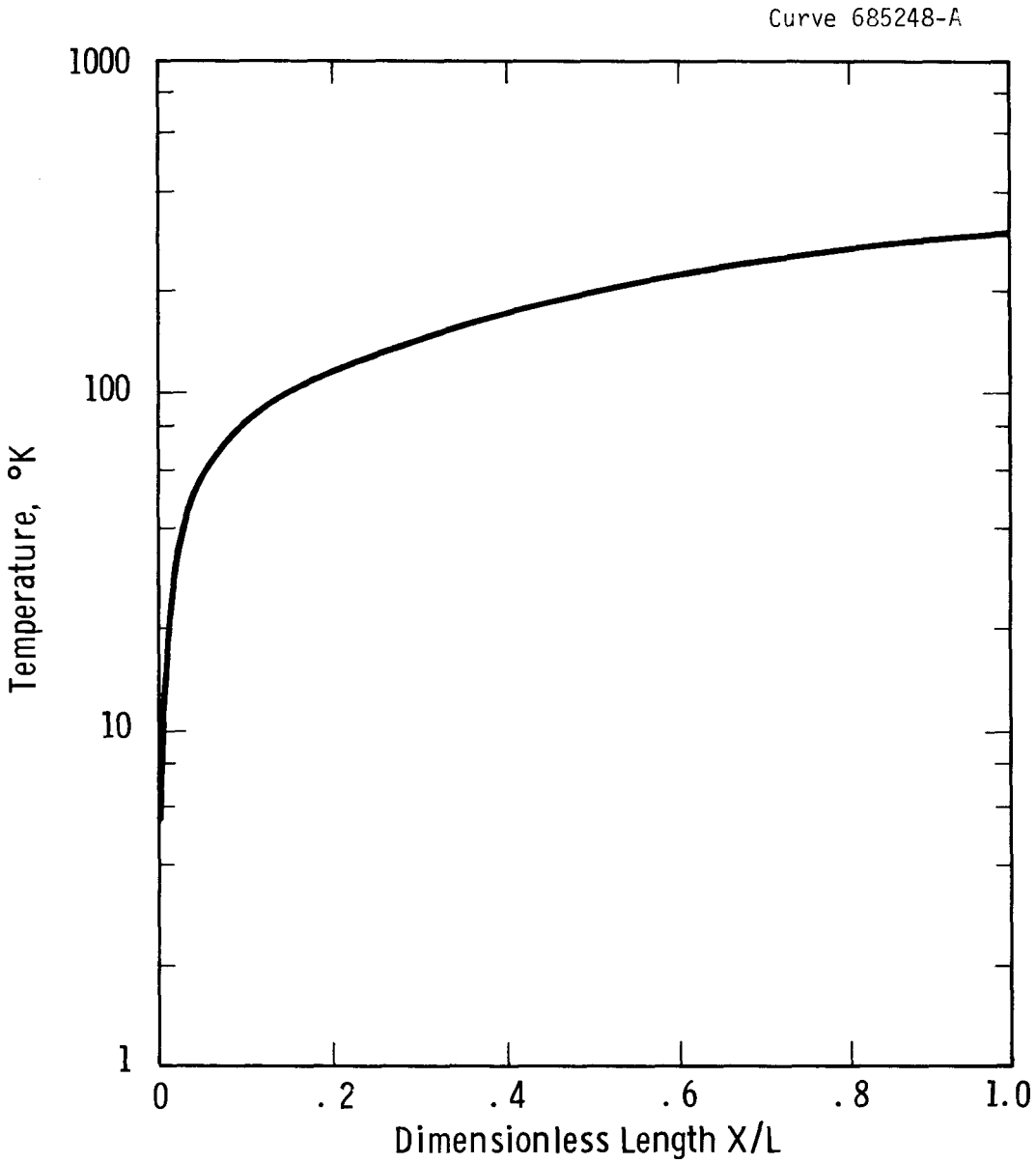

Figure 3-81. Temperature Distribution in 304 Stainless Steel due to Simple Conduction - Hot End at 300°K - Cold End at 4.2°K

is $9.52 \times 10^{-5} \frac{\text{watts}}{\text{cm°K}}$. The heat leak by conduction in the helium $Q_{\text{hcon d}}$ is

$$Q_{\text{hcon d}} = K_h A_c \frac{dT}{dx}\Big|_{4.2}$$

$$= 0.011 \text{ watts}$$

- Convection in the Annular Helium Space. When a temperature difference exists in a space filled with a fluid, some heat transfer by natural convection will occur. This condition exists in the annular space between the rotating and stationary tubes.

  If both tubes were stationary, the relatively narrow annular gap would insure that the convection heat transfer was negligible. With one of the tubes rotating the convection heat transfer may be increased significantly. This effect was observed by Thullen[4] in tests of the 87 kVA alternator constructed at the Massachusetts Institute of Technology.

  The increased convection is thought to be the result of rotational forces segregating the helium into layers of different temperatures. The coldest and densest fluid will be forced to the largest radius and the warmer fluid to the smallest radius. It is assumed that the cold fluid flows axially toward the seal along the outer wall and the warm fluid flows axially away from the seal along the inner wall, thus transporting heat into the liquid helium stream.

  Lee[5] has developed a theory for predicting the magnitude of this heat leak. The heat flux is given by:

$$Q_{\text{conv}} = \frac{P_r}{4\pi} \beta^2 \left(\bar{C}_p \omega T_v P_c\right) \left(\frac{Re_{c\theta} \Delta r}{1.647\ L_w}\right)^3 \left[1 - \left(\frac{T_c}{T_h}\right)^{1.647}\right]^3 \Delta r^3 \qquad (16)$$

The convection loss relation indicates that the gap and annulus radius should be minimized while the bayonet length should be maximized to reduce these losses. The mechanical design requirements would dictate a short, large radius bayonet for mechanical stability with a large gap to prevent rubbing due to misalignment or deflection of mating parts. Therefore the final design for the helium transfer system trades off mechanical design considerations for acceptable heat loss.

The flow coefficient β resulting from integration of the axial velocity profile is given by Lee as .004. A check of this integration gave a somewhat higher value of .004637. The larger value of β has been used as a conservative estimate.

The cold end tangential Reynolds number $Re_{c\theta}$ is given by

$$Re_{c\theta} = \frac{\omega r_1 \rho_c \Delta r}{\mu_c} \qquad (17)$$

For helium vapor at 1 atm (4.2°K), the density and viscosity are approximately:

$$\rho_c = 0.0167 \text{ gms/cm}^3$$

$$\mu_c = 1.26 \times 10^{-5} \text{ gm/sec cm}$$

$$r_1 = 0.79 \text{ cm}$$

$$r = 0.051 \text{ cm}$$

With a rotational speed of 3600 rpm (377 rad/sec), the cold end Reynolds number is:

$$Re_{c\theta} = 20131$$

The average value of the Prandtl number over the range of interest is approximately 0.68. The mean specific heat is 5.23 joules/gm°K: Evaluation of Eq. (16) gives:

$$Q_{conv} = 2.05 \times 10^{-3} \text{ watts}$$

The preceding analysis is based on the assumption of a laminar circumferential velocity profile between the two surfaces.

The concentric cylinders with the outer cylinder rotating produce a highly stable velocity profile. Transition to turbulent flow occurs at very high Reynolds numbers. Schlicting[6] indicates that the critical Reynolds number is a function of r/r_2. For the case being considered, r/r_2 is 0.0645 and the critical circumferential Reynolds number is about 7×10^4. The circumferential Reynolds number is given by:

$$Re_\theta = \frac{\rho \omega r_2^2}{\mu} \tag{18}$$

The highest circumferential Reynolds number will occur at the cold end where ρ is maximum. The viscosity increases with increasing temperature, but this effect is much smaller than the density variation. Thus, the maximum circumferential Reynolds number is given by:

$$Re_\theta = 3.08 \times 10^5$$

This is above the critical Reynolds number. Thus, flow is turbulent and the analysis is conservative.

- Summary of Losses. The total heat losses in the system are given below:

Radiation	0.37	watts
Residual gas conduction	0.015	watts
Axial wall conduction	0.89	watts
Axial helium conduction	0.011	watts
Convection losses	0.02	watts
Total	1.31	watts

In a machine flow of 30 liters/hr (1.04 gms/sec) of liquid helium flow, some will be boiled off to offset the transfer system losses

$$Q = \dot{m}\, h_{fg}$$

$$\dot{m} = \frac{Q}{h_{fg}} = 0.063 \text{ gms/sec}$$

This is about 6% of the total machine flow which is well above minimum quality required for satisfactory operation of the helium coolant system.

Should a lower quality be required to prevent flooding of the gas separation apparatus in the helium management system, a shorter bayonet can be used.

REFERENCES

1. R. Barron, Cryogenic Systems, McGraw-Hill, New York, N.Y., 1966.
2. M. Knudsen, Ann. d. Physik, Vol, 31, p. 205, 1910.
3. R. B. Scott, Cryogenic Engineering, D. Van Nostrand, Princeton, N.J., 1959.
4. P. Thullen, Analysis of the Application of Superconductivity to Commercial Electric Power Generation, Ph.D. Thesis, Massachusetts Institute of Technology, June 1969.
5. W.D. Lee, Continuous Transfer of Liquid Helium to a Rotating Dewar Master's Thesis, Massachusetts Institute of Technology, June 1970.
6. H. Schlicting, Boundary Layer Theory, McGraw-Hill, New York, N.Y., 1960.
7. Thullen, P., Smith, J. L. Jr., and Lee, W. D., "The Design and Testing of a Rotatable Liquid Helium Transfer Coupling for Use at 3600 rpm", 13th International Congress of Refrigeration, 1973.

3.2.1.3 Helium Management System. Among the technical objectives that must be accomplished before the advantages of the air core, superconducting (S.C.) synchronous generator may be secured is the requirement to reliably cool the S.C. winding below its "normal" (resistive) transition or critical temperature. Practical considerations of experience and availability indicate a choice of NbTi in a copper stabilizing matrix at this time. Niobium-titanium has a transition temperature, for example, of about 5.2 K at 3.5 x 10^4 A/cm^2 in a 5.0 T magnetic field. Recently the science of cryogenic cooling in rotating frames has been advancing rapidly with long term operation of cryogenic helium transfer systems, successful laboratory operation of superconducting generators and generator components, cryogenic fluid dynamic and heat transfer experiments in rotating dewars, and a flurry of activity in generator design and analysis for utility operation. Laboratory and utility load operation of generators are significantly different: the most stringent design condition for utility operation is the necessity to provide adequate thermal margin during fault induced transients. Margin, in degrees Kelvin, refers to the difference between the critical temperature and the conductor temperature rise.

A line fault results in the generation of heat in the damper shields, rotor structure and conductor. Because metals have very low specific heats at liquid helium temperatures, any heat generation becomes a potential "normalizing" event. In addition, in certain types of cooling systems the fault heat generation results in a temporary surge in helium flow rate that can cause significant thermal stresses in the structure if not properly controlled. Analysis of the rotor thermal performance during a fault and selection of the optimum thermodynamic cycle for the cooling system are the most significant aspects of the helium cooling system.

Thermal fault transients in the EPRI-W S.C. generator are mitigated by the combined actions of the cold damper shield, structure and damper thermosyphon cooling loops which function in thermal isolation from the winding, a patented helium filled permeable winding bundle which has sufficient specific heat to store fault heat generation locally for subsequent removal and a radiation shield which functions as a regenerator to warm the surge in helium exhaust stream.

The fundamental thermodynamic cooling or refrigeration cycle used within the rotor consists of an isenthalpic expansion from 101 kPa to 51 kPa (3.6 K) and phase separation, followed by an isothermal liquid compression to rotor o.d. pressure, adiabatic expansion then occurs during which the cryogen absorbs heat from the

winding and structure as it moves toward the boiling pool surface. An isentropic compression process then returns all of the exhaust gas to 101 kPa for return passage through the rotating transfer system. The single most important feature of the cooling system is cooling of the conductor by helium at 3.6 K and the significant gain in margin because the conductor approaches that temperature in operation.

General Design Considerations

The primary function of the helium management system is to maintain every portion of the field winding below the superconductor critical temperature under all conditions. Hot spots must be eliminated since a localized normalization of the superconductor requires discharge of the field winding. In addition to this primary function additional design objectives must be considered, including:

- Removal of radiation, structural and lead losses
- Removal of steady state electromagnetic losses
- Removal of transient electromagnetic losses
- Survival of a quench without damage
- Operation compatible with a refrigerator
- Minimum parallel fluid stream paths
- Optimal low temperature loss
- Minimal potential contamination by foreign materials
- Reliable with simple scheduled maintenance
- Prevention of rotor thermal distortion
- Design for adequate cooldown
- Design for a self-regulating demand type system

Each of these desirable objectives may have some attendant disadvantages which are locally addressed in the system component discussions.

The superconducting turbogenerator helium management system was conceived considering reliability as the paramount design criterion. In the conceptual stage, efficiency, manufacturability and cost were all considered secondary to the fact that the first utility operated machine must perform reliably. To determine the type of cooling system most likely to meet the utility's needs, the various cooling systems were compared and an evaluation made. The final result is a combination of two, each of which could provide the cooling function alone but with less margin than the combination. No feature or part of either is incompatible or contrafunctional to the other. Nor does the present design suffer a reduction in efficiency or manufacturability for the initial neglect of these factors, as can be determined from the following text.

The cooling systems for a rotating cryogenic space of the dimensions required for a superconducting rotor may be considered in the general categories of wholly single or two phase refrigerant circuits or combined single and two phase circuits.

Single phase systems have the disadvantage that they do not use the latent heat of vaporization to remove heat leaks and losses and consequently require more refrigerant to be circulated than a two phase system. In addition, certain auxiliary equipment that may be required to achieve supercriticality or subcooling of the refrigerant (pumps, heat exchangers, vacuum pumps) may represent a reduction in system reliability. Wholly two phase systems simply do not exist because of the supercritical pressure levels resulting from rotation. It is helpful to examine the remaining category comprising cooling systems having both single and two phase regions within the rotor from the standpoint of the dominant mode of heat transmission, i.e., conduction, natural convection, or forced convection. Again it is believed that the pump and valves required for a forced convection system seriously diminish system reliability. Thus we are left with either a natural convection or conduction cooled winding and structure. Before proceeding, it is useful to consider some of the major characteristics of each system and their relation to the cooling load.

The most demanding requirement upon the cooling system is that the winding be maintained in the superconducting state through and after a high side transformer fault of 66 ms duration resulting in an expected heat input of 4.1 kJ to the structure and 4.5 mJ/cc of Cu matrix conductor. Sixty-six milliseconds is very small compared to the time constant of either a natural convection or conduction cooled winding and structure. This temperature must be maintained by the cooling system to enable the high side fault losses to be stored as sensible heat in either organic insulation or helium until they are transported from the rotor. In the 300 MVA rotor the target temperature rise due to loss storage is .1 K. Ultimately this conservative choice indicated the use of a cold damper shield which simplifies the design for fault conditions.

Conduction cooling systems have the disadvantage that an excellent heat conductor (copper) must be introduced into the winding thus reducing the conductor packing factor, increasing electromagnetic losses, and affecting reliability through possible ground faults. Unfortunately, electrical insulators are also thermal insulators.

Natural convection becomes an excellent heat transmission mechanism in high "g" fields but also has some disadvantages. Distinct warm and cold passages must be provided to avoid thermal instabilities than can block the natural convection currents. High aspect ratio closed passages must also be avoided. Before any heat is transported by natural convection the neutral thermal lapse rate must be overcome. The thermal lapse rate results from the density increase of expansion cooling the fluid as it moves radially inward and results in a nonconvecting fluid mass if the temperature gradient of the fluid is not larger than the neutral lapse rate. In a helium filled rotor the adiabatic thermodynamic process best describes the neutral lapse rate because of the low thermal conductivity of helium. With the stainless steel teeth of the 300 MVA rotor the neutral lapse fluid density variation with radius would lie between that of the adiabatic and isothermal processes.

In the 300 MVA rotor the adiabatic neutral lapse rate spans approximately 0.9 K from the winding outside radius to the boiling interface and this is a high percent of the allowable temperature rise. Several conclusions may be drawn from the simple considerations above.

First, a cooling system relying solely on natural convection exceeds the allowable 1 K margin above 4.2 K in the summing of the fault losses and overcoming the neutral lapse rate. A conduction cooled system eliminates the temperature rise of the lapse rate but has temperature rises associated with conduction from the winding. It may be concluded that it is desirable to operate the cooling system below 4.2 K. A target value of 3.5 K (0.5 atm saturation temperature) has been selected for the 300 MVA generator and larger units. For reliability reasons a self pumping rotor operating with a suction pressure at the rotor axis of one half atmosphere and a delivery pressure of above one atmosphere at the rotor rotating seals has been selected to provide the necessary additional thermal margin. This decreases the ideal helium refrigerator COP from 0.0142 to 0.0118, but doesn't represent a significant economic penalty.

For reliability reasons a natural convection cooling system is proposed. Considering a liquid-vapor surface near the rotor center line boiling at 3.5 K, the neutral lapse rate would give a helium temperature at the winding OD of 4.4 K. This is considered to be too high for the expected temperature rise of fault loss storage and internal conduction of heat to the winding cooling surfaces, particularly if helium should enter the winding preheated by structural losses. To overcome

the neutral thermal lapse rate, two features have been built into the cooling system. Copper slabs extend into the helium pool from the boiling interface which will maintain the bulk of the helium pool at nearly constant temperature. The copper slabs extend to a radius inside the inner winding support cylinder and thus avoid a significant decrease in reliability due to winding to ground shorting during fault conditions.

The adiabatic neutral lapse rate outside the thermal conduction slabs is reduced in significance by delivering helium to the winding OD through a copper heat exchanger in the pole head. The heat exchanger is sized to deliver helium to the winding with only a 0.1 K rise due to rotational compression. Delivering the helium to the winding OD at 3.6 K has two advantages: the winding can operate through significantly higher fault heat induced losses and the energy (heat) input to the winding to initiate convection is significantly reduced. The penalty paid for these performance improvements is that all of the liquid helium entering the heat exchanger (about 50% of the total helium circulated) must undergo compression. In the subsequent expansion of the helium as it moves toward a smaller radius the fraction of this heat recovered is unknown. It is certain that the intercooled compressor-expander efficiency is not zero nor is it 100%. Frequently in rotating equipment having high Reynolds numbers and extensive flow separation, an estimate of 18-22% thermal efficiency is appropriate. The S.C. rotor compression-expansion cycle should have much higher efficiency because of its low fluid velocities. The thermodynamic performance of the cooling system has been computed for the extremes of cycle efficiency, but is likely to exceed 60%.

The last item in the list of functions of the helium management system relates to the reliability aspects of a demand type cooling system. Monitoring the heat leak and losses through helium flow rate can warn of partial loss of vacuum or component failure. The main disadvantage of a demand system is that if improperly sized, the helium flow through the transfer system may be interrupted. Interrupting the helium flow in the transfer system for extended intervals can lead to erratic restarting of the flow because of the rapid increase in thermal conductivity of materials with temperature and the potential for loss of cyro-pumped vacuum insulation. These problems are not considered insurmountable.

Physical Design Description

Figures 3-82 and 3-83, the helium flow system schematics, and Fig. 3-84, a rotor end view sectional drawing, show the essential features of the rotor as presently configured. Table 3-43 contains a component key which relates to these

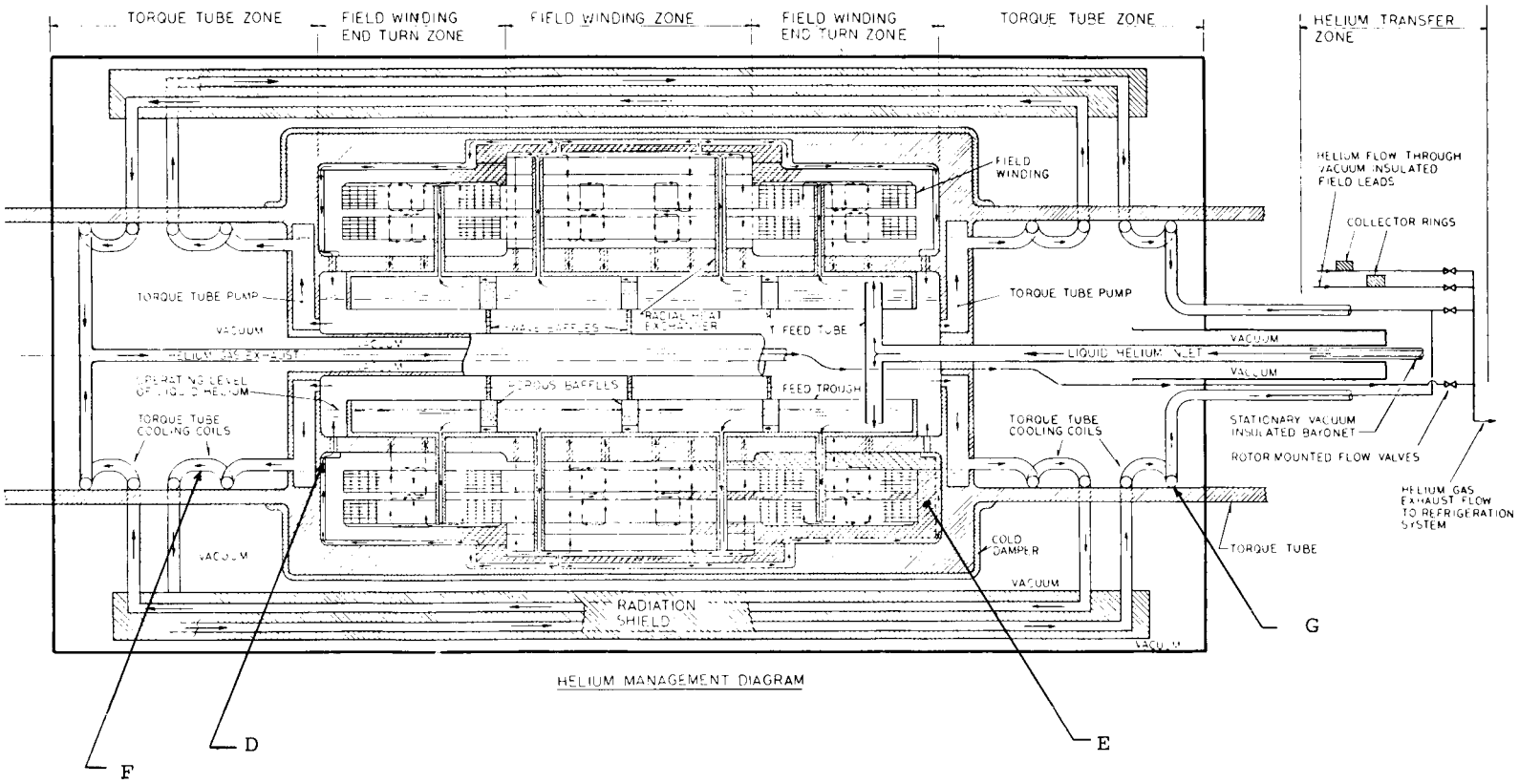

HELIUM MANAGEMENT DIAGRAM

Figure 3-82. Helium Management Diagram

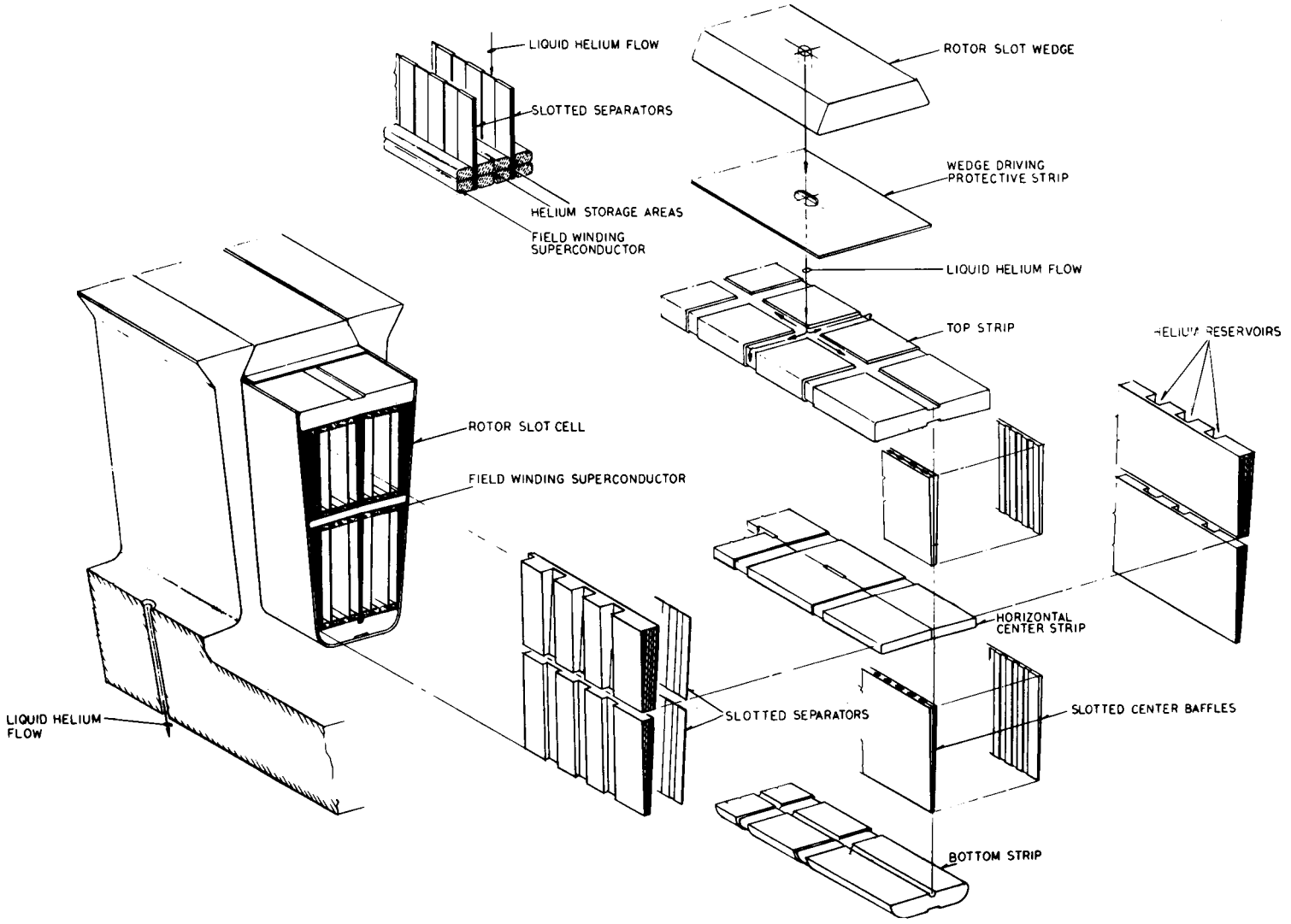

Figure 3-83. Field Winding Slot Subassembly

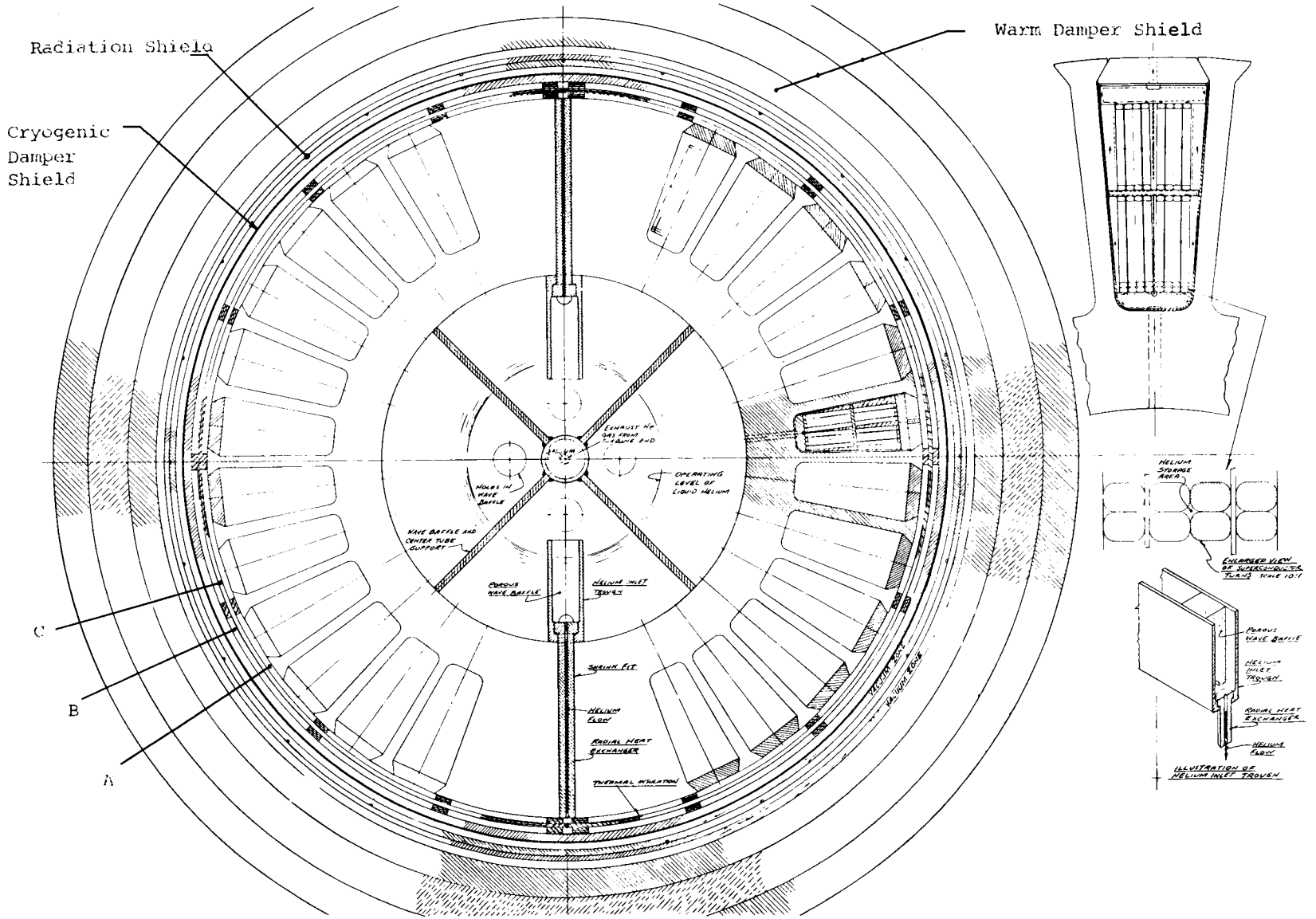

Figure 3-84. Rotor End Sectional View Showing the Helium Inlet Trough

Table 3-43

EPRI-W SUPERCONDUCTING TURBOGENERATOR
COOLING SYSTEM COMPONENT KEY

A. Winding coolant feed chamber gap header - inner annular gap (field winding zone) and groove-slot array (end turn zone).

B. Cold damper cooling gap - outer annular gap (field winding zone) and axial groove array (end turn zone).

C. Thermal insulation - between winding feed chamber and cold damper cooling gap.

D. Torque tube thermosyphon - cooling loop that intercepts the torque tube cold end heat leak.

E. Thermal insulation between torque tube terminus and winding.

F. Convection traps.

G. Exhaust helium warming stations.

figures. The annular helium pool in the rotor receives about 25% vapor quality helium from the "T" tube on the right side of the rotor. It is estimated that 5-10% quality helium will enter the "T" tube from the rotating transfer system. The vapor fraction is not critical to the cooling system operation except that a minimum of 5% vapor must enter the "T" tube. A fixed resistor is included in the inlet tube in case the transfer system is exceptionally efficient. Within the "T" tube, liquid and gas are separated: liquid being attached to the wall and accelerated down the tube with perhaps some splatter; while vapor flows less rapidly and determines the pressure field in the large area pipe. The reader will recognize this as a very simplistic overview of a very complex nonequilibrium thermodynamic problem.

Flowing from the "T" tube, the helium enters an axial inlet trough whose liquid level is maintained at a smaller radius than the liquid level in the "T" tube by the torque tube pumps and that level differential provides a hydrostatic bucking pressure against the inlet transfer tube. Liquid helium traversing this hydrostatic back pressure is expanded and some liquid is evaporated. The separation achieved in the "T" tube is maintained inside the trough and rotor above angular speeds of 1.0 rev/s. From the trough, the only flow path available to the liquid helium is outward in radius through the radial heat exchanger tubes located in the pole head in the slotted part of the rotor. The heat exchanger removes a portion of the work of compression which appears as sensible heat in the helium. It should be noted that the pole head is an advantageous location for the heat exchanger as the magnetic field is oriented radially and has the minimum effect on thermal conductivity there.

Helium which traverses the heat exchangers enters a divided cylindrical chamber (A, Fig. 3-84) between the helium containment structure and the winding. The divider (C, Fig. 3-84) within the annular chamber is a thermal insulator which prevents helium which has been warmed by structural and radiation heating from directly entering the winding and diminishing the operating margin.

Helium adjacent to the rotor slot wedge enters the winding through the hole in the rotor slot wedge shown in Fig. 3-83 and through the aligned hole in the wedge driving strip. A satisfactory voltage creepage path is created by having the helium flow laterally around the top strip (Fig. 3-83) and thence into the winding. Risers and downcomers are designed into the conductor bundle as shown in the upper inset of Fig. 3-84. The downcomers are exceptionally large and the bundle is radially subdivided to provide a local recirculation reservoir available

with less than 0.1 K temperature rise due to compression effects in the thermosyphon. The helium stored in the conductor corner voids and reservoirs (inset of Fig. 3-84) is intended to mitigate the conductor temperature rise during 500 ms events. The stored heat from short events is removed over longer periods by the riser holes in the bottom of the slot which communicate with the main pool. Natural convection systems generally have higher flow rates than boiling systems of comparable heat rates so there is a potential problem in matching the flow rate of the radial heat exchanger and the winding and cold damper loops. It will be shown that constraining the winding and cold damper flow to that through the radial heat exchangers presents no practical limitation on the fault repeat interval. Limiting the flow to the cold damper and winding results in a longer transmittal time for the losses and eases the fault induced flow surge problem.

The steady cooling of the cold damper (1.8 W) is accomplished by flowing helium thru the outer annular space (B, Fig. 3-84) formed by the cylindrical structural loss shield. The outer chamber (B) is fed by holes through the insulation, C, into the inner annular winding feed space (A, Fig. 3-84) near the pole heads. Temperature rise in the cold damper cooling annulus due to a 66 msec three phase fault is less than 0.25 K. This means several faults could occur in succession without influencing the superconductor coolant significantly. In addition, with a 0.25 K rise, expansion upon heating will not cause flood back of warmer helium into the winding. Nor will a significant pressure wave be generated. From the outer annular chamber, the helium warmed by structural losses flows to the rotor ends where it joins the torque tube heat leak cooling channels (Fig. 3-82).

The torque tube cooling channels are designed to transport the torque tube cold end heat leak to the helium pool surface by single phase natural convection cooling with less than 1.0 K temperature rise. Note that interconnecting thermosyphon loops must be designed with extreme care to prevent stagnation or reversal of either syphon.

At this point in the discussion, all of the thermosyphon loops have been traced from the "T" tube inlet to the main helium pool which is maintained at near constant temperature by conduction cooling in the inlet trough walls (Fig. 3-84) and natural convection azimuthal spreading.[1] Helium may exit the rotor by two different paths; the torque tube pumps which draw vapor from the central vapor core in the rotor and the leads which draw liquid from the annular pool. The vapor path will be described first.

As heat is transmitted to the pool surface, evaporation is initiated uniformly by the surface conditioned conduction slabs. Without surface conditioning a uniform distribution of boiling nucleation sites may not exist and boiling could occur preferentially in one location thus unbalancing the rotor. The discharge of liquid from the torque tube pumps could also occur if surging were caused by the boiling instability. Of concern here is that instability due to the storage of heat in superheated liquid which is released by subsequent liquid flashing. It can be the result of too few nucleation sites. The maximum superheat reached, hence the severity of the surge, is increased by fluid purity and reduced pressure and decreased by agitation of the fluid. Assessment of this problem is difficult, but Ogato and Sato[2] mention superheats of 0.4 K (0.72 R) obtained in liquid He at atmospheric pressure and Jakob[3] mentions superheats of 0.6 K (1.1 R) in pure water. Since the volume fraction of steam flashed from water per degree at 1 atm is 2.8 times that produced by flashing helium, at 0.5 atm, it is expected that surge boiling will be less of a problem in helium than in water -- but not necessarily insignificant.

From the vapor core at 0.5 atm located inside the liquid pool, vapor is drawn into the centrifugal pump feeding the torque tube heat exchanger above 1 atm. The pump has a unique configuration in that the radial flow area is much larger than the inlet or outlet areas. This feature enables the pumps to handle momentarily high mass fractions of liquid without pressure surges. The large radial flow area is radially subdivided to prevent excessive fluid slip and consequent deterioration of pump performance.

Heat leak into the cryogenic cold space (cold end heat leak) from the torque tube is controlled by the counterflow of helium vapor in the usual manner (Fig. 3-82). The device may be considered as a counterflow heat exchanger in which the mC_p product of the second fluid is replaced by the temperature dependent conductance of the torque tube, $A\bar{k}(t)/L$. The heat transfer coefficient within the cooling coils is very high due to the coils' location in the high "g" field. Indeed the convection is so good that it is advisable to include convection traps (F, Fig. 3-82) between the axially disposed peripheral cooling stations to prevent countercurrent axial heat transport in the fluid within the tubes.

The cold end heat leak and torque tube temperature distribution are computed by a finite difference computer program which accounts for the temperature variation in the tube thermal conductivity and allows for the inclusion of circumferential heat loads such as occur with the attachment of the radiation shield at about the 110 K thermal station (Fig. 3-82).

The radiation shield, because of its unsupported length, is vapor cooled. Exhaust helium vapor is diverted from the torque tube heat exchanger to flow axially in the shield after the gas reaches the 110 K torque tube station. Two pairs of streams flow in counterflow within the shield. The massive thermal inertia of the shield is used as a regenerative heat exchanger to warm fault induced helium flow surges to 100 K to prevent excessive thermal stress in the torque tubes. Final warming of the surge stream from 100 K to 300 K occurs in the helium warming stations (Fig. 3-82) located in massive uncooled zones of the rotor. Because the shield must be at nearly constant temperature yet have a high effectiveness as a regenerator, the design trade off between sufficient thermal conductance to make the thermal capacity of the shield available to the helium surge stream yet sufficient thermal resistance to preclude thermal shorting of the counterflowing cooling streams during steady operations must be exactly done. Careful design of the radiation shield and torque tube cooling stations enables the generator to be designed to mitigate faults without additional equipment such as a blow off or heat exchanger.

Because the torque heat exchanger and leads represent parallel exits from the rotor which are subject to flow instabilities, the leads are designed as self sufficient with a relatively large pressure drop to isolate the lead flow from the other rotor fluid dynamic interactions. The pressure for motivating a flow in the leads is created by hydrostatic head in the high "g" field pool. The leads are designed to operate in the conduction dominated regime for stability reasons.

It should be noted that throttle valves are provisioned to allow room temperature throttling of all helium outlet streams.

Component Performance Discussion

Inlet "T" Tube Flow Control

Figure 3-85 shows a "T" tube schematic with the associated nomenclature. The thermodynamic condition of the helium at the outlet of the "T" tube is assumed given by the isentropic compression of vapor and liquid in a pressure field set by vapor compression. The actual radial compression process in the "T" tube deviates from the ideal in several respects. First, the temperature rise of vapor and liquid are different during the compression leading to mass transfer between the phases during compression. Secondly, a significant velocity difference (slip) exists between the phases which are centrifugally separated in the "T" tube. These effects are negligible for small radius changes[4]; the temperature difference of adiabatic compression for each phase individually is a maximum of 0.25 K at 3600 rpm, 11.5 cm radius[5] and this is diminished by the conversion of liquid phase kinetic energy to thermal energy through friction at the tube wall.

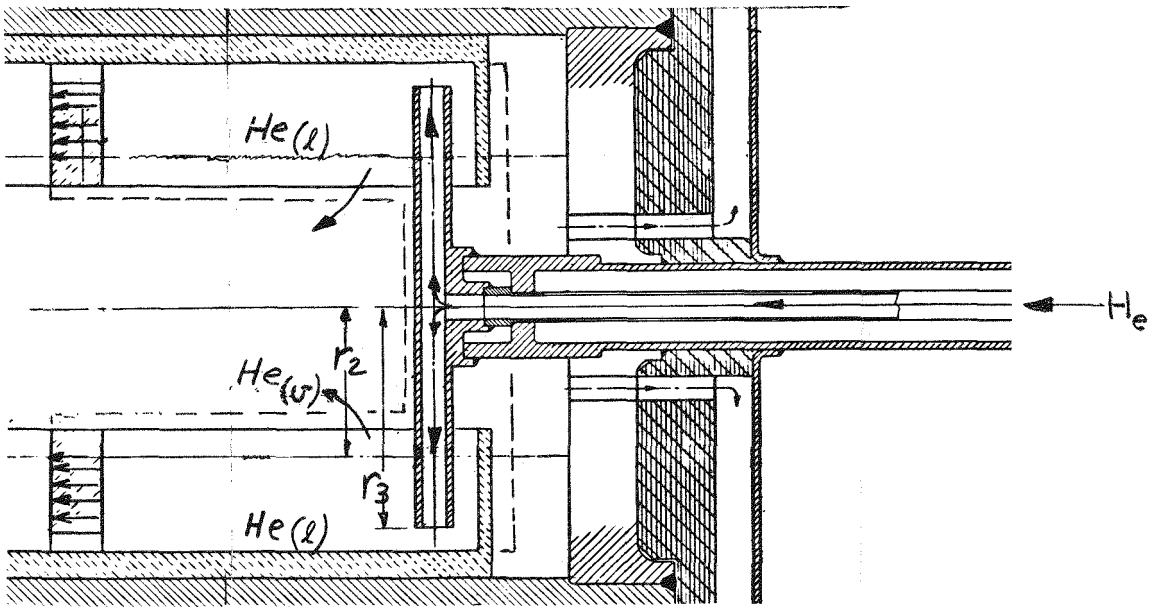

Figure 3-85. Rotor Inlet "T" tube and Trough Configuration Indicating the Control Volume for Eqs. 1 and 2

The liquid level in the feed trough may be calculated by static pressure balances based on adiabatic expansion and compression considerations. For small radius changes these relations have satisfactory accuracy for design purposes.

The sketch above shows the liquid level of the inlet "T" tube for small radius change and shutoff conditions. Summing the hydrostatic pressures relative to a radial datum yields Eq. 1.

$$r_2^2 = \frac{2g_c (P_i - P_o)/\omega^2 + r_3^2(\rho_{(v)_i} - \rho_{(\ell)_o})}{\rho_{(v)_o} - \rho_{(\ell)_o}} \qquad (1)$$

The liquid flow rate is established to maintain approximately 3.8 cm of the "T" tube submerged. Note that the flow rate is very responsive to the heat input to the rotor, i.e., density variation within the pool, because of the area ratio of the trough and main pool.

A first law of thermodynamics analysis of a control volume including the region of the trough and "T tube exerting a back pressure on the inlet gives the quality change from the inlet tube to helium trough as Eq. 2.

$$\Delta\chi = \frac{i_{(\ell)_i} - i_{(\ell)_o} + \chi_i (i_{fg_i} - i_{fg_o}) + \frac{\omega^2 r_3^2}{2g_c J}}{i_{fg_o}} \qquad (2)$$

For the present design, with 10% vapor leaving the rotating transfer system, a quality change of 14.3% occurs in the "T" tube tip expansion.

Radial Heat Exchanger

The incoming liquid helium is constrained to flow between the trough and annular winding feed gap through the radial heat exchanger tubes. These tubes partially remove the sensible heat of compression, 2.56 J/gm (1.1 Btu/lbm), to the evaporating pool surface. A maximum of 10% of the incoming liquid is evaporated by the compression process. A part of this heat is reabsorbed from losses on return to the rotor centerline. Fig. 3-86 indicates the performance of the heat exchanger tubes. The 300 MVA requires a heat exchanger tube pitch of 15.2 cm (6 in). The pitch would increase to 30.4 cm (12.0 in) for the 1200 MVA generator. The equations governing the heat exchanger were first given in the second quarterly report[6] of this project (repeated here as Eqs. 3-10) and subsequently by Haseler, et al.[7]

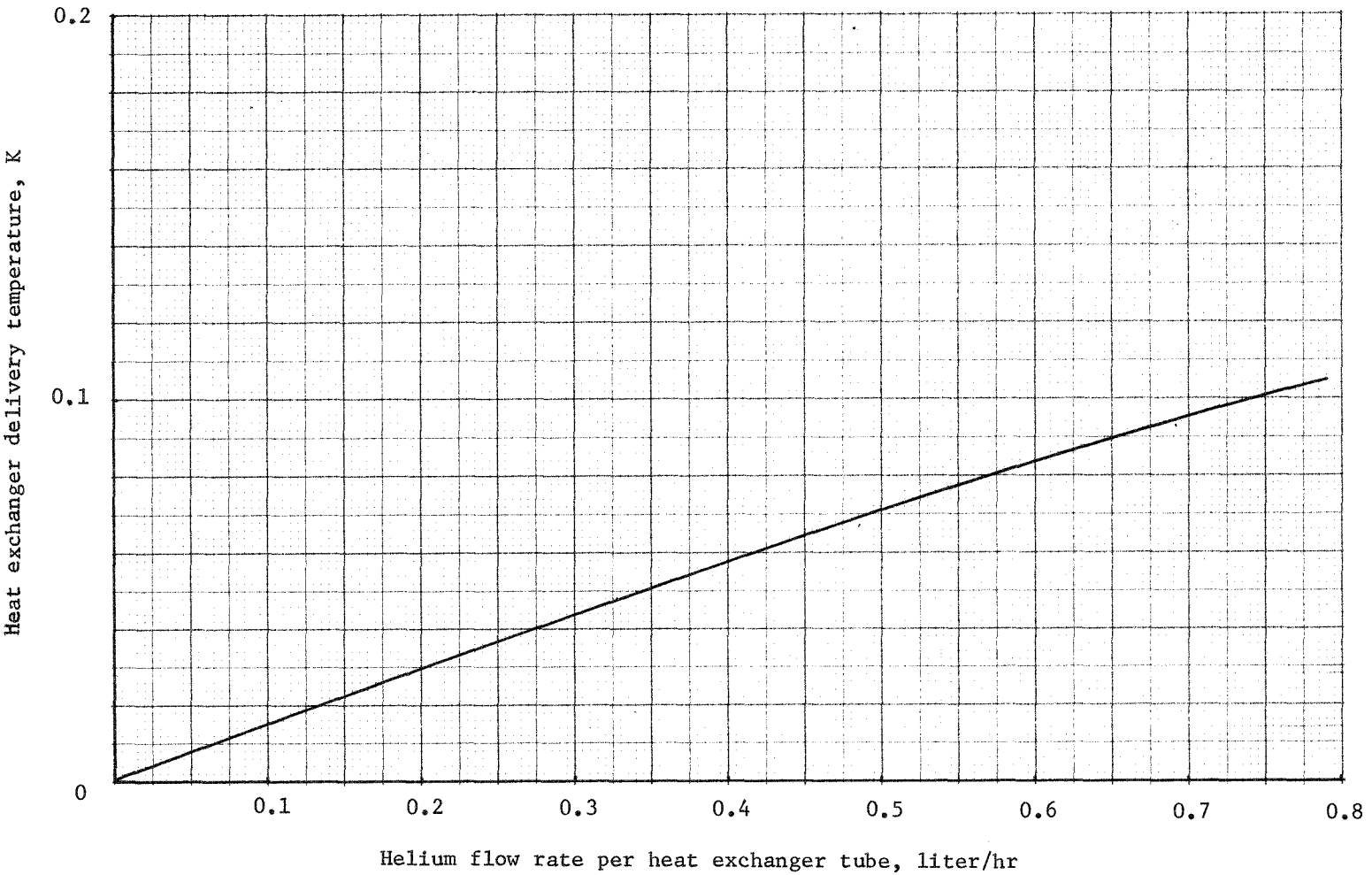

Figure 3-86. Delivery Temperature at the Ouside Radius vs. Flow Rate

$$t_{He} = A + Be^{\lambda^+ r/2} + Ce^{\lambda^- r/2} + N_m r^2 + 2N_m N_\omega / N_k + N_q \quad (3)$$

$$t_{Cu} = A + B(\lambda^+/N_m + 1)\, e^{\lambda^+ r/2} + C(\lambda^-/N_m + 1)\, e^{\lambda^- r/2} + N_\omega r^2 + (N_q + 2N_m N_\omega / N_k) \quad (4)$$

$$\cdot\ (r + 1/N_m)$$

where

$$\lambda^+ = (-N_m + \sqrt{N_m^2 + 4N_k})/2 \quad (5)$$

$$\lambda^- = (-N_m - \sqrt{N_m^2 + 4N_k})/2 \quad (6)$$

$$N_\omega = \frac{\omega^2 f}{2C_p g_c J} \quad (7)$$

$$N_m = \frac{hp}{\dot{m}C_p} \quad (8)$$

$$N_k = \frac{hp}{kA} \quad (9)$$

$$N_q = \frac{\dot{q}''' A}{\dot{m}C_p} \quad (10)$$

Assumptions made by both researchers are equivalent as are the results - including the apparent increase in heat exchanger capacity with helium mass flow rate. Evidently the counterflow of heat and liquid results in considerable fluid preheating at very low mass flow rates and causes the unusual capacity variation. Heat transfer coefficient within the tube is assumed given by the correlation for natural convection within closely spaced, vertical parallel walls (see, for example, Kreith[8]) in this study: Haseler et. al. used a typical forced convection correlation. Equation 11 gives the correlation used to determine the heat transfer coefficient in the exchanger and Table 3-44, the data used in the analysis.

$$\frac{hd}{2k} = 0.0317\ (Gr_d Pr)^{0.37} \quad (11)$$

Table 3-44

HEAT EXCHANGER DATA

radius liquid	12.7 cm (5.0 in.)
radius winding	29.2 cm (11.5 in.)
angular speed	60 rps (3600 rpm)
area Cu wall (for heat conduction)	0.69 cm^2 (0.107 $in.^2$)
diameter of duct	0.165 cm (0.0625 in.)
Cu thermal conductivity	3.0 W/cm - K (173 Btu/hr-ft-°R)
He specific heat	3.01 J/gm - K (0.737 Btu/lbm-°R)
heat transfer coefficient	0.162 W/cm^2 - K (285 $Btu/hr-ft^2$-°R)
He inlet temperature	3.61 K (6.5°R)
heat generation	7.04 μW/cc (0.68 Btu/ft^3-hr)
enthalphy fraction in sensible heat	0.33

Note that Eq. 11 is conservative when compared to an extrapolation of the data of Elenbaas[9] for natural convection in vertical circular ducts. It should also be noted that conduction within the stainless steel teeth which support the copper heat exchanger tubes has been neglected.

Conductor Cooling

The cooling of the conductor bundle in the superconducting mode is conceptually defined in terms of three time intervals, each an order of magnitude different. Cooling during a fault (order of 50 ms time scale) is based on diffusion of heat and local heat storage in stagnate helium. Cooling during recurring faults, i.e., breaker reclosure, is based on the initiation of local convection currents (order of 500 ms scale) to exchange heat with local cold helium reservoirs in the conductor slot. Recovery from fault transients (order of 5^+ s) is predicated upon establishing circulation in the major flow loops of the rotor. Diffusion cooling during the fault is a well known process, similar in nature to scraped film heat exchange. Those cooling mechanisms relying upon thermosyphon action in high "g" fields are less known but adequate data does exist for design purposes.

Temperature rise per 66 ms fault is less than 0.1 K for 10% helium by volume in the winding. The assumption of uniform temperature rise of copper conductor and 10% helium upon which the 0.1 K rise is based is justified by a diffusion time constant across the electrical insulation and corner enclosed helium of 3 ms

and 28 ms respectively. The time constants are based on the time to transfer 62% of the relative energy (Eq. 12 & 13)[9] and therefore are conservative because the low specific heat of the winding results in a large thermal potential to transfer energy.

$$F_o = \frac{\alpha(\Delta\tau)}{L^2} = 0.38 \text{ for slabs} \tag{12}$$

$$= \frac{\alpha(\Delta\tau)}{r_o^2} = 0.05 \text{ for cylinders} \tag{13}$$

Considering that the time constant for initiation of convection is of the order of 500 ms* and the additional 10% volume in the local reservoirs is available in that time interval, the local winding cooling presents no practical limit to operating through multiple faults or breaker reclosures.

Cold Damper Cooling

As mentioned in the introduction, the helium filled annular gap adjacent to the cold damper support structure receives helium from the annular winding feed gap via holes in the thermal insulation between them and exhausts to the torque tube cooling thermosyphon. Neglecting metal specific heats, the temperature rise of the helium in the gap per 66 ms fault is less than 0.25 K, based on uniform local storage of the fault losses. The maximum temperature rise across the Inconel 718 helium containment shell determines the cold damper shield operating temperature and is 8.2 K for steady generation of fault levels. Steady magnetic fluctuations in the cold damper shield produce 1.8 W of heat generation and indicate a temperature rise of 0.15 K at the outlet of the cold shield circuit if the heat exchanger flow should divide and flow equally to the winding and cold shield. Clearly the cold damper poses no cooling problems.

Torque Tube Pumps

The centrifugal pumps that return helium vapor from the rotor at 51 kPa to 101 kPa are located in the end walls of the rotor. They are designed to tolerate momentary ingestion of liquid without liquid delivery to the torque tube heat exchanger or significant pressure variations. Two pumps are used for inherent mechanical balance. The flow passages within the rotor ends are large to prevent liquid bridging (slugging) and have liquid storage capability at their tip. Boiloff of

*See rotor cooling system transient performance section.

ingested liquid occurs because of the small local temperature rise due to torque tube cold end heat leak. The performance of the pumps is estimated using Euler's equation without friction estimates and is presented in Fig. 3-87 as a system characteristic including the effect of torque tube temperature distribution.

Torque Tube and Radiation Shield Cooling

In the 300 and 1200 MVA superconducting rotors, the torque tubes not only transmit torque and control the conduction heat leak into the cryogenic cold space but interact with the radiation shield to mitigate fault transient induced thermal stresses. The details of the design of these two components is complex and fundamental to acceptable rotor performance. For reasons of mechanical balance, parallel pump stability and minimum thermal distortion, two torque tube pumps feed two parallel cooling tubes which are arranged to flow in counterflow to each other around the torque tube periphery at each cooling station. Complete polar thermal symmetry is thus assured if the two parallel cooling paths are at the same temperature. But parallel exhausts from cryogenic spaces to room temperature are known to be among the most unstable thermohydraulic systems: extreme differences in outlet temperature are more likely than similar outlet temperatures. For this reason, two sets of tubes are kept in close thermal contact at each cooling station and are transposed in axial relation to the flow of heat in each successive cooling station. Counterflowing cooling tubes in good thermal contact have a tendency to exchange heat at their ends and come to thermal equilibrium with the piece to be cooled, thus negating any transport of heat by convection (cooling). Offsetting the tube-to-tube exchange problem within each cooling station is high "g" field natural convection tube axial mixing. The length-diameter ratio of one-half the tube station is 60. Rotating helium transfer system analyses[10] have inferred the existence of convective mixing with very high length to diameter ratios. It is expected that each cooling station is essentially isothermal.

Since the rotating seals in the helium transfer system are Ferrofluidic and can only operate above 273 K, helium warming stations are built into the more massive room temperature rotating zones of the rotor.

Figure 3-88 shows the steady state temperature distribution in the torque tube for various helium vapor flow rates. Table 3-45 gives the design data applicable to Figs. 3-88 and 3-89.

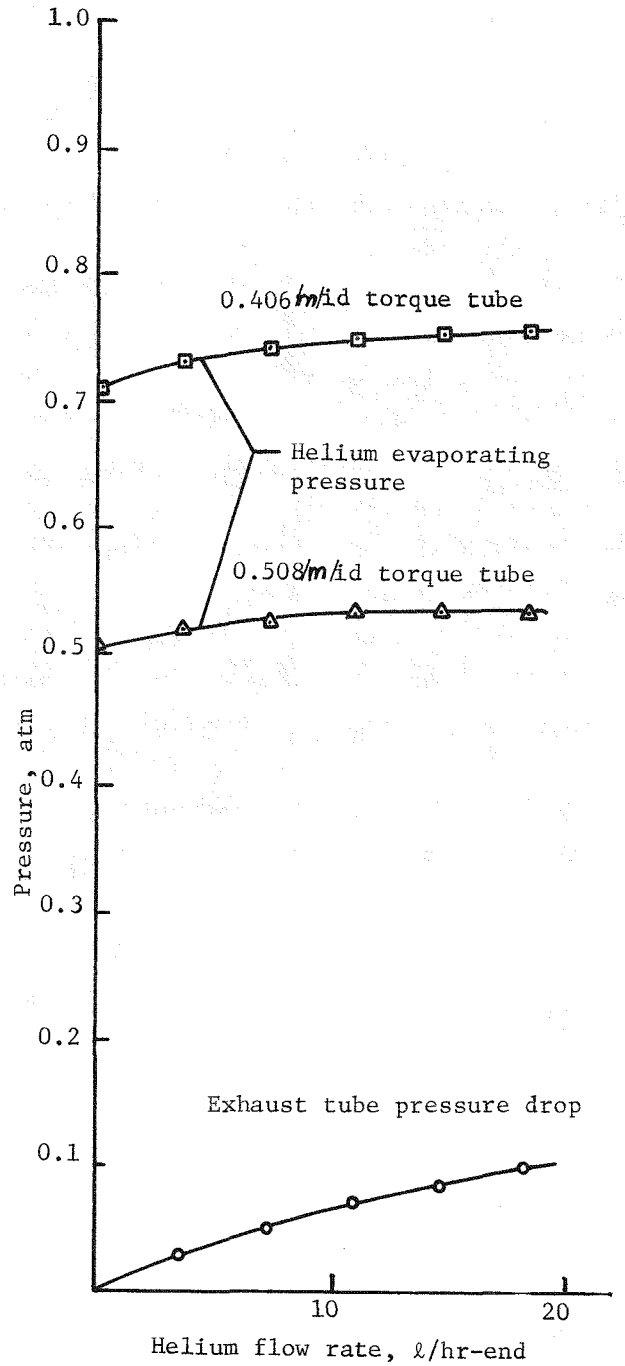

Figure 3-87. Helium Evaporating Pressure and Exhaust Tube Pressure Drop

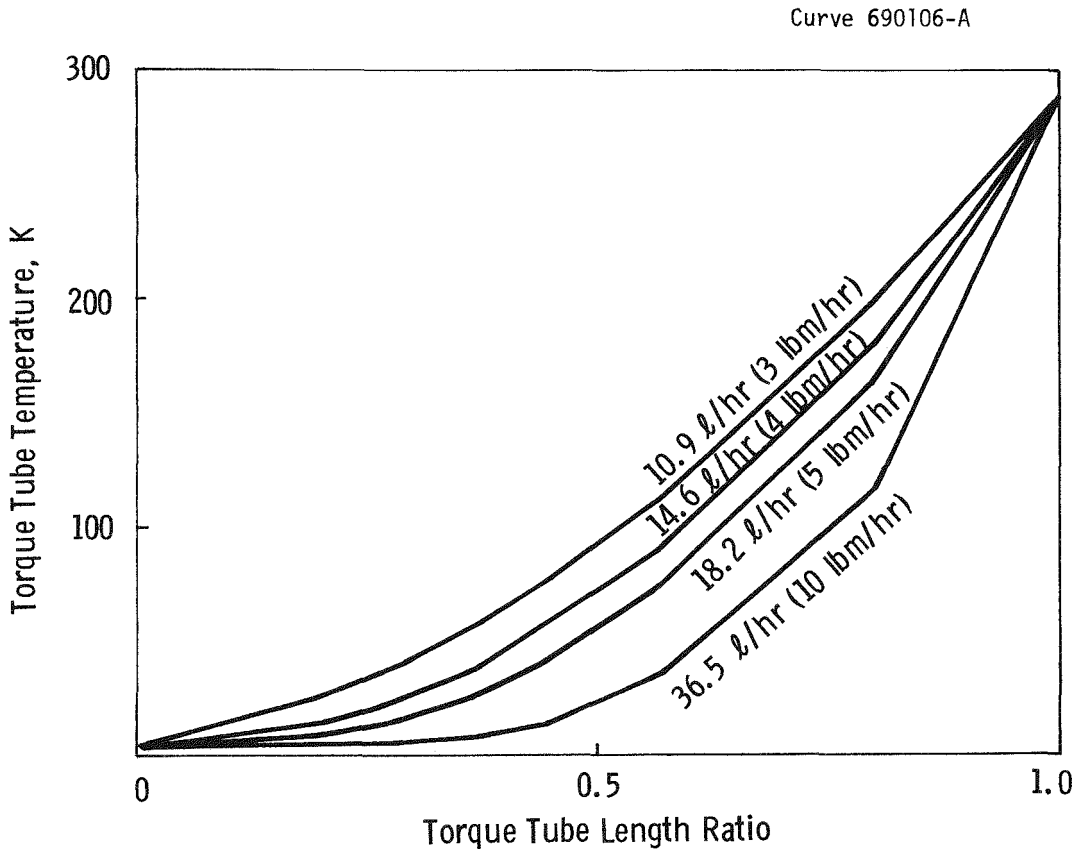

Figure 3-88. Torque Tube Temperature Distribution as a Function of Flow Rate per End

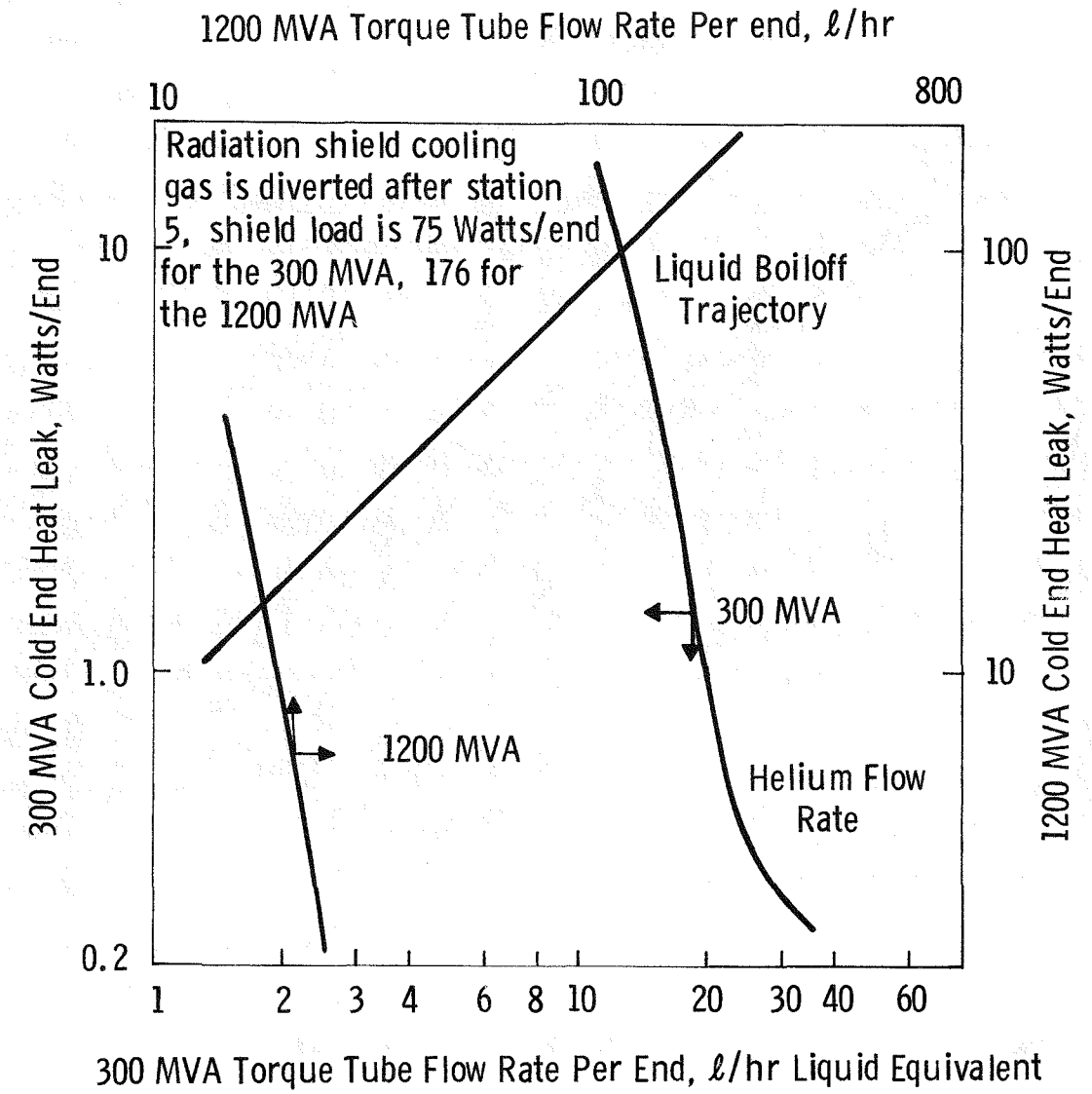

Figure 3-89. Cold End Heat Leak through one Torque Tube as a Function of Flow Rate

Table 3-45

TORQUE TUBE HEAT TRANSFER DATA

	300 MVA	1200 MVA
Material	Inconel 718	Inconel 718
Axial conduction area	200 cm^2 (0.215 ft^2)	506 cm^2 (.545 ft^2)
Overall length (between cooling stations)	26.1 cm (.856 ft)	40.5 cm (1.33 ft)
Length ratio, 1st station	.203	.159
2nd station	.285	.263
3rd station	.367	.366
4th	.449	.468
5th	.566	.594
Radiation Shield tap		
6th	.801	.785
Helium warming stations	1.0	1.0
Heat exchanger tubes, OD x wall	6.35 x 0.825 mm (0.25 x .032 in)	9.53 x 0.825 mm (0.375 x .032 in)
Heat transfer coefficient W/cm^2 -K(Btu/hr-ft^2-°R)	.171 (300)	.171 (300)

The 300 and 1200 MVA torque tubes are geometrically scaled so Fig. 3-88 generally applies to each. The design limit on thermal stress is not exceeded by any of the flow rates shown. Cold end heat leak vs helium flow rate is shown in Fig. 8-89 for the 300 MVA and 1200 MVA generators.

Note that the total heat input from the 300 MVA radiation shield is 150 W or 75 W per end; computed using a polished warm damper emissivity of 0.15 and a gold plated shield emissivity of 0.06. Cooling of the shield is accomplished by the counterflowing of vapor within four groups of cooling passages in the shell (see Fig. 3-90). The equations which describe the temperature field in the shell, including internal heat generation, convection and conduction between the streams are given as Eqs. 14 through 18.

$$\hat{T} = T - \frac{\dot{q}'''\delta}{h_r} = t - t_o - \frac{\dot{q}'''\delta}{h_r} \tag{14}$$

$$N = \frac{h_r}{k\delta} \tag{15}$$

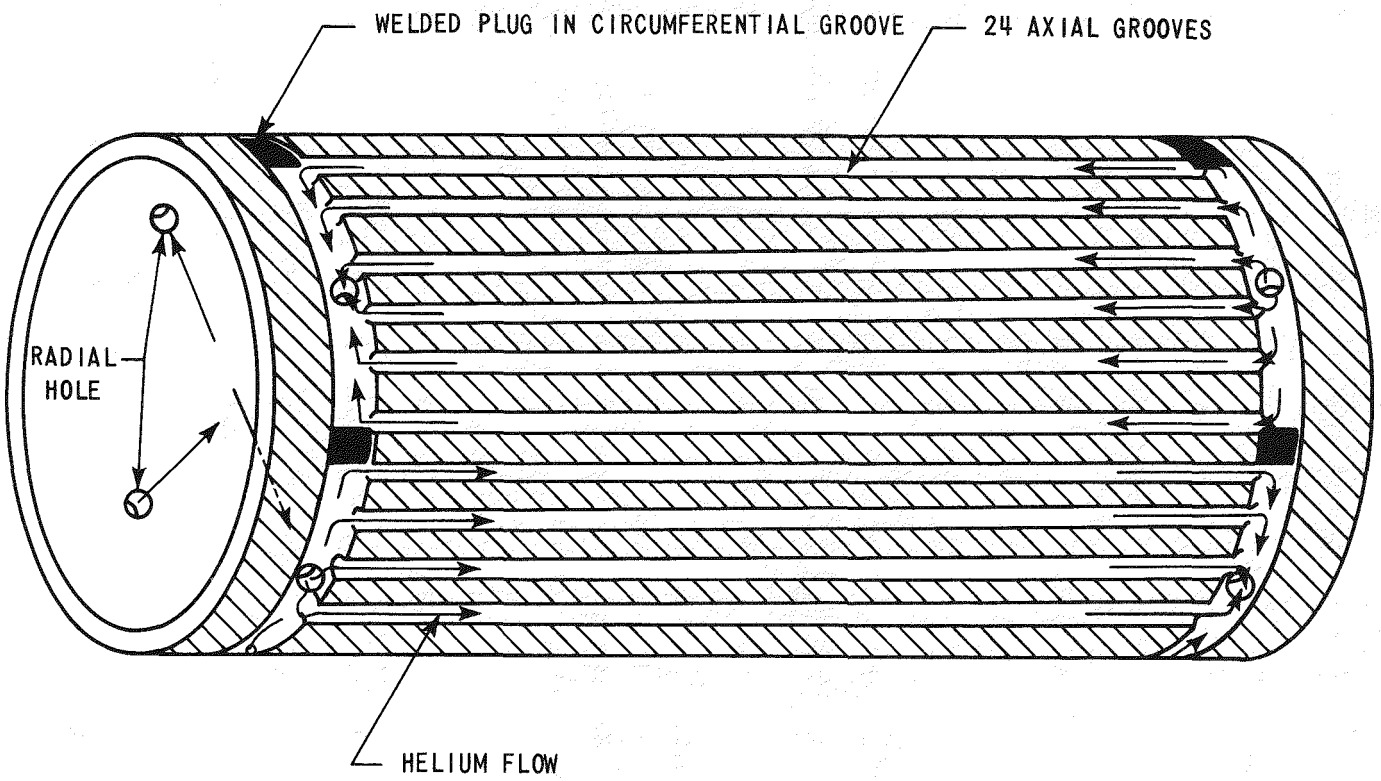

Figure 3-90. Radiation Shield Inner Shell Schematic of Cooling Grooves and Helium Flow

$$\frac{\hat{T}(x,Z)}{\tilde{T}_{He_{in}}} = \frac{\sinh N(L-x)}{\sinh NL} \left[C_3 e^{\lambda Z} + (1 - C_3)\, e^{-\lambda Z}\right]$$

$$+ \frac{\sinh Nx}{\sinh NL} \left[C_3 e^{NL + \lambda Z} + (1 - C_3)\, e^{-(NL + \lambda Z)}\right] \qquad (16)$$

$$C_3 = \frac{(1-e^{-NL})e^{-\lambda l}}{2 \sinh (NL + \lambda l) - \sinh \lambda l} \qquad (17)$$

$$\lambda = 2k\delta N/\dot{m}C_p \qquad (18)$$

Figure 3-91 shows the maximum shield temperature as a function of helium flow rate. In the present design, the average departs very little from the mean of fluid inlet and outlet. It must be noted that Eq. 16 was derived for case of alternate tubes counterflowing. For the present case of banks of counterflowing tubes, the solution may be applied if the actual tube flow is doubled: the modeling is approximate, but the maximum temperature predicted is high. The design condition is 11 ℓ/hr-end and an inlet temperature of 110 K. Between tubes in the same bank, maximum temperature is given $\dot{q}''_{rad}\, L^2/(2K\delta)$ and is the order of 0.5 K. Note that one blank duct is required to control the heat flow between the counterflowing tubes. The maximum radiation shield temperature is 174 K and occurs adjacent to local shield minimum of 123 K.

During a fault transient 4.1 kJ of heat are deposited in the cold space in 5 s and subsequently evaporates 0.4 ℓ of liquid helium. The concept of local storage as sensible heat and longer term transmission of the heat from the rotor results in smoothing the flow of helium resulting from a fault transient. It is expected that the worst possible multiple fault condition, survivable by the turbine and breakers, would lead to no more than five times the steady design flow in the torque tubes. The estimate is based on considerations of the thermal inertia of the rotor, the expected time constant to initiate natural convection and the fact that for local temperature rises of less than 0.5 K the replenishment flow to the cold damper is limited to the evaporation rate from the main pool by the heat exchanger and trough flow circuit.

Figure 3-92 is an example of the steady temperature in the torque tube at fault level flow rates. The steady distribution is a good conservative approximation to the transient condition because of the small thermal mass of the torque

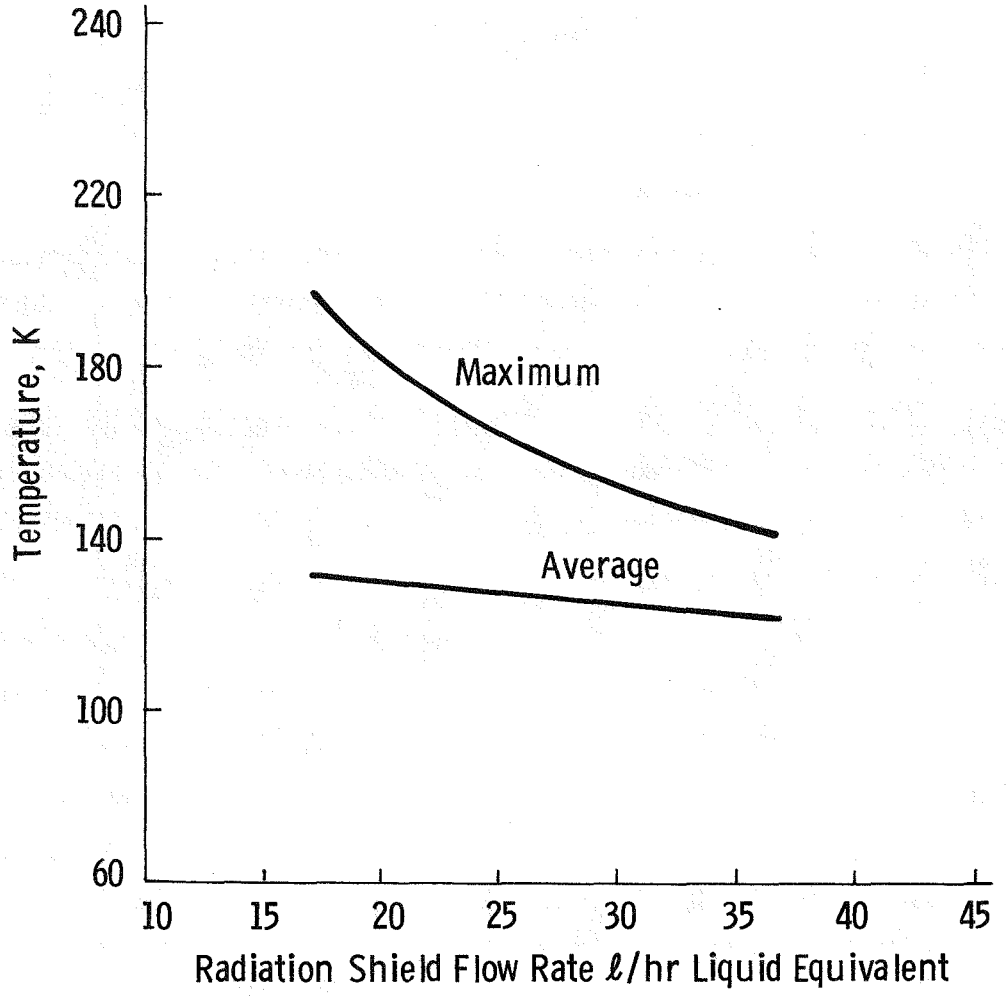

Figure 3-91. Radiation Shield Temperature as a Function of Total Flow Rate

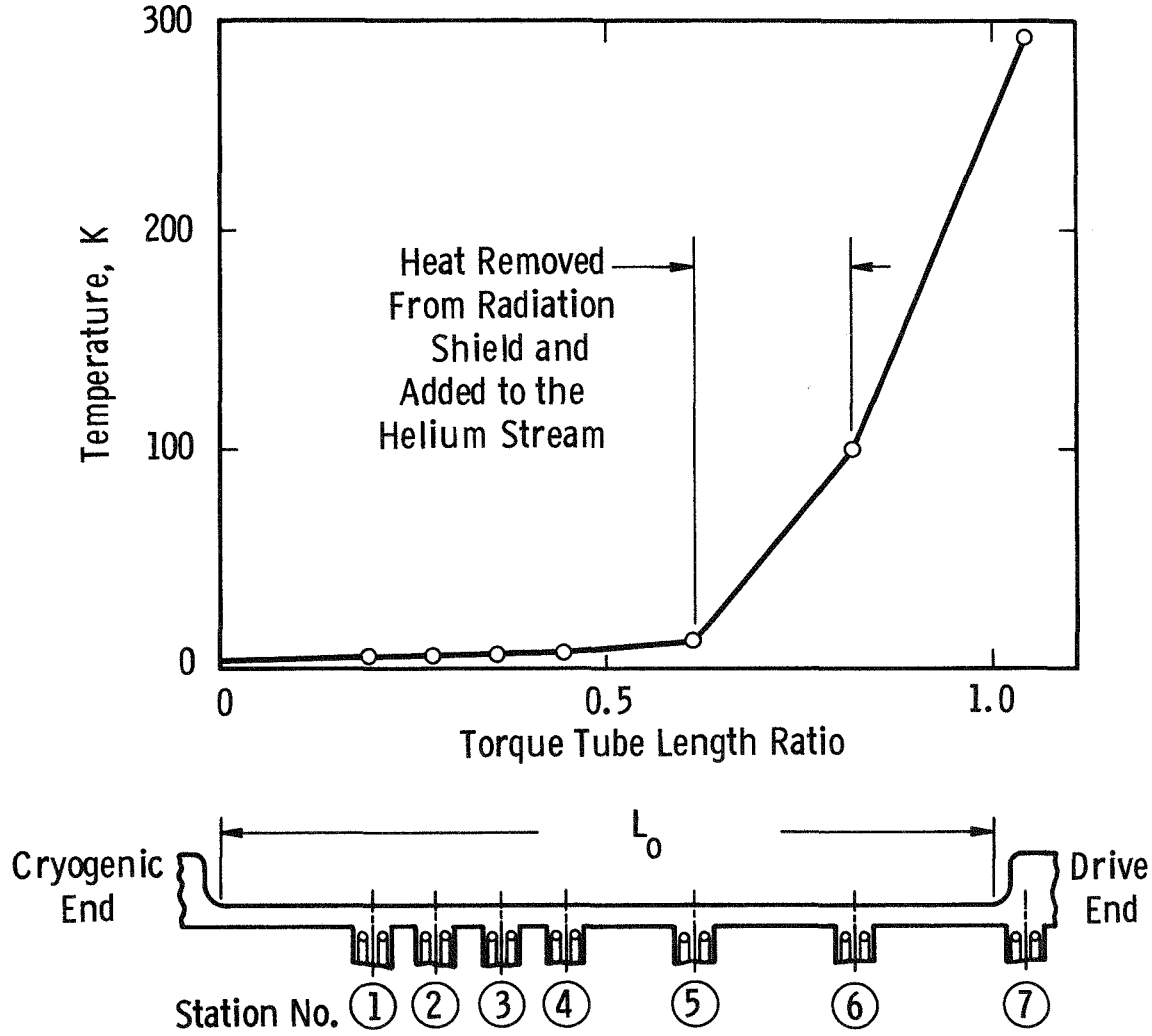

Figure 3-92. Torque Tube Temperature Distribution during a Fault Transient

tube. The heat capacity of the helium surge stream is 0.96 kJ/K and that of the radiation shield is 46 kJ/K. The radiation shield acts as a regenerator during the fault transient to warm the torque tube flow from 12 K to 100 K. Thus station 6 on the torque tube is maintained at a safe temperature level and the final warming of the helium is done in room temperature warming zones. The temperature gradients below station 6 are very high but are of no concern because the coefficient of linear expansion of the material is very small below 120 K. Thus it is that a fault transient can be fully mitigated by passive equipment that performs a necessary function in the steady state design.

Lead Analysis and Design

Electrical penetration to the cryogenic space with a minimum heat leak must be provided by the electrical leads. The leads may be designed for a helium pressure drop type flow rate control or they may be "self sufficient", i.e., the helium flow rate through the lead tube is generated by liquid helium boiled off by the cold end heat leak. Both types have distinct problems; the self sufficient lead is mechanically more simple than the pressure regulated lead, but the cooling capacity is insensitive to changes of temperature at the warm end.

Two heat sources contribute to the cold end heat leak, Joule heating and Fourier conduction and the lead characteristic is determined by the relative contribution of these. For a given lead length and current, two different areas of lead may be found which give the same cold end heat leak. One is heat conduction dominated and the other is electrical heat dominated. The conduction dominated lead is larger in conductor cross-sectional area, is more able to mitigate thermal transients because of higher thermal storage capacity at the warm end, and is more responsive to warm end conditions.

Another less obvious condition must be met to achieve a stable self-sufficient thermo-hydraulic lead system. For any decrease (increase) in lead flow rate the cold end heat leak must increase (decrease) by a sufficient amount to offset the flow decrease (increase).

Although many theoretical treatments of leads have been published, it appears that the most significant factors to be included in the analysis are variable thermal and electrical conductivities. In addition to the zero field temperature variation, the variation of thermal and electrical conductivity with magnetic field intensity have been explored. Since the lead radial section (pressure generating section) is aligned with the field in the end turn pole head region little effect

is expected there. The axial run is transverse to the field for a distance and because of the uncertainties involved, a lead characteristic is shown in which the magnetic field is presumed to be 5 T over the full lead length. The magnetic influence on thermal conductivity ratio is presumed related to electrical conductivity ratio by simple proportionality and electrical conductivity is 50% of that at 4.2 K in a 5 T field. For convenience the 50% conductivity increases linearly with temperature to 100% at 300K. A lumped parameter model of the leads is used to determine their thermo-hydraulic performance map. The digital computer program, CRYOTL, was written by T. J. Fagan[11] and was used to design the Westinghouse 5 MVA and USAF 5 MVA super-conducting leads, structures, and torque tubes as well as those reported herein.

Figure 3-93 is the thermohydraulic performance map computed by CRYOTL for a 1.52 m (5 ft.) lead. The shaded region is the interval of uncertainty associated with magnetostrictive effects at the design condition. The conductor matrix consists of braided 0.508 (20 mil) diameter OFHC strands. The void volume is assumed to be 70% of theoretical close packed cylinders. Ninety percent of the surface is presumed wetted. The matrix heat transfer coefficient is given[12] as:

$$j_h = \frac{h}{C_p G_o} Pr^{2/3} = 0.91\ Re_o^{-0.51}\psi;\quad Re_o < 54.6 \tag{19}$$

$$j_n = 0.61\ Re_o^{-0.41}\psi \qquad Re_o > 54.6 \tag{20}$$

In this case the wake factor ψ is 0.85. Lead pressure drop is computed as

$$\Delta p = \sum_{i=1}^{n} \left(150\ \frac{1-\varepsilon}{D_p G_o/\mu_i\ (T)} + 1.75\right) \frac{(1-\varepsilon)}{\varepsilon^3}\ \frac{L}{D_p}\ \frac{G_o^2}{\rho_i(T)} \tag{21}$$

This is recognized as the Ergun Equation and indicates a pressure drop in the lead of less than 7 mbar. A flow rate of 4.2 l/hr-lead yields a heat transfer coefficient of 17.3 MW/K-cm^2 (3.66 Btu/hr-ft^2-°F) at the cold end according to Eq. 19. Within Westinghouse more operating experience exists with cabled leads. An equivalent lead may be formed from a 19 strand standard cable but would have a 70 mbar pressure drop. Neither type lead has a prohibitive pressure drop.

Exploring the thermohydraulic stability of the lead, it is noted (Fig. 3-93) that for a change of -0.37 l/hr-lead in He flow rate, the cold end heat leak changes by +2.54 watts/lead, or an equivalent of +1.78 l/hr-lead. Satisfactory stability is demonstrated.

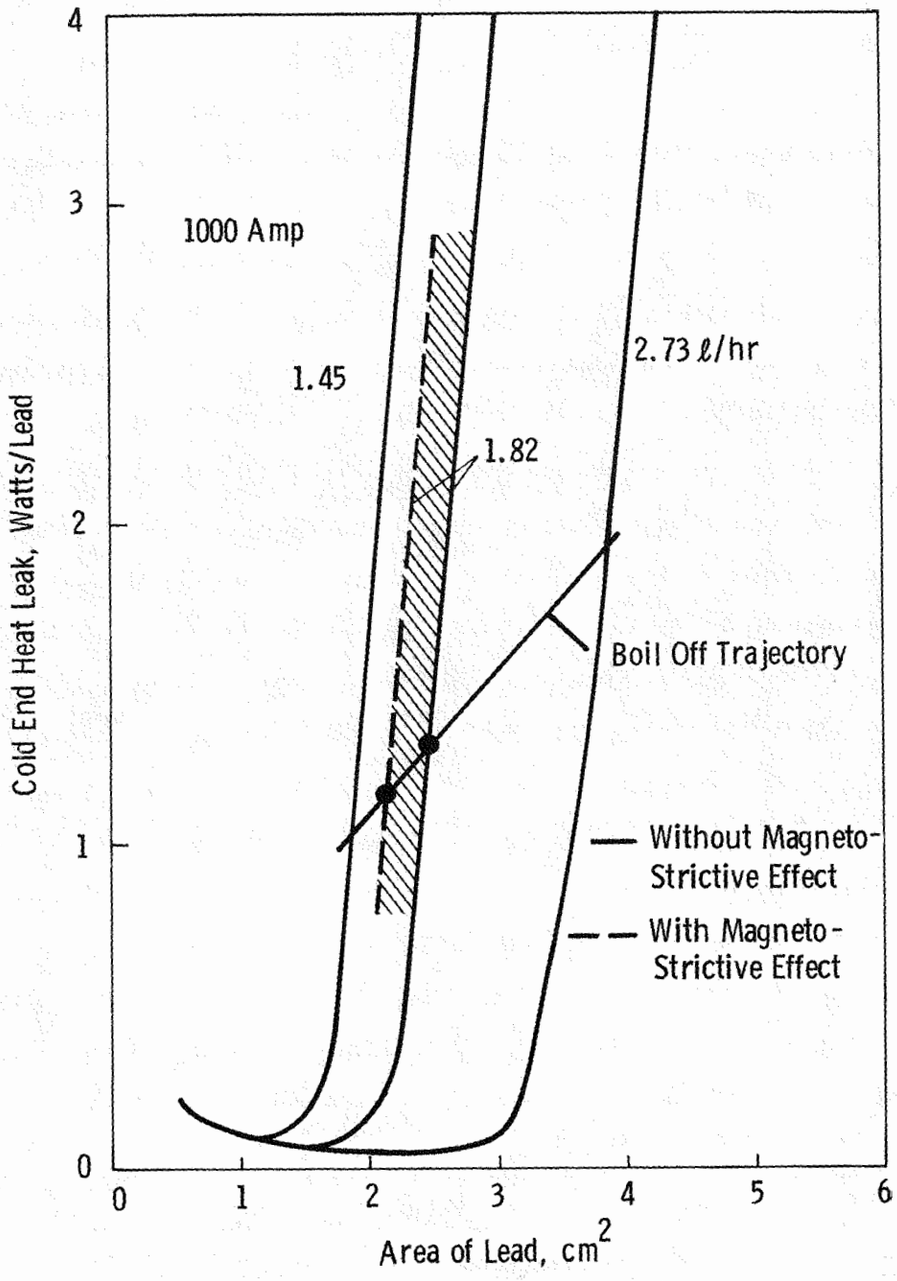

Figure 3-93. Cold End Heat Leak vs. Area of Lead for Various Helium Flow Rates

It should be noted that although Fig. 3-93 indicates the leads could be designed to operate at lower helium flow rates, the minimum in the performance map moves upward very rapidly with decreasing helium flow rate and instability is rapidly approached.

Figure 3-94 shows the lead temperature distribution for various conditions. A satisfactory temperature distribution is shown for the overcurrent condition.

Field Winding Quench Analyses

Under certain extreme fault conditions the generator specifications permit a resistive transition and discharge of the field winding (quench). It is necessary that a quench may occur without an extended outage. The analysis of the quench has been performed from a macroscopic and microscopic point of view. The macroscopic view considers all of the magnetic energy dumped into the winding which is in thermal communication with a vented steel helium reservoir. Back flow out of the inlet "T" tube is permitted above 101 kPa rotor internal pressure. The maximum pressure predicted is 240 kPa (35 psia). This unusually low pressure rise is due to the large thermal mass of the helium pool and long time constant of the fully resistive winding. The computer code used in this analysis was developed by A. Ulke for the USAF.

A more interesting analysis is that which follows the propagation of a local quench zone, but first a look at the cooling system thermohydraulics is instructive. Remembering that the present flow system restricts the winding coolant replenishment flow rate to the inlet flow, it is readily determined that the helium temperature rise in the local propagating quench zone exceeds 20 K, thus inducing a massive convective flow. This flow cannot come from the heat exchanger so it reverses the direction of flow within the winding thermosyphon loops to bypass the radial heat exchangers. In so doing the helium drawn into the winding is heated by compression and the winding operating temperature changes from 3.6 to 4.5 K. The general temperature rise of the winding due to cooling system reversal during quench is valuable as it more than doubles the propagation velocity of the quench zone. It is conceivable that a rotor of sufficient diameter could be designed to thermohydraulically quench the entire winding without external detection equipment. Note that the velocity of propagation used in this analysis does not include the velocity increase of convective heating.

To characterize the quench event, a computer code, written by P. W. Eckels for conductor development, was pressed into service. The program considers one

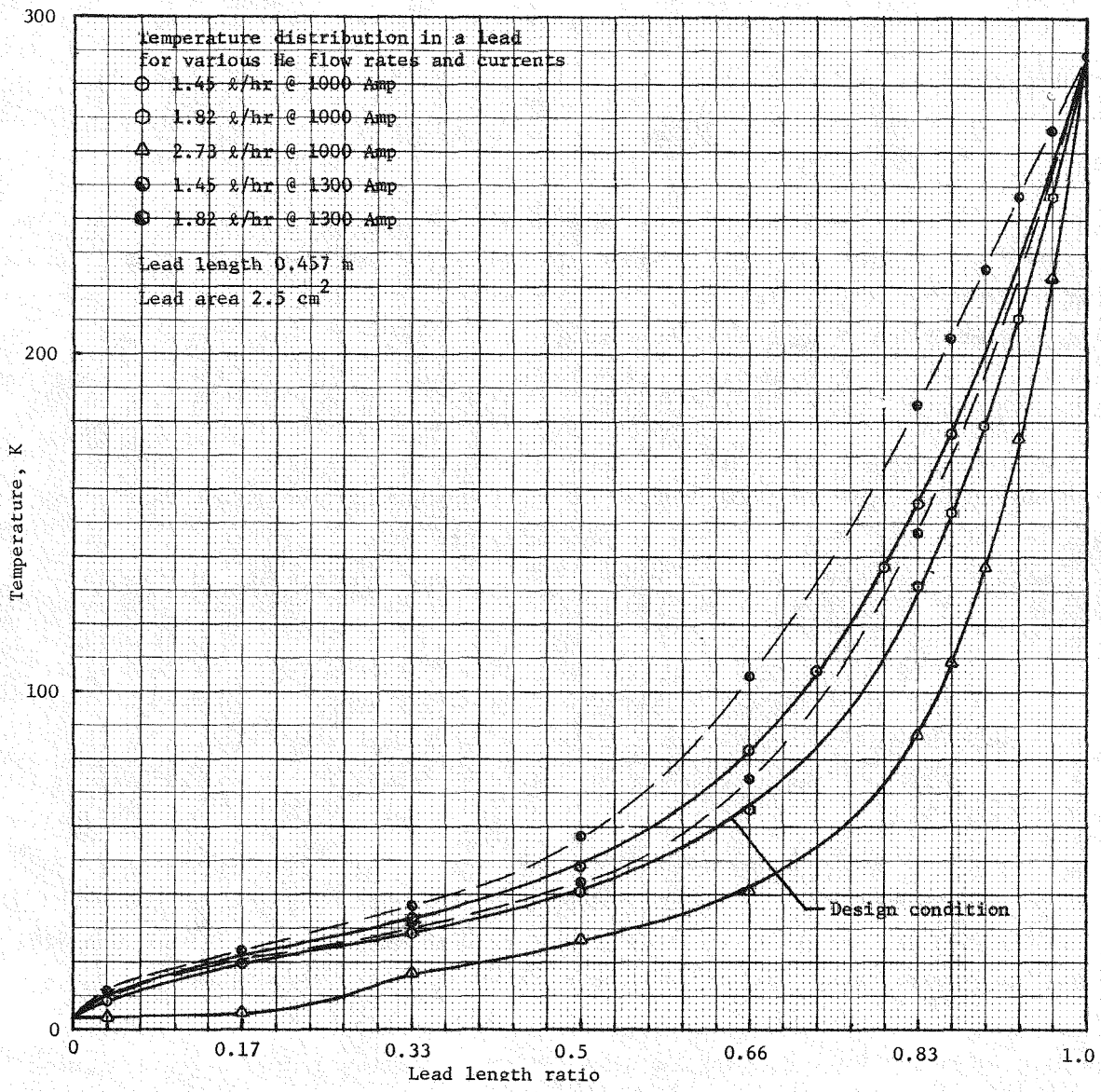

Figure 3-94. Lead Temperature Distribution for Normal and Over Current Conditions

dimensional propagation of the "normal zone" by a velocity which is separately computed. Heat is transferred from the normal zone by conduction and convection as the program marches forward in time. It is possible to simulate an inductive superconducting coil with an intrinsic resistance and to load the coil with a resistor through a simulated quench protection circuit initiated by a preselected coil terminal voltage.

The site selected for quench initiation in the present design is the worst possible in the rotor -- on an insulated edge with initial cooling and lateral propagation from the apex of a single quadrant. The linear velocity of propagation of the resistive zone interface is computed from Equation 21 rewritten after Hagedorn and Dullenkopf.[13]

$$v = \left(\frac{2hk}{r_{eff}^2 c_p}\right)^{1/2} \left[\frac{\rho I^2}{phA\,(t_c - T_b)} - 2\right] \left[\frac{\rho I^2}{phA\,(T_c - T_b)}\right]^{-1/2} \tag{21}$$

$$v = 25 \text{ m/s} \tag{22}$$

The linear velocity is modified for lateral spreading by multiplying the velocity by the ratio of the axial and transverse heat conduction time constants for long thin coils per Kothmann.[14] The final propagation velocity is 33.5 m/s.

For rapid discharge, the field coil of a large generator is paralleled with a nonlinear resistor. If discharge is necessary, the generator excited is tripped out of the circuit. Under these conditions, the resistance of the external load is given by Equation 23, a curve fit to the manufacturers data correlating to 0.9999.

$$R[\text{ohms}] = 193.3\ I^{-0.802} \tag{23}$$

Figure 3-95 is a plot of coil voltage vs. time elapsed since quench initiation. The exciter is in the circuit and the exciter is fully capable of providing the energy dissipated in the resistive zone so that coil energy remains constant. Figure 3-96 is a plot of local hot spot temperature vs. time elapsed since quench initiation.

From the temperatures shown in Fig. 3-95 it is evident that an anchored or nonpropagating resistive zone must be avoided. Hagedorn and Dullenkopf[13] give the minimum current for propagation as Equation 24.

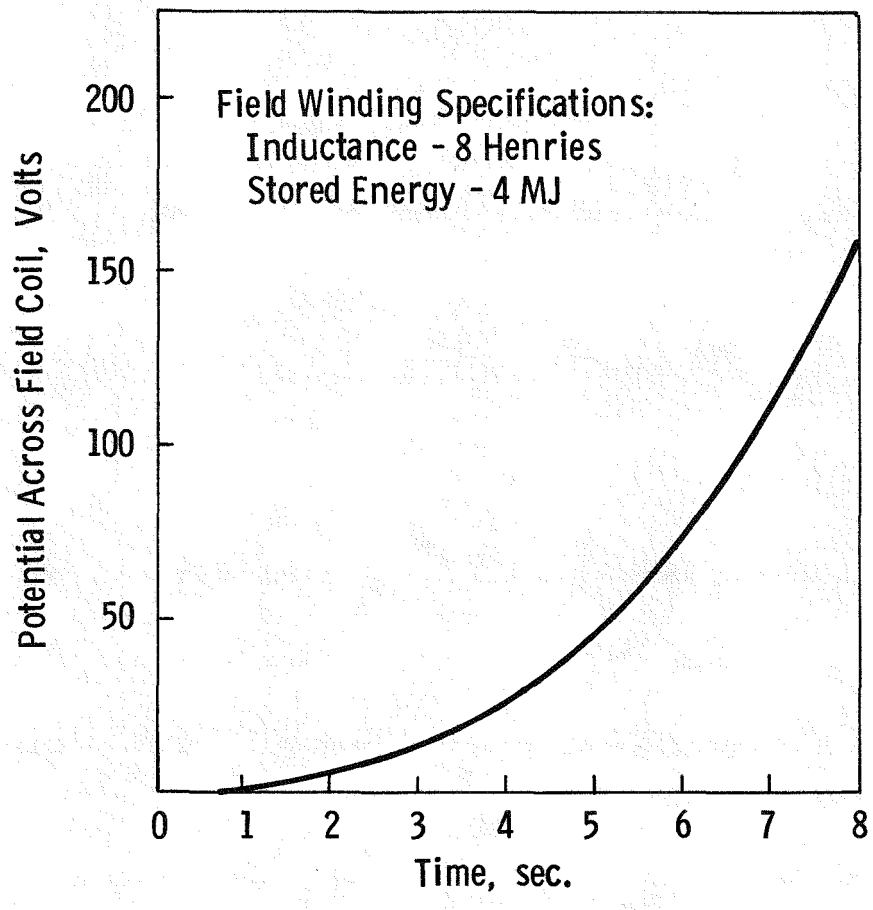

Figure 3-95. Field Coil Voltage vs. Time During Quench

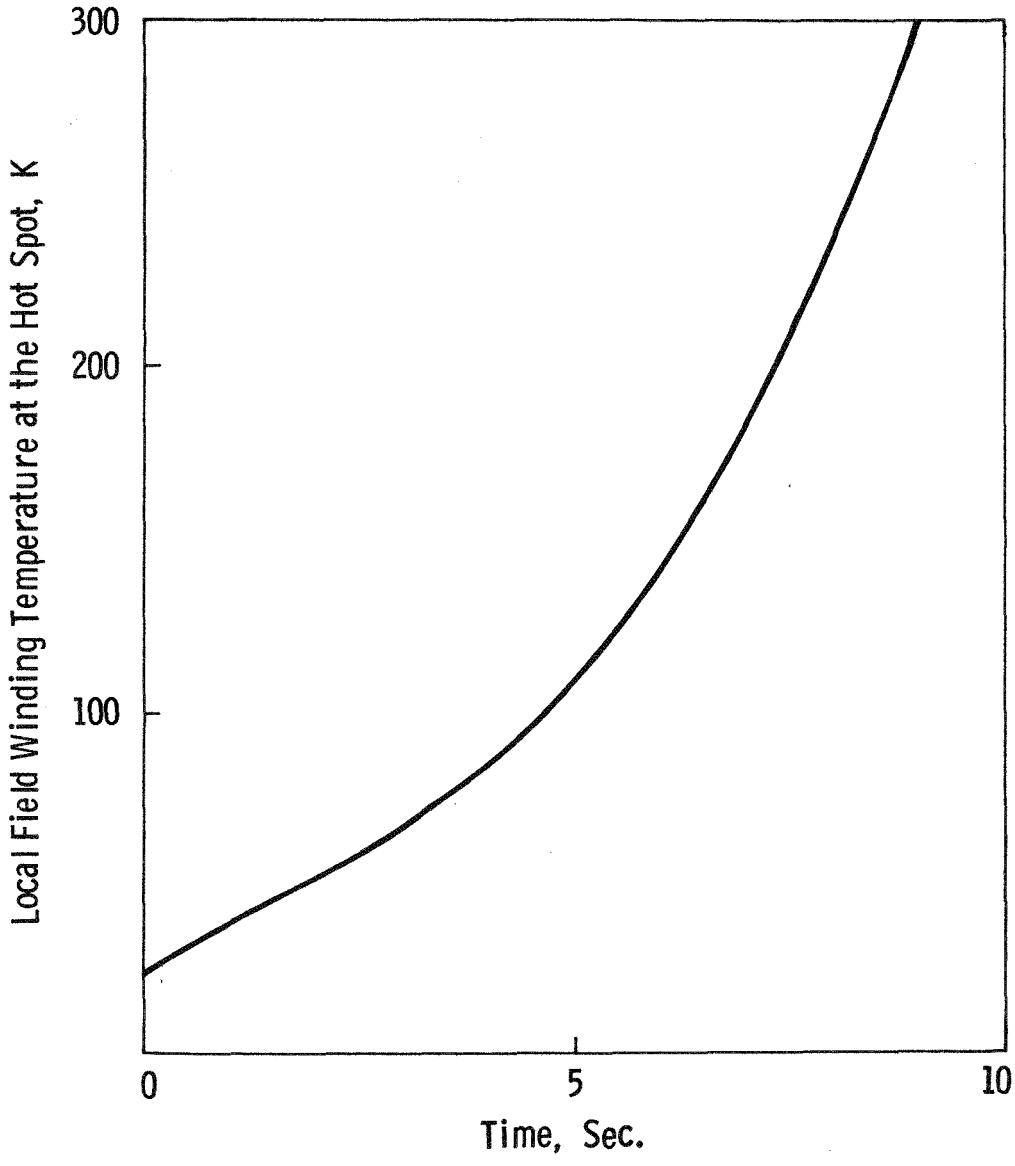

Figure 3-96. Field Winding Temperature at the Hot Spot vs. Time during the Quench Interval

$$I_{min} = \left\{ \frac{2hpA\ (T_c - T_b)^{1/2}}{\rho} \right\} \tag{24}$$

The joints in the superconductor must have a minimum propagating current greater than 10^3 amps.

Rotor Cooldown from Room Temperature

Cooldown may be accomplished from room temperature using plant apparatus or a trucked in helium supply. For reliability considerations nitrogen precooling is not considered a viable technique. Cooldown must also be accomplished at slow roll. Under these conditions the helium would be stratified in the dewar and the effluent may be presumed to be at the metal temperature. An inventory of the cryogenic material yields the following mean heat capacities.

$$_{300}MC_{v_{100\ K}} = 1.1\ MJ/K \tag{25}$$

$$_{100}MC_{v_{10K}} = 0.102\ MJ/K \tag{26}$$

A cooldown estimate can be obtained from the equation

$$\tau_2 - \tau_1 = \frac{\ell n \left(\frac{t - T_2}{t - T_1}\right)}{\frac{\dot{m}C_p}{MC_v}} \tag{27}$$

For a flow rate of 75 ℓ/hr the cooldown time corresponds to 48 hrs. Seventy-five ℓ/hr is readily maintained by the plant refrigerator upon which economic estimates are predicted. Shorter cooldowns can be achieved using purchased batches of liquid helium.

Effect of Transients on the Helium Management System

Apart from the events of a quench and cooldown which are discussed above the major concerns related to transient motions are the dissipative effects produced in the helium pool by damped rotor oscillations and a general time constant estimation for the onset of natural convection. This discussion first appeared in the fourth quarterly report to EPRI[15] and is abstracted there from with some changes.

A summary of those findings indicates the following: the time constant for diffusion of heat from the conductor across the electrical insulation into a very thin layer of helium (10% of the winding by volume) is of order 3 ms; for the start of the thermosyphon flow (cross channel diffusion plus fluid acceleration), 600 ms; and for vapor expulsion, 900 s (15 min). Equations for the dissipative losses due to rotor oscillation have been derived but not solved pending an improved characterization of post-fault rotor oscillation. Note that a positive method for elimination of these losses exists in the inclusion of baffles if later required.

Time Constants of the Cooling System

The literature contains many papers dealing with the time constant associated with the start of natural convection. As would be expected, after heating starts, diffusion is the initial mechanism of heat transmission to the coolant. Buoyancy of the heated fluid then starts the fluid in motion. In the present case the total time constant for convection initiation is that for diffusion of heat into the channel plus that to accelerate the fluid in the channel.

For diffusion the time constant is given for an infinite slab and the transmission of 62% of the relative enthalpy into the fluid. From Figures 4-9 of Kreith,[8] this occurs with the Fourier number equal to 0.38. For a 10 mil cooling channel:

$$F_o = \frac{\alpha(\Delta\tau)}{L^2} = 0.38 \tag{28}$$

$$\Delta\tau = 0.1 \text{ sec} \tag{29}$$

The time constant to accelerate the flow to 62% of the fully developed flow rate, using the relations for impulsively started laminar pipe flow, is taken from Batchelor[16] for $V/V_{max_\infty} = 0.62$.

$$\frac{\nu\Delta\tau}{R^2} = 0.25 \tag{30}$$

$$\Delta\tau = 0.5 \text{ sec} \tag{31}$$

The time constant for cooling the cold damper is based on the replacement rate of helium in the cold damper cooling annulus. Three and six-tenths degree

K helium is presumed to enter the annulus, be perfectly mixed and leave at the mixed temperature. The time constant is defined at the time to remove 62% of the cold damper energy input.

Thus we have

$$\Delta\tau_F = \frac{.97M}{\dot{m}} \qquad (32)$$

$$= 900 \text{ s } (14.8 \text{ min})$$

Note that the 900 s presumes no increase in boiloff rate due to the fault which would shorten the time constant.

REFERENCES

1. Irvine, T. F. and Hartnett, J. P., Advances in Heat Transfer; Convection Heat Transfer in Rotating Systems by Frank Kreith, Vol. 5, Academic Press, 1968, page 216.
2. Ogato H. and Sato, S., Forced Convection Heat Transfer to Boiling Helium, Cryogenics, July 1974
3. Jakob, M., Heat Transfer, John Wiley, Vol. I, 1949, page 616.
4. Smith, J. L., personal communication of work performed in his capacity as EPRI consultant to the Westinghouse Research Laboratories.
5. Fagan, T. J., Thermal Considerations in the Design of Superconducting Generators, ASME Paper No. 74-WA/HT-23, Figure 3, page 6.
6. Parker, J. H. and Towne, R. A., Superconducting Generator Design, EPRI Contract No. RP 429-1, Second Quarterly Report, April 19, 1976.
7. Haseler, L. E., Scurlock, R. G. and Thornton, G. K., Copper Conduction Pre-cooling of Helium Refrigerant in Rotating Superconducting Machines, Cryogenics, June 1976, page 337.
8. Kreith, F., Principles of heat Transfer, International Textbook Co., August 1960, page 319
9. Elenbaas, W., Dissipation of Heat by Free Convection, Parts I and II, Philips Research Report 3, N. V. Philips' Gloeilampenfabrieken, Eindhoben, Netherlands, 1948, pages 338-360 and 450-465.
10. Lee, W. D., Continuous Transfer of Liquid Helium to a Rotating Dewar, MIT Thesis, June 1970.
11. Fagan, T. J., Thermal Considerations in the Design of Superconducting Generators, ASME Paper No. 74-WA/HT-23, November 17-22, 1974, page 8.
12. Bird, R. B., Stewart, W. E. and Lightfoot, E. N., Transport Phenomena, John Wiley & Sons, 1962, page 197, 411.
13. Hagedorn, D. and Dullenkopf, P., The Propagation of the Resistive Region in High Current Density Superconducting Coils, Cryogenics, May 1974, p. 264
14. Kothmann, R. E., Superconducting Magnet Research and Application to MHD Power Generators, USAF Contract 33(657)-10657, Second Quarterly Report, August 15, 1963.

15. Parker, J. H. and Towne, R. A., Superconducting Generator Design, Quarterly Report No. 4, EPRI Contract No. RP 429-1, November 1, 1976.

16. Batchelor, G. K., An Introduction to Fluid Dynamics, Cambridge University Press, 1967.

NOMENCLATURE

A	Constant
A_f	Flow Area
C_D	Constant, $0 < C_D < 1$
C_p	Specific heat at constant pressure
d	Diameter
F_o	Fourier number
G	Mass velocity
Gr	Grashoff number
g_c	Gravitational constant
h	Heat transfer coefficient
I	Electrical current
i	Enthalpy
J	Heat equivalent of work
j	Colburn "j" factor
k	Thermal conductivity
l	1/3 curve linear distance between radiation shield cooling channels
L	Length
M	Mass
$\dot{m}$	Mass flow rate
n_t	Number of tubes
Pr	Prandtl number
$\dot{q}'''$	Heat energy per unit volume
Re	Reynolds number
r	Radius
t,T	Temperature
p	Pressure differential, perimeter
V	Velocity
$\dot{V}$	Volume flow rate

Greek

α	Thermal diffusivity
β	Time constant, sec^{-1}
δ	Radiation shield thickness

ε	Void fraction
λ	Dummy variable
μ	Absolute viscosity
ν	Kinematic viscosity
ρ	Density, lbm/ft^3
τ	Time, sec
Φ	Dissipation function
ϕ	Dummy function
ω	Angular speed, sec^{-1}
χ	Vapor quality

Subscripts

b	Bulk
c	Critical
fg	Phase transition property
i	Inlet
(ℓ)	Liquid phase
o	Outlet, outside
r	Radiation
(v)	Vapor phase

3.2.1.4 Rotor Instrumentation

General

This section reports on the rotor instrumentation and telemetering system requirements for the superconducting turbine generator. This covers available state-of-the-art telemetering systems capable of handling the SCTG requirements, and discussion of the required transducers and sensors. Most of the work involved the search for and the consideration of sensors (transducers) suitable for the measurement of the parameters considered critical to the testing and operation of the machine. This involved discussions with many experts in various specialities at the Westinghouse R&D Center who had experience with specific measurement problems, as well as discussions with suppliers of sensors potentially applicable to the measurement of SCTG parameters.

The report contains a description of a recommended telemetering system approach, and a discussion of possible sensors for each class of measurement problem with some recommendations.

The work is by no means complete and is intended only to serve as a basis for further investigation and final selection of systems and sensors in the next phase of this program.

Quantities to be Measured and Telemetered

The quantities to be measured and telemetered to the outside of the rotor include the following general classes:

Temperature

- Cryogenic 4°K to 100°K (Inner Rotor, Winding, Radiation Shield, Portions of Torque Tube).
- Non-cryogenic (Damper Shield).

Flux Density

- At I.D. of Damper (Non-cryogenic).
- Within inner rotor (Cryogenic).

Displacement

- Inner rotor deflection of center of rotation; normal operation.
- Inner rotor vs. damper shield (radial) under severe fault conditions.
- Inner rotor vs. damper shield (tangential) under fault conditions.

Torque

- Flex shaft.

Vacuum Pressure

- In vacuum space.

Helium Level, Flow and Pressure

- In helium flow circuit.

These quantities can be further classified as "required for engineering test only" and "required for both engineering test and subsequent operation." A further distinction can be made between those quantities which can be multiplexed (i.e., sampled periodically at a relatively low rate) and those which must be measured and transmitted continuously (or sampled at a rate of at least 500 Hz) in order to determine peak magnitudes of transient effects.

Table 3-46 lists the quantities, their probable range, location of sensors, number of sensors, requirement for engineering test only vs. permanent operation, and suitability of multiplexed vs. continuous reading.

Cryogenic Temperature Sensors

Cryogenic temperature sensors considered included semiconductor diodes (gallium arsenide and silicon), semiconductor resistors (germanium), and carbon resistors. All of these are affected to a greater or lesser extent by magnetic fields. The only cryogenic temperature sensor found which is insensitive to magnetic fields is a strontium titanate capacitance type thermometer. However, available space and the complex circuitry required to derive temperature readings from capacitance changes rules out the use of this type of sensor in the SCTG rotor application.

All of the types of sensors mentioned in the preceding paragraph are made by Lake Shore Cryotronics, Inc.[1]

Table 3-46

SCTG ROTOR

Quantities to be Telemetered

Phenomenon	Range or Normal Value	Type of Sensor	Location of Sensor	No. of Sensors		**Reading	
				Permanent	Redundancy or Engrg. Test Only	Multiplexed	Continuous
TEMPERATURES							
Cryogenic	3 to 10°K	Carbon Glass Resistor	Lead Joint	1		Yes	
	3 to 10°K	Carbon Glass Resistor	Fld. Wdg., Center, Inner Surface	1		Yes	
	3 to 10°K	Carbon Glass Resistor	Fld. Wdg., Center, Outer Surface	1		Yes	
	3 to 10°K	Carbon Glass Resistor	Fld. Wdg., End Turns	2		Yes	
	3 to 10°K	Carbon Glass Resistor	Superconducting Joints	2		Yes	
	70°K	Carbon Glass Resistor	Radiation Shield	3		Yes	
	4°K	Carbon Glass Resistor	Torque Tube, Cold End	1		Yes	
	70°K	Carbon Glass Resistor	Torque Tube, Rad. Shield Support	1		Yes	
	275°K	Thermocouple	Torque Tube, Warm End	1		Yes	
Non-Cryogenic	50 to 150°C	Thermocouple	Damper Shield, Cu	1	5	Yes	
			Damper Shield, Steel	1	5	Yes	
DISPLACEMENT							
Inner Rotor Axis of Rotation	±10 mils	Strain Gage	Outer Surface of Inner Rotor	1		No	Yes

Table 3-46 (CONTINUED)

Phenomenon	Range or Normal Value	Type of Sensor	Location of Sensor	No. of Sensors Permanent	No. of Sensors Redundancy or Engrg. Test Only	**Reading Multiplexed	**Reading Continuous
Inner vs. Outer Rotor, Radial Fault Condition	Up to 2 in. at center	Strain Gage	Inner Surf. of Damper Shield	1		No	Yes
Inner vs. Outer Rotor, Tangential Fault Condition	±0.125 in. (±0.01 radian)	Strain Gage	Torque Tube	1		No	Yes
FLUX DENSITY	20-40 kG	Magneto-Resistor (MistoR)	Along I.D. of Damper at Field Winding	1	5 6	? ?	? ?
VACUUM PRESSURE	10^{-3}-10^{-5} Torr	See discussion	Coupled to Vacuum	1		Yes	
Helium Level Flow and Pressure		See discussion					

*Additional sensors included for redundancy or for use during engineering test only. The total of 21 does not imply need for this many additional telemetering channels, since for engineering test purposes a single channel may be manually changed from one sensor to another of the same type for successive tests.

**Readings indicated as continuous may be multiplexed if sampling rate is 500 per second or above.

NOTE: Accuracy of at least 10 percent overall in measurement of mechanical displacements will be considered acceptable.

The carbon glass sensor is much less affected by magnetic fields than the other types considered, with -0.23 K offset at 4.2°K and 15 T, the magnitude of the error varying at a rate somewhat less than the square of the field intensity.

Inasmuch as flux densities in the rotor are to be measured and telemetered, it will be possible to correct temperature indications for the magnetically induced offset, provided the field sensors are located sufficiently close to the temperature sensors to give a reasonably accurate indication of the field intensity at the locations of the latter. Location of the flux sensors near the temperature sensors is desirable, since as will be pointed out, the flux sensors recommended are affected by temperature, and iterative correction between the two may be needed to derive accurate readings for each quantity.

In summary, the carbon glass sensor is recommended for the measurement of cryogenic temperatures in the SCTG rotor. Further information on characteristics and physical dimensions are contained in the Lake Shore Cryotronics brochure.[1]

Non-Cryogenic Temperature Sensors

Sensing of the non-cryogenic temperatures (i.e., those associated with the damper shield) can be accomplished by conventional thermocouples. Telemetering system suppliers can supply thermocouples coordinated with their temperature telemetering systems. For example Acurex Corporation[9] supplies a multi-channel system including chromel/alumel thermocouples, with cold-junction compensation built into the telemetering modules.

Flux Densities

Sensors considered for possible application include sensing coils, Hall effect generators, and magnetic flux sensitive resistors. The latter are small, solid-state thin-film resistors, consisting of a grid of metallic bismuth, which changes resistance directly as a function of ambient magnetic field. The resistance change is independent of field orientation. Operating temperature range is 0°K to 95°C. These sensors are recommended over Hall effect generators because of the more complex wiring and the high control currents required by the latter.

Magnetic flux sensitive resistors are produced by American Aerospace Controls, Inc., under the trade name MistoR[2]. They are available in a wide range of nominal resistance values (1 to 10,000 ohms). Resistance values should be selected to coordinate with the nominal values of the temperature sensors in such a way that a single source of constant current or constant voltage excitation (supplied by the telemetering system supplier) can be used for measuring both phenomena.

As previously discussed, the resistance of the MistoR element has a temperature coefficient, and particularly in the portions of the rotor which are subject to temperature variations, and therefore they should be located near a temperature sensor so that the necessary cross-reference and correction can be made between the two.

Mechanical Displacements

The mechanical displacements of interest are the following:

- Relative motion of the axes of rotation of the inner rotor and the damper shield due to the different stiffness of the two structures. This results in a difference between their centers of rotation and hence relative radial motion at one cycle per revolution. This motion is estimated to be ± 10 mils maximum under normal operating conditions.
- Radial displacement of the damper shield inward toward the inner rotor as a result of the crushing forces developed under fault conditions. This displacement is estimated to be a maximum of .2 inches at the center of the rotor under the most severe conditions.
- Tangential (angular) motion of the inner rotor relative to the damper shield. Under severe fault conditions it is estimated that the inner rotor may be displaced angularly from its normally fixed position with respect to the damper shield by a maximum of ± 0.125 inch at the rotor surface (approximately .01 radian).

A wide variety of electro-optical and other devices were considered in the search for transducers applicable to the measurement of these mechanical quantities. Some of the devices investigated were:

Displacement of Axis of Rotation of Inner Rotor vs. Damper Shield under Normal Operation

A number of capacitive and inductive proximity sensors are available from various manufacturers as standard devices. However, all of these must be closely associated physically with oscillators of which they form an element of the tank circuit, or amplifiers in which they are a feedback element. The severely restricted space and the ambient conditions existing within the SCTG rotor may rule out the use of these devices.

A fiber-optics system of distance and vibration measurement, called a "Fotonic Sensor" is offered by Mechanical Technology, Inc.[3] In this system the probe element is the end of a 0.10 in. diameter bundle of optic fibers up to several feet long, half of the fibers transmitting light from a light source and half returning reflected light back from the target surface to a sensor. Investigation of this

system disclosed that without an auxiliary lens system too bulky for monitoring in the available space, the stand-off distance from the target surface is limited to a maximum of 30 to 50 mils. This system would require a small aperture in the radiation shield. The major limitation of the system, however, is that the required electronic circuitry has not yet been developed for the miniaturization and encapsulation necessary for withstanding the high "g" forces and other ambient conditions involved on the rotor.

An approach which shows some promise but will require more investigation and some development effort is the use of an "optical reflective sensor assembly" manufactured by Spectronics, Inc.[4] This device consists of a solid-state light source and a light sensor in a single assembly, with a built-in lens system focused to provide maximum output from the sensor when a reflective target surface is at an optimum distance from the assembly. Their Model SPX-1180 provides maximum output at a distance of 0.5 inch, with output dropping fairly linearly from 0.5 to distances up to 0.8 inch and possibly beyond. This device would also require an aperture in the radiation shield to allow it, when mounted on the inner surface of the damper shield, to "look at" a polished reflective surface on the inner rotor.

One question with respect to the application of this device is whether the reflectivity of such a mirror surface, mounted on the cryogenic portion of the rotor, would remain sufficiently free of condensation to maintain consistent reflectivity over a long period of time.

The necessary voltages and operating currents for such a device are compatible with those used in the operation of typical rotor telemetering equipment, and could be supplied as a part of the telemetering system.

Questions yet to be answered are the inherent long-term stability of the device and the stabilization of the signal conditioning electronic circuitry (if required by the telemetering system). The standard device is rated for both operation and storage up to 100°C, which indicates that the manufacturer may or may not be able to supply a device which will withstand without damage the 150°C maximum temperature which the damper shield may reach following fault conditions. The mounting details of the SPX-1180 device are not well suited to its attachment to the inside surface of the damper shield, but the manufacturer could no doubt supply a more adaptable mounting arrangement on special order.

A weldable strain gage, suitable for cryogenic temperature, mounted on the inner rotor surface at the axial center of the rotor could be used to sense the deflection of the center of rotation, independently of the deflection of the damper shield. The deflection of the latter could be sensed independently in similar fashion by a strain gage mounted on its inner surface. The two deflections could then be compared to give relative deflection if that quantity is of importance. Strain gages are conventionally used with available rotor telemetering systems, and excitation sources are customarily supplied as part of the telemetering system package.

Since the initial efforts in this investigation were devoted to a search for suitable optical methods, only recently have conversations taken place with strain-gage suppliers, some of whom have supplied literature, specifications, and specific recommendations.

In general, strain gage suppliers feel that it is feasible to use strain gages for deflection sensing on both the inner damper shield surface and the cryogenic surface. As to the question of the behavior of strain gages in heavy, varying magnetic fields, they report that while the strain gages they would recommend are built to be essentially non-inductive, there is some remaining inductance. However, they have used successfully in such applications an identical gage as a dummy gage, mounted flat on top of the active gage and connected with opposite polarity to balance out magnetically induced voltages and currents.

In summary, while the optical device described in this section is potentially applicable approach, the use of strain gages as described is a more direct, time-tested approach, is compatible with standard telemetering systems, and is the approach currently recommended.

Radial Inward Displacement of Damper Shield under Fault Conditions

This problem and the applicable approaches are almost identical to those discussed above. The main difference is that the deflection involved is much greater (up to 0.2 inch at the axial center of the rotor). Similar optical solutions to those described above were investigated, and the most promising optical solution appears to be the Spectronics reflective sensor assembly.

However, the most straightforward solution again appears to be a strain gage (with a different gage factor from those previously discussed) bonded to the

inner surface of the damper shield, with an identical dummy gage superimposed and connected in reverse to neutralize magnetic effects.

The Magnaflux Corporation (Chicago) has supplied literature and specific recommendations for this application.

Tangential (Angular) Displacement of Inner Rotor vs. Damper Shield under Fault Conditions

Possible opto-electronic solutions investigated included the following

- An LED light source, mounted on the inner surface of the damper shield, with a cylindrical lens which focuses a narrow band of light upon the inner rotor through an aperture in the radiation shield. On the inner rotor surface, one of the following:
  - -- A triangular "patch" of photovoltaic material (e.g., a silicon junction photosensor), the output of which would vary depending upon the width of the triangle at the point where the light band strikes it at a given instant.
  - -- A photo-potentiometer or photobridge device (both made by Solar Systems, Inc.,[5]) in which the resistance of a potentiometer of the balance of a resistive bridge is dependent upon the position of an impinging band of light.
    While these devices may be potentially applicable, considerable development would be required. The standard devices are not rated for cryogenic operation, and the manufacturer has not supplied information sufficient to determine whether operation under such conditions is possible with special devices. There is also a question as to the time constant of the response of the standard devices.
  - -- An in-line array of planar photodiodes made on an InAs or InSb crystal. Such arrays are made to order by Spectronics, Inc.[6] (previously referred to in this report). Both InAs and InSb are commonly used at cryogenic temperatures, since they perform best at such temperatures, and the dewars normally supplied with them would be unnecessary. An infrared light source[6] would be used with such a detector array. A major disadvantage of this approach is that a special mask may have to be created for the fabrication of such an array, at a cost of several thousand dollars, unless the manufacturer has already created such a mask. The Spectronics literature on these devices (Reference 6) illustrates such an in-line array with .002" x .020" elements arrayed end-wise which would give .02" resolution, not sufficient for our purposes. A similar array with .01" wide elements arrayed edge-to-edge, would give approximately .01" resolution, sufficient for better than 10 percent accuracy in the ± 0.125 inch maximum excursions expected. This would require 26 leads (including one common lead) from the sensor, however, and is an impractical approach for this reason alone.

A way to reduce the number of required leads would be to make the array in such a way that a binary digital output would be generated. This could be done by dividing the sensitive surface into say 5 separate insulated strips parallel to the working direction, and masking off each strip to separate it into sensitive bands of the width needed so that the presence or absence of an output bit from each strip would indicate in 5 bit binary code the position of the light band across the strip. With 5 such strips, an accuracy of 1 part in 32, or better than 10%, could be obtained for a total 0.25 inch excursion of the light band. Six leads, including a common lead, would be required.
Obviously such a system would require development, but standard integrated circuit packages are available to perform any necessary signal conditioning and the digital to analog conversion such a system would require.

In view of the questions that remain unanswered with respect to the opto-electronic systems described, and the development that any one of them would require, the present conclusion is that the rotor angular deflection should be sensed by the use of two strain gages. One of these could be placed on the torque tube at the exciter end of the inner rotor and the other on the inner surface of the damper shield at the same axial location. The angular deflection can then be determined by comparison of the torque tube strain with the strain on the damper shield.

It is possible that calculation would show that the strain on the damper shield is negligible by comparison with that of the torque tube, and that the strain on the torque tube alone would be sufficient to give the angular deflection with the required accuracy. In this case the second gage on the damper shield would be unnecessary. In either case, however, the problem of calculating deflection taking into account the torque tube temperature gradient will exist, and this will require further study.

Torque (Flex Shaft)

The measurement of torque in the flex shaft is a conventional problem, and no unusual conditions are present. A weldable strain gage should be used since this is to be a permanent installation. Information from manufacturers is forthcoming and will be added to a later version of this report.

Vacuum Pressure

One of the key design features for maintaining the thermal isolation of the inner cryogenic rotor relative to the outer room temperature damper cylinder

is the sealed off vacuum space between these cylindrical shells. It is important to be able to monitor changes in pressure, especially if it falls into the low 10^{-3} Torr range, in order to be able to program an orderly shutdown. The pressure gauge will be measuring only helium gas since the other gases will be cryopumped. Having a pressure monitor will be very important for the first prototype generator as a test of seal weld and container integrity.

The most suitable gauge or sensor for following the pressure (vacuum) in the rotor thermal isolation space appears to be the Phillips Ionization Gauge (PIG). This gauge has the following characteristics that make it suitable for this rotating application,

1. mechanically rugged electrode configuration
2. high output over range of 10^{-3} to 10^{-5} Torr
3. relatively insensitive to variations in magnetic fields axial to the gauge geometry.

The last point deserves further comment. What data that does exist indicates that the axial field can be increased significantly above the $\sim$ 0.1 T level of commercial gauges without sizable changes in sensitivity. However this gauge may be more sensitive to transverse field. Before any decision on final acceptance of this type of gauge, it will be necessary to measure gauge sensitivity to both axial and transverse external fields. It may very well be necessary to build in a magnetic shield around the gauge to reduce the effect of outside fields to a sufficiently low level.

It is possible, with proper alignment and location of the gauge relative to the field winding of the rotor, to utilize the magnetic field from the rotor itself as the gauge bias field. These questions of required shielding and bias field must remain uncertain until experimental studies can be carried out.

Commercial versions of this gauge are available from CVC Bendex and Varian. It may be possible to use commercial gauges with modification and if not, then electrode configuration can be designed special for integration into the rotor.

Helium Level, Flow and Pressure

As important as the cryogenic temperature sensors discussed above, are sensors for measuring and/or monitoring the helium level in the rotor and measuring the flow and pressure in the helium circulation system.

The cryogenic sensors, i.e., temperature, level, flow and pressure are most important for engineering or model tests. Such tests involving a model or test rotor are discussed in the Development Plan Section. While temperature and level sensors would be incorporated into the demonstration machine rotor for monitoring performance during utility system tests, it is likely that flow and pressure sensors will not be required for the demonstration machine.

Level Sensor. The proposed helium management system involves an automatic liquid level control based on the level difference between gas and liquid heads. This concept must be experimentally verified with model rotor test during the "Critical Component Test" phase of the development program. A reliable and rugged level gauge is required for design verification.

The most suitable level indicator for this application is the superconducting wire sensor. Here, current is passed along a length of NbTi conductor which extends part way into the liquid bath. The current through the conductor is adjusted so that the part which is exposed to the gas phase is in a normal state while the remaining length is covered by liquid and is superconducting. Therefore the height of the liquid is proportional to the net resistance of the conductor.

This type of sensor is manufactured by American Magnetics. These sensors have been used at Westinghouse for several years and have proven to be quite reliable under static conditions. There is no reason to believe that they cannot be applied successfully to rotating systems.

Flow and Pressure Sensors. During design verification tests of helium management system, it would be extremely desirable to have sensors for measuring helium flow at critical points in this flow circuit. For example, the proposed design depends on initiation of convection loop flow due to heat loads in the field winding and cold structural support during fault periods. Also under steady state conditions, there is a steady flow of liquid helium to the rotor bath and consequent flow of vapor to the torque tubes and electrical leads. Further there are a few points where the helium divides into parallel paths. All of these features, convection loop flow, steady flow of vapor, division of flow into parallel paths, demand experimental verification of their performance.

Sensors for measuring helium flow and pressure and of a size suitable for integration into a machine rotor are not commercially available at the present time.

One approach to flow measurements is to measure the pressure across a calibrated aperture. There are several prototype cryogenic pressure sensors now under development and test. A pressure sensor that depends on sensing the change in Q of an RF cavity is being worked on at the NBS Cryogenic division at Boulder. A diaphragm sensor using thin film strain gauges is being developed in the Mechanical Engineering Department at MIT.

This latter pressure sensor appears to be the most promising in terms of sensitivity and size. We would propose to explore this type of sensor as part of critical component test phase of the development program.

If this sensor demonstrates sufficient sensitivity, we would propose to attempt to use it, coupled with calibrated apertures, to measure flow at critical points in the model rotor during performance verification of the helium flow circuit. If this sensor cannot meet sensitivity and stability requirements, then other flow sensor concepts, for example those based on time of flight of a heat pulse or ultrasonic phase shifts, must be explored.

Aside from using pressure sensors to determine flow, it is not clear at this time how important it is to measure pressure alone. It is true, that pressure combined with temperature fixes the thermodynamic state of the helium and as such would be valuable to know as a function of position, for example radius, in the rotor. However there is a practical limit to the amount of instrumentation that can be utilized in the contemplated model tests. It is proposed to defer this question until the development phase of the present program.

Telemetering Systems

In view of the large number of quantities to be telemetered from the SCTG rotor, it is apparent at the outset that a multiplexing system approach will be required to minimize the number of radio-frequency carrier signals to be transmitted. In multiplexed systems, individual quantities are sampled periodically at a fixed rate, each in turn altering some characteristic of the transmitted signal in proportion to the magnitude of the quantity. In the receiving equipment, each sample is read in turn and an analog output parameter (e.g., voltage) is set to a corresponding value for that particular output channel, maintaining this value fixed until the succeeding sample is transmitted and read.

If the rate of sampling is at least twice as high as the equivalent frequencies represented by the minimum rise and decay times of the quantities to be measured, the output samples will provide an adequately accurate representation of the varying quantity.

There appear to be two viable companies in the industrial telemetering field which supply equipment basically suitable for the SCTG requirements. Each has a multiplexing system which they claim has been successfully applied to similar applications.

One of these companies is Industrial Metrologists, Inc. (INMET).[8a, 8b] The other is Acurex Corporation.[9]

The basic r-f equipment of both companies operates at a carrier frequency within the standard F-M broadcasting band (88-108 M Hz). Their multiplexing approaches differ somewhat.

INMET supplies a multiplexing system in which one or more audio sub-carrier oscillators (one for each 15 quantities to be telemetered) is used to frequency-modulate an r-f carrier. A four-bit binary code generator is used to switch the sub-carrier oscillator to 16 different signal channels in turn. One of these 16 channels is reserved for a synchronizing signal, leaving 15 channels for the variable quantities. Each channel in its turn shifts the frequency of the sub-carrier oscillator in proportion to the magnitude of the variable input quantity. In the receiver, the synchronizing signal is detected and the sub-carrier frequency shift for each variable channel is converted to an independent output voltage reading for that channel which is maintained until the next sample is available.

INMET states that this system can be supplied for either 15 or 30 independent multiplexed quantities, with sampling rates as required from 2 to 10 samples per channel per second.

INMET states that they will supply, as a part of their telemetering system, signal conditioning and voltage or current excitation sources as required by the sensors finally selected for the SCTG application. They also state that they can supply a proposal on the SCTG system when requirements are more firmly established.

The Acurex system as presently manufactured uses a separate r-f module for each six quantities to be telemetered, with a sampling rate which gives a 25 Hz frequency response for each channel. This is more than adequate for temperature telemetering, but inadequate for the mechanical displacements, where a response of at least 300 and preferably 500 Hz is required to determine peak values.

Thus, it is not possible to specify in detail at this time the complete telemetering system. However, when sufficient information on sensor selection and excitation requirements is developed, both Acurex and INMET are available as suppliers.

REFERENCES

1. "Cryogenic Instrumentation" and "Application Notes for Cryogenic Sensors," Lake Shore Cryotronics, Inc., 9631 Sandrock Road, Eden, N.Y. 14057.

2. "MistoR (TM) Series MRA," American Aerospace Controls, Inc., 129 Verdi Street, Farmingdale, N.Y.

3. "KD-100 Fotonic Sensor," MTI, Mechanical Technology, Inc., 968 Albany-Shaker Road, Latham, N.Y. 12110.

4. "SPX-1180, Reflective Sensor Assembly," Spectronics, Inc., 830 Arapaho Road, Richardson, Texas 75080.

5. "Photo-Potentiometers," Solar Systems, Inc., 1001 East Touhy Avenue, Des Plaines, Illinois 10018.

6. "Infrared Products," SPX-102, Spectronics, Inc., 830 Arapaho Road, Richardson, Texas 75080.

7. "Scientific Foundations of Vacuum Technique," Dushman-Lafferty, J. Wiley and Sons, 1949/1962.

8a. "Multiplexed Temperature Telemeter PAM-7 Model 307 Description and Specifications," INMET, Industrial Metrologists, 987 Pine Treee Drive, Indian Harbour Beach, Florida.

8b. "Multiplexed Temperature Telemeter (Slip-Ring Adapted) PAM 7/15 Model 296 Description and Specifications," INMET, Industrial Metrologists, 987 Pine Tree Drive, Indian Harbour Beach, Florida.

9. "Multi-Channel Temperature Measurement for Rotating Machinery," Acurex Corporation, 485 Cylde Avenue, Mountain View, California 94042.

3.2.2 Stator Design

General Introduction and Requirements

The design opportunities offered by superconducting field windings make armature concepts possible that could not be considered with conventional field conductors. These new concepts include configurations for direct generation at extra-high voltage which permit immediate connection of turbine generators to transmission line terminals or to converter valves for HVDC transmission. The following discussion describes the basis for the design of stator windings. It considers the general requirements applicable to present turbine generators as well as those specified by EPRI Contract No. RP 429-1. Configurations capable of satisfying these requirements are presented and analyzed. Final selection of configurations best suited to the EPRI requirements is predicated on application of a new "spiral pancake" winding concept, which has been disclosed to EPRI for filing of patent applications.

The final designs of armature windings for all applications considered in this report are based on the spiral pancake configuration concept.

EPRI specifications for the design of the 300 MVA machine require that consideration be given to the following criteria in the design of the stator:

- Mechanical stresses on the armature under steady state and transient conditions.
- Electrical stresses at steady state and under switching surges, lightning strikes and other transient conditions.
- Structural and insulation schemes capable of carrying the mechanical and electrical stresses, with at least a 70 kV armature voltage.
- Armature coolant and construction of internal cooling system.
- End connections, their geometry, support, cooling, insulation and connection method.
- Extent of stranding and transposition required and fabrication means for adequately stranded and transposed bars.
- Natural frequencies.

Industry groups, in particular the American National Standards Institute (ANSI) have for many years been active in defining the standard requirements for the windings of electrical machines. These apply to machines of conventional design. They are useful, nevertheless, as a basis for defining requirements for superconducting machines.

The general requirements for armature windings of synchronous machines are defined in ANSI C50.10, and those for cylindrical rotor synchronous generators in ANSI C50.13. These standards specify, amongst other requirements, the insulation systems for windings, methods of temperature determination, voltage wave shape, dielectric test voltage, limiting temperatures or temperature rises, and thermal as well as mechanical requirements applicable during short-time overload or fault conditions. It should be understood that these standards undergo periodic review by panels with full industry participation. Large equipment manufacturers, such as the present contractor, follow these developments closely, and attempt to use the best up-to-date concepts in their design efforts.

The latest revisions (1977) of the ANSI C50 standards specify the following requirements for armature windings of conventional turbine generators:

- For continuous operation at rated load:

  1 — The hottest spot temperature is intended not to exceed 130 C for Class B insulation systems.

  2 — For internally liquid-cooled windings, the inlet temperature of the cold coolant shall be 45-50 C.

  3 — The limiting temperature rise of the liquid coolant shall be 55-50 C (for a total coolant temperature of 100 C).

- For short time overloads:

  The armature shall be capable of operating at 130 percent of rated armature current for at least one minute, starting from stabilized temperatures at rated conditions. For times up to two minutes, the capability to accommodate the same increment of heat storage as that defined for 1 minute is required:

Time (seconds)	10	30	60	120
Armature current (percent)	226	154	130	116

  It is assumed that such conditions do not occur more frequently than two times per year.

- For short circuits:

  The generator shall be capable of withstanding, without mechanical injury, any type of short circuit at its terminals for times not exceeding short-time thermal requirements, when operating at rated kVA and power factor and five percent overvoltage, provided the maximum phase current is limited by external means to a value which does not exceed the maximum phase current obtained from the three-phase fault. In the case of stator windings, the criteria for no injury is that the windings can satisfactorily withstand a normal maintenance hi-potential test. There shall also be no visible abnormal deformation of damage to the winding coils and connections.

- For dielectric test:

  The dielectric test voltage for a new high voltage armature winding is 1000 volts plus twice the rated voltage (rms value of 60 Hz ac wave). For maintenance tests, a dc voltage of 114 percent (1.7 x 0.67) of the rms value of the ac test.

The dielectric test requirements are appropriate for armature windings designed and built according to conventional practices. In terms of insulating and impregnating materials that are used in modern machines, this means a technology that is based on micaceous insulating material in combination with synthetic resin impregnant. Such a technology is not applicable for armature voltage ratings much in excess of 35 or 36 kV. It would not be applicable, in particular, to ratings of 70 kV or above. A new approach for windings suitable for high voltage ratings is described in the following. Standard requirements do not exist for this type of winding. Standard requirements do exist for the high-voltage windings used in transformers, and may be of some value in the eventual definition of standard requirements for the armature windings of high-voltage superconducting turbine generators.

3.2.2.1 Stator Electrical Design

The high mmf capability of the superconducting rotor winding reduces the need for magnetic material in the flux path and thus permits elimination of stator teeth. The space freed thereby can be used for increasing the cross-section of the armature winding. This has provided opportunities as well as challenges to the designer:

- The ground plane no longer interpenetrates the winding. It is therefore possible to reorganize the insulation so as to obtain increased voltage capability.
- More uniform distribution of dielectric stress is made possible by the resulting more uniform spacing and winding capacitances.
- Without the protection offered by teeth, the armature conductors are exposed to high magnetic fields and the resultant stray losses and electromagnetic effects.
- The steps required to control the losses and heating, such as fine stranding of the conductors, tend to reduce ability to withstand electromechanical force effects.

Design opportunities presented by superconducting field windings have been used to advantage to define the armature winding for a 300 MVA turbine generator with a voltage rating of 230 kV. This is about 15 times higher than previously possible with conventional practice, and is high enough to permit direct connection to the transmission system without a step-up transformer. Data for this design are tabulated in Section 3.5.

Increased Voltage Capability - EHV Turbine Generators

History

Interest in the use of high armature voltage ratings for turbine generators dates back to the early years of the industry. Voltage ratings of 16.5 kV were realized in 1906, 22 kV in 1919, and up to 36 kV in 1932.[1] The incentives for this effort were the reduction in armature current, and the accompanying reduction in the current-carrying requirements of associated equipment, as well as the possibility of connection directly to a transmission or distribution system. The arrangements used to achieve up to 36 kV in 1932 are now principally of historical interest, and have not been applied to practical turbine generator construction in recent decades. (The voltage range used in large modern turbine generators of conventional construction is of the order of 24 kV to 30 kV, and is believed to be capable of extension at least to 34 or 36 kV.)

Theoretical studies of superconducting generators and other machines with airgap armature windings have emphasized the opportunity to use the increased voltage capability in order to achieve high voltage ratings. A detailed study, predicated on the use of airgap windings for both the rotor and stator[2], contemplated the rating of 2000 MVA at 60 kV, and the use of an oil-filled encapsulated stator to achieve the high voltage rating. Other studies[3,4,5,6] have encouraged the expectation that superconducting generators could readily be designed to operate at voltage ratings suitable for direct connection to the transmission grids of large power systems. Although moderate increases in rated voltage, to twice or three times the conventional level, might offer some benefits such as:

- Reduced cost of generator main bus
- Easier low voltage circuit breaker application
- Easier application of cable connection to remote transformer

It has been recognized for some time that a major economic gain might be realized by elimination of the main step-up transformer. This requires an increase in voltage of more than 10:1 above the conventional level.

Technical Potential

The design of armature windings for voltage ratings that are an order of magnitude or more higher than those which have proven successful over a period of decades is a major undertaking that must be well founded and adequately substantiated. The need for it must be firmly established, and the means for accomplishing

this objective must be carefully studied and thoroughly understood. In the following, the economic justification for such an effort will be reviewed on the basis of matching generator capabilities to those of the power system. This requires consideration of transmission lines, circuit breakers, and underground cable relays.

Transmission Line Considerations

The choice of transmission voltage depends upon the power that is to be transmitted as well as on the distance between sending and receiving ends. Table 3-47 taken from Reference 7 shows power limits for relatively short, low-voltage lines. Generators in the range of 1200 to 3000 MVA may be expected to require extra-high-voltage (EHV) or ultra-high-voltage (UHV) transmission lines.

The kilowatt capacity of a tie line may be estimated as equal to 4 $(kV)^2$. On this basis, the power capacities of lines at different voltage levels are plotted in Figure 3-97. On the same figure, the levels of transmission line studies reported in Reference 8 are superimposed, and indicate that the estimating equation $4(kV)^2$ is, if anything, optimistic in predicting line kW capability. Therefore, to match required line voltage at its MW capability, generator voltage must be at least equal to $(250\ MW)^{1/2}$. This gives about 520 kV for a 1200 MVA generator, and about 822 kV for a 3000 MVA generator. It will be assumed that these values correspond to the standard voltages of 500 kV and 765 kV respectively.

TABLE 3-47

POWER LIMITS FOR TRANSMISSION LINES

Line Voltage and Characteristics	KW Which Can be Delivered Based on 10% Loss and Equal Voltage at Sending and Receiving Ends			
	Distance in Miles			
	40	80	120	160
132 kV - 16 ft spacing				
Stranded Copper				
4/0	116000	58000	39500	30100
300 MCM	172000	86000	58800	44800
500 MCM	297000	150000	101000	77100
220 kV - 24 ft spacing	80	160	240	320
Hollow Copper				
500 MCM	425000	219000	151000	119000
ACSR - 795 MCM	417000	216000	149000	118500

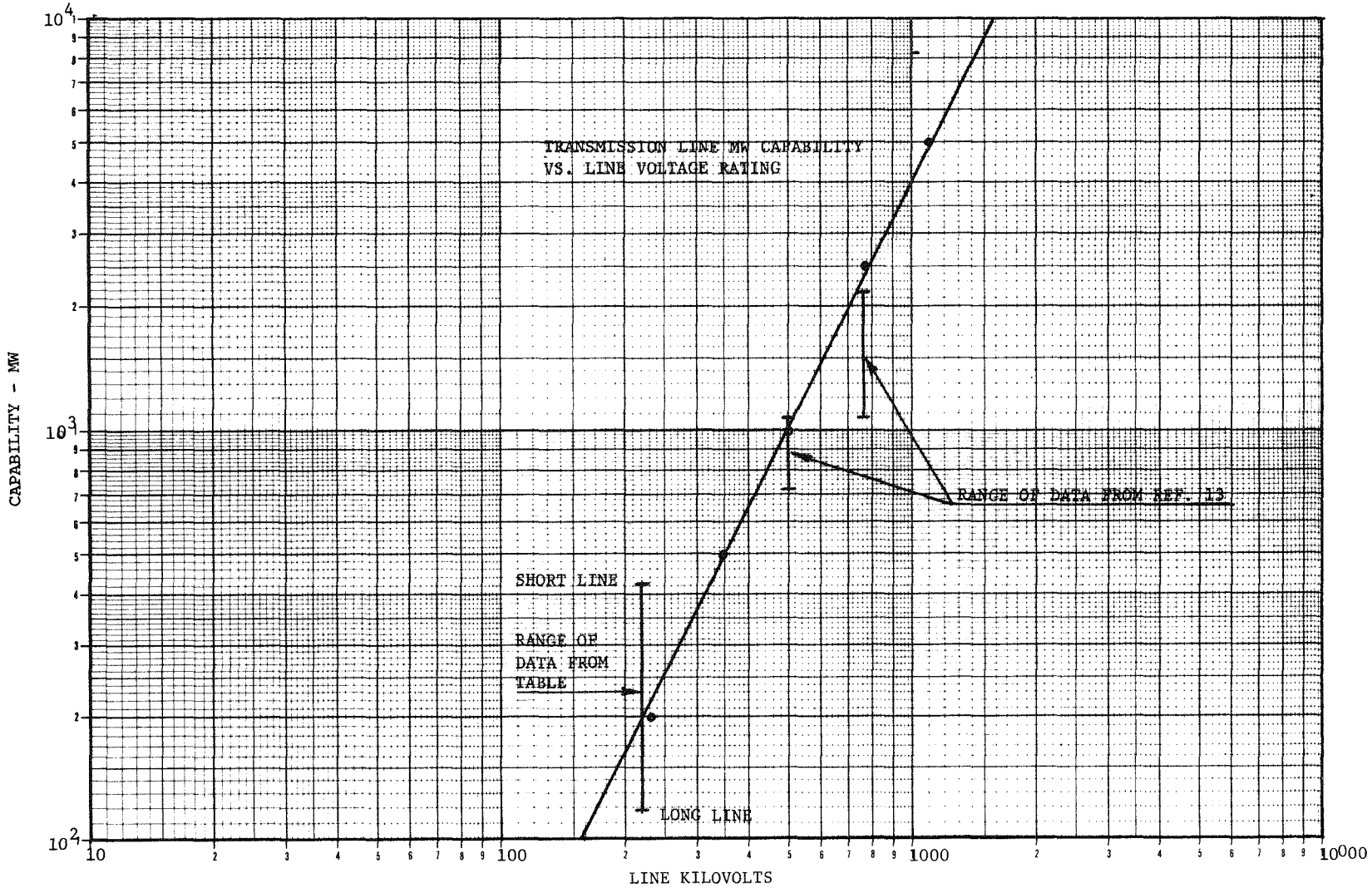

Figure 3-97. Transmission Line NW Capability Vs. Line Voltage Rating.

Transmission lines are exposed to overvoltages of various kinds, in particular, lightning and switching surges. The design and coordination of the insulation used in various power system components proceeds from a knowledge of the surge voltages resulting from these surges at the terminals of the specific apparatus. Protective devices such as lightning arresters[9] and surge capacitors are widely used to reduce the exposure of power system components. Reference 10 gives a detailed bibliography of this subject. To provide a common basis for the design of various types of apparatus, the net effects of lightning exposure and action of protective devices are combined in defining a basic impulse insulation level or basic impulse level (BIL). This level can then be used in designing the insulation for the specific apparatus.

Specific values of BIL are conveniently required for transformers and reactors connected to transmission lines, but not for turbine generators which are normally connected through step-up transformers. It should be noted that the concept of BIL has developed in concern with the development of insulation systems, such as the oil-immersed systems used in many transformers, and is not compatible with the mica-based systems used in conventional generator windings. This will be discussed in greater detail in the following.

Circuit Breaker Considerations

Possible advantages of high terminal voltage ratings and accompanying low current ratings relate to the possibility of applying circuit breakers at the generator terminals. This would permit isolation of the generator from the system more easily and perhaps more quickly[11]. Table 3-48 lists a series of circuit breaker capabilities in the range of 15 to 169 kV. It will be noted that circuit breaker requirements are less restrictive on MVA rating than transmission line requirements.

Table 3-48

CAPABILITY AND RATING OF CIRCUIT BREAKERS
15 TO 169 kV

Voltage Class, kV	Continuous Current Capability, Amperes	Interrupting Rating	Approximate Max. Generator MVA
15	4000	1500 MVA	104
34.5	3000	2500 MVA	180
69	2000	5000 MVA	240
145	3000	63 kA	750
169	2000	50 kA	1000

Underground Cable Relay Considerations

System planning could be facilitated and plant siting given greater flexibility if the generator can be separated from the transmission line terminal by an appreciable distance, of the order of several miles, with an underground cable relay between the power station and the substation. The current status and active development of power cables indicates that high capacity cables for these purposes are likely to be available if and when the need arises.[12,13] Expected capabilities of oil-filled, paper insulated cables in the voltage range of 750 to 1300 kV are illustrated in Figure 3-98.

Economic Analysis

The detailed economic analyses of superconducting generators have identified impressive economies that can be attained with superconducting generators having low-voltage armature windings. For a unit of 1200 MVA rating, costing about $10,000,000, savings of $3,000,000 to $5,000,000 have been shown. The potential savings expected with an EHV armature are an additional $3,000,000 and comes from reductions in capital investment and in fuel costs of the unit transformer.

The potential savings in capital investment are graphically illustrated in Figure 3-99 which shows the simplifications and space savings in power plant design with an EHV superconducting turbine generator as contrasted to one of conventional design. (Solid lines illustrate the EHV SCTG arrangement; dash-dot lines the conventional arrangement.) The additional possibility of further extending the cable connection to the pothead so as to favor the substation or switchyard design is not specifically illustrated.

Economic analyses with respect to alternate armature voltage ratings were done in the second quarter of this contract. The following is based on the information presented in Table I, pp. 3-143 to 3-144 of Quarterly Report No. 2, and on the assumptions that are listed on p. 3-148 of that Report. One possible source of savings was not included in this analysis. This is the reduction in losses and consequent increase in plant output that would result from the elimination of a step-up transformer. At the present stage of the studies of high-voltage armature designs it appears likely that most, if not all, of the losses associated with the transformer could be eliminated. In other words, the armature voltage rating does not appear to affect the generator efficiency greatly. If it is assumed that transformer losses typically amount to 0.15 percent for large power transformers, and that pessimistically only 1/2 of this could be eliminated, it is possible

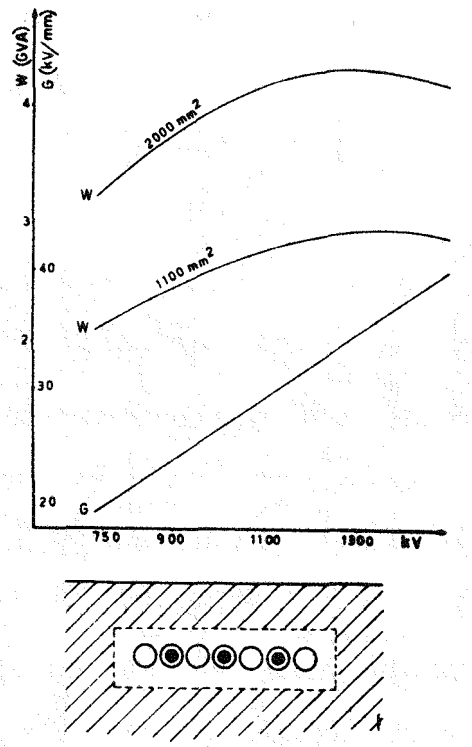

Figure 3-98. Maximum Working Stress and Power Transmitted by Three Single-Core O.F. Cables of the 750 kV Class as a Function of the System Voltage

Source: Reference 13.

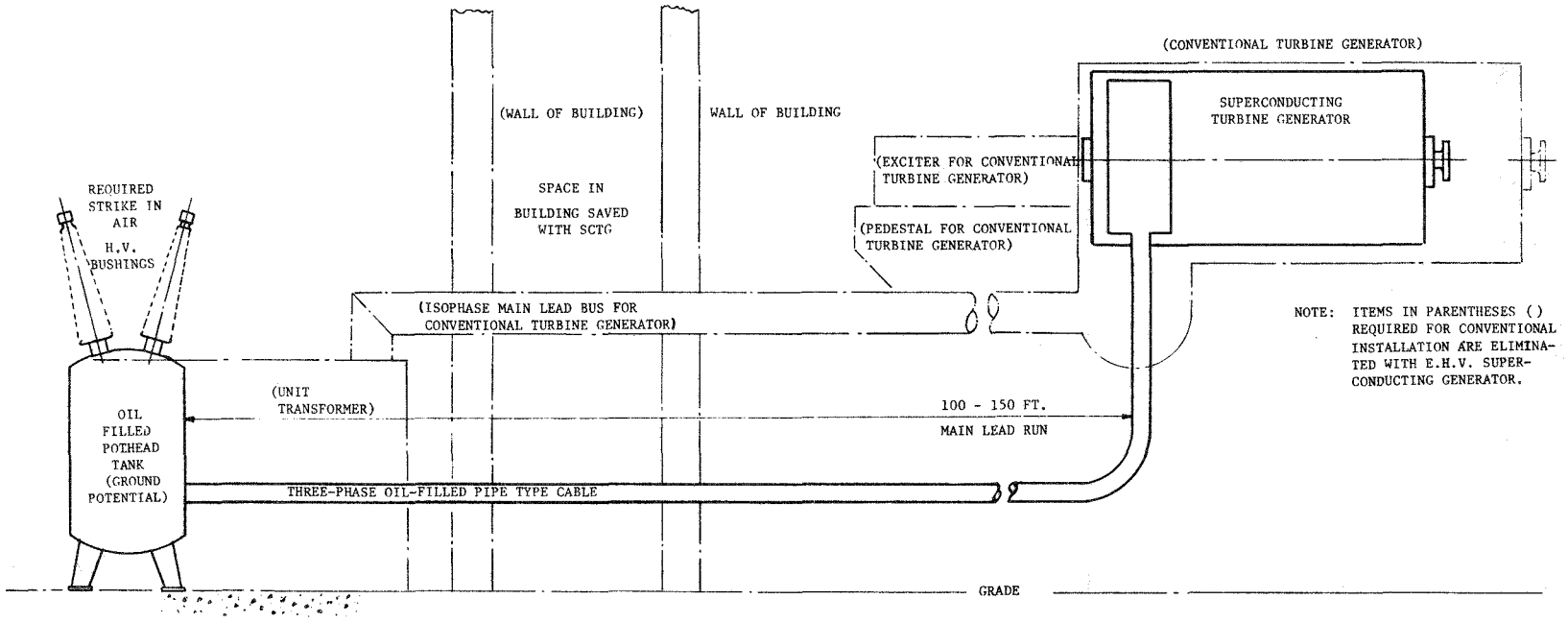

Figure 3-99. Comparison of Conventional Turbine Generator Installation With E.H.V. Superconducting Generator Installation Concept

to calculate total savings, using the average savings per kilowatt listed in Table II page 3-133 of the Report. For a 1000 MW plant, this saving would be 0.0015 x 1000000 x 1373/2 or $1,029,750. Incorporating this into the evaluations listed in Table I on pages 3-143 and 3-144 of the Report changes the overall evaluation in Arrangements J, K, and L. Table 3-49 lists the revised estimated, and compares them to the original estimates for the base case A at 34 kV armature voltage and the alternate case C at 70 kV armature voltage. The basic result of these studies with regard to the economic benefits of 70 kV and 500 kV armature voltage remains, however, unchanged. This result is:

> In order to secure significant improvements in power plant cost it is necessary to increase generator voltage rating to the transmission line level and thereby eliminate the unit transformer and its losses.

Stator Insulation for EHV Generators

This conclusion made a search for new winding concepts imperative. No known turbine generator winding design or concept was demonstrably capable of meeting the EHV objective at that time. An evaluation of the high voltage capabilities of conventional turbine generator windings revealed the following:

Studies of the impulse strength of conventional turbine generator insulation and of the surge exposure of large (normally unit-connected) turbine generators have shown that the insulation of turbine generators as installed in normal system configurations is rather well coordinated to the requirements. The following conclusions are drawn in Reference 14 with regard to mica-based insulation:

> "1. The voltage endurance curve of mica insulations indicates at least a 10-percent increase in insulation level for a decrease in time of voltage application to one-tenth.
>
> 2. From the foregoing it appears that for a 30-percent increase of the impulse level over the 1-minute peak value the cumulative surge time to failure should be about 1/1,000 minute (10^{-3}) which is 0.06 second or 60,000 microseconds.
>
> 3. In correlating the voltage endurance data with the fact that the ground insulation wall has withstood the 1-minute ASA* proof test, it can be concluded that the insulation will withstand many impulses of 100-microsecond duration whose voltage peak does not exceed the peak of the 1-minute proof test by more than 25 percent. (This has also been demonstrated by tests on insulation specimens.)"

Predicated on this level of dielectric strength, it was concluded in Reference 15 that: "Comparison of the winding insulation level with its maximum

Table 3-49

ECONOMIC EVALUATION OF SOME ALTERNATIVE SUPERCONDUCTING GENERATOR TERMINAL VOLTAGES AND STATION LAYOUTS

Arrangement*	A	C	J	K	L
Machine Voltage	34 kV	70 kV	500 kV	500 kV	500 kV
Switchyard Location	1500 ft	1500 ft	1500 ft	5 miles	1500 ft
Method of Power Transfer	Isophase Bus-Overhead Line	Isophase Bus-Over-Head Line	Cable - Overhead Line	Cable	Overhead Line
Item Evaluated					
Overhead Line	0	0	-88,500	-1,646,100	-88,500
Underground Cable	0	0	+1,144,000	+10,780,000	0
Isophase Bus	0	-69,300	-222,600	-222,600	-222,600
Main Step-Up Transformer (incl. foundation and loss eval.)	0	+60,000	-3,499,750	-3,499,750	-3,499,750
Auxiliary Transformer	0	+13,000	+623,000	+623,000	+623,000
Total Difference Referred to Base Case A	0	+3,700	-2,043,850	+6,034,550	-3,187,850

Note: - indicates cost savings, + indicates cost increase.

*Letter designations same as used in Table I, pp. 3-143, 3-144 of Quarterly Report No. 2, April 19, 1976.

attainable surge voltage revealed that in a unit-connected scheme, the generator insulation is well coordinated with its connecting transformer. The lightning arresters at the transformer terminals protect the transformer and the generator as well."

Evidently, the proper coordination of generator insulation level with the level of protection afforded by the lightning arresters and surge protectors must also be assured in the event that the transformer is eliminated by means of a sufficiently high armature voltage rating. This means that a BIL rating would be required for the armature winding.

Basic Impulse Level

A basic insulation level or basic impulse insulation level (BIL) is generally specified for the insulation of apparatus whose dielectric strength must be coordinated for direct connection to the transmission system. ANSI standards include such requirements, for example, for oil-immersed transformers and for outdoor apparatus bushings. Table 3-50 reproduces the requirements of ANSI Standard C57.12.00-1973, "General Requirements for Distribution, Power, and Regulating Transformers" (IEEE 462). In actual practice, voltage ratings beyond the limits of this table are now employed, and variations from the voltage relations specified in the table may be expected, especially in the higher range of voltages. Large Westinghouse power transformers rated at 500 kV may have any one of the following BIL values: 1300, 1425, 1550, or 1675 kV, as specified by the user. In addition, the BIL of the neutral end of a winding may be lower than that of the line end, depending on the method of grounding. For solidly grounded equipment, the difference may be substantial.

High Voltage Insulating Materials

Even a cursory review of the materials and practices used in insulating high voltage apparatus used for power systems reveals the predominance of oil-impregnated cellulose products. An excellent overview of their properties is provided in Reference 16. Applications are discussed in Reference 17. In favorable geometries, oil-impregnated paper insulation can operate at very high dielectric stress. Thus: "A maximum stress at the BIL of 100 MV/m (2500 V/mil) is a reasonable design stress for modern self-contained OF cables..."[13] in addition, the relation between the dielectric strength with respect to surges and the long-time strength coordinates

*American Standards Association, previous name of ANSI.

Table 3-50

Insulation Classes and Dielectric Tests for Oil-Immersed Transformers

Insulation Class* (kV)	Low-Frequency Test (kV rms)	BIL and Full Wave (kV Crest)	Chopped Wave (kV Crest)	Chopped Wave Min Time to Flashover (μs)
(Col 1)	(Col 2)	(Col 3)	(Col 4)	(Col 5)
1.2A	10	30	36	1
1.2	10	45	54	1.5
2.5A	15	45	54	1.5
2.5	15	60	69	1.5
5.0A	19	60	69	1.5
5.0	19	75	88	1.6
8.7A	26	75	88	1.6
8.7	26	95	110	1.8
15A	34	95	110	1.8
15	34	110	130	2
18	40	125	145	2.25
25	50	150	175	3
34.5	70	200	230	3
46	95	250	290	3
60	120	300	345	3
69	140	350	400	3
92	185	450	520	3
115	230	550	630	3
138	275	650	750	3
161	325	750	865	3
180	360	825	950	3
196	395	900	1035	3
215	430	975	1120	3
250	460	1050	1210	3
260	520	1175	1350	3
287	575	1300	1500	3
315	630	1425	1640	3
345	690	1550	1780	3
375	750	1675	1925	3
400	800	1800	2070	3
430	860	1925	2220	3
460	920	2050	2360	3
490	980	2175	2500	3
520	1040	2300	2650	3
545	1090	2425	2800	3

*The letter "A" under Insulation Class refers specifically to distribution levels for distribution transformers.

NOTES:

(1) Section 4.1.3 for regulating taps.

(2) Single-phase distribution and power transformers and regulating transformers for voltage ratings between terminals of 8.7 kV and below are designed for both Y and Δ connection and are insulated for the test voltages corresponding to the Y connection so that a single line of transformers serves for the Y and Δ applications. The test voltages for such transformers when operated Δ connected are, therefore, one step higher than needed for their voltage rating.

(3) Y-connected transformers for operation with neutral solidly grounded or grounded through an impedance may have reduced insulation at the neutral as specified in 4.2.

(4) For series windings in transformers such as regulating transformers, the test values to ground shall be determined by the insulation class of the series windings rather than by the rated voltage between terminals.

well with the ratios of BIL to normal operating voltage. This is illustrated in Figure 3-100. The relationship of short-time to long-time dielectric strengths for micaceous insulation, as described on page 3-326 is not as favorable.

Figure 3-100 also exhibits the relationship of the relative strengths of oil-treated pressboard and clear oil. It will be seen that the pressboard is by far stronger than clear oil and resists direct puncture much better. This superiority is further illustrated in Figure 3-101 reproduced from Reference 16. Unless proper precautions are taken to prevent flashover, however, it may not be possible to realize the high strength of the pressboard. Figure 3-102 from Reference 16 provides some guidance in this respect.

Application Criteria for High Voltage Insulation

As general rules, insulating materials perform best when:

1 - Dielectric stress concentrations are minimized

2 - Ionizable voids are eliminated

3 - Contaminants are excluded

4 - Sources of chemical attack on the insulation are excluded

5 - Thermal degradation effects are minimized

6 - Mechanical vibrations and stresses are controlled so as to prevent rupture of premature mechanical degradation of the insulating materials.

These principles are incorporated in the design of essentially all modern types of high-voltage apparatus. It is, however, probably that the highest values of dielectric strength of oil-impregnated cellulosic insulation are realized in power cables, where other design requirements apparently tend to be subordinated to those appropriate to the insulating function. In transformers other requirements, including the cooling function, may be equally important or take precedence. In a turbine generator, many requirements must be simultaneously satisfied. Nevertheless, it appears that the first objective to be satisfied in defining a high-voltage armature winding concept is to minimize the difference between a turbine generator winding and high-voltage cable. It is believed that this can be accomplished most successfully by using the spiral pancake configuration that is described below. This configuration meets the general principles for successful application of insulating materials in the following respects:

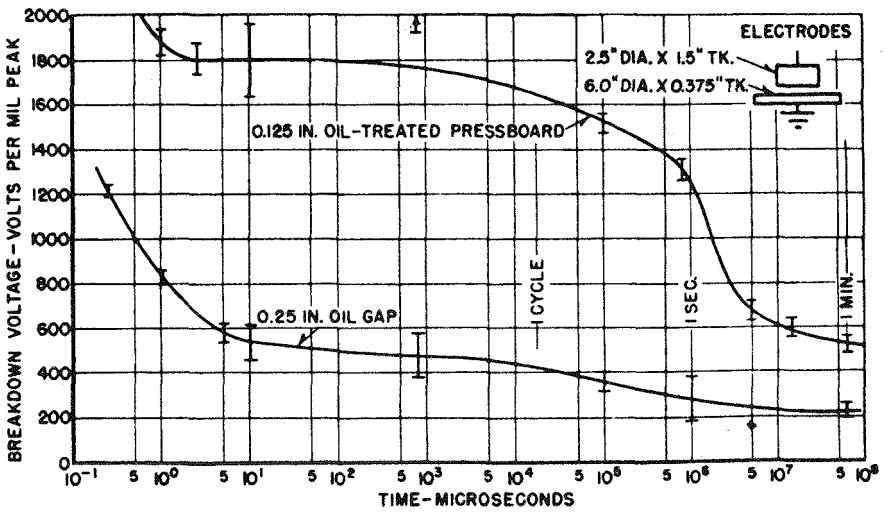

Figure 3-100. Dielectric Strengths of Oil-Treated Pressboard and Transformer Oil as Affected by Time.
(p. 194 of Reference 17)

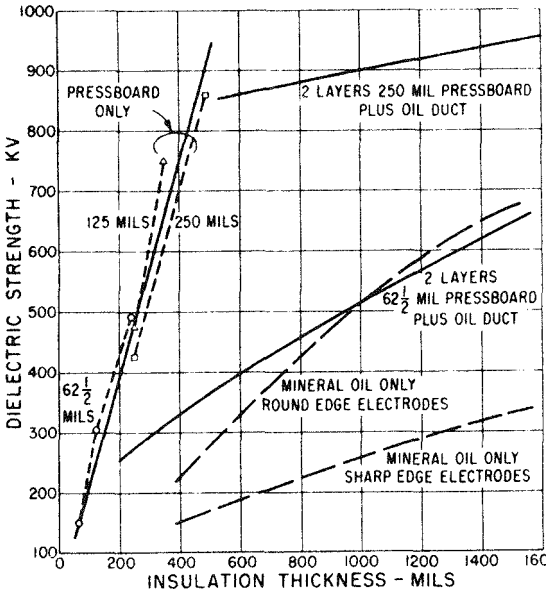

Figure 3-101. Impulse Voltage Breakdown of Oil Treated Pressboard with and without a Series Arranged Oil Duct.
(p. 305 of Reference 16)

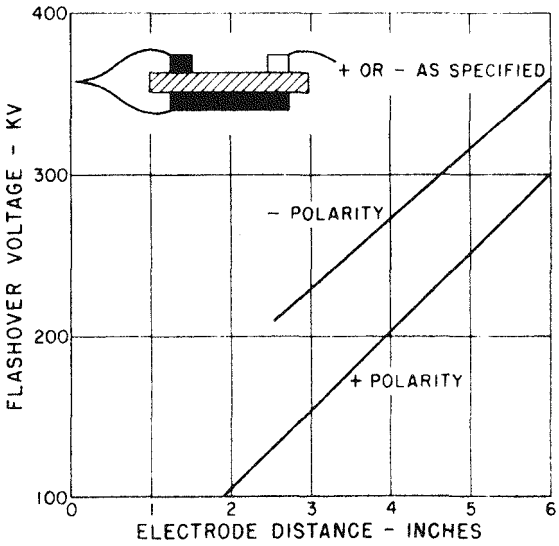

Figure 3-102. Impulse Flashover Characteristics of Oil Treated Pressboard Tested Under Oil.
(p. 313 of Reference 16)

1 - The form of the winding intrinsically produces smooth, continuous, and overlapping layers of insulation between the phase windings, so as to minimize geometric stress concentration factors for dielectric stress. (See Table 3-51)

2 - Creepage paths of relatively great length also follow naturally from the form of the winding. The lengths of these paths could, if necessary, be further extended by local convolution of the insulating layers.

3 - Voids and their detrimental effects are minimized by:

a - use of laminated structures of thin, continuous, overlapping sheets

b - a liquid impregnant

c - pressurization of impregnant (if required).

4 - Dielectric stresses are kept out of the ionizable gap between the armature winding and the rotor by means of an electrostatic shield.

5 - Contamination and chemical degradation effects are minimized by continuous circulation and purification of the dielectric impregnant.

6 - The spiral geometry assists in controlling mechanical effects by providing a wedging action of the winding against the inner surfaces of the flux shield.

In addition, it is possible to provide for cooling and connections without violating the integrity of the insulating structure. This is accomplished in part by using a common liquid as dielectric impregnant as well as coolant.

It is believed that armature windings can be designed for extra-high voltage applications by following these concepts. This is some five to eight times higher in voltage than has been substantiated before by other authors.[2,8] It is possible that the concept can also be extended to ultra-high-voltage applications. These would be adequate for generator ratings of the order of 3000 MVA.

Dielectric Liquids

The types of insulating liquids that may be considered for use in electrical apparatus include hydrocarbon mineral oils, askarels, fluorinated liquids, silicone liquids, and others of lesser importance, such as vegetable oils, organic esters, and synthetic hydrocarbons. The mineral oils have been (and probably continue to be) the most widely used. Their properties are well known.[16] Transformer oil is a good example.

Table 3-51
Maximum Field Strength E with a Potential Difference U Between the Electrodes, for Several Electrode Configurations (Reference 7)

Configuration		Formula for E	Example
Two parallel plane plates		$\frac{U}{a}$	U = 100 kV, a = 2 cm, E = 50 kV/cm.
Two concentric spheres		$\frac{U}{a} \cdot \frac{r+a}{r}$	U = 150 kV, r = 3 cm, a = 2 cm, E = 125 kV/cm.
Sphere and plane plate		$0.9 \frac{U}{a} \cdot \frac{r+a}{r}$	U = 200 kV, r = 5 cm, a = 8 cm, E = 58.5 kV/cm.
Two spheres at a distance a from each other	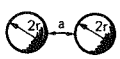	$0.9 \frac{U}{a} \cdot \frac{r+a/2}{r}$	U = 200 kV, r = 5 cm, a = 12 cm, E = 33 kV/cm.
Two coaxial cylinders		$\frac{U}{2.3\, r \lg \frac{r+a}{r}}$	U = 100 kV, r = 5 cm, a = 7 cm, E = 22.9 kV/cm.
Cylinder parallel to plane plate		$0.9 \frac{U}{2.3\, r \lg \frac{r+a}{r}}$	U = 200 kV, r = 5 cm, a = 10 cm, E = 32.8 kV/cm.
Two parallel cylinders	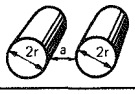	$0.9 \frac{U/2}{2.3\, r \lg \frac{r+a/2}{r}}$	U = 150 kV, r = 6 cm, a = 20 cm, E = 11.5 kV/cm,
Two perpendicular cylinders	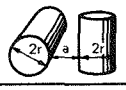	$0.9 \frac{U/2}{2.3\, r \lg \frac{r+a/2}{r}}$	U = 200 kV, r = 10 cm, a = 10 cm, E = 22.2 kV/cm.
Hemisphere on one of two parallel plane plates	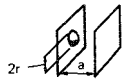	$\frac{3U}{a}$; (a ≫ r)	U = 100 kV, a = 10 cm, E = 30 kV/cm.
Semicylinder on one of two parallel plane plates	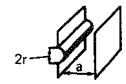	$\frac{2U}{a}$; (a ≫ r)	U = 200 kV, a = 12 cm, E = 33.3 kV/cm.
Two dielectrics between plane plates ($a_1 > a_2$)	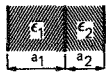	$\frac{U\epsilon_1}{a_1\epsilon_2 + a_2\epsilon_1}$	U=200kV, ϵ_1=2, ϵ_2=4, a_1=6 cm, a_2=5cm, E = 11.8 kV/cm.
Point and Plane $\frac{L}{a}$ =160	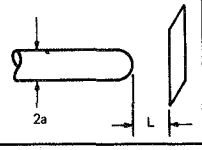	$\frac{0.605\ U}{a}$	U = 1kV, L=160 cm, a=1cm E = 605 volts/cm. Compare parallel plate capacitor with E = 6.25 volts/cm
Ellipsoidal Boss on one of two Parallel Planes [11]	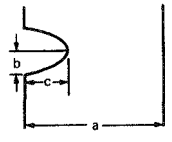	$\frac{U}{a} \times \beta$ $\beta = [n(\coth^{-1} n - 1/n)(n^2-1)]^{-1}$ where $n = c\,(c^2 - b^2)^{-1/2}$	$\frac{c}{b}$ = 10, β ≈ 50

The concept of using oil in a stator winding for insulation as well as cooling is, of course, by no means new, and the possibility of using the properties of oil-impregnated insulating media for very high voltage ratings has been appreciated for several decades. A discussion[19] on a paper[20] on liquid-cooled turbine generators reported in 1947 that tests had been made in 1926 on an oil-cooled stator arranged with an insulating cylinder in the air gap: "This machine functioned quite satisfactorily, but the development did not proceed farther at that time, partly on account of the fire hazard, and partly because no demand developed for the extra high generator voltages originally contemplated." Liquid cooling has been utilized for the internal cooling of conductor strands of conventional machines[21] as well as for the armatures of prototype superconducting generators. As far as known, however, the use of oil in the manner contemplated for the EHV spiral pancake armature winding has not been considered before.

A design criterion that must be followed when oil is used as a coolant as well as an impregnant is that the formation of gas bubbles in the oil must be avoided. Since cavitation phenomena are capable of producing such bubbles, the causes leading to cavitation must be eliminated. This can be accomplished by avoiding local accelerations of the oils streams which would cause negative pressure regions, and can be assisted by pressuring the entire oil volume. Further studies will be required to define these parameters in terms of actual flow paths and their velocity distributions and with respect to possible vibrating surfaces in contact with the oil.

Alternate Material Concepts

Although in the above discussion reference has been made to cellulosic materials, such as pressboard, paper, and the like, impregnated with transformer oil, the ultimate implementation of such a concept may benefit, in terms of power density and possibly other parameters, from the application of materials that will require further development prior to application, such as synthetic papers and oils. The ultimate potential of the concept in conjunction with improved materials may thus be substantially better than the potential based on realization with materials that can be applied in the more immediate future.

Dielectric Stress Distributions

In order to design the insulation structure for an EHV winding in detail, it will be necessary to determine the distribution of electric fields in the insulating media. For simple geometries, such as those shown in Table 3-51 the field

distribution can be obtained by simple formulas. For a complete structure, however, it will be necessary to use some form of mathematical modelling to represent the fields. The detailed model will have to be confirmed by test. (See "Development Plan.")

Dielectric stress distributions must be determined both under steady state operating conditions and under surge conditions. Possible interaction effects of voltage surges followed by high-current faults (and vice versa) must be considered.

The effects of surges on unit-connected turbine generators of conventional design have been studies in detail[14,15]. An equivalent circuit for the surge propagation along the winding of a conventional turbine generator is shown in Figure 3-103 In such machines, which normally use single-turn coils, the mutual inductances and capacitances between successive turns are small and may be neglected. The results of the analysis[15] indicate that maximum surge voltage is within the capability of a standard generator to withstand, but show a considerable piling up of the surge voltage near the line end of the winding (Figure 3-104). A point that is only 20% of the distance from the neutral experiences as much as 63% of the maximum surge voltage at one instant of time.

An analysis of this type is also required for the airgap winding. As far as is known, none has yet been reported in the technical literature. Surge voltage distribution measurements have, however, been carried out on the MIT-EPRI superconducting generator prototype[22], and indicate that surge voltage distributions in airgap windings can be expected to be significantly more uniform than in conventional generator windings.

Equivalent Circuit for Surge Voltage Propagation - Spiral Pancake Winding

The detailed equivalent circuit of a repeatable group of the spiral pancake winding is shown in Figure 3-105. It appears that in this case the turn-to-turn capacitances will predominate and will constitute in essence a capacitive voltage divider. The circuit shown must be replicated six times in order to model the complete winding. Additionally, the end turn portion, with a somewhat different geometry, must be modeled separately.

The analysis of transient voltage distributions would ideally be combined with a geometric analysis of the field distributions. It is, however, likely that practical considerations will require these problems to be analyzed separately. Based on the results, stress grading provisions may be required. Finally, laboratory verification of the results will be essential. Detail proposals for this work are covered in the Development Plan.

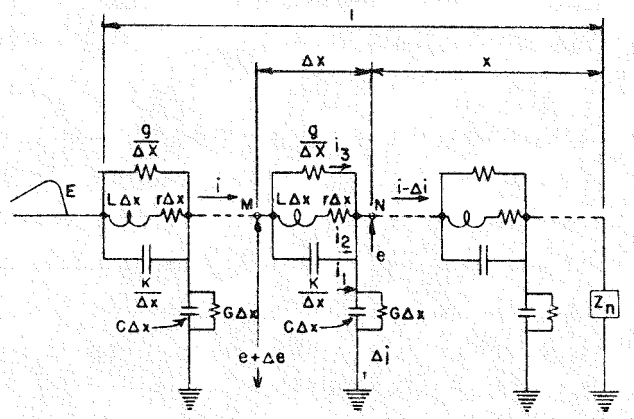

FIGURE 3-103. Equivalent Circuit of One Phase of Conventional Turbine Generator (Reference 17)

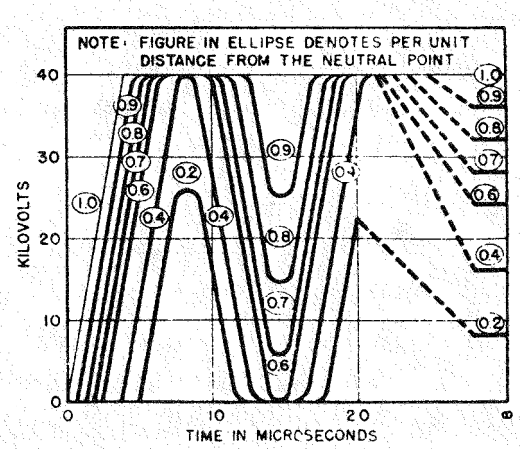

FIGURE 3-104. Surge Voltage Distribution Along Phase Winding of Conventional Turbine Generator (Reference 17)

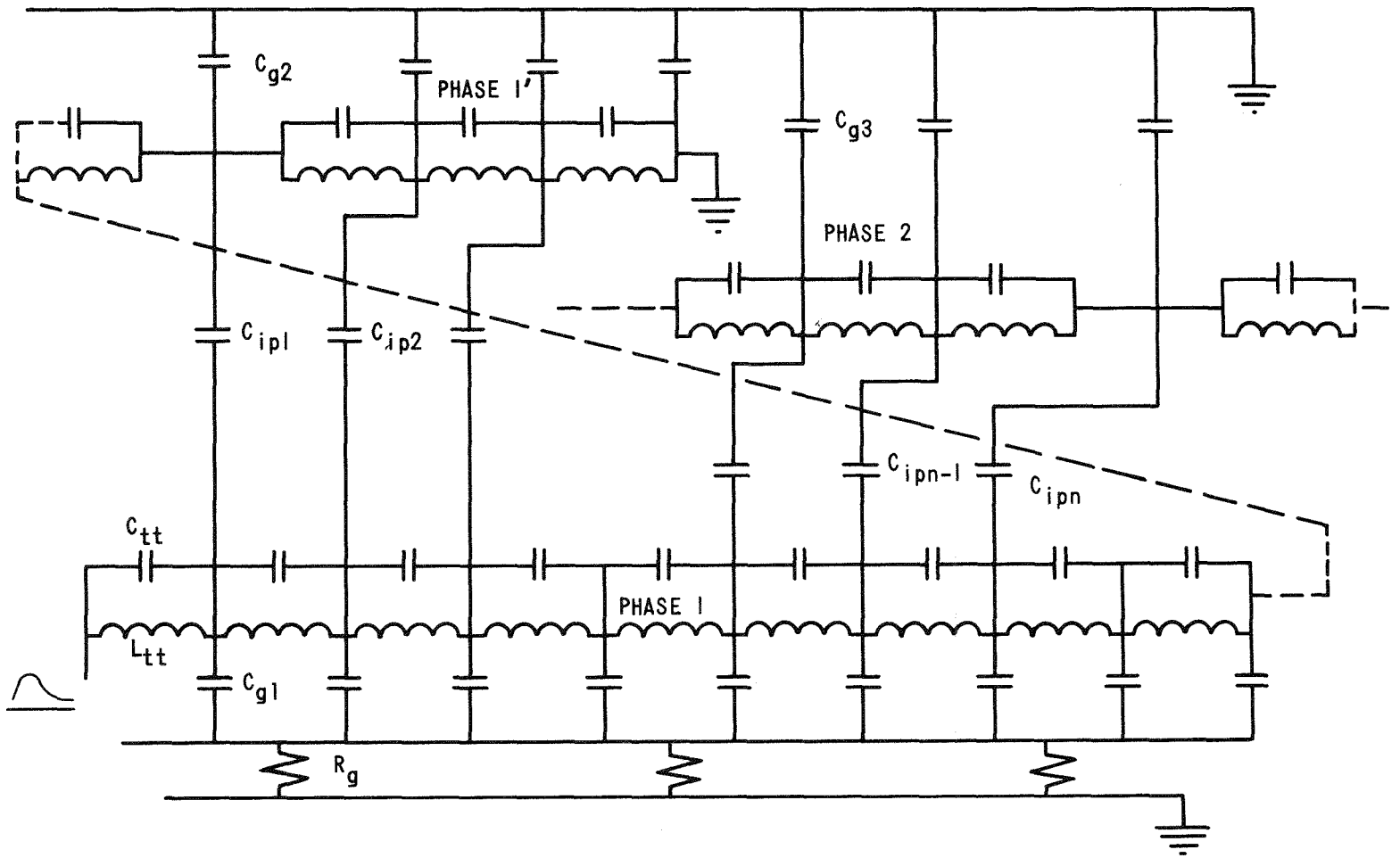

Figure 3-105. Detailed Equivalent Circuit of 60° Portion of 2-Pole High Voltage Spiral Pancake Winding Concept

Avoidance of Localized Dielectric Stress Concentrations

It is possible for high local stress concentrations to be created by surface irregularities or fine foreign objects such as metallic slivers. These must by all means be avoided in the design and by careful processing of insulating and conducting materials, with particular attention to the elimination of all foreign objects and particles from the windings. The need for this precaution is very clearly illustrated in Figure 3-106 which shows the increase in local field strength (field enhancement) due to a minute projection on one plate of an ideal parallel plate capacitor. The hazards of minute particles and of surface irregularities in reducing the dielectric strength of a complex insulating structure cannot be overemphasized. In the case of the present requirements, where armature conductors must be made up of finely stranded subconductors, it may become necessary to apply internal shields around the individual conductors to prevent the formation of local discharges. The need for such treatment must be determined as part of the development program that is proposed in the Development Plan, Section 3.7.

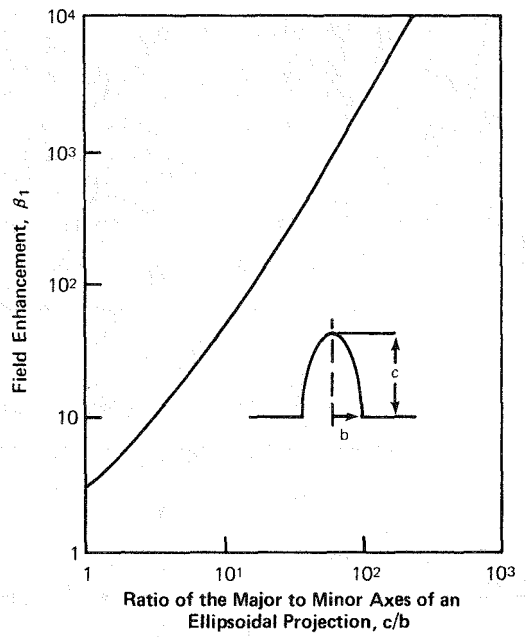

Figure 3-106. Microscopic Field Enhancement as a Function of Geometry for an Ellipsoidal Projection on an Otherwise Flat Infinite Plane.

Stator Insulation for High-Voltage Direct Current Transmission (HVDC)

Transmission of large blocks of electric power over large distances represents a relatively new development in the growth of electric utility power systems. The need for such transmission develops, for example, in order to tap remote and previously inaccessible energy sources. In such cases, the limits for economic transmission via AC high-voltage lines may be exceeded, and HVDC is resorted to. High-voltage DC transmission has also proved to be a promising competitor to extra-high-voltage AC transmission under several conditions:* where long transmission distances from generation to load centers exist; where asynchronous ties are required; and where underground or underwater cables of considerable length are necessary.

Such service imposes design constraints on the generator; for example, the presence of the converter between the transformer and the transmission line introduces harmonics in the phase currents which must either be filtered out or handled by the generator design. One of the effects of the harmonics, as is well known, is to cause additional heating in the damper circuits of the connected generators. With respect to the relative importance of damper windings, they do not form as fundamentally important a part in conventional machines as in superconducting machines, where their presence is essential to the functioning of the field winding. In the case of one HVDC project (with conventional generators) studies showed that filtering was more economical than building the generators to carry the harmonic currents continuously.** In superconducting generators, it is likely that the already rugged damper construction could be given the increased capability for harmonic currents by the addition of water cooling.

Turbine generators with EHV windings could also be applied to HVDC line terminals without transformation. This concept was suggested by EPRI and involves generators installed in plants wholly dedicated to HVDC lines. In this case, the overall line-terminal design can be favored and economized. For instance, special frequencies or numbers of phases could be considered. Superconducting generators with EHV windings are the only candidates for this application because of their following characteristics:

---

*HVDC for the Long Run; by F. J. Ellert and N. G. Hingorani, IEEE Spectrum, August 1976, pp. 37-42.

**Direct Current Transmission, Volume I, E. W. Kimbark, Wiley-Interscience, 1971.

1 - Sufficiently high-voltage capability

2 - Potential ability to accommodate high-current harmonics without overheating (using liquid-cooled dampers)

3 - Reduced reactance (including elimination of transformer reactance) leading to lesser voltage regulation.

The dielectric stress distributions (in time and space) affecting the insulation design of the armature winding must be expected to be different for HVDC transmission than for AC. The phase current harmonics which are introduced by the power converters produce harmonic voltage drops in the internal impedance of the power source, such as the generator. It is also possible that voltage oscillations due to blocking of reverse current would be introduced by the converter equipment. This would depend upon the damping or surge suppression equipment incorporated in the converter design.

It can be assumed at this time that the insulation coordination parameters for a generator for HVDC transmission would need to be different from the concepts presented above.

Insulating Practices for Low Voltages

The potential benefits to the electric utility industry of the application of superconducting generators also apply to generators with low-voltage armature windings. For reasons to be discussed subsequently, these may be designed for exceptionally low subtransient reactance, which would lead to improved critical fault clearing times. Such machines would utilize the insulation technology that has been developed for conventional turbine generators and has been successfully applied to several hundred such units over the past 25 years. The following is a necessarily brief discussion of the principles.

The complete insulation structure of a conventional armature winding is composed of many different materials which act as insulators according to different mechanisms. For example, the major insulation from the high-voltage parts to ground (groundwall insulation) will be composed of solidified resin-impregnated insulation which acts as a dielectric barrier against direct penetration in the straight part of the coil, and may rely extensively on sufficient spacing to keep creepage currents to very low values in the end turns. In the end windings, the gas present between coils may itself play the role of an insulator which, when overstressed, permits partial discharges (corona) to occur. These various functions must be carefully coordinated to secure an adequate insulation design.

Conventional insulation technology as used on a variety of rotating machines, including large turbine generators, relies upon the use of mica which resists the electrically and chemically active substances produced by partial discharges. The qualities of the mica are enhanced and preserved by the use of vacuum-pressure impregnation with synthetic resin. This resin fills all interstices, thus reducing the presence of voids which otherwise might be ionized by the dielectric stress field. In addition, dielectric stress grading is provided by means of surface coatings on the coils, which grade the potential distribution at the coil surfaces down from full armature voltage to ground potential at the end of the core. This stress grading is accomplished by means of surface coatings of selected resistivity which distribute the potential by supporting a surface current. The heating produced by this current sets a limit to the maximum voltage for which a grading system can be designed. This heating, at the test levels required by present ANSI standards, is sufficient to make the ANSI test voltage rather than the operating voltage the design limit. In the core portion of the winding, conducting coatings on the coils assure good grounding to the core, and thus prevent partial discharges to the slot walls.

The type of impregnant exerts a major influence on the dielectric, thermal, and mechanical capabilities of the insulation. Insulation systems using synthetic resin impregnants have replaced the earlier and much more limited asphalt or bituminous insulations. Modern synthetic resin impregnating systems use completely reactive and solventless resin systems, so that no void-forming products can be produced during the polymerization reaction.

Insulation systems using these principles are now routinely applied to large turbine generators with rated voltages in the range of up to 27 kV. Extension to 30 kV is possible with relatively minor development. Further extension at least to 35 or 36 kV is possible, but would require the development of improved surface coatings for dielectric stress grading. In view of the unavailability of good mathematical models for end zone dielectric stress distributions, such a development would involve scale models of end zone configurations. As far as is known, all other components of the insulation technology that is now utilized will be adequate for 35 or 36 kV ratings.

Coil, Conductor and Strand Insulation

Conventional coil construction generally employs fibrous materials, such as glass and synthetic resin fibers, in conjunction with resinous bonding materials for internal insulation which at the same time serves to bond the separate strands of

the conductors and thus to consolidate the coil structurally. With the large numbers of small strands that are required in superconducting generators, it is expected that resin coatings alone may be used for strand insulation, inasmuch as fiber support would occupy excessive space and result in a poor packing factor.

Insulation of Coolant Circuit

The armature winding liquid coolant circuit insulation design must be coordinated with that of the winding itself. The major ground insulation between the grounded coolant supply system and the high potential winding can be provided either at the connections to the individual coils, or near the point of entry into the generator casing. In the latter case, the supply connections to individual coils have to be designed only for turn-to-turn voltage, rather than for full voltage to ground. A choice between these alternatives requires a detailed design study. Insulation is also required between the individual cooling tubes and the strands which they cool.

Corona Protection

Systems of dielectric stress grading for corona protection, as used in conventional armature windings, rely upon making positive electrical connections to the ground plane represented by the grounded stator core. This method would also be applicable to the modified airgap winding previously proposed by Westinghouse.

It would not be applicable to airgap windings of purely monolithic construction which have no direct contact between coil surfaces and the stator shield. Alternative methods of stress control would have to be developed. The more uniform distribution of internal capacitances discussed above under "Dielectric Stress Distributions" provides hope that this would not be an especially difficult problem. In the light of experience with conventional windings, such as development would be primarily empirical, using scale models.

Functional Evaluation of Insulation Systems

The performance and life of an armature winding is determined by the distribution and intensity of a number of stress patterns which are closely interrelated and synergistic. Amongst these, dielectric, electromagnetic, and thermal stress patterns have been individually identified and studied in detail. The accepted method of evaluating effects of a given type of stress on the performance and life of an insulation system is that of functional evaluation. It is based

on the use of physical models which more or less closely approximate the actual conditions, i.e., dimensions, polymer chemistry, and stress distribution, which may be expected in a real machine. Although these may be scale models, full size models provide better assurance of modeling all interactions more accurately. Functional evaluation methods are more advanced with respect to dielectric stresses and thermal stresses than with respect to electromagnetic and consequent mechanical stresses. Various investigators are attempting to define methods for the effective functional evaluation of the latter. During the past two decades, the availability of digital computers has increasingly permitted detailed calculation of electromagnetic and mechanical stress distributions in armature windings, which have been confirmed by use of full-scale models. This has helped greatly in securing a better understanding of the factors which limit the life of a winding. Nevertheless, it is not yet possible to predict the life expectancey of even a conventional winding in absolute terms with complete confidence. Although certain effects, such as fatigue life of metal parts, can be determined with good accuracy, the overall life expectancy is still basically an experience factor based on a study of the performance of reasonably similar machines, which thus become, in a sense, the functional models. Extrapolation of the experience obtained in this manner is possible by considering the relative magnitudes of the various stress patterns in known and new designs.

The models which are available from conventional machine insulating practice provide only a very imperfect insight into the performance to be expected of insulation in superconducting generators. This is obviously true in the case of EHV windings for AC or DC transmission for which alternate models seem more appropriate. It is also true for low voltage windings of the airgap type. This is largely the case because of increased mechanical stress levels and because of the removal of mechanical support that is furnished by the stator teeth and core in conventional machines. Physical models required for functional evaluation for superconducting generators are not yet available. Theoretical studies must in any case precede the design of the physical models. These studies must consider the mechanical as well as the thermal stresses imposed on the insulating materials in addition to the dielectric stress distributions which were discussed above.

Mechanical stresses may originate from purely mechanical causes, such as shaft vibration. In the practical sense, however, the most important mechanical stress patterns are produced by electromagnetic interactions, as between current in armature conductors and the main field in the machine. A knowledge of the magnetic field distributions is therefore basic to an understanding of stator design.

Magnetic Field Distributions in Superconducting Generators

A knowledge of the magnetic fields is required not only for the straight part (for which well known formulas are available) but also for the more complex end portions. This calculation cannot be properly performed with the methods developed for conventional turbine generators. These methods, based on the relatively small gaps found in such machines, consider the end portions to be enclosed in magnetically closed cans, leading to tractable boundary conditions. As an initial step towards a rigorous evaluation of the field distributions, and as an interim tool for design purposes, a method of flux density determination based on repeated application of Biot-Savart's law to the armature conductors and their images was devised and programmed for the digital computer.[24]

A complete description was given in the Preliminary Draft of the Final Report.

Another method of calculating three-dimensional flux distributions, developed by Westinghouse during earlier work on prototype superconducting generators, has been updated and applied to a typical 300 MVA design. A description of the method and a tabulation of results follows under the title: Three Dimensional Magnetic Field Calculation for a Finite Rotating Machine Enclosed by a Magnetic Boundary.

Once the flux density distributions are known in time and space, it is a relatively simple matter to calculate the force vector components from:

$$\underline{F} = I\underline{l} \times \underline{B}$$

where F = instantaneous value of vector force

I = instantaneous peak value of current in conductor

l = vector length of conductor or segment

B = flux density vector at point at which force is determined.

Three Dimensional Magnetic Field Calculation for a Finite Rotating Machine Enclosed by a Magnetic Boundary

A three-dimensional (3D) magnetic field calculation, based on a scalar potential, was previously used at Westinghouse to study end effects in superconducting machines. The machines to which the method can be applied are simplified versions of actual machines. For the simplified machine, the three-dimensional magnetic fields throughout the machine, forces on the windings and winding inductances are calculated. Computer programs implementing this 3D method run as easily and

rapidly as the two-dimensional (2D) method currently in use in this study. The 3D method provides more information than the 2D methods and is therefore a more versatile design tool.

Machine Simplifications

The 3D method is based on analytic solutions of Laplace's equation for the scaler magnetic potential. Only when restrictuions are made on the geometry of the enclosing magnetic boundary and windings and the magnetic and electrical properties of the boundaries is the method useful in practice. The magnetic enclosure around the winding region is to be a finite closed right circular cylinder. The damper is to be a cylinder concentric with the enclosure and extending to the flat end faces of the enclosure. Two types of magnetic boundary conditions have been used.

(1) infinite permeability at the enclosure, and

(2) infinite conductivity at the damper.

Condition (1) and the assumption of infinite resistivity is equivalent to neglecting eddy currents. The second condition models a damper as a perfect flux reflector. With these boundaries and boundary-conditions very simple eigenfunctions can be used to represent the potential for the finite machine.

The actual windings are to be modeled by a number of pairs of filamentary coils distributed in the winding space, the members of each pair are 180 electrical degrees apart. The basic filamentary coil is restricted to lie on a circular cylinder but may have any shape. The restriction is imposed so that the discontinuity in the magnetic scalar potential resulting from a current carrying loop can be used as a simple boundary condition to yield an analytic expression for the potential. A wire with a finite cross-section can be used instead of filaments and was used in some earlier applications of this 3D method.

A partial analysis with this method is still possible if only some of the windings (regular ones) can be sensibly modeled in a way consistent with the 3D method. The fields and forces due to these regular coils can be calculated at the positions of the other or nonregular coils. The flux linkage and therefore inductance between the two types of coils can also be calculated. The forces on the end turns of a "spiral" winding and its mutual inductance with a saddle-type would be a useful case to treat.

Scalar Potential Method

Only a brief sketch of the method is presented since the purpose of this contribution to the final report is to outline the capability of the method. Figure 3-107 shows the machine geometry, the cylindrical coordinates r, θ, Z are used. The field is the negative gradient of the scalar potential. The basic solutions of Laplace's equation for the scalar potential U of a p-pole pair machine are

$$\cos kZ \cos q\theta \times \begin{Bmatrix} I_q(kr) \\ K_q(kr) \end{Bmatrix} \tag{1}$$

where $k = \pi m/2Z_0$, $q = np$ (m, n odd, positive integers) and I_q, K_q are modified Bessel functions. Solutions satisfying the boundary-conditions on the enclosure (with and without a damper) and across the coil surface $r = R_c$ are constructed from a sum over n and m of linear combinations of sets of eigenfunctions containing I_q of K_q. Separate solutions are needed for $r < R_c$ and $r > R_c$.

As in the 2D case there are two boundary-conditions at $r = R_c$ which in 3D is a surface. Across the surface $r = R_c$, the flux on the radial derivative of the potential is continuous. However, U is discontinuous on crossing a coil surface at $r = R_c$, the discontinuity is

$$U(R_c + 0, \theta, Z) - U(R_c - 0, \theta, Z) = If(\theta, Z) \tag{2}$$

where I is the coil current and $f(\theta,Z)$ is ±1 for (θ,Z) inside the loop and 0 otherwise. The sign of f depends on the current direction and the loop location. The next step in determining U is to expand $f(\theta, Z)$ in terms of the complete set $\cos kZ \cos q\theta$. A comparison of the expansions of the left- and right-hand sides of Eq. (2) connect the potentials to the Fourier coefficient of $f(\theta, Z)$. In this way the expansion coefficients of U and therefore U is expressed in terms of f or the coil geometry.

Being in possession of an analytic expression for U, we obtain the fields and forces by differentiation. Inductances are calculated from the fields by an integration over an area enclosed by a coil to obtain the flux linkages.

Model Calculation

To demonstrate some of the capabilities of the three dimensional method, results are presented for one of the proposed 300 MVA machines. Both field and armature are represented by sets of nested saddle coils. Table 3-52 contains the machine dimensions and parameters.

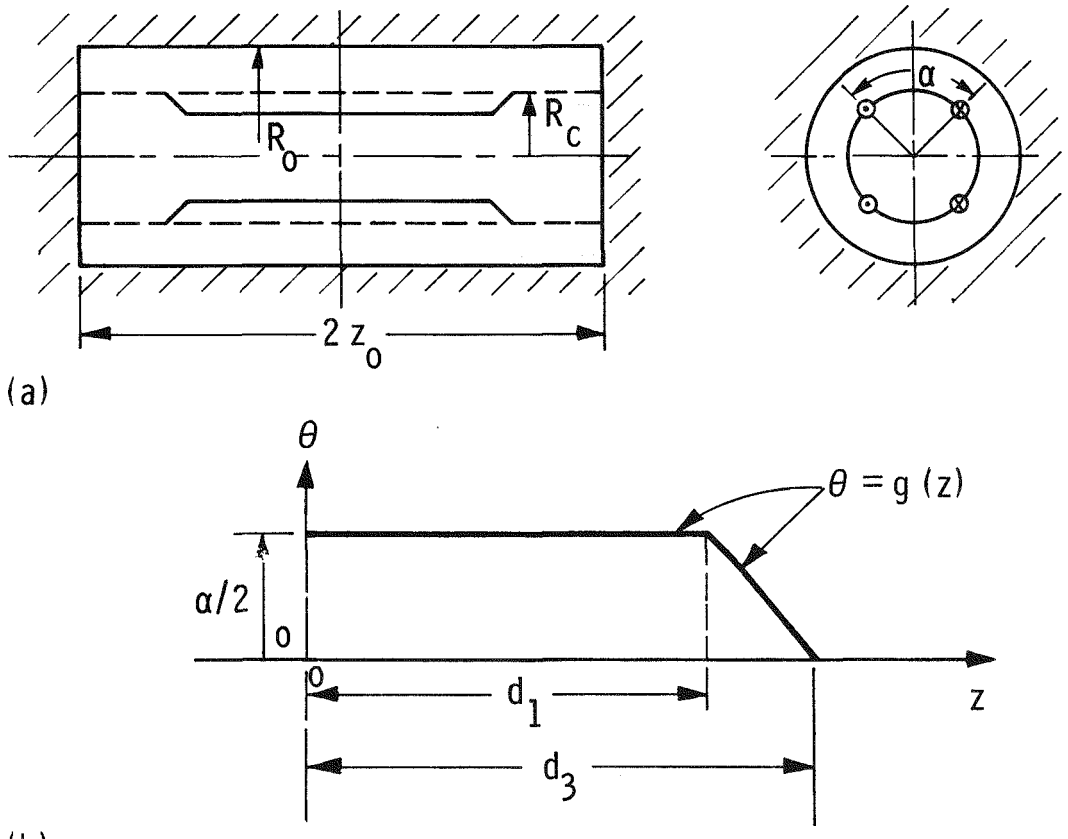

Figure 3-107.(a) Dimensions of magnetic enclosure and coil layout. (b) developed view of one-quarter of a coil. The "straight" section has $0 < x < d_1$, the "end" section has $d_1 < 7 < d_3$

Table 3-52

300 MVA SPIRAL WINDING "SOLID" ROTOR

$X''_d = .16$

Machine Dimensions and Winding Parameters

Armature	
Radius of coil groups	.543 m
Number of stator group pairs	6
Turns/stator group	1
Current/stator group	17.975×10^3 Amps
Length of straight part	1.906 to 3.404 m
Coil type	saddle
Coil angle	100° to 200°
Field	
Radius of coil groups	.212 and .249 m
Number of rotor group pairs	10
Turns/group	161
Current/turn	10^3 Amps
Length of straight part	1.906 to 2.642 m
Pole face angle	49°
Coil type	saddle
Coil angle	62.1 to 166.9°
Damper outer radius	.365 m
Magnetic Boundary	
Inside length	4.724 m
Inside radius	.678 m

Fields calculated by 2D and 3D methods at the mid-plane (z = 0) of the machine are compared in Table 3-53. Since the machine is fairly long compared to its radius, the "finite" effects at the mid-plane are negligible and the two calculations should agree as they indeed do. The first rotor end turn and stator end turn are at Z = 0.953m, the second rotor end turn is at 1.551 m and the second stator end turn is at 1.403 m. Fields at these positions are listed in Table 3-52 and are seen to differ from the corresponding ones at Z = 0.

Table 3-53 also lists inductances. The 3D values are calculated directly, while to obtain the 2D values, a directly calculated inductance per unit length must be multiplies by an effective (arbitrary) length.

As is true of many three-dimensional magnetic field calculations, 3D method generates a large amount of data. Four computer drawn graphs (Figs. 3-108 through 3-111) show some of this data. Figure 3-108 and 3-109 plot the magnitude of the field of one phase of the armature outside the armature. The positions of the stator end turns are marked by heavy lines in Figure 3-108. For all the figures the angular range is $0 \leq \theta \leq 100°$, and the axial range is $0 \leq Z \leq 2.065$ m. The figures clearly show the axial variation of the field components and a peaking of [B] near the first end turn.

Use of Results

The mathematical model used to represent the actual machine leads to accurate calculation of fields, winding forces, and inductances in a rapid, direct, and efficient manner.

Table 3-53

Comparison of 3D and 2D Calculations

First Harmonic Magnetic Field Components (Tesla) $\theta = 0$

Rotor (Field) Contribution

Radius = .193 m (7.60 ins.) - Inside Rotor Radius

	3D			2D	
Axial Distance (Z-meters)	Radial (B_r)	Axial (B_Z)		Radial (B_r)	Axial $B_Z = 0$
0	5.002	0		4.950	0
.953	5.170	-1.297		--	--
1.551	-.152	- .0124		--	--

Stator Contribution

Radius = .589 m (23. 18 ins.) - Outer Armature Radius

	3D			2D	
Z	B_r	B_Z		B_r	$B_Z = 0$
0	.3288	0		.3290	0
.953	.3463	.0423		--	--
1.4030	.1330	.0340		--	--

Radius = .55245 m (21.75 ins.) - Inside Armature

	3D			2D	
Z	B_r	B_Z		B_r	$B_Z = 0$
0	.3536	0		.3486	0
.953	.3741	.0815		--	--
1.403	.1497	.0404		--	--

Table 3-53 (Continued)

Radius = .57048 (22.46 ins.) - Inside Armature

	3D		2D	
Z	B_r	B_Z	B_r	B_Z
0	.3408	0	.3397	0

Inductances (henries)

	3D	2D
Armature		
Without damper - L_a	$.36275 \times 10^{-3}$	$.4560 \times 10^{-3}$
With damper	$.18921 \times 10^{-3}$	
Field - Armature Mutual - M	$.34534 \times 10^{-1}$	$.3658 \times 10^{-1}$

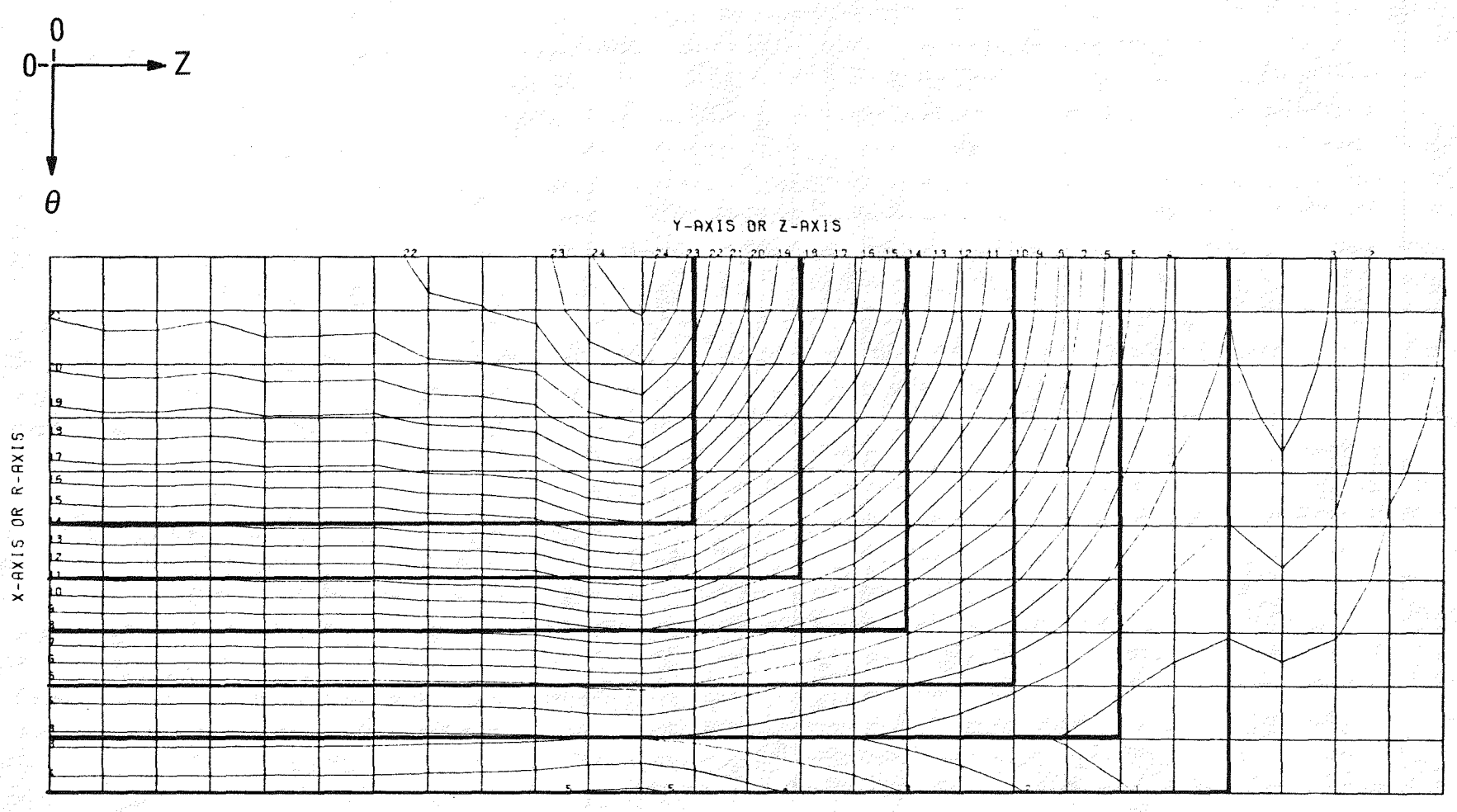

FIGURE 3-108. Contour plot of the magnitude of the armature field | B | at r = .597 m. The vertical axis is the θ-axis (10° increments) the horizontal axis is the z-axis (.0794 m increments). The contours range from number 1 = .02 to number 24 = .24 tesla in increments of .02 tesla. The heavy lines are the positions of the armature coils

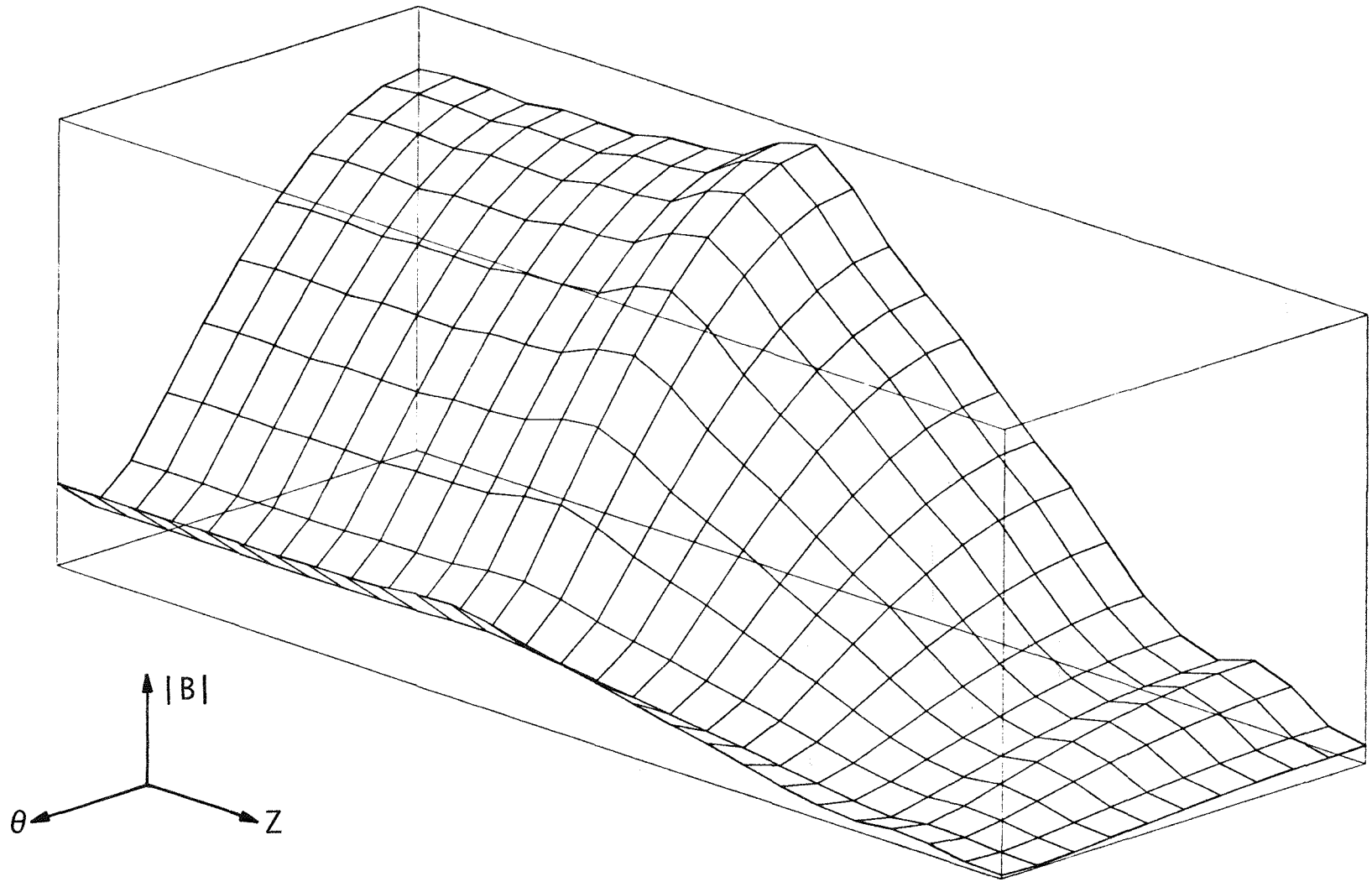

FIGURE 3-109. Perspective plot of the magnitude of armature field | B | at r = .597 m. The triad identifies the axes. The grid spacing and the location of the armature turns are the same as for Fig. 3-108.

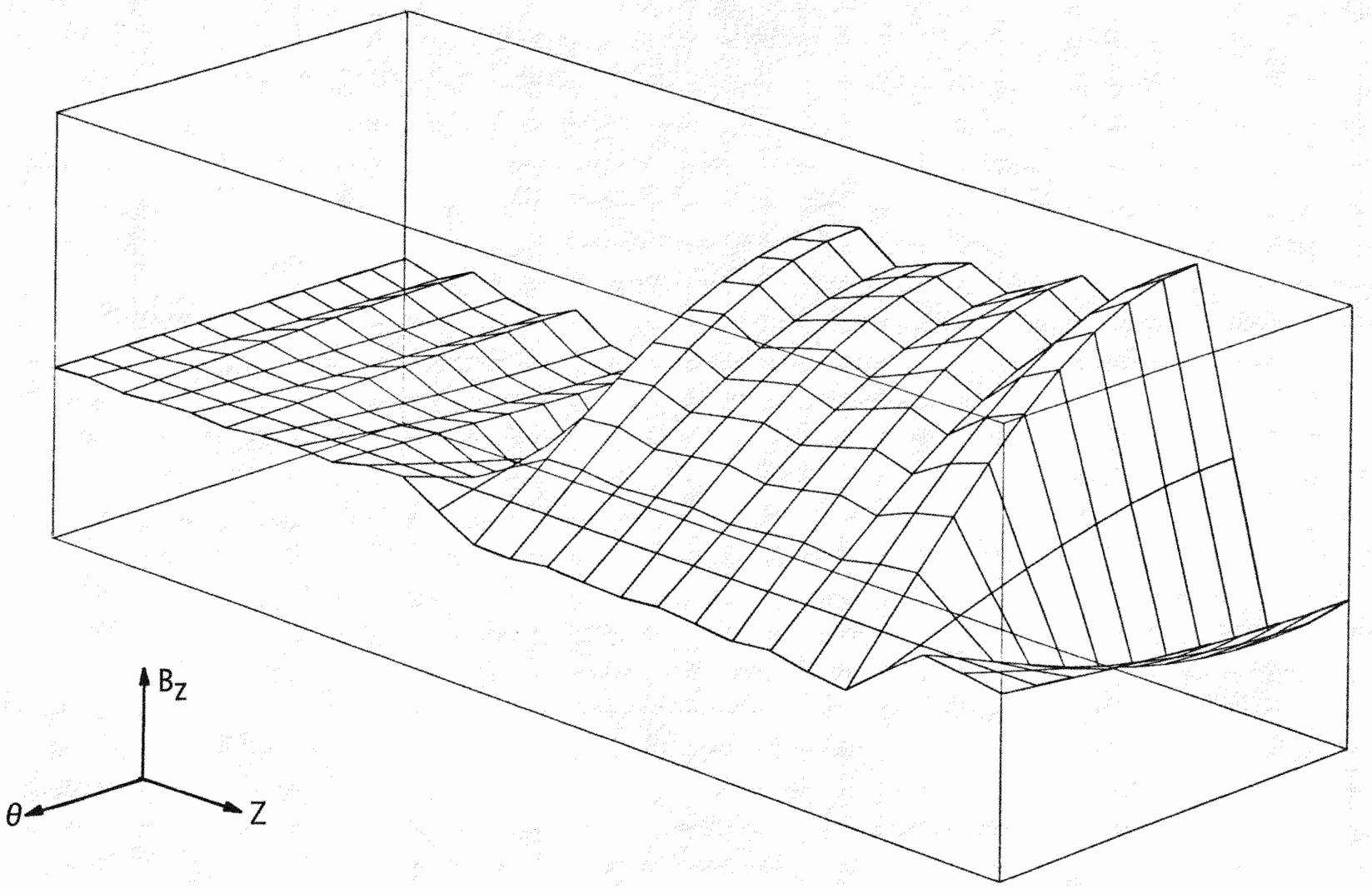

FIGURE 3-110. — Perspective plot of the z-component of the armature field B_Z at r = .597. The triad identifies the axes. The grid spacing and the location of the armature turns are the same as for Fig. 3-108.

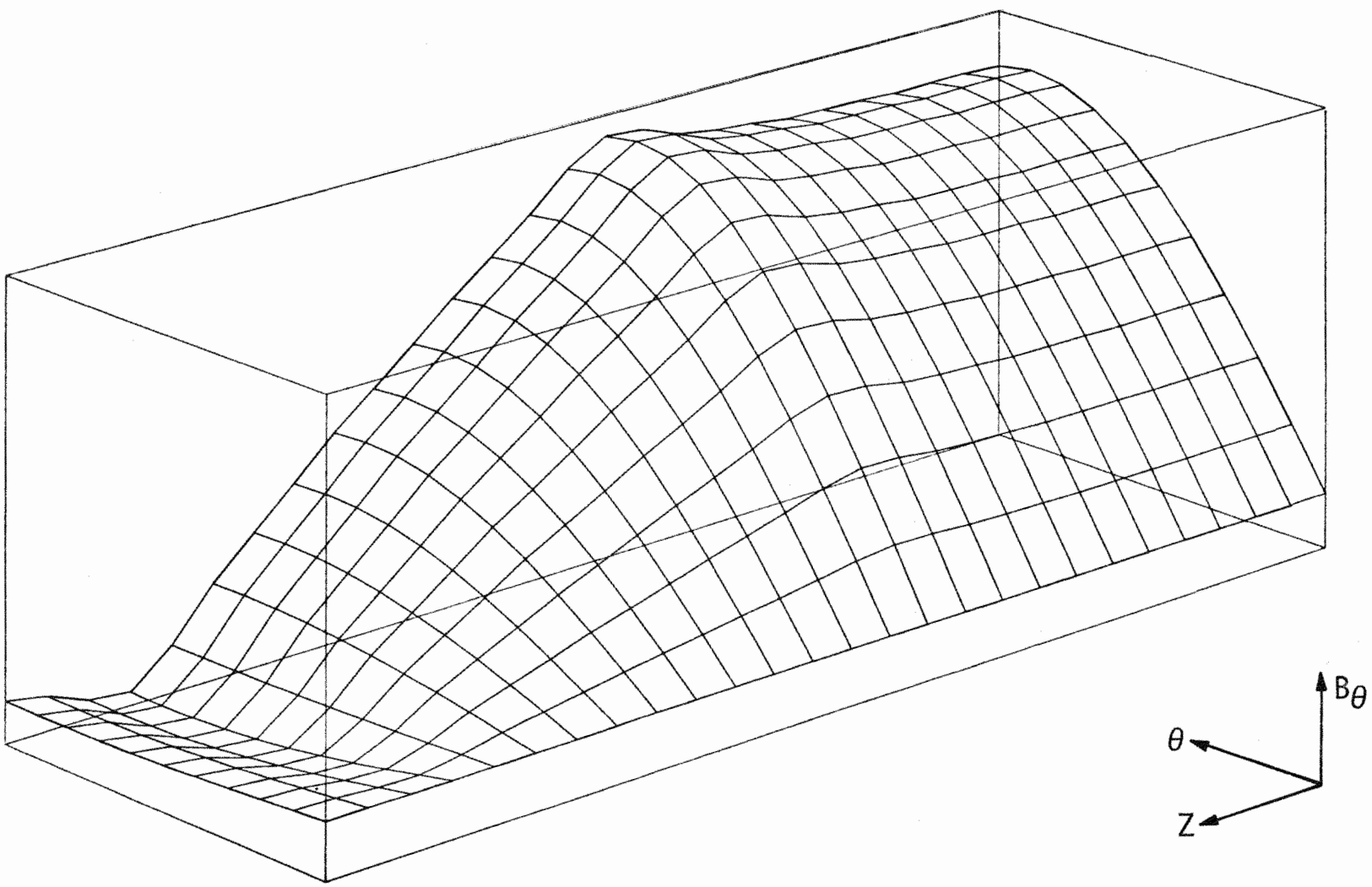

FIGURE 3-111. — Perspective plot of the θ-component of the armature field B_θ at r = .597. The triad identifies the axes. The grid spacing and the location of the armature turns are the same as for Fig. 3-108.

References

1. H. Meyer, "Die Isolierung Grossner Elektrischer Maschinen," (book), Springer-Verlag, Berlin, 1962, pp. 116-118.

2. G. Aichholzer, "New Ways of Building Turbogenerators up to 2 GVA, 60 kV," Elektrotec. u. Maschinenbau, Vol. 89, No. 1, January 1972, pp. 1-11.

3. M. M. Steeves, "A Modified Gramme-Ring Armature for a High Voltage Superconducting Alternator," M.S. Thesis, MIT Dept. of Electrical Engineering, August 1973.

4. J. L. Kirtley, Jr. and M. M. Steeves, "Toroidal Winding Geometry for High Voltage Superconducting Alternators," IEEE Trans. on Power Apparatus and Systems, Vol. PAS-93, No. 6, November-December 1974, pp. 1902-1908.

5. J. L. Kirtley et al., "Rotating Electric Machine Having a Toroidal-Winding Armature," U.S. Patent Application Ser. No. 372,129, filed June 19, 1973.

6. J. L. Kirtley, "Rotating Electric Machine Having a Controlled Gradient Winding and a Circumferentially Segmented Magnetic Core Armature," U.S. Patent Application Ser. No. 372, 130, filed June 19, 1973.

7. Electrical Transmission and Distribution Reference Book, 4th Edition, Westinghouse Electric Corporation, East Pittsburgh, Pennsylvania, p. 7.

8. R. M. Edgell and R. S. Bayless, "AC and DC Transmission Comparison for Kaiparowits Coal-Fired Generation Plant," IEEE Trans. on Power Apparatus and Systems, Vol. PAS-95, No. 4, July/August 1976, pp. 1123 ff.

9. H. L. Rorden, "Lightning Arresters as a Criterion for Insulation Levels," AIEE Trans., Vol. 69, 1950, pp. 84-96.

10. Bibliography of Publications Pertaining to Lightning Protection, IEEE Transmission Sustation Committee of the IEE Substations Committee, IEE Trans. on Power Apparatus and Systems, Vol. PAS-94, No. 4, July/August 1975, pp. 1241-1247.

11. R. O. Berglund, W. A. Mittelstadt, M. L. Shelton, P. Barkan, C. G. Dewey, K. M. Skreiner, "One-Cycle Fault Interruption at 500 kV: System Benefits and Breaker Design," IEEE Trans. on Power Apparatus and Systems, Vol. PAS-93, Paper T 74 176-4, pp. 1240-1251.

12. G. Bahder, G. S. Eager, Jr., D. A. Silver, S. E. Turner, "550 kV and 765 kV High Pressure Oil Filled Pipe Cable System, "IEEE Trans. on Power Apparatus and Systems, Vol. PAS-95, No. 2, March/April 1976, pp. 478-488.

13. G. M. Lanfranconi, G. Maschio, E. Occhini, "Self-Contained Oil-Filled Cables for High Power Transmission in the 750-1200 kV Range," IEEE Trans. on Power Apparatus and Systems, Vol. PAS-93, No. 5, September/October 1974, pp. 1535-1545.

14. G. L. Moses, R. J. Alke, "Studies of Impulse Strength and Impulse Testing Problems on High-Voltage Generators," AISS Trans. on Power Apparatus and Systems, Vol. 72, pt. III, April 1953, pp. 123-121.

15. K. H. Chang, T. B. Thompson, "Surge Protection of Unit-Connected Generators," AIEE Trans. on Power Apparatus and Systems, Vol. 78, pt. IIIB, February 1960, pp. 1580-1590.

16. F. M. Clark, "Insulating Materials for Design and Engineering Practice," (book), John Wiley and Sons, Inc., New York, 1962.

17. L. J. Berberich, "Dielectrics in Power and Distribution Equipment," in "Dielectric Materials and Applications," (book), A. R. von Hippel, Editor, The Technology Press of M.I.T. and John Wiley and Sons, Inc., New York, 1954.

18. J. L. Smith, Jr., "High Voltage Oil Insulated and Cooled Armature Windings," U.S. Patent No. 3,743,867, July 3, 1973.

19. Discussion by H. D. Taylor for Reference 20.

20. C. J. Fechheimer, "Liquid Cooling of A-C Turbine Generators," Trans. AIEE, Vol. 66, 1947, pp. 553-564.

21. C. E. Kilbourne, C. H. Holley, "Liquid Cooling of Turbine-Generator Armature Windings," AIEE Trans., Vol. 75, pt. III, 1956, pp. 646-656.

22. J. L. Kirtley, Jr., "Continuation of the MIT-EPRI Superconducting Generator," IEEE Trans. on Power Apparatus and Systems, Vol. PAS-96, pp. 88-96, January/February 1977.

23. J. F. Sutton and J. E. Stern, "Spacecraft High-Voltage Power Supply Construction," NASA Technical Note TN D-7948, NASA, Washington, D.C., April 1975.

24. C. Flick, "Three-Dimensional Flux Distribution Studies in Superconducting Turbine Generators, IEEE Paper A 77 036-7.

Stator Winding Configuration Selection

The immediate stimulus for initiating a study of basic stator winding configurations was that no existing concepts were found to be entirely appropriate to the requirements for EHV armature windings that were defined in the preceding Section. These studies culminated in the definition of a new "spiral pancake" armature winding configuration with great potential for further development. They incidentally provided further insight into basic aspects of winding configurations.

Final Concept Evaluation and Selection

The following order of priority may be assigned to alternate winding concepts on the basis of these studies:

1 - spiral pancake winding
   a - low voltage application
   b - high voltage AC application (EHV)
   c - high voltage DC transmission application
   d - ultra-high voltage application

2 - modified airgap winding (low voltage only)

3 - monolithic airgap winding with distributed involute coils

4 - Gramme ring armature
   a - low voltage application
   b - high voltage application

5 - pole armature (high voltage only).

This rating is based on a consideration of the following advantages and limitations of the alternate configuration concepts:

Spiral Pancake Winding

- Most orderly configuration of conductors and insulation
  - minimizes dielectric stress concentrations
  - produces smooth, continuous, and overlapping spaces for insulation
  - creates long paths to minimize surface creepage
  - is compatible with high-voltage insulating materials
  - results in excellent support for armature end turns
  - results in simple and easily manufacturable coil shapes

- Versatility of concept allows application to high-voltage as well as low voltage windings and thus
  - permits consideration of EHV turbine generators and substantial savings by elimination of main transformer
  - permits consideration for HVDC transmission application (only candidate for this function)
  - permits consideration for low voltage machines with low reactance design to improve critical fault clearing time
  - is compatible with fully developed insulation technology for low voltage applications
- Requires extensive development of manufacturing technology for low voltage application
- Requires detailed theoretical and experimental concept verification for high voltage application
- Results in somewhat lower power density in active parts of machine than is ideally possible, but:
  - Gives best possible power density when space allocation is dictated primarily by insulation requirements
  - Provides improved end turn dimensions
  - Consequently results in moderate increase in weight, almost no increase in length, and essentially same cost per kVA

Modified Airgap Winding

- Utilizes fully developed insulation technology, which offers:
  - Reliability:
    - Full quality control possible on each coil
    - Assurance against moisture ingress
    - Positive grounding of dielectric stress grading system
    - Positive means of support against radial and tangential electromagnetic forces
    - Accommodation of axial expansion of windings without loss of support
  - Manufacturability
    - More positive control over manufacturing processes and variables than in strictly monolithic windings
  - Maintainability
    - Provisions to accommodate dimensional changes more readily incorporated and continuously acting
    - Better accessibility
- Higher power density possible in active parts than with spiral pancake or other concentric windings
- Limited to maximum rated voltage around 36 kV
- Long, flaring end turns of complex shape are difficult and relatively costly to support. Uniform support at all points virtually impossible to achieve.

Monolithic Airgap Winding with Distributed Involute Coils

- Utilizes same fully developed insulation technology for individual coils as the modified airgap windings, but:
- Requires extensive development of materials, manufacture, and quality control for the support provisions in and around the windings
- Same limit on voltage as modified airgap winding
- May have lower power density than modified airgap winding because of increased space required for support provisions
- Is not as maintainable

Gramme Ring Winding

- Has compact end turns which tend to minimize the end component of armature reactance
- Eliminates crossing of different phases in end turns leading to better management of dielectric stresses
- Requires external damper windings to suppress reactance due to return conductors on outside of armature core, producing:
    - Increased losses
    - Increased machine volume (and cost)
    - Support difficulties
- Does not appear capable of EHV application when both insulation and mechanical support requirements are considered simultaneously

Pole Armature

- May have capability for EHV rating
- Does not appear practical with respect to armature reaction on the rotor
- Appears to have inherently high reactance characteristics

On this basis, the spiral pancake winding concept has been selected as that showing the best potential for future development of superconducting turbine generators. The concept has been reviewed by EPRI's consultants at MIT. Their comments support the foregoing evaluation. Dr. Smith has stated his opinion that the spiral pancake winding is "a major step forward in realizing the full potential of superconductors in large synchronous machines". Dr. Kirtley has stated: "The spiral-winding armature configuration...looks to me as if it may form the basis for successful high voltage armatures. This scheme promises to provide good, full-length support for the armature conductors while affording good electric field management."

The final detailed design studies are based on spiral pancake windings.

Brief History

Early texts[1] on electric machinery recognize the following armature types:

(1) Ring armatures, in which the coils are grouped upon a ring, whose principal axis of symmetry is its axis of rotation.

(2) Drum armatures, in which the coils are wound longitudinally over the surface of a drum or cylinder

(3) Pole armatures, having coils wound on separate poles projecting radially all round the periphery of a disk or central hub.

(4) Disk armatures, in which the coils are flattened into a disk.

Pole armatures may be considered entirely obsolete, and disk armatures are not applicable to large high-spped machines because of the large diameter-to-length ratio.

Different types of ring armatures were first introduced by Pacinotti in 1864 and by Gramme in 1870. The Pacinotti design used a toothed ring with sectionalized coils. The Gramme ring was smooth, with uniformly distributed coils. Ring armatures were popular in the latter decades of the 19th century, but had been gradually displaced by drum armatures by the beginning of the 20th. By that time, the basic form of the conventional drum winding in a toothed core had largely evolved to its present form. For all practical purposes, this form is used in all conventional turbine generators.

Drum windings can be made with concentric or with distributed windings. At present, most drum windings are executed with distributed windings using diamond-type coils with involute ends. It can be shown, at least in principle, that this type of winding evolved from a stretching of the coils of an elongated ring winding. Presumably, the intent was to interlink a larger amount of flux. This transformation is sketched in Figure 3-112.

Spiral Pancake Winding

The spiral pancake armature winding is a drum winding with concentric coils which are curved into the final shape and interleaved so as to form the number of required phase belts at the proper angular separation. The concept is illustrated in Figure 3-113 through 3-117. Each of these windings is, in plane development, a pancake or racetrack coil. In order to make the complete winding, these pancakes must be formed to the correct spiral end view and assembled, together with the necessary insulation, either by axial insertion, or by interleaving after partial and temporary deflection, or by a combination of both.

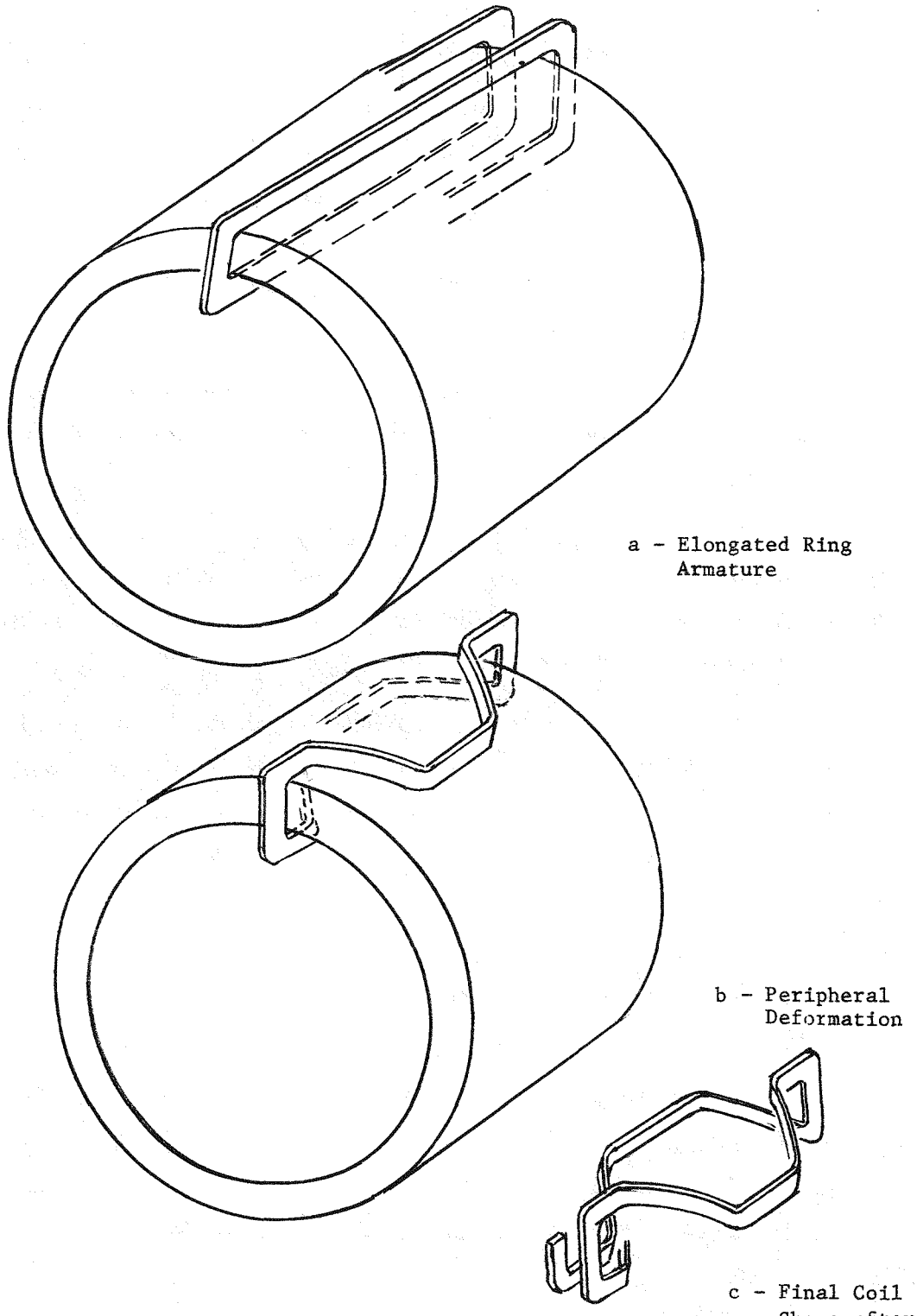

Figure 3-112. Transformation of an Element of a Ring-Wound Armature into a Drum-Type Full Coil.

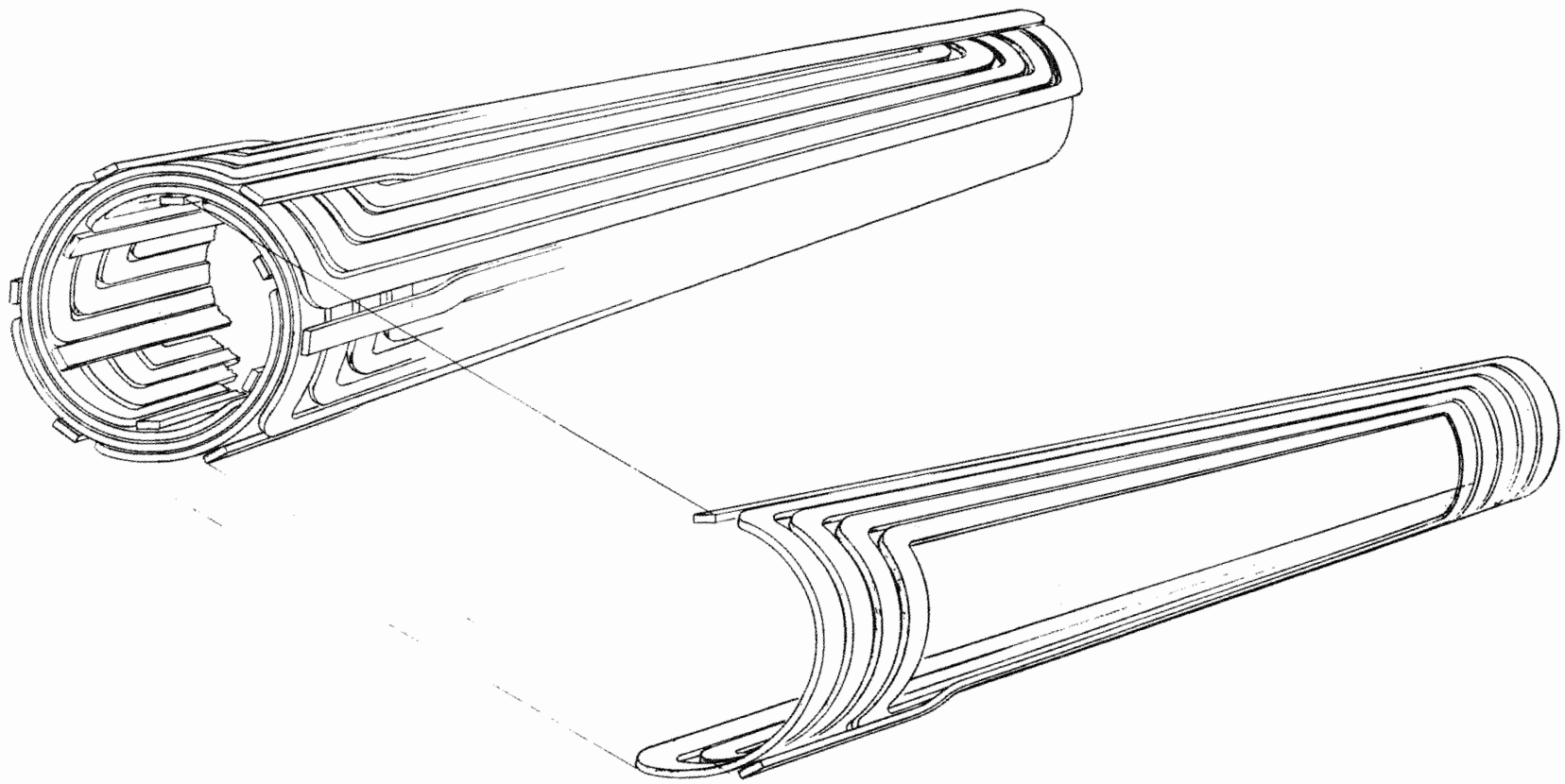

Figure 3-113. Spiral Pancake Winding Concept

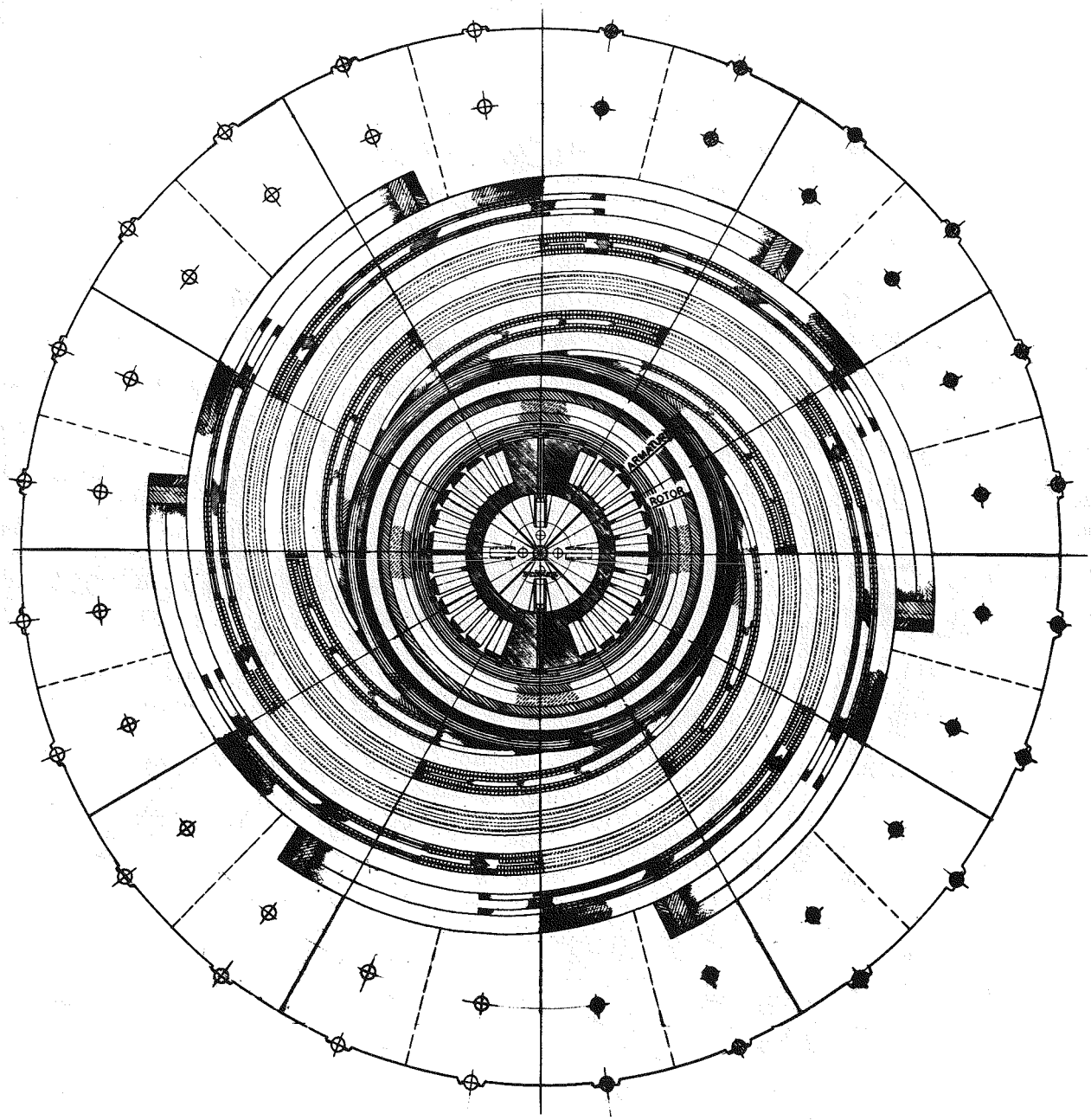

Figure 3-114. Cross Section of Spiral Pancake Winding for EHV Superconducting Turbine Generator Showing Main Components

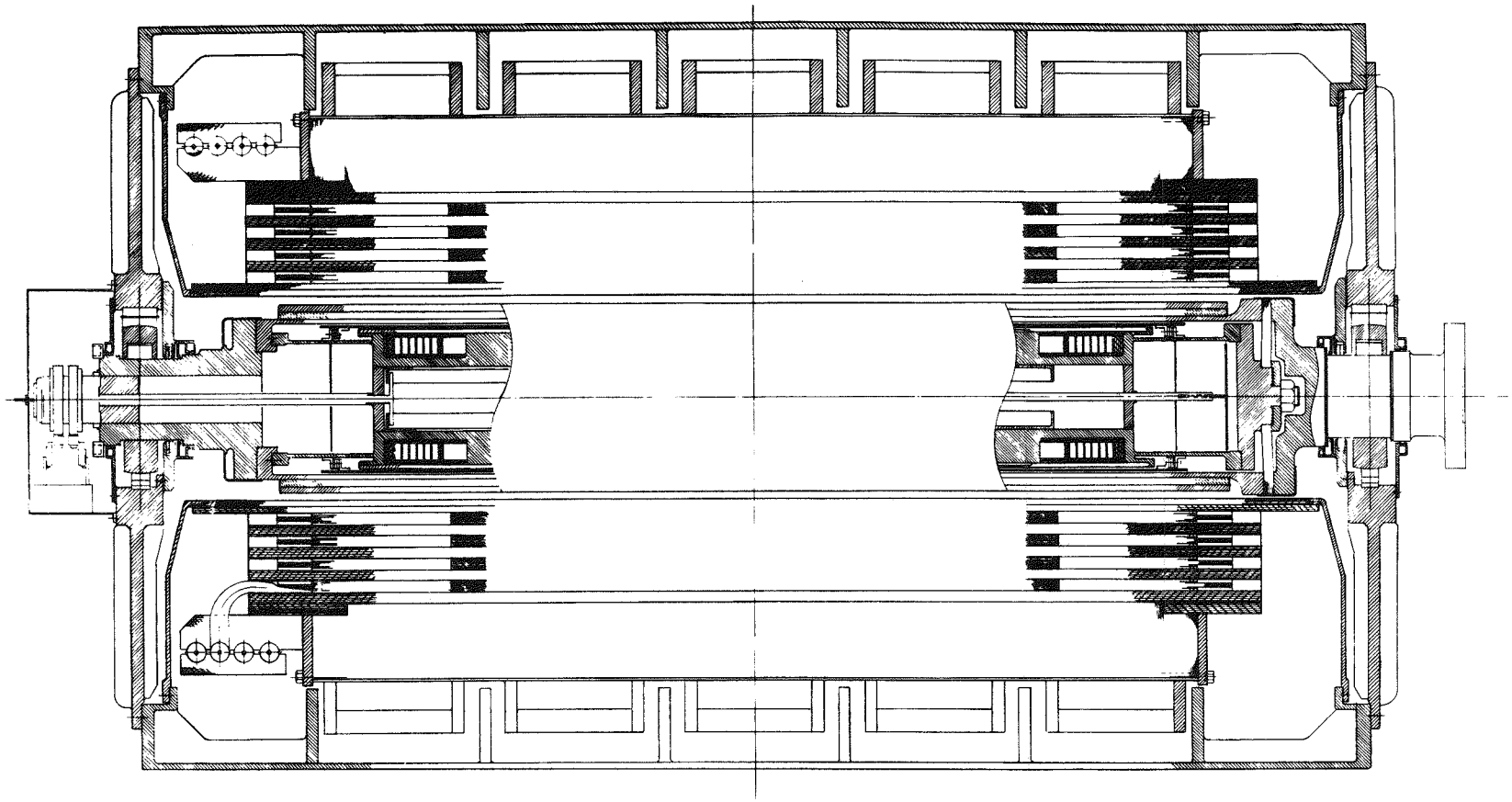

Figure 3-115. Longitudinal Section of Superconducting Turbine Generator with EHV Armature Winding

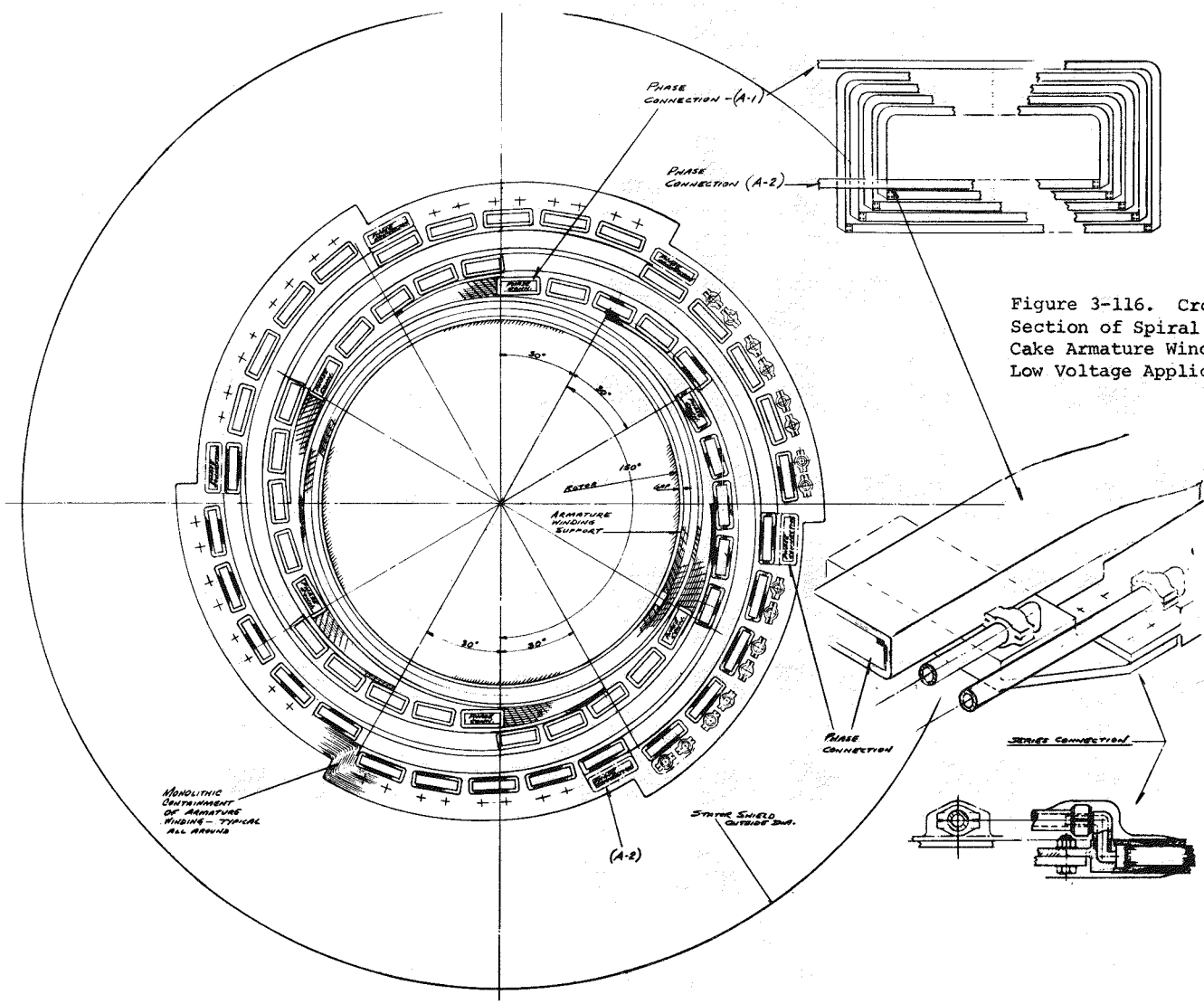

Figure 3-116. Cross Section of Spiral Pan-Cake Armature Winding for Low Voltage Application

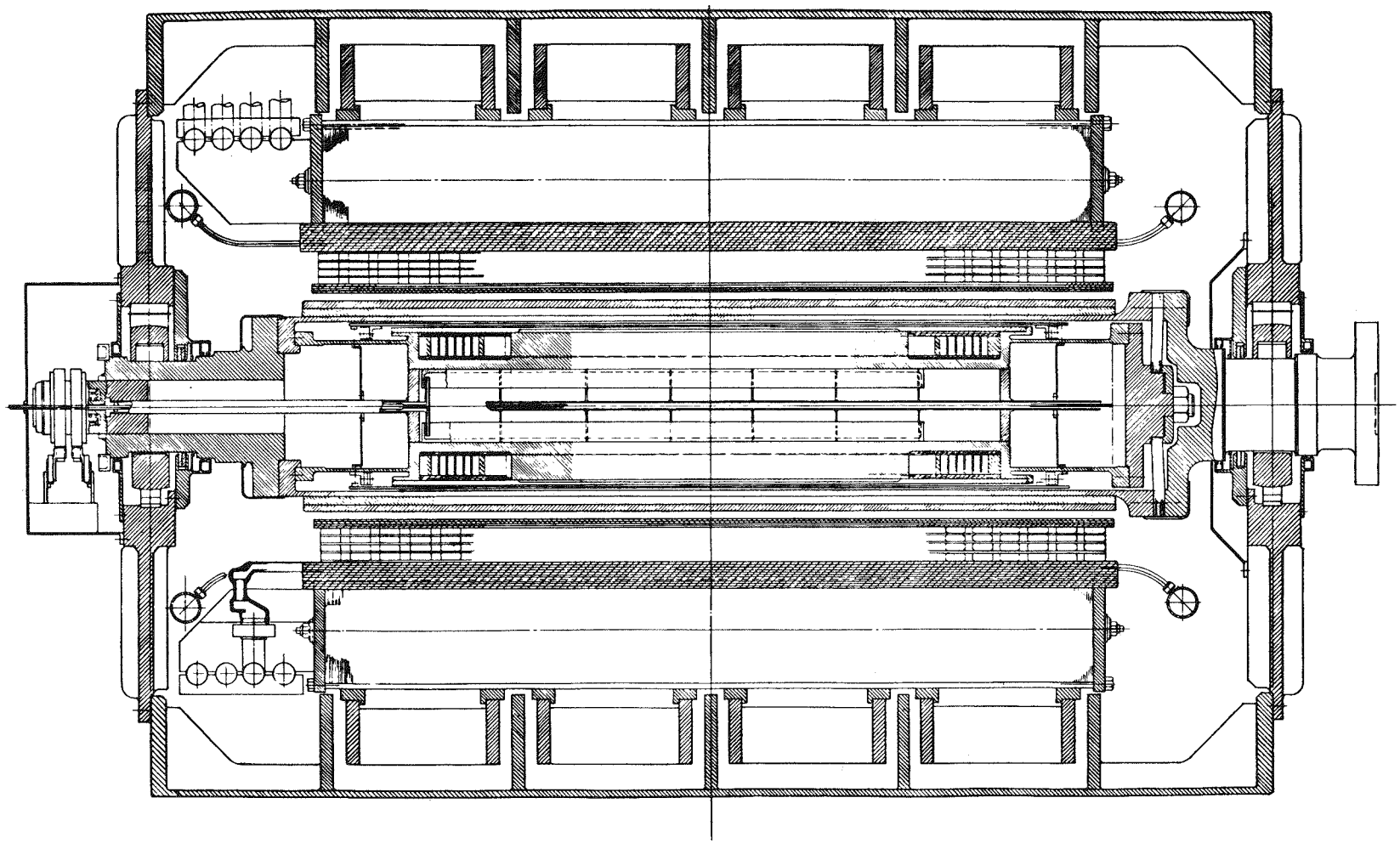

Figure 3-117. Longitudinal Section of Superconducting Turbine Generator with Low-Voltage Armature Winding

A spiral pancake armature winding produces an mmf wave that can be identical with that of a double layer winding. The effects of 5/6 pitch can be obtained, and thus rotor surface heating can be minimized. The effectiveness of space utilization appears to be better, especially at very high voltages, than that of any other known configuration. If only conductors were to be considered, it might be concluded that the space utilization is not as good as that of a double-layer airgap winding, but the space requirements of high voltage insulation are so demanding that this consideration overrides that of filling as much space as possible with active conductors. Unless high voltage insulation is applied to make optimum use of its capabilities, its space requirements quickly lead to impractical results.

The spiral pancake winding configuration is believed to be original. It has been disclosed to EPRI for possible patent protection. It is understood that EPRI is proceeding towards applying for this.

The various design options that can be considered with this spiral pancake winding concept are illustrated in Table 3-54. This table illustrates that the concept can be implemented in the short range with materials that are available from current cable and transformer insulation technology, but is not limited by these choices. As further developments in insulation technology take place, it will be possible to apply improved materials to gain further advantages, either in voltage capability, or power density, or both.

Application of the Spiral Pancake Winding Concept to High Voltage Armature

Please refer to Figures 3-114 and 3-115. The design illustrated therein represents a first-cut approach to the basic engineering problems encountered in designing for an exceptionally high voltage, but does not address the problems that may occur in manufacturing. Manufacturing techniques, including all assembly sequences and procedures, remain to be worked out. It is, however, believed that assembly, though difficult, will prove to be possible.

The complete armature winding concept illustrated in Figures 3-114, 3-115 consists of six pancake type coils wound of many series paper-insulated turns, which are themselves composed of fine copper strands that are mutually insulated with a synthetic varnish film. The fine stranding is required to minimize stray losses which would otherwise be produced by the high flux densities present in the winding. For the same reason, the fine wires are transposed in two directions, as described below. The turns of each coil are arranged in two layers, which are further

TABLE 3-54

SPIRAL PANCAKE WINDING

DESIGN OPTIONS

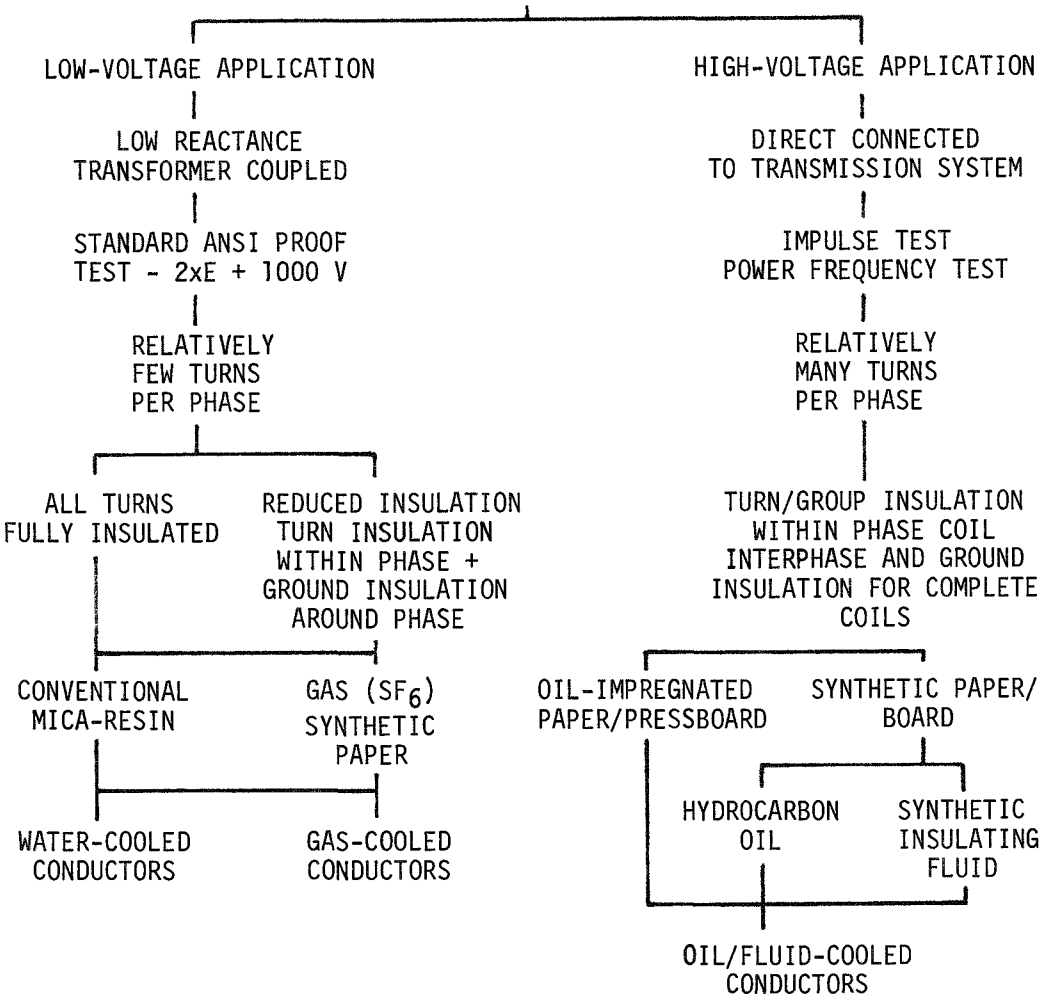

subdivided, as shown in Figure 3-118. The subdivision into multiple layers is done to control dielectric stresses. Each set of two adjacent layers is separated by a duct for cooling and insulating fluid. The conductors of the two layers associated with one fluid duct are wound in the same direction, and are, in effect, electrically in parallel. The voltage of any one conductor is therefore essentially the same as that of its mate on the other side of the duct, so that the potential difference across the duct is close to zero everywhere between the two layers of conductors. The dielectric fluid is thus shielded against dielectric stress. The other fluid duct, which is at a different potential from the first, is shielded in a similar manner. The potential difference between the two is sustained by the stepped intracoil insulation between the sets of conductor-duct layers.

The insulation between the six pancake coils is provided by layers of oil-impregnated cellulosic insulation, such as pressboard, paper, or a combination of both. The insulation, in sheets, is assembled into an inner cylinder that separates the innermost armature conductors from the outer surface of the bore seal tube, and into six layers of interphase insulation. These six layers conform to the basic spiral form of the coils, and their edges overlap the edges of the coils on sides as well as on ends as required by creepage considerations. The edges are tapered out by cutting the component sheets to different widths.

The bore seal tube seals and supports the winding and also controls the dielectric stress in the gap of the machine. This tube is made of a fiber-reinforced synthetic resin and must be essentially oil and gas tight. On the ends, this tube is connected into the stator frame in such a manner as to maintain tightness while permitting thermal expansion. At, or very near, its outer surface, this tube is provided with a suitably arranged conducting or semiconducting layer, which is grounded. This layer effectively excludes electric fields both from the gap and from the main thickness of the bore seal which therefore need not have the high insulating properties that would be required in the absence of this electrostatic shield. Such a shield can be made of a very thin layer of conducting or semiconducting paint. In order to minimize losses in this paint layer itself, it will not be continuous over the surface, but rather subdivided into thin patterns of strips. There may be voltage distributions tending to circulate currents between strips, and this must be resisted by the surface creepage or puncture properties of the bore seal tube itself. The proper control of this voltage is noted as a matter requiring further investigation. The embedment of the conducting strips within the resin-impregnated part of the tube may be enough to prevent partial discharges.

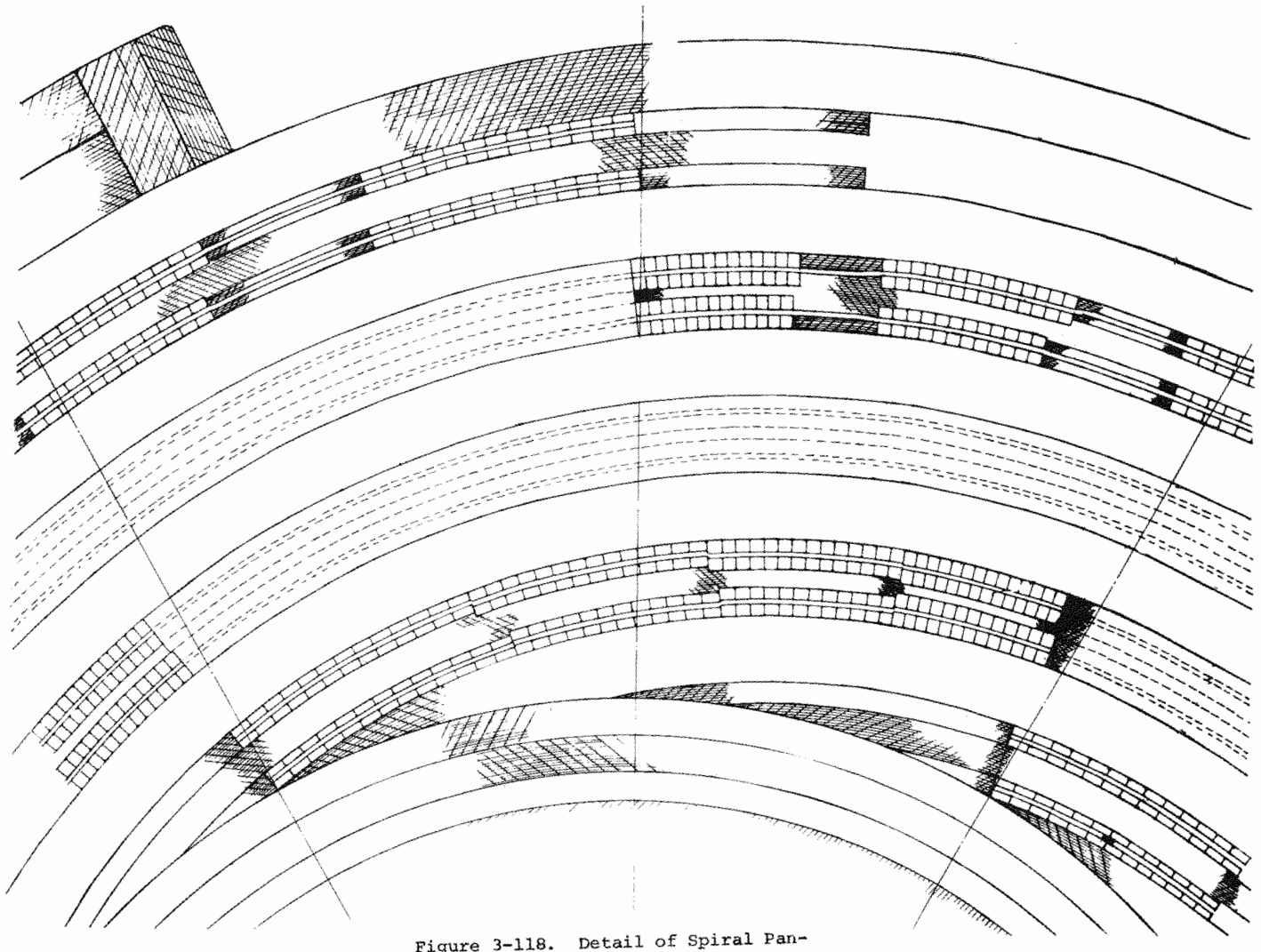

Figure 3-118. Detail of Spiral Pan-Cake Winding Concept for EHV Armature

It may be better to expose the shielding layer to the oil, on the other hand, and thus attempt to gain improved creepage properties. This is an area where theoretical predictions are most difficult, and test models will be required.

The entire space between the bore seal and the outer diameter defined by the flux shield bore or flux shield seal is filled and saturated with insulating oil, for example, of the transformer grade. This oil not only serves as an insulating and impregnating fluid, but also serves as a coolant for the winding. In veiw of the well-known extreme sensitivity of insulating oils to moisture contamination, it is not deemed permissible to combine oil insulation with water cooling of the windings. Although water cooling has proven to be very successful when combined with gas cooling of other parts of the machine, and leak-proof stator windings are now routine, it is judged that the possible entry of even small amounts of water into the oil could have such adverse consequences as to hazard reliability. The cooling oil is circulated through passages which appear naturally at the edges of the coils as a consequence of the spiral geometry, and thence through the two oil ducts present in each double layer of conductors, which are maintained by suitable spacer blocks. It is also possible to create passageways for internal cooling of the individual conductors.

Terminal Arrangements for Large EHV Turbine Generators

The type of terminal arrangement that is used for large turbine generators of conventional design is illustrated in Figure 3-119. Such an arrangement would also be suitable for superconducting generators with armature voltage ratings in the range of 24 to about 36 kV. For voltage ratings at transmission system levels, terminal arrangements suitable for the required BIL and working voltage are required. This requires consideration of the overall plant arrangement, with attention to the transient effects of voltage surges at different points of the connections between the transmission line and the generator windings. Unless it proves possible to terminate the line and connection in a generator surge impedance equal to that of the line, amplification of voltage surges by reflection at the far end of the generator windings must be prevented by installation of surge arresters at or near the generator terminals.

Several conceptual arrangements are presented in the following, using different combinations of oil, gas, and air insulated parts. The most obvious arrangement, that of mounting high voltage bushings directly on the generator enclosure, is not included. It has been omitted because it is considered to be of

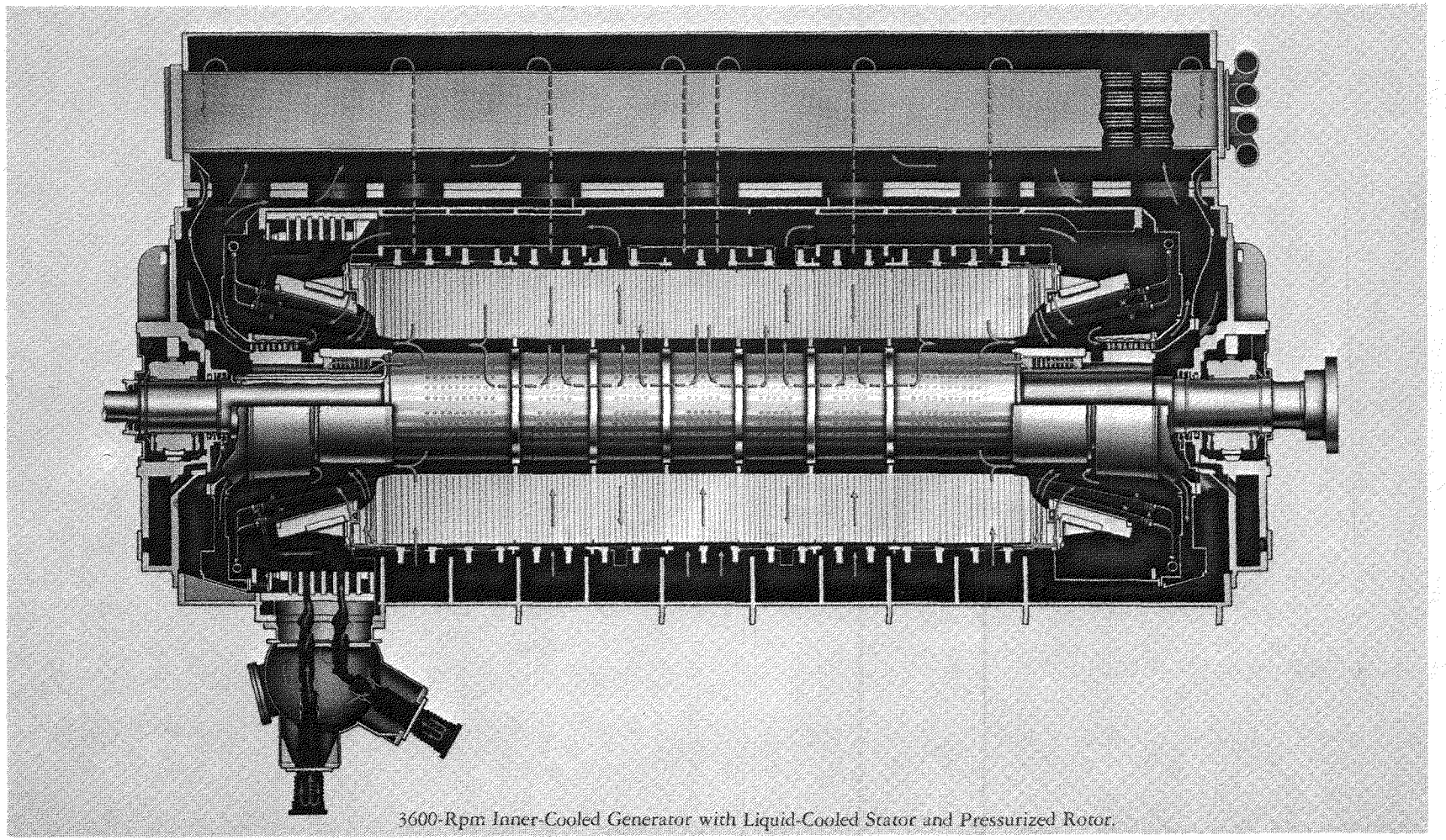

Figure 3-119. Main Lead Terminal Arrangement for Large Conventional Turbine Generator.

questionable practicality and reliability. It would limit the generator installation to a placement of the generator outdoors where the large clearances in air required to withstand the high voltages would be available. It is questionable that this would be generally acceptable. Furthermore, it requires the placement of large and long bushings on a vibrating base, namely the generator frame. The vibration characteristics of such a combination would have to be carefully reviewed to assure success. Alternative arrangements, believed to offer better potential of success, are therefore presented.

Arrangement 1. Oil-filled Connection to Aerial Line

Please refer back to Figure 3-99 . According to this concept. the internal phase connections of the generator are made as oil-impregnated paper-insulated conductors that are, in effect, high-voltage cables. Three of these, the main leads, are continued as a three-phase, oil-filled, pipe type cable through a flexibility loop to a separately encassed oil-filled pothead equipped with the required high voltage bushings. The connections to the power system, including the lightning arresters and the main breaker, as well as the connection to the overhead aerial line, are made via these bushings. The connection between the generator phase connections and the cable continuation is made in an oil-filled enclosure mounted on the side of the machine; this enclosure also provides room for mounting a set of close-coupled lightning arresters, should these be required. A similar enclosure is mounted on the opposite side of the generator and contains the neutral connection.

Arrangement 2. Oil-filled Connection to Gas-Insulated Substation

See Figure 3-120 . This concept is similar to that of Arrangement 1 at the generator end; but the oil-filled cable terminates instead in a set of wall bushings that connect from the oil side to the gas (SF_6) side[2] of a compact tank-enclosed gas-insulated substation, which includes a set of lightning arresters as well as a direct connection to the circuit breaker which is visualized as being incorporated in the compact assembly. According to modern practice, this would be a live-tank breaker at 500 kV operating voltage, and would be directly connected to the 500 kV line.

Arrangement 3. Gas-filled Connection

See Figure 3-121 . According to this concept, the transition from oil to gas is moved back towards the generator, and is accomplished in the enclosure at the side of the generator by means of wall bushings. The remainder of the

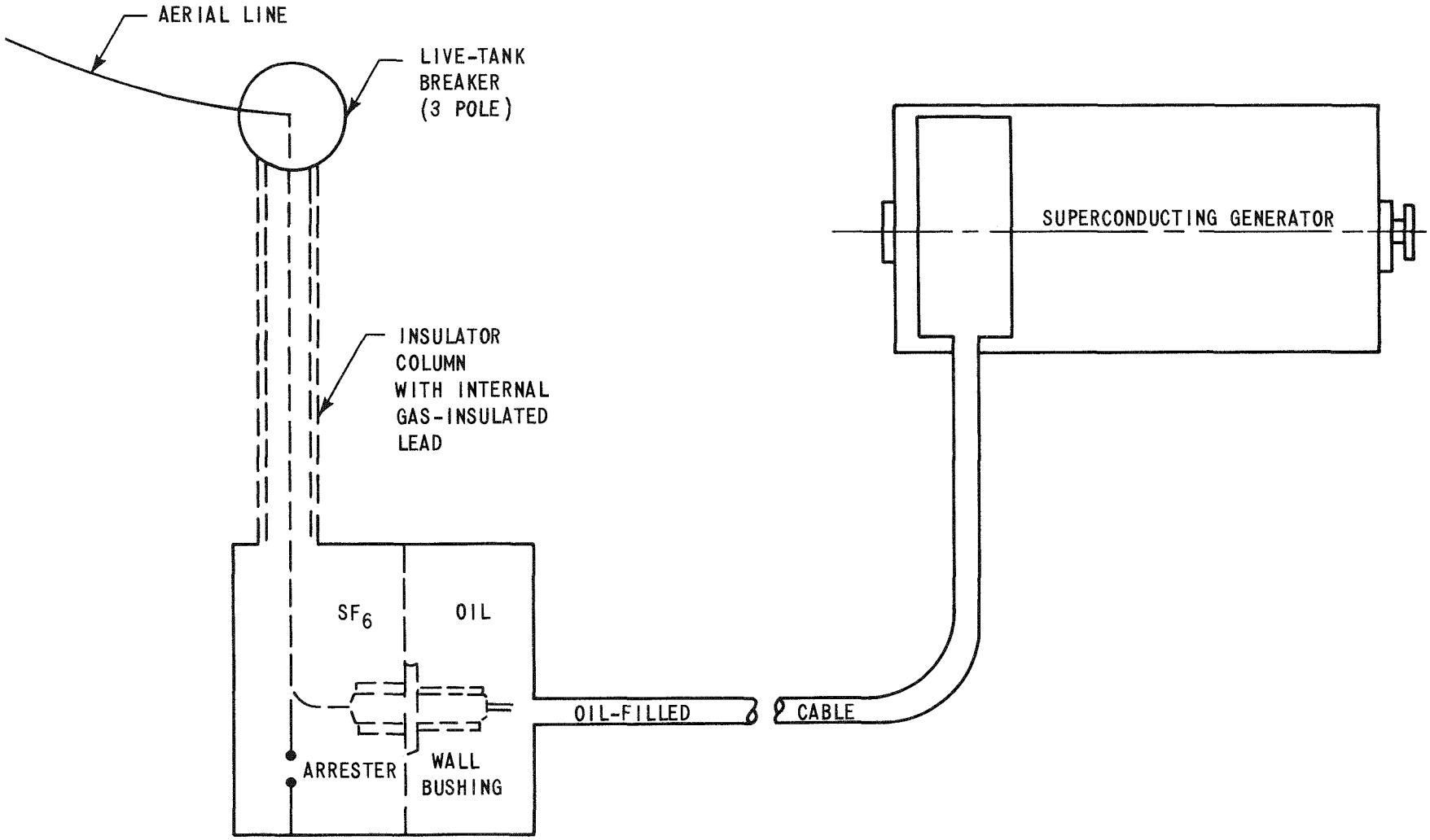

Figure 3-120. Conceptual Arrangement 2. Oil-Filled Connection from Generator to Gas-Insulated Substation

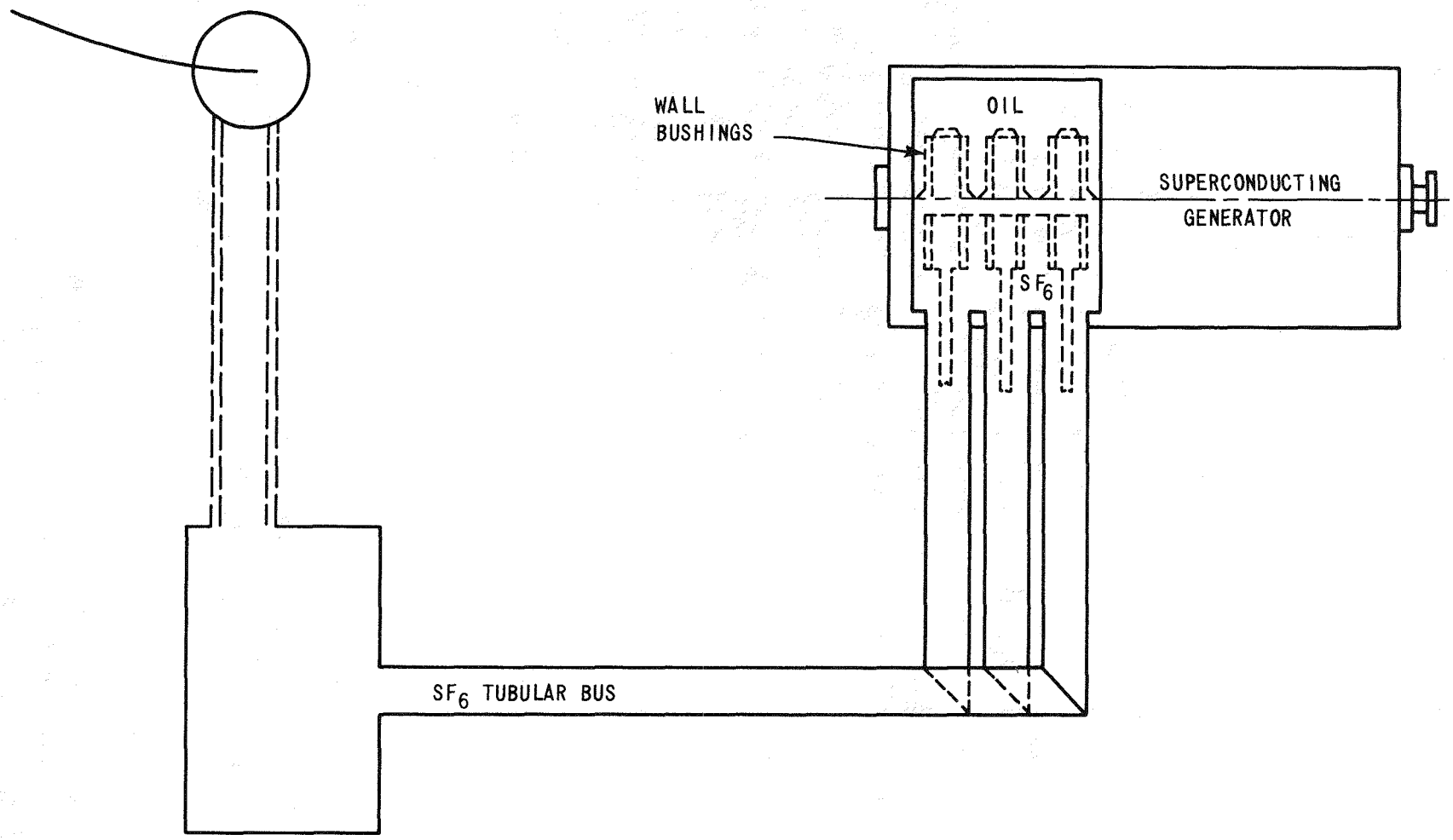

Figure 3-121. Conceptual Arrangement 3. SF_6 Tubular Bus Connection from Generator to GIS. Otherwise same as Conceptual Arrangement 2.

connection scheme would be similar to that of Arrangement 2, except that in this concept an SF_6 tubular bus[3] would be used to connect to the GIS.

Preliminary investigations indicate that, for the realization of any of these concepts, extensive adaption and development of existing types of switchgear would be required, but that no new technology is required. The detail development would have to address such questions as the mounting of instrument transformers in oil, reliability and safety aspects, and cost.

Reduction in Fault Capacity with EHV Armature Windings

An interesting and useful consequence of the type of connection illustrated in Figures 3-99 , 3-120 , or 3-121 is that the maximum current that can flow in any armature winding is limited by the total impedance offered by the generator and the system to the point of fault. In order words, it is no longer possible to have a "high side fault" and a "low side fault" of different severities. Since EHV generators necessarily possess somewhat higher reactance levels than low voltage designs, this will provide a desirable reduction in the maximum electromagnetic forces for which the mechanical supports must be designed.

Scaling of High Voltage Design Criteria for Larger and Smaller Ratings

For the proper definition of a development and application plan for high voltage windings, it is obviously not enough to limit consideration to the single rating of 1200 MVA. In order to estimate the effects on the design criteria of scaling the MVA rating up and down, it is necessary to consider the relation of the BIL to the rated voltage. This relation is not constant; at higher rated voltage levels, the ratio of BIL to rated voltage is reduced. This has a direct bearing on the dominant design criterion for the major insulating barriers.

A possible relationship of rated operating voltage and BIL for generator ratings of 100 MVA to 5000 MVA at voltage ratings that would permit direct generation at transmission system levels is shown in Figure 3-122. This figure also shows the thickness of interphase insulation that would be required at a dielectric stress value of 20 MV/m (500 V/mil) average, and the average stress at the operating voltage. As MVA ratings are reduced from the reference value of 1200 MVA, and at a constant stress at the BIL, the dielectric stress at the operating voltage is also reduced. In this range, therefore, the insulation design tends to be dominated by the BIL requirements, and tends to become more conservative at the operating voltage as MVA rating is reduced. On the other hand, at MVA ratings above the reference value, the

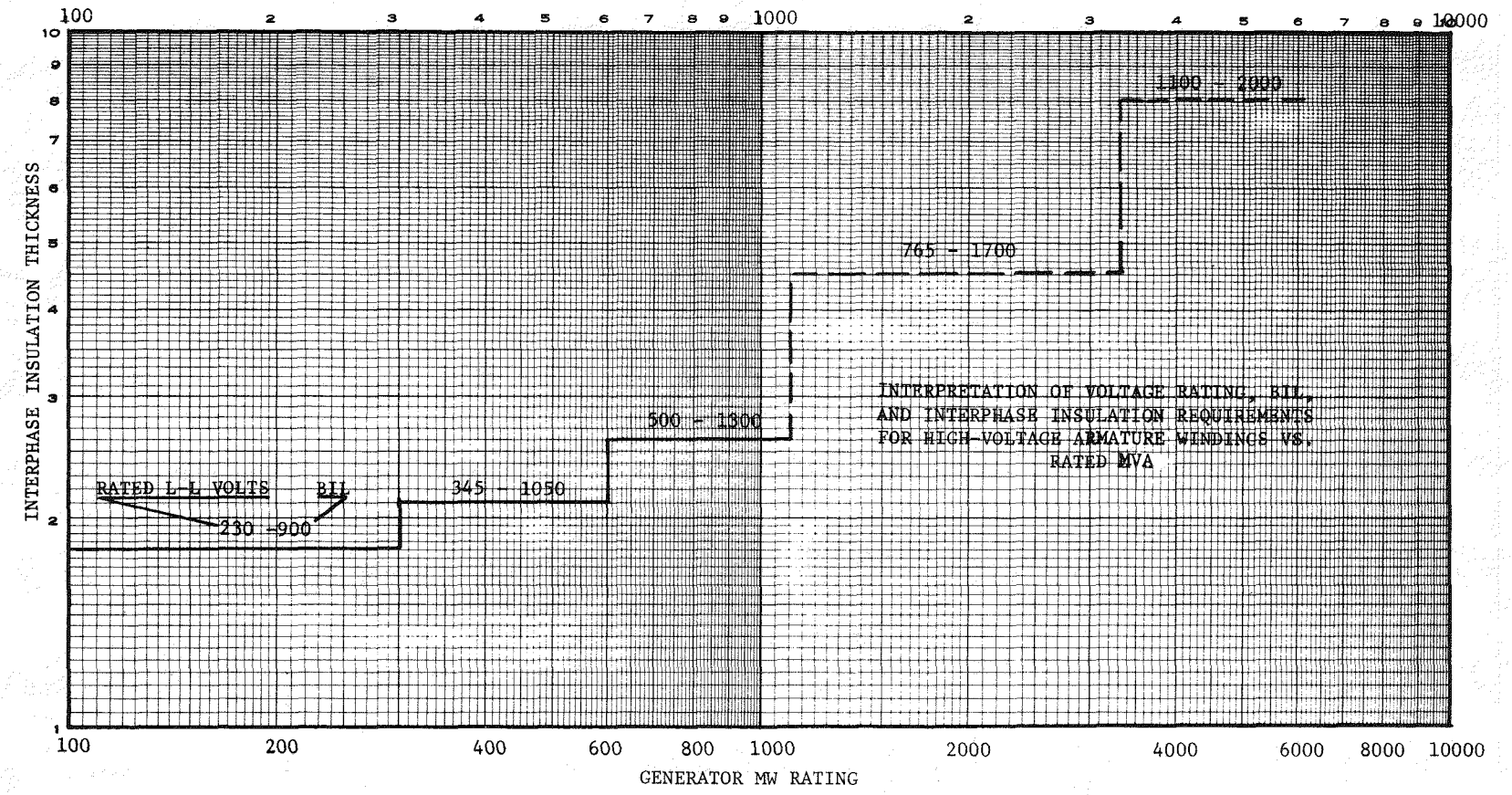
INTERPHASE INSULATION THICKNESS
GENERATOR MW RATING
100
200
400
600
800
1000
2000
4000
6000
8000
10000
1100 - 2000
765 - 1700
500 - 1300
345 - 1050
RATED L-L VOLTS
BIL
230 - 900
INTERPRETATION OF VOLTAGE RATING, BIL, AND INTERPHASE INSULATION REQUIREMENTS FOR HIGH-VOLTAGE ARMATURE WINDINGS VS. RATED MVA

Figure 3-122

insulation design is dominated by the steady-state dielectric stress. Moreover, as insulation thickness is increased, its working dielectric strength in MV/m tends to fall, so that the increased stresses at the normal operating voltage would require more insulation than needed for the surge withstand requirements. At the BIL, the relation is more linear.

On this basis, extrapolation downward should prove relatively easy and safe, but extrapolation upward would require more extensive development of means for controlling the distribution of the dielectric stress, and possibly of material combinations for the insulating and cooling media. It may be necessary to consider also means for subdividing the very thick layers of insulation that would be required and to provide cooling so as to reduce the temperature rise within the insulation produced by dielectric losses. In evaluating the potential of such development, it should be kept in mind that this would go well beyond the state of the art even of current cable insulation technology.

The increasing insulation requirements that are thus encountered as ratings of 3000 MVA are approached tend to enlarge the size of the overall machine, since the effective current density of the armature winding (for a given maximum density in the copper) is reduced. A side effect of the relatively larger machine size is that cooling effectiveness tends to be decreased. The cooling passages tend to be longer, and more temperature rise in the cooling fluid takes place, so that the surface rise must be correspondingly reduced. This tendency must be considered in projecting designs into that size range. On the other hand, the relatively reduced power density of the machine reduces such electromechanical effects as the shaft torques during faults and the crushing force on the damper. These reductions tend to facilitate the mechanical design, and can have some offsetting influences with regard to machine size.

An exploratory set of designs was made at ratings of 300 MVA, 230 kV and 3000 MVA, 765 kV in order to obtain a preliminary indication of the trends as they influence overall machine size and characteristics. These results confirm the practicality of downward extrapolation of the concept. There appears, however, to be a size effect that is somewhat less favorable to high power density at 300 MVA than at 1200 MVA. This size effect appears to be primarily associated with the insulation required to provide the necessary BIL. The 3000 MVA machine is still larger in relation to its reference design with a conventional winding. With current limits on shippable size and weight, it could not be shipped as an

assembled unit. It calculates, however, as a very efficient electrical design (0.3% losses) with low levels of shaft torques and damper stresses, so that there appear to be opportunities for further improving the dimensions and reducing the size.

The discussion presented in this section is based solely on electrical design considerations. Mechanical and thermal analyses have not been performed.

Reliability Factors for EHV Armature Windings: Test, Maintenance, and Fault Anticipation

Experience with large numbers of conventional turbine generators covering a wide range of sizes and types teaches us that the probability of satisfactory operation throughout a normal service life is greatly enhanced by a sound program of quality assurance. The essential elements of such a program include factory testing, periodic maintenance, and early recognition and prevention of potential hazards and incipient damage.

The correct definition and implementation of such a program must naturally proceed from a thorough understanding of the machine construction and of the factors that tend to inhibit its reliable performance or reduce its life. It is generally recognized that the armature windings of conventional machines are vulnerable in this respect. The life expectancy of such an armature winding is usually taken to be shorter than that of most other parts of the machine, so that one or more rewinds are not uncommon. Industry guides have been prepared for the preferred practices for testing and maintaining armature windings[4-7], and are regularly updated. Thus there is a fund of information available to assist in the effort to secure reliable performance from armature windings of conventional design.

This is not, of course, now the case with EHV armature windings which would use the spiral pancake coil configuration. It is therefore necessary to examine the fundamentals which would apply to this in order to frame valid recommendations for safeguarding the reliability of such windings. Consideration of insulation application parameters is basic to such an understanding.

Application of EHV Insulation: Comparison to Conventional Practice

The concepts which govern the application of insulating materials to the EHV armature winding are fundamentally different from those used in designing conventional windings and much simpler to grasp. Their points of reference are high voltage transformers and cables, devices where EHV ratings of 500 kV are well

established. In transformers, ratings of 1100 kV and above are feasible. The application of these concepts results in an orderly and efficient arrangement of windings and insulating materials that is quite unlike any conventional design. These are the underlying reasons for confidence in the potential of EHV armatures to accommodate voltage ratings that would be completely out of the range of conventional practices. (Westinghouse has reiterated for over a year that even a rating of 70 kV, the minimum required by EPRI, would be well beyond the capability of conventional insulation.) It seems rather regrettable that these concepts appear to have no application to generators with conventional field windings.

Before discussing detailed differences, it may be well to point out that the above-mentioned references to high-voltage transformers[18] relate to most of the EHV winding components, as coil construction, turn insulation, shielding, cooling, testing, and maintenance; while the use of insulation to ground and between phases is influenced more by cable design. Also, "low voltage spiral pancake windings" may be built with voltages that overlap the conventional range of ratings. These, while they would use the same basic insulating materials and impregnants as conventional windings, would employ the spiral pancake configuration to achieve other objectives and should not be confused with conventional windings.

Major differences in armature insulation concepts are:

Impregnant

Conventional windings use a solid impregnant, usually a polymerized synthetic resin. This impregnant is applied in what is essentially a one-time impregnation process during manufacture. Even if several impregnations are used, they are done in a time that is short in comparison to the service life of the machine.

EHV spiral pancake windings would use a dielectric liquid impregnant, such as a transformer oil, which would provide continuous impregnation throughout the service life and be in constant communication with the solid insulating components.

Elimination of Ionizable Voids

The initial impregnation of conventional windings effectively eliminates voids in the insulation. Aging processes that occur during the service life of the machine degrade or break some of the bonds that maintain the integrity of the insulating barriers, permitting new voids to arise. Therefore such windings cannot be

kept permanently void-free. The solid insulation must then be chosen so as to resist the attack of products of ionization. Mineral mica and mica products are excellent for this purpose. In EHV spiral pancake windings, on the other hand, the liquid impregnant would diffuse into incipient voids and would prevent the local variations in dielectric constant and strength that support ionization.

Time-Temperature Effects

Thermal aging of the synthetic resin impregnant used in conventional windings tends towards depolymerization and loss of mechanical integrity. This process is irreversible and eventually results in the need to rewind before ultimate failure occurs. At the time of failure, the intrinsic condition of much of the mica may still be excellent.

Thermal aging of the dielectric liquids in an EHV winding would result in decomposition and/or polymerization products such as acids or sludge. While these would be detrimental to the life of the winding if permitted to remain, they can be continuously removed from the oil stream. Thus the life expectancy would be determined by the life of the solid insulation.

Dielectric Stress Concentration

The distribution of dielectric stresses in a conventional armature winding is relatively complex. The physical parameters which determine this distribution vary substantially along the length of the machine, especially at the ends of the stator core where the ground plane abruptly changes direction. The complex bends in the coil shape necessary to effect the end connections change the characteristics of the insulating materials and their impregnants. Manufacturing processes may cause further changes in the finished coils. The use of semiconducting or conducting surface coatings on the coils (or of internal conducting shields) also modifies the stress distribution, and causes it to be different depending upon whether AC or DC voltage is applied to the windings. As a result, it is essentially impossible to predict the electric field distribution theoretically.

The orderly, continuous, and smooth structure intrinsic to the spiral pancake concept tends towards uniform distribution of dielectric stresses and interwinding capacitances. The end turns produce no abrupt changes in the pattern. The dielectric stress patterns may be considered to act in the following manner:

1 - between phase windings, stressing the volume of the interphase insulation and requiring it to resist puncture

2 - between phase windings, stressing the surface of the interphase insulation and requiring it to resist creepage

3 - from phase windings to ground, at the inner and outer peripheries of the armature, stressing the ground insulation volume and surface, and requiring it to resist puncture and creepage

4 - within phases, requiring puncture and creep resistance at somewhat lower voltage levels in the intracoil insulation

5 - between successive turns of each phase winding,

In view of the simple geometry, it appears feasible to make a mathematical model of the dielectric stress distribution of reasonable accuracy.

Contamination

The exposure of conventional windings to external influences, which are present to some degree even in completely closed hydrogen-cooled machines produce deterioration which may also be irreversible in severe cases.

EHV spiral pancake windings would be effectively protected against contamination by the surrounding liquid dielectric (which is continuously purified).

Mechanical Damage

Conventional windings may be damaged by diverse mechanical effects including shock, or by vibration accompanied by abrasion between winding components or even against foreign objects. The service life of a winding may be severely limited by such conditions. Conventional windings typically have large numbers of separate winding components and support elements which may vibrate against each other. Discontinuities in the mechanical support structure, virtually unavoidable in conventional windings with conical end turns, may predispose them to loss of support and consequent vibration.

Faults near the terminals of such machines produce high fault currents which result in severe mechanical shocks to the windings. It is well known that faults which occur on the high side of the step-up transformer between the generator and the power system are much less severe in current and force magnitudes. Certain types of very large generators with conventional windings are expected to survive high-side faults but not low-side faults without damage.

The EHV spiral pancake armature winding, which connects directly to the power system without voltage transformation, could in effect only experience high side faults. The mechanical forces tending to distort the windings would therefore be much smaller than the maximum possible with a generator that had a conventional low-voltage winding and, which in combination with its step-up transformer would offer the same reactance as seen from the power system.

The exceptionally uniform support without discontinuities which is provided by the spiral pancake geometry would further reduce the possibility of mechanical damage from shock or vibration.

Dielectric Test Requirements

Dielectric tests constitute a major tool in the evaluation of the serviceability of armature windings. In principle, such tests predict the long-time voltage endurance of a winding on the basis of its ability to withstand an elevated voltage for a short time. The voltage values that apply are standardized or follow industry practice.

Testing Procedures for Conventionally Insulated Armature Windings

The acceptability of an armature winding for initial delivery, and the determination of its serviceability during maintenance are based on the results of insulation tests. These tests generally include both physical examination of the windings for flaws, weak spots, and the like and electrical tests. Electrical tests are normally not performed until defects which can be observed by other means have been corrected and the windings are clean and dry. Electrical tests consist of those needed to determine the general condition of the winding, such as its dryness and cleanliness, and of final proof tests which verify the physical integrity of the dielectric barriers. Although the final proof test of "hi-pot" is in concept a simple go-no go test, its proper application and interpretation so as to obtain the maximum information on the winding at the least risk is technically intricate and requires experience and judgment.

Standard test voltage for initial factory tests of new apparatus are defined by ANSI Standard C50.1 (including C50.10 and C50.13). It is interesting to note that this standard requires only major ground insulation tests. Thus, in the case of multiturn turbine generator windings, no turn-to-turn dielectric test would necessarily be made.

Testing Procedures for Transformers[18]

The dielectric tests which may be made on transformer windings include impulse testing with full and chopped waves of standardized shape as well as low-frequency applied and induced potential tests. This type of testing therefore stresses turn insulation as well as major insulation to ground and between phases. Tests are made under oil.

Test Requirements for EHV Armatures

These tests would have to include impulse testing in order to confirm the basic impulse level for which the machine is rated. They would also have to include applied potential tests and some means of applying turn-to-turn voltages. Some development will be required to implement the last requirement, since there is no obvious way to induce a voltage in the armature winding short of using the superconducting field winding to generate flux.

Maintenance of Conventional Armature Windings

Manufacturers of large turbine generators generally recommend that such machines be inspected at the end of one year after delivery, and be taken down for periodic maintenance every three to five years thereafter. Between maintenance inspections, continuous supervision of the machine in normal operation is recommended. Abnormal events, such as terminal faults, frequently necessitate additional complete inspection and maintenance.

Maintenance for Transformer Windings[18]

It is not usual to disassemble transformers for inspection or maintenance. Normally, the windings remain submerged for the entire service life. Supervision in operation consists primarily of temperature indication and periodic checks on oil purity. Disassembly is generally not undertaken unless trouble is indicated by supervisory instruments or otherwise.

Maintenance for EHV Armature Windings

An EHV spiral pancake winding would be similar to the windings in a large power transformer so that their service performance should be comparable. It is reasonable to expect that supervisory and diagnostic instrumentation can be developed to eliminate the need for disassembly of the windings for inspection or maintenance during their lifetime.

Fault Anticipation

Although maintenance inspections have in the past constituted the main line of defense against potentially hazardous conditions present in the machine, recent advances, like core monitors, have made it possible to anticipate some such conditions even during operation. There is now considerable interest in developing fault anticipation devices. In principle, fault anticipation can be applied to EHV armature windings at rather small cost: a good system could consist of precise control of oil purity (which is necessary in any case) coupled with continuous supervision of impurity components. Another system would utilize a high-frequency coupler at the terminals of the machine to detect possible RF disturbances that might originate at internal discharges.*

Application of the Spiral Pancake Winding Concept to Low Voltage Armature

The low voltage armature is illustrated in Figures 3-116 and 3-117. In this application, the number of coils per phase is relatively small, the insulation (as compared to the high-voltage application) is relatively thin, and the individual conductors are relatively large in cross-section. Under these circumstances, a more favorable design results with water cooling of the conductors. This requires the use of conventional mica-resin insulation (since water cooling is not compatible with oil insulation). Accordingly, the individual pancakes of the winding would be composed of preformed and fully insulated conductors of alternate C-shape and I-shape that are connected at opposite ends of the machine with combined electrical and water connectors. The detailed view of such a connector is shown in Figure 3-116 . After being connected in this manner, the individual coils would be assembled into pancakes, which would then be assembled into a complete winding external to the shield. After further processing to produce a mechanically strong winding subassembly, this would be inserted into the complete shield in the axial direction, and tightened by wedging against the inner surfaces of the shield bore.

The simple cylindrical form of this winding with straight axial end extensions permits excellent and uniform end support to be applied. See Figure 3-117. As a result, it would be expected to tolerate the electromagnetic force effects due to fault conditions at higher levels than other configurations. This capability may be utilized be designing for lower values of subtransient reactance, and thus improving the critical fault clearing time criterion.

*(These concepts may be developed into patentable inventions and should be treated as such.)

References

1. S. P. Thompson, "Dynamo-Electric Machinery," (book), Spon and Chamberlain, New York, 1896.

2. "Transition from Oil to SF_6," Electrical Consultant, November/December 1976. (Description of Westinghouse type SFO bushing).

3. G. P. Baer, A. Diessner, and G. F. Luxa, "420 kV SF - Insulated Tubular Bus for the Wehr Pumped Storage Plant - Electrical Tests," IEEE Trans. on Power Apparatus and Systems, Vol. PAS-95, No. 2, March/April 1976, pp. 469-477.

4. IEEE Recommended Practice for Testing Insulation Resistance of Rotating Machinery, IEEE Standard 43-1974.

5. IEEE Guide for Insulation Maintenance for Large Alternating-Current Rotating Machinery, IEEE Standard No. 65-1958 (Reaffirmed 1971).

6. Guide for Insulation Testing of Large A-C Rotating Machinery with High Direct Voltage, IEEE Standard No. 95, Dec. 1962 (Reaffirmed June 1971).

7. IEEE Recommended Practice for Insulation Testing of Large AC Rotating Machinery with High Voltage at Very Low Frequency, IEEE Standard 433-1974.

8. E. J. Davies, "Airgap Windings for Large Turbogenerators," Proc. IEE, Vol. 118, No. 3/4, March/April 1971, pp. 529-536.

9. G. Aichholzer, "New Ways of Building Turbogenerators up to 2 GVA, 60 kV," Elektrotec. u. Maschinenbau, Vol. 89, No. 1, January 1972, pp. 1-11.

10. Proposal from Westinghouse Electric Corporation to Electric Power Research Institute, "Superconducting Turbine Generators for the Electric Utilities - Conceptual Designs and Development Plan RFP 429," May 23, 1975.

11. J. L. Kirtley, Jr., "Design and Construction of an Armature for an Alternator with a Superconducting Field Winding," Ph.D Thesis, MIT, August 1971.

12. W. C. Brenner et al, "Development of a 5 MVA Superconducting Generator - Electrical Design and Performance," IEEE Conference Paper C 73 245-8, presented at 1973 PES Winter Power Meeting, New York.

13. French Patent Specification No. 2 287 798 (Application No. 74 33785).

14. H. Spooner, "Fully Slotless Turbogenerators," Proc. IEE, Vol. 120, No. 12, December 1973, pp. 1507-1518.

15. J. L. Kirtley, Jr. and M. M. Steeves, "Toroidal Winding Geometry for High Voltage Superconducting Alternators," IEEE Trans. on Power Apparatus and Systems, Vol. PAS-93, No. 6, November-December 1974, pp. 1902-1908.

16. M. M. Steeves, "A Modified Gramme-Ring Armature for a High Voltage Superconducting Alternator," M. S. Thesis, MIT Dept. of Electrical Engineering, August 1973.

17. M. Furuyama, "A Design Concept of a Damper Shield of a Superconducting Alternator," S. M. Thesis, MIT, August 1974.

18. "Application of Distribution and Power Transformers," IEEE Tutorial Course, IEEE Publication 76 CH1159-3-PWR.

Stator Winding Detail Design

The stator winding configuration studies which are reported in the previous section resulted in the final selection of the spiral pancake arrangement for both the low-voltage and the high-voltage armatures. This configuration concept has been combined with the insulating material application concepts described in the previous sections to define detail configurations for stator windings of 300 MVA and 1200 MVA generator designs. Within each of these ratings, electrical design calculations were made for four different cases. These differ in voltage and in reactance level, as indicated in Table 3-55.

Table 3-55

List of Electrical Designs

Rated MVA	Rated Voltage L-L	Calculated Voltage L-L	Reactances, pu		
			x_d	x_d'	x_d''
300	13,800	13,936	0.225	0.161	0.081
300	13,800	13,628	0.417	0.313	0.160
300	230,000	230,964	0.249	0.202	0.136
300	230,000	230,074	0.492	0.404	0.269
1,200	29,000	28,909	0.221	0.151	0.082
1,200	30,000	29,671	0.405	0.286	0.157
1,200	500,000	501,606	0.261	0.202	0.137
1,200	500,000	496,846	0.497	0.393	0.271

The dimensions and other parameters of these designs are tabulated in Section 3.1.1.

Detailed construction features of the stator windings are described in this section. As may be expected, these features are quite different for the high-voltage winding from conventional practices. The differences are not as pronounced for the low-voltage spiral pancake winding, which would use nearly conventional insulating practices. The differences will be highlighted in the text. All of these stator windings are airgap windings in the sense that no magnetic iron of any kind interpenetrates the space occupied by the winding.

Figure 3-123 shows the general arrangement of a spiral pancake winding for a 2-pole machine. The entire winding consists of six identical spiral pancake coils, which are separately constructed prior to assembly into a complete winding. This method of assembly permits manufacturing operations to be done in parallel rather than in series, and thus permits a reduction in manufacturing cycle time. For a low-voltage winding, each of these coils consists of a few turns, typically five to ten, while in a high-voltage winding the number of turns per coil may exceed 100. Since the armature currents in the two cases also differ by more than an order of magnitude, each of the turns of the high-voltage coil is much smaller in cross-section than each of the turns in the low-voltage coil. The overall appearance of a complete low-voltage spiral pancake coil is suggested in Figure 3-124 which shows five turns per coil. For the sake of clarity, details of end connections, water connections, and the like have been omitted and are shown elsewhere. The shape of the individual coil of the high-voltage winding is suggested in Figure 3-124 The individual turns are not shown separately. The appearance would resemble that of a normal high-voltage transformer coil that is bent around a cylindrical mandrel after winding.

The complete three-phase armature of course requires end connections between the individual phase coils. These will be discussed subsequently. The end connections may be made so as to place the two coils of a given phase either in series or in parallel. For the low-voltage case, either connection is usable, since grading of the voltage distribution is not a constraint in this case. For the high-voltage winding, a series connection would be used so as to divide the terminal voltage between the two halves of a phase winding.

Stranding and Transposition

The high magnetic flux densities that circulate both in the radial and in the peripheral directions through the airgap winding of a superconducting machine require the armature conductors to be finely stranded and properly transposed in order to limit losses that are produced by local eddy currents and parasitic circulating currents. These losses cannot be entirely eliminated with conductors of finite size, but they should be minimized, and must be coordinated with the design of the cooling system.

Local eddy current losses in the individual strands can be calculated by:

$$P_e = \frac{(\pi\, r_{st}\, f\, B_m)^2}{4\rho}$$

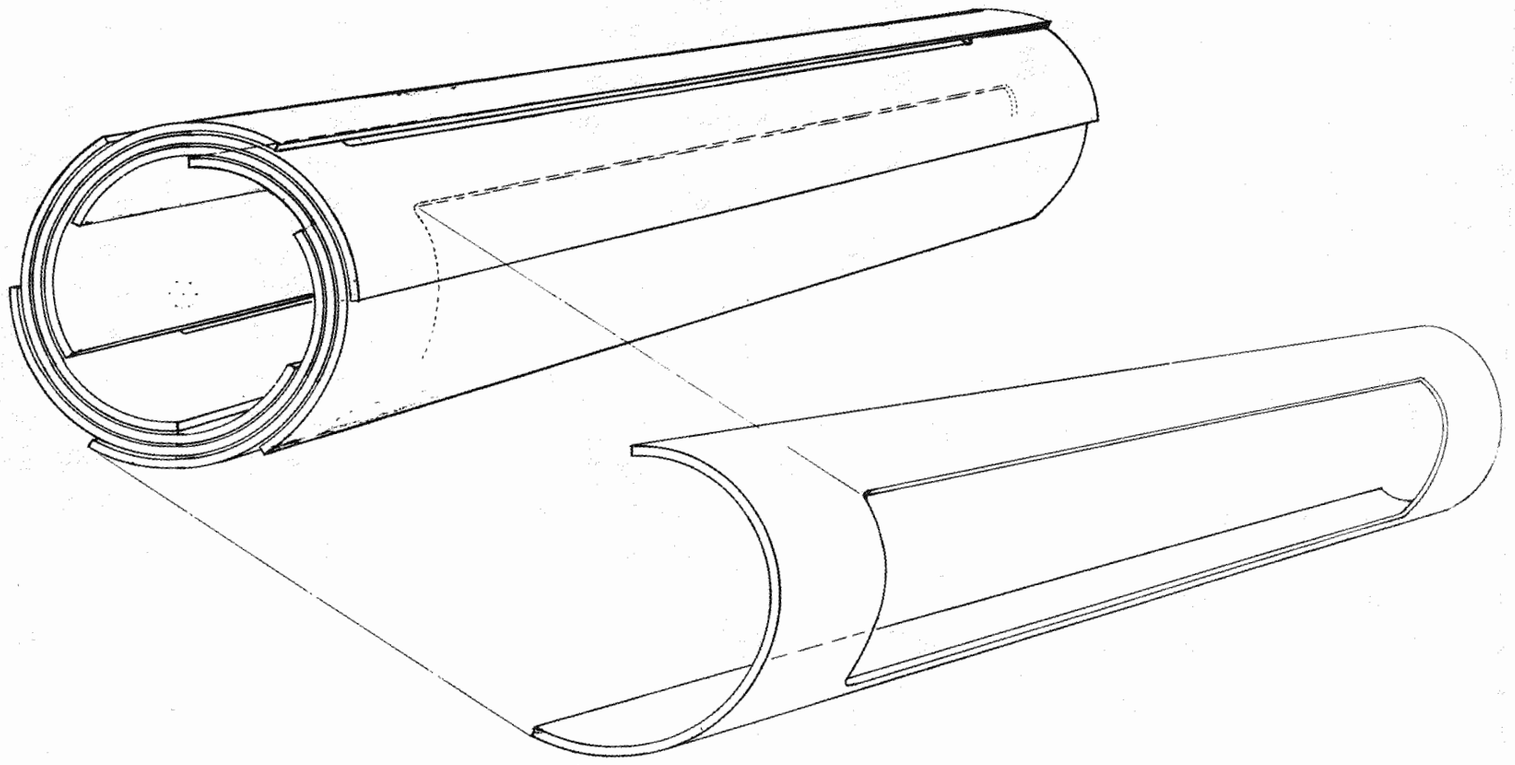

Figure 3-123. General Arrangement of Spiral Pancake Winding for 2-Pole Machine. Also, Overall Appearance of High-Voltage Coil.

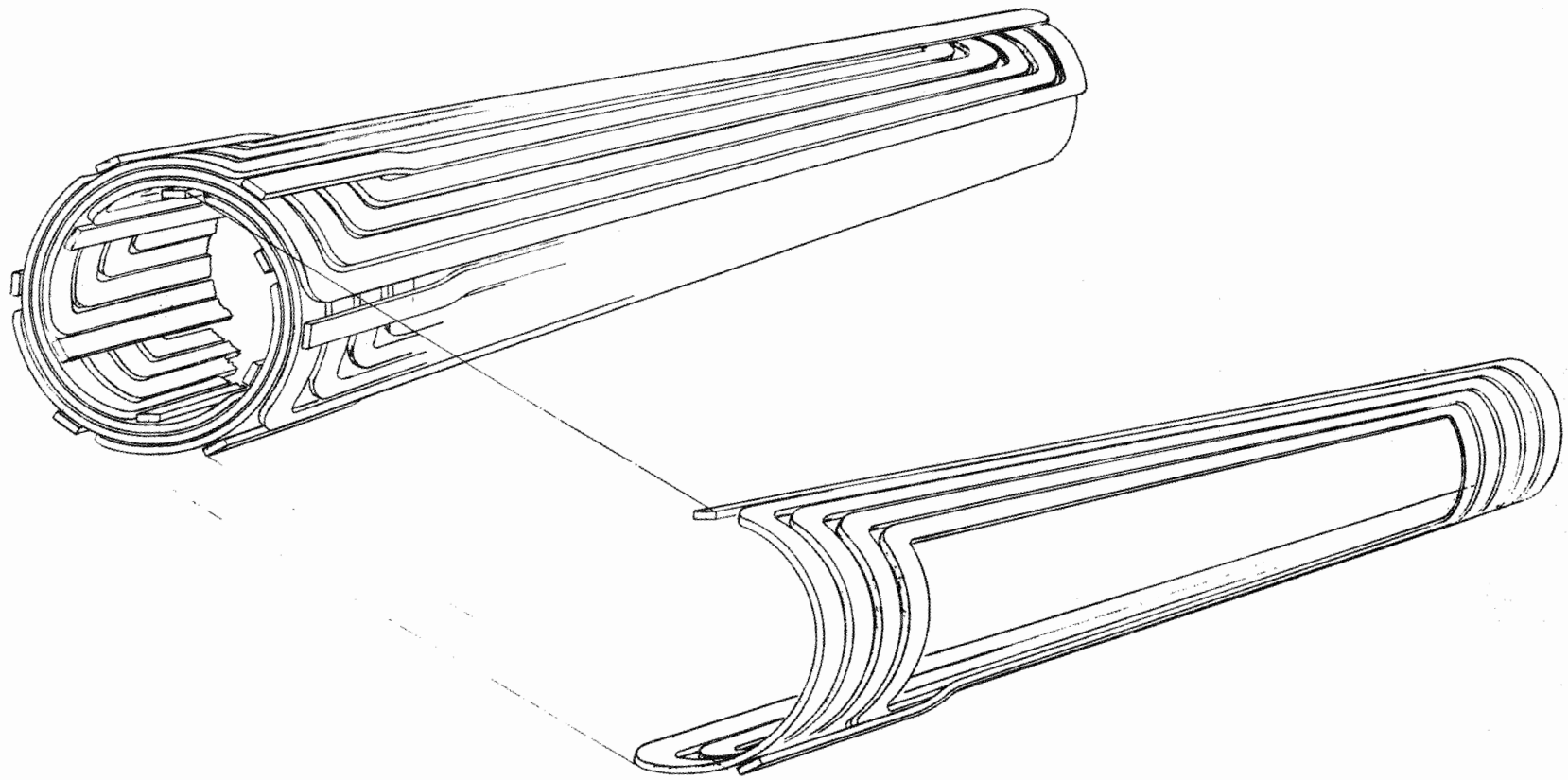

Figure 1-124. Overall Appearance of Low-Voltage Spiral Pancake Stator Winding and of Single Spiral Pancake Coil.

where

r_{st} = radius of strand

f = frequency

B_m = maximum local flux density

ρ = resistivity of strand material

P_e = eddy current loss, w/m^3

In a practical sense, these losses can be reduced only be decreasing either the strand diameter or the local flux density. The latter is not desirable, since it also reduces the power density of the machine. Strand diameters of the order of 1 mm represent reasonable compromises between additional losses and manufacturing requirements with respect to strand insulation and coil assembly. The ratio of a.c. loss (sum of d.c. and eddy current losses) to d.c. (ohmic) loss can be expressed as:

$$\frac{P_{ac}}{P_{dc}} = 1 + \frac{\pi a_{st}}{4} \left(\frac{fB_m}{\rho J} \right)^2$$

where

a_{st} = area of strand

J = current density

For example, with a current density of 10^7 A/m^2 and a flux density of 1.67 T, the total loss increase due to local eddy currents is about 14% with a 1 mm strand diameter.

Additional losses may also be produced by voltage differences between parallel paths in the winding which are shorted together at the ends of a conductor, coil, or winding. An analogous situation occurs in conventional machines, where the straight parts of the armature conductors are located in slots provided in the armature core. The load current produces a cross-slot flux field that increases, approximately linearly, with the height of the slot. Different amounts of cross-slot flux thus circulate between layers of strands which are separated by constant distances but located at different elevations in the slot. If the ends of these strands are shorted at the ends of the coil, for example, in order to make a connection to the next coil, circulating currents are produced by these voltage

differences, and produce additional losses. Various forms of transposition of the strands are used to reduce this effect. The classical solution, using an internal transposition, is due to L. Roebel. The well known Roebel bar uses strands that are transposed both up and down and across the width of the slot so as to occupy all possible positions in the slot for equal intervals. The voltage induced in the various strands, either by cross-slot flux or by radial flux, are thus equalized and losses due to this effect are suppressed.

Additional losses which may be due to flux linking the end turns of the winding can be reduced by one of several possible extensions of the original Roebel concept.

In the airgap winding of a superconducting machine, both radial and tangential components of flux density, which vary continuously in the three dimensions, are in general present everywhere in the stator winding. In order to compensate for voltage differences between conductor strands connected in parallel it is therefore necessary to transpose fully in both directions, and it may furthermore be necessary to transpose from inside to outside in the case of very large conductors. Figure 3-125 shows a conductor where a transposition from side to side and from top to bottom is carried out continuously by rotating the layers of stranded sub-conductors about the axis of the conductor. One and one-half complete rotations (540° transposition) would be required to compensate for both straight portion and end flux distribution effects.

Coordination between Insulation and Cooling Systems

Low-voltage armature coils have relatively few turns, as indicated in Figure 3-124. Each coil, throughout its entire length, is fully insulated to ground. The insulation is designed to meet the requirements of ANSI Standards for turbine generators, in particular, the test voltage requirements. Water cooling, which is used widely for large turbine generator stator windings, is selected in order to obtain a maximum value of current density in the conductors, and thus maximize the power density of the machine. Cooling connections are brought out through headers, which serve simultaneously as electrical connectors, as shown in Figure 3-126. The water conduits between the headers and the external water manifolds are teflon tubes which have excellent insulating properties. Cooling water is highly and continuously purified to maintain a very low conductivity. An epoxy impregnant is selected for the coil insulation to ground to offer the maximum resistance to moisture in the unlikely event of a leak.

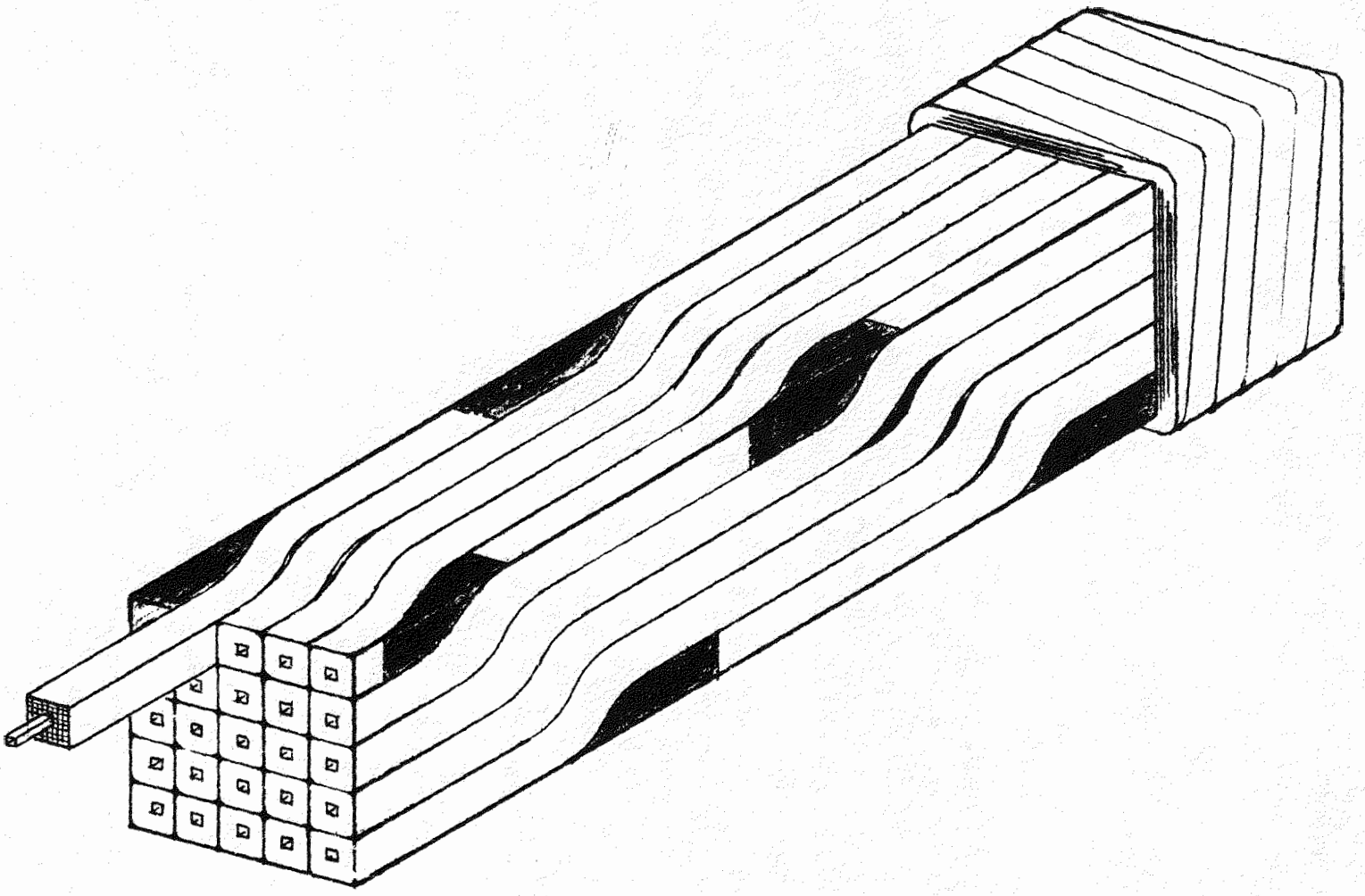

Figure 3-125. Concentrically Transposed Conductor with Water-Cooled Subconductors

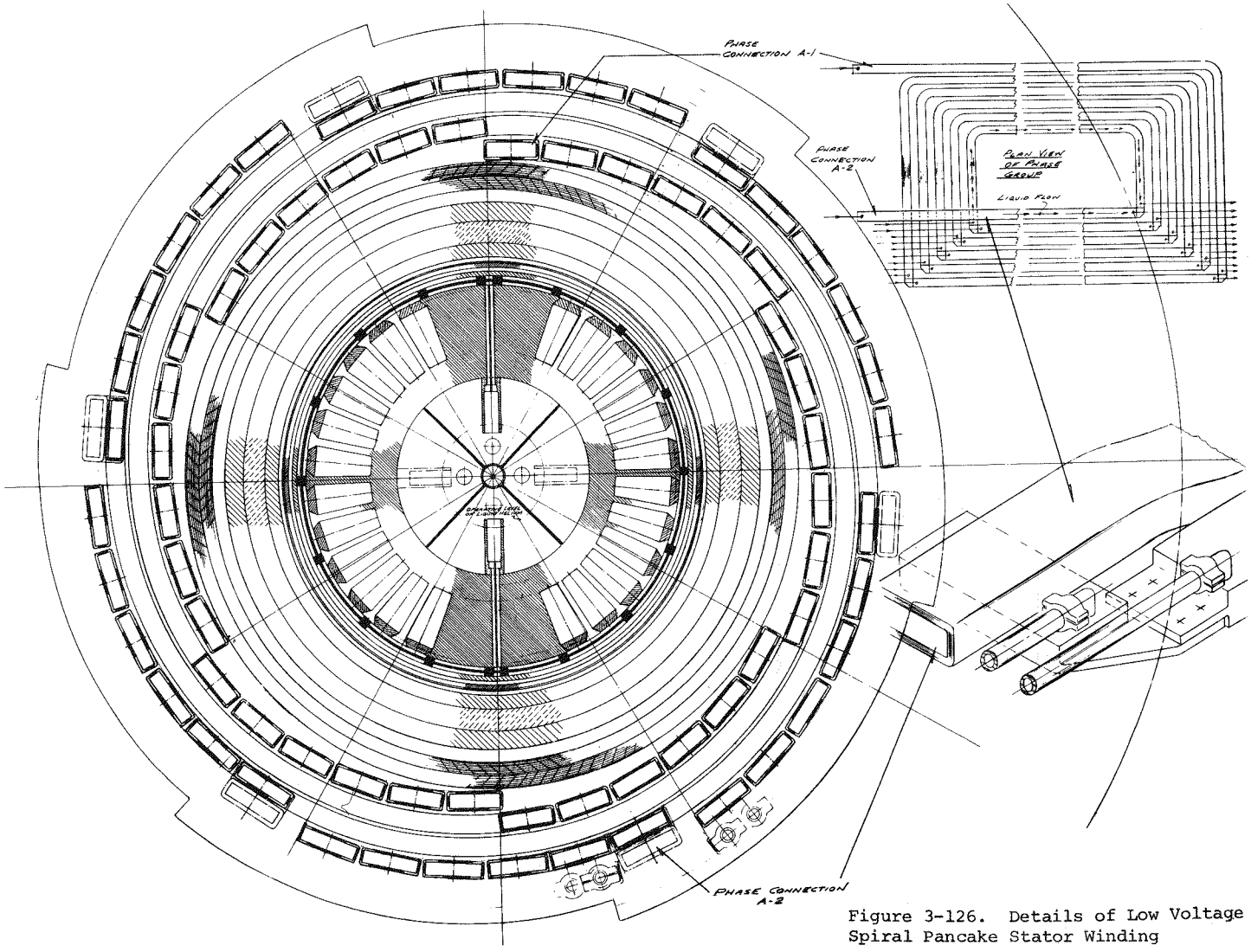

Figure 3-126. Details of Low Voltage Spiral Pancake Stator Winding

The high-voltage armature coils require a large number of turns of relatively small cross-section. Water cooling would not be practical for these, even if no other considerations existed, because of the very much larger number of insulated water connections that would be necessary. In the high-voltage machine, however, a dielectric fluid is required as an impregnant for the insulation, and moisture contamination of this fluid would lead to insulation failure very rapidly. Therefore such contamination must be absolutely avoided, and the only sure way to accomplish this is to exclude water altogether. The high-voltage winding concept is therefore not compatible with water cooling, and the cooling concept is preferably based on the use of the same fluid that serves to impregnate the solid parts of the insulation.

Because of the small cross section required for the strands of the conductors, it is not practical to make these hollow with internal cooling ducts. Rather, the coolant must flow through separate channels. Where water cooling is employed, these must be continuous tubes connected to headers with leaktight joints.

Very careful coordination between insulating and cooling requirements is necessary for the high-voltage armature windings. The channels for coolant flow must be located in such a manner and shaped so as to impact to the minimum possible extent on the insulation system. The cooling passages should not introduce dielectric stress concentrations, and the dielectric fluid in these passages should, as far as possible, be itself shielded against dielectric stresses. At the ends of these passages, stresses that can cause breakdown of the insulating fluid must be appropriately reduced by grading provisions.

An arrangement of cooling passages wherein the dielectric fluid is shielded by the conductors themselves is shown in Figure 3-127. A careful inspection of this figure will show that each of the pancake coils is subdivided into four layers of conductors. Each set of two adjacent layers is separated by a duct for cooling and insulating fluid. The conductors of the two layers associated with one duct are wound in the same direction, and are, in effect, in parallel. The voltage of any one conductor is therefore essentially the same as that of its mate on the other side of the duct, so that the potential difference across the duct is close to zero everywhere between the two layers of conductors. The same applies to the other duct, which is, however, at a different potential from the first duct. This potential difference is sustained by the stepped insulating layer between each set of conductor/duct layers.

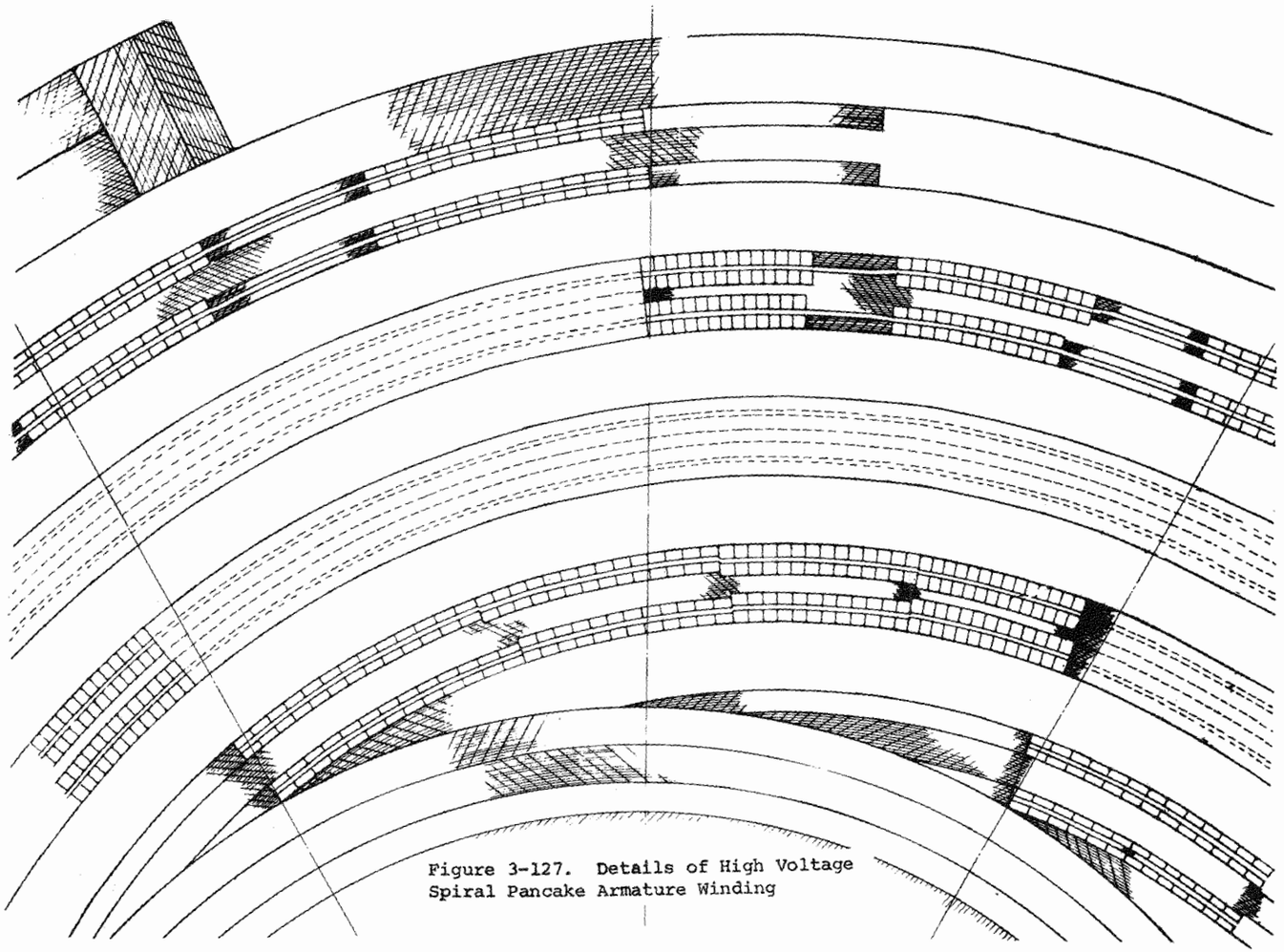

Figure 3-127. Details of High Voltage
Spiral Pancake Armature Winding

Calculation of the Water Flow Path: Water and Surface Rises, Pressure Drop

The following constants and formulas for calculation of the water flow paths required to cool the stator conductors are collected for reference:

Specific heat: 0.9994 kcal/kg°C
1 kcal = 4185 Joule

The water temperature rise is therefore:

$$\Delta\theta = \frac{2.388 \times 10^{-7} \text{ watts}}{A_v \times u_v} \text{ °C}$$

where:

A_v = vent area in m^2

u_v = water flow velocity in m/sec

watts = the power dissipated to vent under consideration.

The Reynolds number is $u_v D_h/\nu$. With the kinematic viscosity $\nu = 0.403 \times 10^{-6}$ m^2/sec, the Reynolds number is:

$$Re = 2.481 \times u_v \times D_h \times 10^6 \text{ (non-dimensional)}$$

where D_h is the hydraulic diameter of the duct in m.

Turbulent flow occurs for Reynolds numbers greater than 4000. The surface heat transfer coefficient for turbulent flow is:

$$h_\infty = 0.023 \, Re^{0.8} \, Pr^{0.4} \, k/D_h \text{ watt/°C-m}^2$$

where

Pr = Prandtl number

k = thermal conductivity in watt/m sec °C

and h_∞ denotes that the heat transfer coefficient is appropriate to fully developed flow. Since the tubes are many times longer than their cross sectional dimensions, this will always be the case.

With k = 0.6605, and Pr = 2.56,

$$h_\infty = 2.888 \times 10^3 \, u_v^{0.8}/D_h^{0.2} \text{ watt/°C-m}^2.$$

The surface temperature rise is $1/h_\infty A_v$ where A_v is the total surface area of the vent that is exposed to the flow of cooling water.

The friction factor for a smooth tube is:

$$f_r = 0.3164/Re^{0.25}$$

and the total pressure required to produce the flow at velocity u_v in the full length of the tube L_v is:

$$\Delta P = 0.5\ u_v^2\ f_r\ L_v\ /\ D_h \text{ kPa.}$$

These formulas will be used subsequently to generate and tabulate the design information for the cross sections of the stator conductors of the low voltage stator windings.

Calculation of the Fluid Flow Path for High Voltage Windings.

Although there are a number of options with respect to the selection of a dielectric fluid for the high voltage winding for detail design it is necessary to select a particular material. Since extensive experience is available with hydrocarbon oils, and their properties are well established, such a fluid is selected. The following characteristics have been selected from the various data that have been published in the extensive literature on these fluids, and apply at 70°C:

Density:	855 kg/m^3
Specific heat:	0.492 kcal/kg°C
Thermal conductivity:	0.114 kcal/m h °C
Kinematic viscosity:	12.64 x 10^{-3} m^2/h

The derived non-dimensional numbers are therefore:

Pr:	46.67
Re:	0.2848 u_v D_h 10^6

The velocities which are used in existing practice with oil-cooled electrical equipment of comparable geometry (such as transformer windings) are well below those used with water cooling, and are of the order of 0.2 m/sec or less. With oil ducts of the order of 0.01 m in width, this corresponds to values of Reynolds number of only a few hundred. Hence, the flow would be treated as laminar, and the surface heat transfer coefficient would vary as the 1/3 power of the volume flow.

Information of a propriety nature, secured from the Westinghouse Large Transformer Division at Muncie, Indiana, includes design data for surface heat transfer from transformer coils to oil that are well above what could be calculated from the heat transfer with laminar flow. This data shows a variation of heat transfer coefficient essentially with the 0.8 power of velocity, as would be the case with turbulent flow, even at very low velocities. It is possible that the fluid is unable ever to reach laminar flow conditions because of the numerous changes of direction that are introduced by the duct spacers. It is also possible that local internal eddies in the flow improve the heat transfer above that which would be expected from purely laminar flow in a (round) duct.

Description of Stator Coils for Low Voltage Windings

Each stator coil consists of several series turns. The number of turns for the specific design is tabulated in the characteristic data, Section 3.1.1. The turns are made up of successive C-sections and straight parts, as indicated in Figure 3-126 in the plan view at the upper right. It will be noted that, in general, the successive C-sections and straight parts are of different lengths. This must be considered in the design of the cooling system, which must have the capability to cool the section with the longest flow path adequately. The complete coil is made up by joining these successive C-sections and straight parts by means of overlapping junctions or joints as illustrated in the detailed view near the right edge of Figure 3-126.

Each of these coil sections is composed of an array of small strands which are multiply transposed and mutually insulated in order to minimize stray losses during operation. Cooling tubes are suitably interspersed in this array at such spacing as is required to secure adequate cooling and to prevent the formation of hot spots at excessive temperature. These cooling tubes, as well as the strands of each section, terminate in "headers" which are at the same time water connections and electrical connections. The headers are joined to the two ends of each coil section by brazing. Header caps, which are complete with connections for current and water flow are in turn brazed to the headers. The detail view in Figure 3-126 indicates both sets of connections.

Each of the C-sections is formed to shape on a suitable tool, called a coil former. The straight sections require no special forming. Each of the sections is subsequently taped with multiple lapped layers of micaceous insulating tape. One or more layers of finish tape are applied to serve as a protective coating. The coil sections are then vacuum-pressure impregnated, using a solventless epoxy resin impregnating system, and cured under pressure and at elevated temperature. During curing, the resin combines with the mica insulation to form Epoxy Thermalastic, an exceptionally strong, temperature, and moisture-resistant insulation system.

After manufacture, each of the coil sections is carefully inspected and given rigorous dielectric tests. Thereafter, the individual sections are assembled into pancake coils. All six pancake assemblies are identical and interchangeable. The assemblies are then installed in the complete armature winding, which is installed in the stator shield.

The strand and tube details and the results of the calculation of the cooling path are shown in the following Table 3-56 for the four low voltage designs. In each case, the longest coil section, i.e., the C-section of the second turn, is considered. This constitutes a worst-case consideration of the cooling design. Refinements in the stranding and coil construction are, of course, possible to favor the longer sections, but have not been considered for these designs. The inclusion of such refinements would be expected to offer a reduction in machine size, but, because of the additional manufacturing complexities, might offer no economic benefit.

The detailed internal construction of the stator conductors is also illustrated in Figures 3-128 and 3-129 which show, respectively, the complete conductor cross sections and enlarged sections of the individual subconductors.

Winding Connections for Low Voltage Windings

The windings for the generator designs designated as A, B, and F are connected in wye (Y). The winding for design E is connected in wye with two parallel paths (YY). To accomplish this, the two ends of the two coils belonging to the same phase are joined together by means of the phase conductor arrangement. For the series wye (Y) connection, the coils are joined end to end.

Table 3-56

ARMATURE WINDING DESIGN DATA

Low Voltage

Machine Designation		A	B
Rating			
MVA		300	300
Line Volts		13800	13800
Calculated Line Amps		12551	12551
Stator Winding Design Data			
Mean Outside Radius	m	0.5588	0.5888
Mean Inside Radius	m	0.4978	0.4978
Turns/Coil		4	6
Conductor Cross Section	m^2	0.00172	0.00176
Space Factor		0.60	0.60
Copper Cross Section,	m^2	0.00103	0.00106
Current Density in Copper	A/m^2	12.042×10^6	11.877×10^6
Conductor Design Data			
Width of Uninsulated Conductor	m	0.117	0.075
Depth of Uninsulated Conductor	m	0.014	0.021
Width of Insulated Conductor	m	0.123	0.081
Depth of Insulated Conductor	m	0.020	0.027
Number of Subconductors/Conductor		41	24
Strands/Conductor		1353	1152
Strand Size, bare	m	0.00095 square	0.00104 square
Total Strand Area/Conductor	m^2	0.00104	0.00106
Eddy Factor		1.073	1.087
Total Loss per Conductor	watts/m	3408.	3387.
Length of Longest Conductor	m	6.845	6.722
Total Loss for Longest Conductor	watts	23326.	22767.
Cooling Tube Data			
Outside Dimensions	m	0.0029 square	0.0031 x 0.0042
Inside Dimension	m	0.0021 square	0.0021 x 0.0032
Cross Section Area	m^2	4.39×10^{-6}	6.70×10^{-6}
Total Flow Area/Conductor	m^2	1.80×10^{-4}	1.608×10^{-4}
Hydraulic Diameter	m	0.0021	0.0025
Water Velocity	m/sec	2.30	2.30
Reynolds Number		11983.	14427.
Pressure Drop	kPa	260.7	205.3
Maximum Water Rise	°K	13.45	14.70
Surface Rise	°K	0.52	0.72
Flow/Conductor	m^3/sec	4.14×10^{-4}	3.70×10^{-4}
Summary Data			
Maximum Temperature Rise	°K	24.	26.
Total Water Flow	m^3/sec	1.37×10^{-2}	1.63×10^{-2}
Total Pressure Drop	kPa	275.	210.

Table 3-56 (Continued)

Machine Designation		E	F
Rating			
MVA		1200	1200
Line Volts		29000	30000
Calculated Line Amps		23890 (YY)	23094
Stator Winding Design Data			
Mean Outside Radius	m	0.7671	0.7976
Mean Inside Radius	m	0.6477	0.6350
Turns/Coil		6	5
Conductor Cross Section	m^2	0.00166	0.003344
Space Factor		0.60	0.60
Copper Cross Section	m^2	0.0010	0.0020
Current Density in Copper	A/m^2	11.945×10^6	11.547×10^6
Conductor Design Data			
Width of Uninsulated Conductor	m	0.090	0.103
Depth of Uninsulated Conductor	m	0.018	0.027
Width of Insulated Conductor	m	0.105	0.119
Depth of Insulated Conductor	m	0.033	0.043
Number of Subconductors/Conductor		27	33
Strands/Conductor		972	2079
Strand Size, bare	m	0.0011 square	0.00104 square
Total Strand Area/Conductor	m	0.00102	0.00192
Eddy Factor		1.103	1.099
Total Loss per Conductor watts/m		3235	6401
Length of Longest Conductor	m	11.90	9.69
Total Loss for Longest Conductor	watts	38488	62025
Cooling Tube Data			
Outside Dimensions	m	0.0033 x 0.0044	0.0031 x 0.0052
Inside Dimension	m	0.0023 x 0.0034	0.0021 x 0.0042
Cross Section Area	m^2	7.82×10^{-6}	8.82×10^{-6}
Total Flow Area/Conductor	m^2	2.11×10^{-4}	2.91×10^{-4}
Hydraulic Diameter	m	0.0027	0.0028
Water Velocity	m/sec	2.30	2.30
Reynolds Number		15657	15978
Pressure Drop	kPa	330.	258.
Maximum Water Rise	°K	18.94	22.13
Surface Rise	°K	0.57	0.84
Flow/Conductor	m^3/sec	4.85×10^{-4}	6.69×10^{-4}
Summary Data			
Maximum Temperature Rise	°K	30.	35.
Total Water Flow	m^3/sec	2.52×10^{-2}	2.68×10^{-2}
Total Pressure Drop	kPa	345.	270.

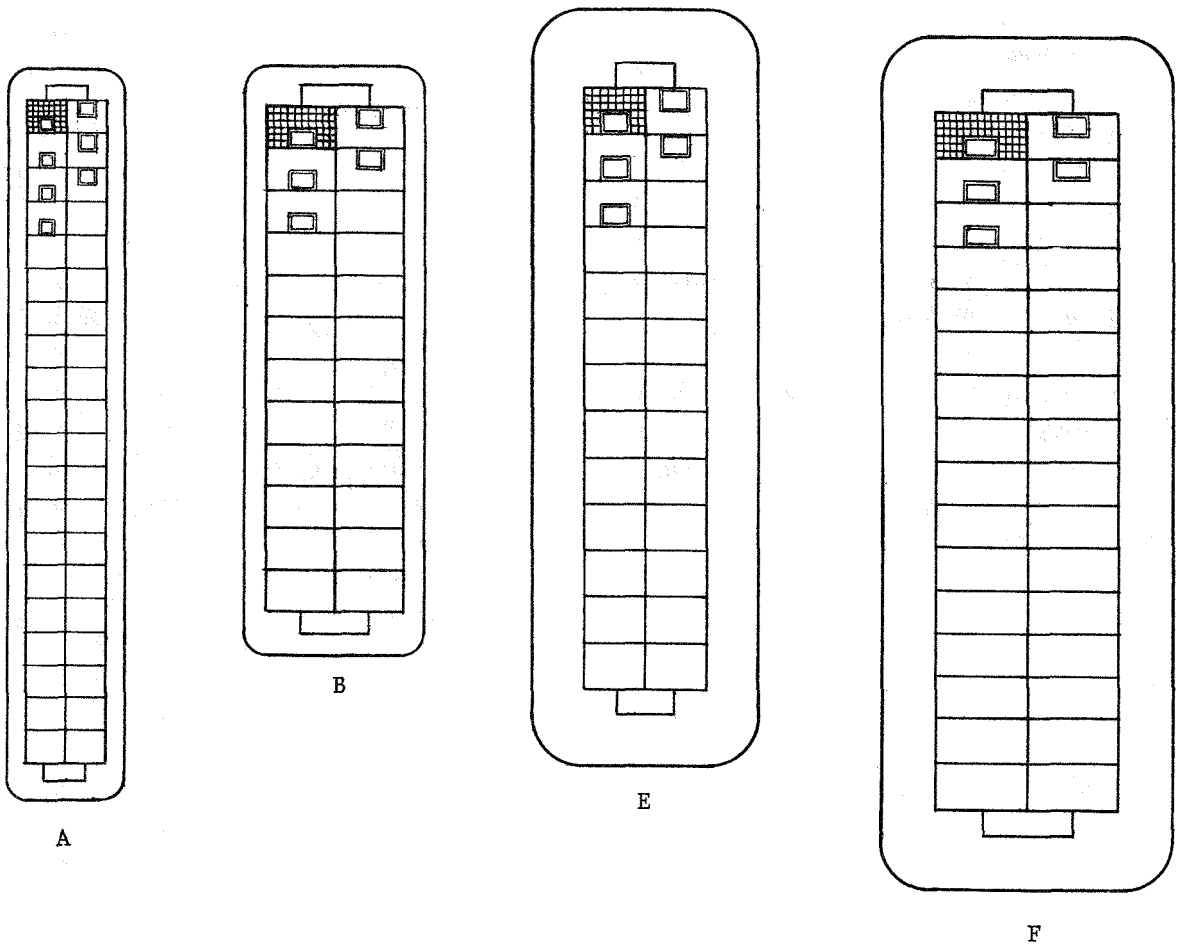

Figure 3-128. Cross Sections of Stator Conductors for Low-Voltage Armature Windings A, B, E, and F. See Tabulated Data for Detailed Dimensions.

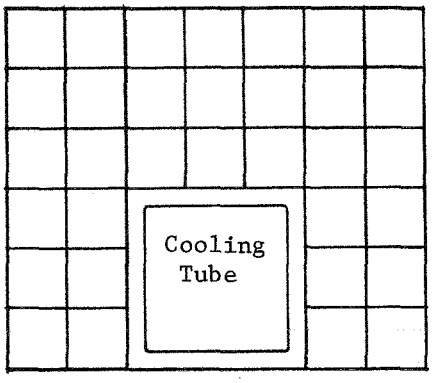

A

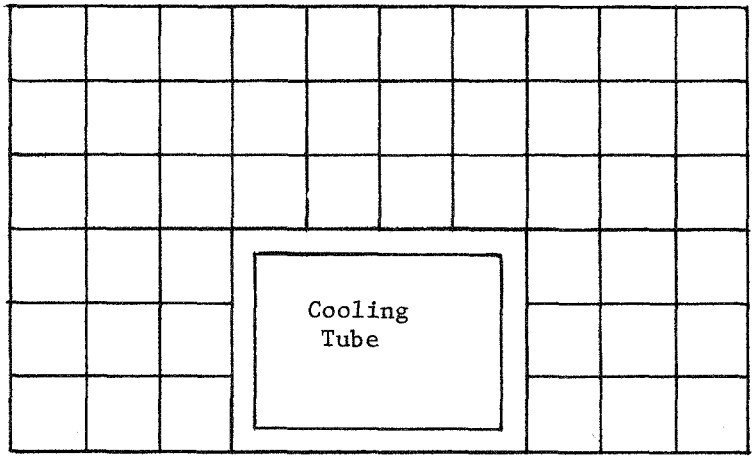

B

Figure 3-129(A). Cross Sections of Stator Subconductors for Low-Voltage Armature Windings A and B

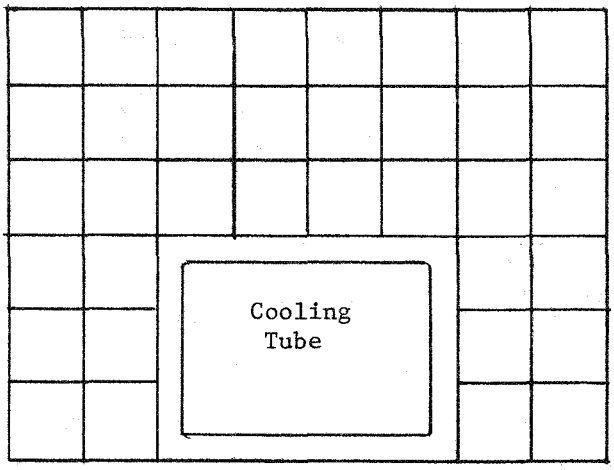

E

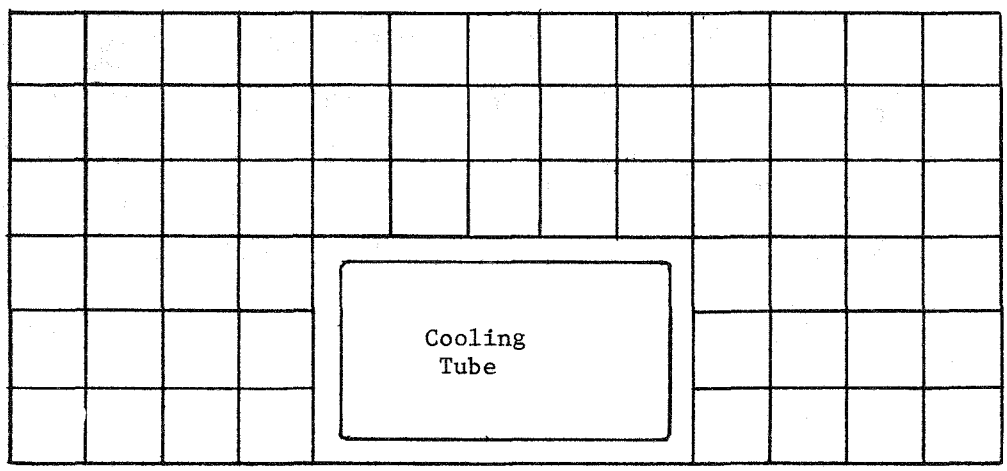

F

Figure 3-129(B). Cross Sections of Stator Subconductors for the Low-Voltage Armature Windings E and F

Construction of the Subconductors for Low Voltage Windings

It has been assumed in the foregoing that sufficient manufacturing development will be performed prior to the construction of a prototype generator to achieve routine economical production of the subconductors in the required quantities and of the complete coils made by assembling these subconductors with the required transpositions. At this time, only preliminary experiments to establish feasibility of forming small strands into a compact transposed assembly with a central cooling tube have been performed. The results are illustrated in Figure 3-130 which is the enlarged photograph of the polished cross section of such a conductor. The actual full size cross section is about 1 cm square. From a detailed study of this photograph, a space factor for the copper cross section was deduced. The value was found to be approximately 0.85, and is used in the design of the stator conductors.

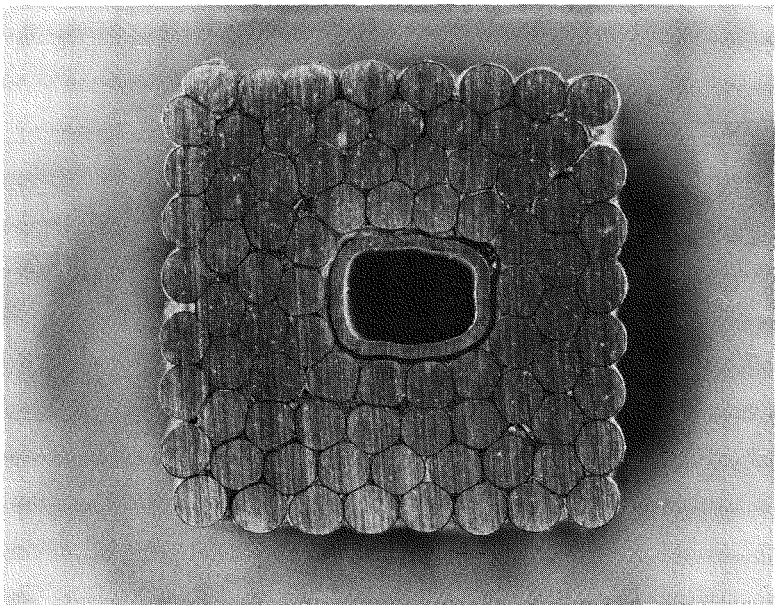

Figure 3-130. Experimental Stranded and Transposed Subconductor.

Description of Stator Coils for High Voltage Windings

Each stator coil consists of a large number of series turns. The number of turns, from 112 for Generator G to 210 for Generator D, is shown in the tables of characteristic data, Section 3.1.1. Each of the turns is subdivided into two parallel conductors, one on each side of the oil duct, as illustrated in Figure 3-127 This is done to control the potential gradient across the oil duct (see "Coordination between Insulation and Cooling Systems). The complete coil thus consists of four layers of conductors in two pairs. Each pair of layers is separated by a cooling duct, whereas the two pairs are separated by the intracoil insulation. Successive turns are wound in the proper sense so that the voltages of the two halves of the coil are additive; i.e., starting at the lead end, which is on the outside of the coil, the successive turns spiral inward in the first pair of layers, then cross-connect to the other pair of layers, and finally spiral back out in the second pair. The finish lead is consequently also on the outside of the coil, and no problems with lead crossing exist.

With this construction, each coil is made up of two parallel paths of conductors. In order to prevent the possibility of circulating currents between these parallels, the winding is arranged in a pair of series-parallels. This is accomplished by connecting the parallel paths to each other only at the terminals of each complete phase winding, and connecting the two halves of the phase in series internally, using a transposition so as to assure that each parallel path contains an equal number of conductors in the same relative positions. A connection scheme which accomplishes this is shown in Figure 3-131.

The intracoil insulation requirements that are established by the internal turn-to-turn voltage distribution from one pair of layers can be satisfied by a tapered or stepped insulating layer, as shown in Figure 3-127. A stepped insulator has been used to favor mechanical and manufacturing considerations. This dictates that the conductor aspect ratio (height/width) must change at intervals if the conductor cross section is to remain constant. (A further refinement could consider the possibility that the cross section changes continuously or at intervals as determined by the surface area in contact with the coolant, but this refinement has not been considered in the present calculation.) For the present study, a constant cross section has been used, and the conductor dimensions are varied to distribute the conductors in the space defined by the intracoil insulator and the cooling ducts. For calculation purposes, an "average conductor" of the appropriate cross section is used.

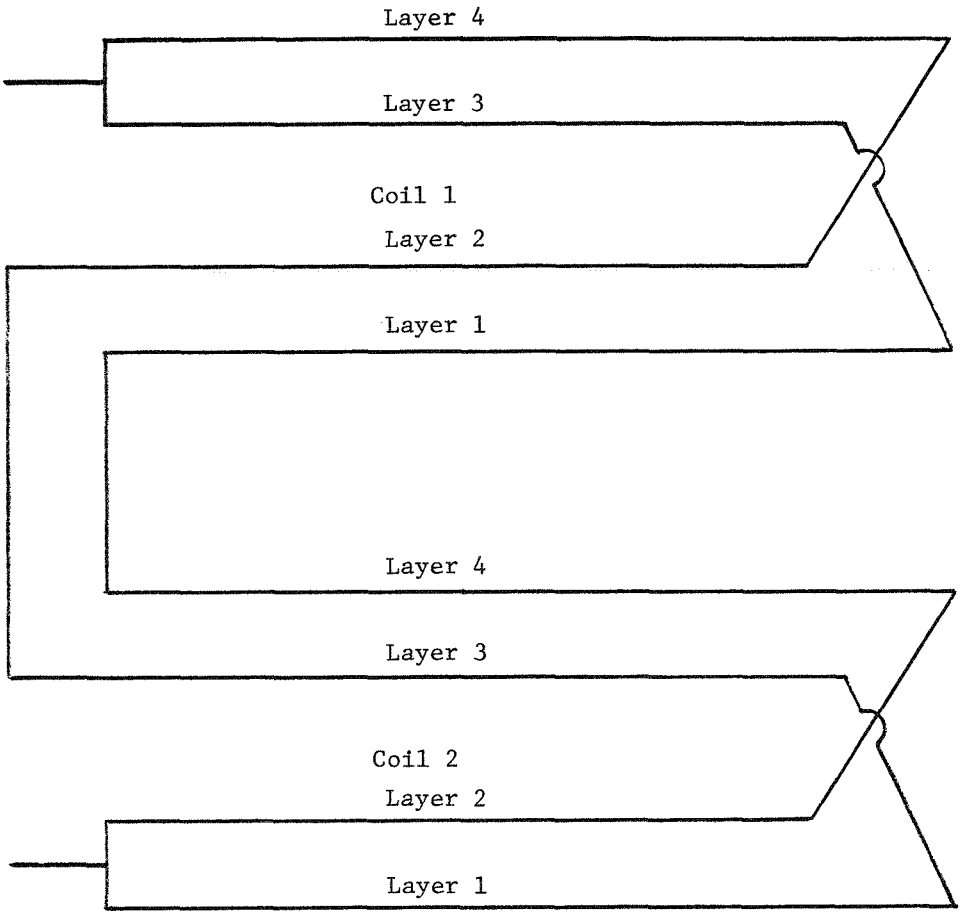

Figure 3-131. Parallel-Series Connection with Transposition for Two Phase Coils of High-Voltage Spiral Pancake Stator Winding

Each of the conductors is formed of an array of small strands which are multiply transposed, mutually insulated with varnish, and compressed to shape and size so as to obtain the best possible conductor space factor. Further development work is required to accomplish this, as is also the case for the subconductors for the low voltage windings. The successive turns are insulated with lapped layers of insulating tape; for example, Kraft paper. The coils are wound on appropriate forms, and then consolidated with a heat-curing synthetic resin prior to further assembly.

Conductor details for the generator designs designated as C, D, G, and H are shown in Table 3-57.

Shield Design

The electrical design of the flux shield must be such as to assist in obtaining the maximum power density from the active parts of the machine at the best achievable efficiency, while at the same time assuring that permissible temperatures will not be exceeded. These requirements can often be satisfied in conventional machine practice with stator cores which are smaller in cross section than those which are actually employed. The additional thickness of stator core is often required in order to provide enough stiffness against ovalizing forces.

Flux shield designs have been made for the eight generator designs designated in the tables of Section 3.5 as A through G. All but one of these designs have the shield thickness limited by magnetic saturation effects. Design D (300 MVA, 230 kV, $x_d"$ = 0.269° required additional depth in the shield in order to provide sufficient stiffness.

The limiting flux density used for the remaining seven designs is 1.6 Tesla. The iron loss (hysteresis and eddy current) loss intensity at this flux density is taken as 2.5 watts/lb.

Shield Cooling

In the very large number of designs of conventional machines of various types that have been made over the past 70 to 80 years, one encounters an almost unlimited variety of cooling schemes for the stator core. It is, in principle, possible to cool magnetic cores or shields with air, hydrogen, other gases, water, oil or other dielectric fluids, by conduction to cooler surroundings, or with heat pipes. From a practical design point of view, there is considerable merit in

Table 3-57

ARMATURE WINDING DESIGN DATA

High Voltage

Machine Designation		C	D
Rating			
MVA		300	300
Line kV		230	230
Calculated Line Amps		753	753
Stator Winding Design Data			
Mean Outside Radius	m	0.7912	0.7874
Mean Inside Radius	m	0.5418	0.5334
Turns/Coil		65	105
Conductor Cross Section	m^2	0.000065	0.00008
Space Factor		0.75	0.60
Copper Cross Section	m^2	0.495×10^{-4}	0.480×10^{-4}
Current Density in Copper	A/m^2	7.691×10^{6}	7.781×10^{6}
Conductor Design Data			
Average Width of Uninsulated Conductor	m	0.018	0.011
Average Depth of Uninsulated Conductor	m	0.0036	0.0056
Strands/Conductor		80	66
Strand Size, bare	m	0.00089 square	0.00094 square
Total Strand Area	m^2	0.537×10^{-4}	0.495×10^{-4}
Eddy Factor		1.103	1.094
Loss/Coil Length	watts/m	7936	13794
Straight length of coil	m	5.035	3.776
Total Loss for Strand Length	watts	39960	52081
Cooling Duct Data (for Straight Part)			
Width	m	0.5674	0.5585
Depth	m	0.0034	0.0034
Area	m^2	0.00194	0.00191
Number per Coil		2	2
Total Duct Area/Coil Half	m^2	0.00388	0.00382
Hydraulic Diameter	m	0.0068	0.0068
Oil Velocity	m/sec	0.45	0.45
Reynolds Number		871.5	871.5
Pressure Drop	kPa	3.9	2.9
Maximum Oil Rise	°K	12.99	17.19
Surface Rise	°K	4.46	7.88
Flow/Coil Side	m^3/sec	1.75×10^{-3}	1.72×10^{-3}
Summary Data			
Maximum Temperature Rise	°K	27.5	34.0
Total Oil Flow	m^3/sec	4.5×10^{-2}	4.5×10^{-2}
Total Pressure Drop	kPa	3.9	2.9

Table 3-57 (Continued)

Armature Winding Design Data (Continued)

Machine Designation		G	H
Rating			
MVA		1200	1200
Line kV		500	500
Calculated Line Amps		1386	1386
Stator Winding Design Data			
Mean Outside Radius	m	1.012	1.055
Mean Inside Radius, m	m	0.6629	0.6629
Turns/Coil		56	89
Conductor Cross Section	m^2	0.000144	0.000145
Space Factor		0.75	0.75
Copper Cross Section	m^2	1.08×10^{-4}	1.09×10^{-4}
Current Density in Copper	A/m^2	6.417×10^{6}	6.399×10^{6}
Conductor Design Data			
Average Width of Uninsulated Conductor	m	0.0245	0.0159
Average Depth of Uninsulated Conductor	m	0.0058	0.0090
Strands/Conductor		150	144
Strand Size, bare	m^2	0.00097 square	0.0010 square
Total Strand Area	m^2	1.2×10^{-4}	1.22×10^{-4}
Eddy Factor		1.246	1.254
Loss/Coil Length	watts/m	11708	18730
Straight Length of Coil	m	8.488	6.414
Total Loss for Strand Length	watts	99377	120133
Cooling Duct Data (for Straight Part)			
Width	m	0.694	0.694
Depth	m	0.0036	0.0036
Area	m^2	0.0025	0.0025
Number per Coil		2	2
Total Duct Area/Coil Half	m^2	0.0050	0.0050
Hydraulic Diameter	m	0.0072	0.0072
Oil Velocity	m/sec	0.45	0.45
Reynolds Number		922.8	922.8
Pressure Drop	kPa	6.0	4.6
Maximum Oil Rise	°K	25.1	30.3
Surface Rise	°K	5.4	8.6
Flow/Coil	m^3/sec	2.25×10^{-3}	2.25×10^{-3}
Summary Data			
Maximum Temperature Rise	°K	40.5	49.0
Total Oil Flow	m^3/sec	6.0×10^{-2}	6.1×10^{-2}
Total Pressure Drop	kPa	6.0	4.6

selecting a means of cooling that is most nearly compatible with that used for other, perhaps more critical, components of the machine. In the present case, this approach is best implemented by using the same medium for the shield as is used for at least one other major part of the machine. Although water could thus be used for the shields of the low voltage machine designs, the use of the same hydrogen that is used to cool the gap is preferred in that it leads to a simple construction and better reliability against the change of accidental water leaks. For the high voltage machines, the use of the same dielectric fluid that is used to cool the windings is the obvious choice. In both cases, the simplest and most reliable design is obtained by matching the pressure drops across the two fluid flow paths that are fed in parallel. For the low voltage designs, the drop across the shield ducts should match the drop across the gap, which is tabulated as the last line of Table 3-56 (Designs A, B, E, and F). For the high voltage designs, the drop across the shield ducts should match the drop across the stator coils, shown in Table 3-58 for Designs C, D, G, and H. To the extent that this can be accomplished, it is not necessary to use special orifices for flow control.

Properties of Cooling Media

The following constants and derived numbers for hydrogen gas at a pressure of 30 PSIG (3.14 kp.cm^2 abs.) are listed for reference:

Density ρ	0.2405 kg/m^3
Specific heat c_p	3.424 kcal/kg °K
Thermal conductivity k	0.1676 kcal/m h °K
Kinematic viscosity ν	0.142 m^2/h at 60°C
Absolute viscosity η	0.03427 kg/m h at 60°C
Reynolds number Re	$25.28 \times 10^3 \, u_v \, D_h$
Prandtl number Pr	0.700
Nusselt number Nu	$0.0199 \, Re^{0.8}$
Heat transfer coefficient	$12.9 \, u_v^{0.8} / D_h^{0.2}$
Friction factor f_r	$0.3164/Re^{.25}$

The major dimensions and heat losses to be dissipated are listed for each of the flux shields in the tables of Section 3.1.1. Using this information, together with the above properties of the cooling gas, it is a straightforward matter to select an appropriate number of cooling ducts. The calculations are indicated in tabular form, Table 3-58.

Table 3-58. FLUX SHIELD VENTILATION FOR LOW VOLTAGE STATOR DESIGNS

Generator Designation	A	B	E	F
MVA	300	300	1200	1200
Inner Radius of Shield, m	0.6477	0.6777	0.8560	0.8865
Outer Radius of Shield, m	1.0523	1.0414	1.4038	1.3820
Length m	4.173	3.532	7.390	5.531
Loss kW	357.7	275.2	1140.	774.7
Cooling Duct Diameter m	0.0254	0.0254	0.0254	0.0254
Number of Ducts total	111	102	210	156
Number of Rows (Circles)	3	3	3	3
Ducts/Row	37	34	70	52
Gas Velocity m/s	45	45	55	55
Re	28895	28895	35316	35316
f_r	0.0243	0.0243	0.0231	0.0231
Heat Transfer Coefficient h, $w/m^2-°K$	565.6	565.6	664.1	664.1
Surface per Duct m^2	0.333	0.282	0.590	0.441
Total Duct Area m^2	0.056	0.052	0.106	0.079
Total Flow, m^3/sec	2.52	2.34	5.85	4.35
Gas Rise °K	41.2	34.1	56.5	51.7
Surface Rise °K	17.1	16.9	13.9	17.0
Total Rise °K	58.3	51.0	70.4	68.7
L/D_h ratio	164.3	139.1	290.9	217.8
Friction Drop, v.h.	3.99	3.38	6.72	5.03

Table 3-58. FLUX SHIELD VENTILATION FOR LOW VOLTAGE STATOR DESIGNS - CONTINUED

Generator Designation	A	B	E	F
Total Drop, velocity heads	5.99	5.38	8.72	7.03
Differential Pressure, mm H_2O	698.9	619.6	1500.	1209.
Compare to Differential Pressure across gap (Table 3-18.	708.7	637.5	1508.	1200.

Calculation of Cooling Passages for Stator Shield for High Voltage Windings

The dielectric fluid that is used to insulate and cool the stator windings for the high voltage armature provides a simple and effective means for cooling the flux shield also. For this purpose, passages for flow of this fluid are provided by means of holes punched in the appropriate locations of the individual stator shield laminations. These holes overlap to constitute complete passages from end to end of the shield. Since the entire stator is immersed in the dielectric fluid, no leakage problem would be introduced by this construction.

Hole diameters of the order of 0.02 to 0.03 meters are well compatible with manufacturing technology for stator cores of conventional generators. The use of special means to control the flow through the flux shield can be avoided by designing the passageways in such a manner that essentially the same differential pressure appears across these passages as across the vents in the stator coils. Application of these criteria to the parallel passages in the flux shield and in the armature winding leads to flow velocities in the shield that are roughly double the velocities in the coil vents. In conjunction with the larger vents (larger hydraulic diameters) Reynolds numbers are obtained that imply turbulent flow. Actually, the characteristics of the flow may be in the transition region between laminar and turbulent flow, but in this range of Reynolds numbers, the difference in heat transfer coefficient becomes negligible. Therefore, with thermal conductivity $k = 0.114$ as before, the heat transfer coefficient becomes:

$$h = 3.277 \times 10^2 \, u_v^{0.8} / D_h^{0.2} \text{ watt/°C-m}^2.$$

(See page 3-399 ff. for fluid flow data for the dielectric fluid.) The cooling duct design is, as before, carried out in tabular form. See Table 3-59 . It is evident that the shield can easily be cooled with a dielectric fluid of the type for which characteristics have been given. The low calculated temperature rises indicate that a somewhat lower flow rate or reduced number of cooling ducts would be acceptable.

3.2.2.2 Stator Mechanical Design

Superconducting generators with water-cooled windings will tend to have higher current densities and higher flux densities, thus much higher electromagnetic forces than those for the conventional generators during a short circuit. Also the coils are more flexible and the modified airgap windings will cause end turns to be longer. It is obvious that a sound and strong stator bracing system,

Table 3-59. FLUX SHIELD COOLING FOR HIGH VOLTAGE STATOR DESIGNS

Generator Designation	C	D	G	H
MVA	300	300	1200	1200
Inner Radius of Shield, m	0.8928	0.8890	1.1519	1.1951
Outer Radius of Shield, m	1.1946	1.2446	1.5646	1.5509
Length m	4.986	3.944	8.407	6.464
Loss kW	391.5	205.4	1175.	787.
Cooling duct Diameter m	0.0254	0.0254	0.0254	0.0254
Number of Ducts total	81	57	144	129
Number of Rows (Circles)	3	3	3	3
Ducts/Row	27	19	48	43
Fluid Velocity m/s	1.03	0.95	1.03	1.00
Re	7451	6872	7451	7234
f_r	0.0341	0.0348	0.0341	0.0343
Heat Transf. Coeff. h	699.5	655.6	699.5	683.1
Surface per Duct m^2	0.398	0.315	0.671	0.516
Total Duct are m^2	0.041	0.029	0.073	0.065
Total Flow m^3/sec	0.042	0.027	0.075	0.065
Fluid Rise	5.3	4.2	9.1	6.9
Surface Rise	17.4	17.4	17.4	17.3
Total Rise	22.7	21.6	26.5	24.2
L/D_h Ratio	196.3	155.3	331.0	254.5
Friction Drop, v.h.	6.69	5.40	11.3	8.73
Total Drop, v.h.	8.69	7.40	13.3	10.73

Table 3-59 FLUX SHIELD COOLING FOR HIGH VOLTAGE STATOR DESIGNS - CONTINUED

Generator Designation	C	D	G	H
Differential Pressure, kPa	3.94	2.86	6.03	4.87
Compare to Differential Pressure across Stator Coil (Table 3-57.	3.9	2.9	6.0	4.6

or a continuous support system will be required for a superconducting generator. Under steady state, the corresponding forces are small in comparison with those during a short circuit and are estimated to be less than one percent. Therefore one of the objectives is to design the braces to resist the short circuit loads without causing excessive stresses and strains in the structure. Another objective is to construct and maintain the end winding assembly tight against the vibratory forces of normal operation so that wear of insulation and any contact surfaces will be prevented. In addition, means must be provided to re-tighten the windings, if necessary, to accommodate the shrinkage and the creep of the materials used in the winding structure during the life of the machine. It is desirable to have the natural frequencies of the stator winding structure above 150 Hz. If this is not feasible, resonance must be avoided near the principal excitation frequencies.

Forces on the stator windings resulting from a three-phase short circuit have radial, tangential and axial components. The radial force components are by far, the largest. Their magnitude varies approximately as a sinusoidal curve along the periphery as shown in Figure 3-132. The maximum force acts outward while the minimum force is very small and may act inward. The radial force distribution in the axial direction remains constant at the straight portion of the winding, and is preliminarily assumed to be linear at the end turns with a maximum value just outside the slots and diminishing to almost zero at coil ends. These radial forces are resisted by coil support extending out from the end of the core assembly. The use of external rings to resist this load is usually not sufficient because the sinusoidal load distribution tends to bend the rings into ellipses, thus resulting in large displacements of the coil ends.

The tangential forces on the bottom coils (outer basket) tend to oppose those on the top coils (inner basket). Consequently, the resulting moment on the entire end windings becomes very small. The opposing forces on the outer and inner baskets indicates that the two baskets should be keyed together to cancel these forces. The entire end winding assembly will then be keyed to the braces to resist the small resultant moment.

The relatively small axial forces tend to act outward together on the top and bottom coils. Without the proper support this would tend to cause relative motion of the coil ends in the tangential direction. The type of keying designed to lock the inner and outer baskets to cancel the opposing tangential forces, should also resist motions induced by the axial force components.

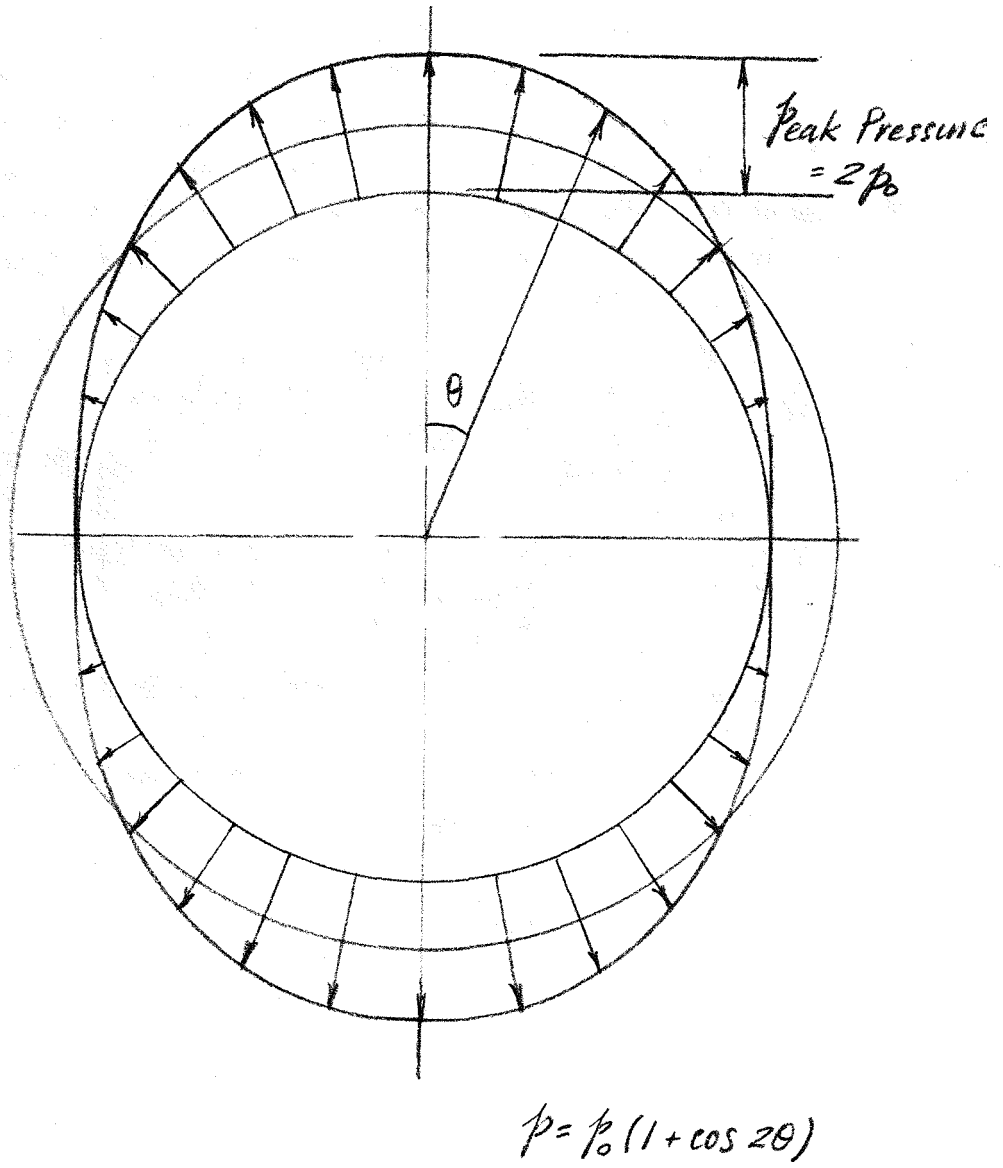

Figure 3-132. Radial Force Distribution

Spiral Pancake Winding and its Support

The spiral pancake winding consists of six phase windings or coils which are interleaved in a spiral fashion to form the complete armature. All coils have full insulation. Having each of these windings manufactured and tested as a sub-assembly, they can be inserted axially into the frame in a vertical position. The spaces in between the phase windings are impregnated with resin and the complete armature may be cured into a monolithic structure in the frame with induction heating. The armature should be so positioned in the core that the operating torque will tend to tighten the winding between the core and the bore ring against the vibrating forces. Wedges and ripple springs are provided at the edge of each phase winding against the ledges projected from the core to maintain the winding tight under normal operating conditions and to prevent excessive angular displacement of the coils during a short circuit. In addition, this facilitates the re-tightening of the armature if necessary, to accommodate the shrinkage and the creep of the material used in the winding structure during the life of the machine.

One of the advantages of using spiral winding in the stator is the improvement in the support of the armature windings, particularly in the end-turn regions. In a conventional stator, the straight portion of the coils is supported by the core and the frame, while the end turns are kept in place by the braces. Due to the difference in the spring constants of the core and the braces, the end turns are subjected to high stresses due to bending and twisting. The maximum stress usually occurs in a coil at a location just outside the slot. While the conventional braces may be strong enough for the generators of medium transient reactance, it remains to be proved that the similar bracing system will be sufficient for the low reactance machines. Since in the spiral winding stator, the end turns are brought out on the same radius as the straight part of the coils, the entire coil is continuously supported by the core assuming that sufficient blocks are provided at the end turn regions. Thus, the cause for the high stress is iliminated. The end turns are subjected to forces equal to or less than those for the straight portion of the winding. Consequently, the stress and the displacement of the end turns will be no more than the corresponding values for the straight portion. The core vibration and its displacement will be discussed in next section.

High Voltage Armature Mechanical Development

The high voltage armature has the spiral pancake winding, which consists of six phase coils wound of paper insulated turns. The insulation between the six pancake coils is provided by layers of oil-impregnated insulation. The entire

winding assembly will be tightly clamped between the core and the bore seal tube. The armature should be so positioned in the core that the operating torque tends to further tighten the winding. Provisions must be made to accommodate the shrinkage and the creep of the materials used in the stator so that the winding will be maintained tight under normal operating conditions. In addition, the winding and its supporting structure must be designed to withstand short circuits. It is desirable to have the natural frequencies of the stator winding structure above 150 Hz. If it is not feasible in the case of high voltage machines of large ratings, resonance and consequent magnification forces and displacements must be avoided near the principal excitation frequencies.

The resulting forces and displacements on the winding and its supporting structure due to conductor forces, are interrelated and their relation is dependent on the mechanical properties of the materials used in the stator and the compression and the shear strength developed by clamping between the coils and the insulation. Porous insulation with low modulus yields large displacements which can cause abrasion and wear and may produce fatigue failures of the insulation during normal operation. A dense insulation transmits large forces which can cause crushing of the insulation layers with consequent loosening of the coil assembly. Both large forces and large displacements must be avoided because they lead to mechanical breakdown, flashover and coil failure. It is important to select the suitable insulation to fulfill the mechanical as well as the electrical requirements.

In order to properly design the stator winding and its supporting structure, it is essential to accurately predict their resulting forces and displacements. A mechanical development plan outline can be found in Section

Shield and Frame

The construction of the shield and frame of a superconducting generator is similar to that of a conventional generator except that the shield is extended to continuously support the end turns of the spiral winding. The end turns are subjected to forces equal to or less than those for the straight portion of the winding. Consequently, the stress and the displacement of the end turns will be no more than the corresponding values for the straight portion. The forces acting on the straight portion of the winding are obtained from force = $I \underline{\ell} \times \underline{B}$ and are listed in Tables 3-60 and 3-61 for the various superconducting designs and their comparative conventional designs. The core natural frequency of the various designs are estimated from the thin ring formula. The calculated static and magnified shield displacements appear to be within the allowable limit except that for the 1200 MVA unit with the high voltage stator which should be modified to reduce the core displacement.

Table 3-60

Stator Core Vibration - 300 MVA

(Toothed Rotor - Spiral Winding Stator)

	Conventional	Superconducting X''_d = .16, 13.6 kV	Superconducting X''_d = .27, 230 kV
Stator Shield, R_o	130 (51.0)	104 (41.0)	124 (49.0)
Stator Shield, R_i	81 (32.0)	68 (26.7)	89 (35.0)
Core Natural Frequency, cps	203	263	155
$p_1 = p_2$, MPa (psi) $p = p_1 + p_2 \cos 2\theta$	.106 (15.5)	.184 (26.7)	.070 (10.0)
Maximum Static Displacement	.0010 (.00042)	.0019 (.00073)	.0018 (.00071)
Magnified Displacement	.0015 (.0006)	.0023 (.0009)	.0046 (.0015)

All dimensions are in centimeters. Dimensions in parentheses are inch equivalents.

Table 3-61

Stator Core Vibration - 1200 MVA

(Toothed Rotor - Spiral Winding Stator)

	Conventional	Superconducting X''_d = .16, 30 kV	Superconducting X''_d = .27, 500 kV
Stator Shield, R_o	150 (59.0)	138 (54.4)	155 (61.1)
Stator Shield, R_i	90 (35.3)	89 (34.9)	120 (47.1)
Core Natural Frequency, cps	230	205	88
$p_1 = p_2$, MPa (psi) $p = p_1 + p_2 \cos 2\theta$	.163 (23.7)	.200 (29.1)	.073 (10.6)
Maximum Static Displacement	.0014 (.00056)	.0024 (.00094)	.0046 (.0018)
Magnified Displacement	.0020 (.0008)	.0036 (.0014)	.0050 (.0025)

All linear dimensions are in centimeters. Dimensions in parentheses are inch equivalents.

3.3 AUXILIARIES

3.3.1 Exciter and Voltage Regulator

The discussion of the generator excitation system has been split into two parts. First, the functional requirements of the excitation system are defined. The second part involves the selection of the most appropriate type of excitation system given the functional requirements and a brief overview of actual equipment selection.

The functional requirements of the excitation system are presented below.

Steady State Requirements

The excitation system must be capable of supplying steady state excitation power. The 300, 1200, and 3000 MVA Westinghouse Superconducting generators will require approximately 3 kW of excitation. This is extremely low compared to the excitation power required by conventional machines of similar rating. Construction of an excitation system to supply 3 kW will be no problem.

Excitation System Forcing Requirements

Positive forcing requirements will be determined by transient stability considerations and the permissible time for charging the generator field. Transient stability considerations will be discussed first.

References 1 and 2 indicate that the transient stability of a superconducting machine is not a strong function of the excitation system ceiling voltage. The reasons for this are: First, the superconducting generator field time constant is very long compared to a conventional machine. The Westinghouse cryogenic machine may have an open circuit time constant of over 2000 seconds. The long time constant will tend to nullify the effects of a high ceiling voltage on the generator field.

Second, a damper shield surrounds the cryogenic field winding. An attempt to change the flux through the main field winding will be countered by an MMF in the damper winding. Because of this, the damper winding will reduce the effectiveness of any fast field forcing.

Extremely high per unit ceiling voltages can be obtained on a superconducting generator. The high per unit ceiling voltage can be achieved because the generator field no load and full load field voltages are quite low. For the Westinghouse machine, full load voltages may be three volts mainly due to brush drop. No load voltage will be slightly lower.

A large per unit ceiling will tend to cancel the effects of the large field time constant and the effects of the damper shield. However, References 1 and 2 indicate that large per unit ceiling voltages will not significantly improve transient stability.

The excitation system will also have to charge the generator field before the machine is synchronized. A high voltage may have to be applied to the generator field if rapid charging is deemed to be essential. The actual voltage will depend upon the open circuit field time constant and the maximum permissible charging time.

Very high voltages may not be required. Assume a T'_{do} of 20 minutes. Application of no load field voltage would result in a charging time of about 60 minutes. It takes approximately one hour to bring a machine up to rated speed. Hence, if excitation were applied immediately after the unit were started, no load field current would exist when the operator wished to synchronize. A higher field voltage would produce shorter charging times.

The results of the preceding preliminary analysis indicate that high positive ceiling voltages will not improve transient stability. In addition high ceiling voltages are probably not required to change the superconducting field. However, the voltage regulation characteristics of the superconducting machine following a sudden load change must be analyzed before a ceiling voltage is specified.

The excitation system must also be capable of rapidly reducing generator field current following a loss of load or when a fault occurs within the generator protective zone. In a superconducting machine, a rapid reduction in excitation can only be accomplished by applying a large negative voltage to the generator field. This negative voltage is required to overcome the large field time constant. Negative forcing can be accomplished directly by the excitation system or by using a field breaker and discharge resistor. The maximum negative forcing permitted would be a function of the insulation strength of the field winding.

To meet the functional requirements discussed above, the following types of excitation systems have been considered.

- Static Excitation System
- Rotating Rectifier Excitation System
- Rotating Thyristor Excitation System

At the present time, the static excitation system appears to be the most promising alternative. The technology required to build a static system already exists. The system is capable of forcing both negative and positive. In addition, a field breaker and discharge resistor can be added. The static system is also the least complicated of the three alternative excitation systems to design and construct.

The rotating rectifier excitation system probably cannot be utilized because it is not capable of forcing negative. A field breaker and discharge resistor cannot be used. The rotating thyristor system can force negatively. However, the system has not yet been perfected. Because of this and because of the problem of access to the excitor shaft end due to interference with the helium transfer system, a rotating excitation system will not be considered further.

Operation of Excitation System and Voltage Regulator

In choosing a type of excitation system for the superconducting generator, several things had to be considered. Most importantly, because of the extremely long open circuit time constant of the generator field (T'_{do}), the response time is very slow compared to a conventional generator. The response time is greatly improved by applying a field forcing voltage of, say, 400 volts of either a positive or negative voltage depending upon whether the voltage regulator calls for a forcing up or a forcing down of excitation. Satisfactory results can readily be obtained utilizing a full converter thyristor amplifier in a potential-source-rectifier static excitation system.

The full converter thyristor amplifier's unique ability for negative field forcing is defeated if a diode bridge rectifier is connected in parallel with the full converter thyristor amplifier three phase full wave bridge configuration. When the full converter applies negative field forcing, the diode bridge acts like a short circuit and no negative forcing is accomplished. A three phase

full wave bridge rectifier assembly would be the means through which short circuit support would be accomplished along with power current transformers in a compound rectifier static excitation system.

In addition to not being able to accomplish a conventional means of short circuit support, it appears that short circuit support would not be a benefit. The superconducting generator has a direct axis synchronous reactance (X_d) of approximately 25% of a conventional generator. This may result in a fault current of approximately 60% more than a conventional generator. Also, due to the long time constant of the generator field, the excitation would not decay as fast permitting the breakers more time to remove the fault.

The voltage regulator operates in an excitation system which includes the static exciter. When the voltage regulator is out of service, the manual control is set by a separate input to the static exciter. The manual control utilizes a dc current regulator which monitors the generator field current. The level of excitation is controlled remotely by a control switch in the motor circuit of the motor operated dc current adjuster.

The voltage regulator sensing circuit responds to average three-phase voltage and is frequency insensitive. Three-phase voltage from potential transformers is rectified and compared to a constant reference derived from a temperature compensated zener diode. The difference between the sensing and reference quantities is applied to a solid-state push-pull amplifer.

The output of the preamplifier is applied through a signal mixing module to the static firing circuits of the power amplifiers in series with an ac signal which is synchronized with the ac supply voltage to the associated thyristors. This input signal is amplified and applied to pulse circuitry. The output of the firing circuit is a dc pulse variable from 0 to 180 degrees with respect to the positive (anode positive) supply to the thyristors.

The power amplifiers employ thyristors in a three-phase full converter bridge configuration. This will provide full positive and negative forcing. The thyristors operate in a switching mode. They are turned on or rendered conducting once each cycle at a variable angle in the cycle as determined by the amplified error signal from the regulator. The earlier in the cycle that the thyristors are turned on, the greater is the amount of energy delivered to the field. Thus, the regulator controls excitation by varying the output of the power amplifier by controlling the associated firing circuits.

Another aspect of the excitation system that is unique to the superconducting generator is a requirement on the current ripple from the exciter. Current ripple must be at a sufficiently low level that the total field winding conductor loss, due to the ripple magnetic field, is kept below about one watt. The limit for the current ripple is dependent on the conductor type.

Figure 3-133 shows the total heat input to the field winding of the 300 MVA machine for a monolithic and cabled mixed-matrix conductor and for a copper-matrix conductor as it depends on the ratio of peak ripple at 360 Hz to the dc field current. This plot is based on a "six-pulse" thyristor, full wave bridge power amplifier with the lowest ripple frequency at 360 Hz. The higher ripple harmonics are multiples of this base frequency and fall off as one over frequency.[3]

The dominant loss for these conductors is due to eddy currents in the matrix. This loss goes as the square of the product of frequency and field up to the skin effects shielding limits for the specific conductor.[4] Above this limit the loss drops off with frequency. For example, for the cabled, mixed matrix the highest harmonic that contributes to the loss is 5760 Hz and each harmonic (multiples of 360 Hz) below this, down to 360 Hz, contributes equally. The curves in Figure 3-133 for the two mixed-matrix conductors represent the sum of all of the harmonics to the eddy current (and hysteresis loss) that contribute.

With the copper matrix conductor 360 Hz is already above the shielding limit. The curve for this conductor is therefore for only the eddy current loss for 360 and 720 Hz, the higher components dropping off fast enough to be neglected.

The conductor that has been chosen as optimum for the 300 MVA machine is a copper-matrix conductor. With a six-pulse thyristor bridge, the maximum current ripple at 360 Hz relative to the dc current, using 15 h as the field inductance and 400 volts as the exciter ceiling is 10^{-5}. Referring to the copper matrix curve in Figure 3-133, it is evident that the total loss in the field winding is below 1 watt.

This loss could be reduced even further if necessary by going to a 12-pulse thyristor bridge.

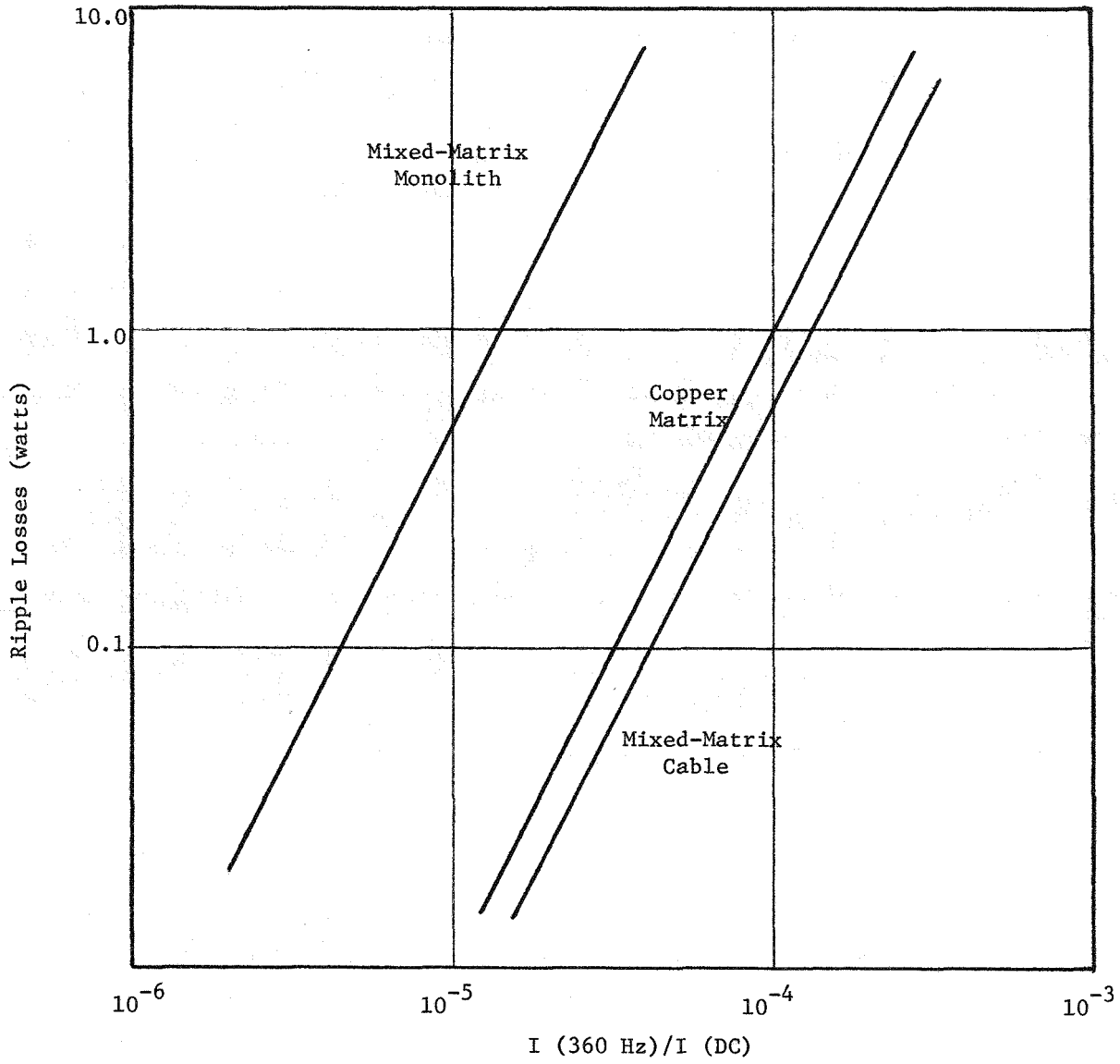

Figure 3-133. Field Winding Ripple Losses.

Because of the extremely long open circuit time constant of the generator field in this application (approximately 500 times that of a conventional generator) and the electronic speed of regulator and static exciter circuitry, it has been determined that excitation system damping for stability is not required.

Signal summing, limiting, and auctioneering is accomplished in a solid-state logic circuit whose output controls the firing circuit of the power amplifier.

A static minimum excitation limiter is included as standard design in the voltage regulator. This limiter prohibits lowering of the excitation of the a.c. generator below the level which would result in loss of synchronism of the generator with the system. This limiter responds to a circular kVA characteristic, similar to and following the same laws as that of the static stability limit. The inputs to the limiter are taken from machine potential and current transformers. The limiter output bids against the voltage sensing signal output in an auctioneering circuit for control of the power stages of the regulator. The control of the power stages by the limiter prevents the voltage regulator elements from decreasing machine excitation below the adjustable set value.

A static maximum instantaneous current limiter is also included in the design of the voltage regulator. This limiter acts through the regulator to return the value of excitation to a preset value somewhat above the preselected value for field forcing. The limiter operates instantaneously. Input to this limiter is taken from a generator field shunt through the isolating transducer described above. The output of the limiter is auctioneered with the regulator in the signal mixing module.

The instantaneous overexcitation limiter is not intended for overall thermal protection of the generator field. For overall protection, the limiter is supplemented by instantaneous overexcitation protection equipment. These serve to protect the generator field from excessive thermal stress during periods of overexcitation and under all modes of excitation control.

Volts per hertz limiting is included in this proposal as standard design. It is applied to a regulator when it is visualized that the station will have to operate under adverse circumstances with the system frequency below normal operating range. In such cases voltage regulation should be subordinated

to volts per hertz regulation. Avoidance of the heating effects of excessive a.c. current in windings of transformers and other magnetic devices is the reason for operating at reduced voltage during underfrequency conditions. The input to the maximum volts per hertz limiter is machine terminal voltage and its output is a signal that auctioneers with the voltage regulator output signal in the signal mixer.

Independent of the volts per hertz limiter in standard design is the volts per hertz protection. This device provides alarm and trip in the event that under-frequency operation reaches low levels without adequate retreat of terminal voltage level. The volts per hertz protection includes a sensing relay and a time delay relay. Time delay is introduced into the alarm function to prevent false alarms due to transient voltage or frequency changes. The delay for the trip circuit is set long enough to allow the limiter to function. The volts per hertz relay is left in service when on manual control of voltage, even though the limiter under these circumstances, is out of service.

A block diagram of the exciter and voltage regulator system is shown in Figure 3-134. This represents the implementation of the above discussion.

One of the problems arising for a superconducting generator excitation system is how to monitor system for normalization. Schemes for normalization or quench detection are discussed in a separate section. The output signal from the quench detection circuit would, of course, be used to operate a relay which trips the generator field breaker. The energy in the field winding is then absorbed in the non-linear shunt resistor.

References

1. System Performance Characteristics of Superconducting Alternators for Electric Utility Power Generation, T. H. Einstein, IEEE Trans. Power Apparatus and Systems, Vol. PAS-94, No. 2, March/April 1975, pp. 310-319.
2. Transient Stability of Superconducting Alternators, M. Furuyama, J. L. Kirtley, Jr., IEEE Trans. Power Apparatus and Systems, Vol. PAS-94, No. 2, March/April 1975, pp. 320-328.
3. Thyristor Phase-ontrolled Converters and Cycloconverters, B. R. Pelly, Wiley-Interscience, Chap. 4, p. 69.
4. See Section 3.2.1.2, Superconductor Application, for a full discussion of conductor losses.

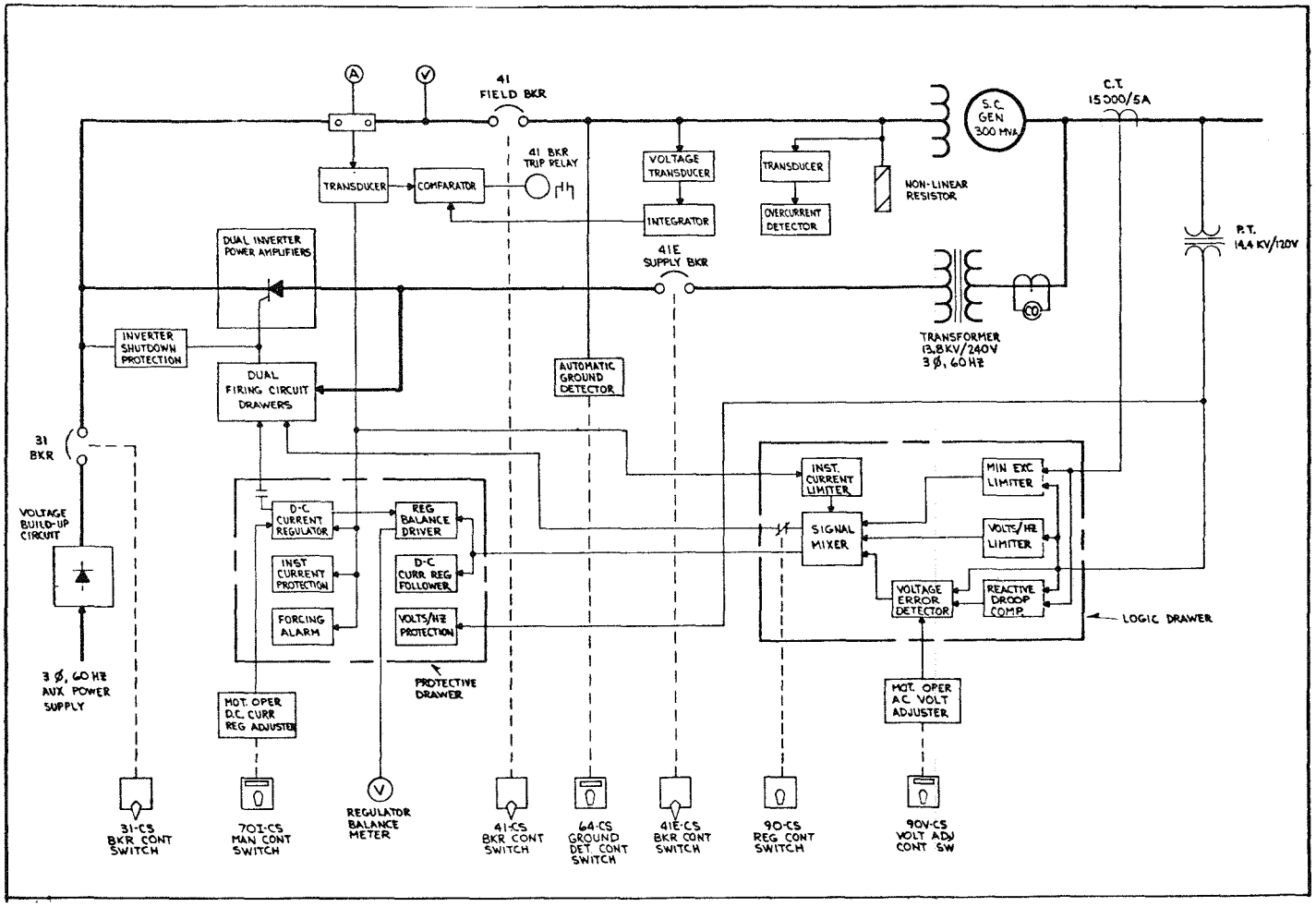

Figure 3-134 - Generator Control and Excitation System.

Quench Detection

Introduction

Our design philosophy for the superconducting field windings has been to push, as far as is judged advisable, toward high current densities in order to realize high machine power densities. In adopting this approach, it was recognized that, based on the present uncertainties in designing and fabricating field windings that will be stable against internal heat generation due to conductor motion, a normalization or quench can occur. Also, a quench under a terminal fault condition due to conductor or support structure heating and the subsequent temperature rise is also a possibility. Therefore it is necessary to plan that quenches may occur for early demonstration machines and to design to handle the consequences of this event.

When a quench is initiated, the normal zone will grow and propagate through the winding and therefore the resistance of the coil will increase with time. This leads to heat generation and to rapid vaporization of helium as well as to a rapid temperature rise in the winding. Handling the pressure increase is addressed in the section on the rotating seal system. The purpose of this section is to discuss quench detection schemes that will be sufficiently fast to catch and therefore dump the energy stored in the winding before a hot spot develops that can lead to coil burnout.

In the rotor design section the time dependent quench analysis predicted that if the quench could be detected within the order of a few seconds after initiation, the hot spot temperature would be well within the safe limits ($\lesssim$ 300°K). Therefore in the following discussion it will be assumed that the quench will be detected at times of less than $\sim$ 5 seconds.

Quench Detection

The following basic requirements must be met by a quench detection scheme.

- The quench must be sensed and action taken before the maximum temperature in the winding rises to 300°K.
- Detection must be effective no matter where the quench initiates in the winding.
- The detection scheme must distinguish a real quench from effects due to systems disturbances, e.g. faults and load changes, and subsequent exciter action.

It is possible to base quench detection on measured changes in thermal, mechanical or electrical quantities. For example, the change in winding temperature could be detected by a number of sensors in series placed throughout the winding, or the change in the pressure in the helium system by placing sensors in the bath or in the exit gas stream. It may well be that the first few large machines that are built and tested will be instrumented for sensing temperature and pressure for design verification and as such, this instrumentation could also serve for quench detection. However, looking further into the future, schemes that do not involve sensing in the winding or in the cold space would be desirable. This then leads to consideration of electrical methods.

The electrical quantity that changes as a quench proceeds is, of course, the resistance of the winding. Therefore any electrical scheme must ultimately be based on detecting this resistance change.

Quench detection for dc magnets uncoupled to other electrical systems is simple and direct. Detecting a change in current (for constant voltage supply) is all that is required.

Magnets driven by time varying voltages or currents, but still uncoupled to other electrical systems, represent the next stage of complication. If the drive is sinusoidal, measuring the change of the in phase component of voltage (or current) will suffice. If the drive is non-sinusoidal, then either a "bucking" technique or a separately injected signal approach could be used.

A "bucking" or difference approach could utilize an electronic simulation of the field coil. Here the actual field current would be the input to the simulator and the voltage output would be compared with the actual voltage across the field winding. The electronic inductance would be adjusted to match the field winding in inductance and Q. Then the voltage difference would be proportional to the change in field winding resistance.

The other method would consist of injecting a small sinusoidal current into the winding and then measuring the in phase voltage across the field to yield the resitance change. It would be essential with this method to be able to reject or discriminate against the variation of coil voltage from the time varying supply by narrow band techniques. Also the level of injected current must be sufficiently low so as not to impact on the helium requirement to any significant degree.

Another approach to this time varying case would be to use a series of voltage taps on the coil, e.g. divide the coil into four parts, and to sample voltage difference between alternate section pairs. This approach is similar to an external "bucking" conductor discussed above.

The field winding of a generator connected to a power system represents a much more complex case for quench detection. This is due to the fact that the currents through field windings are driven not only by the exciter but also through coupling to the armature and thereby to the power system. Further, the effective inductance and resistance parameters for the field winding are frequency dependent due to coupling of the field to the shield system and the armature. Both of these aspects imply that most quench detection methods that can be utilized for dc or ac isolated coils are not applicable to a generator field winding.

The method briefly covered above utilizing a separate injected current signal is applicable to the generator. The problem is again to be able to inject sufficient current without excessive heating and still be able to detect the voltage signal in the presence of large exciter swings. With proper narrow band techniques this method might be workable, but two other methods appear more straight forward.

The first of these methods has been proposed by D. T. Ching (MIT Bachelor of Science Thesis, 1976). This scheme recognizes that the field winding current is a function of both the direct axis armature current and exciter voltage. It is then proposed that an electronic simulation of the generator be utilized to predict the field current using the field voltage and the direct axis current as inputs. Then a difference between the predicted field current (output of the simulator) and the actual field current will indicate the initiation of a quench. This method has been tested by a computer simulation of both the machine and detector dynamics under worst case system and exciter conditions.

The second method for the coupled field winding case would utilize voltage taps on the field winding. By measuring the voltage difference between alternate pairs, it would be possible to detect the start of normalization. Here it is recognized that each winding subsection will respond in an equal way to the exciter and system changes. With two or more taps, a normal section can be detected any place in the coil. This method would, of course, require the difference voltage to be transmitted from the rotor by slip rings or telemetering. Aside from this aspect, the method is passive.

The above three methods are schematically diagrammed in Figures 3-135, 3-136 and 3-137 along with a schematic of the field coupled to the shield and armature in Figure 3-138.

It is not possible at this time to make a definite choice between the machine simulation (Ching) and the voltage tap approach. Each have certain advantages and disadvantages and only further computer or experimental work can lead to the best choice.

Superconducting Machine Dynamic Stability

Introduction

Previous analytical studies conducted on EPRI Contract No. RP 429-1 have included investigation of the sensitivity of superconducting machine transient stability limits to changes in unit electrical and mechanical parameters and also a comparison of the stability limits of a superconducting machine to a conventional machine.[1] This section describes a study comparing dynamic stability of a superconducting machine to that of a conventional machine operating in the same environment.

One way of evaluating the relative stability of a synchronous machine, including the effects of the excitation system, is by examining synchronizing and damping torque coefficients over the range of oscillation frequencies typically 0.2 to 2 Hz, likely to be encountered in power systems. The stability of a generator connected to a power system requires that both the synchronizing and damping components of accelerating torque be positive over the range of oscillation frequencies encountered. Synchronizing torques are in phase with rotor angle. Positive synchronizing torque is necessary to insure restoration of the rotor angle following a disturbance. Damping torques are in phase with rotor velocity. Positive damping torque is necessary for the decay of rotor oscillations following a displacement in rotor angle.

Analytical techniques for evaluating synchronizing and damping torque coefficients have been developed for simplified models of a single machine and infinite bus.[2,3,4] A similar analysis (developed by R. T. Byerly, Westinghouse Advanced Systems Technology) is included here. This analysis differs from references 2, 3, and 4 in that subtransient circuits are included in the machine model.

METHOD #1 MACHINE SIMULATOR (MIT)

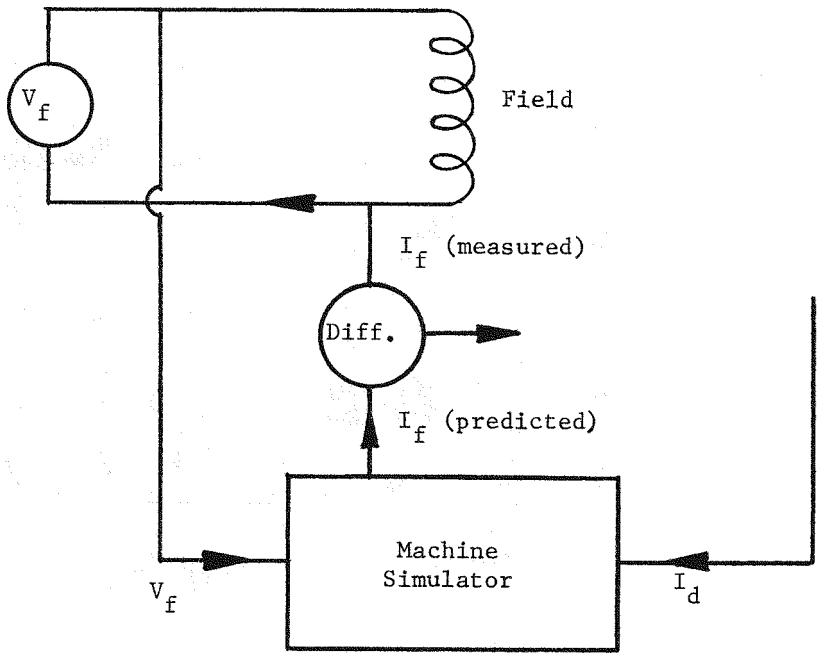

Figure 3-135. Schematic of Quench Detection Scheme #1

METHOD #2 VOLTAGE TAPS

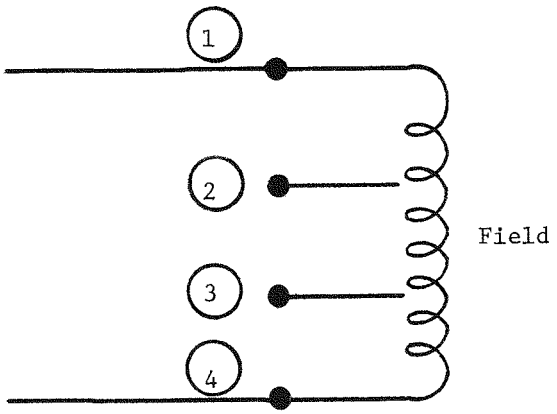

Alternately measure $(V_{34} - V_{23})$ and $(V_{12} - V_{23})$ at $\approx$ 1 Hz

Figure 3-136. Schematic of Quench Detection Method #2

METHOD #3 INJECTED SIGNAL

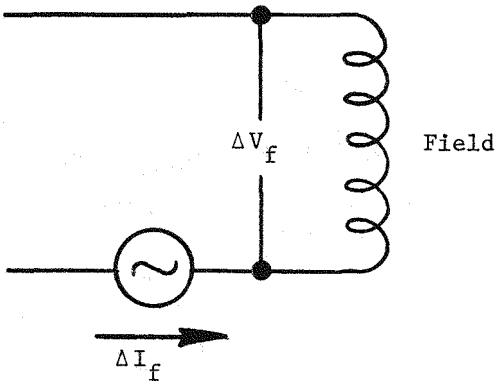

Real $\left(\frac{\Delta V_f}{\Delta I_f}\right)$ $\propto$ Field Resistance

Utilize Narrow Band Techniques

$\Delta I_f < 0.1$ Amp

$Q < 1$ Watt (Field Heating)

Figure 3-137. Schematic of Quench Detection Method #3

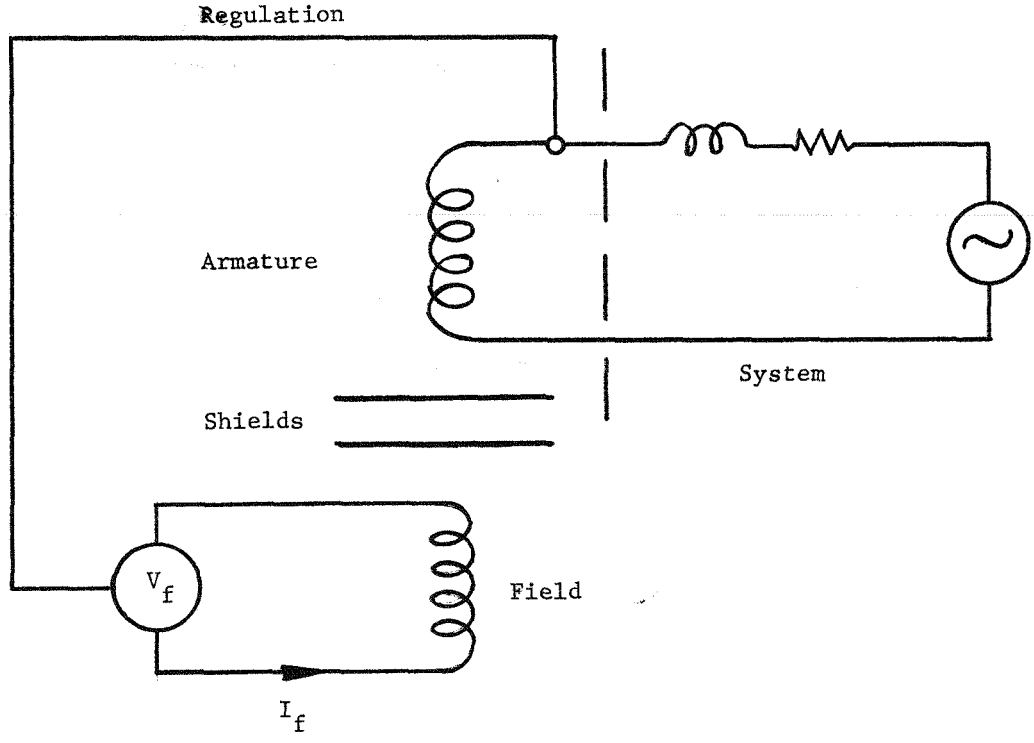

Figure 3-138. Schematic of Field Coil Coupled to Armature and System

Method of Analysis

In this simplified analysis, the generator is assumed to be connected through a reactance to an infinite bus. A stability model for a machine and infinite bus is shown in Figure 3-139. Electrical torque is calculated from equivalent circuit equations using the model shown in Figure 3-140 for the synchronous machine and infinite bus and the model shown in Figure 3-141 for the excitation system.[5,6] Constants assumed for the machine,[1] excitation systems, and operating conditions[1] are listed in Table 3-62.

In these calculations, the generator inertia constant (H) is treated as a variable. At low (< 0.5 Hz) frequencies, the model is representative of a large sub-system connected radially to another large system. At higher frequencies, the model is representative of a single machine connected to a large system.

Referring to Figure 3-141 and Table 3-62, the forward gain (K_A) excitation system stabilizer gain (K_F) and time (T_F) values used in this study for the conventional generation are typical values currently being used in actual applications. The forward gain (K_A) used for the superconducting generator excitation system was chosen, somewhat arbitrarily, such that ceiling voltage would be obtained with approximately 0.06 p.u. generator terminal voltage error. Consideration of the off-line, open circuit, frequency response characteristics of an excitation control system with a superconducting generator shows that application of an excitation system stabilizer is neither required nor desirable due to the very large open circuit field time constant of the superconducting machine.

In this analysis, the transfer function of the power system stabilizer was chosen to provide good though not necessarily optimum damping in the region of the natural frequency of the local made oscillations i.e., oscillations of a single machine against the system. Improved damping at low frequencies corresponding to inter-area oscillations could be obtained by adjusting the time constants of the stabilizer; however, less positive damping would then exist at the higher frequency corresponding to the local mode.

Discussion of Study Results

Calculated synchronizing and damping torque coefficients for the model of the conventional machine are shown as functions of frequency in Figures 3-142 (a) and (b). In Figure 3-142, the solid curves labeled "constant excitation" show

DYNAMIC STABILITY MODEL FOR AN EXCITATION CONTROL SYSTEM AGAINST AN INFINITE BUS WITH ELECTRICAL TORQUE DERIVED FROM SYNCHRONOUS MACHINE EQUIVALENT CIRCUITS

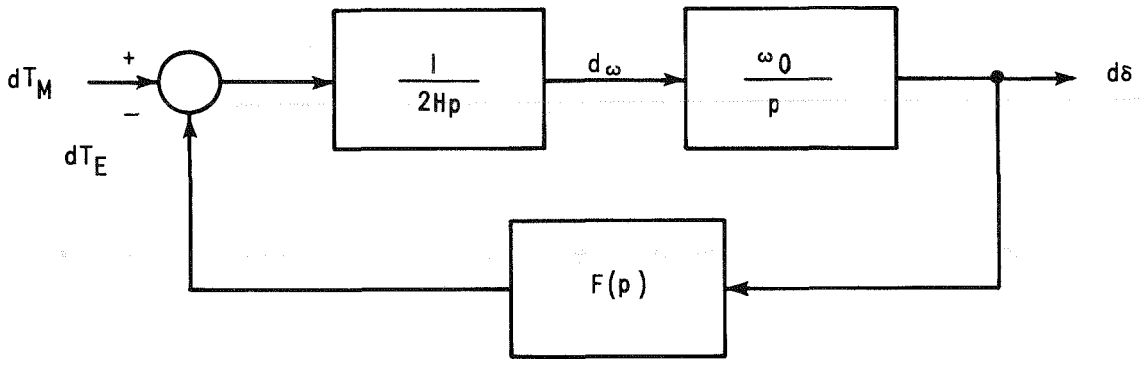

T_M = MECHANICAL TORQUE

T_E = ELECTRICAL TORQUE

δ = ROTOR (TORQUE) ANGLE

H = INERTIA CONSTANT

ω = ROTOR SPEED

p = OPERATOR d/dT

F(p) = FUNCTION OF MACHINE CONSTANTS, EXTERNAL IMPEDANCE, OPERATING LEVEL & EXCITATION SYSTEM CONSTANTS

Figure 139 A

DYNAMIC STABILITY MODEL OF AN EXCITATION CONTROL SYSTEM AGAINST AN INFINITE BUS WITH SYNCHRONIZING AND DAMPING COMPONENTS OF ELECTRICAL TORQUE SEPARATED

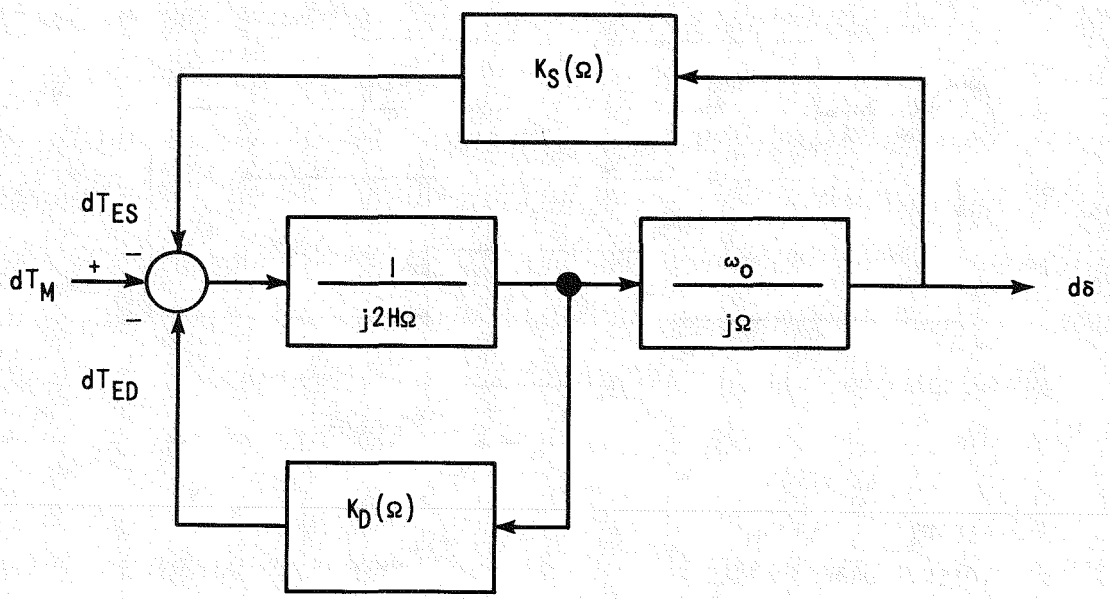

FOR FREQUENCY RESPONSE ANALYSIS $p = j\Omega$

$K_s(\Omega)$ = REAL $[F(j\Omega)]$ = PER UNIT SYNCHRONIZING TORQUE FUNCTION

$K_D(\Omega) = \frac{I_{MAG}[F(j\Omega)]}{(\Omega/\omega_o)}$ = PER UNIT DAMPING TORQUE FUNCTION

Figure 139 B

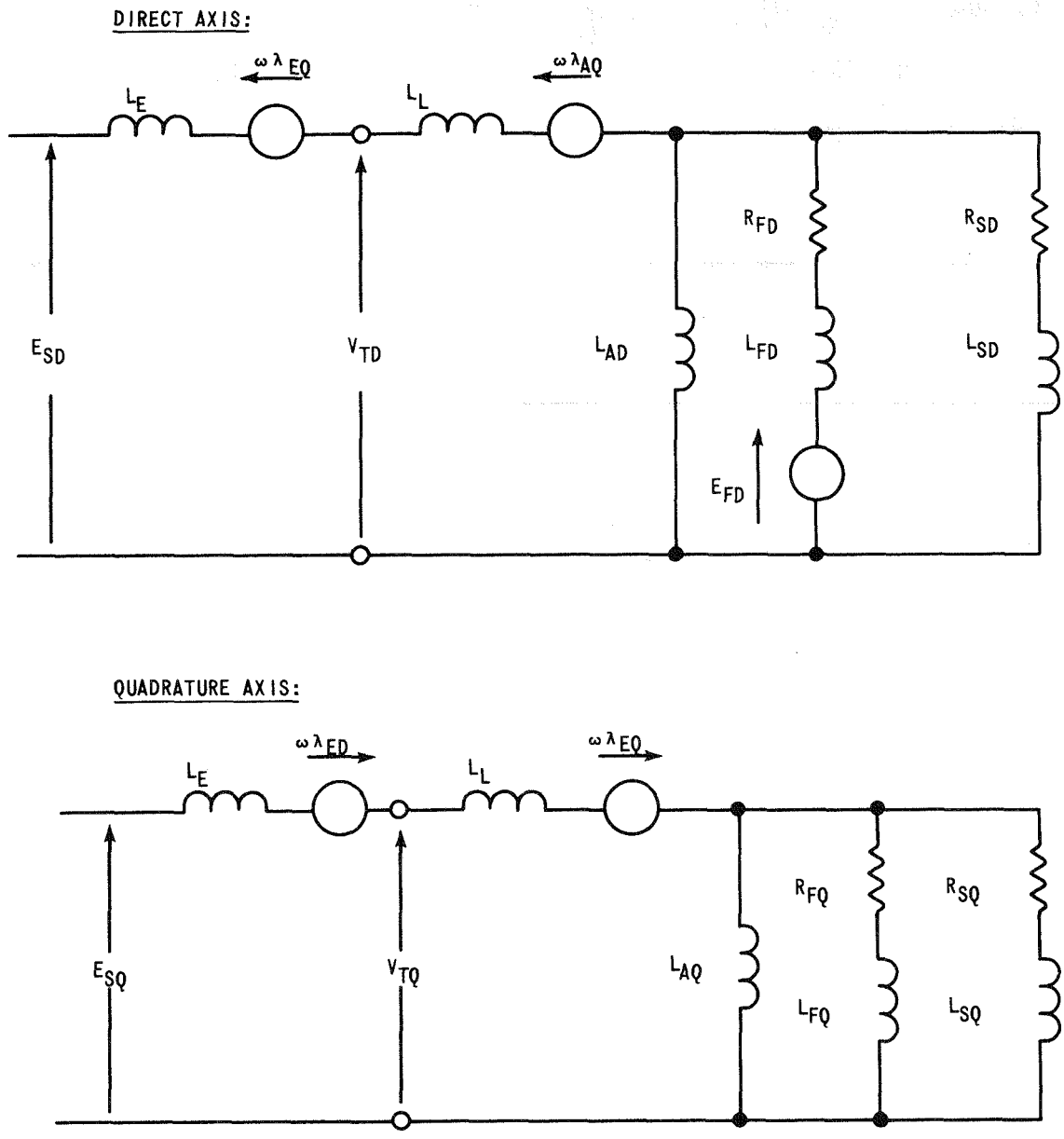

Figure 3-140. Model of Conventional Synchronous Machine Against an Infinite Bus

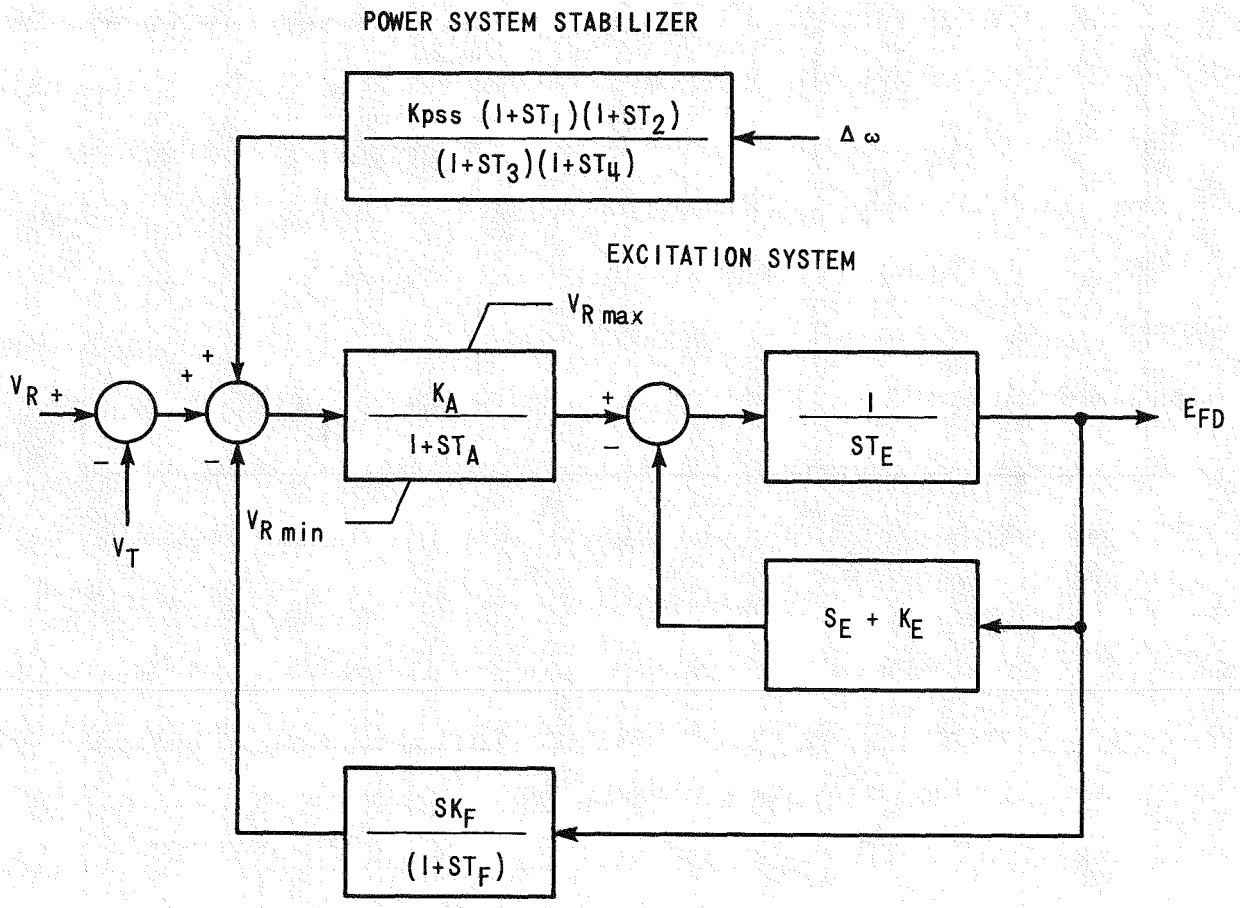

Figure 3-141. Excitation System Model

Table 3-62

CONSTANTS ASSUMED FOR DYNAMIC STABILITY ANALYSIS

	Superconducting Generator	Conventional Generator	Operating Conditions
X_D	0.453	1.701	X_E = 0.37
X_D'	0.303	0.281	P = 0.90
X_D''	0.161	0.239	Q = 0.37
X_Q	0.453	1.674	E_T = 1.05
X_Q'	0.453	0.458	E_S = 0.978
X_Q''	0.161	0.237	
T_{DO}'	2800	5.30	
T_{DO}''	0.205	0.04	
T_{QO}'	0	1.50	
T_{QO}''	0.205	0.068	
X_L	0.081	0.197	
H	Variable	Variable	
K_A	2000	200	
T_A	0.05	0.05	
K_F	0	0.04	
T_F	0	1.0	
K_E	1.0	1.0	
T_E	0	0	
SE_{MAX}	0	0	
$SE_{.75MAX}$	0	0	
VR_{MAX}	+125	+4.29	
VR_{MIN}	-112	-3.86	
K_{PSS}	10	10	
T_1, T_2	0.50	0.50	
T_3, T_4	0.05	0.05	

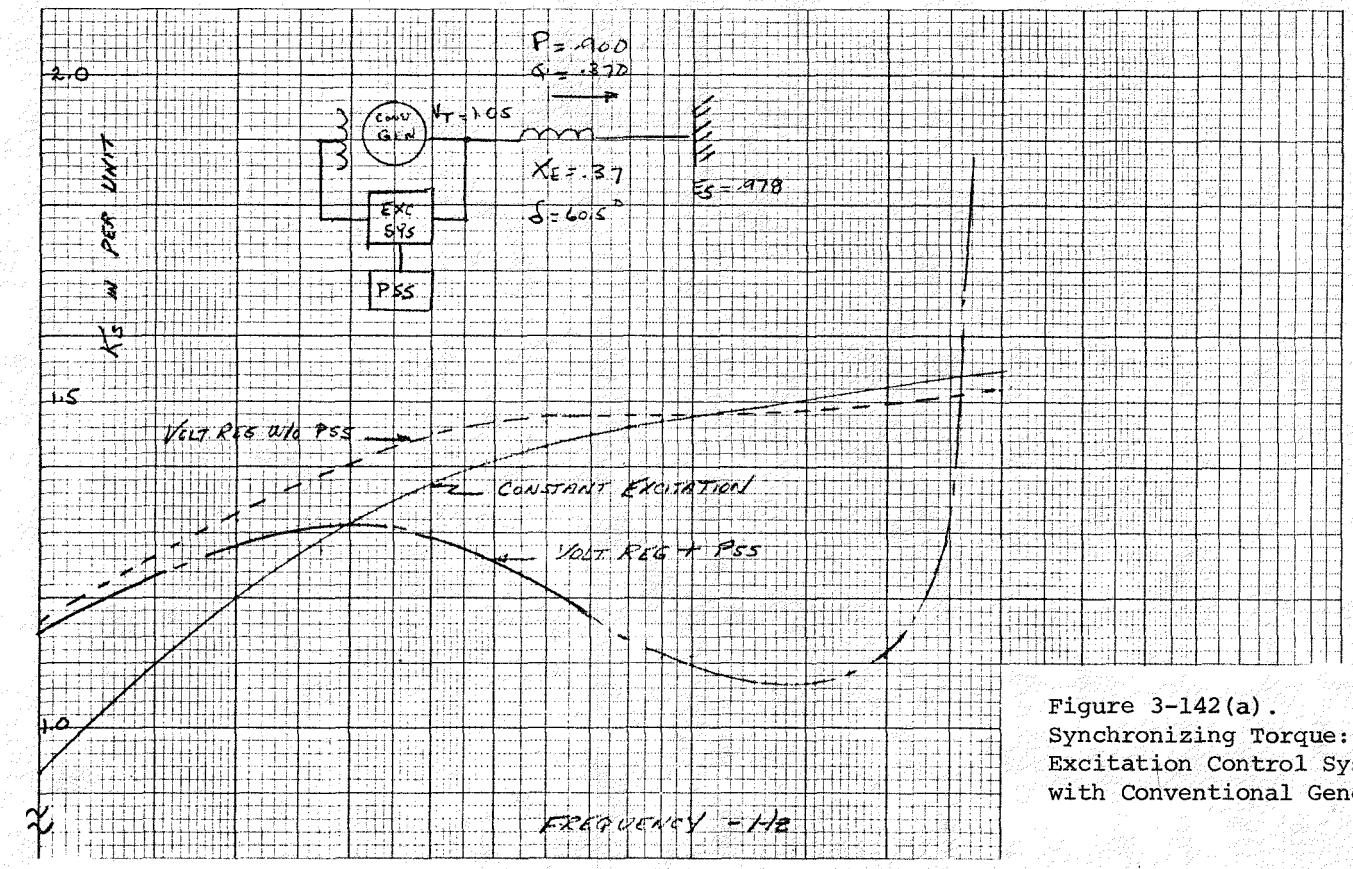

Figure 3-142(a).
Synchronizing Torque:
Excitation Control System
with Conventional Generator

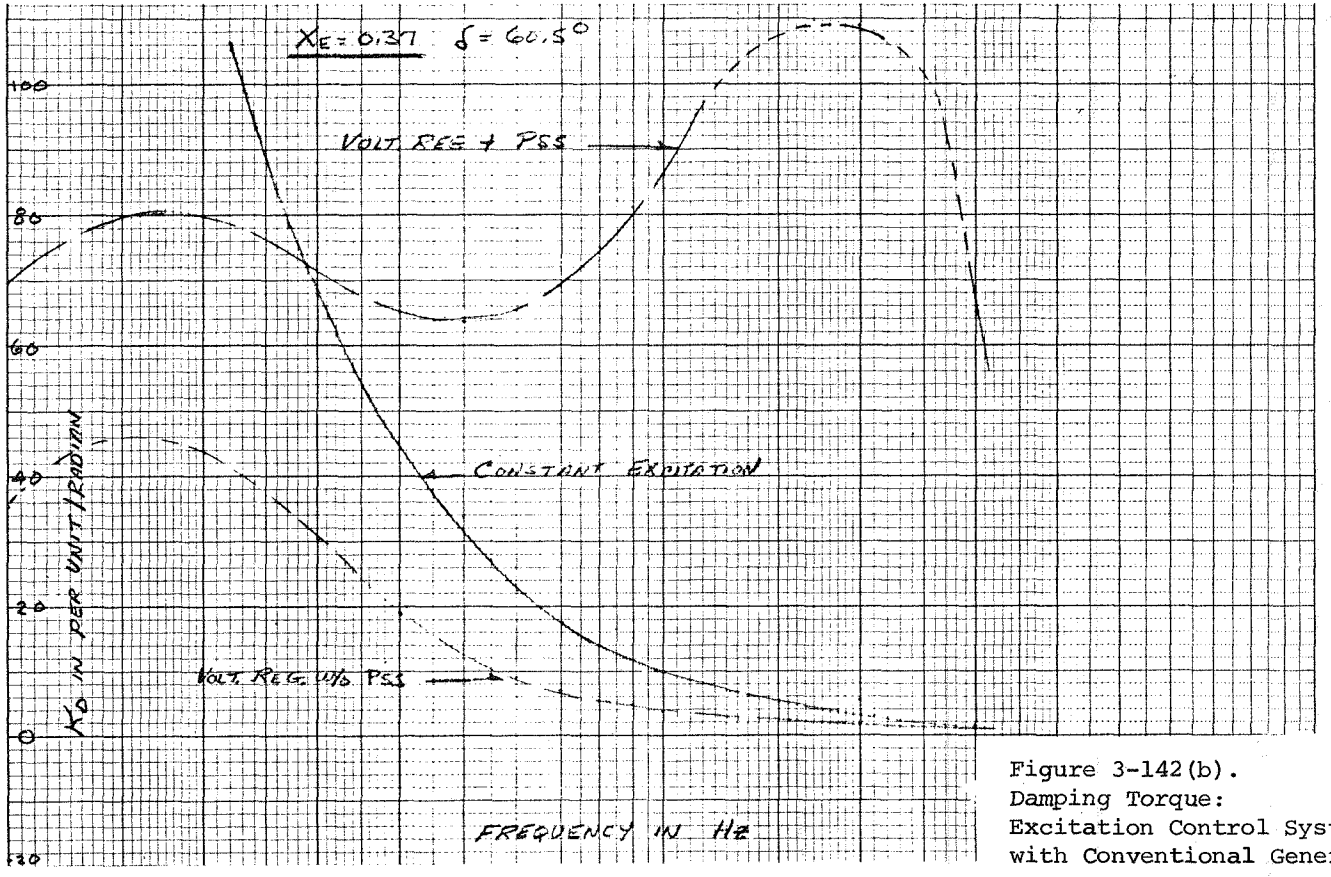

Figure 3-142(b).
Damping Torque:
Excitation Control System
with Conventional Generator

the performance of the machine itself with no regulator or governor action, the broken line curves labeled "without power system stabilizer" show the effect of adding a voltage regulator, and the broken-line curve labeled "with power system stabilizer" show the effect of adding a power system stabilizer to the excitation system. Natural frequencies of power system electromechanical oscillations generally are in the range of 0.2 to 2.0 Hz for which these functions are shown.

The rate of growth or decay of oscillations at a natural frequency is strongly dependent on synchronizing and damping torque coefficients and a decay function calculated from these coefficients is shown in Figure 3-142(c). At the low end of the frequency range, say from 0.2 Hz to 0.5 Hz, this function is representative of inter-system oscillations. At higher, say 0.8 to 2 Hz, it is representative of oscillations involving a single-unit or plant.

The synchronizing and damping torque coefficients and decay function calculated for the superconducting generator are shown in Figures 3-143(a)3-143(b) and 3-143(c).

Figures 3-142 and 3-143 show that in the frequency range above 0.8 Hz in Figure 3-142 and above 0.2 Hz in Figure3-143, the effect of the excitation system without a power system stabilizer on the synchronizing torque is slight. This is due to the attenuation attributable to the field time constant of the generator and is, of course, more pronounced in the case of the superconducting generator. The increase in synchronizing torque above 2 Hz with the addition of the power system stabilizer is due to the compensating phase lead and increased gain provided by the stabilizer.

The effect of automatic voltage regulation, without supplementary control provided by a power system stabilizer, is to reduce positive system damping as shown in Figures 3-142 and 3-143. Comparing Figures 3-142 and 3-143, it is seen that in the frequency range from 0.3 Hz to 3 Hz the reduction in damping is less pronounced in the case of the superconducting machine. Recent years have seen wide application of supplementary control devices, (power system stabilizers) to improve system damping. Figure 3-142(b) shows a dramatic increase in positive damping with the addition of a power system stabilizer in the excitation control system with a conventional generator, Figure 3-143(b), as expected, that the improvement in damping provided by the power system stabilizer is much less in the case of the superconducting generator; however, it is interesting to note that some improvement is indeed attainable.

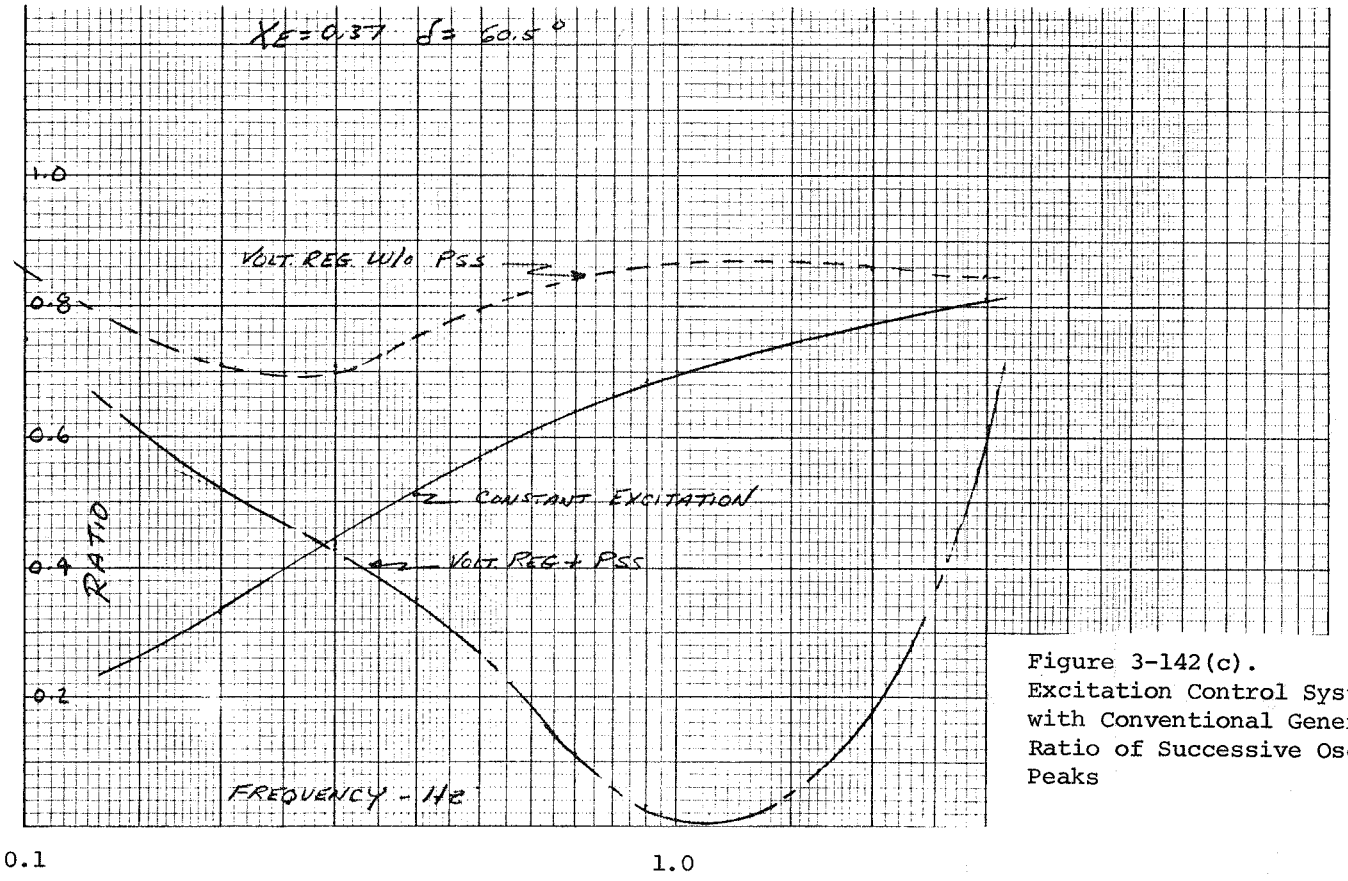

Figure 3-142(c).
Excitation Control System
with Conventional Generator:
Ratio of Successive Oscillation
Peaks

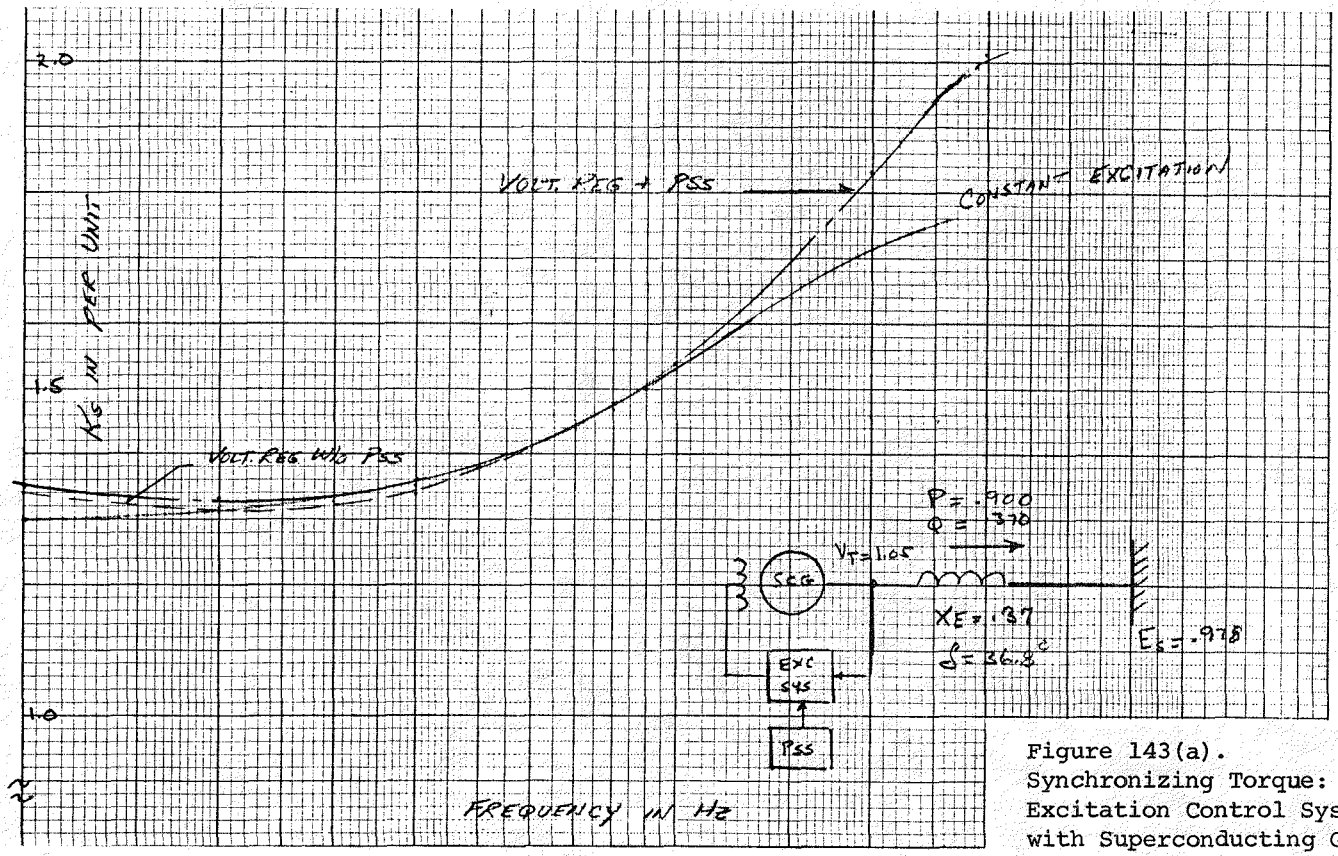

Figure 143(a).
Synchronizing Torque:
Excitation Control System
with Superconducting Generator

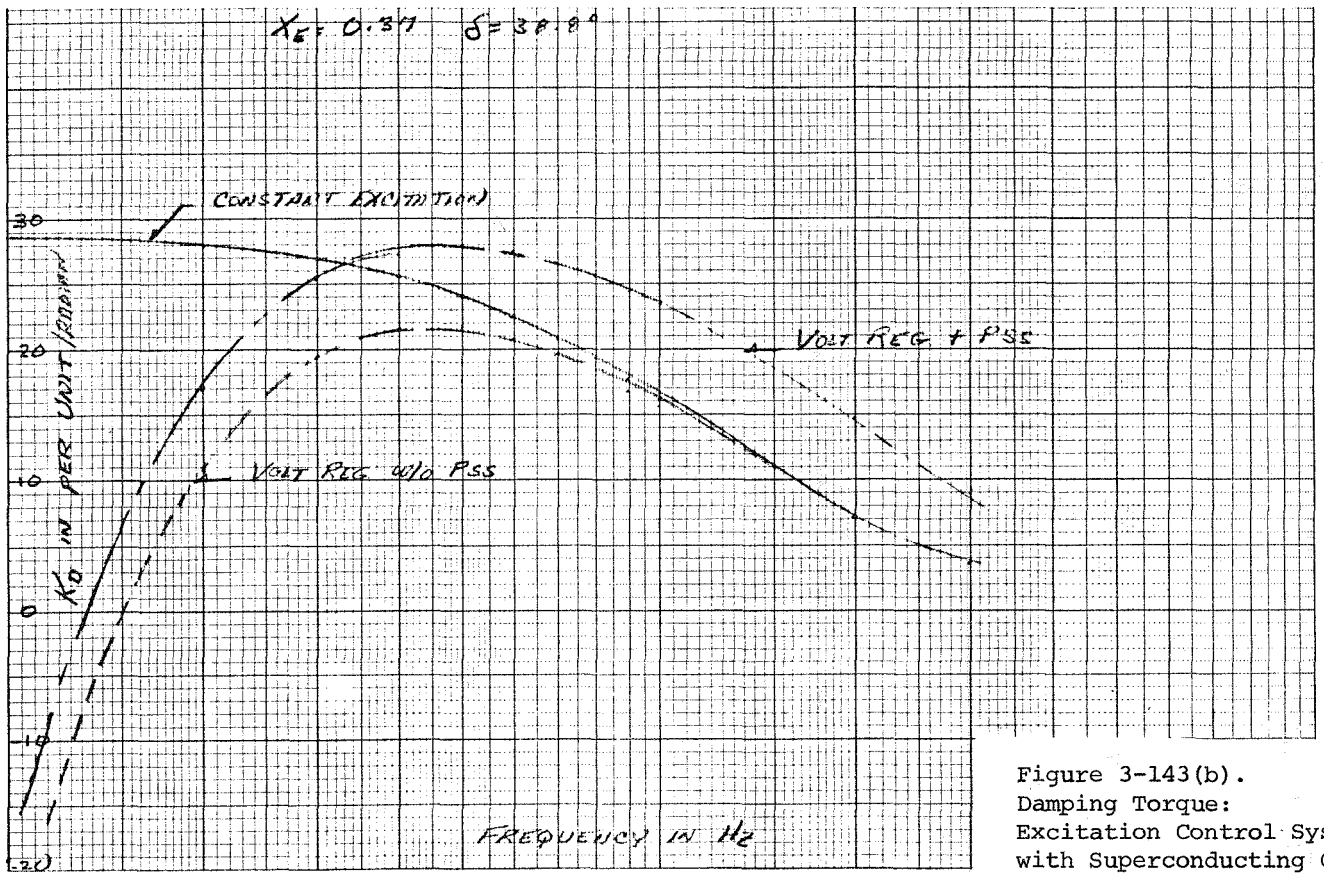

Figure 3-143(b).
Damping Torque:
Excitation Control System
with Superconducting Generator

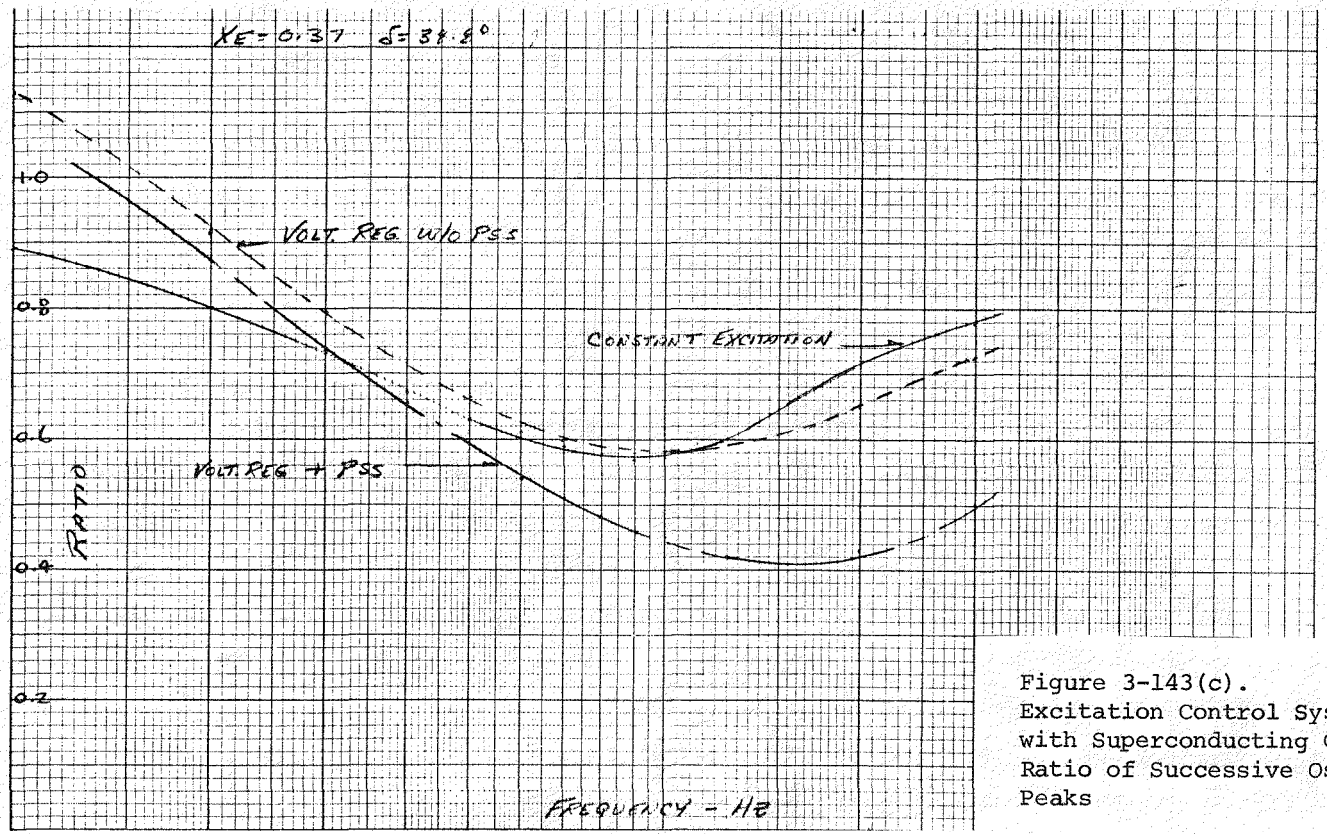

Figure 3-143(c).
Excitation Control System
with Superconducting Generator:
Ratio of Successive Oscillation
Peaks

In evaluating relative damping, the ratio of successive peaks data of Figures 3-142(c) and 3-143 (c) is perhaps somewhat easier to interpret than the plots of K_D. Also, this data provides a means of correlation between this frequency response analysis and a real time transient performance simulation.

Conclusions

In general, the results of this analysis are in agreement with the conclusions drawn in references 7-10. In particular, unlike conventional machines, the superconducting alternator will have no dynamic stability limit when operating within its MVA rating. To further illustrate this, an additional case was analyzed comparing superconducting generator performance with that of a conventional machine (one that is actually in operation) operating into a power system over a very high (X_E 0.82 p.u.) reactance. Complete results of this case are not included here, but may be summarized as follows: The conventional machine operating at power output of 0.61 p.u. (torque angle of 72°) is unstable without the addition of a power system stabilizer whereas the superconducting generator (torque angle of only 45.8°) is stable without a power system stabilizer.

References

1. J. H. Parker, Jr. and R. A. Towne, Superconducting Generator Design, EPRI Contract No. RP 429-1, Quarterly Reports Nos. 2 and 3, March/June, 1976.
2. F. P. DeMello and C. Concordia, "Concepts of Synchronous Machine Stability as Affected by Excitation Control," IEEE Transactions on Power Apparatus and Systems, Vol. PAS-88, pp. 316-329, April, 1969.
3. W. K. Marshall and W. J. Smolinski, "Dynamic Stability Determination by Synchronizing and Damping Torque Analysis," IEEE Transactions on Power Apparatus and Systems, Vol. PAS-92, #4, pp. 1239-1246, July/Aug., 1973.
4. M. K. El-Sherbiny and D. M. Mehta, "Dynamic Stability, Part I - Investigation of the Effect of Different Loading and Excitation Systems," IEEE Transactions on Power Apparatus and Systems, Vol. PAS-92, #5, pp. 1538-1546, Sept./Oct., 1973.
5. D. C. White and H. H. Woodson, "Electromechanical Energy Conversion" New York: Wiley, 1959.
6. IEEE Committee Report, "Computer Representation of Excitation System," IEEE Trans. Power Apparatus and Systems, Vol. PAS-87, pp. 1460-1464, June, 1968.
7. T. H. Einstein, "Excitation Requirements and Dynamic Performance of a Superconducting Alternator for Electric Utility Power Generation," MIT Thesis (ScD), Department of Mechanical Engineering, December, 1970.

8. T. H. Einstein, "System Performance Characteristics of Superconducting Alternators for Electric Utility Power Generation," IEEE Transactions on Power Apparatus and Systems, Vol. PAS-94, No. 2, pp. 320-329. March/April, 1975.

9. M. Furuyama and J. L. Kirtley, Jr., "Transient Stability of Superconducting Alternators," IEEE Transactions on Power Apparatus and Systems, Vol. PAS-94, No. 2, pp. 320-329, March/April, 1975.

10. T. H. Einstein and T. A. Keim, "Effect of Field Winding Electromagnetic Shield on the Excitation Requirements of a Superconducting Alternator," IEEE Paper A 75-578-5 presented at the IEEE Summer Power Meeting, July 20-25, 1975.

3.3.2 Generator Gas, Oil and Water Systems

Gas System

The low voltage generator will be filled, in the region outside the damper shield, with a low pressure, low density gas to perform the following functions:

- Remove eddy current losses from the damper shield
- Remove miscellaneous inductive heating losses from the stator shield end region and the enclosure
- Minimize windage loss
- Provide a good dielectric environment for the armature

A pressure slightly above ambient (i.e., 0.5 psig) should be adequate and will result in a low gas leakage rate. The low pressure will also allow the design of a relatively lightweight stator enclosure.

The required gas circulation through the rotor damper shield will be obtained by means of differential pressure maintained between the two ends of the generator frame, which will provide a flow of cooling gas through axial grooves. An external blower will provide the required differential pressure for circulation through the machine proper and external coolers. Figure 3-144 shows the proposed gas system.

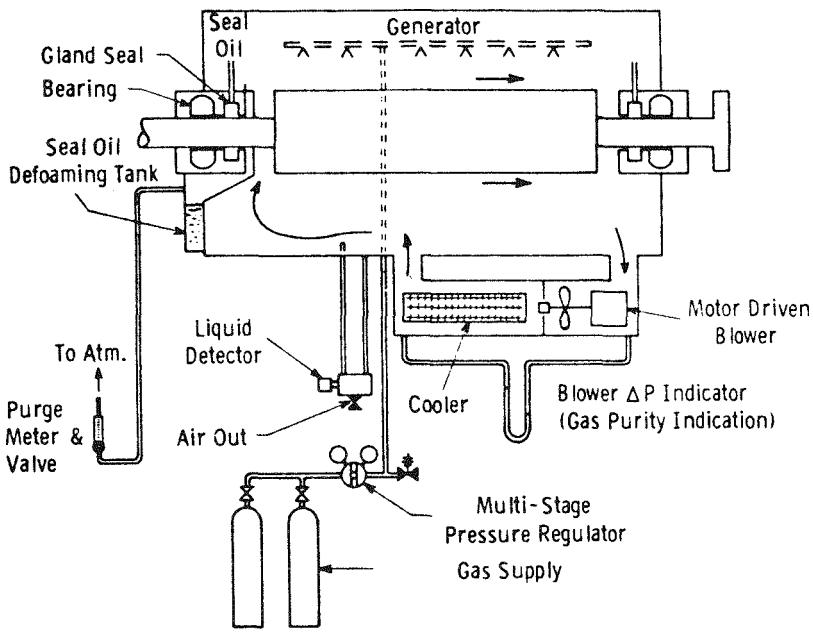

Figure 3-144. Gas System for Use with Superconducting Generator

The high voltage generator stator will be filled for the most part with insulating oil as described in the armature section. The region between the armature and the damper shield will be filled with gas, however, to remove damper shield losses and to minimize windage losses, and will have a similar gas system.

Gland Seal System

Containment of the cooling gas within the generator shell will be accomplished by shaft oil gland seals of conventional design. Because of the relatively low gas pressure, low oil pressures and low oil flows will be required. The seal oil system will be relatively small and of the single flow type. Gas purity would be maintained by continuous purge of a small amount of impure gas from the helium side seal oil drain tanks.

Figure 3-145 is a diagram of the proposed seal oil system. The bearing oil supply system will serve as the primary seal oil supply. Both ac and dc motor driven pumps are provided to serve a back-up function only.

Water System

Water will be used to directly cool the armature winding parallel and lead connections and lead bushings. Water cooling technology is well established and may be applied directly. The water system diagram would be as shown in Figure 3-146. The water supply unit would have the usual dual centrifugal pumps, heat exchangers, main flow filters and demineralizers to ensure reliable continuity of service. Water purity and flow would be monitored with appropriate alarm and trip provisions as indicated.

3.3.3 Refrigeration System

In order for generators to operate in a superconducting mode, the windings of the generator must be cooled to cryogenic temperatures. In this application, the superconducting winding is designed to operate at or below the temperatures of liquid helium.

To date, liquid helium for cooling prototype superconducting generators has been supplied by the batch method. This approach is acceptable for experimental or short operating periods but is not practical for long term steady state generator operation. Reliable long term cryogenic refrigeration is essential to the development of a successful superconducting generator system. Therefore, Westinghouse engaged CTI-Cryogenics to develop a conceptual design for a complete refrigeration system to supply cryogenic cooling to their proposed superconducting generator.

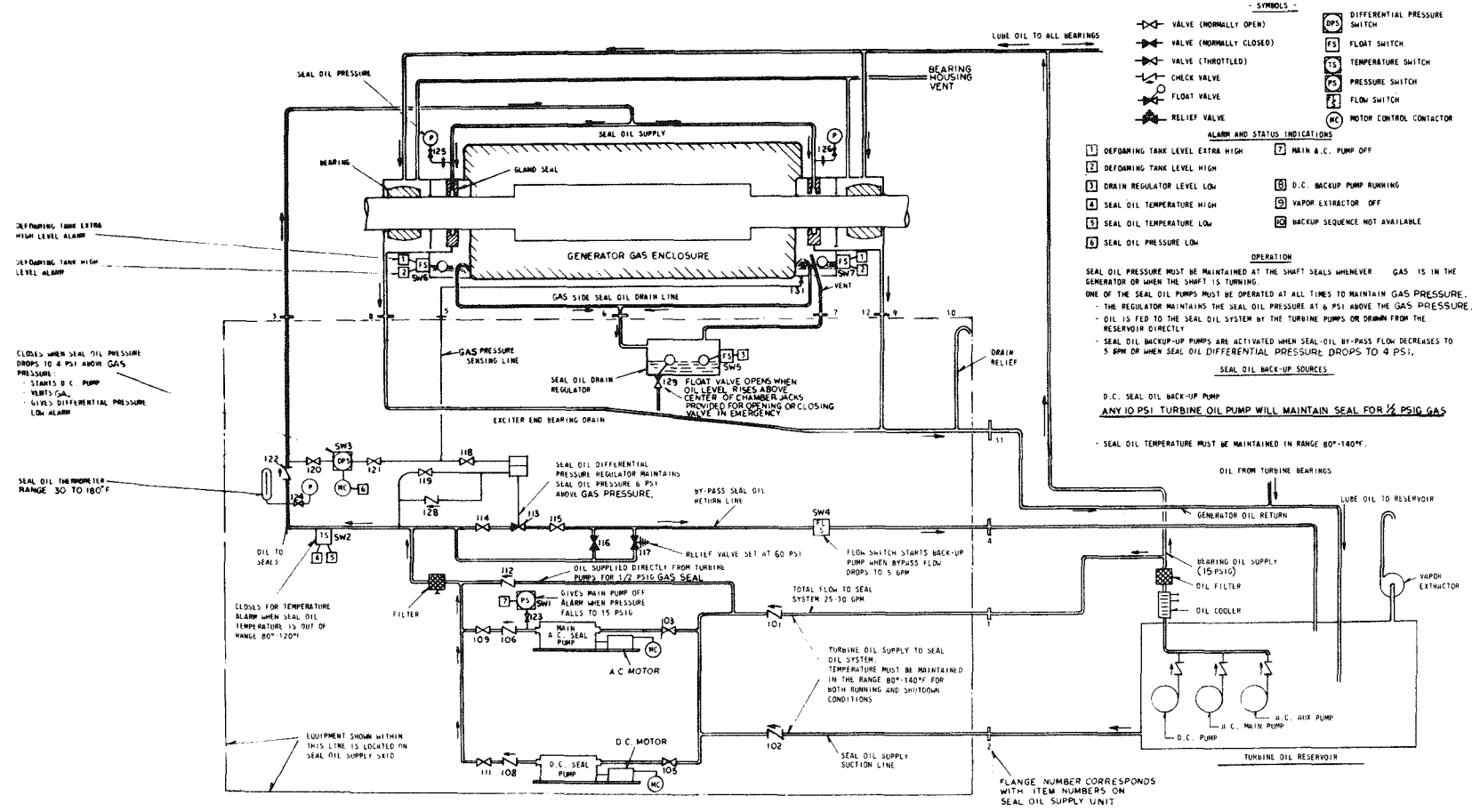

Figure 3-145. Diagram of Gland Seal Oil System

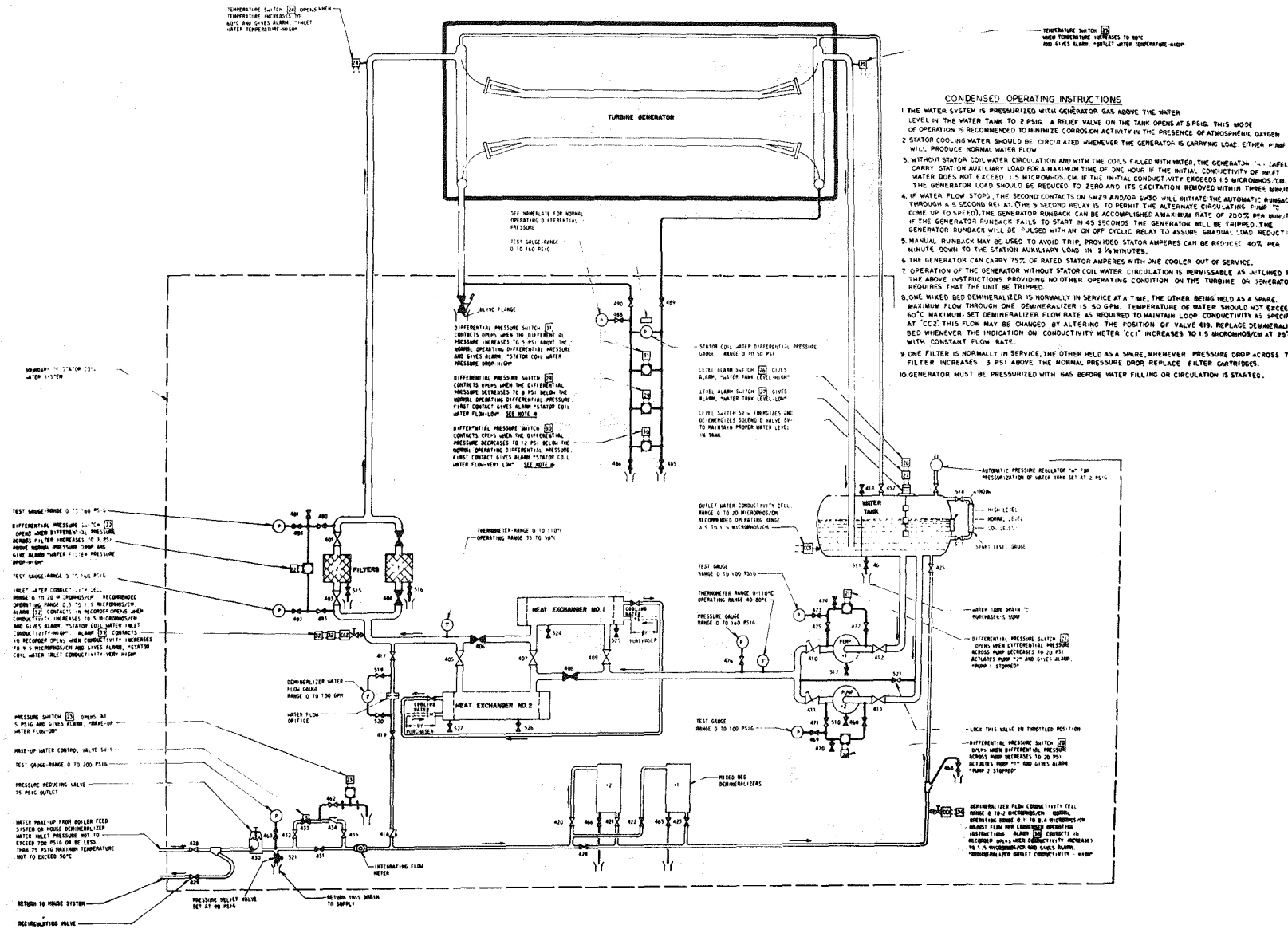

Figure 3-146. Diagram of Armature Cooling Water System

The technology of liquefying helium is well known at the present time. The purpose of this contract, therefore, was to develop a conceptual design of a complete refrigeration system capable of supplying practical and long-term cryogenic cooling to a superconducting generator.

Scope of Work

The tasks to be defined in the study were: system design, system description, key component identification, reliability, maintenance, and cost evaluation.

In the initial phase of this study, CTI-Cryogenics representative met with the Westinghouse representatives to review and define the process and operational requirements for the refrigeration system. They were:

- 300 MVA and 1200 MVA cooling requirements
- Unattended operation
- Planned maintenance interval
- Alternate source of cooling
- The grade of helium to be provided
-

The design study was divided into seven phases and has been reported in that manner:

- Compressor System
- Cold Box
- Instrumentation
- Storage Dewar and Liquid Control
- Reliability
- Maintenance
- Cost Estimate

System Design

Process and Operational Requirements

The process requirement of the refrigeration system as defined jointly by Westinghouse and CTI-Cryogenics is to deliver to the superconducting generator two phase helium at a temperature of 4.35K. For the 300 MVA generator, the flow requirement is 47 liters per hour. For the proposed 1200 MVA generator system the flow requirement is 79 liters per hour of helium at 4.35K. The two phase

helium flow in both cases is comprised of 95% liquid and the remaining flow as saturated gas. Included in the liquefaction rate requirement is a 50% safety margin, to allow for unpredictable losses and possible future changes in the superconducting generator cooling requirements.

As part of the refrigeration system requirements it was agreed that: (1) the system will operate automatically with unattended operation and (2) the equipment selected for the conceptual design shall be based upon the maximum reliability obtainable with an on-stream continuous operating period of approximately 3 years. Also agreed was that planned maintenance intervals would be scheduled yearly. However, the planned maintenance intervals must not interfere with the steady flow of 4.35K helium fluid to the generator over the three year period.

In the event of a power outage, the refrigeration system must be designed to supply liquid cooling to the generator from an alternate source. Additionally, the helium gas exiting from the generator, and the excess gas in the liquefier, resulting from equilization of the pressure levels within the liquefier will also be vented to the atmosphere.

It was also agreed that the use of liquid nitrogen precooling to increase the system efficiency, would add complexity and adversely affect system reliability, this approach was therefore ruled out.

Westinghouse also specified that the helium process gas supplied to the refrigeration system would be Grade E vaporized liquid helium. Therefore, no cryogenic charcoal adsorbers (purifiers) for removal of contaminants in the gas, have been included in the refrigerator. However, it may be necessary initially to provide an external cryogenic charcoal adsorber in the exit stream of the generator to remove any contamination introduced in the system from the generator electrical windings.

Thermodynamic Process Cycle

Figures 3-147 and 3-148 depict the proposed thermodynamic process cycle for the refrigerator for the 300 MVA generator and the proposed 1200 MVA generator. These cycles have been developed based upon the specific refrigeration requirements for each generator and without the use of liquid nitrogen precooling.

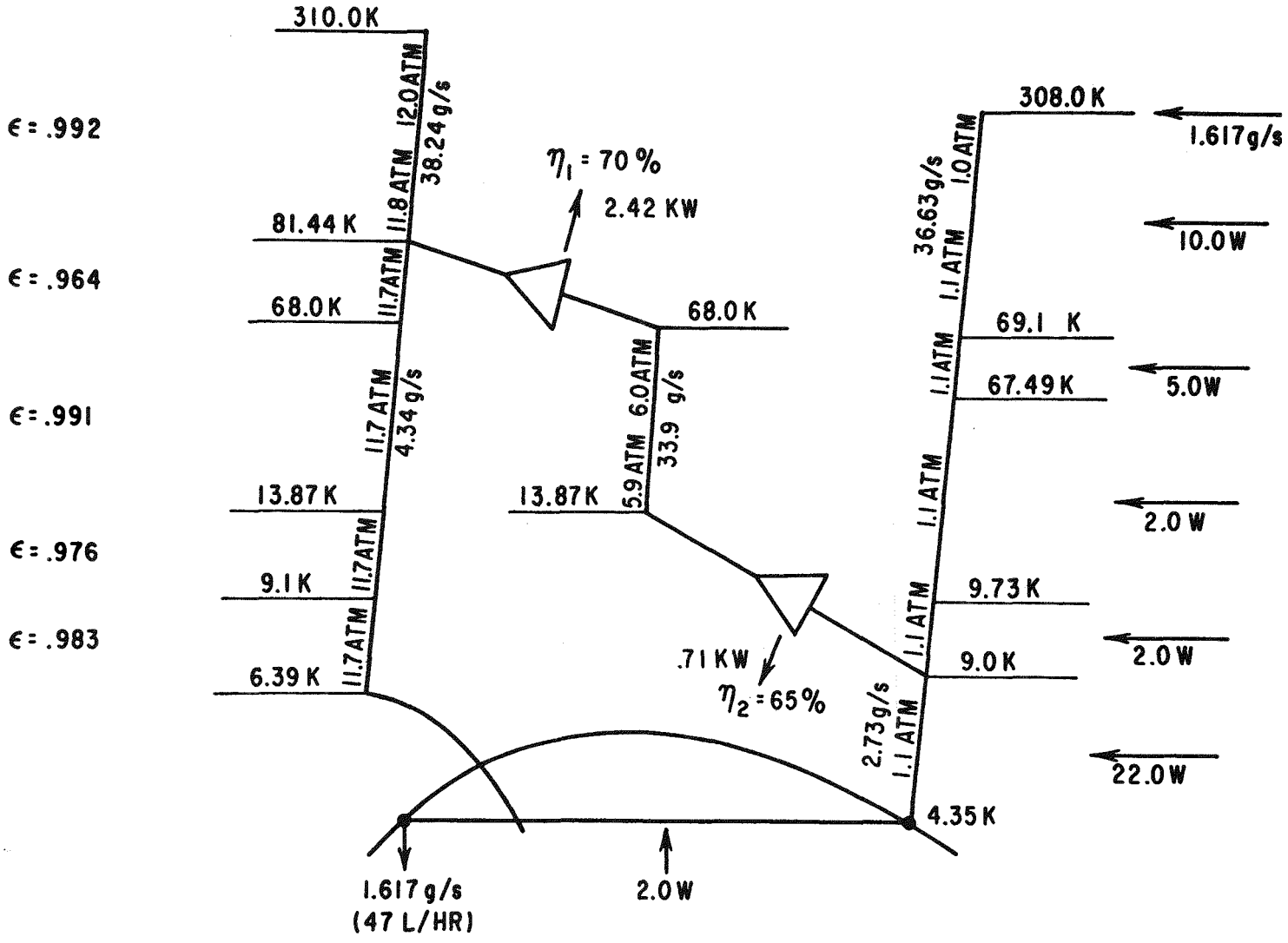

Figure 3-147. Thermodynamic Process Cycle for 300 MVA Generator

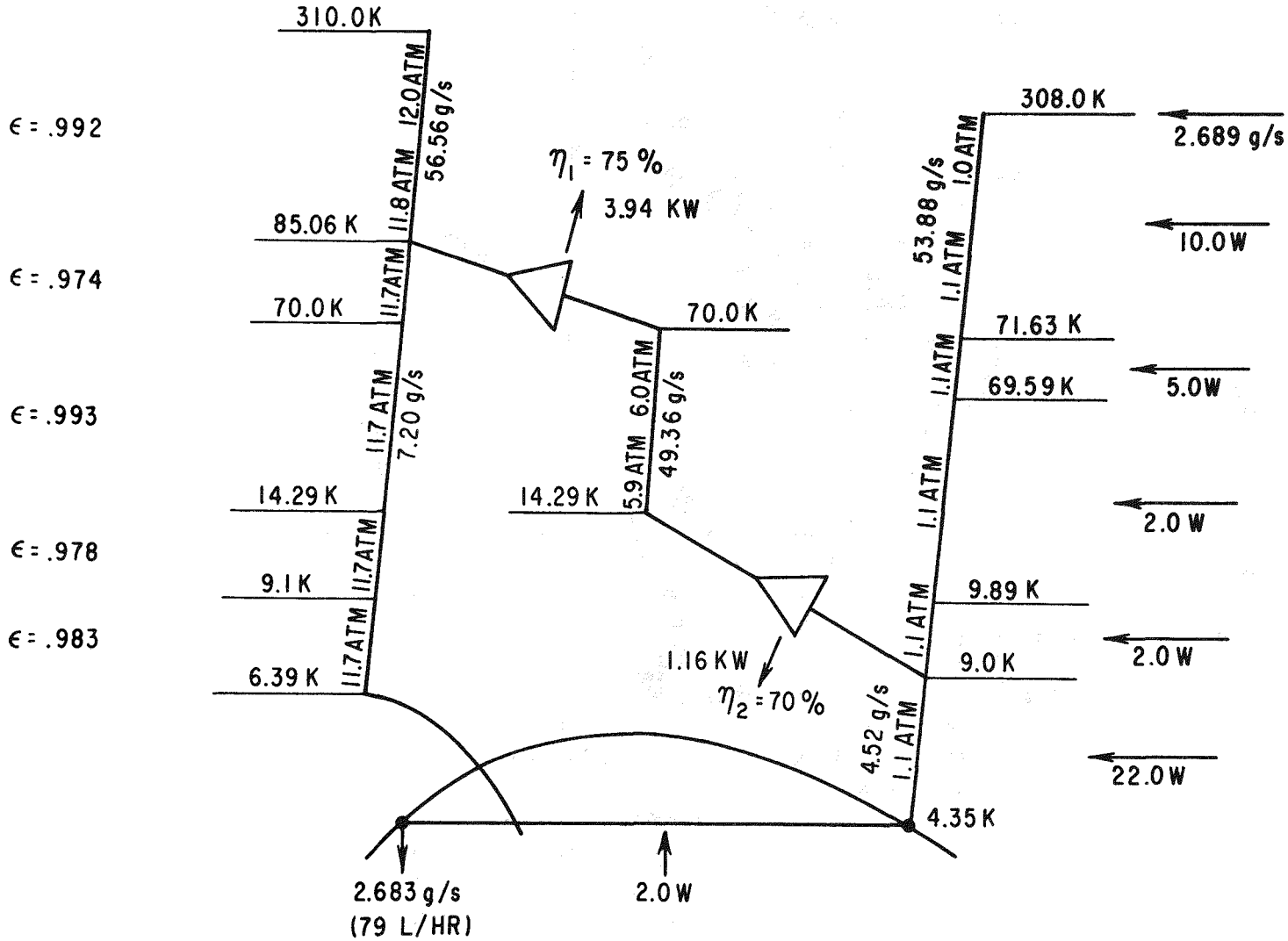

Figure 3-148. Thermodynamic Process Cycle for 1200 MVA Generator.

Both cycles are similar in concept i.e., two expanders, heat exchangers operating at the same pressure level and a single Joule Thomson valve. The basic differences between the two cycles are the turbine efficiencies and slight temperature differences in the heat exchanger. These variations are due to the fact that as the refrigeration requirements (liquefaction rate) increase, the mass flow through the turbines is also increased, resulting in a higher turbine efficiency. The efficiency in turn causes the heat exchangers to operate at slightly different temperatures.

These cycles were developed using CTI-Cryogenic's computer program. This approach enabled us to evaluate the optimum pressure level, the inlet temperature to the turbines, the temperature differences of the heat exchangers, and the inlet temperature to the Joule Thomson valve. Each of these parameters were investigated for the optimum condition.

Realistic heat losses to the system were included including the 2.0 watts required to provide 5% gas in the process stream to the generator. Heat exchanger efficiencies were then calculated to ascertain that the heat exchanger requirements were within the present state of the art.

The carnot efficiency of the cycle has been calculated to be 9.81%. The efficiency of the cycle could be increased by opting to use more expanders or by retaining the same number of expanders and selecting expanders which are more efficient. Reciprocating expanders are more efficient than turbo expanders in cycles requiring a low mass flow through the expander to develop the required refrigeration. Rotary turbine expanders are intrinsically more reliable than reciprocating expanders. Therefore in our opinion it is more prudent to sacrifice carnot efficiency, lower expander efficiency, than to compromise on system reliability.

System Description

Refrigeration System

Figure 3-149 illustrates in schematic form the key components of the refrigeration system. They consist of a two-stage compressor, with redundancy, an oil removal system, with redundancy, the cold box which houses the heat exchangers and turbines, the 12 meter transfer lines to and from the helium storage dewar, and the lines to and from the phase separator which are close

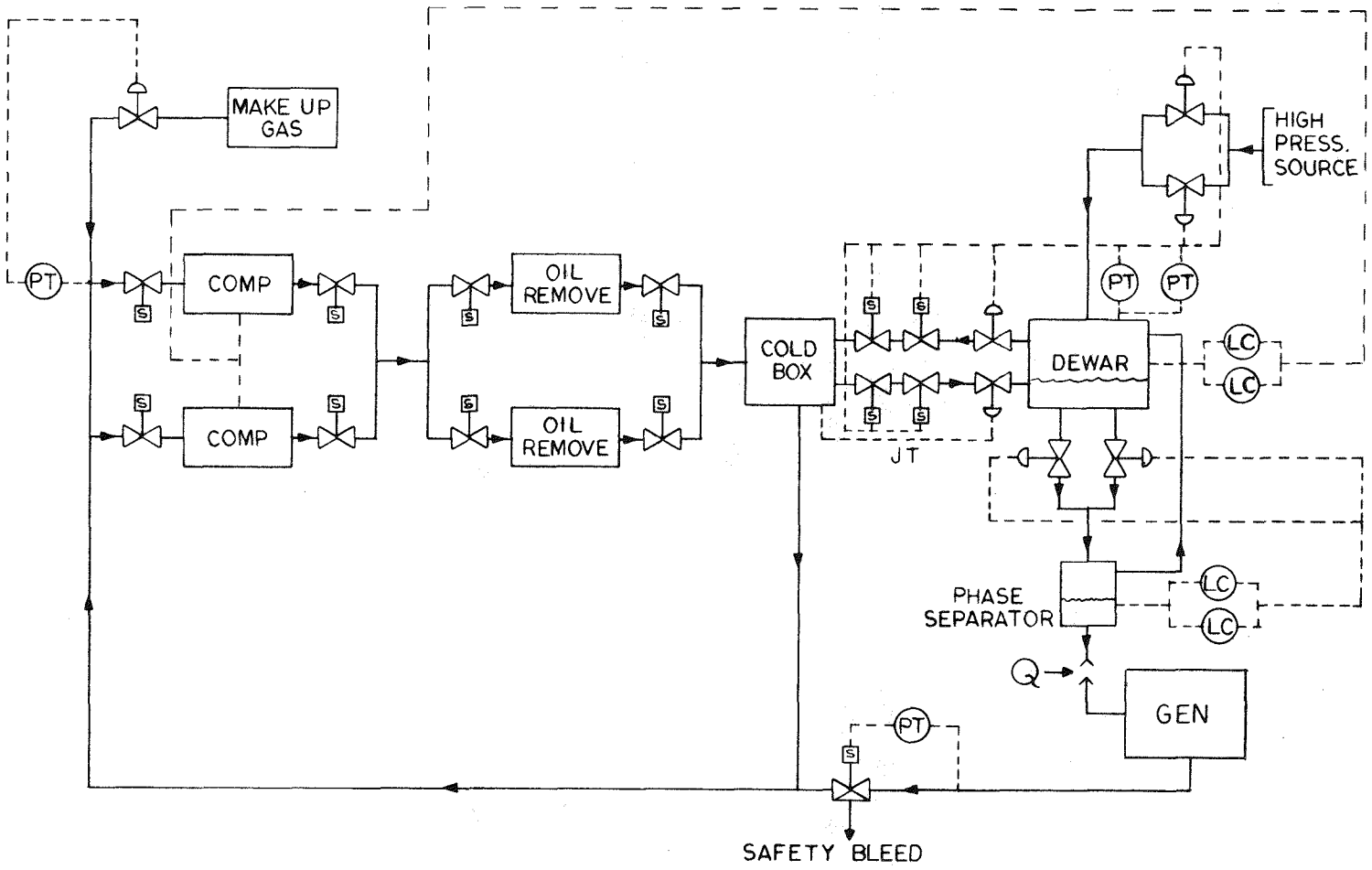

Figure 3-149. Refrigeration System Block Diagram.

coupled to the generator. In addition, the Figure shows the helium make-up gas requirement, the pressure gas requirement for the storage dewar and the return line from the generator to the suction side of the compressor.

Also represented in the system block diagram (Figure 3-149) are the isolation valves, with redundancy, the Joule Thomson valve, the dewar pressure regulating valve, the redundant liquid flow control valve to the phase separator and their appropriate controllers.

Briefly, helium gas introduced into the system from the make-up supply is compressed in a two-stage, oil-lubricated rotary compressor from 1 atmosphere to 12.5 atmospheres. The gas then passes through the oil removal system to the cold box where it is cooled by heat exchange with the returning gas. The inlet gas passes through the first section of the exchanger where a portion is directed to the expansion turbine and a portion to the Joule Thomson valve. The gas entering the turbine is expanded in two expansion turbines to 1 atmosphere and returned to the compressor to cool the incoming gas. The portion of gas directed towards the Joule Thomson valve previously cooled by the return stream, then passes through the transfer lines to the Joule Thomson valve where partial condensation takes place. The two phase flow then enters the storage dewar where the liquid is separated by gravity. The remaining gas returns to the heat exchanger via the return transfer line.

Liquid helium then flows from the storage dewar through a control valve to the phase separator and generator. The level controller in the phase separator maintains a constant level, thereby maintaining a steady flow of helium to the generator. The vaporized liquid helium flows through the various passages within the generator and exits at approximately 300K where it then returns to the compressor.

Compressor System

Figure 3-150 shows in schematic form the key components of the compressor system. A complete and detailed schematic diagram of the compressor flow system is shown in Figures 3-151A and 3-151B.

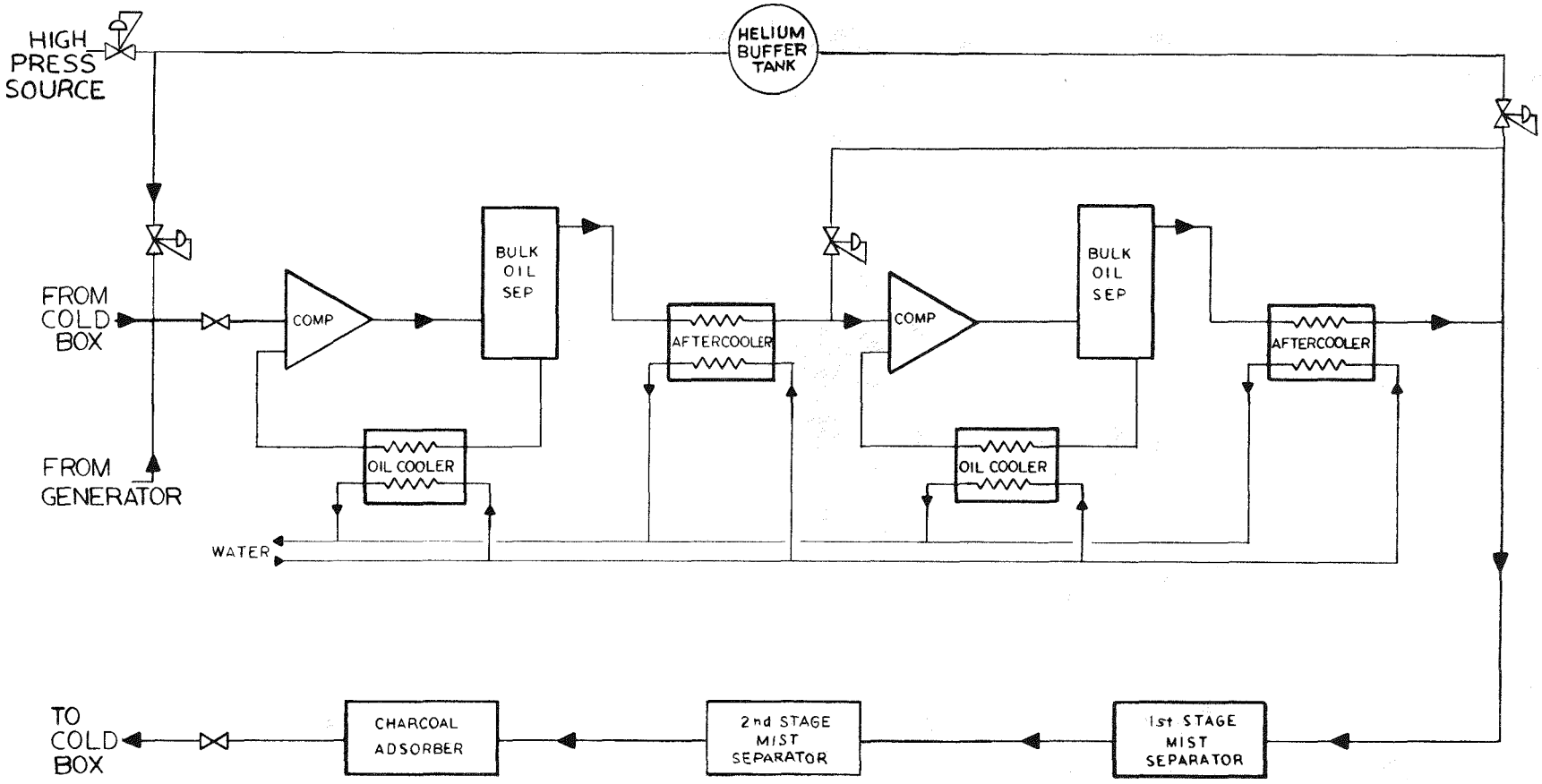

Figure 3-150. Compressor System Block Diagram.

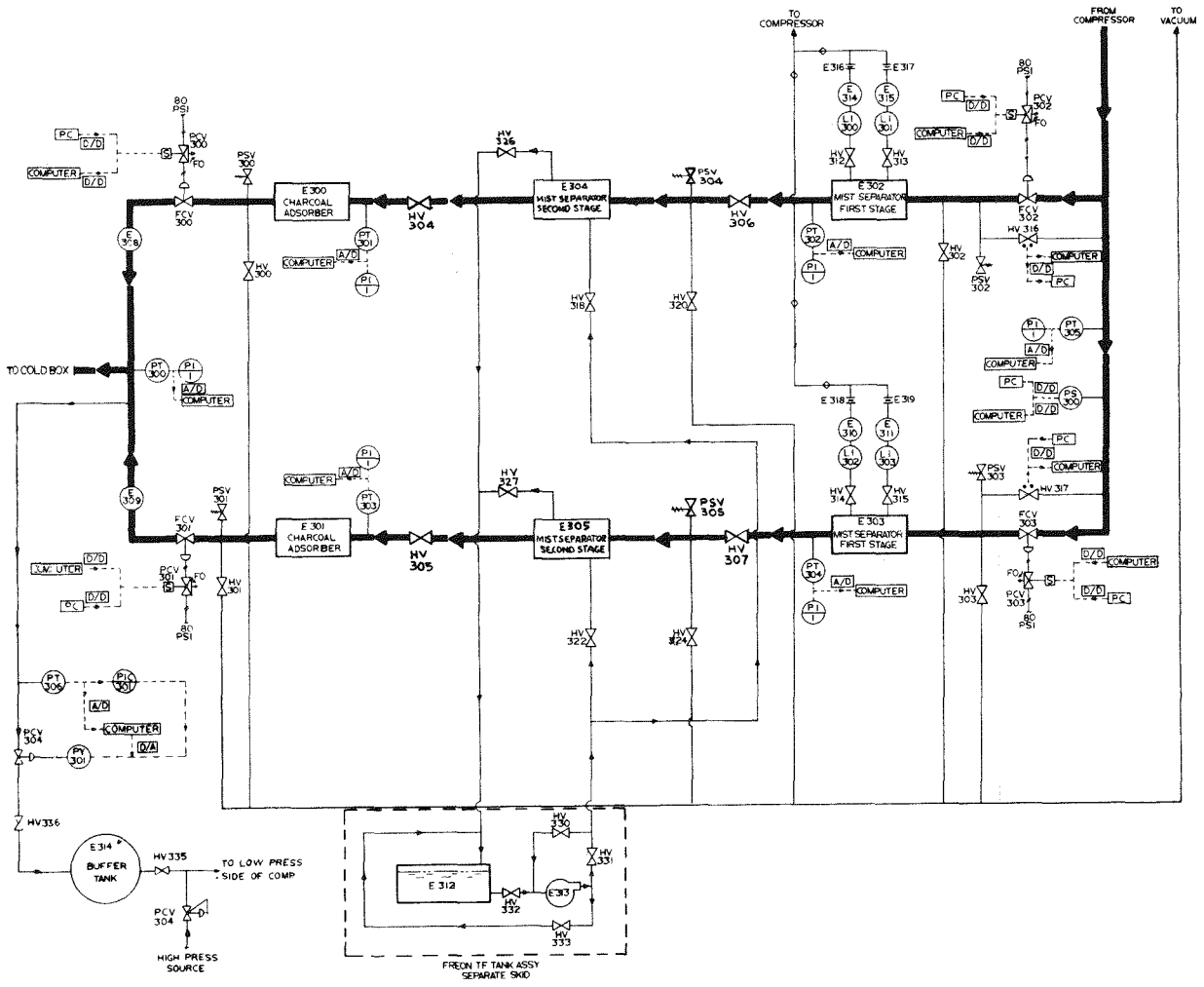

Figure 151A. Compressor Flow Diagram

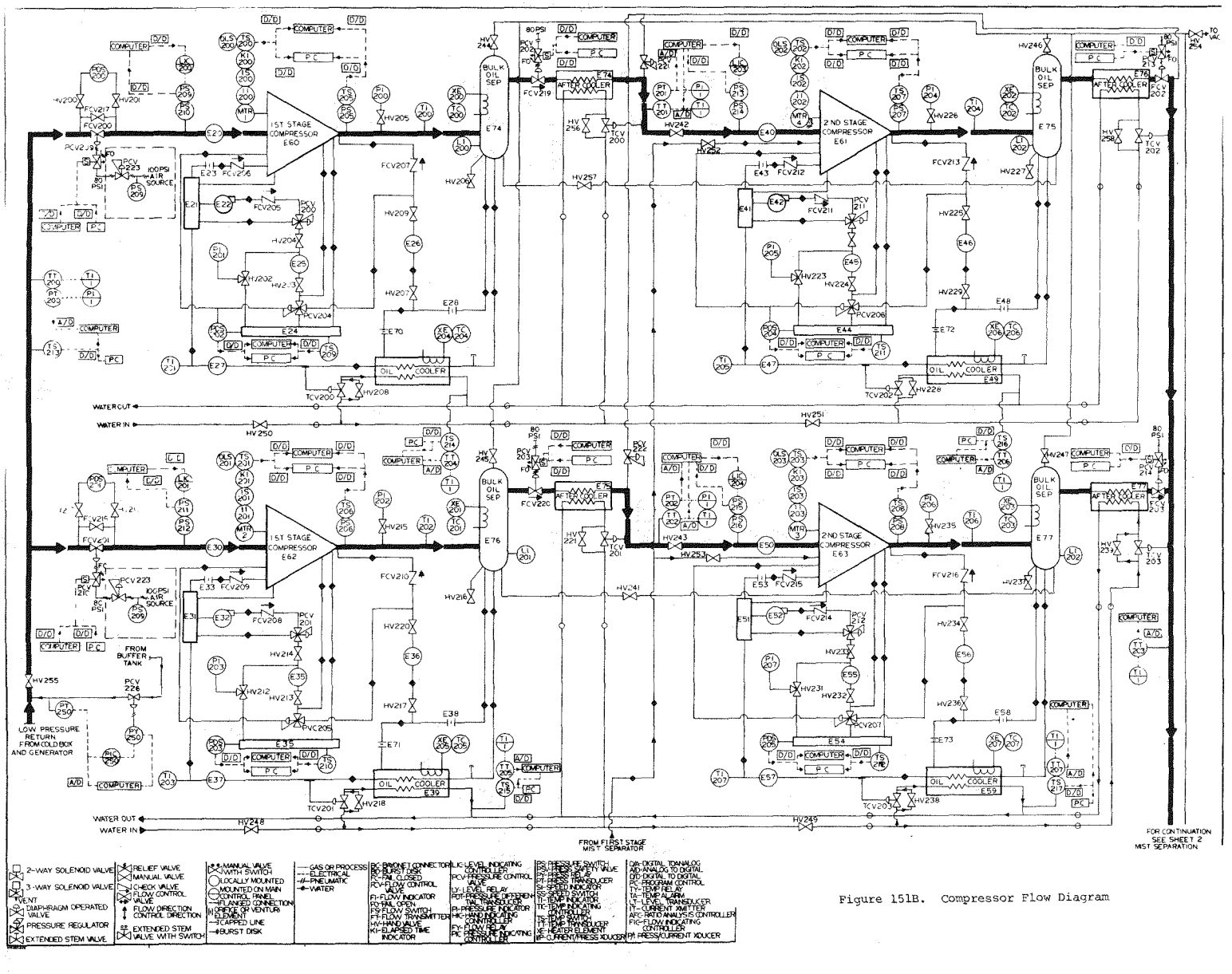

Figure 151B. Compressor Flow Diagram

Figure 3-150 does not show the redundant compressor and oil removal systems. The compressor system consists of two oil-lubricated and oil cooled rotating screw compressors each having a bulk oil separator and after-cooling at their respective discharge. Each compressor has an oil cooler to cool the oil separated in the bulk oil separator before it returns to the suction side of the compressor.

In describing the helium compression and oil injection in the compressor system the 300 MVA generator cooling requirement will be described. The concept for the 1200 MVA system will be identical; only the flow rates, gas, oil and water, and the power requirement will vary.

Helium gas, 38.2 g/s, at 306K and 1 atm enters the suction side of the first stage compressor and is compressed to 3.5 atm. In order to minimize the discharge temperature of the helium gas, and to provide cooling and sealing for the screw compressor rotor, oil is injected into the compressor. The work required to compress the gas and oil to the 3.5 atm level is 55.4 kW with an adiabatic compression efficiency of 70%.

The gas and oil then flows to the bulk oil separator where the velocity of the gas is reduced sufficiently to enable the bulk of the oil to settle out by gravity and to be returned via the oil cooler to the suction side of the compressor.

Before entering the second stage compressor, the helium gas is directed to the intercooler where its temperature is lowered from 361K to 310K.

In the second stage compressor, the helium gas is compressed to 12.5 atm. The work required to compress the oil and gas in the second stage is 56.5 kW with an adiabatic compression efficiency of 70%. After the bulk oil contained in the helium gas stream has been separated and returned to the compressor, the heat of compression is removed in the water-cooled aftercooler; the gas then flows to the first stage mist separator at 310K.

The water requirement for the inter and after coolers is 30 liters/min at a maximum temperature of 302K. The water requirement for the oil cooler is 115 liter/min.

The compressed helium gas containing oil particles is next directed to the three stages of oil removal. In the first and second stage mist separators, agglomeration and coalescing of the oil particles into a size that can be separated by gravity occurs. The oil that is separated in these two stages is returned to the suction side of the first stage compressor. These staged separators are capable of reducing the oil contamination level in the helium stream to 0.1 to 1.0 ppm by weight.

The third and final stage of separation occurs in the charcoal adsorber where the oil vapor contained in the helium gas stream is removed by adsorbtion.

The compressed helium gas, with the heat of compression removed and properly purified, is now acceptable for entry into the cryogenic cold box.

In order to provide a safety margin in the compressor flow rate, we have selected compressors which have the capability of delivering 52.6 g/s instead of the 38.2 g/s specified in the design.

Included as part of the compressor system are the high pressure and low pressure regulating valves controlling the suction and discharge pressure of the compressor system. A compressor bypass valve is also included for start-up and shut down purposes. Each compressor is equipped with a slide valve capable of adjusting the mass flow through the compressor.

Cold Box System

The cold box for the refrigeration system consists of a carbon steel vacuum vessel in which the heat exchangers, turbines, bypass valves and instrumentation are housed. All of these components are insulated by a high vacuum of 10^{-6} Torr by multilayer super insulation.

Figure 3-152 shows in block diagram form the key components located within the cold box. A more detailed flow diagram of each component within the cold box is shown on Figure 3-153.

In describing the cold box, for clarity reasons only, the 300 MVA refrigeration cycle (refer to Figures 3-147 and 3-152) will be described. Once the 300 MVA cycle is understood, the 1200 MVA cycle paralleling the preceeding description will become obvious.

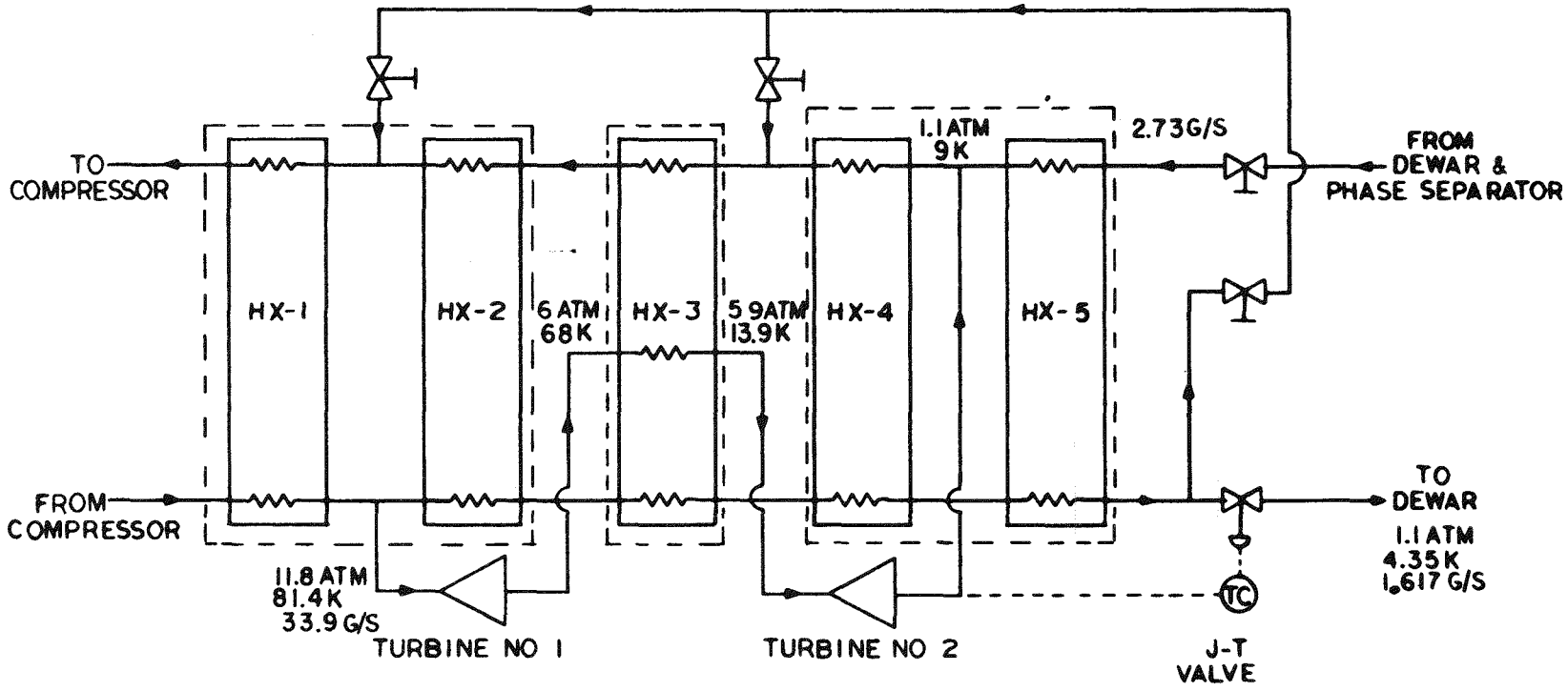

Figure 3-152. Cold Box Block Diagram.

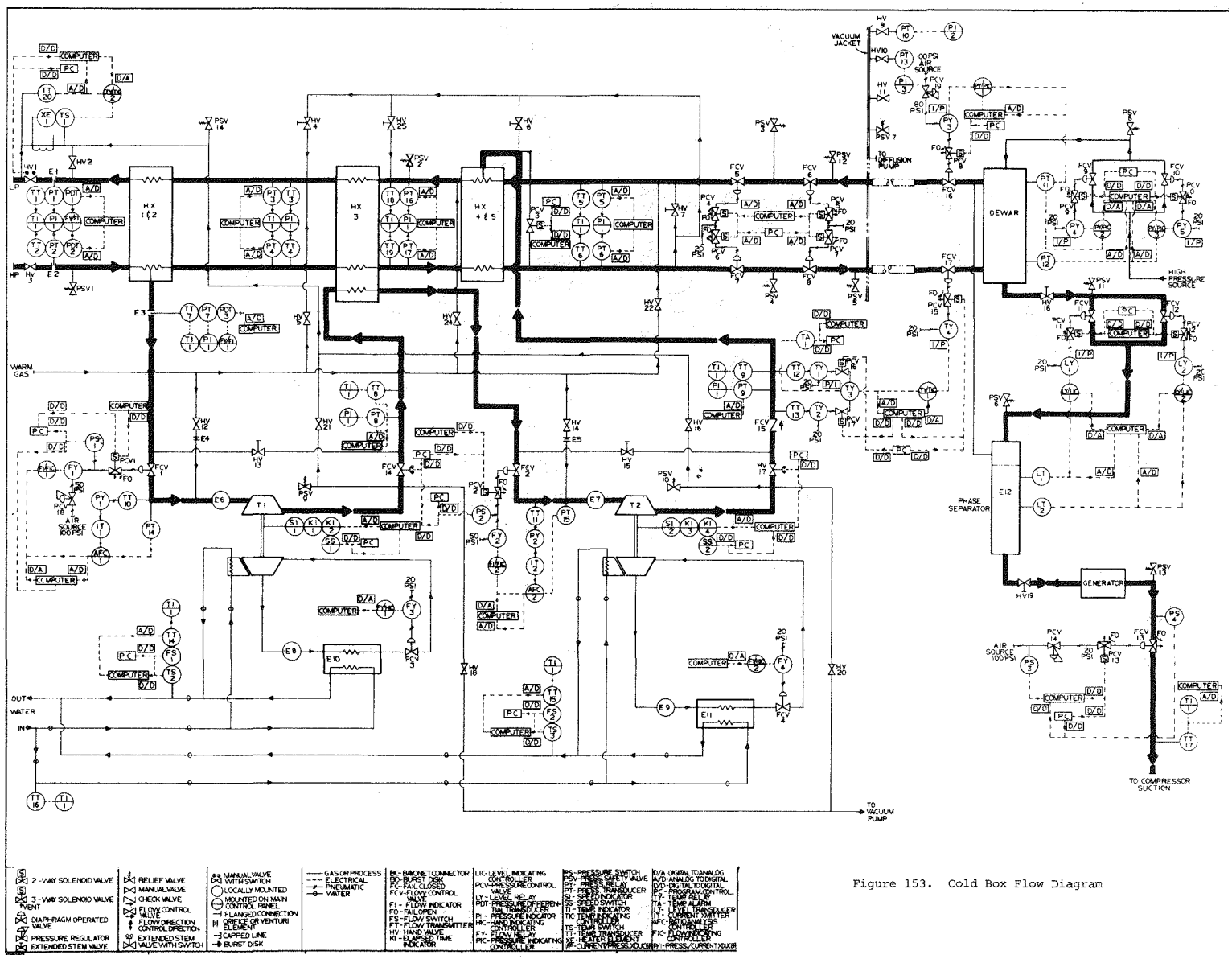

Figure 153. Cold Box Flow Diagram

As stated previously compressed helium gas at a pressure of 12.0 atm and 310K enters the first exchanger identified as HX1 where the gas is cooled to 81.4K. At this point 33.9 g/s of the gas is directed to the upper turbine and 4.3 g/s is directed to the Joule Thomson valve. The 33.9 g/s stream is expanded from 11.8 atm to 6.0 atm in the upper turbine to a temperature of 68K. The energy extracted from the gas via the water cooled brake circuit heat exchanger, described in the turbine section, is shown to be 2.42 kW. The helium gas is expanded isentropically at an efficiency of 70% in a Sulzer gas bearing turbine. Gas bearing turbines are used in this application instead of oil bearing turbines because of the small size of turbine required.

The portion of gas, 4.3 g/s, directed to the Joule Thomson valve enters heat exchanger HX2 and is cooled from 81.4K to 68.0K by the return low pressure stream in heat exchanger HX2.

The gas expanding from the upper turbine at 68K then flows through a three pass exchanger identified as HX3 to the inlet of the lower turbine at a temperature of 13.9K. The 6.0 atm stream was cooled to 13.9K by the low pressure return stream.

As the gas enters the lower turbine it is expanded from 5.9 atm to 1.1 atm and to a temperature of 9.0K. As before, the gas expands isentropically at an efficiency of 65% and 0.71 kW of energy has been extracted from the helium process stream.

After leaving heat exchanger HX2 the Joule Thomson directed stream, 4.3 g/s, is cooled in exchangers HX3, HX4 and HX5 to a temperature of 6.4K. At this point the helium gas enters the Joule Thomson valve and expands from 11.7 atm to 1.1 atm where partial condensation takes place. The liquid portion of this stream is deposited in the storage dewar and the vapor portion is returned to the heat exchanger at 4.3K, mixed with the gas exhausted from the lower turbine at 9K and returned to the compressor at 308K.

As shown in Figure 3-152, the Joule Thomson valve is controlled by the exhaust temperature of the lower turbine. If the temperature of the gas exhausting from the lower turbine is below the prescribed operating temperature, it indicates that the Joule Thomson valve is not allowing enough gas to pass through heat exchanger HX5 and the valve is opened accordingly. Conversely,

if the exhaust temperature is too warm, the valve is open too far passing too much and will be modulated closed until the prescribed temperature set point has been reached.

By-pass valves are located within the cold box to by-pass sections of heat exchanger's during cool down to decrease the time to cool down the refrigerator. The heat exchangers piping and valves located in the cold box have been designed to accommodate the increased flow from the redundant compressor during cool down. This will also decrease the time to cool down the refrigerator.

Liquid Helium Control System

The liquid helium control system, reference Figure 3-149, for controlling the flow of helium to the generator consists of a set of 12 meter transfer lines, a 1000 liter helium storage dewar, a helium flow control valve, with redundancy and a 50 liter volume phase separator.

In the present configuration it is assumed that the cold box is located approximately 12 meters away from the helium storage dewar which will be mounted at approximately the same elevation as the superconducting generator. At the end of each of these transfer lines will be three valves; two shut off or block valves and one regulating valve. Regulating valves are positioned at the end of the line for Joule Thomson expansion and control of the dewar pressure.

The block valve with its accompanying redundancy is used to isolate the storage dewar from the cold box in the event unpredictable maintenance or power outage occurs. Should either of these conditions occur, both block valve and the high pressure source regulating valve will close. The accompanying redundant valve, will open and maintain a constant pressure in the helium storage dewar as the liquid level drops in the dewar. The redundant high pressure source control valve will open only if the other valve is not controlling the dewar pressure. In that case, the normal operating valve will be shut off and signaled for repair.

It is anticipated that the transfer lines between the storage dewar and the phase separator are short; any liquid vaporized will be redirected back to the storage dewar. The flow of liquid from the dewar to the phase separator is controlled by the liquid level in the separator. If the demand for liquid

cooling to the generator is increased or decreased, the liquid level in the separator will sense this change and adjust the flow control accordingly. This is a key control point in the system, therefore redundancy has been included.

To provide a system with automatic refrigeration, redundant liquid level controls are installed in the storage dewar to maintain the level in the dewar. If the level in the dewar falls below the prescribed set point, it indicates the cooling requirement has increased and therefore additional refrigeration is required. The signal from the level control will thereby actuate the slide valve on the first stage compressor. The total system mass flow will not increase and develop more refrigeration. Conversely, if the level increases the slide valve of the compressor will open reducing the system mass flow.

Instrumentation and Process Control System

Control of the process system is accomplished by a computer located on the main control panel in the control room. Control information and commands are exchanged between the compressor, the cold box and the liquid helium control system located at the generator, and the main control panel.

Figure 3-154 illustrates the process control system block diagram, the figure represents the transmission of data to and from the various subsystems to the process computer. The control instrumentation located at the control panel has been selected to ensure complete data acquisition, safety monitoring and control over the entire process. Each type of process task has been designed for computer control as well as manual operator control.

The transmission of data from the various sub-systems to the computer is divided into four groups. The first group is the electrical analog inputs to the main control panel. This group includes all of the temperatures, pressures, and valve position transmitters which are relaying variable process information to the control panel for data logging, malfunction annunciation or process control.

The second group includes electrical analog output data from the control panel to the control valves based upon the analog inputs from the first group.

The third group includes digital input from the various sub-systems to the control panel. This group includes the pressure and temperature switches and relay contact information that is digital in nature, i.e., on or off.

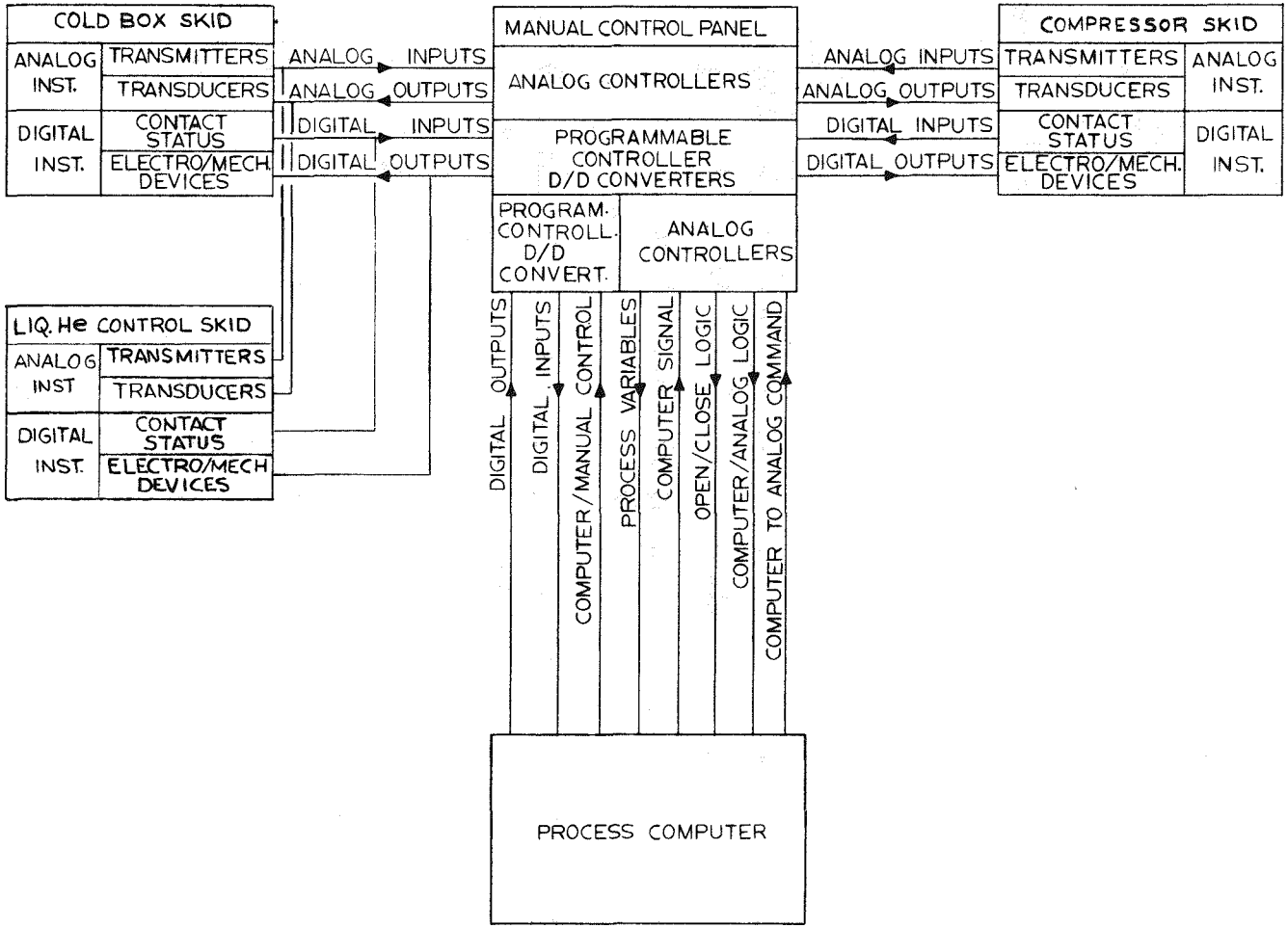

Figure 3-154. Process Control System Block Diagram.

The fourth group includes the digital output from the control panel to the various sub-systems. These signals include the on/off commands to electro-mechanical solenoids, contactors and relays.

All four groups of transmission have been designed for computer and manual interface, low signal attenuation for long distances, and for universally accepted design approach.

The control panel is designed to monitor and operate the process by either computer command or manual operation supervision. Key control point for system operation are equipped with redundancy to maintain process control at all times. Transfer of the computer to manual operation will be accomplished by operator command. If the computer cannot control the process within the prescribed control points an alarm will sound giving the operator warning of a pending control problem.

Key Component Identification

Compressor Discussion

Compressors are important components in cryogenic process equipment, in particular for helium refrigeration or liquefaction systems. The type of compressors used for helium service are: (1) reciprocating compressors with teflon rings, oil-lubricated metal rings, or labyrinth pistons, and (2) regenerative compressors and screw compressors utilizing either hermetic or open drive. In the past, the reliability of the compressor determined the maximum reliability of the entire helium refrigeration system. However, the application of rotary screw compressors has improved the reliability characteristics of the entire refrigeration system.

Oil lubricated screw compressors may be separated into two categories: semi-hermetic and open drive. The motor in the semi-hermetic compressor is located in the same housing as the compressor and is cooled by oil. The disadvantage of using hermetic compressors is that they are only available with 480 volt motors and have a size limitation of 600 HP at the present time.

The open drive compressor on the other hand has a motor and a shaft seal located external to the compressor housing.

The advantage of using an open drive compressor is in the ability to select higher voltage motors and motors having horsepower ratings greater than 600.

Within the last ten years, these compressors have been applied to compressing refrigerants in commercial air conditioning systems competing with reciprocating compressors. During their use in commercial applications the screw compressors have consistently demonstrated and have established good seal life characteristics.

Both types of oil-lubricated screw compressors require oil injection for effective sealing and rotor cooling. With oil injection, the clearance between the rotors is reduced resulting in improved volumetric and adiabatic efficiencies.

The compressor system we are proposing consists of two oil-lubricated screw compressors with an efficient oil removal system capable of removing all but trace quantities of oil from the process system i.e., less than 0.1 ppm by weight. The oil-lubricated screw compressor was selected because we feel it has the highest reliability of all compressors at the present time. Although the isentropic efficiency and volumetric efficiency of the screw compressors is not as high as some reciprocating compressors, the reliability of the screw compressor clearly out weighs the slight sacrifice in effieiency.

The compressors selected for the 300 MVA design are equipped with 150 HP motors.

Screw Compressor Operation

The screw gas compressor consists of two intermeshing helical rotors; a male helix or lobe, and a female helix or flute. The rotors are fitted into a housing provided with gas inlet and discharge ports and means for driving one of the rotors. There are no valves.

The screw compression process may be divided into three phases (suction, compression, and discharge) and is described as follows:

In the suction phase a volume of gas is introduced into and trapped in the interlobe space at the operating suction pressure. During the compression phase, the gas trapped in the interlobe space is carried circumferentially

around the compressor housing. As the male rotor is revolved, the volume occupied by the trapped gas within the interlobe space is decreased, thereby increasing gas pressure. For the discharge phase of the compression process the discharge port is uncovered, the compressed gas is thereby forced into the discharge plenum by the advancing rotor mesh.

The screw compressor also contains a slide valve for capacity control. When the compressor is fully loaded, the slide valve is in the closed position, and all of the gas in the screw compressor is compressed in the manner described above. The opening of the slide valve creates a port in the bottom of the rotor housing to the inlet port. The compression process is then delayed until the trapped interlobed space moves beyond the slide valve opening. The opening of the slide valve reduces the effective compressor displacement thereby by-passing a portion of the trapped inducted gas before appreciable compression has taken place. Since no significant amount of work is done on this return gas, there are no appreciable losses incurred for reduced compressor capacity.

Figure 3-155 illustrates an outline of the compressor system including the redundant system. Although the figure does not reflect the complete system i.e., piping and valves, its intent is to show the approximate location of major components, outline pertinent dimensions and to give the weight of the system.

The various valves, pipes, oil and water coolers used in conjunction with the compressor are standard off-the-shelf items and will be completely defined during the design phase of the program.

The oil-removal system for separating the injected oil from the helium gas stream will be similar to units which CTI-CRYOGENICS has designed for other systems. The concept of this system has been successfully utilized in hundreds of oil injected compressors by CTI-CRYOGENICS.

Cold Box Discussion

The cold box assembly consists of: a vacuum shell known as the cold box; aluminum plate fin heat exchangers; gas bearing turbines; welded piping and valves; instrumentation and a suitable vacuum insulation to minimize the heat leak from the warm environment.

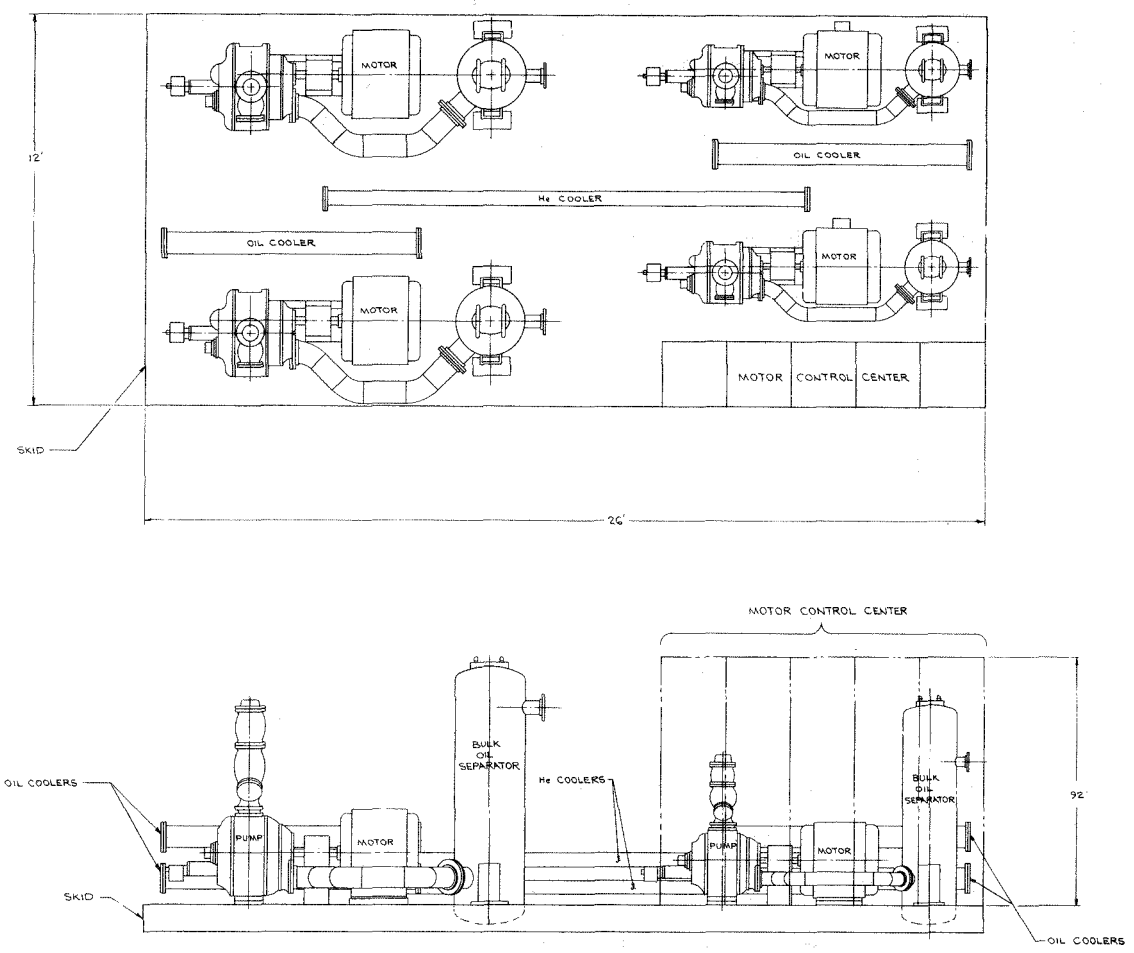

WT. 60,000 LB.

Figure 3-155. Compressor System.

The cold box as presently conceived (reference Figure 3-156), will be constructed of carbon steel and will enclose the heat exchanger assembly components; it will be approximately 1.8 meters in diameter and 4.7 meters long. Accessibility to the cold box interior is possible by removing one or both of the two flanged ends of the cold box, which are sealed by O-rings. The cold box has a flange for the installation of vacuum pumping equipment. It is also equipped with a relief valve to prevent an internal pressure greater than 0.35 Kg/cm^2 from developing within the cold box, in the event of a line failure.

Heat Exchanger

The heat exchanger like the compressor and expander is a key component in any refrigeration or liquefaction system. Unlike the compressor and the expander, the heat exchanger is a passive component as its performance does not change with time unless it is subjected to contamination. The technology of designing and manufacturing heat exchanger is well understood and available in many forms i.e., plate finned heat exchangers, fin tube heat exchanger, pin finned heat exchangers and regenerative type heat exchangers. The type we have selected for this application is the aluminum plate fin exchanger. These exchangers are available from several manufacturers.

Our reasons for selecting these heat exchangers are: (1) demonstrated performance and leak tightness, (2) ability to accept higher levels of contamination without degradation in performance, and (3) ability to specify smaller heat exchanger temperature pinches which are not as easily obtained in the finned tube type exchanger. One of the disadvantages of this type of exchanger is its length. In order to keep the end to end heat loss to a minimum on an aluminum exchanger, its length must be appreciable longer than the coiled fin tube exchanger which is mounted on a stainless steel mandrel. Both types of exchangers have exhibited good performance with respect to leak tightness even though the aluminum exchanger has extensive brazed joints. Satisfactory manufacturing is accomplished by furnace brazing the entire assembly in one operation.

The pin finned and regenerative type exchangers are typically used in smaller applications and were not considered for this design.

Heat Exchanger Assembly

The heat exchanger will consist of three brazed aluminum heat exchanger cores. Each core will consist of a number of passages of plate type serrated fins. The core material will be type 3003, aluminum alloy.

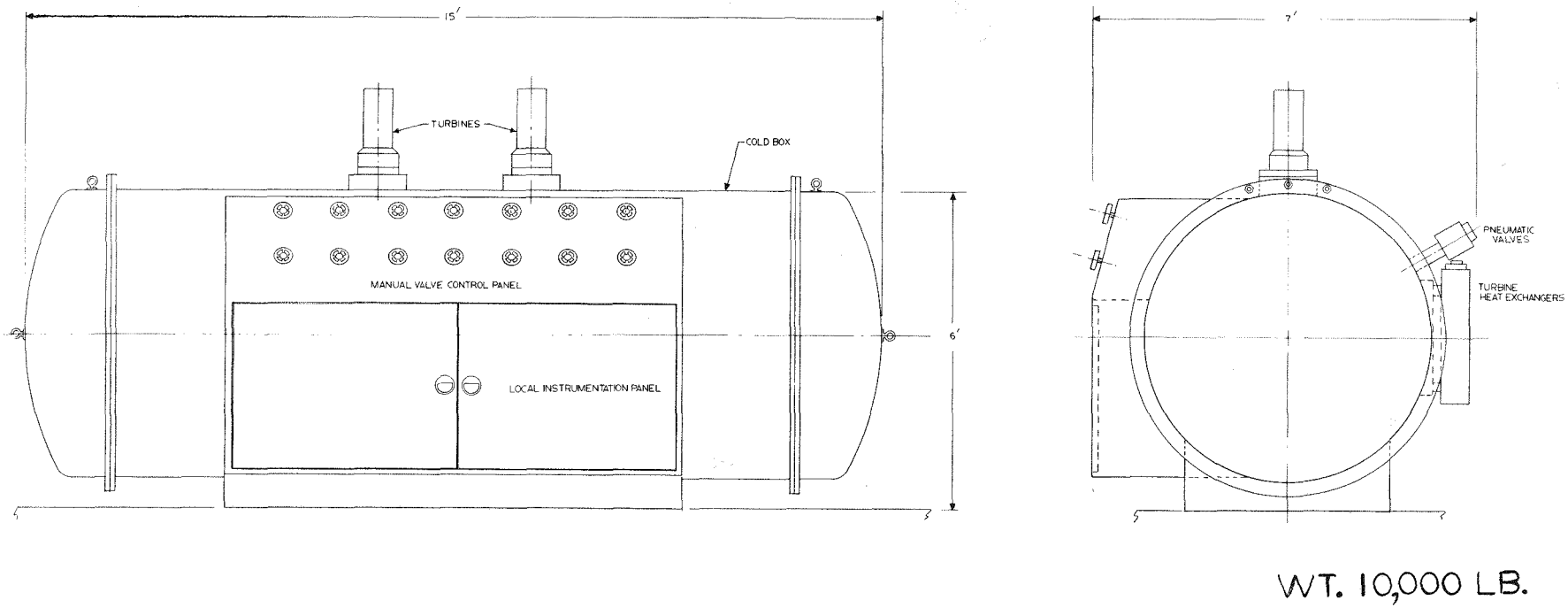

Figure 3-156. Cold Box.

First Heat Exchanger (HX1 and HX2)

The first section of the heat exchanger, HX1 and 2 (see Figure 3-152) consists of a core 30.48 cm wide by 22.86 cm deep, by 3.05 meters long. This section of heat exchanger cools the incoming high pressure helium stream from 310K to 68K. Located approximately at the 81K temperature level, is a connection to enable a portion of the high pressure helium stream to be directed to the upper turbine. The low pressure returning gas enters this exchanger at 67K and is warmed up to a temperature of 308K before leaving the cold box.

Second Heat Exchanger (HX3)

The second heat exchanger identified as HX3, is a counterflow helium heat exchanger which cools the incoming helium from 68K down to 13.9K. This section of the heat exchanger is similar in construction to the first exchanger except that the heat exchanger has three passes. The middle pass of this heat exchanger operates at 6.0 atmospheres and is located between the exhaust end of the upper turbine and the inlet end of the lower turbine. The low pressure gas return stream cools this stream as well as the high pressure stream from 68K to 13.9K.

The low pressure returning gas enters this exchanger at 9.7K and is warmed up to 67.5K in cooling the high and medium pressure streams.

Third Heat Exchanger (HX4 and HX5)

The third exchanger identified as HX4 and HX5 is again a counterflow helium heat exchanger in which the incoming helium is cooled from 13.9K to 6.4K by the return low pressure stream entering at 4.35K and warming up to 9.7K. Located at a point approximately two-thirds along the length of the exchanger is a connection for the gas exhausting from the lower turbine to enter the heat exchanger.

Heat Exchanger Installation

All three of the heat exchangers will be mounted horizontally within the cold box and interconnected with aluminum or stainless steel piping. Connections to the stainless steel piping and the aluminum heat exchangers are made with aluminum to stainless steel transition joints. The heat exchangers will be mounted on a stainless steel support frame. The exchangers are anchored at only one end during operation enabling the heat exchanger and associated piping to contract as the exchanger is cooled down. The opposite end of all heat exchangers will be anchored for shipment. These shipping supports will be removed prior to operation.

In order to minimize the heat leak into the heat exchanger assembly, an aluminized mylar assembly is fabricated and installed around the inner surface of the cold box. In addition, several layers of aluminized mylar are wrapped around the warm exchanger, HX1 and HX2, in order to minimize the heat leak from that exchanger to the colder portions of the system.

Turbine Discussion

The theory and practice of turbo-expansion machinery is well developed for helium refrigeration and liquefaction system. It has been used successfully in the hydrocarbon processing and air separation industry for many years. The basic difference between these two operations is the temperature level at which the turbines operate; the principle is the same for either operation.

There are basically two types of turboexpanders. The first to be developed was the oil bearing turbine which operates at a speed of approximately 120,000 rpm. This type of turbine has been used successfully in the hydrocarbon processing, air separation and the large helium liquefaction industry.

In recent years the newly developed gas bearing turbine has been used successfully in smaller helium refrigeration and liquefaction systems. These turbines depend upon gas to lubricate the bearings and operate at approximate speeds of 200,000 rpm.

Reciprocating expansion machinery has also been used successfully in helium refrigeration and liquefaction systems. They are not being used today in the hydrocarbon processing and air separation system for practical reasons i.e., they typically operate at lower speeds and therefore their size would necessarily have to be enormous in order to handle the same mass flow.

In general, the reciprocating engines used in helium refrigeration or liquefaction systems are more efficient than the turbine; however, the turbine exhibits better long-term reliability characteristics and require less maintenance.

The system we are proposing utilizes two gas bearing turbines. We have not selected oil bearing turbines because their efficiency would be extremely low at such low mass flow rates.

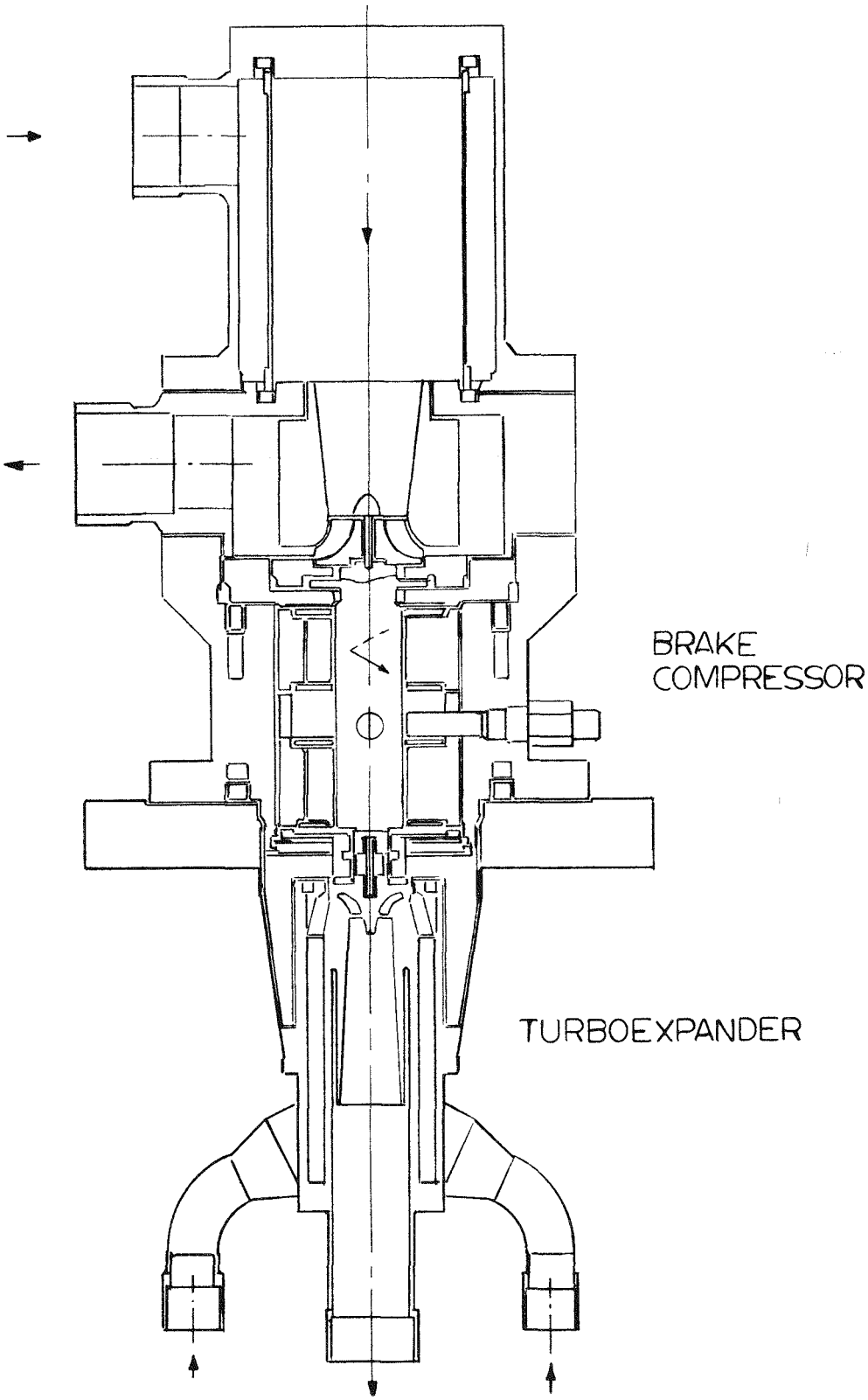

Figure 3-157. Gas Bearing Turbine.

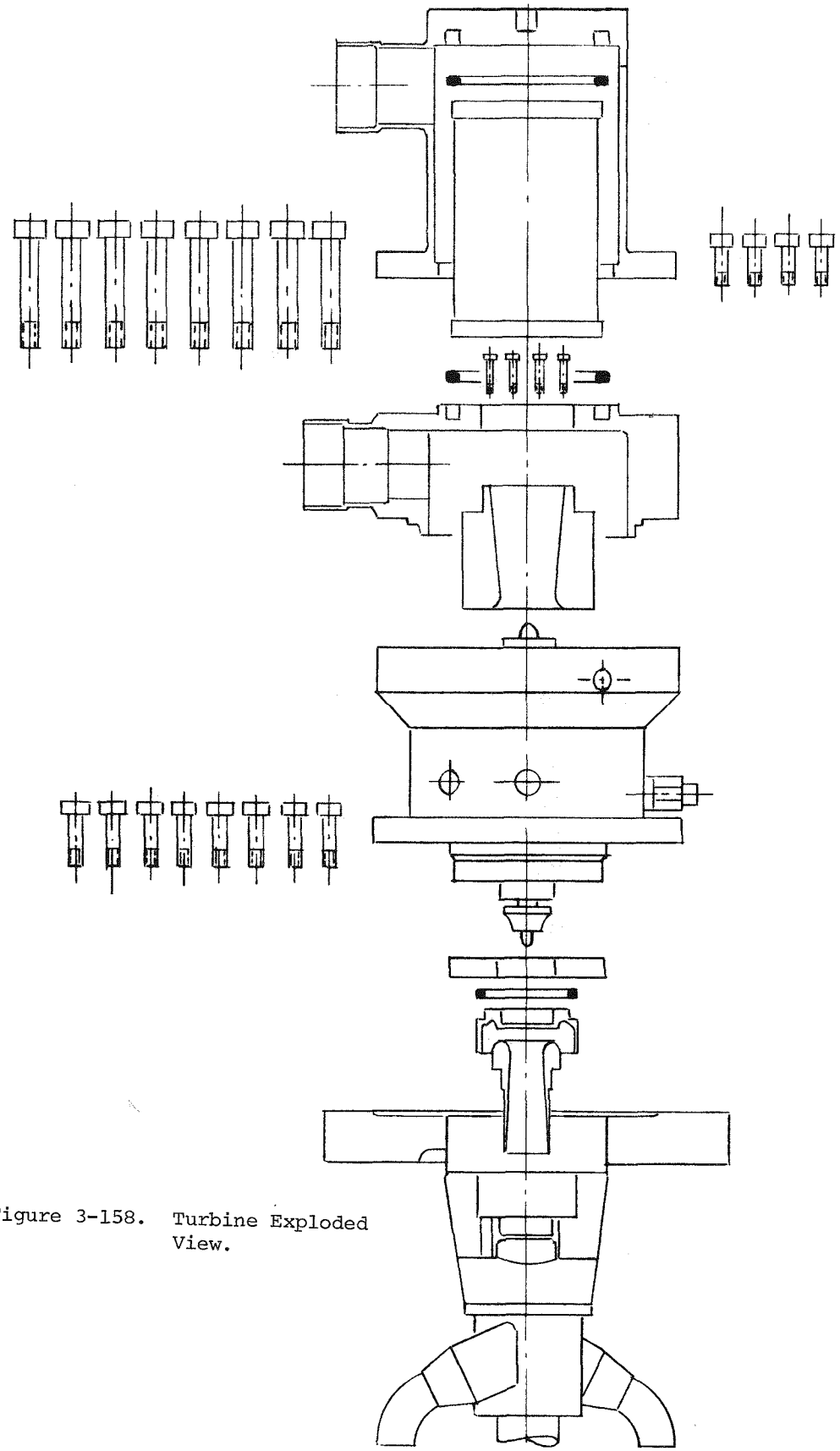

Figure 3-158. Turbine Exploded View.

We have based our design on Sulzer gas bearing centripetal (radial inflow) turbines. A schematic and an exploded view of the turbine assembly is shown in Figures 3-157 and 3-158. The turbine assembly consists of a turbo-expander wheel at the cold end, a brake compressor wheel at the warm end; the two wheels are connected by a common shaft. The turbine wheel may operate at temperatures as low as 5K. The temperature drop between the turbine wheel and compressor wheel occurs along the thinner part of the connecting shaft which is approximately 20mm long. There are two axial bearings and two radial bearings which operate at ambient temperature. Depending on the direction of thrust, the rotor is supported by either the upper or lower axial bearing. Both axial bearings are self-acting gas bearings of the normal spiral-grooved type. At low speeds the lower axial bearing uses a pressurized gas supply. The radial bearings have three tilting pads and are self-acting for all operating conditions.

High pressure helium process gas is allowed to expand through the turbine wheel which rotates the interconnecting shaft. The shaft speed is controlled by the turbine brake circuit. The brake circuit consists of a throttle valve and a water-cooled heat exchanger to cool the helium gas in the brake circuit. Brake valve adjustment controls the helium flow and compression ratio across the brake compressor wheel thereby controlling the turbine wheel speed. The work extracted from the helium process gas is transferred to the brake circuit helium gas via the compressor wheel and is dissipated in the cooling water.

Replacement of a gas bearing turbine cartridge is a relatively simple operation and does not require entering the vacuum case. To replace the gas bearing turbine cartridge, the valves before and after the turbine are closed; removal of the turbine cartridge is then accomplished, when ambient temperature is reached, by removing the bolts on the turbine cover, removing the cover, and extracting the turbine cartridge.

The time required for the cartridge replacement is less than two hours.

The gas bearing turbine does not require programmed maintenance.

Control Panel Discussion

The concept of the control panel we have developed for this application is shown on Figure 3-159. We have assumed that the control panel will be remote and locate in the power generating station control room. The overall configuration of the control panel can be modified to match an existing control panel in the power station.

The control panel will contain the process computer for controlling the refrigeration system and the instrumentation, including the programmable controller, required to operate the system in a manual mode. This includes all of the start and stop switches, indicating lights and controllers, and system alarm annunciation.

The compressors will be capable of being started locally or at the remote panel. Included at the local compressor panel will be the necessary instrumentation to determine operating conditions during start-up of the compressor. These controls will be interlocked so that start-up cannot occur simultaneously from either panel. Shut down of the compressor, however, can be accomplished from either panel.

Storage Dewar Discussion

The standby storage facility for liquid helium to supplement refrigeration in case of power outages or component repair or replacement is based on the current commercial techniques for bulk storage, using vacuum insulated, gas cooled shielding, with multi-layer superinsulation.

Heat leaks equivalent to steady boil-off losses of one percent or less of the full content of the dewar are achievable. Vacuum insulation is usually static as the cryopumping of the helium inner tank usually is sufficient to maintain pressures at or below 10^{-5} Torr.

Helium storage dewars are available in many sizes and in horizontal or vertical configuration depending upon the size selected. Based upon our evaluation of the length of time to repair or replace a component, or the time to bring additional liquid helium to the power generating station, we would recommend as a minimum a storage dewar of 1000 liter capacity. Figure 3-160 shows the approximate size and weight of a typical 1000 liter storage dewar.

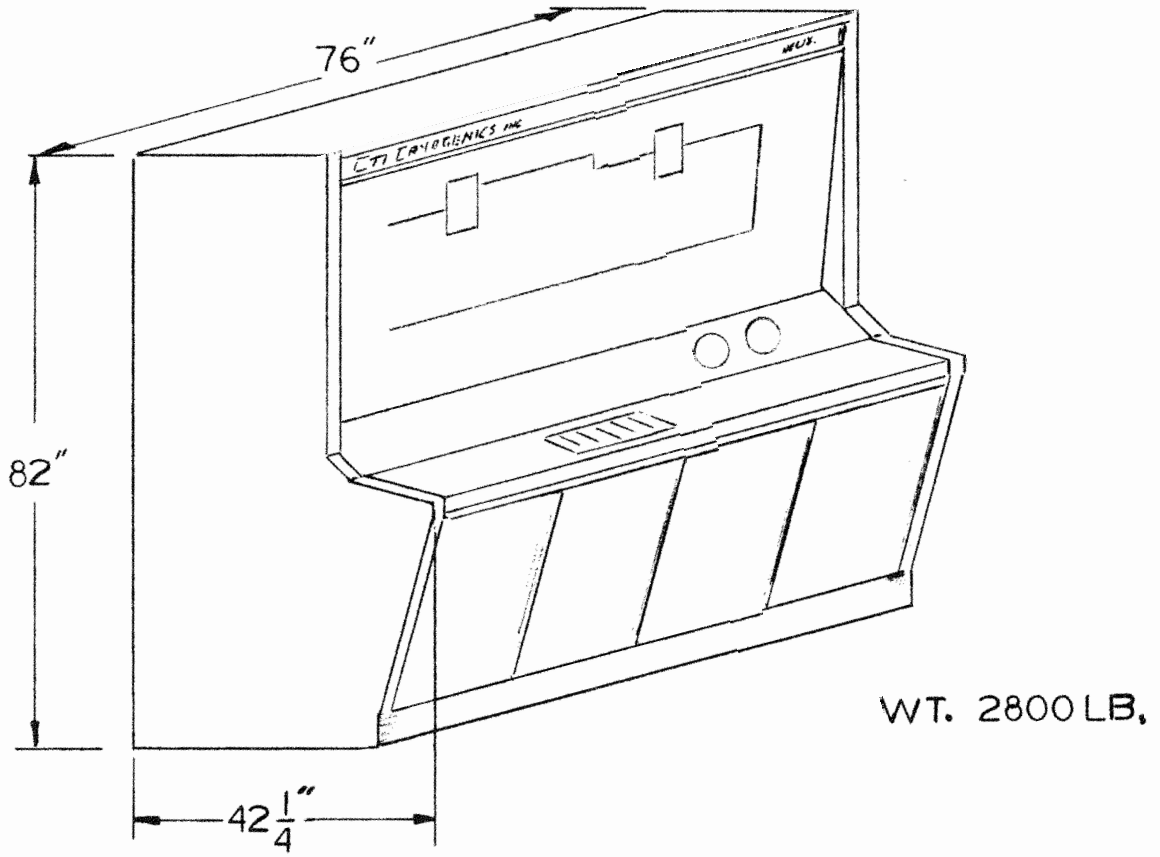

Figure 3-159. Control Panel.

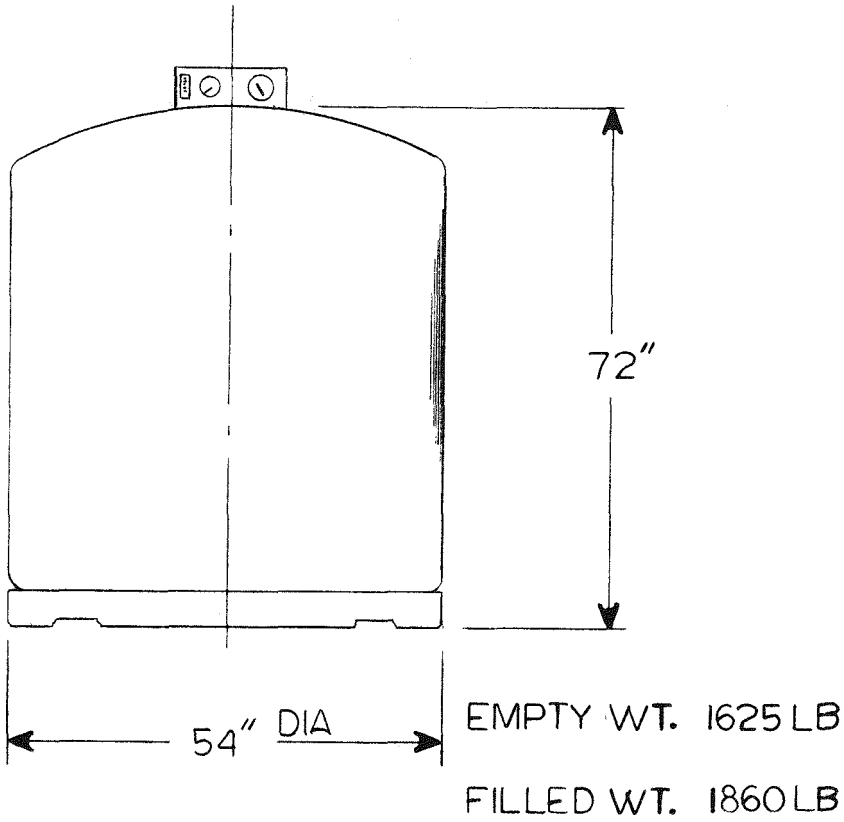

Figure 3-160. Storage Dewar (1000 Liters Capacity).

If the delivery time of helium to the power generating station is questionable, larger additional capacity up to 3785 liter (1000 gallons) helium storage may be appropriate. Our reliability analysis has been based upon the assumption that the dewar size is sufficient to keep the generator supplied with liquid helium between liquid helium replacement.

The refrigeration system we have developed has approximately 10% additional liquefaction capacity over the specified 47 liter per hour requirement. If power outages or component replacement depletes a major portion of the liquid stored in the dewar, the additional compressor capacity can be utilized to bring the level of the liquid helium back to the design operating level. The redundant compressor may also be utilized in restoring the liquid level at a faster rate. The heat exchangers and turbines have been designed oversize for this operation.

Reliability Discussion

An indepth reliability analysis of the refrigeration system was not included as part of the scope of work of this design study. We did, however, agree to present an overview on the question of reliability, make recommendations regarding redundancy, and to assess the reliability of the system.

To this end, we have reviewed some of the literature which has been written regarding reliability of process equipment, in particular, cryogenic process equipment.

Numerous articles have been written regarding system reliability in the hydrocarbon processing industry. A recent report for ERDA, addresses the question of reliability in assessing cryogenic refrigeration for superconducting transmission cables.[1] It points out, and we tend to agree, that the development of historical operating data on large helium refrigeration plants is minimal because of the small number of large helium plants operating and the limited data documented by those plants. Therefore, in assessing the reliability of large cryogenic plants, the report examines and documents the operating data of other large plants using comparable technologies.

---

[1] The U.S. Energy Research and Development Administration Under Contract No. E(11-1)-2552 "An Assessment and Study of Existing Concepts and Methods of Cryogenic Refrigeration for Superconducting Transmission Cables."

These plants although operating at a higher temperature level, have similar types of equipment and can be taken as indications of the reliability of cryogenic systems. Also included in the report, is an analysis of the failure records of six randomly chosen air separation plants operating over a 30 year period. They report that the overall onstream record for these plants was 98.27 percent. They also report the percentage of off-stream time due to failures by categories and the outage duration versus time for the six plants. The report states that only 4.3% of all of the outages lasted more than 24 hours.

It is worth noting that the report addresses and substantiates the need for redundant key components and the use of liquid helium storage as back up refrigeration, for the cryogenic cooling for superconducting power transmission cables.

Reliability Overview

Reliability of a system is achieved by: (1) selecting reliable components, (2) properly integrating those components into a well engineered system, (3) providing appropriate redundancy, and (4) establishing and executing a proper maintenance program.

We have selected the most reliable components available at the present time and have integrated them into a well engineered system. To assure that continuous refrigeration is delivered to the generator, redundancy has been provided in a component or sub-system where failure of that component or sub-system individually, or in conjunction with, any other component or sub-system, would prevent the continuous delivery of refrigeration to the generator. Several examples of this design philosophy can be seen by examining the system block diagram Figure

Within the total system concept, the storage dewar is a passive component, providing the system with additional assurance that continuous refrigeration will be supplied to the generator. The dewar has the capability of providing liquid helium to the generator for a period of up to 20 hours in the event of a power outage or component replacement. The ERDA report states that 94.6% of the outages experienced on the six nitrogen plants lasted less than 24 hours. Our experience with the KRH and Cities Service helium liquefaction plants, also indicates that most of the experienced outages last for a period of less than 24 hours. It is important that those components which support the storage dewar

and provide delivery of liquid helium to the generator are provided with redundancy. Thus, duplicate level controls are provided to maintain a constant level of liquid helium in the phase separator, as well as duplicate pressure controls, to assure the correct pressure in the storage dewar. The 1000 liter dewar is sized for the 300 MVA system. For the 1200 MVA system the dewar size should be adequate to continue operation between dewar refilling operations.

Since the dewar has a finite liquid capacity, it is important to provide redundancy for those components which have a time to repair in excess of the dewar capacity. Thus, we have provided redundancy for the entire compressor and oil removal systems for the following reasons:

- The time to repair is in excess of dewar delivery capacity
- To provide excess capacity during cooldown periods
- To provide alternate hardware during periods of scheduled maintenance.

Our experience has shown that the turbine can be replaced within the time period allotted to use liquid helium in the storage dewar to provide refrigeration to the generator. The critical instrumentation within the cold box is redundant. For these reasons we do not believe the cost of a redundant cold box can be justified and is not included as part of the system. This rationale is based upon the fact that we have selected reliable heat exchangers and turbines and have developed the necessary manufacturing techniques to establish vacuum integrity in the cold box. To assure vacuum integrity, we have proposed the cold box be equipped with an appropriately sized vacuum pump system. This feature will maintain the proper insulating vacuum in the event a small helium leak should occur after years of operation.

Reliability Analysis

Table 3-63 presents some of the system concepts studied with their corresponding reliability characteristics. The reliability figures are based on the following assumptions:

- There is sufficient reserve cooling to allow for minor on-line maintenance and correction to minor component failures.
- The dewar system is of sufficient capacity to provide adequate cooling during a major equipment repair; or the dewar can be refilled with commercially supplied liquid helium to provide cooling as required.

Table 3-63

SYSTEM CONCEPT RELIABILITY STUDY

CASE	SYSTEM	RELIABILITY (%)
1.		57.1
2.	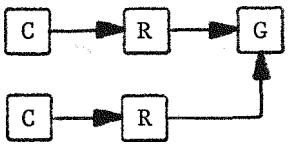	81.6
3.	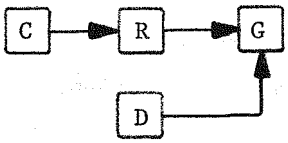	94.4
4.	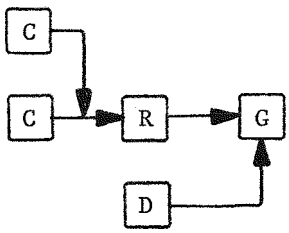	96.6
5.	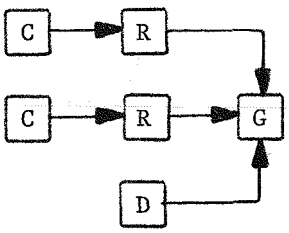	97.7

NOTES: Reliability is defined as the probability that the system will be able to provide cooling over a one year period.

C = Compressor R = Refrigerator G = Generator D = Dewar

- The dewar connections and controls are either redundant or sufficiently high in reliability so as to not be limiting.
- Sufficient alarms will be provided to force attention and necessary action in the event of operator error when operating in the manual mode.

Conclusion

CTI-CRYOGENICS concludes that a refrigeration system designed with redundant compressors and a helium storage dewar should assure high reliability. The redundant compressor will also provide additional gas for cooldown operations. Additional component redundancy, cold box, can be utilized to further improve the system reliability; although it appears that it is of limited benefit. The reliability characteristics of the system are consistent with achieving a high plant availability.

Maintenance Schedule

To assure that the refrigeration system performs reliably for extended periods of time, it is necessary to establish and conduct a preventive maintenance program.

Table 3-64 presents typical areas of interest to the maintenance personnel and suggested inspection frequency intervals.

Table 3-64

INSPECTION FREQUENCY INTERVALS

Component	Inspection Interval (Hours)	Areas of Concern
Screw Compressor	4400	Excessive oil or gas leakage
Filters	8800	Excessive pressure drop
Cold Valves	8800	Excessive leakage at stems
Turbine Filters	8800	Excessive pressure drop
Vacuum and Diffusion Pumps	4400	Cleanliness and quantity of oil
Instruments and Controls	4400	Instrument and control accuracy

Cost Evaluation

In order to determine the cost to design and manufacture the described refrigeration system, we have subdivided the effort into the following major categories:

- Engineering
- Manufacturing
- Computerized Process Control

The categories were further subdivided in order to develop a detailed cost estimate. Table 3-65, lists a complete breakdown of the cost of each of these categories as well as the total cost.

Table 3-65

PRICE BREAKDOWN

Discipline	Price ($)* ($1,000)
Engineering	200
Manufacturing	800
Subtotal	1,000
Computerized Process Control (Including Software Engineering)	300
Total System Price	1,300

*1977 Dollars

It is worth noting that the cost is based upon the design and manufacturing of the first system. Subsequent systems would definitely cost less. We would expect that the cost of the second system could be reduced by 24 percent. We have evaluated the mature cost of future systems and would anticipate they could be reduced to approximately $600,000 in 1977 dollars, not including installation assistance and start-up supervision.

Conclusions and Recommendations

The component that has the most important influence on system reliability is the helium storage dewar system. For this reason a 3785 liter (1000 gallon) helium storage dewar is recommended, space permitting, for maximum reliability.

The refrigeration system we are proposing, excluding the storage dewar, has been developed utilizing components which require minimum maintenance and have the highest reliability. In some cases, such as the compressor and turbo-expanders, we have sacrificed efficiency for reliability. As a result, our reliability analysis shows that the system has a 96.6 percent probability of providing cooling to the generator over a one year period. Our analysis also indicates that a complete redundancy, including cold box, only increases the reliability 1.1 percent to 97.7 percent probability. This results in no more than one refrigeration system induced outage over the life of the superconducting generator system.

Since the helium refrigeration system will be designed for unattended operation, computer control will be needed to perform necessary functions such as, monitoring the system status; ability to switch to a back-up system in priority sequence; control components (such as expanders) during cooldown, transients, and warm up; call for maintenance; and diagnose faults. We envision computerized process control of helium refrigeration systems as being developed over the next five years.

3.4 GENERATOR AND SYSTEM INTERACTIONS

Introduction

There are a number of aspects of the interaction of the superconducting generator with the system that must be evaluated and be compared with that of a conventional generator. The most important of these are transient stability, steady state stability, dynamic stability. A feature of the 300 MVA generator as developed by Westinghouse that requires separate attention in terms of system disturbance is the flexible shaft utilized for transient torque attenuation. Here the question of the damping of the oscillatory mode associated with this shaft and of the torque that the shaft is subjected under fault conditions must be covered.

Transient stability is concerned with the ability of the generator to remain in synchronous with the system after a severe system disturbance. One of the most severe disturbances that the generator can be subjected to is a system fault and the subsequent clearing of that fault. The parameter that can be used to quantify the performance of the generator in this case is the critical fault clearing time (CFCT). This number gives the longest time that the fault

can be sustained and the generator remain synchronous after the fault is cleared. This quantity will be utilized below for comparing the transient stability of a superconducting with a conventional generator.

The steady state stability limit represents the maximum power that the generator can deliver to the system without going out of synchronous with the system under steady state conditions. A brief discussion of this aspect is given below.

Dynamic stability is the ability of the machine to stay in synchronous with the system under the action of low frequency system disturbances (0.2 to 2 Hz). Dynamic stability for the superconducting generator was discussed above in Section 3.3, Exciter and Voltage Regulator.

The push toward low reactance machine requires special consideration of the large transient torques that are present during and after fault periods. A special aspect of this is consideration of the flexible shaft utilized with the 300 MVA superconducting generator. The purpose of this shaft is, in combination with the rotor inertia, to attenuate the transient torques to a level that can be handled by the 3 pu torque of existing steam turbines. This is in anticipation that the 300 MVA unit must be tested in an existing plant without modification of the turbine shaft. While the main discussion of the flexible shaft design and its ability to handle the torques is presented in Section 3.2.1.2, in this section, some results from machine-system computer runs are given which show the flexible shaft torque as functions of time during and after a fault.

Another aspect of the flexible shaft is the damping of the new oscillatory mode introduced by this shaft. It is important that this mode is positively damped so that sustained oscillation will not occur. Calculations of the damping of this mode is discussed below.

The transient stability limit of a cryogenic machine is affected by the value of the unit electro-mechanical parameters. These parameters and hence transient stability limits, can vary over a wide range as unit design is changed. The value of the parameters will generally differ from those of a conventional machine. The possibility therefore exists that the stability limits of the cryogenic unit will differ from those of a conventional unit.

One objective of the Superconducting Generator Project is to select a machine design that yields the best CFCT that can be justified economically. To accomplish this, the transient stability limits and cost of a large number of superconducting generator design variables must be determined and evaluated. It is also desirable to compare the CFCT of the cryogenic machine design selected to the CFCT of a conventional unit. The comparisons will aid the system planner in determining the impact of the superconducting machine on the power system.

The purpose of this study was to determine how cryogenic unit critical fault clearing time changed as machine electrical and mechanical parameters, and hence unit design, were varied, and to compare the transient stability performance of a cryogenic machine to a typical conventional unit.

The Parametric Study

The transient stability limits of a superconducting machine depend primarily upon the value of the machine reactances, the time constants, and the unit inertias. The effect of varying these parameters on turbine generator transient stability limits as measured by CFCT will be examined in this section of the report.

A power system consisting of a single 300,000 kVA superconducting machine connected through a main step-up transformer and equivalent system reactance to an infinite bus was utilized. The study consisted of placing a three-phase bolted fault on high side of the main step-up transformer. The fault duration was varied to determine the machine critical fault clearing time.

The step-up transformer reactance selected was 12 percent and the system impedance used was 5 percent. Both quantities are based on the machine rating. Five percent represents a typical system impedance for a 300 MVA unit.

For this study only, a base or reference superconducting generator design was developed. The electrical and mechanical constants for this design are depicted in Table 3-66. For such a unit, operating at rated power and 0.90 power factor lag, a critical fault clearing time of 13.5 cycles was obtained.

The manner in which the CFCT varied as unit electrical and mechanical parameters were changed is displayed in Figures 3-161 and 3-162. In all cases, the unit was initially operating at rated power and 0.90 power factor lag.

Table 3-66

SUPERCONDUCTING GENERATOR ELECTRICAL CONSTANTS - REFERENCE DESIGN

MVA Base = 300		
X_d = 0.423	X'_d = 0.278	X''_d = 0.139
X_q = 0.423	X'_q = 0.423	X''_q = 0.139
X_L = 0.076	R_A = 0.0023	
T'_{do} = 1500 seconds	T'_{qo} = 0.0	
T''_{do} = 0.219	T''_{qo} = 0.447	
H = 3.00		

The first parameter varied was unit inertia. In Figure 3-161 critical fault clearing time is depicted as a function of unit inertia constant. The unit CFCT increases as machine inertia is increased. The Figure indicates that an increase in CFCT of approximately two cycles occurs when the turbine generator inertia constant is increased by one. Such an increase in inertia could be achieved by adding a flywheel.

The next parameter to be varied was machine reactance. Figure 3-162 depicts a plot of critical fault clearing time versus generator impedance. The number 1.0 on the x-axis indicates the reactances used were those shown in Table 3-66 for the reference design. The number 0.50 indicates that a machine design with one-half the reference machine reactances was considered while the value 1.50 indicates the unit design considered used reactances 50 percent greater than the reference design values. The generator time constants utilized were those shown in Table 3-66.

The CFCT is not sensitive to changes in machine reactances. Decreasing or increasing the reactance 50 percent compared to the reference design, increases or decreases, respectively the CFCT about 1.50 cycles.

The previous results assumed a system impedance of 5 percent. If system reactance were increased, the change in CFCT associated with a 50 percent change in machine reactance would be less than 1.5 cycles. The reason is that

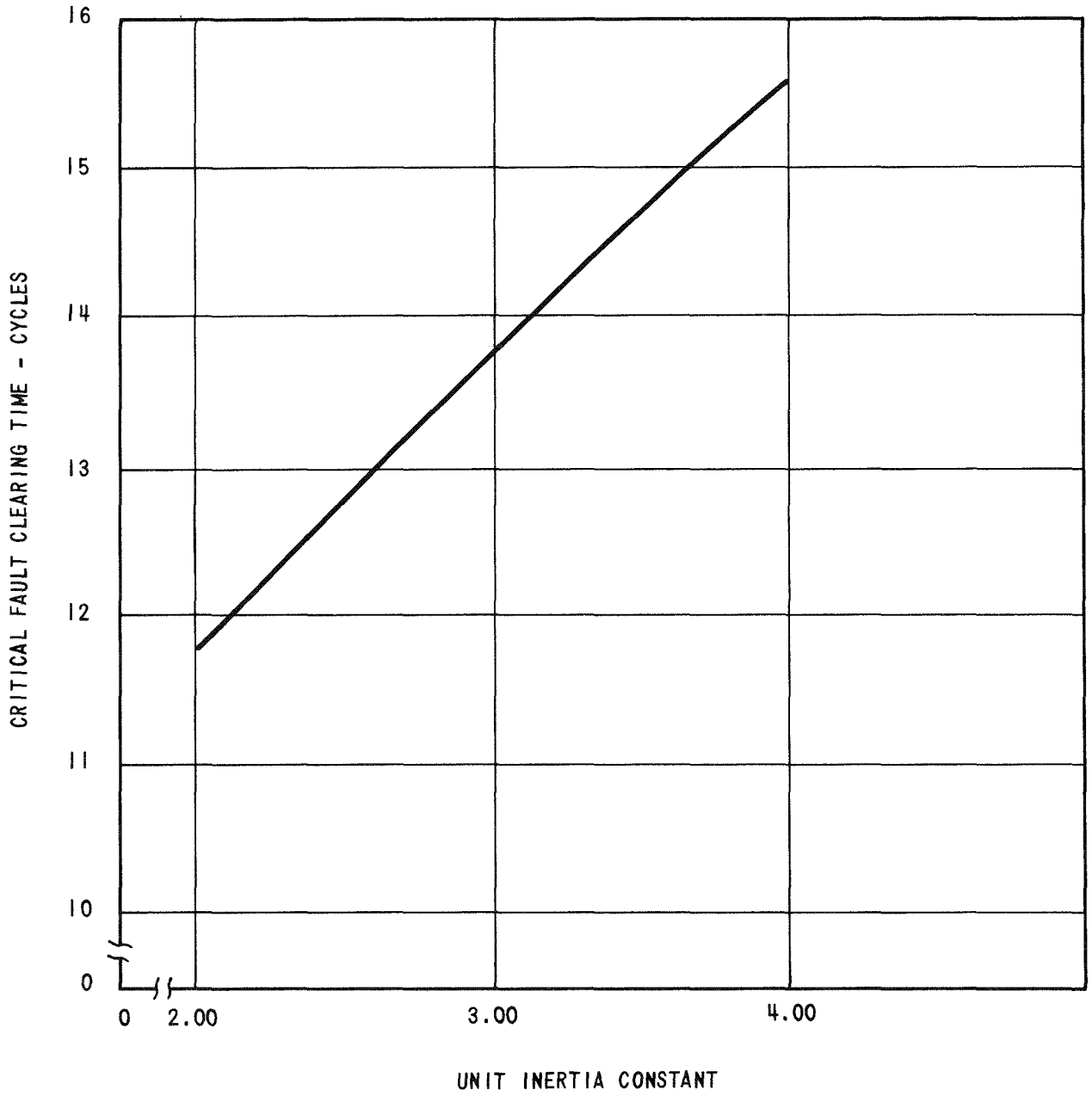

Figure 3-161. Critical Fault Clearing Time as a Function of Unit Inertia.

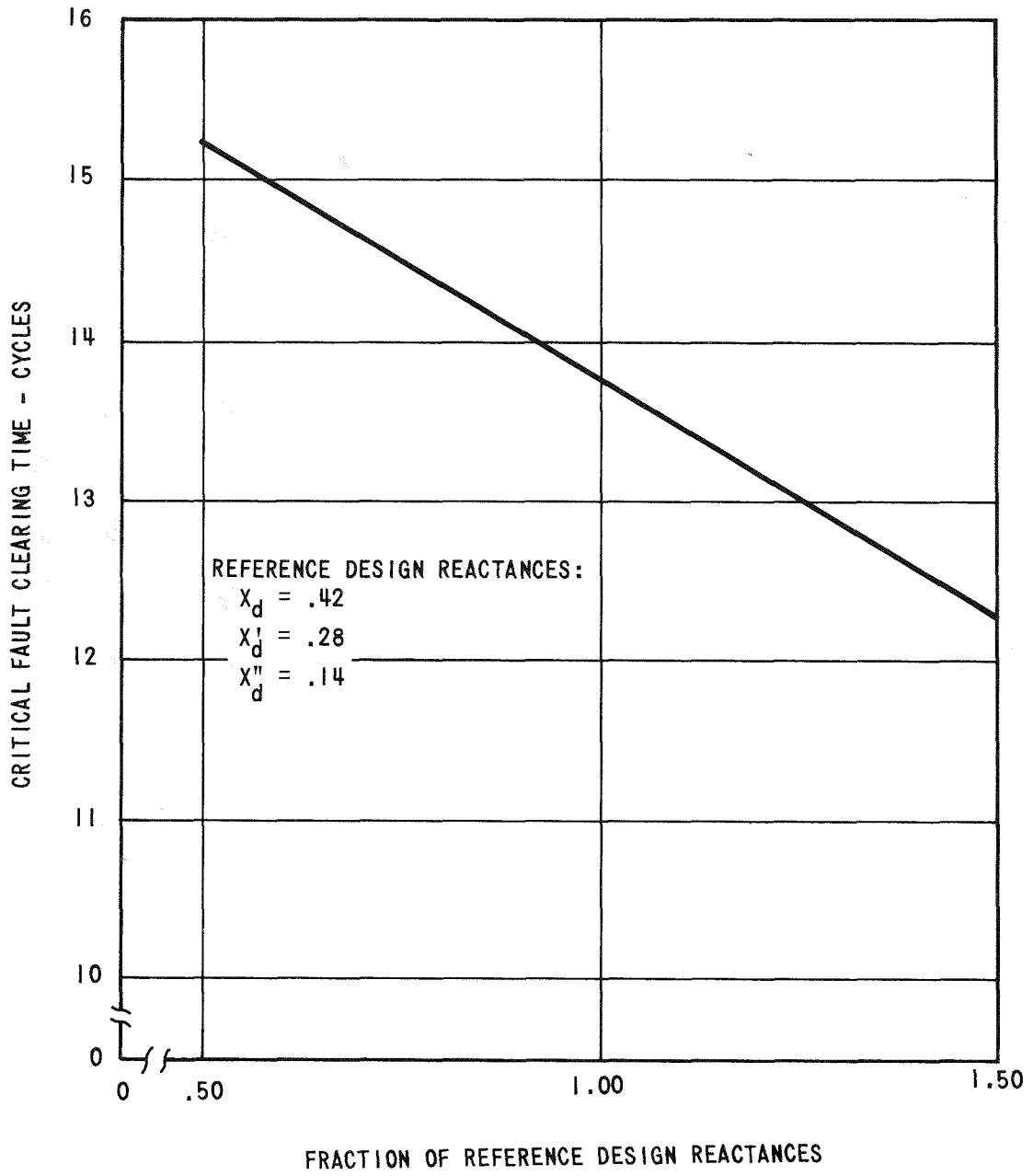

Figure 3-162. Critical Fault Clearing Time as a Function of Generator Reactance.

the generator reactance would represent a smaller fraction of the total reactance between the machine internal voltage and infinite bus. Conversely, if system reactance were reduced below 5 percent, a larger change than 1.5 cycles would occur for the same change in generator reactance.

The effect of varying the generator sub-transient time constant (T''_{do}) on unit CFCT was analyzed. In Figure 3-163 a plot of critical fault clearing time versus generator T''_{do} is shown. The value of T''_{do} is related to the physical characteristics of the shield surrounding the cryogenic field winding. The generator reactances and field time constant utilized are shown in Table 3-66.

Figure 3-163 indicates that as T''_{do} is increased, machine CFCT is increased. The increase in CFCT is the result of a higher machine rotor flux. The higher flux increases the power transfer capability of the unit and therefore enhances machine transient stability. Figure 3-163 indicates that the unit CFCT can be increased approximately one cycle by increasing T''_{do} from the reference machine value of .219 seconds to .50 seconds. Decreasing T''_{do} from .219 seconds to .10 seconds reduces the critical fault clearing time by .50 cycles compared to the CFCT associated with the reference machine design.

The last parameter to be varied was excitation system ceiling voltage. Figure 3-164 depicts a plot of machine critical fault clearing time as a function of excitation system ceiling voltage. The machine reactances and time constants are shown in Table 3-66. The figure indicates that a generator field ceiling voltage of 1500 volts will increase the machine critical fault clearing time by about .5 cycle compared to a case in which the unit voltage regulator is on manual control. This result assumes a generator T''_{do} of .219 seconds.

If the generator sub-transient time constant is increased to .50 seconds, the gain in machine CFCT diminishes when a high ceiling voltage is utilized. This occurs because the large time constant makes it more difficult for the excitation system to increase rotor flux and therefore CFCT. Computer simulations indicate that if T''_{do} equals .50 seconds, an excitation system ceiling voltage of 1500 volts will increase the machine critical fault clearing time by only .1 cycles.

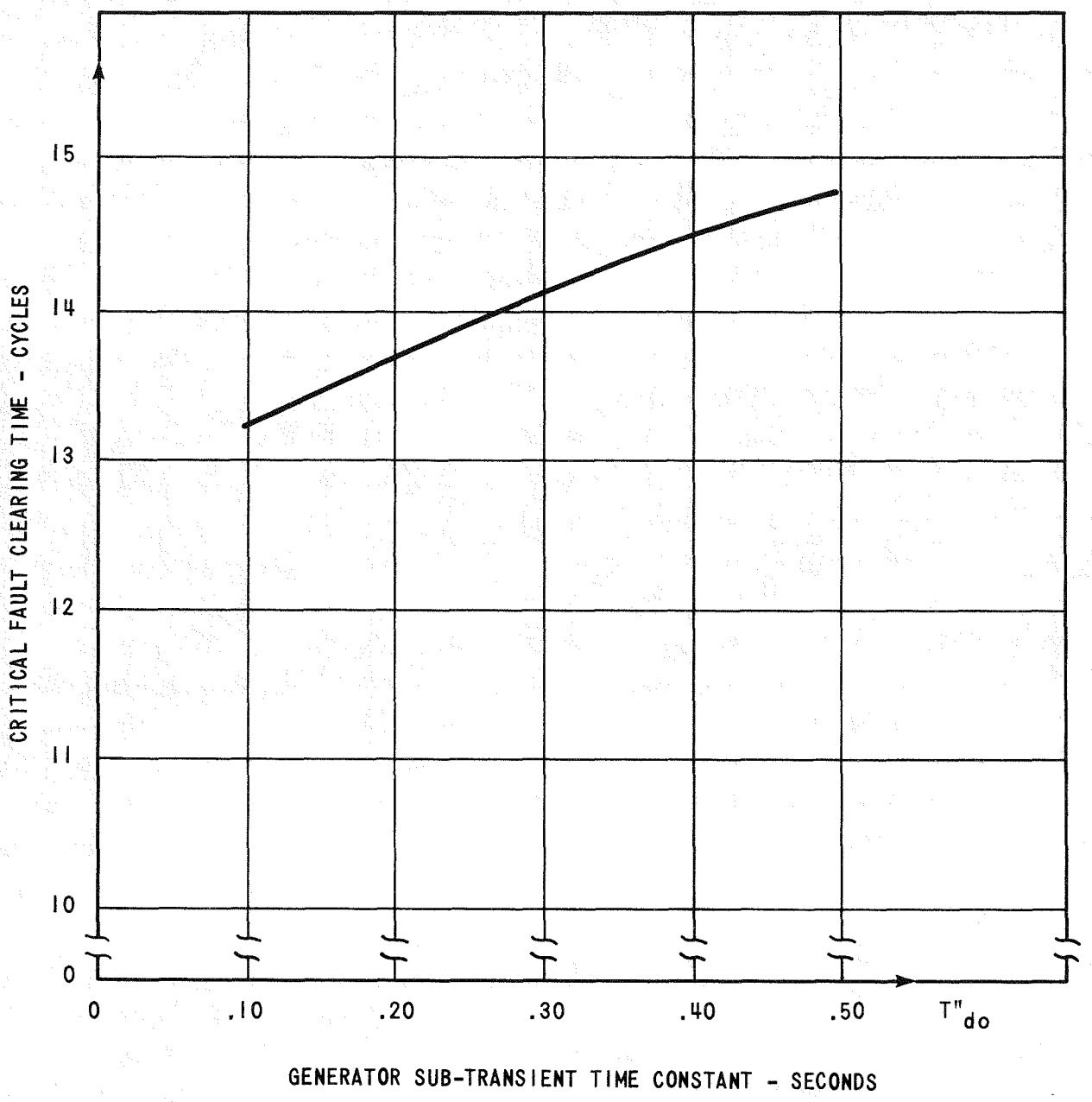

Figure 3-163. Critical Fault Clearing Time as a Function of Generator Subtransient Time Constant.

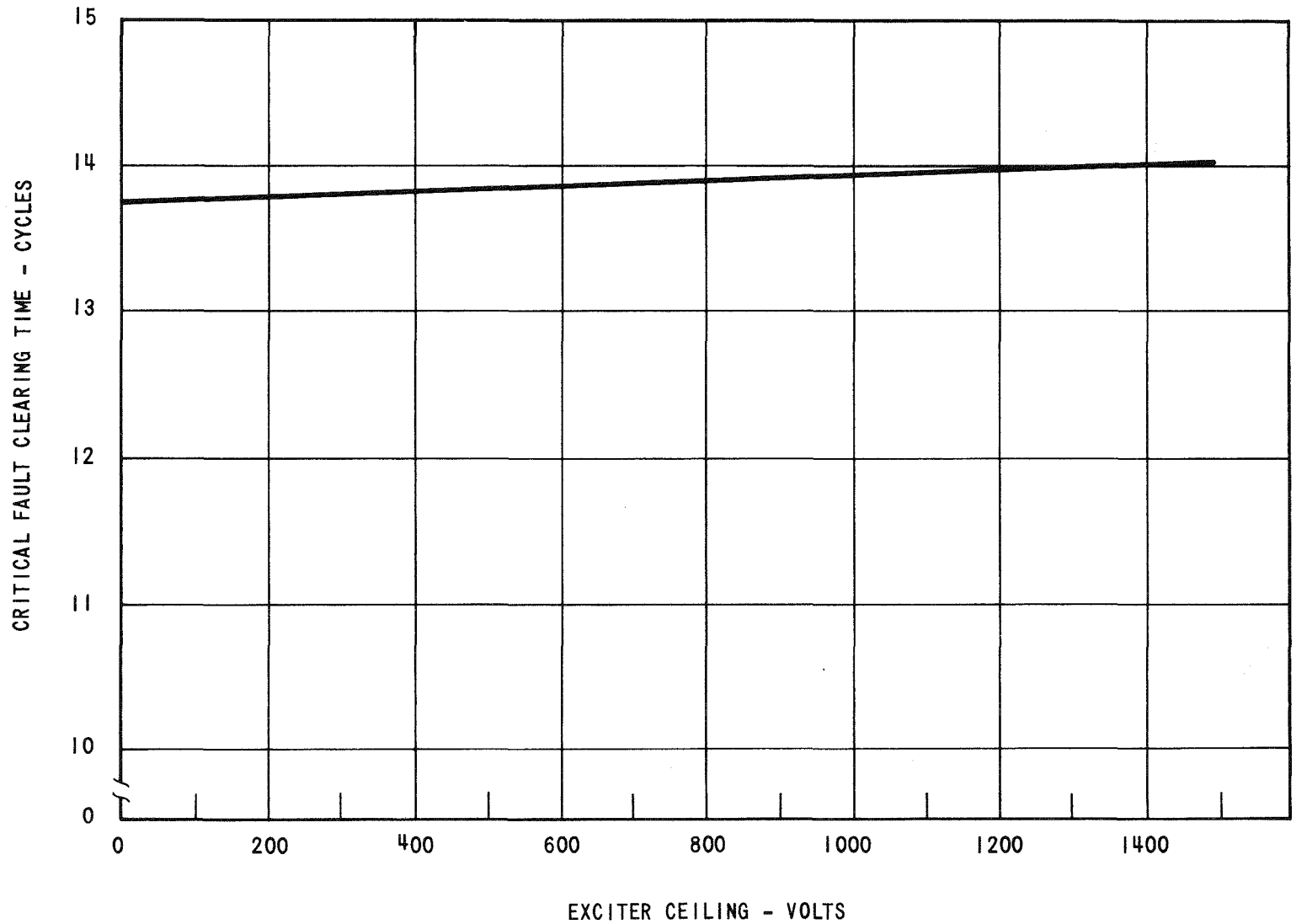

Figure 3-164. Critical Fault Clearing Time as a Function of Exciter Ceiling Voltage.

If two or more machine parameters are varied at one time, a reasonable approximation of the total change in CFCT can generally be determined by adding the changes in CFCT that occur if each parameter is varied alone. One important exception exists: the change in CFCT resulting from variations in generator T''_{do} (Figure 3-163) cannot, in general, be added to the change in CFCT when the generator field ceiling voltage is varied (Figure 3-164). This occurs because a change in T''_{do} will affect the ability of the voltage regulator to change rotor flux. As a result, the slope of Figure 3-164 will change appreciably as T''_{do} is varied.

It is tempting to draw the conclusion from the previous analysis that the design selected should have low reactance, a high inertia constant, and a large T''_{do} to achieve the maximum critical fault clearing time. For instance, compared to the reference case, the CFCT could be increased 4.5 cycles by using a machine with one-half the reactance, and inertia constant of 4.0, and a T''_{do} equal to .50 seconds. However, such a design might be uneconomical or technically infeasible.

The analysis presented in this section provides the engineer with information required to analyze machine CFCT variations as unit parameters are changed and select a machine design, so far as is practical with favorable transient stability.

The design selected may have a CFCT that is different from a conventional unit of the same rating connected to the power system. The effect that this difference in CVCT may have on the power system can be assessed by comparing the CFCT of the cryogenic unit to the conventional machine. This is done in the next section.

Comparison of a Superconducting Machine to a Conventional Unit

In this analysis, the critical fault clearing time of a cryogenic unit and a conventional machine were compared. A power system consisting of a single 300,000 KVA unit (either conventional or superconducting) connected through a main step-up transformer and system reactance to an infinite bus was utilized. Transformer and system reactances used were identical to those used in the previous section. The study consisted of applying three-phase bolted faults of varying duration at the high side bus of the main step-up transformer to determine unit CFCT. The machine was initially operating at full turbine power and either .90 lagging or .95 leading power factor.

In Table 3-67, the conventional machine parameters utilized for the study are shown. These parameters are for a typical 300 MVA unit with an inertia constant of 3.0. The reference superconducting plant electrical parameters shown in Table 3-66 were utilized with the exception that the cryogenic unit inertia constant was taken as 2.40 and not the value given in the Table 3-66. The value of 2.40 was obtained assuming the cryogenic and conventional generators utilized the same turbine.

Table 3-67

CONVENTIONAL GENERATOR ELECTRO-MECHANICAL CONSTANTS

MVA Base = 300

$X_d = 1.701$	$X'_d = 0.281$	$X''_d = 0.239$
$X_q = 1.674$	$X'_q = 0.458$	$X''_q = 0.237$
$X_L = 0.197$	$R_A = 0.0015$	$H = 3.0$
$T'_{do} = 5.3$ seconds	$T''_{do} = 0.09$	
$T''_{do} = 0.04$	$T''_{qo} = 0.068$	

The results of this portion of the study are depicted in Table 3-68. When the initial power factor is 0.90 lag, the CFCT of the superconducting machine is equal to the critical fault clearing time of the conventional unit. At 0.95 leading power factor, the CFCT of the cryogenic unit is approximately 3 cycles longer than the conventional unit CFCT.

Table 3-68

COMPARISON BETWEEN SUPERCONDUCTING AND CONVENTIONAL UNITS

System reactance = 5% on machine base
Conventional unit inertia constant = 3.00
Cryogenic unit inertia constant = 2.40
Turbine initially at rated power

Initial Generator Power Factor	Superconducting Unit (Cycles)	Conventional Unit (Cycles)	Difference
0.90 lag	12.75	12.75	0
0.95 lead	11.75	8.75	3.0

The preceding results assumed a system reactance of 5 percent. When the reactance was increased to 25 percent, the machine critical fault clearing times decreased; however, the difference in CFCT between the superconducting and conventional units were similar to those found when system reactance was 5 percent. It therefore appears that the CFCT of the superconducting generator is equal to or greater than the CFCT of a conventional unit over a wide range of initial machine operating points and system impedance.

What this improvement in CFCT means to an electric utility system planner is difficult to determine. It may eliminate the need for stability enhancement techniques such as fast valving or main step-up transformer reactance reduction in certain cases. This would result in savings to the user. The stability enhancement techniques actually eliminated will vary from plant to plant and cannot be analyzed on a generic basis.

The comparison between the conventional and cryogenic machines will be affected by variations in the superconducting unit electromechanical parameters. The analysis described in the previous section of this report can be utilized to determine how these variations will effect the comparison with the conventional unit. While the results presented in the previous section were determined for a unit initially operating at 0.90 power factor lag, the results should be approximately valid for the 0.95 leading power factor case if percent change in CFCT is obtained from Figures 3-161 through 3-164 and not absolute change in cycles. An examination of these figures indicates that small variations in cryogenic unit parameters would not affect the comparison between the superconducting and conventional units previously described.

Damping of Superconducting Generator Rotor Oscillations Following a Distrubance

In this section, damping of machine rotor oscillations following a three-phase bolted fault was analyzed.

The system utilized is shown in Figure 3-165. The superconducting generator is rated at 300 MVA and 0.9 power factor. Initially, the machine is operating at rated load and rated power factor. The transformer impedance is 0.12 per unit on the generator MVA base. Three cases were run utilizing different system impedances. The different prefault impedances used are shown on Figure 3-165. The post fault impedance is 30 percent greater than the prefault value. The fault was applied at the high side of the main step-up transformer.

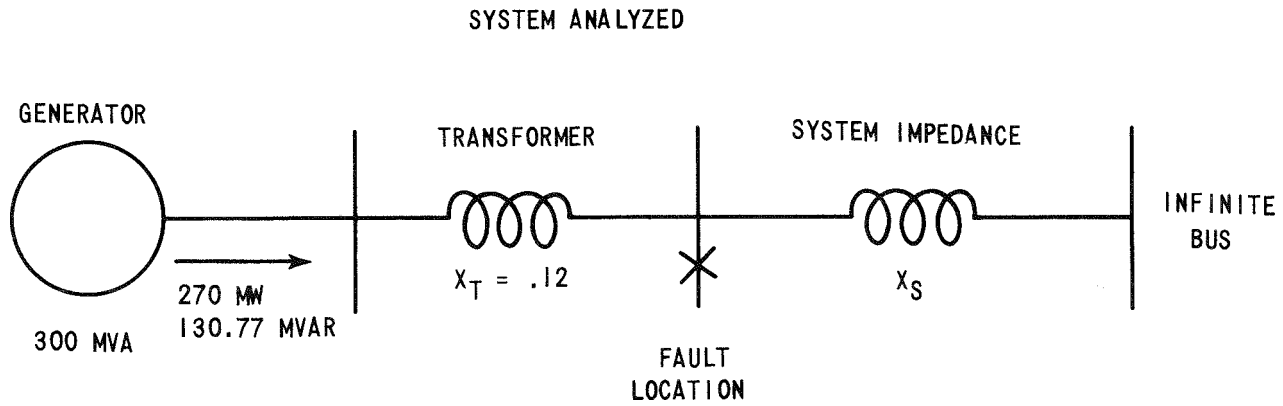

NOTE: ALL PER UNIT VALUES ARE BASED UPON AN MVA EQUAL TO 300.

PRE-FAULT VALUES OF SYSTEM IMPEDANCE STUDIED:

X_S = 5%

X_S = 15%

X_S = 25%

Figure 3-165. Diagram of System Analyzed.

Generator constants used are shown in Table 3-69. Excitation voltage and turbine power are assumed constant for the duration of the study.

The results of the study are depicted in Figure 3-166, 3-167 and 3-168. The fault times are shown on the figures. Each fault time is close to the critical fault clearing time. The swing frequencies are shown in Table 3-70. Damping at these swing frequencies is adequate.

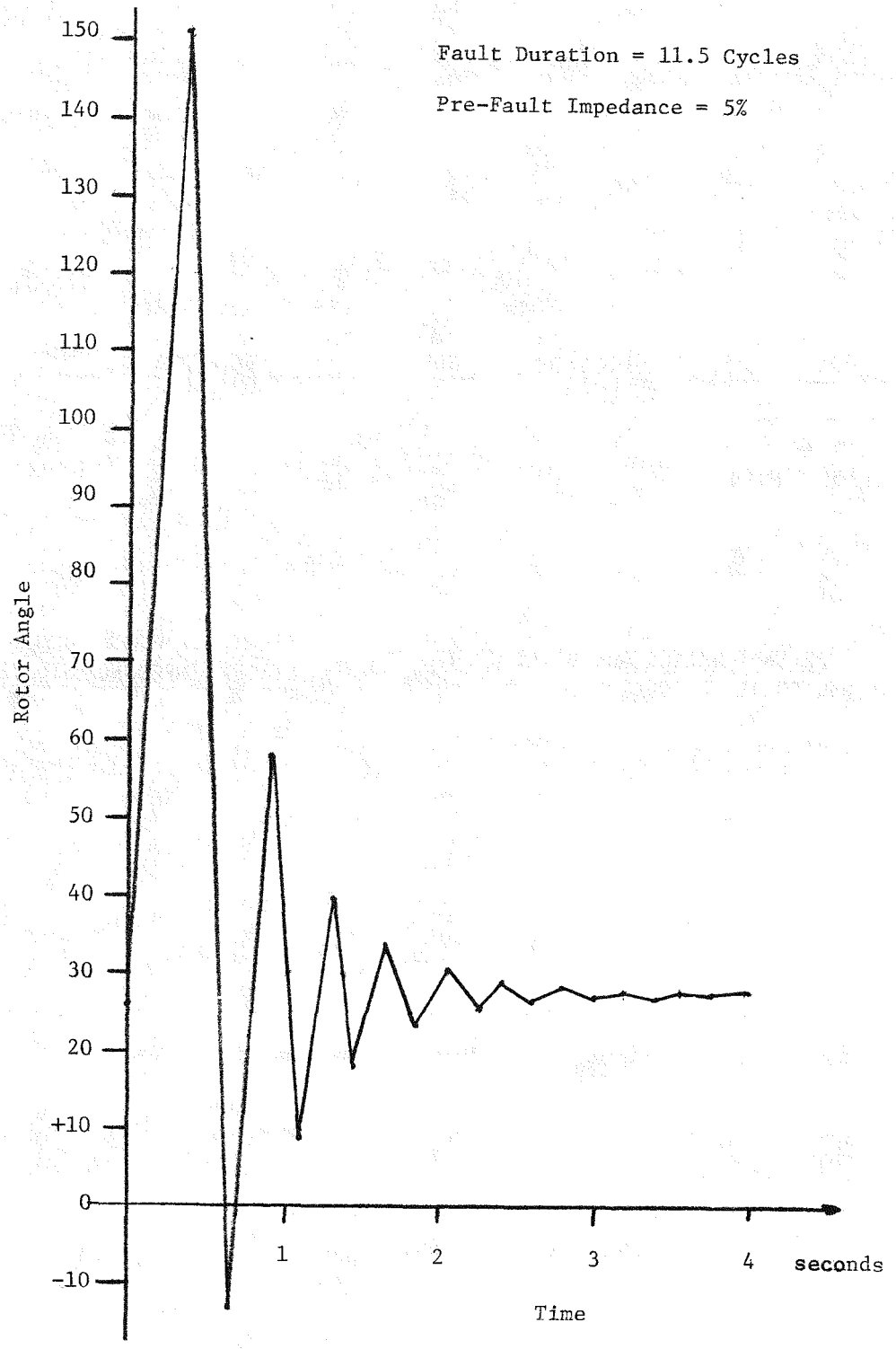

Figure 3-166. Rotor Angle Versus Time.

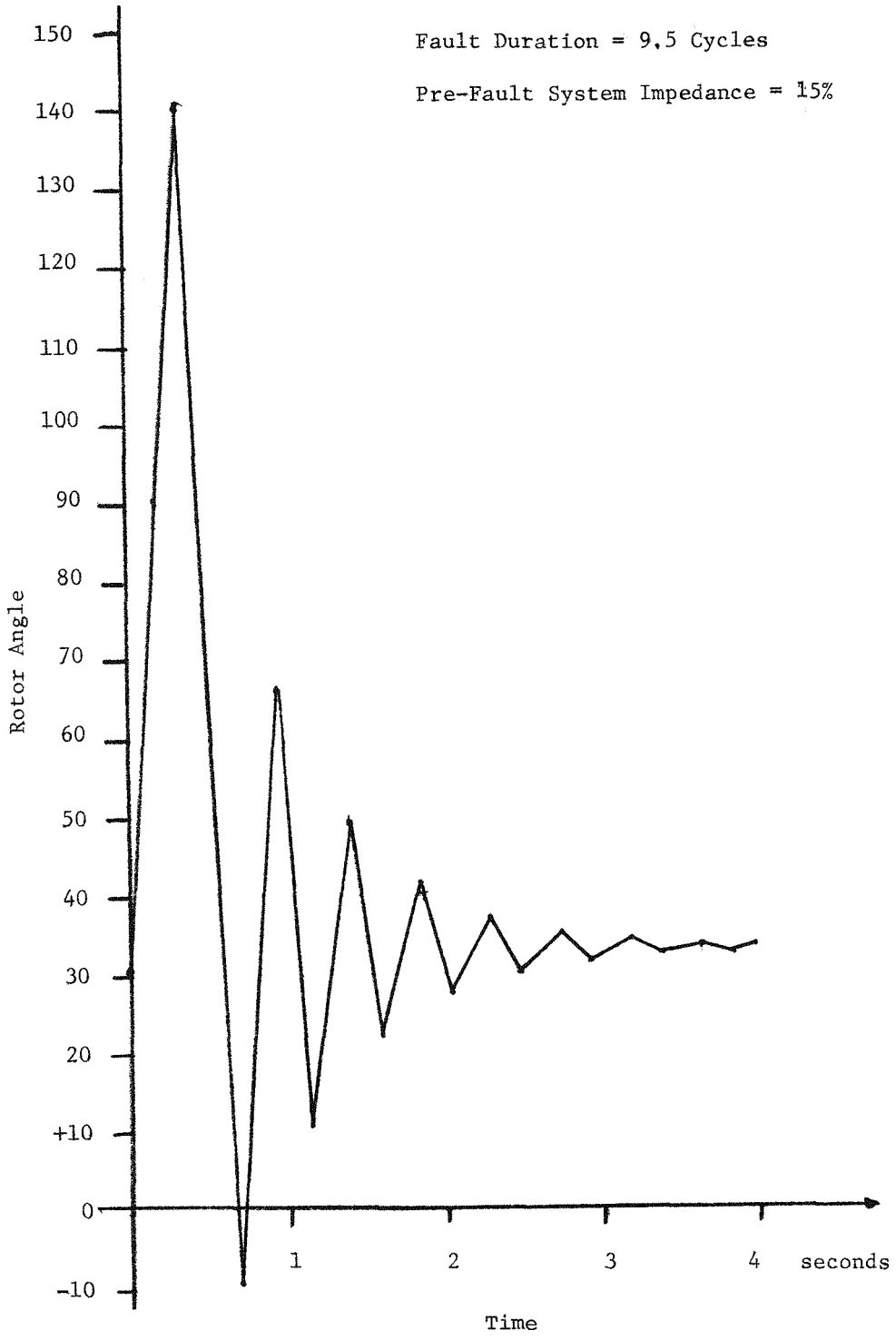

Figure 3-167. Rotor Angle Versus Time.

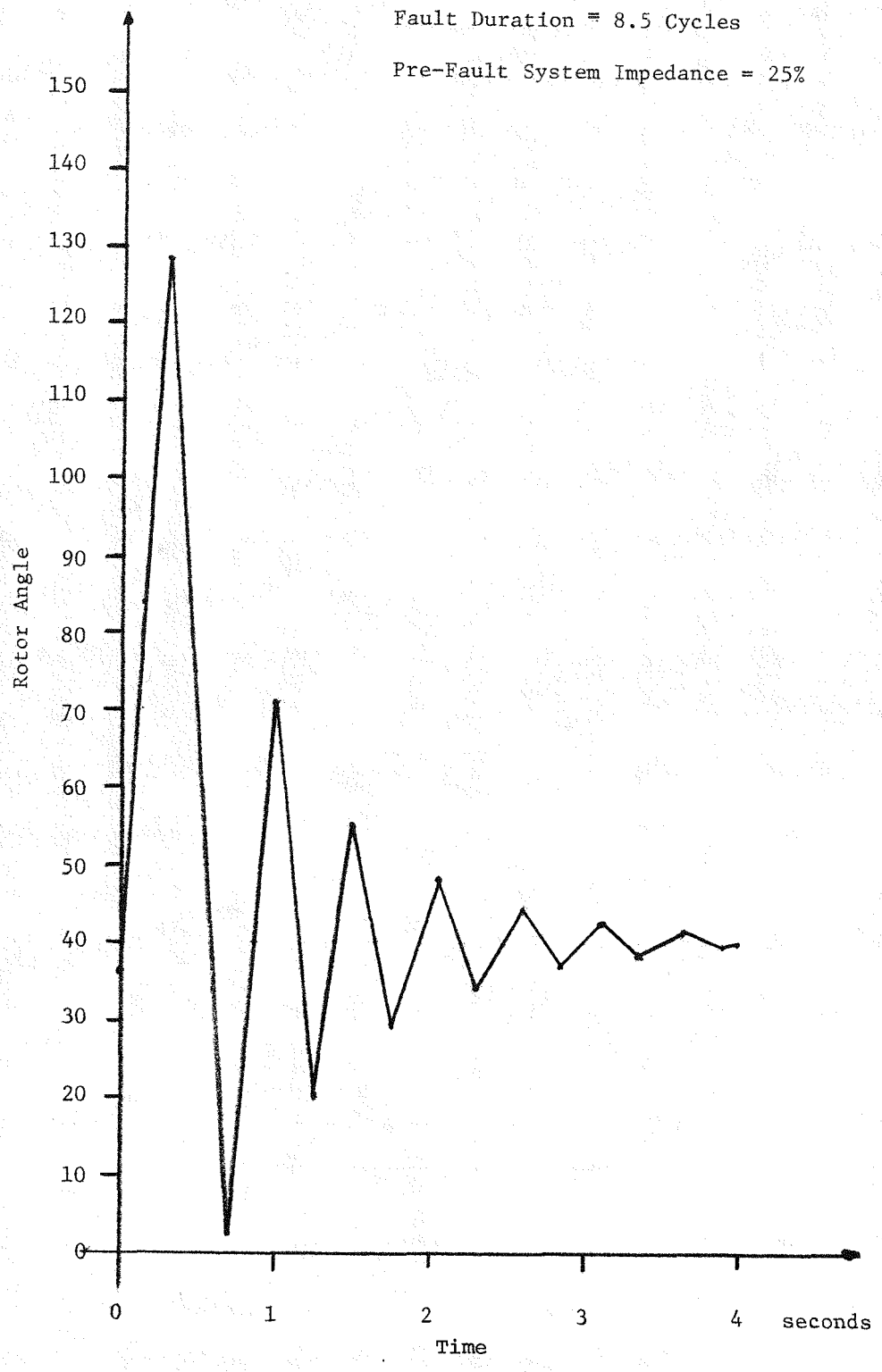

Figure 3-168. Rotor Angle Versus Time.

Table 3-69

GENERATOR CONSTANTS

MVA Base = 300

$X_d = .453$	$X'_d = .303$	$X''_d = .161$
$X_q = .453$	$X'_q \quad .453$	$X''_q = .161$
$X_L = .081$	$R_A \quad .003$	
$T'_{do} = 2800$ seconds	$T'_{qo} = 0.0$	
$T''_{do} = .205$*	$T''_{qo} = .205$*	
$H = 2.0$		

*Damper Time Constant

Table 3-70

SWING FREQUENCY OF GENERATOR

System Impedance	Fault Duration (Cycles)	Swing Frequency (Hertz)
.05	11.5	2.86
.15	9.5	2.17
.25	8.5	2.0

Fault Torques and Further Results on CFCT

The machine model used to carry out the parametric studies and to obtain the CFCT's and the swing curves as reported above incorporated rigid mechanical connection between the generator and the turbine. In order to obtain additional information on shaft torques over that discussed in Section 3.2, a more elaborate model was used. This incorporated mechanical compliance between the high pressure and low pressure turbine stages, between the generator rotor and the low pressure turbine (flexible shaft) and between the inner cold rotor and the warm outer rotor (damper shield). The electrical part of the model was expressed in terms of real phase quantities, e.g., i_a, i_b, i_c and the output of the program gave the time evolution of the electrical and mechanical quantities during and after a fault. Critical fault clearing times could also be obtained by running the program for varying fault periods.

The generators studied with this program were all 300 MVA and included a low voltage, conventional end turn armature unit and the two high voltage, spiral armature units with low (X''_d = 16%) and with high reactance (X''_d = 26%).

The CFCT's for these units are listed in Table 3-71. The parameters for the superconducting, conventional end turn machine are very close to those listed in Table 3-69 for a similar machine that was used in the shaft mode damping studies discussed below. Parameters for the spiral armature machines are given in Table 3-1 above in Section 3.1.1.

Table 3-71

CRITICAL FAULT CLEARING TIMES FOR 300 MVA GENERATORS

	CFCT	Cycles
Conventional	0.226 sec	13.6
Superconducting Conventional End Turn	0.233 sec	14.0
High Voltage Spiral Armature High Reactance	0.252 sec	15.2
High Voltage Spiral Armature Low Reactance	0.320	19.2

Figures 3-169 and 3-170 display the type of results that were obtained with the program with Figure 3-169 showing the air gap power and Figure 3-170 showing the shaft torques as functions of time. The generator in this case is the superconducting unit with a conventional end turn armature. The fault is on the high side of the unit transformer and is cleared in 0.229 sec.

Both figures display positive damping for the low frequency rotor swings (2 Hz) and for the oscillatory shaft mode (20 Hz). It must be pointed out that T''_{do} was taken as 0.07 sec, a value that is smaller than the actual value associated with the warm damper. The reason for using a smaller time

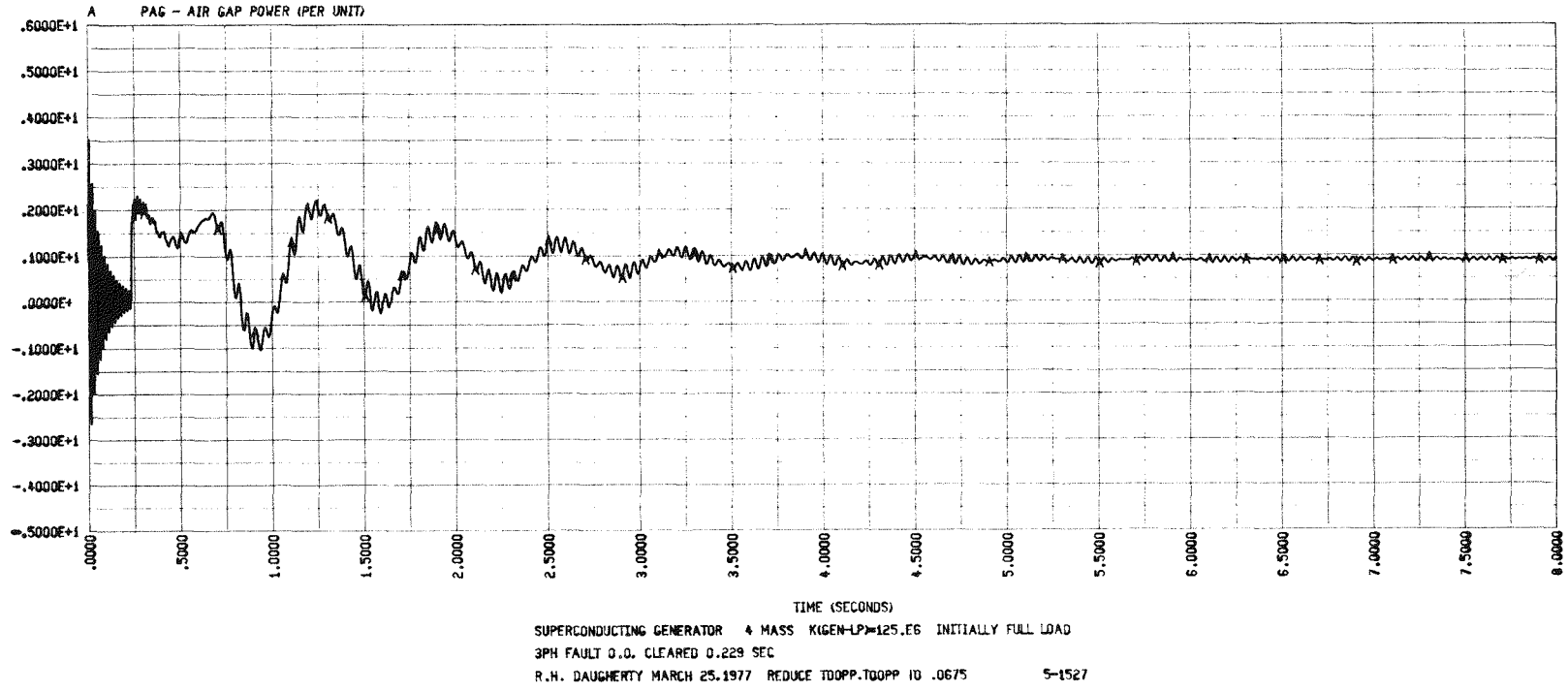
A PAG - AIR GAP POWER (PER UNIT)
.6000E+1
.5000E+1
.4000E+1
.3000E+1
.2000E+1
.1000E+1
.0000E+
-.1000E+1
-.2000E+1
-.3000E+1
-.4000E+1
-.5000E+1
.0000
.5000
1.0000
1.5000
2.0000
2.5000
3.0000
3.5000
4.0000
4.5000
5.0000
5.5000
6.0000
6.5000
7.0000
7.5000
8.0000
TIME (SECONDS)
SUPERCONDUCTING GENERATOR 4 MASS K(GEN-LP)=125.E6 INITIALLY FULL LOAD
3PH FAULT 0.0. CLEARED 0.229 SEC
R.H. DAUGHERTY MARCH 25.1977 REDUCE TDOPP.TQOPP TO .0675 5-1527

Figure 3-169

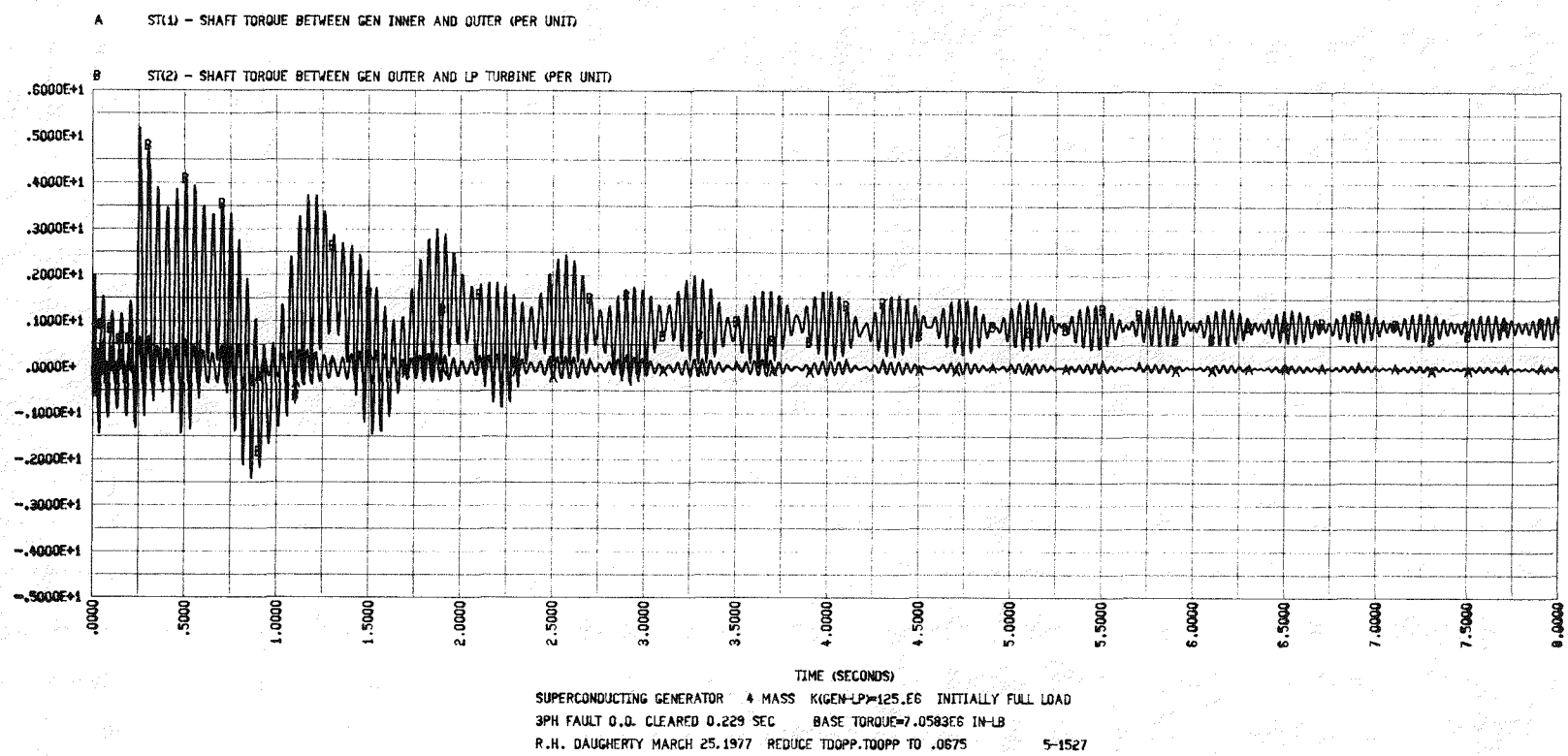
A ST(1) - SHAFT TORQUE BETWEEN GEN INNER AND OUTER (PER UNIT)
B ST(2) - SHAFT TORQUE BETWEEN GEN OUTER AND LP TURBINE (PER UNIT)
.6000E+1
.5000E+1
.4000E+1
.3000E+1
.2000E+1
.1000E+1
.0000E+
-.1000E+1
-.2000E+1
-.3000E+1
-.4000E+1
-.5000E+1
.0000
.5000
1.0000
1.5000
2.0000
2.5000
3.0000
3.5000
4.0000
4.5000
5.0000
5.5000
6.0000
6.5000
7.0000
7.5000
8.0000
TIME (SECONDS)
SUPERCONDUCTING GENERATOR 4 MASS K(GEN-LP)=125.E6 INITIALLY FULL LOAD
3PH FAULT O.C. CLEARED 0.229 SEC BASE TORQUE=7.0583E6 IN-LB
R.H. DAUGHERTY MARCH 25,1977 REDUCE TDOPP,TQOPP TO .0675 5-1527

Figure 3-170

constant was to approximate the damping that would be expected from both electromagnetic and mechanical. Since the present machine program cannot take mechanical damping directly into account, reducing the subtransient time constant is a means for representing the net mechanical and electro-mechanical damping. In the section below on calculations of the damping of the flexible shaft mode, the conclusion is that this mode is positively damped when both mechanical and electromagnetic losses are taken into account.

Table 3-72

ROTOR, SHAFT, AND SYSTEM CONSTANTS

Moment of Inertia

Inner rotor, 150 Nm sec^2

Outer rotor 730

LP turbine 1.0×10^4

HP turbine 2.7×10^3.

Spring Constant

Inner to outer rotor, 2.8×10^8 Nm/rad

Rotor to LP, 1.4×10^7

LP to HP, 4.6×10^7

System After Fault

x = 0.17 pu (includes transformer)

r = 0.09.

Figure 3-170 shows the large torques in the flexible shaft immediately after the fault has been cleared at times close to the CFCT for the machine. If the fault is cleared earlier, at about 0.07 sec, then the maximum torques are appreciably smaller. This is illustrated in Figure 3-171 where the clearing time is varied from 0.065 sec up to 0.080 sec. This data is again for the superconducting generator with the conventional end turn armature.

Runs have also been made for the 300 MVA machines with the high voltage, spiral armature. Here the unit transformer is removed and the fault is at the terminal of the generator. For the high reactance design (X''_d = 0.27 pu) the peak torques are close to those shown in Figures 3-170 and 3-171. However, for the low reactance design (X''_d = 0.16) the peak torques are appreciably larger as would be expected.

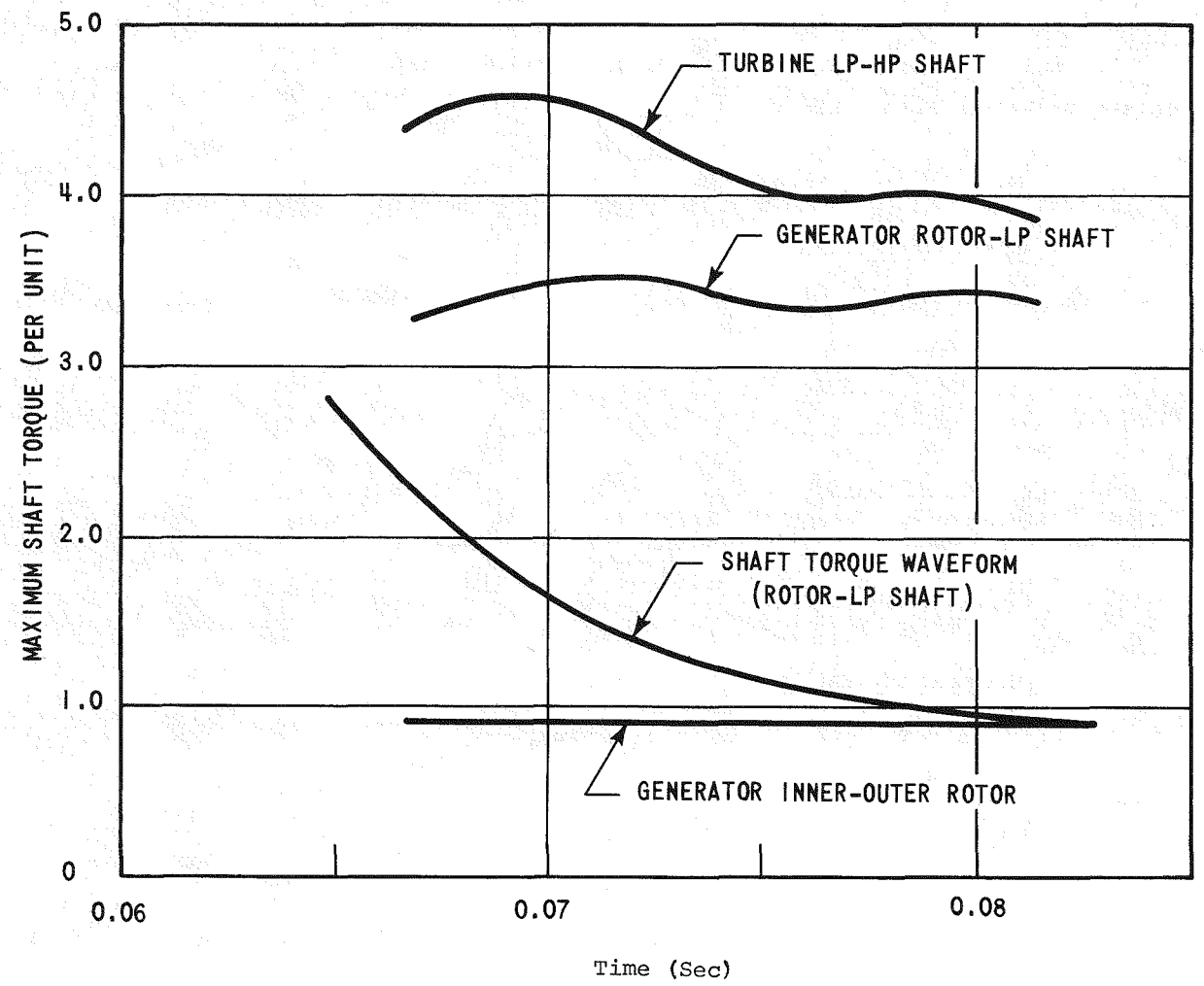

Figure 3-171. Torques Versus Clearing Times, 300 MVA Superconducting Generator.

Frequency of Faults and Line Interruptions

Low frequency oscillation of the superconducting generator rotor with respect to the system will produce eddy currents in the rotor surface. These currents will generate heat and impose a burden on the refrigeration system used to cool the cryogenic winding. The refrigeration equipment must be capable of handling this extra heat burden. It is therefore important to determine what system conditions can cause the rotor to oscillate at low frequency and how often such conditions can occur.

Rotor oscillations will occur whenever a transient mismatch occurs between the electrical power flowing from the machine and the turbine power. Such a mismatch can occur under the following conditions:

Faults

Faults on the transmission lines leaving the generating station will produce rotor oscillations. Little information concerning the frequency of transmission line faults is available. Small quantities of data were obtained from the IEEE working group on "High Speed Switching Effects on Turbine Generators". The data are for one power system and are depicted in Table 3-73.

Table 3-73

FAULT FREQUENCY

Transmission Line Voltage (kV)	Fault Frequency Per 100 Circuit Miles Per Year
230	4
500	1.5

Assume three 100 mile long transmission lines are used to transmit power from the generator to a load center. Then one would expect 12 faults per year if the transmission voltage is 230 kV or about 5 faults per year if the transmission voltage is 500 kV.

Assuming high speed reclosing is not utilized, the frequency of fault occurrence depicted in Table 3-73 is a valid measure of how often the rotor will be subjected to rotor oscillations as a result of transmission line short circuits. If high speed re-closing is used, a single fault could result in multiple disturbances to the generator rotor over a short time interval. The machine could suffer several additional shocks over a period of time ranging from 1 to 30 seconds.

False Line Interruptions

False line interruptions could be caused by personnel error or equipment failure. Such a line interruption would cause the machine rotor to oscillate. From the IEEE working group on "High Speed Switching Effects on Turbine Generators", the following data on the frequency of false line interruptions were obtained. The data are for one power system.

Table 3-74

FREQUENCY OF FALSE LINE INTERRUPTIONS

Transmission Line Voltage (kV)	False Line Interruption Frequency per 100 Circuit Miles Per Year
230	3.8
500	3.5

Assume three 100 mile long transmission lines send power from the plant to the load center. Then one would expect approximately 11 false line interruptions per year if the transmission voltage is 230 kV, or about 10 false line interruptions per year if the transmission voltage were 500 kV.

Line Switching Due to Maintenance

Occasionally a line must be switched out of service so repairs can be made. This operation will result in machine oscillations. How often this event occurs is difficult to determine. Utilities try to avoid removing a line from service for repairs.

Steady State Stability

The choice of generator reactance will affect the stability of the superconducting machine. The lower the generator reactance, the more stable the machine will be.

For a superconducting generator, the per unit synchronous reactance will be approximately 1/3 the synchronous reactance of a conventional machine of similar rating. This will result in an improvement in the steady state ability of the superconducting machine compared to a conventional machine. The cryogenic generator will be capable of operating more under-excited or on a weaker power system than a conventional unit. This assumes that the machine

thermal capability will not limit generator operation. Therefore, steady state stability considerations indicate that the synchronous reactance of the superconducting machine be as low as possible.

Regulation Under Load Change

Figure 3-172 compares the performance of a superconducting generator with a conventional generator, both 300 MVA, for a 20% VAR overload. The superconductor generator is limited by a 300 volt excitor ceiling while the conventional generator utilizes a standard response ratio. It is to be noted that the superconducting generator has better performance than the conventional for this type of overload.

Figure 3-173 shows the performance of superconducting generator and Figure 3-174 the performance of a conventional unit after full load rejection. The figures give the generator voltage, the volts/Hz and the speed as a function of time after load rejection for these two units. The performance differs mainly in that the superconducting generator overshoots in voltage by 18% while the conventional maximum is 12%.

Generator-Turbine Shaft Mode Damping

While low reactance designs have the advantage of improved system stability, e.g., longer CFCT's, they have the disadvantage of being subjected to large oscillating fault torques. One crucial question that the designer is faced with is whether these torques are higher than can be handled by turbine shafts. This may not be a problem for the higher rated superconducting genertors that will be on line 10 to 15 years from now and at which time turbine shafts could be designed to accommodate these torques. However for the first demonstration machine that will be tested on an existing turbine, it is a problem when the fault torques on the rotor can be as high as 7 pu while the turbine is designed for only 3 pu torques.

One solution to this problem, which proposed by Westinghouse, is to insert a flexible shaft between the rotor and turbine. By setting the resonant frequency of rotor mass-shaft spring constant low enough, the 60 Hz fault torques can be attenuated to below 3 pu at the turbine.

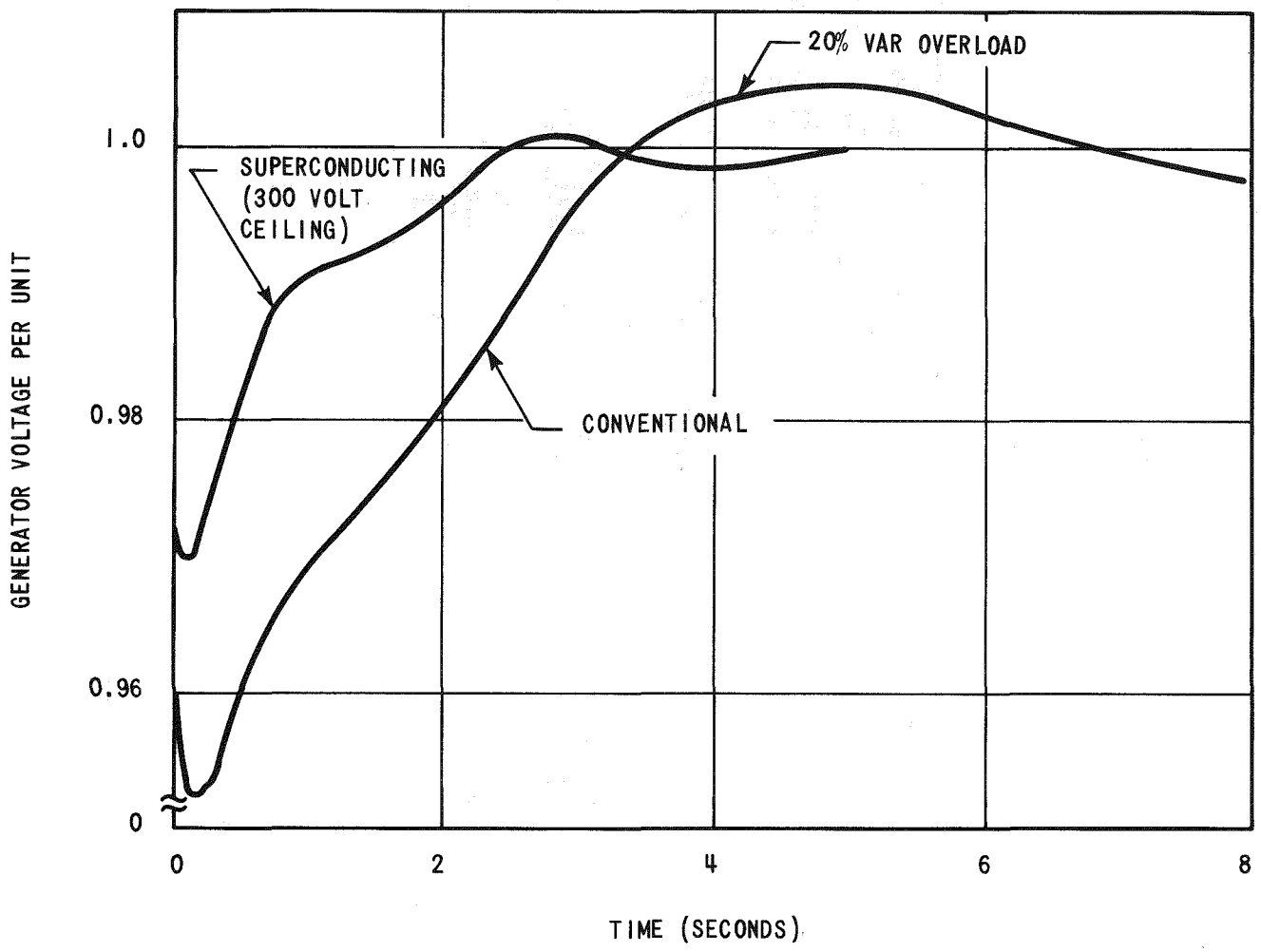

Figure 3-172. Generator Voltage Versus Time for 20% (60 MVAR) VAR Overload.

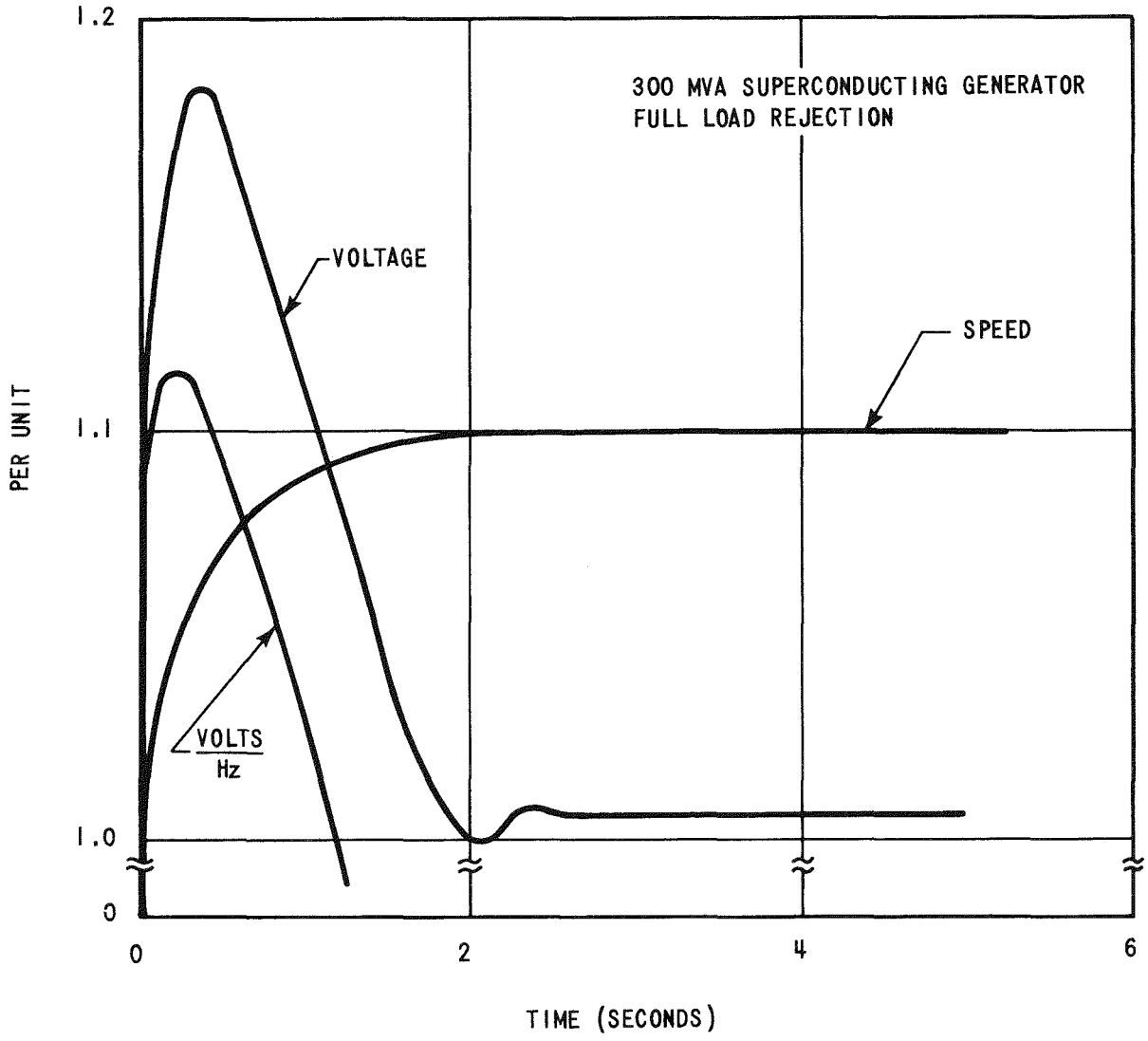

Figure 3-173. Generator Voltage, Volts/Hz and Speed Following a Full Load Rejection-Superconducting.

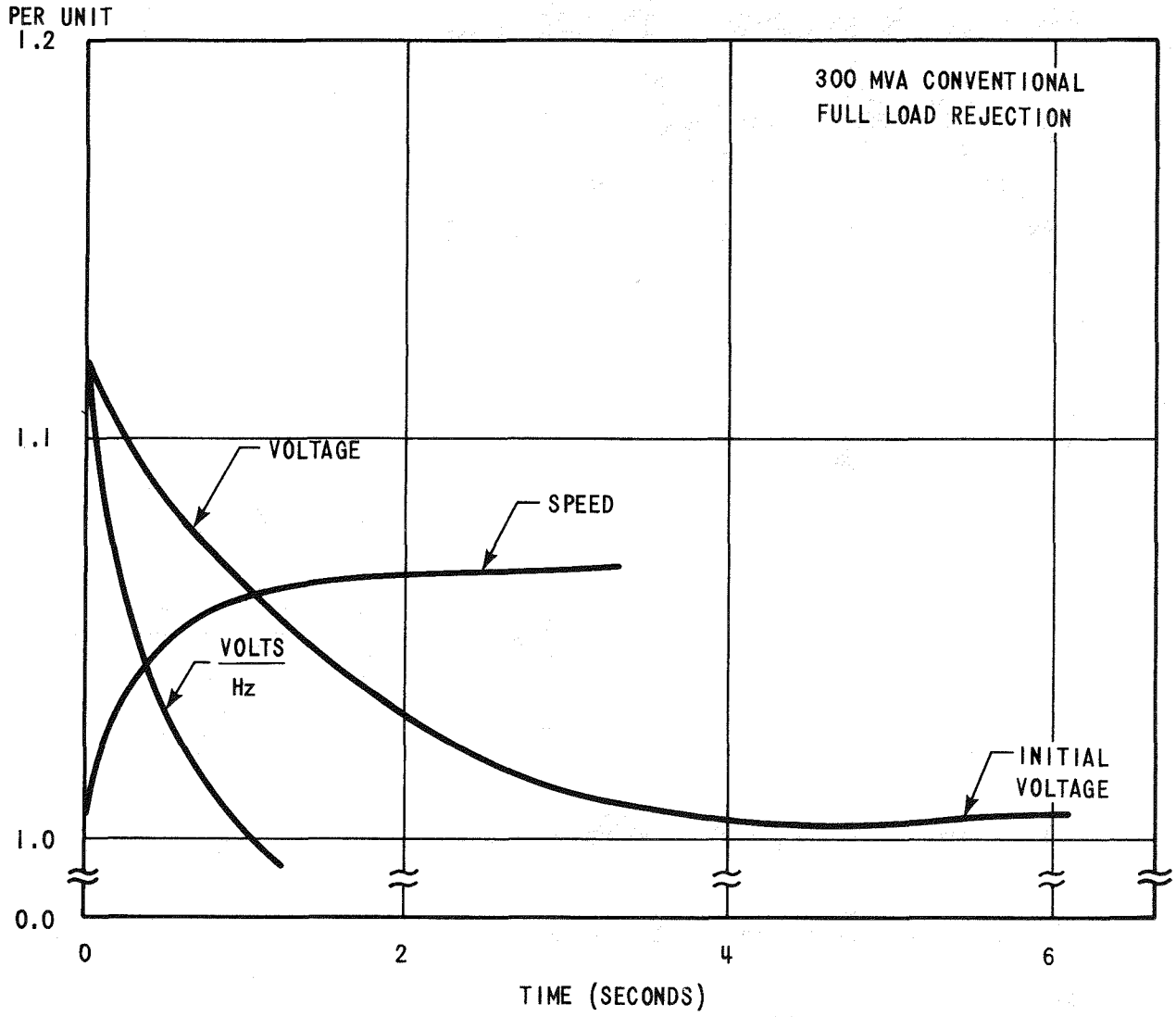

Figure 3-174. Generator Voltage, Volts/Hz and Speed Following a Full Load Rejection-Conventional.

While it appears that this design feature does give adequate torque attenuation, there arises the question of whether this new mechanical mode will be sufficiently damped so as not to go in self-oscillation and thereby lead to excessive shaft stresses. The purpose of the present section is to analyze the electromagnetic damping for the 300 MVA design in the region of this flexible shaft mode, i.e., about 20 Hz.

During conditions of rotor oscillations about its operating point, there are currents induced which react with the machine flux to produce spring torques and damping torques. The damping torques arise through those components of current associated with the system resistances; power dissipation is a necessary requirement for damping. The damping associated with the damper shield resistance is positive, tending to reduce the oscillations. That associated with the armature and external circuit resistance is negative, tending to accentuate the oscillations. There has been concern expressed that in a superconducting generator, with its relatively low damper resistance, the negative damping may be greater than the positive damping, leading to the "self-excited instability." This phenomenon has been observed on a small, experimental superconducting generator.*

Three approaches have been developed to study this problem. The first is a relatively simple equivalent circuit approach similar to that used in induction motor analysis. The second approach involves a complete solution of the currents and flux linkages in a thin winding, two-phase machine. The third approach linearizes the Park's equations to obtain the damping torques. These three approaches, and the results obtained, are discussed below.

Equivalent Circuit Method

The rotor is assumed to be oscillating at a frequency ω_M with an amplitude Δ. Using the principle of superposition, a voltage can be injected in the stator to cancel any current induced by this oscillation. Since it is unopposed, the flux change at right angles to be flux trapped by the damper, E", will be ΔE". (E" is the "voltage behind subtransient reactance".) We can solve the equivalent circuit of the machine for this voltage applied in reverse to get the oscillating components of current.

---

*P. Thullen, J. C. Dudley, D. L. Greene, J. L. Smith, Jr., "An Experimental Alternator with a Superconducting Rotating Field Winding," IEEE Trans. P.A.S., Vol. PAS-90, No. 2, March/April 1971, p. 611.

The slip of the oscillation as seen by the rotor is defined by

$$S = \omega_M/\omega_o$$

where ω_o = line frequency

Thus, the equivalent rotor resistance will be r_2/S, when r_2 is the damper shield resistance. The stator sees the oscillation as two half amplitude ($\Delta/2$) waves rotating in opposite directions, one at a frequency $\omega_o + \omega_M$, and one at a frequency $\omega_o - \omega_M$. Thus, there are two equivalent stator resistances, one for the forward traveling wave and one for the backward traveling wave, given by

$$r_+ = \frac{r_1}{1 + S}$$

$$\text{and } r_- = \frac{r_1}{1 - S}$$

where r_1 = primary resistance, including both stator winding and external circuit resistance.

The components of induced current due to the oscillating flux can be found using the complex impedances

$$i = \frac{\Delta E"}{Z_r} + \frac{1}{2}\Delta E" \left(\frac{1}{Z_+} - \frac{1}{Z_-}\right)$$

where

$Z_r = x + r_2/S$

$Z_+ = x + r_+$

$Z_- = x + r$

$x = x" + x_e$

$x"$ = subtransient reactance

x_e = external circuit reactance

These currents are induced primarily on the direct axis, but there are in-phase components on the quadrature axis which react with the direct axis flux (E") to produce the damping torques. The in-phase components are proportional to the ratio of resistance to impedance of the circuit. The torque thus produced is given by

$$T = E"\left[\frac{\Delta E"}{Z_r}\left(\frac{r_2}{SZ_r}\right) + \frac{\Delta E"}{2Z_+}\left(\frac{r_+}{Z_+}\right) - \frac{\Delta E"}{2Z_-}\left(\frac{r_-}{Z_-}\right)\right]$$

Since the impedance is primarily reactive, the resistive component can be neglected to simplify the expression to

$$T = \Delta\left(\frac{E''}{x}\right)^2 \left(\frac{r_2}{S} - \frac{Sr_1}{1 - S^2}\right)$$

There is another smaller component of damping torque resulting from the reaction of the quadrature axis load current with the small oscillation of flux which is out of phase with the initial $\Delta E''$. The assumed initial flux change induces currents causing the actual flux change to be ahead in time phase. This fraction (in time phase with velocity) will be $\Delta r_1/A$, and the resulting torque is

$$T = E'' \frac{\Delta}{2Z} (r_+ - r_-) \; I \sin \alpha$$

where I = load current

α = angle between I and E" = $\Theta + \delta$

Θ = power factor angle

δ = load angle

The total damping torque is thus given by

$$T = \Delta\left(\frac{E''}{x}\right)^2 \left[\frac{r_2}{S} - \frac{Sr_1}{1 - S^2} \left(1 + \frac{x}{E''} \; I \sin \alpha\right)\right]$$

and the damping constant T/Δ is

$$D = \left(\frac{E''}{x}\right)^2 \left[\frac{r_2}{S} - \frac{Sr_1}{1 - S^2} \left(1 + \frac{x}{E''} \; I \sin \alpha\right)\right]$$

Thus, when the quantity r_2/S^2 is less than the term proportional to r_1, we can expect a net negative electrical damping.

Complete Solution Method

In this method, which was described in detail in Quarterly Report No. 4, the torque is found from a complete solution of the current and flux densities in the machine. The generator is modeled as a system of five coils: a field coil, direct and quadrature axis damper coils, and direct and quadrature axis stator coils. The rotor direct axis is displaced from the stator direct axis by an angle Θ, which varies as

$$\Theta = \Delta \sin \omega_M t$$

The currents in each coil are found by solving the voltage balance equation

$$\text{TERMINAL VOLTS} = \text{IR drop} + \frac{d}{dt}\ (\text{flux linkage})$$

An iron shield is included in the model for the flux linkage calculation.

The force on a coil element is found by the relationship

$$dF = BL\ dI$$

where B = flux density at the element

L = coil length

dI = current in the element

The tangential component of force is multiplied by the moment arm (radius of the coil), and integrated over the entire coil to compute the torque. The component of torque which varies as cos $\omega_M t$ is in phase with the oscillation velocity, and is identified as damping torque. The damping constant is this damping torque divided by the amplitude Δ of the oscillation.

Park's Equation Approach

The third approach to calculating damping torques is by linearizing Park's equations for a small angular oscillation of the rotor relative to the synchronous, steady state rotor position. That is, the rotor position angle can be expressed as

$$\Theta = \omega_o t + \phi$$

and

$$\phi = \phi_o \sin \omega_m t$$

where ω_o is the synchronous shaft rotational frequency, ω_m is the frequency and ϕ_o is the amplitude of the shaft mode. The expression for Θ, when used as the angle variable in the Park's transformation, leads to zero and first order equations in ϕ. The zero order equation represents the steady operation of the machine while the first order equations express the incremental changes in direct and quadrature axis quantities in terms of the angular driving time ϕ and $\dot{\phi}$. The incremental amplitudes can then be used to obtain the damping torque using the general torque expression

$$T = \frac{3}{2}\ (i_d \Psi_q - i_q \Psi_d) \qquad (1)$$

The frequencies of interest for ω_m are sufficiently high so that the skin depth in the warm damper is less than its thickness. It is therefore a good approximation to take the field current as constant and the inner cold shield currents as zero. This leaves only four Park's equations that are first order in ϕ which must be considered and solved for the incremental changes in i_d, i_q, i_{ds} and i_{qs}.

Utilizing the above approximations, the Park's equations, first order in ϕ, can be written (in absolute units and with generator current convention) as

$$\phi V_q = - rI_d + M_s \frac{dI_{sd}}{dt} - L \frac{dI_d}{dt} - \omega_o M_s I_{sq} + \omega_o L I_q + Li_{qo} \frac{d\phi}{dt}$$

$$-\phi V_d = - rI_q + M_s \frac{dI_{sq}}{dt} - L \frac{dI_q}{dt} + \omega_o M_s I_{sd} - \omega_o L I_d + (M_f I_{fo} - Li_{do}) \frac{d\phi}{dt}$$

$$0 = r_s I_{sd} + L_s \frac{dI_{sd}}{dt} - \frac{3}{2} M_s \frac{dI_d}{dt}$$

$$0 = r_s I_{sq} + L_s \frac{dI_{sq}}{dt} - \frac{3}{2} M_s \frac{dI_q}{dt}$$

where

$$i_d = i_{do} + I_d$$

$$i_q = i_{qo} + I_q$$

with i_{do} and i_{qo}, the steady state current and I_d and I_q are the first order (in ϕ) currents.

The generator is taken as being connected to the system with series external reactance and resistance and terminating in an infinite bus. This is illustrated in Figure 3-175 along with a steady state phasor diagram of the generator and system. It is to be noted that V_s is the infinite bus voltage and δ' is the phase angle between the machine internal voltage $\omega_o M_f I_{fo}$ and the bus voltage. The quantities in the equation L and r are

$$L = L_d + L_{ext}$$

$$r = r_d + r_{ext}.$$

M_s is the mutual inductance between armature and warm shield, L_s is the self inductance of the shield, L_f is the field winding self inductance and I_{fo} is the dc field current.

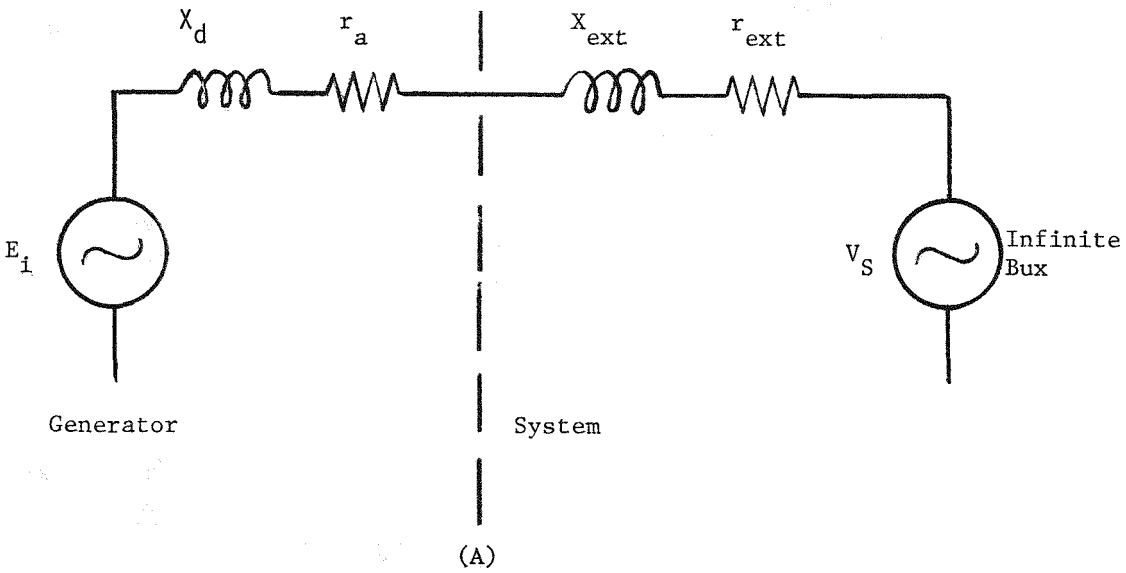

(A)

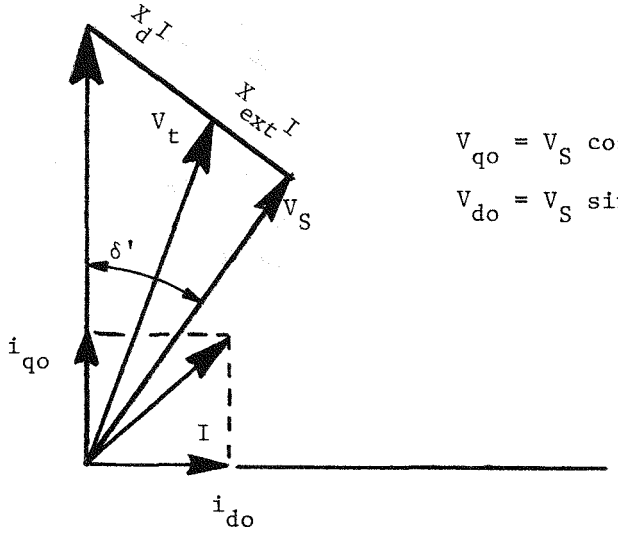

$E_i = \omega_o M_f I_{fo}$

$V_{qo} = V_S \cos \delta'$

$V_{do} = V_S \sin \delta'$

(B)

Figure 3-175. (A) Schematic of Generator - System
(B) Steady State Phasor Diagram

The torque [Eq. (1)] when expressed to first order in ϕ can be written as,

$$T = \frac{3}{2}\left(M_s i_{do} I_{sq} - M_s i_{qo} I_{sd} - M_f I_{fo} I_q\right) .$$

Putting $\phi = \phi_o e^{j\omega mt}$, and solving the Park's equation for the current amplitudes required in the torque equation, gives the following expression for the complex torque.

$$\left(T/\frac{d\phi}{dt}\right)\frac{2\omega_o^2\,(Y_1^2 + Y_2^2)}{3} = \left[\left(E_i i_{do} - XI^2\right) - \frac{j}{\beta}\left(V_{qo} i_{qo} + V_{do} i_{do}\right)\right] Y_1 Z_s$$

$$+ \left[-E_i i_{qo} + \frac{j}{\beta}\left(V_{do} i_{qo} - V_{qo} i_{do}\right)\right] Y_2 Z_s$$

$$+ \left[-E_i\left(E_i - X i_{do} i_{qo}\right) + \frac{jV_{do}E_i}{\beta}\right] Y_1$$

$$+ \left[E_i X i_{qo} + \frac{jV_{qo}E_i}{\beta}\right] Y_2$$

where

$$Y_1 = j\beta X'' + (r + \bar{r}_s)$$

$$Y_2 = X'' - j\frac{\bar{r}_s}{\beta}$$

$$Z_s = \bar{X}_s + j\frac{\bar{r}_s}{\beta}$$

with

$$X = \omega_o L$$

$$X'' = X - \bar{X}_s$$

$$\bar{X}_s = \frac{3}{2}\left(\frac{M_s}{L_s}\right)^2 \omega_o L_s$$

$$\bar{r}_s = \frac{3}{2}\left(\frac{M_s}{L_s}\right)^2 r_s$$

and

$$\beta = \frac{\omega_m}{\omega_o}$$

Note that this expression is still in absolute units but it can be easily transformed to the per unit system.

It should be evident from the above expression that the real part of T is the damping term and the imaginary part is the spring constant term, i.e.,

$$\text{Real } (T) = - R \frac{d\phi}{dt}$$

and

$$I_m \ (T) = - k_{em} \ \phi$$

The quantity R can also be expressed as

$$R = \frac{D}{\omega_m} = \frac{2I}{\tau}$$

where D is the damping constant (Nm/rad), I is the rotor moment of inertia and τ is the shaft mode decay time.

The electromagnetic spring constant K_{em} can be used to calculate ω_s from

$$-I \ \omega_m^2 + k + k_{em} \ (\omega_s) = 0$$

where k is the mechanical spring constant of the shaft. This model assumes that the inertia of the turbine is large in comparison to the rotor moment of inertia.

The approach given above to calculate the damping torque, takes the angular oscillation as given and uses it as a steady state driving term in the equations for direct and quadrature axis currents. These currents are then used to obtain the torque as a function of shaft mode frequency, ω_m. This approach seems simpler than to obtain the complete set of eigenvalues for the system of equations made up of the Park's equations plus the mechanical equation. Both of these methods should yield identical results if applied correctly.

Results, Early Reference Design

In order to obtain results from each of these three methods, the damper resistance referred to the armature must be determined. This is done by calculating the power dissipated under full armature current at the oscillation frequency (with respect to the rotor), using the methods developed in the second quarter of this program for calculating damper shield loss. The per unit value of the damper resistance is then equal to this power dissipated, in per unit. The variation of the resistance with frequency for the damper shield of the 300 MVA reference generator is shown in Figure 3-176. Also plotted is skin depth, illustrating the increase in resistance as skin depth is decreased.

The simplified method of analysis gives a damping constant in per unit torque per unit displacement. Therefore, it must be multiplied by rated torque to give the damping constant D, in newton-meters/radian.

All three methods have been used to compute the damping constant for the first 300 MVA reference generator design as a function of oscillation frequency, f_m. Three conditions have been considered:

- No load, primary resistance of 2%
- Full load, primary resistance of 1%
- Full load, primary resistance of 2%

The results are plotted in Figures 3-177 and 3-178.

As can be seen from these figures, all three methods agree very well for the no load condition, but the circuit method deviates significantly for the full load conditions. This suggests that the equivalent circuit method does not correctly represent the effect of load current.

It is felt that if the damping constant is positive, or only slightly negative, then the performance will be stable, because there is still mechanical positive damping. The mechanical hysteresis in the shaft contributes to the positive damping, and thus will compensate for slightly negative electrical damping. Since all methods indicate only a slight negative damping at the expected frequency (20 Hz) and at the upper limit of expected primary resistance (2%), it is felt that the damping in this machine will be adequate.

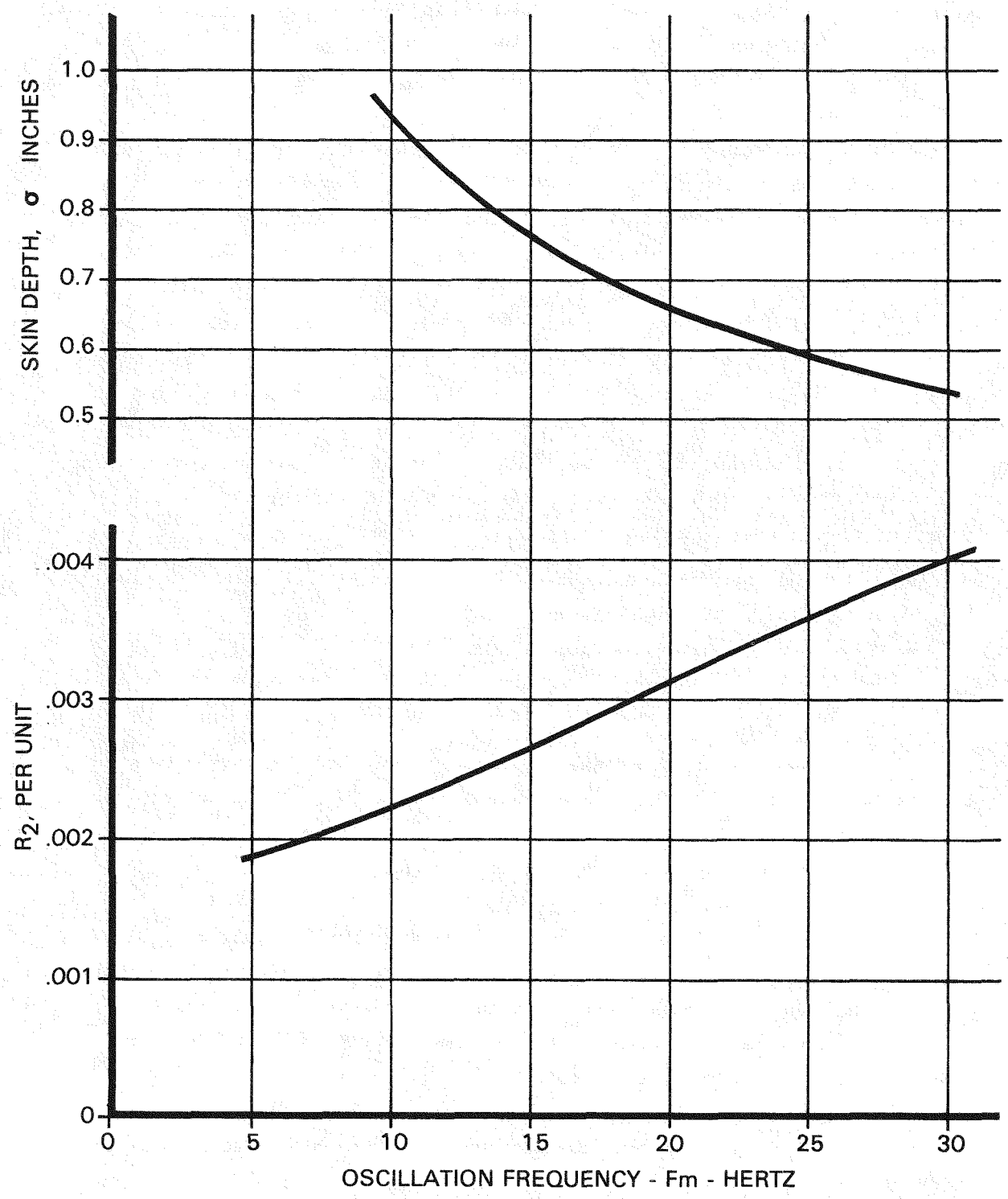

Figure 3-176. Secondary Resistance and Skin Depth Versus Frequency.

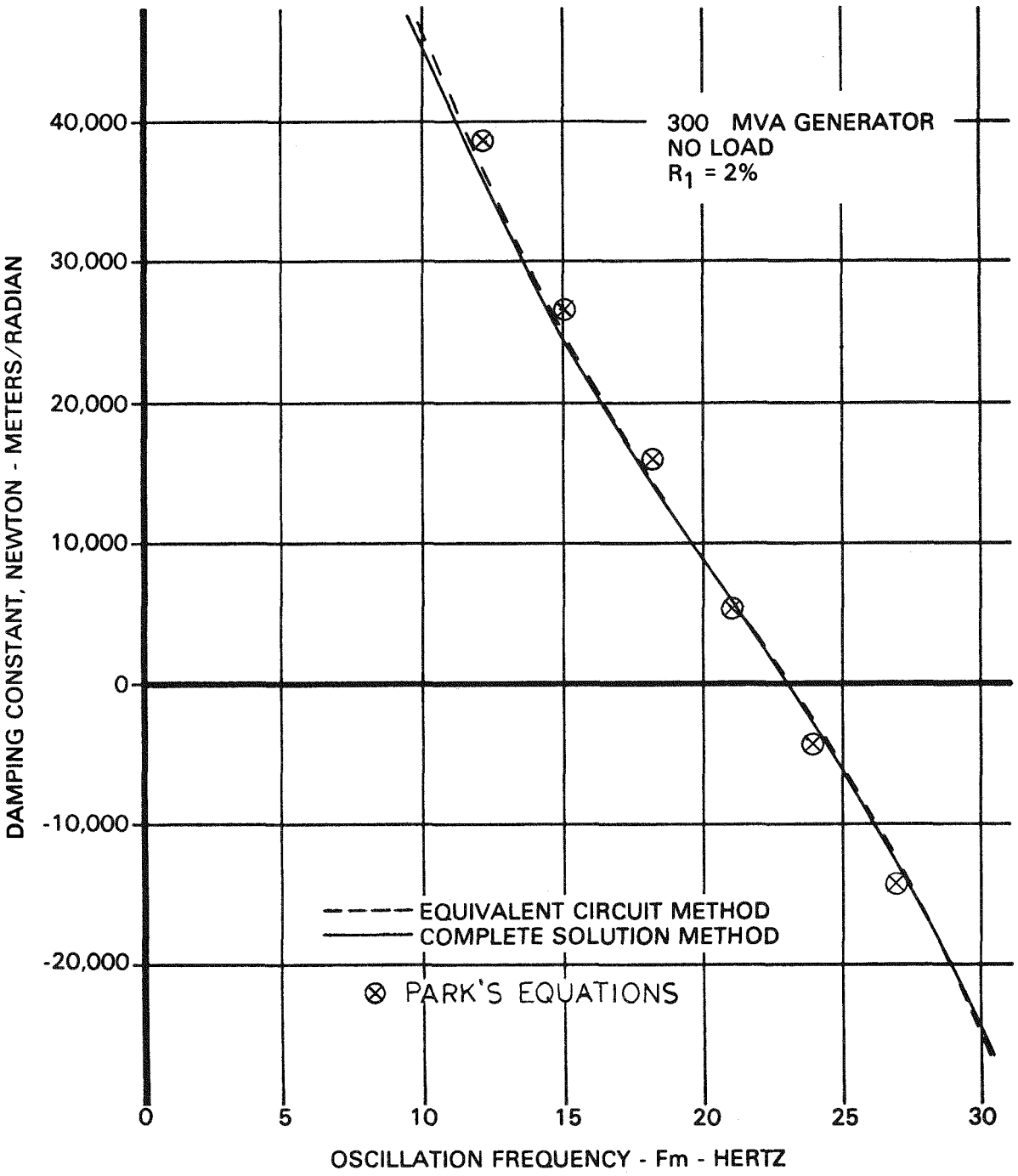

Figure 3-177. Damping Constant Versus Frequency - No Load.

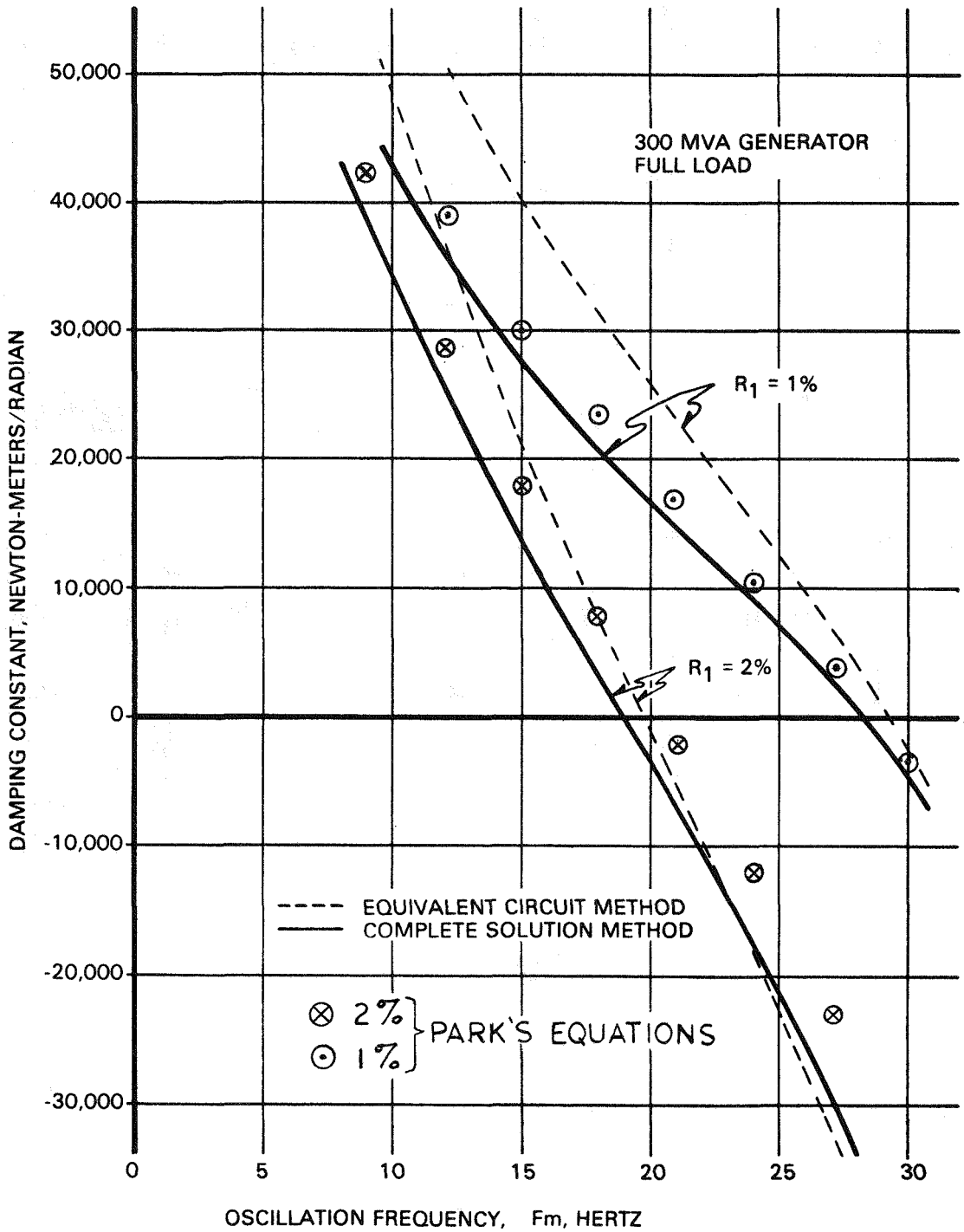

Figure 3-178. Damping Constant Versus Frequency - Full Load.

Machine Parameters

The damping results given in Figures 3-177 and 3-178, as given by the three independent approaches, are for a conventional end turn, 300 MVA early reference design. Its parameters are listed in Table 3-75 along with the parameters for the low-voltage and high-voltage spiral armature designs.

Results, Low- and High-Voltage Spiral Armature Design

Damping results are given for the low- and high-voltage spiral armature designs in Figures 3-179 and 3-180. These results are for 1% and 2% system resistance and were obtained using the Park's equation approach. The relevant parameters for these two machines are given in Table 3-75.

It is evident from the plots that with a 2% resistance, which is taken as representative of a long transmission line case, that the electromagnetic damping is just on the borderline of yielding stable operation with a shaft mode of 18 Hz. It is to be noted that the high-voltage machine is more stable than the low-voltage machine.

These results do not, of course, include mechanical damping. A representative number for mechanical damping can be taken as a logarithmic decrement (L) of 0.008. This is about equally split between shaft damping and steam damping. The damping constant, D, can be expressed in terms of the logarithmic decrement, L, as

$$D_{mech} = \frac{I\ L\ \omega_m^2}{\pi}$$

This gives $D_{mech} \simeq 33{,}000$ for the high- and low-voltage machines with f_m 18 Hz. With this positive mechanical damping, the net damping for all of the machines covered in this section will be positive at the shaft mode frequency of 18 Hz.

Impact of Flexible Shaft Oscillation on CFCT

The potential and kinetic energies for the model system shown in Figure 3-181 are,

$$V(\theta_g, \theta_t) = K_m(1 - \cos \theta_g) + 1/2\ K_S(\theta_g - \theta_t)^2,$$

$$KE = 1/2\ I_g \dot{\theta}_g^{\,2} + 1/2\ I_t \dot{\theta}_t^{\,2}$$

Table 3-75

300 MVA MACHINE PARAMETERS FOR SHAFT DAMPING

Parameter	Conventional End Turn	Low-Voltage Spiral	High-Voltage Spiral
Rotor Resistance (referred to stator)	0.003 pu @ 18 Hz	0.0023 pu @ 20 Hz	0.0020 pu @ 20 Hz
Armature Plus System Resistance	0.01 pu 0.02	0.01 pu 0.02	0.01 pu 0.02
Synchronous Reactance	0.45 pu	0.42 pu	0.493 pu
Subtransient Reactance	0.16 pu	0.16 pu	0.27 pu
System Reactance	0.25 pu	0.25 pu	0.13 (No Transformer)
PU Reactance Base	0.67 Ω	0.62 Ω	176 Ω
Terminal Voltage (L-N)	8182 V RMS	7868 V RMS	133 kV
Power Factor	0.9	0.9	0.9
Damper Dimensions			
• Copper Alloy Radius (2×10^{-8} Ω-m)	0.33, 0.36 m	0.35, 0.38 m	0.35, 0.38 m
• Support Shell Thickness (10^{-6} Ω-m)	0.03 m	0.029 m	0.029 m
Armature Induction (1 pu)	0.51 T	0.36 T	0.29 T
Rotor Inertia (kg-m^2)	870	994	1160

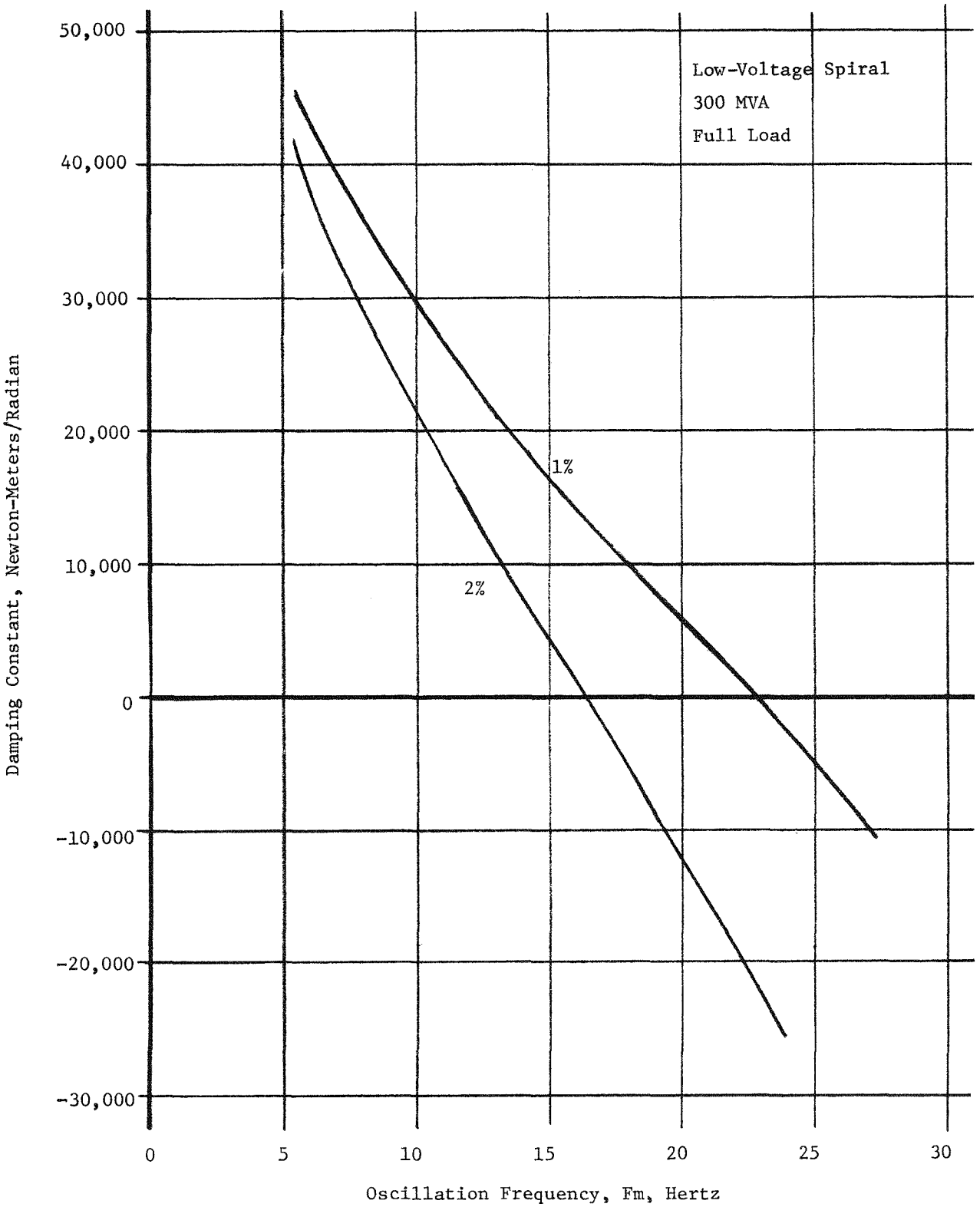

Figure 3-179. Damping Constant Versus Frequency - Low-Voltage Spiral, Full Load.

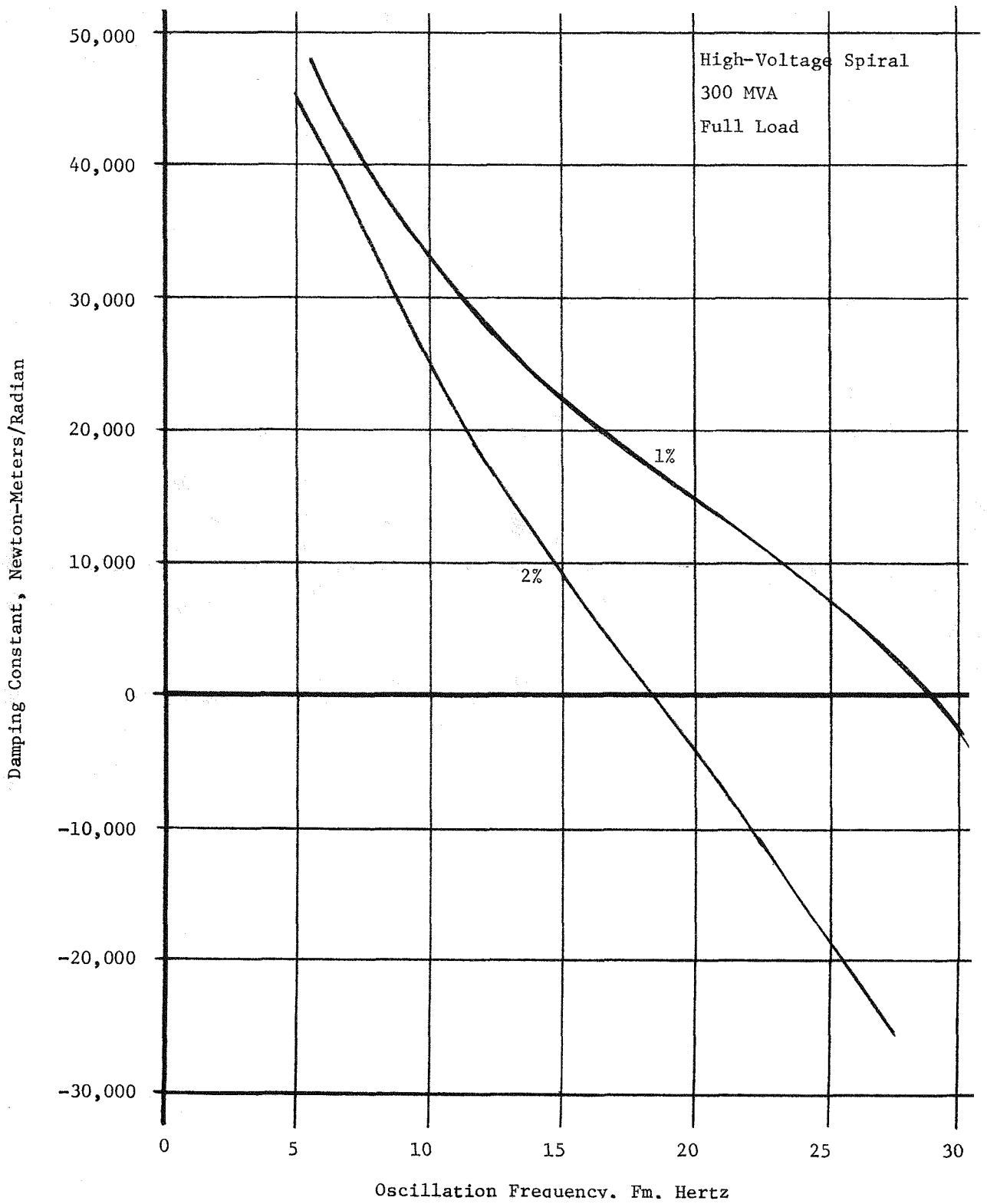

Figure 3-180. Damping Constant Versus Time - High-Voltage Spiral, Full Load.

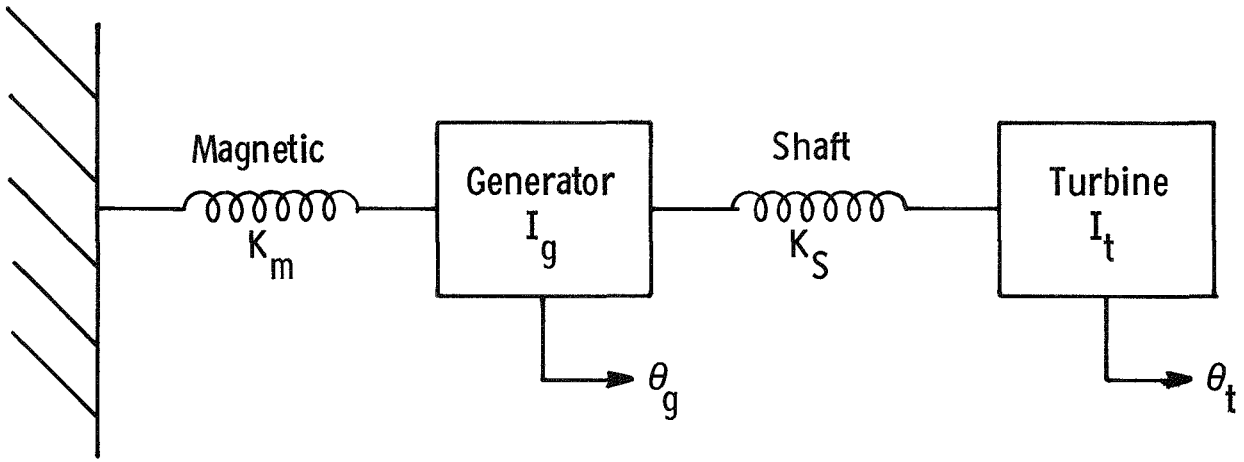

Figure 3-181. Model System.

where K_m and K_S are the magnetic and shaft spring constants and I_g and I_t are the moment of inertia for the generator and turbine respectively. The coordinates θ_g and θ_t are the angular position of the generator and turbine rotors relative to the synchronous shaft position. The kinetic energy expression represents that part of the total kinetic energy suitably for discussing shaft deviations from this synchronous position.

We can now transform to new coordinates S and Δ.

$$\theta_g = S + \frac{I_t}{I}\Delta$$

$$\theta_t = S - \frac{I_t}{I}\Delta \qquad (1)$$

or

$$S = \frac{I_g}{I}\theta_g + \frac{I_t}{I}\theta_t$$

$$\Delta = \theta_g - \theta_t$$

where

$$I = I_g + I_t$$

Then the potential and kinetic energies become

$$V(\Delta, S) = K_m[1 - \cos(\frac{I_t}{I}\Delta + S)] + 1/2\ K_S\Delta^2 \qquad (2)$$

$$KE = 1/2\ I_R\ \dot{\Delta}^2 + 1/2\ I\ \dot{S}^2$$

where

$$I_R = I_g I_t / I$$

As is evident, Δ is the relative coordinate between the generator and turbine and S is the center of mass (inertia) coordinate. The coordinates Δ and S are appropriate zero order coordinates, since for the linearized problem (small S) and in the limit of small K_m/K_S, these are the normal coordinates. It is to be noted that in the present case K_m/K_s is about 1/10. Therefore the approach is to consider both the effect of finite K_m/K_S and the non-linearity of the magnetic spring as the perturbation away from the zero order case.

Expanding Equation (2) yields

$$V(\Delta, S) = K_m[1 - \cos (\frac{I_t}{I} \Delta) \cos S + \sin (\frac{I_t}{I} \Delta) \sin S] + 1/2\ K_S\ \Delta^2$$

Now using $L = KE - V$ and (3)

$$\frac{d}{dt} \frac{\partial L}{\partial \dot{q}_i} - \frac{\partial L}{\partial q_i} = 0$$

where $q_i = \Delta$ or S, gives the homogeneous equations of motion.

$$I_R \ddot{\Delta} + K_S \Delta + K_m \frac{I_t}{I} [\sin (\frac{I_t}{I} \Delta) \cos S + \cos (\frac{I_t}{I} \Delta) \sin S] = 0 \qquad (4)$$

and

$$I\ddot{S} + K_m [\cos (\frac{I_t}{I} \Delta) \sin S + \sin (\frac{I_t}{I} \Delta) \cos S] = 0 \qquad (5)$$

During the fault period, $K_m = 0$ and the driving torques are the steady turbine torque and the 60 Hz oscillating torques (3ϕ fault). Under these conditions Δ and S are to a very good approximation the normal coordinates. These time dependent torques as appropriately applied to Equations (4) and (5) give initial values for Δ and S and their time derivatives at the start of rotor swing period when $K_m \neq 0$. It is during this later period that the non-linearity of the magnetic spring and its impact of mixing Δ and S and the resulting change in CFCT occurs. During this period the steady torques continue to be applied to the turbine while the 60 Hz torques are small and can be neglected.

First consider the Equation (4) for Δ. The zero order solution neglecting the mixing terms in S is,

$$\Delta = \Delta_1 \sin (\omega_S t + \psi) - \Delta_o$$

where $\omega_S = (K_S/I_R)^{1/2}$ and Δ_o is a constant equal to $I_g T_o / IK_S$. Equation (4) can be rewritten as

$$I_R \ddot{\Delta} + K_S (1 + \frac{K_m}{K_S} (\frac{I_t}{I})^2 \cos S)\ \Delta = -K_m \frac{I_t}{I} \sin S \qquad (6)$$

where the approximation has been made that

$$\sin \frac{I_t}{I} \Delta \simeq \frac{I_t}{I} \Delta$$

and

$$\cos \frac{I_t}{I} \Delta \simeq 1$$

It is evident that the effect of the first perturbing term is to produce a small and slowly varying modulation of the natural frequency for Δ, i.e.,

$$\omega' = \omega_S\left(1 + \frac{K_m}{K_S}\left(\frac{I_t}{I}\right)^2 \cos S\right),$$

where it is recognized that S(t) is slowly varying in comparison to sin $\omega_S t$. The effect of the second mixing term on the righthand side of Equation (6) is to add a term proportional to sin S, i.e.,

$$\Delta = \Delta_1 \sin(\omega' t + \psi) - \frac{K_m}{K_S}\frac{I_t}{I}\sin S - \Delta_o \qquad (7)$$

This form of Δ will now be used to evaluate the impact of the Δ variation on the time dependence of S in Equation (5). It is important to note that Δ is bounded even if S is not.

Returning to Equation (5) and using the form for Δ as given by Equation (7), the perturbing effect on S(t) due to the torques involving Δ can be evaluated. The trigometric term involving Δ are approximated as,

$$\sin\left(\frac{I_t}{I}\Delta\right) \simeq \frac{I_t}{I}\Delta$$

and

$$\cos\left(\frac{I_t}{I}\Delta\right) \simeq 1 - \left(\frac{I_t}{I}\right)^2 \frac{\Delta^2}{2}$$

Then Equation (6) can be written as

$$I\ddot{S} + K_m \sin S - \frac{1}{2}K_m\left(\frac{I_t}{I}\right)^2 \Delta^2 \sin S + K_m \frac{I_t}{I}\Delta \cos S = 0 \qquad (8)$$

Putting in Δ as given by Equation (7), Equation (8) can be rewritten as

$$I\ddot{S} + K_m\left[1 - \frac{1}{4}\left(\frac{I_t}{I}\right)^2 \Delta_1^2 - \left(\frac{I_t}{I}\right)^2 \frac{K_m}{K_S}\cos S\right]\sin S$$

$$= \Sigma \text{ high frequency terms.}$$

Here we have collected the slowly varying terms (up to first order in K_m/K_S) as part of a new magnetic spring term on the left-hand side and have indicated all of the high frequency terms on the right-hand side. These latter terms cause S to have a high frequency variation that is bounded and therefore will

not impact on the CFCT. It is the change in the magnetic spring term that will yield the change in CFCT due to the flexible shaft oscillation. A new magnetic spring torque term can be written as

$$T(S) = K_m \left[1 - \frac{1}{4} \left(\frac{I_t}{I} \right)^2 \Delta_1^2 - \left(\frac{I_t}{I} \right)^2 \frac{K_m}{K_S} \cos S \right] \sin S \qquad (9)$$

It is to be noted that we have neglected the effect of Δ_o since it is small in comparison to Δ_1.

This torque expression reduces to the "stiff shaft" limit when

and $\frac{K_m}{K_S} \to 0$, i.e.

$$T(S) = K_m \sin S \qquad (10)$$

Either of these expressions when multiplied by ω_o give the conventional "power angle" relationship.

It is evident that θ_g and θ_t are both bounded if S is bounded. Therefore S and its torque relation as given by Equation (9) can play the role of the conventional machine angle δ and its power angle relation. A simple formulation of the CFCT problem can be used to obtain the magnitude change in CFCT due to this change in magnetic torque.

The discussion can be based on an "equal area" approach as diagrammed in Figure 3-182 . This approach assumes a single reactance for the machine after the fault is cleared to establish one power angle curve. Further, it takes an initial machine angle δ_o starting from which the generator and turbine are accelerated to the critical angle δ_c due to the steady turbine torque. The fault is then cleared, and the turbine generator, with the turbine torque still active, is deaccelerated by the magnetic spring to synchronous speed. This occurs at a machine angle of δ_1. The equal area criteria follows from equating the work done by the turbine during the fault period to the work by the turbine against the magnetic spring during the first quarter of a rotor swing. If this criteria can be met, the rotor swing will be bounded and the machine can return to synchronous with the system.

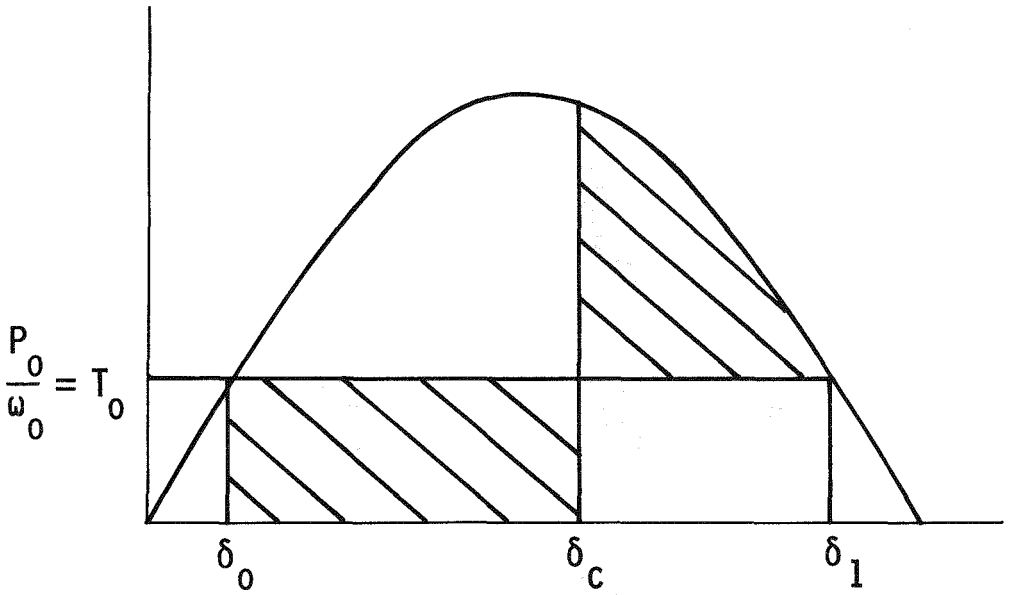

Figure 3-182. CFCT Diagram.

The CFCT is related to the critical angle in this approach as

$$\delta_c - \delta_o = 1/2 \frac{T_o}{I} t_c^2$$

and therefore

$$\frac{dt_c}{t_c} = \frac{1}{2} \frac{d\delta_c}{\delta_c}$$

The energy relation can be expressed as

$$T_o (\delta_1 - \delta_o) = \int_{\delta_c}^{\delta_1} T(\delta)\, d\delta = V(\delta_1) - V(\delta_c) \qquad (11)$$

where $T(\delta)$ is given by Equation (9) or (10) and $T_o = T(\delta_o)$.

Using Equation (11), it can be shown that

$$d\delta_c = \frac{dV(\delta_1) - dV(\delta_c)}{T(\delta_c)}$$

where $d\delta_c$ is the incremental difference for δ_c in going from the torque given by Equation (10) to that of Equation (9).

Therefore

$$\frac{dt_c}{t_c} = \frac{1}{2} \frac{dV(\delta_1) - dV(\delta_c)}{\delta_c T(\delta_c)}$$

where

$$dV = K_m \left[\frac{1}{4} \left(\frac{I_t}{I} \right)^2 \Delta_1^2 \cos S - \frac{1}{2} \left(\frac{I_t}{I} \right)^2 \frac{K_m}{K_S} \sin^2 S \right]$$

and

$$T = K_m \sin S$$

Then

$$\frac{dt_c}{t_c} = \frac{\frac{1}{2}\left(\frac{I_t}{I}\right)^2 \Delta_1^2 \left(\cos \delta_1 - \cos \delta_c\right) - \left(\frac{I_t}{I}\right)^2 \left(\frac{K_m}{K_S}\right) \left(\sin^2 \delta_1 - \sin^2 \delta_c\right)}{4\delta_c \sin(\delta_c)}$$

The critical time is taken as 12 cycles = 0.2 sec to evaluate δ_c from the expression

$$\delta_c - \delta_o = \frac{1}{2} \frac{T_o}{I} t_c^2$$

with $\delta_o = 20°$.

We take $\delta_1 = 180° - \delta_o$ then the fractional change in t_c is calculated as

$$\frac{dt_c}{t_c} = 0.01$$

The constants used in the above calculations are appropriate for the 300 MVA machine. It should be pointed out that the largest term in dV is the second which is associated with finite K_m/K_S. This term is about three time and of the opposite sign of the first term which is associated with the non-linearity of the magnetic spring.

Generator Transient Performance

Electromechanical Transients

As is now well known, the complete description of the transient performance of an electrical machine is obtained by the solution of the set of coupled differential equations for the electromagnetic circuits and the mechanical system. These systems are described, for these purposes, by lumped parameters, namely self and mutual inductances, masses, and springs. Dissipation effects are described as resistances. The solution is normally carried out by means of high-speed digital computers.

For routine design purposes, where many iterations may be required before a successful design is achieved, it is more practical to consider particular events of high severity, leading to large mechanical stresses, and to design for these. This is a form of "worst case" analysis, and is consistent with the requirements specified in ANSI Standards. With regard to the stresses experienced by mechanical components, including the shaft, the armature windings, and the armature mounts, terminals faults represent a very severe occurrence. Faulty synchronizing may indeed impose still higher stress levels, but occurs so rarely in the American utilities and can be avoided so easily that, by common concensus, it is not a practical design requirement. High speed breaker reclosure is a more frequent occurrence. Analysis of this condition is presently under consideration in the industry, but has not been standardized.

Terminal short circuits produce airgap torques which are transferred to the shaft, ovalizing or "crushing" forces on the damper, and forces on the armature windings. Calculation methods have been devised for all these effects.

The stress tensor, as indicated above, requires evaluation of the differences of the squares of the internal and external tangential fields at the damper. Reference 6 made this evaluation by assuming a phase relationship of the traveling wave and standing wave components of the fields themselves. It is, however, not difficult to carry out the calculation of the square terms without making this assumption. For this purpose, it is convenient to omit the internal field at the inside of the damper, whose square in any event is much less than the square of the external field and has very little influence on the result.

Letting, as in Reference 6:

$$H_{\theta o} = \sqrt{A^2 + B^2} \cos\left(\omega t + \phi - \theta + \tan^{-1}\frac{B}{A}\right) - C \cos(\phi - \theta)$$

where

$$A = H_{ao} \sin\psi + \frac{2 H_{al}}{1 + \left(\frac{R_s}{R_{mi}}\right)^2} + H_f \cos\delta$$

$$B = H_{ao} \cos\psi + H_f \sin\delta$$

$$C = \frac{2 H_{al}}{1 + \left(\frac{R_s}{R_{mi}}\right)^2}$$

and further letting $\xi = \tan^{-1}\frac{B}{A}$, we obtain:

$$H_{\theta o}^2 = (A^2 + B^2)\cos^2(\omega t + \phi - \theta - \xi) + C^2 \cos^2(\phi - \theta) - 2C\sqrt{A^2 + B^2}\cos(\omega t + \phi - \theta + \xi) \cdot \cos(\phi - \theta)$$

$$= \frac{A^2 + B^2 + C^2}{2} - C\sqrt{A^2 + B^2}\cos(\omega t + \xi) + \frac{C^2}{2}\cos 2(\phi - \theta)$$

$$-C\sqrt{A^2 + B^2}\cos(\omega t + 2\phi - 2\theta + \xi) + \frac{A^2 + B^2}{2}\cos 2(\omega t + \phi - \theta + \xi)$$

In rotor coordinates, $\theta = \omega t + \theta_r$, so that, from the rotor reference, the components of the radial stress appear as:

$$H_o^2 = \frac{A^2 + B^2 + C^2}{2} - C\sqrt{A^2 + B^2}\cos(\omega t + \xi) + \frac{A^2 + B^2}{2}\cos 2(\theta_r - \phi - \xi)$$

$$- C\sqrt{A^2 + B^2}\cos(\omega t + 2\theta_r - 2\phi - \xi) + \frac{C^2}{2}\cos 2(\omega t + \theta_r - \phi)$$

The first two terms of this expression have no angular dependence in the rotor coordinates. The first is a compression, uniformly around the rotor, of constant amplitude. (The decay factors which presumably apply to all the transient fields have been neglected in this analysis. This approximation is justified inasmuch as the mechanical parts must in any event withstand the maximum stresses.) The second term of the expression is a pressure which alternates with time, but is uniform in magnitude around the periphery of the rotor. The third term is a 4-pole wave that is stationary with respect to the rotor coordinates. The last two terms are traveling force waves. Both are 4-pole waves, but they travel with different speeds over the rotor periphery. The 4th term travels at one-half synchronous speed, and thus causes damper deformations at line frequency. The 5th term travels at synchronous speed, and causes double-line-frequency deformations.

These results are somewhat different from those given in Reference 6. This difference was not found until near the termination of the present studies. The latest studies of flux compression by the damper shield are based on a recognition of the above. The "crushing force" values which have formed the basis for the mechanical design of damper supports are, however, based on the results stated in Reference 6. Since the same maximum stresses would apparently be obtained in either case, this is considered acceptable.

Calculation of Forces on High-Resistivity Rotor Parts

Forces experienced during fault conditions on such metallic parts as the radiation shield must also be evaluated for the mechanical design. The above equations for the forces on the damper assume complete exclusion of the radial component of transient magnetic field. This is not the case for high-resistivity parts. For this case, it is necessary to base the force calculation on a current density in the high-resistivity shell. Since such shells are mainly needed in the region between the inner diameter of the room-temperature damper and the outer diameter of the field winding or of the cold damper, this current density can be estimated.

A thin shell approximation (see Section 3.2.1.3) is used to estimate the current density in the high-resistivity shield:

$$J_z = \frac{2\ \omega\ \tau/d}{\sqrt{1 + (\omega\tau)^2}}\ \frac{\Delta B}{\mu o}$$

and

$$P_m = B_\theta J_z d$$

where

P_m = peak pressure due to magnetic interaction, n/m^2

J_z = induced current density in axial direction

ΔB = change in flux density due to transient interaction (see below)

B_θ = peripheral flux density prior to fault

d = thickness of structural shell

ω = frequency at which the field change ΔB occurs

R = average radius of structural shell

$\tau = \frac{\mu_o Rd}{2\rho}$

ρ = resistivity of structural shell

The change in flux density at the appropriate frequency is estimated from the flux compression produced by damper ovalizing, in the same manner as indicated in Section 3.2.

Forces on Armature Windings

Forces on stator windings of electrical machines are, in principle, calculated from the simple relationship

$$F = I\ell \times B$$

where

F = instantaneous value of vector force

I = instantaneous peak value of current in conductor

ℓ = vector length of conductor or conductor segment

B = flux density vector at point at which force is evaluated.

The flux density B is the net vector flux density at the point at which the force is being evaluated, due to all currents which can produce flux at that point. Means of evaluating this flux density distribution have been developed during the present studies, and are reported in Section 3.2.2.

References

1. T. H. Einstein, "Excitation Requirements and Dynamic Performance of a Superconducting Alternator for Electric Utility Power Generation," MIT Sc.D. Thesis, December 1970.

2. N. Dagalakis, "Electromechanical Design for an Inertial Spool Superconducting Generator," MIT Thesis, Ph.D., November 1974.

3. H. S. Kirschbaum, "Transient Electrical Torques of Turbine Generators during Short Circuits and Synchronizing," AIEE Technical Paper 45-14, December 1944.

4. R. E. Doherty, C. A. Nickle, "Synchronous Machines, Part IV, Single-Phase Short Circuits," AIEE Transactions, Vol. 47, 1928, pp. 457-87.

5. R. E. Doherty, C. A. Nickle, "Synchronous Machines, Part V, Three-Phase Short Circuit of Synchronous Machines," AIEE Transactions, Vol. 49, 1930, pp. 700-14.

6. M. Furuyama, "A Design Concept of a Damper Shield of a Superconducting Alternator," S.M. Thesis, MIT, August 1974.

3.5 RELIABILITY

Achieving a reliability that equals or surpasses that of conventional generators is mandatory for superconducting generators for utility application. There is no technical basis at this time for believing that this goal cannot be achieved. It will, of course, require a major long-term investment in engineering and manufacturing to push this technology toward commercial ratings and reliabilities. The question of reliability at this point is not so much can it be achieved, but how much will it cost and what are the consequent long economic benefits if achieved. These last two questions are discussed, as best they can at present, in Section 2.5 of this report.

With respect to reliability itself, it was our earlier intent to attempt to develop a formal fault tree analysis and in the Fourth Quarterly Report we had started to lay the formalization for this. However, in trying to expand from this starting point, it was realized that it was all but impossible to quantify at this time, the various probabilities that would be required for obtaining numerical values for failure rates, etc. This due to the lack of reliability data on the subcomponents that make up the rotor, stator and auxiliaries of a superconducting generator. This lack of data stems from the fact that there is at present no real long-term experience with such components under real machine operating conditions.

It might be possible with further effort to extrapolate experience that does exist for certain components as utilized in other applications, e.g., stationary cryogenic dewars, refrigeration plants for liquification of gases and stationary superconducting coil systems. However, it was judged more expedient to expend the funds under the present program in further engineering verification of the machine concepts being proposed than that on a detailed reliability analysis of questionable long range value.

Some small effort has been applied to cataloguing initiating events that can result in generator failure and/or outage. These are listed in the charts that follow and divided into those associated with rotor, stator and auxiliaries. These lists can be considered as a starting point for future reliability studies as well as a useful check list for the design engineer during future design studies.

Table 3-76

LIMITED FAILURE - REPAIRABLE

STATOR

ELECTRICAL CAUSE	MECHANICAL CAUSE	THERMAL CAUSE
Insulation Failure Terminal-Terminal To Ground Phase-Phase	End Turn Support	Core Overheating
Water Leak into Coil	Coil Vibration Steady Transient	Hot Spot on Structure
Bond Degradation	Bore Support Retaining Ring	Foreign Objects Loose Fastener Other
Insulation Shrinkage	Strand Fatigue	
Creep	Blocked Fluid Passages	
Corona	Water System Failure	
Harmonic Heating and Vibration	Coolant Tube Failure	
Excessive TIF*	Machine Misalignment	
	Flexible Mounting	
	Self-excited Instability	
	Frame Vibration	

*Telephone Influence Factor

Table 3-77

LIMITED FAILURE - REPAIRABLE

ROTOR

ELECTRICAL CAUSE	MECHANICAL CAUSE	THERMAL CAUSE
Collector Rings and Leads	Damper Structure Overheating and Loss of Structure Integrity	Quench
Connection Failure	Weld Crack	Loss of Vacuum
Insulation Failure Terminal-Terminal To Ground	Unbalance Inner Rotor Thermal Damper Structure	Helium Transfer System
Coil Degradation	Flange Bolt Failure	Radiation Shield
	Gland Seals	Plugged Helium Passages
	Torque Tube Yielding	Internal Pipes
	Lateral Vibration	
	Shaft Misalignment	
	Torsional Oscillations	
	Subsynchronous Resonance	
	Solid Air Buildup	

Table 3-78

LIMITED FAILURE - REPAIRABLE

AUXILIARIES

Refrigeration	Loss of Coolant
Broken Transfer Lines	Failure of Auxiliaries
Plugged Transfer Lines	Maintenance
Refrigerator Failure	Instrumentation Failure
Back-Up Storage Failure	Control System Failure

3.6 MATERIAL SELECTION

General Comments

Material Utilization and Selection Criteria

The utilization criterion for materials employed in superconducting turbine generators will be that the minimum mechanical and physical properties will be met or exceeded in the final fabricated and assembled condition. The materials selection criteria for each component depends upon the critical design requirements for that component and tradeoffs in cost, manufacturing ease, and other impinging design requirements. Most components have conflicting design requirements and optimization can only be achieved with experience. The material selection criteria for the main structural components in the 300 and 1200 MVA SCTG rotors are shown in Table 3-79.

There are many material choices that would appear to fill the selection criteria in Table 3-79. Availability and finished cost eliminate metal matrix composites from consideration for the 300 MVA machine; the need to use well characterized materials to achieve failure-safe designs eliminates many others. Preliminary material selections for the 300 MVA unit are shown in Table 3-80. A discussion of each component and alternative material choices follows.

Metal Alloy Designation Terminology[1]

A common problem in materials programs is the selection of terminology used to refer to various alloys so that machine designers, metal producers, and fabricators all understand exactly what material is being discussed. In general we will use common commercial trade designations because of their recognition value, however, this is not in any way an endorsement of any particular company's product nor is it always definitive. Inconel 718 is the commercial designation (trade name) for a nickel-base superalloy produced by Huntington Alloys Division of International Nickel Corp., it is also marketed under the names Udimet 718 (Special Metals Corp.), Unitemp 718 (Universal-Cyclops, Speciality Steel Div.), Pyromet 718 (Carpenter Technology Corp.), and Haynes Alloy #718 (Stellite Division of Cabot Corp.) among others. While all the producers use the same basic composition, the melting, mill equipment and the microstructures; and hence structure sensitive properties, may vary widely.

Table 3-79

REQUIRED MATERIAL PROPERTIES

COMPONENT (TEMPERATURE RANGE)	PROPERTIES REQUIRED AND APPROXIMATE DIMENSIONS	MVA 300	MVA 1200
DAMPER SHIELD SUPPORTS (0°C-200°C)	NONMAGNETIC		
	HIGH EL. RESISTIVITY		
	HIGH YIELD STRENGTH - ksi(MPa)	125 (861)	170 (1171)
	FRACTURE TOUGHNESS - ksi$\sqrt{in}$ (MPa$\sqrt{m}$)	100+(110)	100+(110)
	WELDABLE		
	APPROXIMATE DIMENSIONS (OUTER CYLINDER) in.(cm)		
	INSIDE DIAMETER	29 (73.6)	38 (96.5)
	THICKNESS	1.37 (3.48)	2.38 (6.05)
	LENGTH	132 (335.3)	180 (457.2)
	APPROXIMATE DIMENSIONS (INNER CYLINDER) in.(cm)		
	INSIDE DIAMETER	24.25 (61.6)	32.75 (83.2)
	THICKNESS	.88 (2.24)	1.37 (3.48)
	LENGTH	132 (335.3)	180 (457.2)
DAMPER SHIELD (0°C-300°C) (CONTINUOUS OPERATION AT APPROXIMATELY 100°C)	HIGH EL. CONDUCTIVITY (IACS%)	80% APPROX.	80% APPROX.
	HIGH YIELD STRENGTH - ksi(MPa)	50 (344.5)	50 (344.5)
	HIGH DENSITY - lb/in^3(g/cm^3)	.32 (8.86)	.32 (8.86)
	APPROXIMATE DIMENSIONS OF CYLINDER in.(cm)		
	INSIDE DIAMETER	26 (66)	35.5 (90.2)
	THICKNESS	1.25 (3.18)	1.25 (3.18)
	LENGTH	130 (335.3)	180 (457.2)
FIELD WINDING RETAINER AND TORQUE TUBE (4°K-300°K)	NONMAGNETIC		
	HIGH EL. RESISTIVITY		
	YIELD STRENGTH - ksi(MPa)	170 (1171)	170 (1171)
	FRACTURE TOUGHNESS - ksi$\sqrt{in}$ (MPa$\sqrt{m}$)	100 (110)	100 (110)
	WELDABLE		
	APPROXIMATE DIMENSIONS OF TOTAL CYLINDER in.(cm)		
	INSIDE DIAMETER	20.7 (52.6)	29.5 (74.9)
	THICKNESS	.5 (1.27)	.75 (1.51)
	LENGTH	96 (244)	128 (325.1)
THERMAL RADIATION SHIELD (70°K-300°K)	NONMAGNETIC		
	HIGH EL. RESISTIVITY		
	YIELD STRENGTH - ksi(MPa)	77 (530)	129 (889)
	FRACTURE TOUGHNESS - ksi$\sqrt{in}$ (MPa$\sqrt{m}$)	100 (110)	100 (110)
	WELDABLE		
	GOOD THERMAL CONDUCTIVITY		
	APPROXIMATE DIMENSIONS OF CYLINDER in.(cm) (MAKE AS SANDWICH FOR GAS PASSAGES)		
	AVERAGE DIAMETER	23.4 (59.4)	32 (81.3)
	THICKNESS	.37 (.94)	.37 (.94)
	LENGTH	130 (335.3)	180 (457.2)

Table 3-80

PRELIMINARY MATERIAL SELECTIONS

Component	Material	Mechanical Properties								Physical Properties	
		UTS		YS		El	RA	K_{IC}		Elec. Resist. @ 25°C (μΩ-cm)	Mag Perm
		MPa	KSI	MPa	KSI	%	%	MPa$\sqrt{m}$	KSI$\sqrt{in.}$		
Flexible Shaft	Ti-6Al-4V	1033	150	999	145	11	30	101.46	92	NA	NA
	250 Grade Maraging Steel	1757	255	1722.5	250	12	45	77.2	70	NA	NA
Damper Support	ASTM A289	1240.2	180	861.2	125	40	55	220+	200+	90-95	1.002
Torque Tube and Field Winding Retainer	Inconel 718	1274.6	185	1205.7	175	12	15	77.2	70	124	
Damper Shield	Pd-135	461.6	67	378.9	55	10	40			2.3	NA
Radiation Shield	A286	969	140	645	94	21					

Table 3-81

METAL ALLOY DESIGNATION CROSS REFERENCE SUMMATION TABLE

TRADE NAME	UNS	AMS	ASTM	OTHER
AISI 310S	S31008	5521 5572 5577 5651	A167 (310S) A240 (310S) A276 (310S) A314 (310S) A473 (310S) A479 (310S) A580 (310S)	AISI 310S SAE J405 (30310S)
INCONEL 706	N09706	5605 5606 5701-3		
INCONEL 718	N07718	5383 5589 5590 5596 5597 5662-4 5832	A637 A670	MIL-N-24469
A286	K66286	5525 5731 5732 5734 TO 5737 5804 5805	A638 (660)	SAE J467 (A286)
W 545	K66545	5545 5741	- -	AISI 665
DISCALOY	K66220	5733	A638 (662)	AISI 662 SAE J467 (DISCALOY)
V-57				AISI 663
NITRONIC 33	S24000	- -	A240 (XM-29)	- - -
(18Mn-5Cr)		- -	A289	
TRM-45		- -		
MULTIPHASE MP 35N	R30035	5844 5845 5758		
TI-6AI-4V (ELI)	- -	- -	- -	- - -
TI-5AI-2.5 Sn (ELI)	- -	- -	- -	- - -
OFHC - Cu	C10200	4500 4701	B1-3 B12 (102) B13 (102) B33 B42 (102) (+26 OTHERS)	CDA 102 SAE J461 (CA102) SAE J463 (CA102) QQ-B-825 QQ-C-576 MIL-B-18907 MIL-R-19631
AMZIRC - Cu	C15000	- -	- -	CDA 150 SAE J461 (CA150) SAE J463 (CA150)
PD - 135	- -	- -	- -	- - -
250 GRADE MANAGING STEEL			A579 GRADE 72	

Other alternative ways of designating such alloys rather than by commercial trade designations are:

- Primarily metal producer sponsored organization specifications such as the Aluminum Association (AA), The Cooper Development Association (CDA) and the American Iron and Steel Institute (AISI).
- Primarily metal user sponsored organization specifications such as the Society of Automotive Engineers (SAE), American Society of Mechanical Engineers (ASME) and Federal and Military Specifications (QQ and MIL Specs).
- Combined user and producer sponsored specifications such as American Society for Testing and Materials (ASTM), American National Standards Institute (ANSI), and the American Welding Society (AWS).

Using such "standard" specifications for the purpose of alternative alloy designation terminology is not without its own inadequacies, however. For example, a given alloy may be included in several different specifications originating from the same society (Oxygen Free Copper is covered by over 30 ASTM specifications depending on the product form and intended use). Furthermore, the alpha-numerical designation used in a particular specification often bears no resemblance to the commonly known alloy designation (trade name). For example, the precipitation hardening stainless steel referred to as A-286 is designated as Alloy 660 by AISI, A638 by ASTM, J 467 (A286) by the SAE and is covered by approximately nine different Aerospace Materials Specifications (AMS).

A relatively recent and comprehensive metal alloy designation system has been advanced jointly by the Society of Automotive Engineers, Inc. (SAE) and the American Society for Testing and Materials (ASTM).[2] This system, identified as the Unified Numbering System for Metals and Alloys, provides a systematic means of correlating the various alpha-numerical systems mentioned above and will hopefully avoid the confusion associated with more than one designation for the same material and having the same designation assigned to more than one material. This system does not replace nor serve as a product specification but rather serves only as a unified identification system for metals and alloys meeting a certain chemical composition range. A cross reference is included as Table 3-81 in this report which contains the commercial designation, the Unified Numbering System (UNS) designation and various society specification designations for those candidate cryogenic structural materials listed in Table 3-80.

If there are reservations to the use of commercial trade designations for engineering alloys, then the UNS alloy designation system is the most potentially useful alloy designation technique. The UNS System does not, at present, include metal matrix composite materials or any non-metallic materials.

PRELIMINARY MATERIAL SELECTION

Flexible Shaft

The flexible shaft, if chosen for use, is a component where two different materials might easily be used. They are both presented and a final material choice would be dictated by the expected total cost at the time of manufacture.

As a titanium base alloy, Ti-6 - 6-2 or Ti-6-4 the shaft would be 27.93 cm (11 in.) in diameter and 152.39 cm (60 in.) long. Its procurement presents no problem.

As a steel component the shaft would be only 24.12 cm (9.5 in.) in diameter, and would still be 152.39 cm (60 in.) long. The 250 grade maraging steel would need a protective coating, paint or other organic coatings would serve.

Outer Damper Shield Support

The outer damper shield support will operate between ambient temperature and 200°C (392°F). It should be non-magnetic to reduce losses and it must have a minimum 861 MPa (125 KSI) yield strength so that the total imposed stress is no more than 70% of the yield strength.

Three distinct material systems appear to fulfill these requirements.

- Titanium alloys are readily available with yield strengths in excess of 861 MPa (125 KSI). However, excessive deflections and limited fracture mechanic data make them at best an alternative choice.
- Nickel-base superalloys, preferably Inconel 706, and some iron-base superalloys, V57 (Cartech) and W545 (Universal-Cyclops) develop the necessary strength levels, however, the geometry of the component; a cylindrical shell, 79.37 cm (31.25 in.) O.D., 3.49 cm (1.375 in.) wall thickness, 330.19 cm (130 in.) in length cannot be fabricated by standard hot working methods used with these alloys. Welding data on Inconel 706 is not available, the data on the iron-based alloys indicates that they are not easily welded and base metal properties are difficult to achieve.

- The material/fabrication combination that is most promising in the near term is a cold worked austenitic steel cylindrical shell. Four specific alloys on which there is enough data to justify their consideration are:

  -- 18 Mn - 5 Cr steel (ASTM A289 Composition A)

  -- 15 Mn - 5 Ni steel (TRM-45, Crucible steel)

  -- 18 Cr - 12 Mn - 3 Ni stainless steel (Nitronic 33, Armco Steel)

  -- AISI 310S stainless steel.

At the required strength level all of the alloys provide exceptional toughness. They are extremely stable magnetically and have comparable electrical resistivities ($\approx$ 90 $\mu\Omega$-cm).

The ASTM A289 alloy has a very successful history in conventional generator applications. Its cost and availability are well known.

The TRM-45 steel was developed by Crucible Steel Research to provide a more microstructurally stable austenitic steel than a 12 Mn - 8 Ni alloy and it has been used in electric utility items for several years.

The two stainless steels are included for completeness, the application does not require resistance to atmospheric corrosion. In addition their base cost is two to two and a half times the base cost of either of the high manganese steels.

Inner Damper Shield Support

The inner damper shield support has the same mechanical and physical property requirements as the outer support. Its smaller size, 66.03 cm (26 in.) O.D., and thinner wall 2.35 cm (.88 in.) makes it more amenable to being cold formed. The material choices are the same as were outlined for the outer support.

Damper Shield

The minimum conductivity desired in the damper shield is 80% of the conductivity of pure copper at any temperature in its operating range. It is necessary only to assure that this condition is met at the lowest operating temperature, since the thermal coefficient of resistance is highest in pure copper.

The size and shape of the damper shield; 2018 kg (4450 lb), 69.18 cm (27.25 in.) O.D., 3.17 cm (1.25 in.) wall thickness, 330 cm, (130 in.) long is not within current fabrication practice. The mechanical strength requirement, σy = 275.6 MPa (40 KSI) dictates the use of a high strength, high conductivity copper alloy:

- PD-135 (Phelps-Dodge)
- Zirconium Copper (CDA 150)
- Chromium Copper (CDA 182)

Suppliers indicate that these materials are not available in billet sizes large enough to produce the damper as a monolithic structure. Data on heavy section welded material is not readily available, however, all of the alloys require 25 to 80% cold reduction before aging to develop optimum conductivity, such that considerable refinement of a welded structure will be possible. This component then will be cold formed from a welded blank.

Damper Design - Fabrication

The composite damper developed by Westinghouse, represents several fabrication problems. The first and foremost problem is procurement of non-magnetic, 834 MPa (125 KSI) yield strength, 110.2 MPa $\sqrt{m}$ (100 KSI $\sqrt{in.}$) plane strain fracture toughness material in the required geometry for the inner and outer supports.

The other major problem is to ensure that the entire assembly acts as a unit during steady state or transient operation. The interface between the copper alloy damper shield and the austenitic steel supports must transfer shear loads during bending and torque loading and tensile loads during the short circuit crushing forces. Consideration is being given to low temperature joining methods but the large surface area, 14.35 sq. m. (154.4 sq. ft.) appears to be too severe a condition for capillary flow soldering or brazing. A low temperature diffusion bonding system utilizing gold or an amalgam-type of bonding agent could be used if the autofrettage method proves unsuitable.

Radiation Shield

The critical design requirement for the radiation shield is that it be non-magnetic. The stresses involved are fairly low and an A286 structure is considered suitable for the 300 MVA machine.

Torque Tube and Field Winding Retainer

The design requirement of 1205.75 MPa (175 KSI) yield strength and non-magnetic properties severely constrains the material choices for the torque tube and field winding retainer. The unfortunate occurrence of the highest stresses at the warm region prohibits taking advantage of the increase in yield strength with degreasing temperature seen in many austenitic materials.

In the slotless rotor configuration, the torque tube to field winding retainer weld would be made after the completion of the inner rotor structure. Therefore excessive working of the weld and complete heat treatment of the structure could not be accomplished. The necessity of making that weld eliminated cold worked components from consideration.

Only one nickel-base superalloy meeting the design requirements of yield strength and non-magnetic character has sufficient data existing to enable its use in a safe and logical engineering design. This material, Inconel 718, unfortunately, does not possess the level of fracture toughness that is desired. Careful consideration of flaw sizes, duty cycle, and out ability to non-destructively find such flaws must be undertaken.

The final design configuration is a slotted inner rotor. If this part, with integral torque tubes cannot be made of Inconel 718, then welded on or bolted on torque tubes may be used. The slotted inner rotor could then be made of a different, possibly magnetic, material.

POTENTIAL FUTURE MATERIALS

Titanium Base Alloys

Titanium base alloys possess several inherent advantages over austenitic alloys for high strength structures where cold forming is not a feasible manufacturing process and non-magnetic characteristics are needed. The major advantage is the capability of using two-phase alloys where strength is derived by any of three methods; precipitation of a stable phase from a metastable phase, reversion of a metastable phase, or by compound formation. This variety of microstructural modifiers can produce a wide range of properties in a given alloy composition. In addition solid solution hardening may also be used. This allows the achievement of moderate yield strengths, 620.1 - 826.8 MPa (90-120 KSI) in annealed material.

Calculation of Airgap Torques During Short Circuit[3]

Values of airgap torque during three-phase or unbalanced short circuits are conveniently obtained by means of formulas derived from the Doherty and Nickle treatment of the synchronous machine.[4,5] The formulas that apply are:

For Three Phase Fault:

$$T = \frac{E^2}{X_d''} FA \sin \omega t + \sqrt{2}\left[\frac{\sqrt{2}EA}{2X_d''}\right]^2 (R_2-R_1) + \left[\frac{EF}{X_d''}\right]^2 R_1 \text{ per unit torque}$$

$$F = \left[\frac{X_d''}{X_d} + \frac{X_d''(X_d-X_d')}{X_d'X_d}\varepsilon^{-\frac{t}{T_{do'}}\frac{X_d}{X_d'}} + \frac{(X_d'-X_d'')}{X_d'}\varepsilon^{-\frac{t}{T_{do}''}\frac{X_d'}{X_d''}}\right]$$

$$A = \varepsilon^{-2\pi f \frac{R_a}{X_d''} t}$$

For Line-to-Line Fault on Phases b and c:

$$T = \frac{E^2}{(X_d''+X_2)}\left[2 FA \sin(\omega t+\alpha) - F^2 \sin 2(\omega t+\alpha)\right] + 2\left[\frac{EF}{X_d''+X_2}\right]^2 (R_2-R_1) + \sqrt{2}\left[\frac{\sqrt{2}EA}{X_d''+X_2}\right]^2 (R_2-R_1) + 2\left[\frac{EF}{X_d''+X_2}\right]^2 R_1 \text{ per unit torque}$$

$$F = \left[\frac{X_d''+X_2}{X_d+X_2} + \frac{(X_d''+X_2)(X_d-X_d')}{(X_d'+X_2)(X_d+X_2)}\varepsilon^{-\frac{t}{t_{do'}}\frac{X_d+X_2}{X_d'+X_2}} + \frac{(X_d'-X_d'')}{(X_d'+X_2)}\varepsilon^{-\frac{t}{T_{do}''}\frac{X_d'+X_2}{X_d''+X_2}}\right]$$

$$A = (\cos\alpha)\,\varepsilon^{-2\pi f \frac{2R_a}{X_d''+X_2} t}, \quad \alpha = \text{angle between quadrature axis of rotor and phase } a$$

The symbols used in these equations, except as noted, are the usual machine constants, i.e., reactances, resistances, and time constants. Reactances and resistances are per-unit values. The voltage E is the appropriate machine voltage "behind subtransient reactance".

It should be noted that these formulas differ slightly from the form given in the original derivation[3] in that the exponents of terms proportional to damper resistance $(R_2 - R_1)$ have been changed from 1.8 to 2. This is to account for a difference in damper characteristics between conventional turbine generators and superconducting generators. See Section 3.2 and the subsequent material on Electromagnetic Transients.

Calculation of Ovalizing Forces on Damper and on Rotor Structural Parts

The magnitude of the crushing force appearing at the damper during short circuit can be estimated by means of the Maxwell stress tensor evaluated at the inner and outer surfaces of the damper:[6]

$$\sigma_r = \frac{\mu_o}{2} (H_{\theta o}^2 - H_{\theta i}^2)$$

The general expressions for the field distributions H_θ were listed in Table Section 3.2. If the exciting currents known to exist during short-circuit conditions are applied to these expressions, it is possible to calculate the magnitude and distribution of the stress σ_r which corresponds to a distribution of radial force on the damper shell.[6] For the case of a three-phase short circuit, it has been shown that the following expressions are obtained for the transient fields:

$$H_{\theta o} = H_{ao} \cos (\omega t + - \theta + \frac{\pi}{2} - \psi) + \frac{2H_{al}}{1 + (\frac{R_s}{R_{mi}})^2} [\cos(\omega t + \phi - \theta) - \cos (\phi - \theta)] + H_f \cos (\omega t + \phi - \theta + \delta)$$

$$H_{\theta i} = H_f \cos (\omega t + \phi - \theta + \delta) + H_{ao} \cos (\omega t + \phi - \theta + \frac{\pi}{2} - \psi)$$

where

$$H_{ao} = \frac{3\sqrt{2}}{\pi} \sin (\frac{\theta_{wae}}{2}) R_{ao} J_{ar} [1 - x + \frac{1}{3} (1 - x^3) \cdot (\frac{R_{ao}}{R_{mi}})^2]$$

$$H_{al} = \frac{H_{ao}}{X_d''}$$

$$H_f = \frac{2}{3\pi} \sin (\frac{\theta_{wfe}}{2}) R_s J_f (\frac{R_{fo}}{R_s})^3 (1 - y^3) [1 - (\frac{R_s}{R_{mi}})^2]$$

The symbols are the same as used in Reference 1 for Section 3.2 and in Table except for the angles ϕ, δ and ψ which are:

ϕ = phase angle at instant of fault

δ = power angle

ψ = power factor angle

all expressed in radians.

Major disadvantages are the difficulty of achieving high fracture toughness and the ductile-to-brittle transition seen in high or all beta-phase alloys. Interstitial content would seem to be the key to fracture toughness, although respectable values, 101.38 - 106.89 MPa $\sqrt{m}$ (92-97 KSI $\sqrt{in.}$), have been developed by microstructural control in standard alloys (Ti-6-4).[3] In addition, the low modulus of titanium alloys, 103.35 - 124.02 x 10^3 MPa (15 - 18 x 10^6 psi) in comparison with iron or nickel base alloys dictates that designs be developed specifically for their application; they cannot be substituted for standard structural materials without incurring large deflections or specifying thicker sections. Since the object of using titanium alloys is to take advantage of their high strength, using heavier sections to limit deflections is an inefficient method.

Specifically for superconducting structural components, titanium alloys are more nearly non-magnetic than either iron or nickel-base alloys, they may have electrical resistivities of 150-180 μΩ-cm (150% that of Inconel 718), and have coefficients of thermal conductivity 50% that of Inconel 718 (6.74 W/m°K vs, 11.24 W/m°K for Inconel 718).

Further work on interstitial control in primary processing and on low temperature properties will be necessary before titanium alloys are extensively used in cryogenic structures.

Composites

A. Reinforced Resin Structures

The use of fiber glass reinforced plastics in cryogenic structures is attractive because of their high strength at low temperatures.[4-6] Yield strengths of several hundred thousand psi are available with certain glass-epoxy systems. These composites, however, have a low modulus of elasticity of the order of 3 to 8 x 10^6 psi (20.67 to 55.27 x 10^3 MPa). The introduction of new exotic fibers such as graphite and boron have resulted in composites with high mechanical strength as well as a modulus comparable with that of structural steels. The design of fiber reinforced plastic composite structures must consider other factors in addition to strength and elasticity:

- Thermal conductivity
- Thermal contraction
- Directional properties
- Fracture toughness
- Sealing capabilities
- Long term stability

The ratios of yield strength and modulus of elasticity to thermal conductivity are important parameters in selecting materials for cryogenic structures. Fiber glass reinforced plastic composites have a high strength-to-conductivity ratio permitting light, low heat leak support structures. However, the low modulus of elasticity of these structures permits them to deflect readily under load. Composites fabricated from boron and graphite fibers have high ratios for both parameters and therefore are acceptable for stiff, low heat leak structures required for the field winding support.

The coefficient of thermal contraction of fiber reinforced plastics is significantly lower than that of most structural metals. In addition, the contraction is anisotropic, being governed primarily by the fibers in the direction of the fibers, and by the resin system perpendicular to the fibers. The directional variation of contraction can be minimized by cross weaving of the fibers. The difference in thermal contraction between composites and structural metals requires careful joint designs to prevent high local stresses if the metal-to-composite joint is to be cycled through a large temperature range. Work has been done by NASA[8] to evaluate the effect of resin-fiber ratio on the physical and mechanical properties. Increasing the resin binder weight in a composite will reduce the difference in contraction between composites and structural materials. As the ratio of resin to fibers also affects the mechanical properties, the structures utilizing composites and structural metals must be carefully designed.

In addition to directional thermal properties, the mechanical properties of composites also show considerable differences in strength and modulus perpendicular and parallel to the fibers. The strength of composites is very high in the direction of the fibers but is significantly lower perpendicular to the fibers where the tensile strength of the resin dominates.

The design of a composite structure with multidirectional stresses is difficult. In structural metals, the principal stresses can be determined and allowable stresses can be established using a failure theory such as the maximum shear theory. Because of their directional properties, the effect of multidirectional stresses is very complex for composites. The structure is normally cross weaved to provide fibers parallel to each of the principal stresses. However, this is not always possible, and can result in high stresses on the composite binder which may result in failure.

The fracture toughness and failure mode in composites is significantly different from those in structural metals.[9] Fiber glass composite failure is characterized by a loss of bond between the fibers and the binder which leads to fiber rupture. Once this occurs, damage is irreversible and the structural integrity is reduced. Since fiber glass composites are relatively brittle, they are not stress limited due to local yielding. The design stresses, therefore, on structures subjected to impact loads, are normally very conservative so that the impact stresses will not exceed the material yield stress resulting in permanent damage to the structure.

One of the most important factors in the design of composite structures for long term use is the variation of mechanical and physical properties with time. Some work has been done in these areas for temperatures above room temperature. However, very little work has been done on the variation of composite properties with time at cryogenic temperatures.

Considering the relative levels of development and knowledge of metallic and plastic composite structural materials, the metallic materials would be expected to dominate in applications in the near future.

B. Metal Matrix Composites

Metal matrix composites are distinguished from the more extensively developed resin matrix composites by virtue of their metallic nature in terms of physical and mechanical properties and by their ability to lend themselves to conventional metallurgical processing operations. Electrical conductivity, thermal conductivity, matrix shear strength, ductility (providing a crack blunting mechanism) and abrasion resistance; the ability to be coated, joined, formed, and heat treated; are some of the properties that differentiate metal matrix composites from resin matrix composites. Typical tensile data from diffusion bonded metal matrix composites in Table 3-82 illustrate impressive strength and stiffness values that can be achieved.

The ability to "tailor" both electrical and mechanical properties by suitable matrix/reinforcement choice may overcome classical material problems where there are conflicting design objectives. The damper shield assembly is an example; a combination of high strength and electrical conductivity not available in conventional materials is needed.

Table 3-82

ROOM TEMPERATURE PROPERTIES OF SEVERAL CURRENT METAL MATRIX COMPOSITES REPORTED IN THE LITERATURE

Material	Density		Longitudinal Tensile		Tranverse Tensile		Longidutinal Modulus		Transverse Modulus	
	lb/in^3	g/cm^3	MPa	KSI	MPa	KSI	MPa x 10^3	PSI x 10^6	MPa x 10^3	PSI x 10^6
50% B/6061 Al	.096	2.66	1136.8	165	137.8	20	227.3	33	124	18
50% B/Ti-3Al-2.5 Sn	0.128	3.54	1240.2	180	454.7	66	241.1	35	179.1	26
SiC/Ti-6Al-4V	0.130	3.60	1309.1	190	516.7	75	248	36	199.8	29
50% Be/Ti-6 Al-4V			689	100			190.8	27.7	174	26
60% Al_2O_3/2024 Al	.125	3.46	654.5	95	130.9	19	199.8	29	103.5	15
50% Al_2O_3/Mg	.101	2.80	551.2	80	130.9	19	199.8	29	103.5	15
30% Thornel 50 (Graphite Fiber 6061 Al	.080	2.21	757.9	110	82.6	12	165.3	24		
30% T-50/Cu	.240	6.64	964.6	140	34.4	5	165.3	24		

Raw material costs eventually dictate the utility of a new product and it should be recognized that the current cost barrier is represented by the fiber reinforcements. Many types of reinforcements have been considered, both as continuous fiber reinforcements and as whisker materials. Currently whiskers do not represent an important reinforcement for metal matrix composites because of fabrication problems -- sorting, alignment, breakage, and reaction. At this time boron, Borsic (SiC coated boron), and carbon are the most important fibers. The former are available in diameters of 100 to 140 microns (0.0004 - 0.0056 in.) and carbon fibers, depending on the precursor fiber, are $\sim$ 7 microns (.0002 in.). One process, chemical vapor deposition (CVD) yields fibers in the 25 micron (.001 in.) range, but little data on metal matrix composite properties utilizing this fiber reinforcement is available.

The major shortcoming of current metal matrix composites is cost. For the relatively mature boron/aluminum system the current cost is $180 per pound. Price projections for 1980, based on an annual production of 200,000 pounds (100 tons), are $60 per pound for B/Al plate. In addition basic design data must be established. Standard test procedures must be developed for;[10]

- Static mechanical properties
- Dynamic and time-dependent properties
- Combined stress tests
- Joint tests
- Electrical tests

Specifically, the areas in greatest need of additional work are:

- Combined state of stress - Biaxial and triaxial tests conducted over the entire stress envelope.
- Fracture mechanics data
- High strain rate loading, fatigue, creep
- Mechanical properties of joints, particularly at elevated Temperatures
- Electrical conductivity, magnetic properties

In addition to the basic design data needs, work is required for the understanding of the failure process and for nondestructive testing. The definition of the failure processes which control local composite failure are necessary to allow the material to be tailored according to the end use environment.

Nondestructive testing capability must be developed to insure composite quality.

Problems which exist are:

- Detecting and defining the significance of defects and their relationship to composite performance.
- Developing techniques for inspecting multilayered structures and individual bondlines.
- Providing a capability for inspecting complex shapes.
- Overcoming the difficulties of determining a weak fiber bond and a strong fiber bond.

References

1. This Section is from:

   J. M. Wells, W. A. Logsdon, R. Kossowsky, and M. R. Daniel, "Structural Materials for Cryogenic Applications, Fourth Semi-Annual Report," Westinghouse Research Laboratories 75-904-CRYMT-R2 (October, 1975).

2. Anon., Unified Numbering System for Metals & Alloys, ASTW DS-56, SHEJ1086, published by Soc. of Automotive Engineers, Warrendale, Pa., January, 1975.

3. R. A. Wood & R. J. Favor, Titanium Alloys Handbook, MCIC-HB-02, Metals and Ceramics Information Center, Battelle Memorial Institute, Columbus, Ohio, December, 1972.

4. J. E. Campbell "Handbook on Materials for Superconducting Machinery," Battelle Handbook MCIC-HB-04 (November, 1974).

5. Fred R. Schwartzbeck et al., Cryogenic Materials Data Handbook, Vols I and II, Martin Marietta Corp., Denver, Colo., July, 1970.

6. M. B. Kaser, "Mechanical and Thermal Properties of Filamentary Reinforced Structural Composites at Cryogenic Temperatures," Cryogenics Division Institute for Basic Standards, National Bureau of Standards, Boulder, Colo.

7. K. E. Hofer, "Development of Engineering Data of the Mechanical and Physical Properties of Advanced Composite Materials, "Air Force Materials Laboratory, AFMC-TR-72-205 (Sept., 1972).

8. L. M. Soffer and L. Molho, "Cryogenic Resins for Glass Filament Wound Composites," NASA CR-72114 (1967).

9. C. C. Chamis, M. P. Hanson, and T. T. Serafine, "Designing for Impact Resistance with Unidirectional Fiber Composites," NASA-TN-D-6464 (Aug. 1971).

10. R. L. Kolek, "Fibrous Metal Matrix Composites - Review and Status", Westinghouse Research Laboratories 75-1B7-HETSM-R1 (Dec., 1975).

3.7 DEVELOPMENT PLAN

Introduction

The next step in the superconducting generator development is to build, test, and observe in service a prototype unit of sufficient size to credibly demonstrate the features of the design. A prototype will demonstrate:

- That a full-size superconducting field winding, and its cryogenic system, can operate successfully under power system conditions.
- That the armature configuration can match the power density capability of the field winding, and withstand system transient forces, and
- That the expected economic and system dynamic performance goals can be achieved.

The purpose of the present section is to layout and describe the necessary steps leading to this goal.

It is proposed that the development program for the 300 MVA demonstration machine be divided into two parts. These are:

Part A: Design, construction and test of a 300 MVA low-voltage generator.

Part B: Design, construction and test of a 300 MVA high-voltage (transmission level) generator. This machine would utilize a duplicate of the rotor developed in Part A.

Each part would take six years for completion (not including the extended utility test period). They could be run in parallel or Part A could be initiated first with a delay before the start of Part B.

Each part would be divided into two successive phases.

Phase I - Premanufacturing Development

A. Critical Component Development - consists of building and testing models and certain critical components for the purposes of confirming predicted performance and developing fabrication techniques. This will require considerable time to complete and should start immediately upon the initiation of work on the project. The output of this work will be needed in developing the final machine design.

B. Engineering Development - consists of extending the present machine performance analysis technique to obtain a more exact determination of machine performance, particularly during transient conditions, thus permitting the fullest exploitation of the superconducting concept with increased assurance that the design has been properly specified and that performance has been accurately predicted.

C. Materials and Manufacturing Development - consists of determining and specifying the particular materials and manufacturing methods to be used in the construction of the machine.

Phase II - Manufacture and Installation

D. Manufacture and Test

E. Field Installation

F. Evaluate Field Performance

The overall plan as applicable to the development of both the low-voltage generator (Part A) and the high-voltage generator (Part B) is diagrammed in Figure 3-183.

The development costs are given in Table 3-83 for Phases I and II for the low- and the high-voltage case.

The performance of the generator under power system conditions is preferably established by placing it in generating service with a turbine. We would propose to accomplish this utilizing the Westinghouse Large Turbine Test Facility located in the Chester Generating Station of the Philadelphia Electric Company. With this arrangement, the transient performance of the unit can be monitored conveniently, and the generated output is not critical to the power system.

Phase I - Premanufacturing Development

This section outlines the major tasks to be carried out in Phase I. The tasks that refer to the rotor are associated with Part A, the low-voltage generator development. The tasks that refer to the high-voltage armature are associated with Part B, the high-voltage generator development.

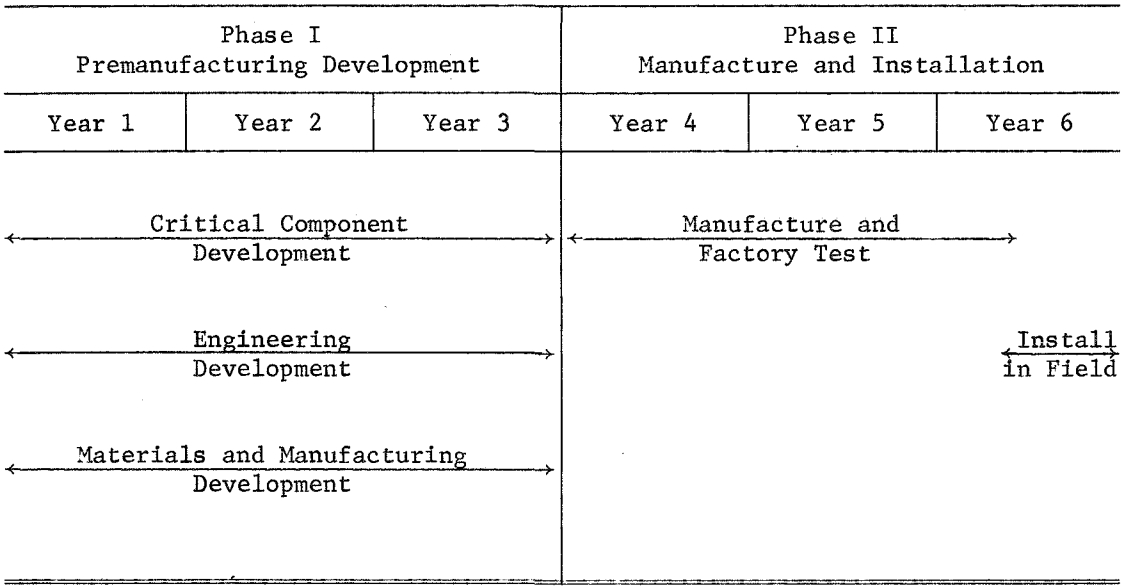

Figure 3-183. Development Plan.

Table 3-83

Development Cost
300 MVA - 3600 RPM

	Part A	Part B
	Low-Voltage	High-Voltage
	Rotor and Stator	Armature Only
Phase I (three years)		
Critical Component Development	$ 2.0 x 10^6	$ 2.0 x 10^6
Engineering Development	1.0 x 10^6	0.7 x 10^6
Material and Manufacturing Development	0.5 x 10^6	1.0 x 10^6

	Part A	Part B
	Low-Voltage	High-Voltage
Phase II (three years)		
Manufacturing, Installation and Test		
Rotor	$ 3.0 x 10^6	$ 1.2 x 10^6
Stator	3.0 x 10^6	
Armature		2.0 x 10^6
Frame		1.5 x 10^6
Auxiliaries	1.5 x 10^6	1.0 x 10^6
Installation and Test	1.0 x 10^6	1.0 x 10^6
	$12.0 x 10^6	$10.4 x 10^6

A. Critical Component Development - Rotor

The critical components of the rotor that require model tests, evaluation and design verification are:

- The helium management system
- The superconducting field coils
- The helium transfer system
- The electrothermal shield system and
- Rotor instrumentation

The schedule for this phase of the plan is given in Figure 3-184.

Model Rotor. A full-size model rotor will be designed and constructed in order to carry out tests and studies of the helium management system and the superconducting field coils. This test rotor will differ in design from the ultimate machine rotor. Since the emphasis will be on electrical and thermal performance, this test facility will consist of the inner cryogenic rotor, rotating inside of a stationary, room temperature non-metallic cylinder. Incorporation of vacuum rotating seals along with continuous dynamic pumping will provide the required vacuum thermal isolation for the inner relative to the outer structure. The inner rotor will be designed for demountability so that design changes can be more easily accommodated for the components being tested.

It is planned that the complete helium-flow system will be the first component to be tested with this facility. Heaters will be installed within the rotor and will be used to simulate fault heating. The resultant thermal disturbance to the coolant system can thus be studied. Such tests will require temperature, pressure and flow sensors for monitoring the helium system's response and performance. The thermal response of the radiation shield will also be an important part of this study.

The test rotor will be supplied with helium from a closed-cycle refrigeration system. As such, the operation of this rotor will also act as a test of interfacing of the refrigeration with the machine and as a partial test of the helium rotating seal transfer system. The main tests on the rotating transfer system will be carried out on a separate model that will be discussed further on in the present section.

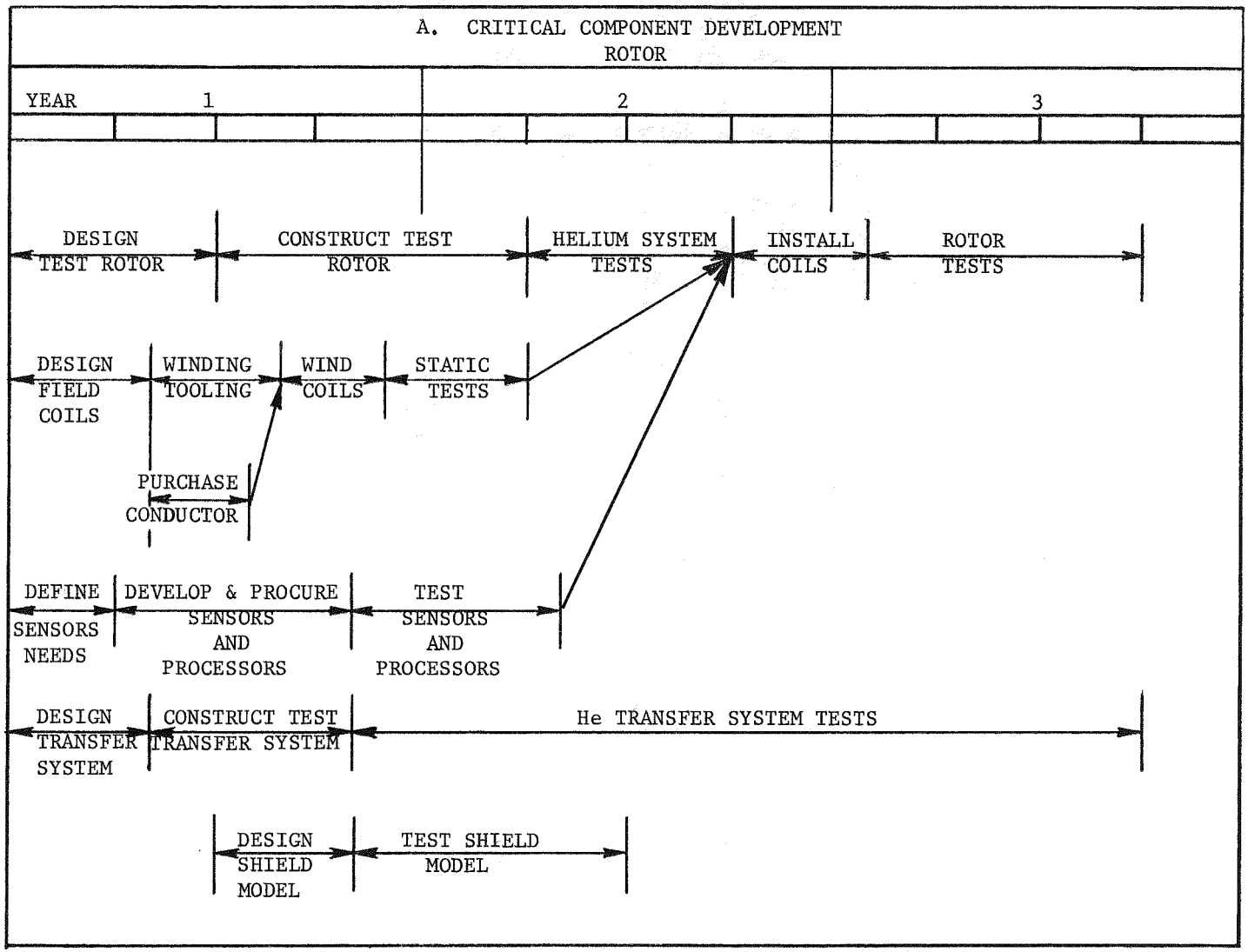

Figure 3-184. Critical Component Development - Rotor.

After the required studies of the rotor helium system are carried out, full-size field coils will be incorporated into the test rotor and rotational tests of the field winding carried out.

The field coils will first be tested statically to verify current and charge capability before being mounted for the rotational tests. Also quench behavior will be studied statically and dynamically. This latter aspect is important for verification of the seal system performance under quench and for the quench detection method.

Helium Transfer System. A double ended, full-size model of the rotating seal, transfer system will be built and run for an extended period. It is essential to demonstrate the reliability of this component over as long a period as possible. It is anticipated that initial tests will indicate certain modifications are required and it is therefore essential to build this rig immediately at the start of Phase I to give ample time for changes and running.

A good fraction of the test time of this unit would be with the unit in a close-cycle refrigeration loop.

Electrothermal Shield. While the design of the electrothermal shield would depend mainly on analytical studies of its mechanical, thermal and magnetic behavior, still it is essential to carry out model verification of some of its performance characteristics.

Such model tests would be carried out with existing two-pole stators. The purpose of the test would be to verify performance under simulated (and scaled) fault conditions in terms of mechanical static deflection and vibration modes as well as design confirmation of shield calculations for finite length shields. It is anticipated that as part of the Engineering Development task 2 for Phase I, numerical or analytical approaches will be developed for finite cylinders. It will be important to carry out experimental verification of these theoretical methods.

Rotor Instrumentation. The final component of the rotor that requires development and test is the rotor instrumentation and associated telemetering apparatus.

While there are a number of temperature sensors that can be used "off the shelf", commercial sensors for determining helium pressure and flow do not exist. It is planned to develop such sensors as are needed for the helium management system tests.

Telemetering equipment does exist for the rotating systems, and it is anticipated that such commercial equipment can be modified to suit the needs of the cryogenic rotor test.

Critical Component Development - Stator

Development by means of model tests and studies of material properties and configurations is required for the high voltage armature winding, including:

- The insulation system
  - -- to ground
  - -- between phases
  - -- within each phase
- The cooling system
- The mechanical support system
- The treating system for dielectric fluid

These studies are expected to result in defining further innovative approaches and solutions to the problem of building large, reliable, high voltage turbine generators. The following problem areas will be addressed:

Insulation System. Design parameters for a practical insulation system designed for high electrical stresses must be determined by model tests on simulated armature winding configurations. The refinement of the configuration must proceed simultaneously with the testing of candidate materials in order to develop the final arrangement of conductors, insulating materials, fluid ducts, and dielectric stress distribution provisions.

The insulation concept that has been devised for the high voltage armature windings is predicated on the possibility of approaching the dielectric strength of insulating materials that is achieved in high voltage cables. This is a requirement if generator designs of acceptable power density and size are to be achieved. High voltage cables have a very orderly geometry that can be accurately calculated and predicted and that is very favorable to the control of dielectric stress. Power transformers, on the other hand, have a more complex

insulation geometry, and make use of design stresses in the insulating materials that are considerably lower than those encountered in cables. The design stresses permitted in power transformers are too low to realize a practical design for a high voltage superconducting generator. It remains to be proven by test that these design objectives for the high voltage windings can be practically realized.

The dielectric test program of Phase I of the Development Plan will be formulated to design, manufacture, process, and test full scale models of parts of the insulation system under simulated operating conditions. The primary goal will be to verify the insulation system design, with respect to ac and impulse dielectric strength, corona or discharge inception voltage, and pulse charge magnitude. Since these parameters may be functions of operating variables such as temperature, pressure, fluid flow, and mechanical force effects, provisions to include or simulate these operating conditions will be included in the model. The results of this testing will be factored into the engineering development continuously, and adjustments will be made in the initial model as the engineering evaluation of the results requires. Qualitative analyses of the winding and insulation geometry indicate the probability that the most important refinements in the configuration will apply to the elimination or minimization of spaces in which continuous volumes of the dielectric fluid can exist.

Cooling System. As part of an overall insulation system development effort, the design parameters for the cooling system must be determined and their compatibility with the insulation function must be established. In particular, the possibility of bubble formation either by local velocities or, possibly, by dielectric stress itself must be checked and eliminated. The possibility of generation of electrostatic fields due to fluid flow must also be investigated. It would be expected that confirmation of the surface heat transfer characteristics from windings to fluid would constitute a logical part of this phase of the development.

Mechanical Support System. The parameters required for the reliable design of the stator winding support structure must be established by test. The types of tests which are required include:

- Measurement of friction between coils and insulation
- Abrasion tests on insulation materials
- Thermal cycling tests

Although extensive information exists on the mechanical properties of the insulating materials used in transformers, the geometry of the stator windings using a spiral-pancake arrangement is sufficiently different so that this information is not applicable. Therefore, material properties must be determined afresh.

Treating System for Dielectric Fluid. The testing program for the high-voltage armature insulation will include construction of a test facility consisting of a test tank and a dielectric fluid degassing and purifying plant. The test tank will be designed for vacuum-processing of the insulating models, i.e., heating under vacuum as well as vacuum-impregnation. The treating system will be designed for the elimination of gases and impurities from the dielectric liquid on a continuous basis.

B. Engineering Development

The analytical and numerical approaches that have been developed and applied during the conceptual design work must be expanded and refined to yield more accurate and thereby more reliable design procedures in the first phase of the development effort. These improvements, which apply to several different design areas, are outlined in the following.

Magnetic Analysis. The computer codes that have been developed for three-dimensional magnetic field problems will be broadened and their results integrated into machine design programs. This will provide a more accurate and realistic determination of the magnetic fields, inductances, and end turn forces than is now available. Accurate calculations of the end turn forces become especially important as the design parameters are adjusted to favor lower reactances, and hence improved critical fault clearing time. These calculations form the basis for reliable design of the winding insulation and support components, and for the development of new support arrangements. The three-dimensional field analysis must also be integrated into any meaningful program for machine optimization.

Refinements in the calculation of eddy current shields are required. At present, there are no satisfactory methods to account for end effects. An approach will be developed and applied to obtain greater accuracy in the calculation of time constants, shielding coefficients, heating, and damping performance for the multiple electrothermal shield system.

Superconductor heating calculations have so far been made with a "worst-case" type of analysis. It is planned to extend this analysis by means of more sophisticated magnetic and thermal approaches to obtain better values for field winding heating.

System Stability. Further work will be performed on the shaft oscillation modes in order to assure that acceptable shaft life will be realized in the presence of repeated system faults. This would require further extension of the present approach by solving a complete system of Park's equations and mechanical equations under worst case parameter and system conditions. These techniques will be used to supplement the "time evolution" codes that are now available for evaluating fault, fault clearing, and reclosure events.

Heat Transfer and Coolant Flow. Further refinements will be carried out in the present approaches to predicting the cryogenic cooling of the field winding and its support structure.

Dielectric Stress Distribution. An analytical method, to be used in conjunction with the test program on high-voltage insulation is required in order to predict the distribution of dielectric stresses in the armature under steady-state and transient conditions. Such methods are now in use in the design and analysis of transformer and reactor windings, but must be modified to suit the particular geometry of the spiral-pancake winding configuration.

Dynamic Analysis of Stator Windings. The high electromagnetic force levels that will be experienced by the stator windings under fault conditions, and that will be especially severe in low-reactance machines, require a thorough analysis of the forces and the resulting stresses. Such methods are in existence, but must be modified for the spiral-pancake winding arrangement. The mechanical performance of the high-voltage stator windings must also be calculated in detail, so that a reliable insulation and support structure can be designed.

C. Materials and Manufacturing Development

There are several important areas that require the development of manufacturing techniques. These relate to rotor components as well as to stator components.

Rotor. One of the critical areas for the rotor is the development of tooling and techniques for winding the field conductors into the radial slot configuration. This involves not only the winding tooling but also the techniques for forming low loss and reliable superconductor joints. The latter is especially critical for this configuration where it presently appears that in order to wind in this configuration, it will be necessary to incorporate many joints as the winding proceeds.

Fabrication of the high strength inner rotor shells represents both a materials and manufacturing task. This would involve working with the vendor in working out the metal shaping procedures to give the required geometries and mechanical properties.

Fabrication of the warm damper shield is another component that requires development work. Here the problem is as above in forming large cylinders plus the problems in developing the techniques for bonding the steel support shells to the copper alloy damper shell.

Along with the above must of course, be mechanical and metallurgical characterization of the structural materials as the processes are developed.

Stator. Manufacturing development for the stator centers on the stranded armature conductor, the fabrication of the race-track coils for the spiral armature configuration and the assembly of the coils and insulation system into a completed stator.

With the low-voltage armature the conductor is stranded, twisted and inner cooled. The development of the tooling and techniques for fabricating long lengths of this type of conductor will require significant effort. Also there will be need for tooling during the winding of the coil in order to handle the end turn bends without strand separation. The fabrication of the conductor for the high voltage armature should be less complicated since there is no inner cooling tube in this case.

Procedures and methods must be developed for winding these large race-track coils and for handling the placing of the finished coils into the stator structure. This latter step will involve both the insertion of coils and the insulation for the high-voltage armature.

Section 4.0

REVIEW QUESTIONS AND RESPONSES

During the course of this program, the completion of each quarter's work, and its documentation by means of the Quarterly Report, was followed by a Quarterly Review Meeting. These meetings were attended by the EPRI Project Manager, Dr. Mario Rabinowitz, his Advisory Group, and the Westinghouse Project Group. The memberships of these Groups are listed in the "Preface" and "Acknowledgements" Sections at the front of this Report. The review meetings included informal presentations of the project status and the technical progress as well as question and answer periods. A principal objective of this procedure was to identify technical aspects of the design that might require special attention or consideration. The questions and comments which developed during these sessions were recorded and collected, together with Westinghouse responses, and this material was then included in the final versions of the Quarterly Reports which are referenced in the "Preface." It is thus completely documented, and the interested reader is referred to the several Quarterly Reports for details.

A large proportion of the questions and comments have in fact been dealt with in a significant manner by inclusion of the appropriate components and considerations in the final report. Examples are:

- Replacement of the sliding joint between the cold inner rotor and the warm outer rotor by a flexible member.
- Inclusion of several electrical designs with low subtransient and transient reactances.
- Evolution of a concept for high-voltage armature windings.
- Application of a second method of three-dimensional flux mapping.

- Development of additional calculation methods for fault losses in the field winding and cryogenic components.
- Development of additional calculations regarding self-excited oscillations.

There are thus a relatively few areas of investigation which relate to review questions or comments to which responses are not complete. They are listed below. It should be noted, however, that these are mostly recognized in the Development Plan, Section 3.7, whose satisfactory performance would thus complete action on these items also. They are listed here primarily for completeness of the report:

- Effect of Presence of Flexible Shaft between Generator and Turbine.
- Overall Utilization Effectiveness of Spiral Winding in Comparison to Other High-Voltage Armature Winding Concepts.
- Field Winding Insertion and Assurance of Uniform Support.

A flexible shaft between the generator and the turbine has been used primarily for the purpose of limiting the shaft torque following a fault to a value that is consistent with turbine design practice; in the anticipation that the 300 MVA prototype generator will have to be connected with a turbine of conventional design. It has been pointed out that larger torques have been calculated to occur as a result of the clearing of faults and consequent reclosing. It is, however, a fact that such high-speed reclosing is not now a recommended operating practice and probably could not be safely recommended in connection with a turbine of existing conventional design. With respect to later applications to larger sizes, redesign of the appropriate parts of the shafting to withstand the torques that would result without the additional shaft flexibility is a definite possibility.

While studies reported in Section 3.4 of the Report have shown that the 300 MVA generator would be at least marginally stable and would damp out vibrations at the critical frequency of the first torsional shaft mode, even without considering mechanical damping, further studies along these lines, using more detailed models, have been recommended in the Development Plan.

As regards the overall effectiveness of space utilization of the spiral pancake winding, our studies to date have shown that, in terms of an overall

machine design for a low-voltage application, there is no significant increase in machine size, weight, or cost, as compared to a more nearly conventional modified airgap winding, our earlier choice. This is in spite of the fact that the airgap winding using diamond ends is obviously more efficient in its use of space in the straight part of the machine. The various complicated bends required in the ends, however, considerably degrade this advantage, and this degradation tends to increase with the size of the conductors and the voltage rating. With respect to the high-voltage application, we have seen no calculations that would substantiate the superiority of any other practical concept based on an existing or reasonably anticipated insulation technology. We do, however, intend to remain alert to possible alternatives for achieving the objective of a high-voltage armature winding in the optimum manner.

The method of installation of the field winding into rotor slots has been identified in our Development Plan as a critical area for the manufacturing development of the rotor. This area cannot, we believe, be further effectively pursued without the use of full-sized winding component models, for which funds must be provided. While we anticipate numerous problems in the development of the detailed assembly method, we have selected this approach because we believe that more problems, and the likelihood of reduced reliability, inhere in any other approach so far proposed. Again, we intend to remain alert to any developments which would tend to alter this view.